

**Structural Studies of Molecular Crystals of  
Inositol Derivatives and Their Inclusion  
Complexes**

*A Thesis Submitted to the University of Pune*

*for*

*the Degree of*

**Doctor of Philosophy**

*in*

Chemistry

*by*

**Rajesh G. Gonnade**



**Center for Materials Characterization  
National Chemical Laboratory  
Dr. Homi Bhabha Road, Pune - 411008  
October 2006**



"The most important thing in science is not  
so much to obtain new facts as to discover  
new ways of thinking about them."

- Sir William L. Bragg

***Dedicated to***

***My Brother Eknath...***





राष्ट्रीय रासायनिक प्रयोगशाला  
(वैज्ञानिक तथा औद्योगिक अनुसंधान परिषद)  
डॉ. होमी भाभा मार्ग पुणे - 411 008. भारत  
**NATIONAL CHEMICAL LABORATORY**  
(Council of Scientific & Industrial Research)  
Dr. Homi Bhabha Road, Pune - 411 008. India.



**CERTIFICATE**

This is to certify that the work incorporated in the thesis entitled “**Structural Studies of Molecular Crystals of Inositol Derivatives and their Inclusion Complexes**” submitted by **Rajesh G. Gonnade** was carried out by him under our supervision at the National Chemical Laboratory, Pune, India.

[M. M. BHADBHADE]

Research Guide

Center For Materials Characterization

National Chemical Laboratory

Pune-411 008

Date: 16.10.06

[M. S. SHASHIDHAR]

Research Co-guide

Division of Organic Chemistry (Synthesis)

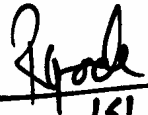
National Chemical Laboratory

Pune-411 008

Date: 16 Oct 2006

## DECLARATION

I hereby declare that the matter embodied in this thesis entitled “**Structural Studies of Molecular Crystals of Inositol Derivatives and their Inclusion Complexes**” is the result of investigations carried out by me in the Center for Materials Characterization, National Chemical Laboratory, Pune, India, under the supervision of **Dr. M. M. Bhadbhade** and **Dr. M. S. Shashidhar** and it has not been submitted elsewhere for the award of any degree or diploma, membership etc. In keeping with the general practice in reporting scientific observations, due acknowledgements has been made whenever the work described is based on the findings of other investigators.

  
16/10/06

---

[RAJESH G. GONNADE]

## Acknowledgements

*Journey is easier when you travel together. Interdependence is certainly more valuable than independence. This thesis is the result of five years of work whereby I have been accompanied and supported by many people. It is a pleasant aspect that I have now the opportunity to express my gratitude for all of them.*

*It is a great pleasure to express my sincere thanks and a deep sense of gratitude to my direct research supervisor **Dr. M. M. Bhadbhade** for introducing me to the exciting field of X-ray Crystallography. His overly enthusiasm and integral view on research and his mission for providing 'only high-quality work and not less', has made a deep impression on me. I owe him lots of gratitude for having me shown this way of research. I am very proud to have him as my research supervisor. Without his constant support and encouragement it would not have been possible to complete my research work and finally this thesis. His cheerfulness and jovial and friendly nature is greatly appreciated. Besides of being an excellent supervisor he is guardian to me and my family.*

*I also acknowledge **Dr. M. S. Shashidhar** my co-supervisor for introducing me to the exciting field of inositol chemistry and providing me lab space to carry out synthesis work. He is not only a great scientist with deep vision but also most importantly a kind person. His trust and scientific excitement inspired me in the most important moments of making right decisions and I am glad to work with him.*

*I am grateful to **Dr. K. M. Sureshan**, for his earlier crucial observations on the inclusion of the dihalomethane by the myo-inositol derivative which has triggered off the work in this thesis.*

*I am very thankful to **Dr. (Mrs.) V. G. Puranik**, who greatly supported me personally as well as scientifically during my thesis work. Her politeness, overly enthusiasm and dedication to the work are cherished. Its my pleasure to thank **Mrs. Renu Pasricha** for her valuable help, advices and maintaining cheerful atmosphere during the work.*

*I would like to thank **Dr. S. D. Pradhan** and **Dr. Ms. S. Mule** for providing me TGA/DTA and DSC data in time and for the fruitful discussions and valuable suggestions. I also thank Central NMR, Elemental Analysis and FTIR and Library Facilities, NCL for providing me the respective data in time.*

*It is my great pleasure to thank **Prof. T. N. Guru Row** and **Dr. P. Munshi**, Solid State and Structural Chemistry Unit, Indian Institute of Science, Bangalore for introducing me to the exciting field of X-ray Charge Density Study. Their valuable hints, suggestions and timely help on carrying out charge density analysis were gratefully acknowledged. Also the help from **Mr. Deepak Chopra** and **Mr. Diptikanta Swain** is greatly appreciated.*

*I am very thankful to Prof. **Dr. Martin U. Schmidt**, Institut für Anorganische und Analytische Chemie der Universität Frankfurt, Germany for his valuable help and interest in lattice energy calculations. I gratefully acknowledge **Dr. Michael Ruff**, Bruker-AXS, Karlsruhe, Germany, for X-ray data of two crystal structures on Bruker 1000 CCD diffractometer.*

*I express my sincere gratitude to **Director, NCL** and Modernization Grant from **CSIR** for the X-ray diffractometer CCD facility in NCL, Pune; this facility has enabled me to collect diffraction data for all the compound studied here. Special thank to the efforts taken by **Dr. (Mrs.) V. G. Puranik** and **Dr. Mohan. M. Bhadbhade** in installing X-ray Diffractometer Facility at CMC, NCL.*

*Special thanks to **Dr. P. Ganguly** and **Dr. S. K. Date**, earlier Heads of Physical Chemistry Division and **Dr. M. M. Bhadbhade** Head, CMC and **Dr. S. R. Sainkar**, former Head, CMC for their constant encouragement and allowing me to complete my thesis work in time. I sincerely thank all the colleagues of CMC for helping me during the course of my research work. I am thankful to **Dr. K. N. Ganesh**, former Head, OCS, NCL for allowing me to use their divisional lab facilities for synthesis work.*

*I express my sincere gratitude to DST, New Delhi for financial assistance to the project. I take this opportunity to thank IUCr, for supporting my active participation in International School of Crystallography, Eliche (2001) and IUCr general assembly at Florence (2005), Italy.*

*I thank **Prof. K. Venkatesan**, **Prof. Gautam R. Desiraju**, **Prof. Roland Boese**, **Prof. Dario Braga**, **Prof. Joel Bernstein**, for fruitful discussions either during their visit to our lab or in the conferences. I also wish to thank **Prof. S. Gadre** and **Dr. Babu** for the fruitful discussions on estimating nature of halogen bonding contact. I also would like to*

*thank Dr. C. G. Suresh and his group for their valuable help. Special thanks to Dr. E. Suresh, CSMCRI, Bhavnagar, for his encouragements and suggestions.*

*I sincerely thank to earlier lab mates Dr. Praveen, Dr. Sureshan, Dr. A. K. Sanki, Dr. R. Barman, Dr. Manash Sarmah, Gaurav, Sachin and Devaraj, for their help and encouragement. My present lab-mates Manoj, Shailesh, Murali, Rajendra, Shobhana, Madhuri and Bharat made the working atmosphere in the lab extremely enjoyable. I am very thankful to Manoj and Shobhana for proof reading of this thesis. Manash and Manoj were also very good friends to me, who were available for help and advices both within and outside NCL whenever needed. I take this opportunity to thank them for their kind co-operation. I am very grateful to Mr. Prakash, (M. Sc. Project Student) for his kind help in setting up the crystallization of some inclusion crystals discussed in the Chapter 8 of this thesis. Special thank to all the friends and colleagues at NCL who directly or indirectly helped me during doctoral research work.*

*A very special thank to my brother, **Prof. Eknath M. Gonnade** and vayni **Kalpana**, for their immense help during my education. I am dedicating this thesis to them because their unforgettable help in providing me excellent educational platform. I don't know where I would have been, if they had not taken the responsibility of my studies. I am very much thankful to my beloved wife **Jaya** (Vaishali) for her constant encouragement and patience. I am very fortunate to have her as my life partner. During last three years of my research work, she gave me strong and emotional never-ending support.*

*The hospitality and encouragement from Dr. Mrs. Ranjana M. Bhadbhade madam, Dr. Mrs. Vidya Shashidhar madam and the enjoyable company of Megha, Malhar, Shishira and Archana are sincerely acknowledged.*

*Finally, I express my deepest sense of gratitude to my parents, elder parents, in-law's, Anil bhau, Manda vayni, Sister- Kunda, brother-in-law Raju for their encouragements and care throughout my life. Special Thanks to sweet nieces, Sonu, Tinu, Sherya, Shruti, Sakshi, Komal, nephews - Kapil, Yash and brother-in-law Nishikant for making pleasant atmosphere at home.*

October 16, 2006, Pune, India.

[**RAJESH. G. GONNADE**]

## TABLE OF CONTENTS

	PAGE
<b>Abstract</b> .....	<b>i-x</b>
<b>Chapter 1. Understanding ‘Halogen Bonding’ Interactions</b>	<b>1</b>
1.1 Intermolecular Interactions.....	<b>2</b>
1.2 Non-covalent Interactions Involving Halogens.....	<b>7</b>
1.3 Halogen Bonding: A Historical Background.....	<b>12</b>
1.4 Halogen Bonding Interactions from Cambridge Crystallographic Database.....	<b>16</b>
1.5 Halogen Bonding: Theoretical Calculations.....	<b>20</b>
1.6 Halogen Bond: Applications in crystal engineering and Designing Functional solids.....	<b>23</b>
1.7 Halogen Bonding in Biological Systems.....	<b>24</b>
1.8 Halogen Bonding and Implications for Drug Design .....	<b>26</b>
1.9 Insight into ‘Halogen Bonding’ Contacts: Path Followed in the Present Thesis.	<b>27</b>
<b>Chapter 2. Spontaneous Formation of Stable Inclusion Crystals of Racemic 1, 2, 3, 4, 5-penta-<i>O</i>-benzoyl-6-<i>O</i>-tosyl <i>myo</i>-inositol Induced only by Dihalomethanes via C-Halogen...O=C and C-H...O Short Contacts.</b>	<b>30</b>
2.1 Introduction.....	<b>31</b>
2.2 Experimental Section.....	<b>37</b>
2.2.1 Synthesis.....	<b>37</b>
2.2.2 Crystallization.....	<b>38</b>
2.2.3 Thermal Analysis.....	<b>40</b>
2.2.4 Hot Stage Microscopy.....	<b>44</b>
2.2.5 X-ray Data Collection, Structure Solution and Refinement.....	<b>44</b>
2.3 Results and Discussion.....	<b>50</b>
2.3.1 Intramolecular Geometry.....	<b>50</b>
2.3.2 Host Organization.....	<b>53</b>
2.3.3 Role of Guests in the Assembly of Dimers.....	<b>55</b>
2.3.4 Significance of ‘Halogen Bonding’ in Host-Guest Interactions.....	<b>56</b>
2.3.5 Other Host...Guest (C-H...O and C-H...halogen) Interactions.....	<b>59</b>

2.3.6	Channel Formation.....	59
2.3.7	Other Weak Interactions that Stabilize Molecular Packing.....	62
2.3.8	Spontaneous Crystallization of <b>3</b> Induced by CH <sub>2</sub> X <sub>2</sub> .....	65
2.3.9	Trace of Dihalomethane Induces Self Assembly.....	66
2.4	Conclusions.....	68

**Chapter 3. Polymorphic and Pseudopolymorphic Behaviour of hexa-*O*-benzoyl *myo*-inositol: Conversion of Chiral to Achiral Crystals, Gradual Escape of Guest from Inclusion Crystal Lattice** **69**

3.1	Introduction.....	70
3.2	Experimental Section.....	72
3.2.1	Synthesis.....	72
3.2.2	Crystallization.....	73
3.2.3	Thermal Analysis.....	76
3.2.4	Data Collection, Structure Solution and Refinement.....	77
3.3	Results and Discussion.....	85
3.3.1	Structure of Dimorphs of <b>4</b> (Form I and Form II).....	85
3.3.2	Structures of Dihalomethane Inclusion Crystals Before and After Guest Escape.....	92
3.3.3	Structural Changes Upon Guest Escape in Dihalomethane Inclusion Crystals of <b>4</b> .....	109
3.3.4	Structures of Chloroform and Bromoform Inclusion Crystals of <b>4</b> .....	113
3.3.5	Structure of Dioxane Solvated Crystals of <b>4</b> .....	127
3.4	Conclusions.....	132

**Chapter 4. Pseudopolymorphic Behaviour of Racemic 1, 2, 3, 5, 6-penta-*O*-benzoyl-4-*O*-benzyl-*myo*-inositol: Synthesis, Crystallization and X-ray Crystallographic Studies** **134**

4.1	Introduction.....	135
4.2	Experimental Section.....	135
4.2.1	Synthesis.....	135

4.2.2	Crystallization.....	137
4.2.3	Differential Scanning Calorimetric Analysis (DSC).....	138
4.2.4	Data Collection, Structure Solution and Refinement.....	139
4.2.5	Thermal Response on Hot Stage Microscopy.....	141
4.3	Results and Discussion.....	141
4.3.1	Structure of Solvent Free Crystals of <b>7</b> .....	142
4.3.2	Structures of Form II Inclusion Crystals of <b>7</b> .....	147
4.3.3	Structures of Form III Inclusion Crystals of <b>7</b> .....	156
4.3.4	Comparison of Conformations of Molecules of <b>7</b> in its Crystals <b>7</b> , <b>7·CH<sub>2</sub>Br<sub>2</sub></b> and <b>7·CHCl<sub>3</sub></b> .....	167
4.4	Conclusions.....	168

## **Chapter 5. Single Crystal to Single Crystal Phase Transition of Room Temperature**

	<b>Form to High Temperature Form and Solvatomorphism in Hexa-<i>O-p</i>-toluoyl -<i>myo</i>-inositol: Synthesis, Crystallization and X-ray Studies</b>	<b>169</b>
5.1	Introduction.....	170
5.2	Experimental Section.....	170
5.2.1	Synthesis.....	170
5.2.2	Crystallization.....	171
5.2.3	DSC of Solvent Free Crystals.....	172
5.2.4	Thermal Response on Hot Stage Microscopy.....	173
5.2.5	Data Collection, Structure Solution and Refinement.....	174
5.3	Results and Discussion.....	177
5.3.1	Structures of Forms I and Form II crystals of <b>8</b> .....	177
5.3.2	Structure of Dioxane Inclusion Crystals (Form III) of <b>8</b> .....	184
5.3.3	Difference Between Structures of Form I and Form III Crystals of <b>8</b> ....	191
5.3.4	Conformational Difference in Molecules of Form I, Form II and Form III of <b>8</b> .....	192
5.4	Conclusions.....	193



<b>Chapter 6. Exploring the Inclusion Behaviour of 4,6-di-<i>O</i>-benzoyl-<i>myo</i>-inositol-1,3,5-orthoformate and its Orthoacetate Analog: Isostructurality in Host Organization and Self-Inclusion Phenomena</b>	<b>194</b>
6.1 Introduction.....	195
6.2 Experimental Section.....	196
6.2.1 Synthesis.....	196
6.2.2 Crystallization.....	196
6.2.3 Thermal Analysis of Inclusion Crystals of <b>9</b> .....	198
6.2.4 Hot Stage Microscopy.....	200
6.2.5 X-ray Data Collection, Structure Solution and Refinement.....	201
6.3 Results and Discussion.....	205
6.3.1 Intramolecular Geometry in Solvates and Solvent Free Crystals of <b>9</b> ...	205
6.3.2 Dimer Formations.....	208
6.3.3 Difference in Association of Dimers in Inclusion Crystals of <b>9</b> .....	212
6.3.4 Host-Guest Association in <b>9</b> .CH <sub>2</sub> Cl <sub>2</sub> and <b>9</b> .CH <sub>2</sub> CIBr.....	216
6.3.5 Host-Guest and Guest-Guest Interactions in <b>9</b> .CHCl <sub>3</sub> , <b>9</b> .CHBr <sub>3</sub> and <b>9</b> .CHCl <sub>2</sub> Br.....	220
6.3.6 Stability of Dihalomethane and Trihalomethane Inclusion Crystals of <b>9</b> .....	224
6.3.7 Association of Dimers in solvent free crystals of <b>9</b> : When Host becomes Guest.....	225
6.3.8 Crystal Structure of <b>10</b> .....	229
6.4 Conclusions .....	235
<b>Chapter 7. Concomitant Dimorphs of tri-<i>O</i>-[<i>p</i>-halobenzoyl]-<i>myo</i>-inositol 1,3,5-orthoformates with Different Halogen Bonding Contacts: First Order Crystal-to-Crystal Thermal Phase Transition of Kinetic Form to the Thermodynamic Form</b>	<b>236</b>
7.1 Introduction.....	237
7.2 Experimental Section.....	238
7.2.1 Synthesis.....	238

7.2.2	Crystallization.....	239
7.2.3	Thermal Analysis (DSC Study).....	241
7.2.4	Data Collection, Structure Solution and Refinement .....	243
7.2.5	Thermal Response on Hot Stage Microscopy.....	245
7.3	Results and Discussion.....	246
7.3.1	Intramolecular Geometry.....	246
7.3.2	Dimer Formation via Halogen Bonding Contacts.....	247
7.3.3	Association of Dimers.....	248
7.3.4	Conformational Differences.....	252
7.3.5	Proposed Mechanism of Transition from Form I to Form II Crystals of <b>11</b> .....	253
7.3.6	Lattice Energy Calculations.....	256
7.3.7	CSD Survey on Different Types of Halogen Bonding Contacts.....	258
7.4	Conclusions.....	261

**Chapter 8. Polymorphic and Pseudopolymorphic Behaviour of racemic 2,6-di-*O*- (*p*-halobenzoyl)-*myo*-inositol 1,3,5-orthoformates: Different Halogen Bonding Contacts in Molecular Associations and Crystal-to-Crystal Phase Transition**

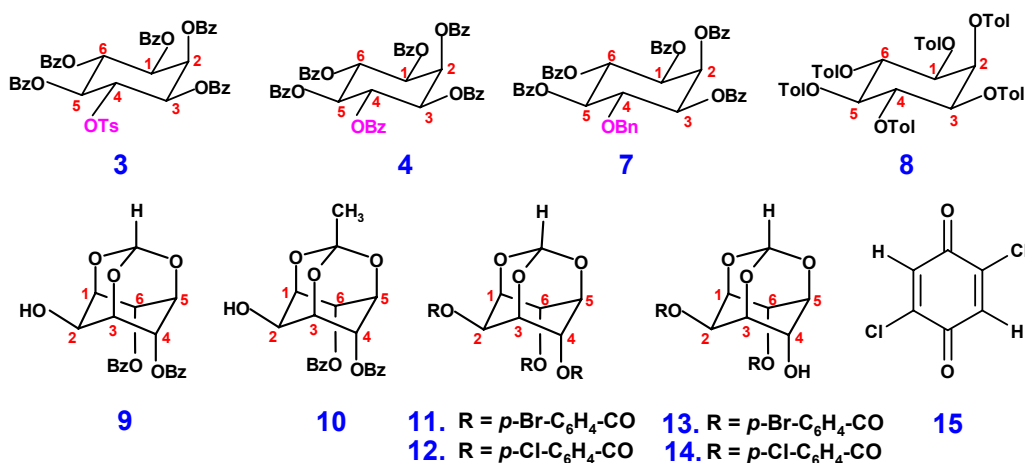
		262
8.1	Introduction.....	263
8.2	Experimental Section.....	264
8.2.1	Synthesis.....	264
8.2.2	Crystallization of <b>13</b> and <b>14</b> .....	265
8.2.3	DSC Studies <b>13</b> and <b>14</b> .....	268
8.2.4	Thermal Response on Hot Stage Microscopy .....	271
8.2.5	X-ray Data Collection, Structure Solution and Refinement .....	273
8.3	Results and Discussion.....	280
8.3.1	Structures of Polymorphs of <b>13</b> and <b>14</b> .....	280
8.3.1.1	One-Dimensional Isostructurality.....	281
8.3.1.2	Differences in Dimer Formation.....	285
8.3.1.3	Dimeric Association via C-H···X and C-X···O Contact.....	289

8.3.1.4 Possible Pathways of Nucleation .....	291
8.3.1.5 Conformational Differences .....	293
8.3.1.6 Proposed Mechanism for Transition from Form I Crystals to Form II Crystals of <b>13</b> .....	294
8.3.2 Structures of Solvates of <b>13</b> and <b>14</b> .....	296
8.3.2.1 Conformational Difference.....	296
8.3.2.2 Host Organization.....	298
8.3.2.3 Host-Guest Assembly and Intermolecular Interactions in Solvates of <b>13</b> and <b>14</b> .....	311
8.3.2.4 Difference in Association of molecules in Polymorphs and Solvates of <b>13</b> and <b>14</b> .....	324
8.4 Conclusions.....	326
<b>Chapter 9</b> .....	<b>327</b>
<b>Part A: General Conclusion</b> .....	<b>328</b>
9.1 On exhibiting (Pseudo) Polymorphic Behaviour.....	328
<b>Part B: Charge Density Study of Model Compound</b> .....	<b>332</b>
9.2 Introductions.....	332
9.3 Charge Density and Weak Intermolecular Interactions.....	334
9.4 System Chosen for Charge Density Studies.....	335
9.5 Experimental Section.....	336
9.6 Results and Discussion.....	338
<b>Part C: Scope of Future Work</b> .....	<b>343</b>
9.5 Working on Guest Specificity for Molecular Selectivity / Separations.....	343
9.6 Spontaneous Resolution – Implications in Producing Organic Chiral Crystals..	343
9.7 Crystal-to-Crystal Phase Transitions Between Polymorphs.....	344
9.8 Insight into Halogen Bonding Interactions – it’s Implications in Drug Binding.	344
9.9 Study of Other Isomers of Inositol .....	344

<b>Appendix I: Lattice energy Calculations</b>	<b>345</b>
<b>Appendix II: Charge Density Analysis: Overview</b>	<b>348</b>
<b>References.....</b>	<b>369</b>
<b>List of Publications.....</b>	<b>390</b>

## Abstract

The research work reported in the thesis entitled “**Structural Studies of Molecular Crystals of Inositol Derivatives and Their Inclusion Complexes**” originated after a serendipitous discovery<sup>1</sup> of highly selective encapsulation of dihalomethanes by the *myo*-inositol derivative **3** (see below). Selective inclusion of guest molecules in crystals via intermolecular weak interactions<sup>2</sup> has always been of interest for both chemical and pharmaceutical industries<sup>3</sup> because of their potential applications in molecular separation and improving drug-receptor binding. A relatively new type of weak interaction, C-halogen...oxygen contact or what is termed as ‘halogen bond’<sup>4</sup> plays a vital role in forming a stable host-guest assembly as in crystals of **3**, a bonding recognized as a strong driving force in the formation of co-crystals and controlling the construction of supramolecular architectures.<sup>4d</sup> This thesis depicts the role of halogen bonding interactions in promotion and growth of (inclusion) crystals and their stabilities along with some interesting observations on concomitant polymorphs and their crystal-to-crystal phase transition. Highly selective encapsulations of dihalomethanes by **3** prompted us to investigate inclusion behaviour of some more hexa-*O*-substituted *myo*-inositol derivatives and *myo*-inositol 1,3,5-orthoesters. This thesis describes the crystal structure of inclusion complexes and polymorphs of *myo*-inositol derivatives **3**, **4**, **7-14** and the charge density analysis of 2,5-dichloro-1,4-benzoquinone (**15**).



Bz = C<sub>6</sub>H<sub>5</sub>CO, Ts = *p*-CH<sub>3</sub>-C<sub>6</sub>H<sub>4</sub>-SO<sub>2</sub>, Bn = C<sub>6</sub>H<sub>5</sub>-CH<sub>2</sub>, Tol = *p*-CH<sub>3</sub>-C<sub>6</sub>H<sub>4</sub>CO

**Chapter 1** reviews intermolecular halogen interactions with various functionalities, with a special reference to the C-halogen...O (halogen bonding) interactions. The subsequent four **Chapters (2,3, 4 and 5)** report the results of inclusion behaviour of analogs of **3**; their crystal structures and (pseudo) polymorphic behaviour. **Chapters 6, 7 and 8** describe the inclusion and interesting polymorphic behaviour of *myo*-inositol 1,3,5-orthoesters including crystal-to-crystal structural phase transitions. To probe the C-Cl...O interactions further, the X-ray charge density analysis of the model compound, 2,5-dichloro-1,4-benzoquinone, possessing good halogen-bonding contacts was also undertaken which is described in **Chapter 9**. Highlights of each of the chapters are given below.

**Chapter 1** gives a brief review on various non-bonding interactions in molecular crystals with emphasis on halogen bonding interactions. It was recognized as early as in 1950s,<sup>4a</sup> that halogens could form complexes with hydrogen-bond acceptors. This behaviour was rationalized on the basis of anisotropic charge distribution of halogens. Thus, heavier halogens (Cl, Br, and I, not fluorine due to extreme electronegativity and limited polarizability) exhibit electrophilic character along axis of C-X bonds and nucleophilic character perpendicular to these bonds.<sup>4bc</sup> Hence, halogen-bonding interactions with nucleophiles (e.g. O, N, S, Se) display roughly linear geometries. ‘Halogen bonding’ is an attractive interaction between the atoms possessing one or more lone pair of electrons, which donate their lone pair to a halogen atom. The review illustrates these interactions and their applications in crystal engineering, supramolecular synthesis and biological molecules.

**Chapter 2** reports selective encapsulation of dihalomethanes by racemic 1,2,3,4,5-penta-*O*-benzoyl-6-*O*-tosyl-*myo*-inositol (**3**).<sup>1</sup> The compound **3** resisted crystallization from most of the common organic solvents but spontaneously crystallized in the presence of dichloromethane (even when present at a concentration level of ~0.01% in other solvents) to yield highly stable good quality single crystals. DSC studies showed that the solvent molecules were retained in the crystal lattice close to the melting point of the crystals, suggesting a strong association of guest molecules with the host. Crystal structure of **3** showed formation of open channels containing CH<sub>2</sub>Cl<sub>2</sub> guests

(**Figure 1A**), which makes two notable interactions with the host molecule, C-H $\cdots$ O and C-Cl $\cdots$ O, the later termed as ‘halogen bonding’ appear to play a significant role.<sup>4</sup> In order to explore the halogen selectivity in host-guest crystal formation, **3** was also crystallized from CH<sub>2</sub>Br<sub>2</sub>, CH<sub>2</sub>ClBr, CH<sub>2</sub>ICl and CD<sub>2</sub>Cl<sub>2</sub>, which yielded highly stable good quality inclusion crystals. These experiments revealed that brominated solvents were preferentially included over chlorinated solvents, and the order of selectivity is CH<sub>2</sub>Br<sub>2</sub> > CH<sub>2</sub>ClBr > CH<sub>2</sub>Cl<sub>2</sub>. Notably, all the guests have C<sub>2</sub> symmetry axis which coincides with the crystallographic two-fold in space group C<sub>2</sub>/c (crystals with CH<sub>2</sub>ClBr and CH<sub>2</sub>ICl showed two-fold statistical disorder), other halogenated guests such as CHCl<sub>3</sub>, CCl<sub>4</sub>, which lack C<sub>2</sub> symmetry did not yield crystals. An inclusion crystal with the lowest observed occupancy (5%) of CH<sub>2</sub>Cl<sub>2</sub> is also reported, which seems to suggest that guest molecules induce the host assembly (**Figure 1B**).

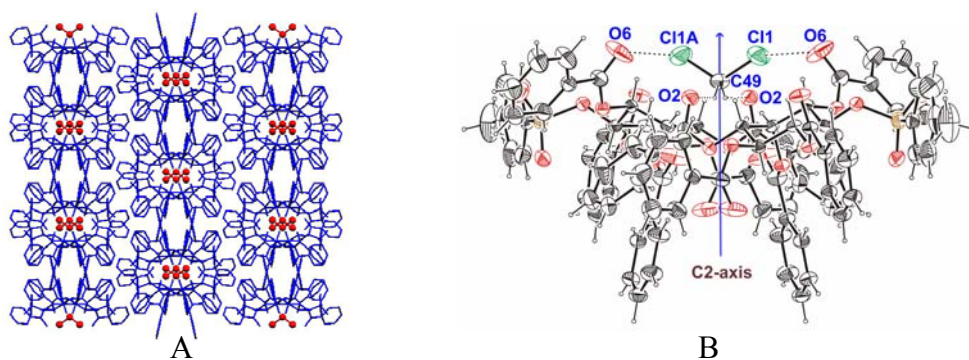


**Figure 1.** A) View of molecular packing down c-axis showing presence of guest molecules (red) in the channels formed by host molecules (blue) and B) Host-guest association across two-fold axis in CH<sub>2</sub>Cl<sub>2</sub> inclusion crystals of **3**.

**Chapter 3** reports the effect on inclusion tendency by replacing tosyl group at C4 position in **3** by benzoyl group. Hexa-*O*-benzoyl-*myo*-inositol (**4**) also formed inclusion complexes exclusively with halogenated solvents CH<sub>2</sub>Cl<sub>2</sub>, CH<sub>2</sub>Br<sub>2</sub>, CH<sub>2</sub>ClBr, CHCl<sub>3</sub> and CHBr<sub>3</sub> as well as with dioxane. Unlike crystals of **3**, inclusion crystals of **4** were highly unstable (in the open atmosphere). X-ray intensity measurements of fresh crystals of dihalomethane revealed the presence of two molecules of CH<sub>2</sub>X<sub>2</sub> (X = Cl, Br, **Figure 2A**, green and red), while the data collection after six to eight hours (standing the crystals in paraffin oil) showed presence of only one molecule of CH<sub>2</sub>X<sub>2</sub> (**Figure 2B**, green). Inclusion crystals with CHCl<sub>3</sub> and CHBr<sub>3</sub> as guests make good halogen bonding contacts

with the host along with C-H $\cdots$ O and C-H $\cdots$ X contacts. But due to bigger size of these guests compared to dihalomethanes, the host assembly expands breaking up host $\cdots$ host interactions seen earlier.

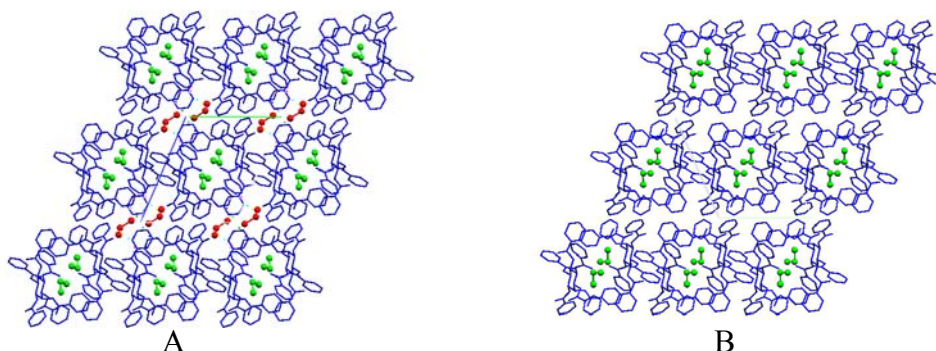


**Figure 2.** View of molecular packing down a-axis of CH<sub>2</sub>Cl<sub>2</sub> inclusion crystals of **4**, A) immediate data collection and B) data collection after six hours.

The compound **4** exhibited fascinating polymorph conversion; a metastable chiral polymorph formed under kinetic conditions slowly transformed to an achiral form upon standing in the mother liquor.<sup>5</sup> Supersaturated solution of **4** in ethyl acetate yielded long needle like crystals (**Figure 3A**) within one hour, belonging to a chiral space group P6<sub>1</sub>. These crystals gradually disappeared with the simultaneous appearance of small plate like crystals (**Figure 3B** and **3C**) belonging to the achiral space group P-1. Formation of both polymorphs is discussed with respect to their differences in molecular associations.

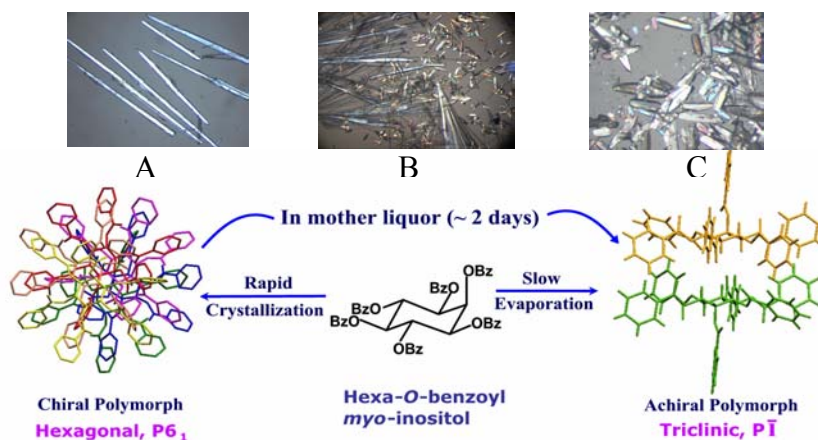


**Figure 3.** Photomicrographs of crystals of solvent free form of **4**, A) long and thin needles (chiral form), B) needles and plates (chiral and achiral forms) in mother liquor and C) only plate like crystals, achiral form.



**Chapter 4** reports structures of highly unstable inclusion complexes of racemic 1,2,3,5,6-penta-*O*-benzoyl-4-*O*-benzyl-*myo*-inositol (**7**) exclusively with halogenated solvents such as CH<sub>2</sub>Cl<sub>2</sub>, CH<sub>2</sub>Br<sub>2</sub>, CH<sub>2</sub>ClBr, CHCl<sub>3</sub> and CHCl<sub>2</sub>Br. Crystallization from other common solvents produced solvent free crystals. Thus, by replacing tosyl group at C4 position in **3** by benzyl group maintained its pseudopolymorphic behavior but lost the specificity and stability of inclusion formation. The stoichiometry of host to guest was 1:1 in CH<sub>2</sub>Cl<sub>2</sub>, CH<sub>2</sub>Br<sub>2</sub> and CH<sub>2</sub>ClBr crystals, whereas 2:1 in crystals of CHCl<sub>3</sub> and CHCl<sub>2</sub>Br. In the former, guest molecules occupy all the cavities formed by the host molecules (**Figure 4A**), whereas in the latter only alternate cavities are occupied by the guests (**Figure 4B**). It is interesting that there are no ‘halogen bonding’ contacts between the host and guest molecules, the guest molecules are associated with the host via C-H···O, C-H···halogen and C-halogen···π contacts. The solvent free crystals of **7** have completely different molecular packing from the ones described earlier.

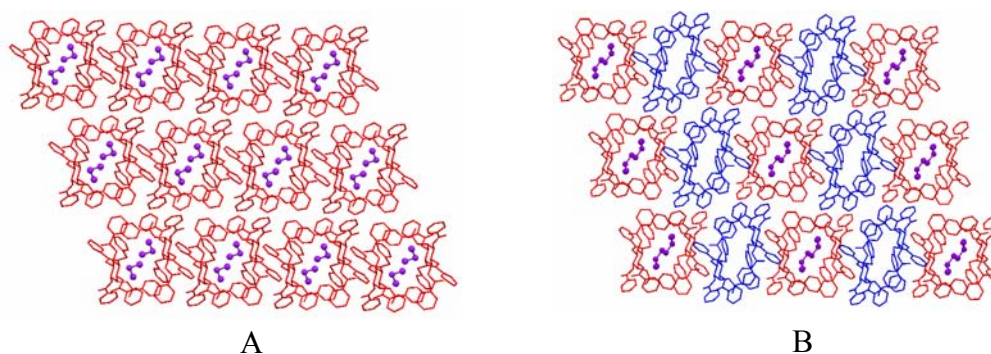


**Figure 4.** View of molecular packing down a-axis in inclusion crystals of **7**, A) **7**·CH<sub>2</sub>Br<sub>2</sub> and B) **7**·CHCl<sub>3</sub>

**Chapter 5** reports inclusion tendencies of symmetric hexa-*O*-toluoyl-*myo*-inositol (**8**). Crystallization from most of the solvents, **8** produced solvent free crystals (Form I). Interestingly, this form showed single crystal to single crystal phase transition upon heating to ~ 260 °C giving crystals of a new form (Form II). The Form II crystals could also be obtained by cooling the melt of **8**. Also crystallization of **8** from dioxane produced highly unstable inclusion complex (Form III). The association of host molecules in the inclusion crystals creates open framework structure (**Figure 5A**), which accommodates dioxane molecules that make C-H···O contacts with the host. Molecular

organization in both solvent free crystals (Form I and Form II) does not leave any voids for even a small guest inclusion (**Figure 5B**).

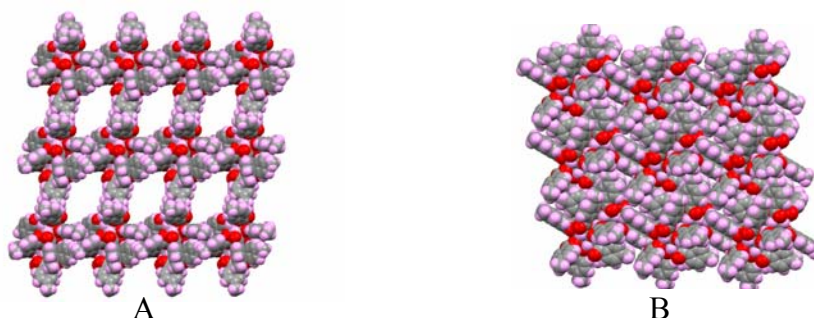


**Figure 5.** View of molecular packing down a-axis in crystals of **8**, A) open framework structure in dioxane inclusion crystals and B) in solvent free form with no voids.

**Chapter 6** describes inclusion complexes of 4,6-di-*O*-benzoyl *myo*-inositol 1,3,5-orthoformate (**9**) and the crystal structure of its orthoacetate analog **10**. Compound **9** forms inclusion crystals (Form I, monoclinic  $P2_1/n$ ) with  $\text{CH}_2\text{Cl}_2$ ,  $\text{CH}_2\text{ClBr}$  (highly unstable) and  $\text{CHCl}_3$  (moderately stable). It also forms moderately stable inclusion crystals with  $\text{CHBr}_3$  and  $\text{CHCl}_2\text{Br}$  (Form II, Triclinic,  $P-1$ ). Crystallization of **9** from most other solvents gave stable solvent free crystals (Form III, monoclinic  $P2_1/c$ ). It is striking that inclusion crystals with trihalomethane solvent were moderately stable showed halogen-bonding contacts ( $\text{C-X}\cdots\text{O}$ ) along with  $\text{C-H}\cdots\text{O}$  contacts (**Figure 6A**), whereas highly unstable inclusion crystals with dihalomethane contained only  $\text{C-H}\cdots\text{O}$  contacts between the guest and the host. A remarkable one-dimensional isostructurality<sup>6</sup> is present in all the structures; the orthoformate moieties form centrosymmetric ‘head to head’ dimers via intermolecular  $\text{O-H}\cdots\text{O}$  and  $\text{C-H}\cdots\text{O}$  contacts reflected in a conserved b-axis in all the forms. However, linking of these strings along c-axis diverges to yield monoclinic and triclinic forms. In monoclinic form, these one-dimensional strings (red, **Figure 6B**) have  $2_1$ -screw relation with the other string (blue, **Figure 6B**), whereas they are centrosymmetrically related in the triclinic form (**Figure 6C**). In both systems, the head-to-head dimeric association creates cavities to accommodate the guest solvents. Solvent free crystals of **9**, present an interesting structure where molecules of **9** play the role of host as well as guest (‘self inclusion’). (**Figure 6D**).

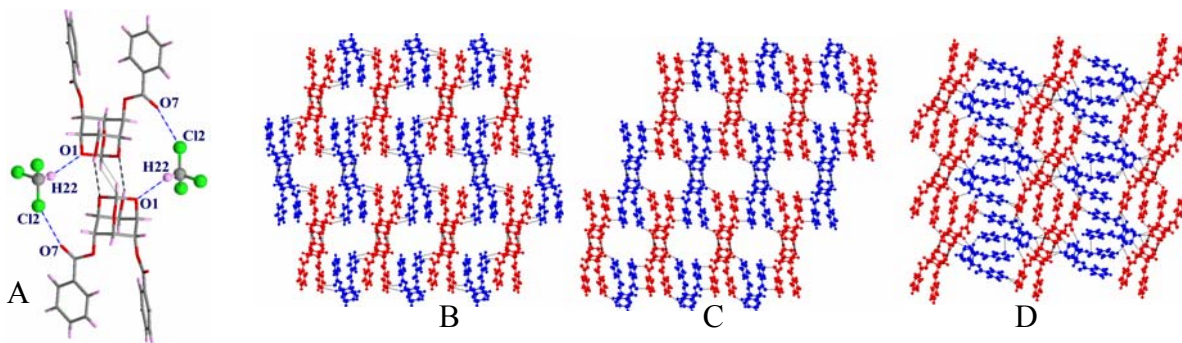


**Figure 6.** A) Host-guest association in  $\text{CHCl}_3$  inclusion crystals of **9**, B) packing mode of host molecules of **9** in monoclinic system, C) packing mode host molecules of **9** in triclinic system and D) self-inclusion type packing mode in solvent free crystals of **9**.

In crystals of **10** because of the bulkier methyl group, the head-to-head association is lost showing a totally different packing mode that leaves no room for solvent inclusion. Molecules of **10** show helical assembly around crystallographic  $2_1$ -screw axis via  $\text{O-H}\cdots\text{O}$  and  $\text{C-H}\cdots\text{O}$  interactions (**Figure 7A**) and neighboring helices are linked via  $\text{C-H}\cdots\text{O}$  contacts (**Figure 7B**). Along b-axis the molecules form endless chain of dancing pairs linked via  $\text{C-H}\cdots\text{O}$  contacts (**Figure 7C**).

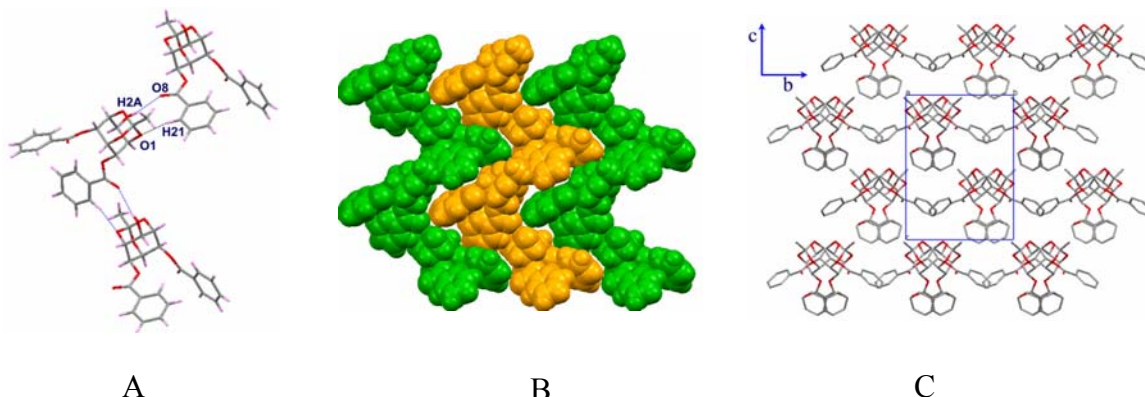


**Figure 7.** A) Helical assembly of molecules via  $\text{O-H}\cdots\text{O}$  and  $\text{C-H}\cdots\text{O}$  contacts in crystals of **10**, B) Inter-helical packing and C) molecular packing showing infinite chain of dancing pairs along b-axis.

Since many of the inclusion complexes discussed in the previous chapters showed halogen bonding contacts between the guest and the host, it was thought to make halogenated host derivatives of *myo*-inositol to examine their molecular association and inclusion behavior. **Chapter 7** describes interesting structural properties of 2,4,6-tri-*O*-

[*p*-halobenzoyl]-*myo*-inositol 1,3,5-orthoformates (bromo, **11** and chloro, **12**). Both **11** and **12** gave concomitant dimorphs (needles, Form I and octahedral blocks, Form II) when crystallized from ethyl acetate-petroleum ether solution (**Figure 8A**) but no inclusion of small molecules was observed in any of the crystals. Form I crystals were kinetically produced (within few hours), whereas Form II crystals were obtained by slow evaporation (~ 2 days). Single Crystal X-ray studies of **11** revealed that both forms utilized ‘halogen bonding’ contacts, C-Br···O-C (ether oxygen) in Form I (**Figure 8B**) and C-Br···O=C (carbonyl oxygen) in Form II (**Figure 8C**). DSC studies suggested an irreversible structural phase transition at ~ 185-186 °C (**Figure 8D**). Form I crystals (**Figure 8F**) upon heating at 185-186 °C, underwent crystal-to-crystal phase transition to Form II crystals (**Figure 8G**).<sup>7</sup> The complete crystal structure analysis and possible mechanism of phase transition is discussed.

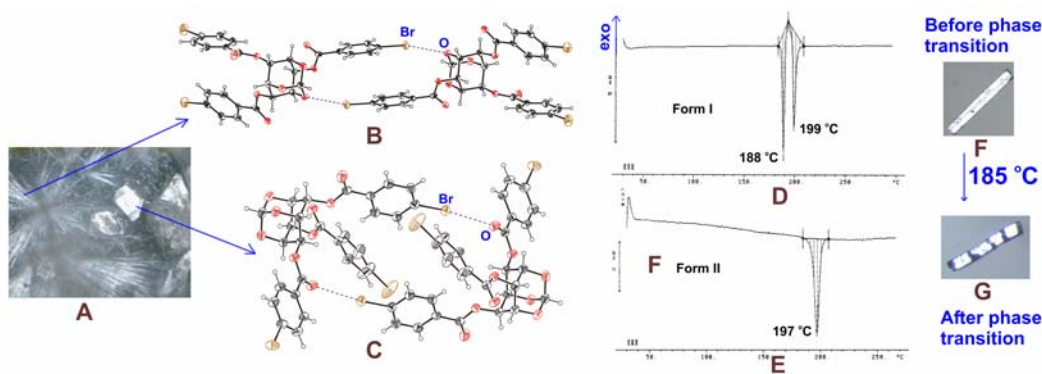


**Figure 8.** A) Photomicrographs showing concomitant dimorphs in **7**, B) dimeric association of molecules of **11** (Form I) via C-Br···O-C contacts, C) dimeric association of molecules of **11** (Form II) via C-Br···O=C contacts, D) DSC of Form I crystals of **11**, E) DSC of Form II crystals of **11**, crystal photographs, before phase transition (F) and after phase transition (G).

**Chapter 8** reports structures of dimorphs and pseudopolymorphs of racemic-2,4-di-*O*-[*p*-halobenzoyl]-*myo*-inositol 1,3,5-orthoformates. Both bromo **13** and chloro **14** derivatives form polymorphs when crystallized from methanol (thin needles, Form I) and ethyl acetate (small blocks, Form II), whereas crystallization from various other solvents produced pseudopolymorphs, which were stable up to one week (in open atmosphere). Crystal structure analysis revealed Form I crystals of **13** make centrosymmetric dimers via



C-H...halogen contacts (**Figure 9A**), whereas molecules in Form II crystals of **13** centrosymmetrically associated via dimeric halogen bonding contacts (**Figure 9B**). DSC studies of Form I crystals of **13** suggested an irreversible structural phase transition at ~ 223-224 °C. Form I crystals of **13** upon heating at the transition temperature, underwent crystal-to-crystal phase transition to Form II crystals of **13**. The Form I crystals of **14** did not show such behaviour. Interestingly, inclusion crystals of both **13** and **14** showed helical assembly of the host molecules around the crystallographic two-fold screw axis making O-H...O and C-H...O contacts (**Figure 9C**). The associations of the neighboring helices create voids to accommodate guest solvents (**Figure 9D**).

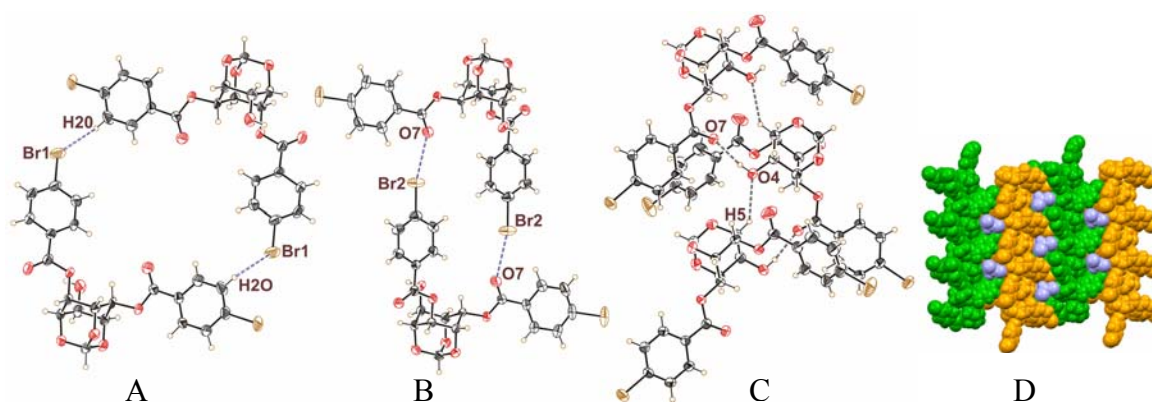


**Figure 9.** Molecules of **13** associated via dimeric, A) C-H...Br (Form I), B) C-Br...O (Form II) interactions, C) helical assembly of host molecules of **13** (Form III) via O-H...O and C-H...O contacts and D) packing of helices with guest included in **14**·CHCl<sub>3</sub>.

**Chapter 9** reports the charge density studies on the model compound 2,5-dichloro-1,4-benzoquinone (**15**).<sup>8</sup> The crystal structure contains catameric arrangement of molecules via excellent halogen-oxygen contacts. It was realized that only geometrical short contact between Cl...O is not sufficient in understanding the nature of the ‘halogen bonding’ interaction.<sup>9</sup> In order to observe experimentally the distribution of charge densities in the vicinity of the Cl, O and along the direction of halogen bond (C-Cl...O), we attempted the charge density analysis on crystals of the model compound **15**.

**Appendix I** describes the methodology followed for the lattice energy calculations.

**Appendix II** contained theoretical as well as experimental aspects of X-ray charge density analysis.

References:

1. K. M. Sureshan, R. G. Gonnade, V. G. Puranik, M. S. Shashidhar, M. M. Bhadbhade, *Chem. Commun.* **2001**, 881
2. G. R. Desiraju, T. Steiner, *The Weak Hydrogen Bonds: In Structural Chemistry and Biology*, Oxford University Press: Oxford, New York, 1999
3. E. Weber, in Kirk Othmer Encyclopedia of chemical technology, 4<sup>th</sup> Edn, Vol. 14 (Eds: J. L. Kroschwitz), Wiley, New York, **1995**, pp. 122-154.
4. (a) H. A. Bent, *Chem. Rev.* **1968**, 68, 587; (b) N. Ramasubbu, R. Parthasarathy and P. Murray-Rust. *J. Am. Chem. Soc.* **1986**, 108, 4308; (c) J. P. M. Lommerse, A. J. Stone, R. Taylor, F. H. Allen, *J. Am. Chem. Soc.* **1996**, 118, 3108; (d) P. Metrangolo, H. Neukirch, T. Pilati, G. Resnati, *Acc. Chem. Res.* **2005**, 38, 386 and references therein.
5. R. G. Gonnade, M. S. Shashidhar, M. M. Bhadbhade, *Chem. Commun.* **2004**, 2530.
6. (a) L. Făbiăñ, A. Kălmăñ, *Acta Crystallogr.* **2004**, B60, 547. (b) G. V. Bhosekar, C. Murali, R. G. Gonnade, M. S. Shashidhar, M. M. Bhadbhade, *Cryst. Growth & Des.* **2005**, 5, 1977.
7. R. G. Gonnade, M. M. Bhadbhade, M. S. Shashidhar, A. K. Sanki, *Chem. Commun.* **2005**, 5870.
8. R. Bees, *Acta Crystallogr.* **1970**, B26, 1304.
9. P. Munshi, T. N. Guru Row, *J. Phys. Chem. A* **2005**, 109, 659.

# **Chapter 1**

## **Understanding 'Halogen Bonding' Interactions**

# Chapter 1

## 1.1 Intermolecular Interactions

Investigating ‘Intermolecular Interactions’ in understanding the structure activity relationship of a given system is central to practically every branch of research, ranging from metallurgy to molecular biology, or from material science to chemistry. An exhaustive listing of the all types of interactions that are observed experimentally or estimated theoretically in different physical states of matter would be arduous task. Single crystal structure analysis by X-ray diffraction is one of the most suitable techniques that provide us accurate information on the process of molecular association that balances all possible intermolecular interactions in the solid state. This dissertation is concerned with crystal structure analysis of *myo*-inositol derivatives, most of which lack strong conventional hydrogen bonding *Donor/Acceptor* groups. Investigation of such systems could provide us with a wealth of valuable information on weak intermolecular interactions. In particular we have investigated molecular assemblies involving halogen atoms in the present thesis.

It is rather intriguing that in spite of large number of crystal structures (~360000, deposited in the Cambridge Crystallographic Data Centre), the blind tests given to predict the crystal structure of simple organic molecules posed a formidable challenge.<sup>1</sup> Several workers, Gavezzotti<sup>2</sup> and Dunitz,<sup>3</sup> have discussed the complexities involved in predicting a crystal structure. The non-covalent intermolecular interactions that lead to crystal formation can typically be divided into strong, moderate and weak interactions,<sup>4</sup> although the demarcation between is not sharp.<sup>5</sup> ‘Hydrogen bonding’ is a classical example of



strong, specific and highly directional intermolecular interaction. This has emerged as the most important organizing principle not only for the crystal structures (or engineering) but also for structure of biologically important molecules and supramolecular chemistry and crystal engineering. Hydrogen bonding patterns are differentiated based on geometrical, energetic and thermodynamic features. The strongest hydrogen bond is believed to be the  $[F\cdots H\cdots F]^-$  bond in the hydrogen bifluoride ion. It has an energy near  $50 \text{ Kcal mol}^{-1}$  and an  $F\cdots F$  distance of  $2.27(6) \text{ \AA}$  in potassium hydrogen bifluoride ( $KHF_2$ ).<sup>6</sup> The hydrogen atom appears to be symmetrically located between the two fluorine atoms.<sup>7</sup> Another very strong hydrogen bond is the  $O-H\cdots O$  hydrogen bond in certain carboxylates and organic hydrogen anions. The  $O-H\cdots O$  bond, in its strongest bonding environment (bond energy  $15-40 \text{ Kcal mol}^{-1}$ ), with an  $O\cdots O$  distance of  $2.2$  to  $2.5 \text{ \AA}$ , the bond lengths  $H\cdots O$  and  $O-H$  are nearly the same and the geometry of  $O-H\cdots O$  is nearly  $180^\circ$ .<sup>8</sup> These hydrogen bonds demonstrate pronounced covalency and generate rigid frameworks. In hydrogen bonds, donor (D) to acceptor (A) distances in the range  $2.5$  to  $3.2 \text{ \AA}$  (e.g. H bonds of the type  $O-H\cdots O$ ,  $N-H\cdots O$ ,  $N-H\cdots S$  and  $N-H\cdots N$ ) with bond energies ranging from  $4-15 \text{ Kcal /mol}$ , the interactions are mainly electrostatic with almost all the bonds shorter than the sum of the van der Waals radii. Hence, the strength of the hydrogen bond lies between weak covalent bond and a van der Waals interactions.<sup>9</sup>

Latter part of 19<sup>th</sup> century investigation of hydrogen bonding systems was more or less restricted to interactions involving F-H, O-H and N-H as proton donors and F, O, N as proton acceptors.<sup>10</sup> Weak interactions such as  $C-H\cdots O$ ,<sup>4</sup>  $C-H\cdots N$ ,<sup>11</sup>  $C-H\cdots F$ ,<sup>12</sup>  $C-H\cdots \pi$ ,<sup>13</sup>  $C-H\cdots X$  ( $X = Cl, Br, I$ ),<sup>4</sup>  $\pi\cdots\pi$ ,<sup>14</sup> halogen-halogen<sup>15</sup> are of considerable importance in the absence of classical hydrogen bonds as they play an important role in

molecular packing arrangement. The ability of carbon atoms to act as proton donors depends on the hybridization at the C-atom site ( $C(sp)-H > C(sp^2)-H > C(sp^3)-H$ ). The presence of electron withdrawing groups on the adjacent atoms also appears to play a role in the proton donating ability of the carbon atom. However, non-conventional hydrogen bonds have been the subject of controversy for many years.

D. J. Sutor<sup>16</sup> conducted a survey of crystal structures containing short  $C-H\cdots O$  contacts in 1963. According to her, these short contacts could best be described as weak hydrogen bonds and are generally attractive in nature rather than repulsive, with roughly one third the energy of conventional  $O-H\cdots O$  hydrogen bond. However, if there are a large number of such interactions, their contribution to the stability of a system could be substantial. The importance of  $C-H\cdots O$  interactions in supramolecular chemistry,<sup>17</sup> crystal engineering,<sup>9</sup> biological systems,<sup>18</sup> nucleic acid and protein structures<sup>19</sup> has been well documented.

Other types of weak interaction such as  $\pi\cdots\pi$  interaction,<sup>20</sup> which involves interaction between the  $\pi$ -electron systems (aromatic as well as aliphatic), are generally called  $\pi$ -complexes. They are characterized by short intermolecular distance perpendicular to the stacking direction. The two molecules forming such a  $\pi$ -complex consist of a donor molecule with a low ionization potential so that an electron can be readily lost (a delocalized  $\pi$ -electron of the polycyclic aromatic hydrocarbon) and an acceptor molecule with a high affinity for electrons. As a result, stacks of alternating donor and acceptor molecules are found in the crystal.

Hydrogen bonds formed with electrons in  $\pi$  bonds acting as the acceptor are attracting much interest currently, both in the fields of structural chemistry and structural

biology. The most important amongst these are those with  $\pi$  cloud of the phenyl rings, X-H $\cdots$ Ph (aromatic hydrogen bonds), which occur in many chemical and biological systems.<sup>21</sup> C-H $\cdots\pi$  interactions come under the category of weak interactions where hydrogen atoms points towards electron rich aromatic ring and mostly results in herringbone type arrangement of molecules in crystals. Like other weak interactions, these also play a crucial role in the formation molecular assemblies,<sup>13c</sup> group transfer reactions,<sup>22</sup> stability of peptides,<sup>23</sup> proteins<sup>24</sup> and conformation of small organic molecules.<sup>13</sup> Other weak interactions, O-H $\cdots\pi$ , (small molecules<sup>25</sup> and several proteins structures reported in PDB<sup>26</sup>) and N-H $\cdots\pi$ ,<sup>27</sup> are also observed in the crystal structures. The other weak intermolecular interaction includes C=O $\cdots$ C=O,<sup>28</sup> C-F $\cdots$ C=O<sup>29</sup> and S=O $\cdots$ C=O<sup>30</sup> (dipole-dipole interactions). These dipolar contacts have also been suggested to play an important role in the molecular aggregation and the formation of stable host framework.

The strength of various interactions discussed above was systematically reviewed by Munshi et al.<sup>5</sup> using X-ray charge density analysis of coumarin derivatives as model systems. They characterized the interactions (15 types) of varying strengths. The exponential dependence of electron density, ( $\rho_b$ ) on interaction length, ( $R_{ij}$ ) is shown in **Figure 1.1**. Based on the values of  $R_{ij}$ , in the range of 1.6 to 3.8 Å and the corresponding values of  $\rho_b$ , lie between 0.3 to 0.005 eÅ<sup>-3</sup>, they separated the range interactions from hydrogen bonds to van der Waals interactions into three categories. The hydrogen bonds such as, O-H $\cdots$ O, N-H $\cdots$ O, N-H $\cdots$ N and N-H $\cdots$ S fall in the region of strong hydrogen bonds ( $R_{ij} < 2.3$  Å,  $\rho_b > 0.08$  eÅ<sup>-3</sup>), region 1. The C-H $\cdots$ O interactions reside in the weak hydrogen bond region ( $2.3$  Å  $< R_{ij} < 2.75$  Å,  $0.07$  eÅ<sup>-3</sup>  $> \rho_b > 0.02$  eÅ<sup>-3</sup>), region 2. The

interactions like, C-H $\cdots\pi$ , C-H $\cdots$ S and  $\pi\cdots\pi$  (O $\cdots$ C, N $\cdots$ N, C $\cdots$ C, O $\cdots$ O, S $\cdots$ S, S $\cdots$ C, S $\cdots$ N and N $\cdots$ C) are among the weakest types of interactions and belong to the van der Waals interaction region ( $R_{ij} > 2.75$  Å,  $\rho_b < 0.05$  eÅ $^{-3}$ ), region 3.

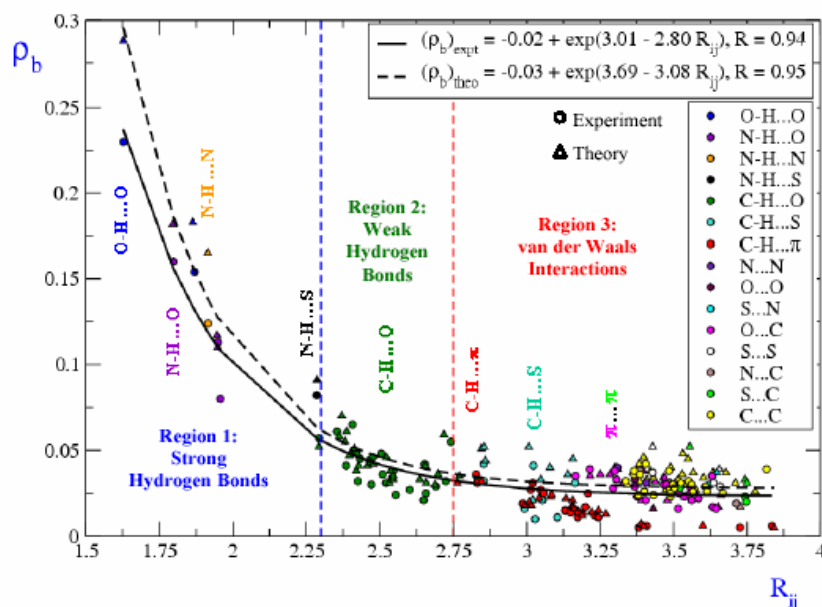


**Figure 1.1.** Exponential dependence of electron density,  $\rho_b(\mathbf{r})$  [eÅ $^{-3}$ ] on interaction length,  $R_{ij}$  [Å] of 15 types of interactions and 114 data points, the circles and triangles represent experimental and theoretical values respectively and the solid and dash black lines represent the corresponding fittings. The inset gives the details of the fitting models along with correlation coefficients  $R$  and the color code for each type of interactions. The interactions, categorized are marked accordingly.

## 1.2 Non-covalent Interactions Involving Halogens

It has long been known that the halogens Cl, Br and I form short non-bonded contacts with hydrogen bond acceptors in crystals.<sup>31</sup> This behavior has been rationalized based on anisotropic (non-spherical) charge distribution in halogen atoms.<sup>32</sup> Thus, heavier halogens (except fluorine, due to extreme electronegativity and limited polarizability)

exhibit electrophilic character along the axis of C-X bonds and nucleophilic character perpendicular to these bonds. Hence, electrophiles in general tend to approach halogens at angles of *ca* 100° and nucleophiles at 165°. <sup>33</sup> Calculation of electrostatic potential surfaces of methyl halide by Hunter et al. using STO-3G basis set in Spartan (**Figure 1.2**) supports this view. <sup>31</sup> According to their calculations, the heavier halogens have more positive region on the surface opposite to the C-X bond and negative region perpendicular to this bond. The magnitude and area of the zone of positive potential increases with the size of the halogen, so that iodine, in particular makes relatively strong interactions with hydrogen-bond acceptors. Thus, halogens can act as hydrogen-bond donors or acceptors depending on the angle of approach. <sup>34</sup>

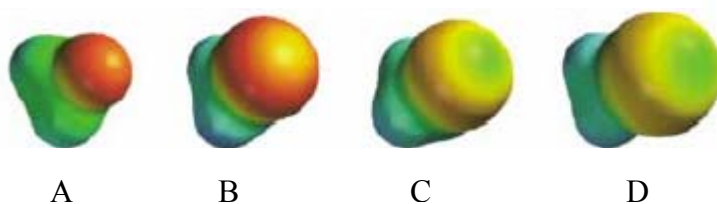


**Figure 1.2.** Molecular electrostatic potential surfaces of A) methyl fluoride, B) methyl chloride, C) methyl bromide and D) methyl iodide calculated by using the STO-3G basis set in Spartan. The red regions represent negative electrostatic potential, the blue regions positive electrostatic potential and yellow is neutral.

Hence, interactions of halogens with nucleophiles (e.g. O, N) display roughly linear geometries with respect to the halogens, capable of forming a variety of intermolecular interactions, whereas interaction with electrophiles occur in side-on fashion. <sup>35</sup> Some of the (now) recognized weak intermolecular interactions involving halogens are mentioned below.

### 1.2.1 C-H...Halogen Interactions

C-H...X (X = F, Cl, Br and I) type interactions occur when halogen atom acts as hydrogen atom acceptors. However, the existence of C-H...Cl hydrogen bonds has been questioned.<sup>36</sup> Gibb et al. carried out a systematic survey of Cambridge Crystal Structure Database, which established the extensive occurrence of C-H...Cl hydrogen bonds.<sup>37</sup> Furthermore, they have shown that C-H...X interactions are real and they do play an important role in molecular aggregation and prediction of molecular structure. It is observed that chloride anions are shown to be better hydrogen-bond acceptor systems than neutral chloride-containing molecules and a similar situation pertains for the other halides. The number of examples for C-H...halogen bonding with F and Cl are more compared to that of bromine and Iodine, probably as the size of the halogen atom increases (decrease in electronegativity) it becomes electron pair acceptor rather than donor.<sup>37</sup> In C-H...F type interactions, the C-F bond acts as proton acceptor and it is one of the predominant interactions in fluorine containing compounds. Further, it is considered as one of the tools in crystal engineering.<sup>38</sup> It is still under debate that the chlorine or other halogen atoms can also be H-bonding acceptors. In summary, C-H...X (X = Cl, Br and I) hydrogen bonds can be added to the range of tools available to the supramolecular chemistry and crystal engineering.

### 1.2.2 C-Halogen... $\pi$ Interactions

The involvement of halogen atom is also found in C-halogen... $\pi$  type interactions. The nature of this interaction depends on the halogen atom and electron withdrawing or electron donating substituents on the aromatic ring. The existence of such interactions was first noted by Dastidar et al.<sup>39</sup> while analyzing the structure of Zinc-tetra(4-

bromophenyl) porphyrins. The close approach of C-Br $\cdots\pi$  as a possible specific interaction to result in well defined packing modes was noted by them. Guru Row et al. carried out a systematic Cambridge Crystallographic Database<sup>40</sup> and Protein Data Bank study<sup>41</sup> on the intra and intermolecular geometries of C-halogen $\cdots\pi$  contacts. The intramolecular contacts involving fluorine were relatively abundant as compared to other halogens. Their study showed that C-X $\cdots\pi$  interactions are highly directional. The organic fluorine showed greater propensity for the formation such interactions rather than accepting hydrogen bonds as well as compared with other halogens. The C-F $\cdots\pi$  intramolecular interactions appeared to spread across the histogram, while the other halogen atoms showed a tendency to cluster near  $D_{max}$  (cut-off values of distance). The intermolecular C-X $\cdots\pi$  interactions for all the halogen atoms clustered around  $D_{max}$ . C-X $\cdots\pi$  appears to play an important role in the stability of host guest complex.<sup>42</sup> The directional nature of the halogen $\cdots\pi$  contacts makes these relatively weak interactions capable of influencing the packing of organic molecular crystals decisively, thus providing a new tool for crystal engineering of both homomolecular and supramolecular organic solids.<sup>41,43</sup>

### 1.2.3 Halogen $\cdots$ Halogen Interactions

As a consequence of the spatially segregated regions of complementary electrostatic potential, interhalogen bonding is also observed with halogen groups acting as both nucleophiles and electrophiles. Desiraju et al.<sup>44</sup> carried out systematic CSD search on the geometries of these contacts and deduced that the short X $\cdots$ X intermolecular distances arise from the specific attractive forces between the two halogen atoms in

crystals and the non-spherical shape (polar flattening) of the halogen atoms was the consequence of this interaction. Price et al.<sup>45</sup> showed that for X...X short distances especially chlorine-chlorine interactions could originate from anisotropic effects (non-spherical atomic charge distribution) between elliptically shaped chlorine atoms. Murray-Rust and coworkers classified X...X interactions based on the two C-X...X angles  $\theta_1$  and  $\theta_2$  with the classes being denoted as type I ( $\theta_1$  or  $\theta_2 = 90^\circ$ ), type II ( $\theta_1$  or  $\theta_2 = 180^\circ$ ) and type III ( $\theta_1 = \theta_2$  and the two halogen atoms being related by crystallographic center of inversion).<sup>46</sup> The nomenclature for these X...X interactions was subsequently simplified by Desiraju and coworkers;<sup>44</sup> type I interactions ( $\theta_1 = \theta_2$ ) and type II interactions ( $\theta_1 \cong 180^\circ$  and  $\theta_2 \cong 90^\circ$ , **Figure 1.3**). The type II contact is consistent with the polarization of adjacent X atoms as  $\delta(+)$  and  $\delta(-)$  while type I contact is a consequence of crystallographic symmetry, the X atoms being located across a centre of inversion.



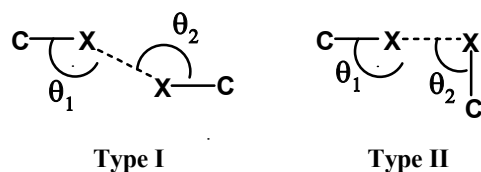


**Figure 1.3.** Schematic representation of halogen...halogen interactions.

The role of X...X contacts, appears to be important (irrespective of their cause) in determining supramolecular structures and it may be possible to exploit them directly in crystal engineering and for the design of supramolecular aggregates.<sup>47</sup>

#### 1.2.4 ‘Halogen Bonding’ Interactions

There has been growing interest (over the last two to three decades) in a newer type of weak interaction between halogen and oxygen atom. This contact was earlier categorized as charge transfer or electron-donor-acceptor bond, but now it is generally termed as ‘halogen bonding’ interaction. This is also regarded as one of the supramolecular glues useful in designing functional solids. The term “Halogen bonding” was introduced by Dumas et al. in 1983<sup>48</sup> and latter used by several others<sup>49</sup> to stress its similarity with hydrogen bonding.<sup>50</sup>

Halogen bonding is the attractive donor acceptor interactions<sup>51</sup> that involving an atom possessing one or more lone pair of electrons (such as O, N or S, which donates electrons, Lewis base) and a halogen atom (F, Cl, Br or I functioning as Lewis acids accepting the lone pair of electrons).<sup>52</sup> Like hydrogen bond, in which H-atom covalently bonded to an electronegative atom approaches another electronegative atom,<sup>9</sup> in halogen

bond, the halogen atom bonded to an atom approaches a more electronegative atom (**Figure 1.4**). The stronger the electron-withdrawing environment around the halogen atoms, their ability to be engaged in halogen bonding interactions is higher. The resulting complexes were considered by Prout and Kamenar as belonging to the  $n\sigma^*$  type.<sup>53</sup> The halogen bond seems to be mainly electrostatic in origin with some contribution from dihalogen polarization upon complex formation.<sup>54</sup> Since this thesis reports the importance of the halogen bonding contact in host-guest complex formation and their stability, crystal growth, polymorphism and crystal-to-crystal phase transitions, this interaction is reviewed in some detail below.

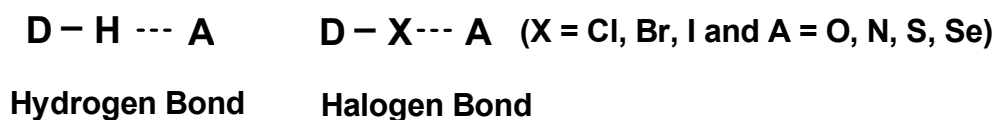


**Figure 1.4.** Analogy of halogen bond with hydrogen bond

### 1.3 Halogen Bonding: A Historical Background

The first unequivocal report on the ability of halogen atoms to form well-defined adducts with electron donor species dates back to 1863 when Guthrie described the formation of the  $\text{NH}_3 \cdots \text{I}_2$  complex.<sup>55</sup> Remsen and Norris<sup>56</sup> in 1896 proved the general tendency of amines to form adducts with bromine and chlorine; pale yellow crystals of composition  $(\text{CH}_3)_3\text{N} \cdot \text{Br}_2$  were obtained by directly adding trimethylamine to bromine. While its implications have an impact on all the fields where design and manipulation of aggregation phenomena play a key role, halogen bonding has become subject of serious study only recently. It has been recognized as a well-defined, strong, specific and

directional interaction for assembling complex supramolecular architecture. The crystallographic studies of Hassel are a landmark in the study of the halogen bond phenomenon. He first demonstrated that halogen bonding is a powerful tool in driving the self-assembly of endless chains of alternating donor and acceptor modules.<sup>57</sup> He studied the X-ray crystallographic structure of molecular addition compound containing dihalogens and electron pair donor molecule 1,4 dioxane. The crystal structure investigation of bromine - 1,4 dioxane complex revealed the presence of endless chains consisting of alternating dioxane and bromine molecules (**Figure 1.5**). The oxygen-bromine-bromine-oxygen arrangement is linear. The most striking feature of the structure was the short contact between the oxygen atom of the dioxane and a bromine atom. The O...Br distance in the crystal is only 2.71 Å, which is very much less than sum of van der Waals radii (3.35 Å) and the angle at the bromine atom making short contact is almost linear. Each bromine atom is involved short O...Br interactions, off each end of the Br-Br bond and each dioxane molecule is involved in two O...Br interactions.

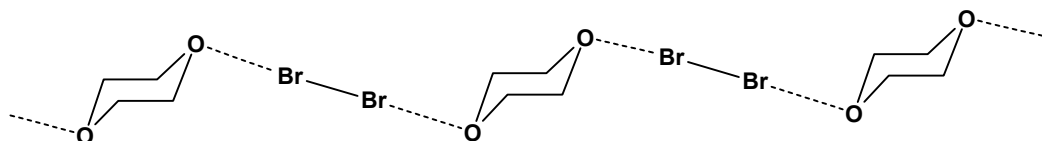


**Figure 1.5.** Formation of O...Br-Br...O bridge in molecular complex of dioxane and bromine.

Hassel and coworkers concluded that charge transfer from the donor atom (O) to the acceptor (Br) takes place since the molecular complex possesses appreciable dipole moment while Br<sub>2</sub> and dioxane lack dipole moment. They studied crystal structures of

several addition compounds involving dihalogens and ether as well as carbonyl oxygens; in all the complexes the halogen...oxygen distance was much less than the sum of van der Waals radii and the halogen bond between oxygen and halogen was stronger with heavier halogen atoms. Like halogen bonding between dihalogen and ether oxygen, the bonding between dihalogen and carbonyl oxygen is linear. They concluded that the complex formation was due to the charge transfer interactions between electron pair donor atoms and halogen atoms belonging halide molecules. In Hassel's Nobel lecture,<sup>58</sup> he stressed the similarities between the interactions where halogen and hydrogen work as electron acceptors. Thus, his solid-phase structural studies (using X-ray crystallography) unequivocally established the existence of a  $D\cdots X$  ( $D$  = electron-pair donor,  $X$  = electron-pair halogen acceptor) interaction with a defined linear geometry. Bent et al. have reviewed halogen bonding interactions, establishing the analogy between halogen bonding and conventional hydrogen bonding.<sup>50a</sup>

R. N. Brown<sup>59</sup> first observed halogen bonding contact in a single component system. In crystals structure of N-chloro-succinimide, the chlorine atom bound to nitrogen makes short contact (2.88 Å) with carbonyl oxygen atom forming zig-zag chains (**Figure 1.6A**). He concluded that the close approach of chlorine to oxygen was because of electrostatic attraction due to charge separation; both N-Cl and C=O bonds display large dipole moment wherein chlorine is positive and oxygen is negative. Later Pritzkow et al.<sup>60</sup> also observed similar features in crystal structure of N-bromo-succinimide ( $\text{Br}\cdots\text{O} = 2.80 \text{ \AA}$ ). Padmanabhan et al.<sup>61</sup> also reported very short  $\text{I}\cdots\text{O}$  contact [ $\text{I}\cdots\text{O} = 2.580(6) \text{ \AA}$  which was much shorter than the sum of their van der Waals radii (3.50 Å) and  $\angle\text{N-I}\cdots\text{O} = 175.7(2)^\circ$ ], in crystals of N-iodo-succinimide (**Figure 1.6B**).

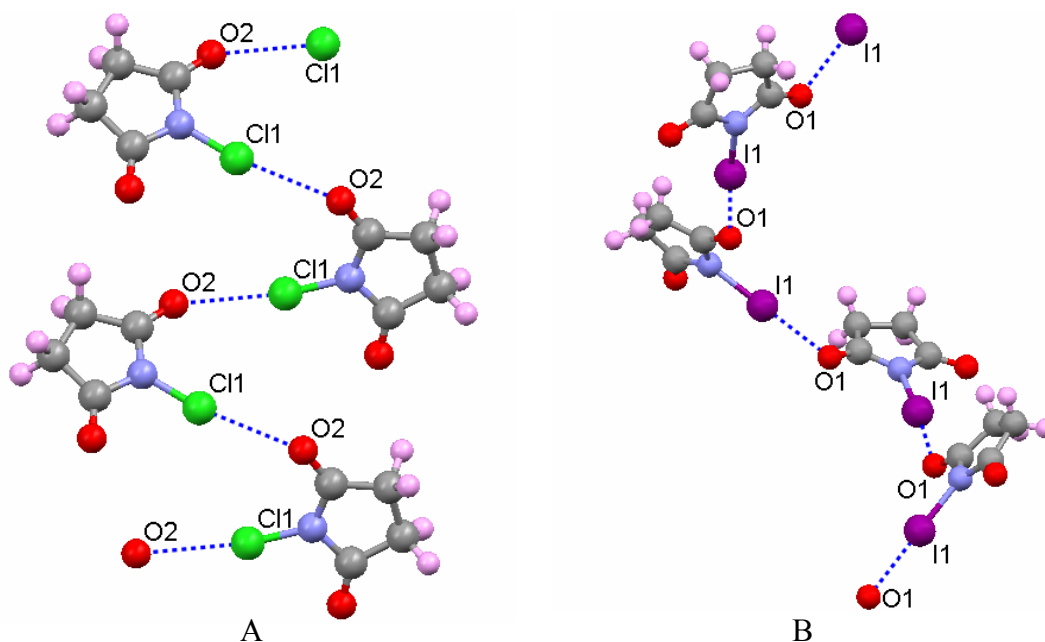


**Figure 1.6.** A) Endless chain of N-chloro-succinimide molecules formed via C-Cl $\cdots$ O contacts (N-bromo-succinimide also has similar crystal structure) and B) polymeric layer formed in N-iodo-succinimide crystals via C-I $\cdots$ O short contact.

Sabesan and Venkatesan<sup>62</sup> also observed short Br $\cdots$ O contact in 3-*p*-bromophenyl-1-nitroso-2-pyrazoline and assumed it was a charge transfer type weak interaction. Pascal et al. also noticed, nitrogen-chlorine donor-acceptor interactions in the crystal structure of cyanuric chloride (2,4,6-trichloro-1,3,5-triazine) which dominate the complete crystal packing.<sup>63</sup>

The gas-phase structures of 60 complexes of F<sub>2</sub>, Cl<sub>2</sub>, Br<sub>2</sub>, BrCl, ClF and ICl with Lewis bases have been determined by rotational spectroscopy by the Legon's group and important generalizations about the angular and radial geometries in these complexes

have been drawn.<sup>64</sup> They systematically reviewed the properties of complexes  $B \cdots XY$  ( $B$  = Lewis Base, gaseous molecule like  $\text{NH}_3$ ,  $\text{CO}$ ,  $\text{C}_2\text{H}_2$ ,  $\text{HCN}$ ,  $\text{H}_2\text{S}$  and  $XY$  = gaseous dihalogen molecule like,  $\text{Cl}_2$ ,  $\text{ClF}$ ,  $\text{F}_2$ ,  $\text{Br}_2$ ,  $\text{BrCl}$ ) changes with varying  $B$  and  $XY$  to deduce the nature of  $B \cdots XY$  interaction and its dependence on the Lewis base and the halogen involved.<sup>64d</sup> They analyzed the  $B \cdots XY$  interaction by varying  $B$  and  $XY$  and found that the electrophilic region of the halogen atom ( $\delta^+$  in  $X^{\delta^+}-Y^{\delta^-}$ ) interacts with the  $n$ -pair of  $B$  in such a way that  $B \cdots XY$  has linear arrangement similar to  $B \cdots \text{HX}$  complex (**Figure 1.7**).<sup>65</sup> They concluded that the geometry of the halogen bond is similar to hydrogen bond.

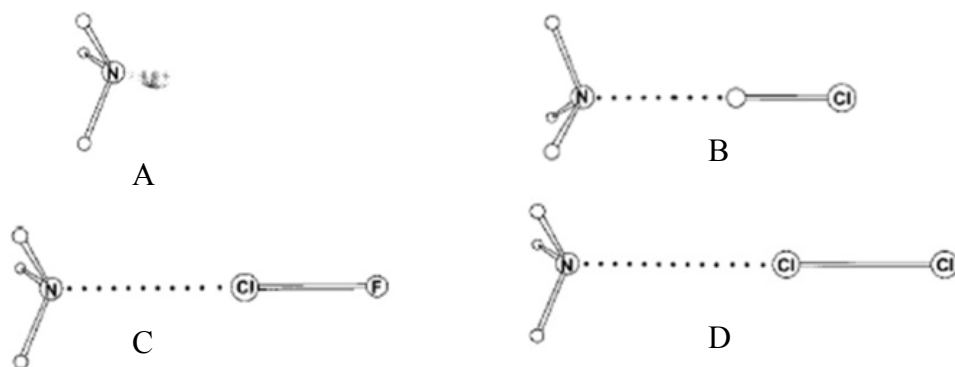


**Figure 1.7.** A) Non-bonding pair electron density model of  $\text{NH}_3$  and the observed  $C_{3v}$  geometries of B)  $\text{H}_3\text{N} \cdots \text{HCl}$ , C)  $\text{H}_3\text{N} \cdots \text{ClF}$  and D)  $\text{H}_3\text{N} \cdots \text{Cl}_2$ .

#### 1.4 Halogen Bonding Interactions from Cambridge Crystallographic Database

Murray-Rust and Motherwell<sup>66</sup> found about 219 crystal structures containing O and C-I bond in the Cambridge Crystal Structure Database. They analyzed these structures for  $\text{I} \cdots \text{O}$  contacts ( $< 5 \text{ \AA}$ ) along with the  $\text{C-I} \cdots \text{O}$  angle. They found over 500 contacts in this range and the sharp variation of  $\text{I} \cdots \text{O}$  distance with the  $\text{C-I} \cdots \text{O}$  angle. At

90° the minimum I...O distance is 3.6-3.7 Å, whereas at 180° it is as low as 2.8 Å. When the halogen to oxygen approach is linear the halogen...oxygen distances are much less than the sum of van der Waals radii. Similar results were found for C-Br...O and C-Cl...O contacts with over 3000 examples of each, although the minimum X...O distance did not approach that of I...O. Further, they did not find any difference in the distribution when the analysis was carried out with different chemical nature of oxygen (ether, ester and carbonyl). They concluded that the distribution is independent of the nature of oxygen atom. They also analyzed the environment around halogen centers in hundreds of crystal structures<sup>67</sup> and found the angular preferences of intermolecular forces around halogen centres; nucleophiles approach X of C-X along the back side of the bond whereas the electrophile approach of X nearly perpendicular to C-X. Thus, the contacts of O or N with X are nearly “head on” with O, N approaching X along backside of C-X and the angle of approach is about 165°. The directionality has been explained qualitatively in terms of charge-transfer between the highest occupied molecular orbital (HOMO) of the electronegative atom (O or N) and the lowest unoccupied molecular orbital (LUMO) of the halogen. This interpretation was largely based on molecular orbital studies of the dimer H<sub>3</sub>N...F<sub>2</sub>.<sup>33</sup>

A decade latter, Allen et al.<sup>32</sup> carried out systematic analysis on the nature and geometry of intermolecular interactions between carbon bonded halogens (C-X, X = F, Cl, Br or I) and electronegative atoms (El = N, O and S) using Cambridge Crystal Structure Database. They found that the electronegative atoms in various hybridization states clearly prefer to form contacts with Cl, Br and I (but not F) in the direction of the extended C-X bond axis, at interatomic distances less than the sum of the van der Waals

radii. The scattergram of C-Cl $\cdots$ O geometry (**Figure 1.8**) represents a hemisphere around the nucleus of the chlorine atom at the terminal side of the covalent C-Cl bond, up to a maximum Cl $\cdots$ O distance of  $d = 4.12$  Å.

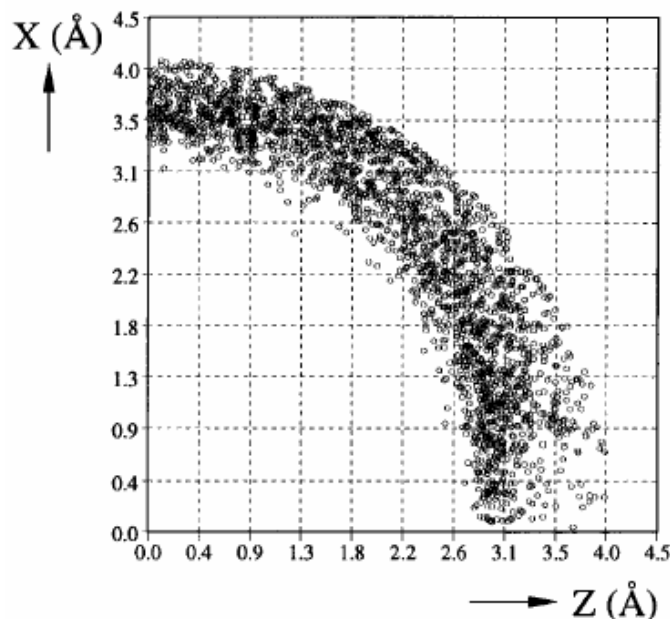


**Figure 1.8.** Distribution of  $sp^2$  hybridized oxygen atom around carbon-bonded chlorine atoms found in the crystal structures in the CSD. Each circle represents one unique contact of an oxygen atom to the chlorine atom, placed at the origin.

Allen et al. also performed *ab initio* intermolecular perturbation theory (IMPT) calculations, which showed that the attractive nature of the X $\cdots$ El interaction is mainly due to electrostatic effects, but polarization, charge-transfer and dispersion contributions all play an important role. They calculated the interaction energy for the chloro-cyanoacetylene dimer and found it to be about 2-3 Kcal/mol, which is about half the magnitude of an average hydrogen bond, highlighting the potential importance of these kinds of non-bonded interactions. The directionality of the interaction was explained by



the anisotropic electron distribution around the halogen atom, causing a decreased repulsive wall and increased electrostatic attraction for electronegative atoms in the observed preferred position. The fact that tendency to form short  $X\cdots El$  interactions ( $I > Br > Cl$  [ $>F$ ]) parallels the order of their polarizabilities. This suggests that polarization and/or charge-transfer energies related to the halogen atom play a significant role in the interaction. They ruled out the concept of 'polar flattening' (short contact merely due to consequences of close packing of anisotropic X atom, as observed by Price et al.<sup>45</sup>) in  $Cl\cdots Cl$  intermolecular contact, in case of  $C-X\cdots El$  ( $El = N, O$  and  $S$ ) bond and also demonstrated that it is not a consequence of close packing by closely analyzing the structure of 2,5-disubstituted-1,4-benzoquinones.<sup>33</sup> In 2,5-dichloro-1,4-benzoquinone crystal structure, all chlorine and oxygen atoms are involved in 1:1 contacts (**Figure 1.9A**). Similarly, in 2,5-dibromo-1,4-benzoquinone, all bromine atoms form 1:1 contacts with oxygen atoms (**Figure 1.9B**). Thus, despite the much larger volume of bromine atoms, the crystal is isostructural with the dichloro analog and shows  $X\cdots El$  to be an essential driving force in the formation of the crystal structure. This was supported by the structure of 2,5-dimethyl-1,4-benzoquinone, although the volume of methyl groups is comparable to that of chlorine atoms, it has completely different crystal packing (**Figure 1.9C**). Furthermore, the electrostatic nature of the halogen bond was confirmed due to the fact that the order in which interaction becomes stronger ( $S < N < O$ ) corresponds to the increase in electro-negativities of the atoms. Also the hybridization state of the  $El$  atom has an effect on the nature of the halogen bond.  $El$  atoms in  $sp$  and  $sp^2$  hybridization states attract electrons by resonance. This is not possible in  $sp^3$  hybridized state because of steric crowding and hence  $El$  cannot approach halogen atoms at shorter distances.

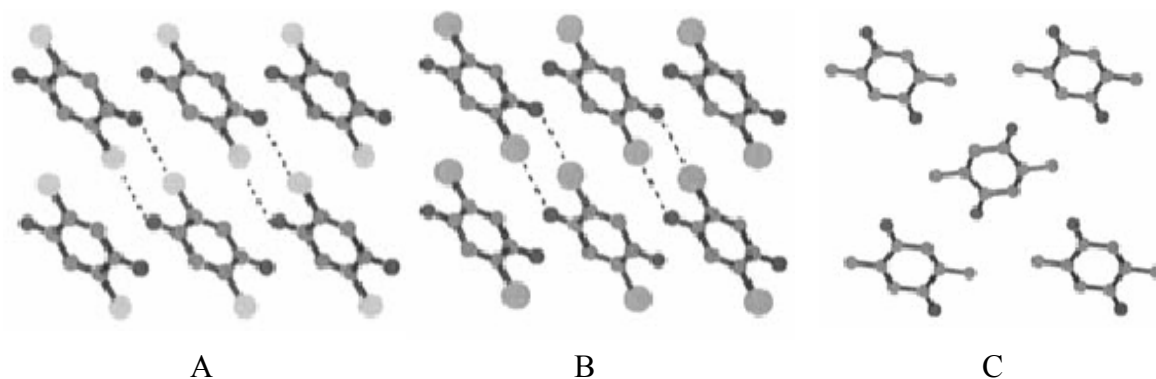


**Figure 1.9.** Packing of 2,5-disubstituted-1,4-benzoquinones in their crystals. The dotted lines show the contacts of oxygen and halogen atoms, A) 2,5-dichloro-1,4-benzoquinone, B) 2,5-dibromo-1,4-benzoquinone and C) 2,5-dimethyl-1,4-benzoquinone.

Lourence et al.<sup>68</sup> also carried out the analysis of the halogen bonding geometry of dihalogen complexes  $Y-X\cdots B$  using CSD. From the analysis they concluded that,

- i) In the solid state, the  $I-I\cdots B$  halogen bond is more linear compared to  $O-H\cdots B$  bond by  $10-38^\circ$  and the halogen bond appears to be stronger than hydrogen bond.
- ii) The direction of the halogen bond (vector  $X\cdots B$ ) is very close to the axis of the non-bonding electron pair of B.
- iii) The lengthening (weakening) of the  $Y-X$  bond when the  $X\cdots B$  interactions shortens (strengthens).

### 1.5 Halogen Bonding: Theoretical Calculations

Theoretical investigation into charge transfer and electron donor-acceptor interactions of halogen-bonded complexes was performed earlier by Mulliken and Parson.<sup>51</sup> Price et al.<sup>45</sup> and Allen and co-workers.<sup>33</sup> They used intermolecular perturbation

theory calculations on the complexes formed between chlorine containing molecules and electronegative atoms (N and O). Resnati and coworkers<sup>69</sup> conducted theoretical calculations (DFT and MP2) on the halogen-bonded complexes formed between fluoroalkyl halides and ammonia and examined the effect of increasing the fluorine substitutions on halogen bonding. They found that equilibrium C-X...N geometries were linear and the X...N distances are shorter than the sum of the van der Waals radii (**Figure 1.10**). The binding energies of  $\text{CF}_3\text{X}\cdots\text{NH}_3$  increase from 2 to 6 Kcal/mol on following the sequence  $\text{X} = \text{Cl}, \text{Br}, \text{I}$ . Also, progressive introduction of fluorine atoms in methyl iodides raised the interaction energy from 2 Kcal/mol for  $\text{CH}_3\text{I}$  to 6 Kcal/mol for  $\text{CF}_3\text{I}$ .

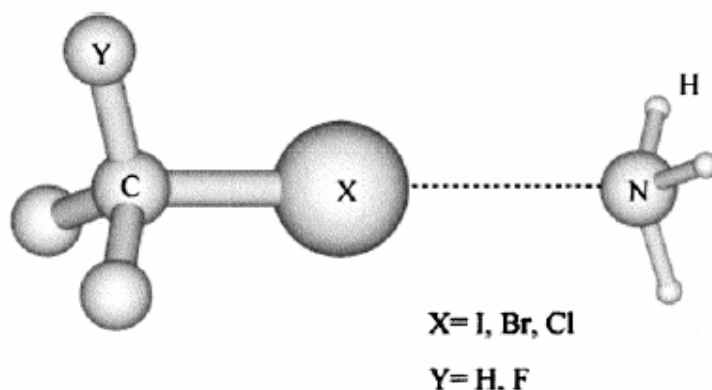


**Figure 1.10.** Schematic representation of the halogen-bonded complexes

Chu et al.<sup>70</sup> carried out the theoretical calculations on fluorine containing donor-acceptor complexes. Their investigation revealed that the electron density is anisotropically distributed around the halogen nucleus and the effective atomic radius of X-atom along the C-X bond axis is smaller than that in the perpendicular direction. When electron donors are involved in the halogen bonding is preferentially along the axis of

orbital containing the lone pair of donor. Romaniello and Lelj<sup>71</sup> analyzed the halogen bond between CF<sub>3</sub>I adducts and several electron donors (N or O). These theoretical calculations revealed that the most important contribution to the intermolecular interactions of halogen atom is electrostatic, whereas the contribution from charge-transfer type interactions is minor and even negligible in some cases. Further in addition to provide qualitative understanding of the electron-accepting nature of the carbon-bound halogen atoms, the molecular surface electrostatic potential (ESP) of some halogen containing molecules have been reported.<sup>49b,72</sup> Their results clearly reveal that there is positive cap at the end regions of the halogen atoms along the C-X (X =Cl, Br and I) bond vectors.

Recently Zou and coworkers<sup>73</sup> performed *ab initio* study of a series of complexes formed between halogen-containing molecules and ammonia to gain a deeper insight into the nature of halogen bonding and the electron-accepting propensities of covalently bonded halogen atoms. They found that the dihalogen molecules form the strongest halogen bonding complexes with ammonia; followed by HOX and that charge-transfer-type contribution is predominant in halogen bonding. However, for carbon bound halogens (RX), the interaction energy mainly stems from electrostatic interactions. They also explored the influence of the hybridization state of the carbon atom bonded to the halogen and substitution upon the electron-accepting ability of the halogen atom. It has been disclosed that,

- i) sp-hybridized carbon-bound halogen atoms form the strongest halogen bond, followed by sp<sup>2</sup>- and then sp<sup>3</sup>-hybridized carbon-bound halogen atoms, which very

much resembles the behavior of the corresponding hydrocarbons as hydrogen-bond donors.

- ii) The halogen-bond strength is significantly enhanced by progressive fluorine substitution, the substitution of a hydrogen atom by a methyl group in the  $\text{CH}_3\text{X}\cdots\text{NH}_3$  complex weakens the halogen bonding in the  $\text{CH}_3\text{X}\cdots\text{NH}_3$  complex.

They also investigated positively charged systems to explore the effect of charge on halogen bonding and found that the charged complexes have significantly larger interaction energies than the corresponding neutral complexes, which indicates the electrostatic nature of the halogen bond in carbon bound halogen systems.

## 1.6 Halogen Bond: Applications in Crystal Engineering and Designing Functional Solids

The strong, directional and selective nature of halogen bonding interactions makes it effective and reliable tool in crystal engineering and can be considered as a new type of palette glue to achieve supramolecular architecture and designing of functional solids.<sup>74</sup> These non-covalent interactions can be strong enough to control aggregation of organic molecules in solids,<sup>75</sup> liquid,<sup>76</sup> liquid crystals<sup>77</sup> and gas phase.<sup>50e,f, 78</sup> Pedireddi et al.<sup>79</sup> first successfully reported the importance of this new supramolecular cement in crystal engineering. They designed the supramolecular assemblies via  $\text{NO}_2\cdots$ halogen contacts in several co-crystals of halo and nitro derivatives of aromatic compounds and concluded that the halogen-oxygen linked assemblies are useful supramolecular synthons in developing strategies for systematic and general crystal engineering.<sup>79</sup> Resnati and coworkers have done remarkable work by successfully utilizing features of halogen

bonding contacts in supramolecular architecture,<sup>35d,80</sup> molecular recognition<sup>81</sup> and solid state synthesis.<sup>82</sup> They experimentally proved the domination of halogen bond over hydrogen bond under appropriate conditions in molecular recognition controlling self-assembling process.<sup>80e</sup> The complete account of halogen bonding interactions with its vital applications is recently published.<sup>74b</sup> Prof. Pennington and coworkers also have used halogen-bonding contact (one of the supramolecular glue) in designing functional solids.<sup>84</sup>

### 1.7 Halogen Bonding in Biological Systems

The X-ray crystal structures of complexes between halogen substituted drugs and their specific proteinaceous receptors unequivocally proved the existence of halogen bonding interactions that optimizes the receptorial fitting. Understanding the mode of action of naturally occurring biologically active substances by designing of active synthetic compounds has been the aim of many studies modeling small molecule substrate (hormone, drug agonist or antagonist) interactions with their macromolecular (binding protein, enzyme or receptor) active sites.<sup>85</sup> Thyroid hormones form a special class of molecules because they are the only naturally occurring biologically active iodine containing compounds which bind with the macromolecules. The iodine atoms in thyroid hormone thyroxin (T4) binds via short I...O contact with the carbonyl oxygen of the amino acid residue in the pocket of transthyretin (TTR), the major transporter of T4 (**Figure 1.11**) in human body.<sup>86</sup> Structure-function studies have been carried out on several thyroid hormone analogues in order to determine those features that are required for binding and activity.<sup>87</sup> These data showed that successive removal of the four iodines

dramatically reduces their serum transport protein-binding affinity as well as affect their nuclear binding and biological activity. However, replacement of the iodines with alkyl groups of roughly equivalent size neither significantly reduces their biological activity, nor does it restore equivalent transport protein binding.

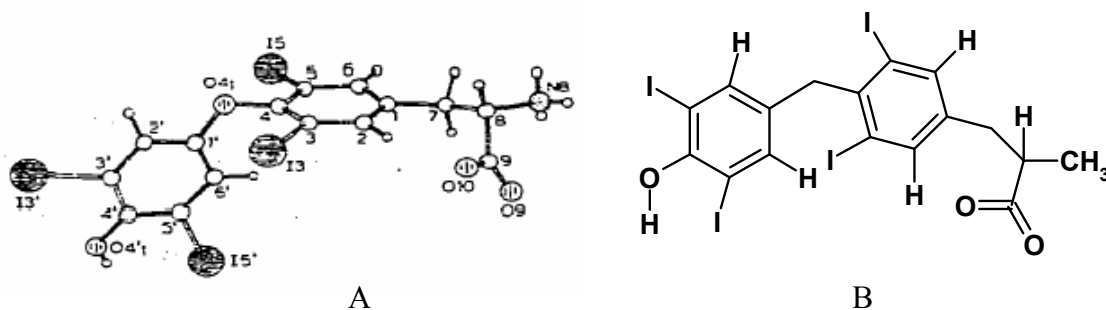


**Figure 1.11.** A) Crystals structure of 3,5,3',5'-tetraiodo-L-Thyronine (T4) and B) ISIS draw of the same.

Short  $O\cdots Cl$  and  $S\cdots Cl$  contacts have been detected in the crystals structure of the complex between the factor *Xa* of the human blood coagulation cascade and a trichloro substituted inhibitor, which is used in the treatment of thrombotic diseases.<sup>88</sup> Polyhalogenated organic compounds are used as general anesthetics. Halothane is a common volatile anesthetic used in therapy in the racemic form. The two enantiomers have different pharmacological activities and the measured eudismic ratio has been attributed to the specific binding with proteinaceous receptor sites.<sup>89</sup> The enantioselective recognition of the drug *in vivo* may be mediated by the formation of halogen-bonded complexes with electron-pair donors present in the receptor pockets. The survey of the single crystal structures of proteins and nucleic acids in the PDB for halogen bonds,

resulted many hits which clearly demonstrates the potential significance of this interactions in ligand binding and recognition as well as molecular folding.<sup>90</sup>

### 1.8 Halogen Bonding and Implications for Drug Design

The diversity of short  $X\cdots O$  interactions that are involved in protein-ligand recognition is illustrated by the four short  $\text{Br}\cdots\text{O}$  contacts between the inhibitor 4,5,6,7-tetra-bromobenzotriazole and the ATP binding site of phospho-CDK2-cyclin A (2.2 Å structure, PDB ID code 1P5E).<sup>91</sup> Two  $\text{C}-\text{Br}\cdots\text{O}=\text{C}$  interactions (middle) involve the lone pair electrons of oxygen atom and one (right) involves the  $\pi$  electrons of a peptide  $\text{O}=\text{C}$  group. In addition, one halogen bond to a water molecule ( $\text{C}-\text{Br}\cdots\text{O}_w$ , left, **Figure 1.12**) also exists.

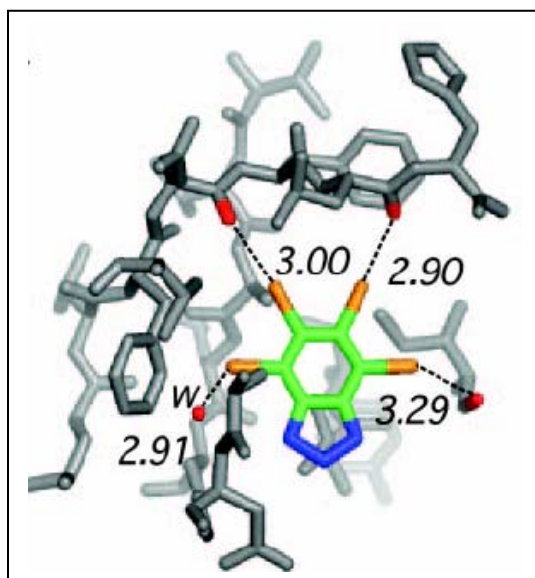


**Figure 1.12.** The 2.2-Å structure of phospho-CDK2/cyclin A in complex with the inhibitor 4,5,6,7-tetrabromobenzotriazole. The inhibitor is shown with three bromine halogen bonds to peptide carbonyl oxygens of the protein. Two interactions (middle)



involve the lone pairs of the oxygen atom and one (right) involves the  $\pi$  system of the C=O group. In addition, one halogen bond to a water molecule (w) is seen (left).

In this case, the halogenated inhibitor very efficiently displaces the charged ATP ligand, mainly through halogen bonding interactions, stressing the potential role of halogen bond in the design of new drugs and inhibitors. Thus, electrostatic-type nature of halogen bond interactions, which is strong enough to compete with standard hydrogen bonds<sup>68</sup> along with their abilities to serve as electron withdrawing substituents or their supposed “hydrophilic” properties, would contribute to the design of ligands by providing a framework for the use of this inter atomic interaction.

### 1.9 Insight into ‘Halogen Bonding’ Contacts: Path Followed in the Present Thesis

The work reported in this thesis triggered from the observation that racemic 1,2,3,6,5-penta-*O*-benzoyl-4-*O*-tosyl-*myo*-inositol (Chapter 2) spontaneously formed very stable inclusion crystal exclusively with dihalomethane solvents.<sup>81b</sup> So much was the dependence on dihalomethanes, that even a trace of dihalomethane (0.01%) solvent induced crystallization. DSC studies showed a strong association of guest molecules with the host. The revelation came from the crystal structure analysis, which showed the presence of short C-Cl $\cdots$ O contact (Cl $\cdots$ O=2.962 Å), along with a weak C-H $\cdots$ O interaction that held the guest molecule. Analogues of **3** were synthesized to examine the effect on inclusion behaviour and guest selectivity. Hexa-*O*-benzoyl-*myo*-inositol (Chapter 3) also formed solvates with dihalomethanes but were highly unstable in open atmosphere. The crystal structure showed C-H $\cdots$ O as a major binding interaction in the host-guest systems, with marginal halogen bonding contacts. The inclusion crystals could

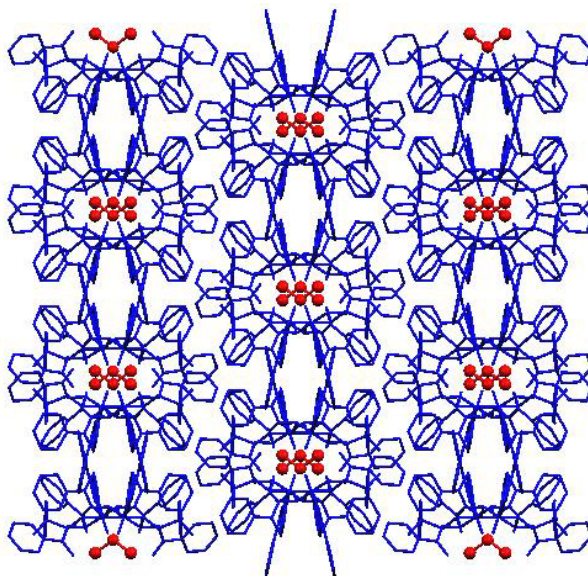
also be obtained from chloroform and bromoform. The chloroform inclusion crystals were highly unstable amongst all but the bromoform crystals were more stable (~ 10-15 minutes). However, the halogen atom of the guests in these structures made good halogen bonding contacts with the host molecules. Other hexa substituted *myo*-inositol derivatives such as 1,2,3,5,6-penta-*O*-benzoyl-4-*O*-benzyl *myo*-inositol (Chapters 4) and hexa-*O*-toluoyl-*myo*-inositol (Chapter 5) also produced inclusion crystals, which were highly unstable. The absence of halogen bonding interactions was consistently noted in these crystals showing high instability. This observation was strengthened from the pseudopolymorphic behaviour of 4,6-di-*O*-benzoyl-*myo*-inositol-1,3,5-orthoformate (Chapter 6), in which inclusion crystals obtained from dihalomethanes were highly unstable compared to the inclusion crystals obtained from trihalomethanes (stable upto 2-3 days in the open atmosphere, Chapter 6). Again here, their stability could be correlated with the presence of halogen bonding interaction between guest and the host molecules. The inclusion of other guests making C-halogen...O contacts reinforced the point. For example, higher stability was observed for trihalomethane inclusion crystals. Later chapters showed preference between halogen bonding contacts with differently hybridized oxygen atoms (Chapter 7). Crystals obtained with halogen bonding with carbonyl oxygen were large chunks, whereas crystals containing halogen bonding with ether oxygen were very thin needles. Interestingly, the crystals having halogen bonding with ether oxygen underwent single-crystal-to-single-crystal phase transition (on heating) to the crystal having halogen bonding with carbonyl oxygen. One more halogen containing *myo*-inositol derivative (Chapter 8) formed polymorphs (thin needles and blocks), one having C-H...halogen contact (thin needles) and other having

halogen...oxygen contact (blocks). This derivative also showed crystal-to-crystal phase transition from the crystals containing C-H...halogen contact to the crystal having halogen...oxygen contact. Thus this thesis investigates the role of halogen bonding interactions in promotion and growth of (inclusion) crystals, their stabilities along with some interesting observations on concomitant polymorphism and their crystal-to-crystal phase transitions.

To gain more insight into this intermolecular interaction, C-halogen...O, we also aimed to measure experimental charge densities involving these atoms. For this purpose, a model compound 2,5-dichloro-1,4-benzoquinone (Chapter 9) which exhibited excellent geometry for C-Cl...O short contact was chosen. The good quality crystals were grown in our laboratory and the intensity data were measured at 100K for obtaining more details on this intermolecular interaction (Chapter 9).

## Chapter 2

**Spontaneous Formation of Stable Inclusion  
Crystals of Racemic 1, 2, 3, 4, 5-penta-*O*-benzoyl-  
6-*O*-tosyl *myo*-Inositol Induced only by  
Dihalomethane via C-Halogen $\cdots$ O=C and C-H $\cdots$ O  
Short Contacts**



# Chapter 2

## 2.1 Introduction

Organic compounds often crystallize by the inclusion of one or more solvent molecules in the crystal lattice. For many of the compounds, the inclusion of solvent molecules in their crystals is of vital importance for successful crystallization. This has to do with the principle of close packing of organic molecules that is followed in their crystals.<sup>91</sup> Some inherently stable crystals do allow inclusion of small molecules,<sup>92</sup> however in others, the host framework is stable only in the presence of certain guests.<sup>93</sup> In the latter case, host is said to be guest sensitive. In such cases, the guest specificity and selectivity of host could provide valuable insight into the design of functional materials.<sup>94</sup> During the formation of crystals of a single compound, solute-solvent interactions are replaced by solute-solute interactions. However, when non-covalent interactions between the solute and the solvent molecules are more favorable than solute-solute interactions, solvated crystals result. Molecular recognition lies at the heart of the inclusion chemistry and this process occurs in solution during crystallization. Formation of inclusion crystals is an intermolecular recognition process, as a result of a number of non-covalent interactions that exist between the molecules in a crystal lattice.<sup>95</sup> The affinity of a host molecule for a given guest depends on the nature of host, guest and the medium of

crystallization under defined conditions of temperature, pressure and concentration as well as steric requirements of host and guest molecules. In addition to the topological interactions as well as directed binding forces, e.g. of dipole-dipole, ion-dipole and ion-ion type, H-bonding between host and the guest component and other van der Waals interactions gives rise to controlled guest selectivities.<sup>96</sup> Identification and characterization of weak interactions between functional groups in molecular crystals is the key for successful crystal engineering and design of new supra molecular assemblies with unusual properties.<sup>97</sup> Attempts to identify or synthesize novel 'host' compounds with specific properties,<sup>98</sup> which exhibit selectivity and specificity towards the inclusion of 'guest' molecules have resulted in the development of areas such as 'Supramolecular Chemistry'<sup>95</sup> and 'Crystal Engineering'.<sup>97</sup>

Since this thesis discusses pseudopolymorphic behaviour of *myo*-inositol derivatives, a brief introduction to this phenomenon is given below.

Host molecules can be broadly classified into two main types: (i) those which form molecular complexes by fitting guest into host cavity (ex. cyclodextrin, cyclophanes, calixarenes),<sup>99</sup> (ii) those which form lattice inclusion compounds by packing in such a manner as to leave cavities, channels or layers that accommodate various guest molecules.<sup>100</sup> There is no covalent bonding between the guest and the host, the attraction being generally due to non-covalent *intermolecular interactions*. These weaker intermolecular forces, which have impact on host-guest systems, have been systematically reviewed.<sup>101</sup> The strength of these interactions vary from strong ionic interactions (100-350 kJmol<sup>-1</sup>), through hydrogen bonding (10-40 kJmol<sup>-1</sup>), cation- $\pi$ , and  $\pi \cdots \pi$  stacking, to weak van der Waals forces (<5 kJ mol<sup>-1</sup>). Of these, hydrogen bonding is

the most important in material as well as biological activities and a number of recent texts deal with various aspects of this subject.<sup>102</sup>

Study of inclusion phenomena and host-guest chemistry has grown dramatically in last two decades, for example there are about 53000 entries under the term solvate in the November 2005 release of CSD v5.27. Several books and monographs are available including the authoritative 11 volume publication of *Comprehensive Supramolecular Chemistry*.<sup>103</sup> This well known phenomenon has wide applications in the areas of research as well as in chemical and pharmaceutical industries, which includes, purification and resolution of drugs, trapping and storage of toxic materials, matrices for slow drug release, solid-state reactivity, polymorphism, and the construction of functional materials.<sup>104</sup> This phenomenon (inclusion) involves the choice of a suitable host compound which, when exposed to a mixture of guests, combines selectively with a particular guest to form a crystalline inclusion compound.<sup>105</sup>

Since this thesis report is a study of polymorphic and *pseudo*-polymorphic behaviour of inositol derivatives, a brief introduction to inositols is given below.

Inositols are cyclohexane-hexols; there are nine known as stereoisomers (Chart1). Four isomers, viz., *myo*-, *neo*-, *chiro*-, and *scyllo*-Inositol, have been recognized to occur in nature while the others, viz., *cis*-, *epi*-, *allo*-, and *muco*-Inositol are unnatural synthetic isomers.<sup>106</sup> *myo*-Inositol being the most abundant, occurs widely in nature in both free and combined forms. *myo*-Inositols has five equatorial hydroxyl groups and an axial hydroxyl group. Although it has the *meso* configuration, in the combined form it occurs almost always as an optically active derivative. There is a plane of symmetry passing through C-2 and C-5 atoms (Chart 2). The carbon atom at the axial position is labeled as

C-2 and the other ring carbon atoms are numbered C-1 to C-6 starting from C-1 atom and proceeding around the ring either in clockwise or anticlockwise fashion. According to convention, an anti-clockwise numbering in unsymmetrically substituted *myo*-inositol leads to the D-configuration and the clockwise numbering leads to L-configuration.<sup>107</sup> However, International Union of Biochemistry (IUB) nomenclature allows all biologically relevant compounds to be denoted as the D-isomer.<sup>108</sup>

### Chart 1

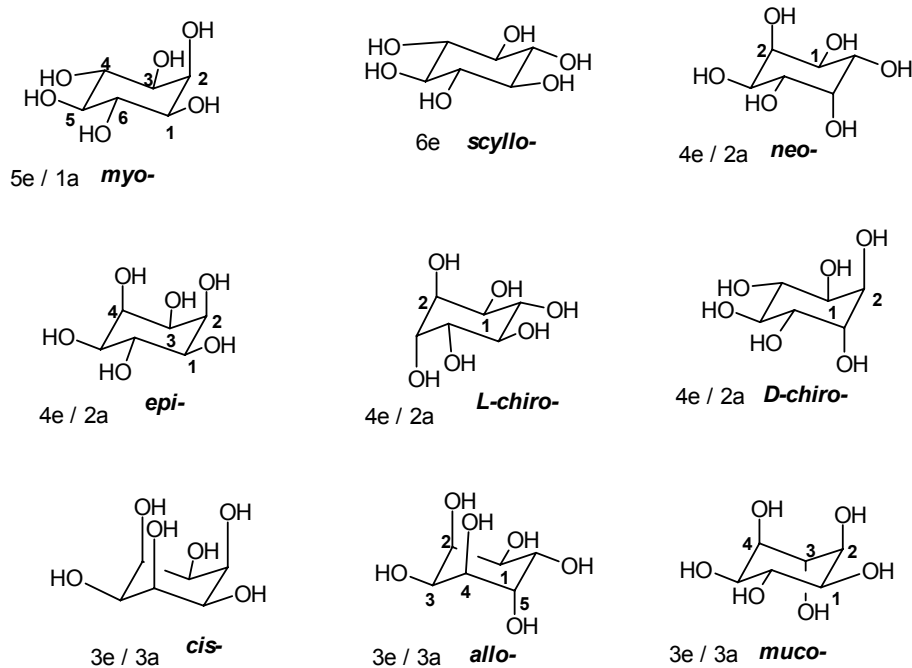
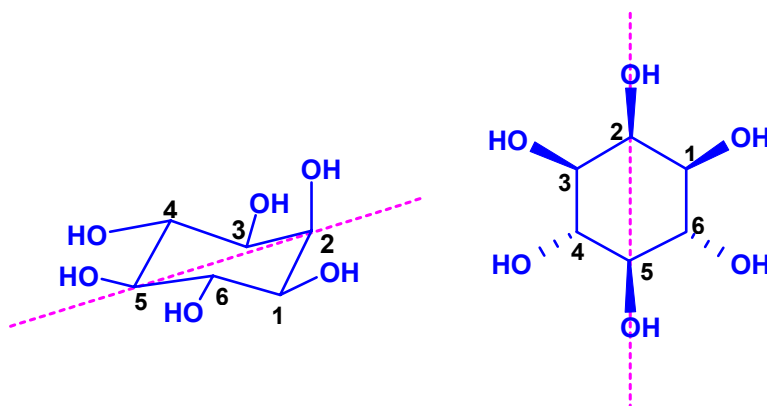


### Chart 2



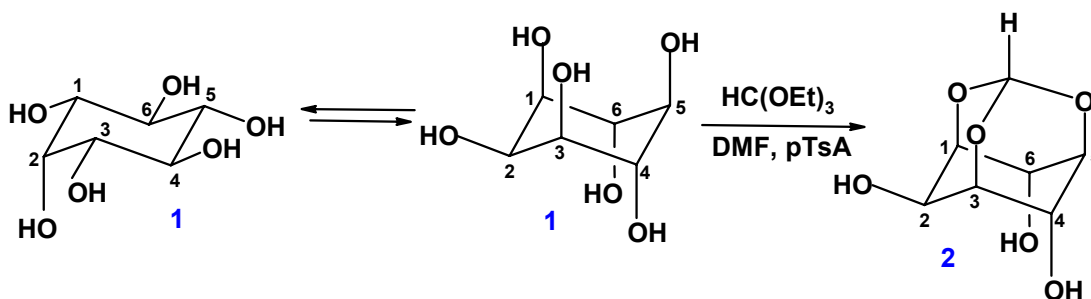


Synthesis and study of *myo*-inositol derivatives has attracted a great deal of attention recently, due to the establishment of the role played by the phosphorylated *myo*-inositol derivative in biologically important phenomena like cellular signal transduction<sup>109</sup> and anchoring of proteins to cell membranes.<sup>110</sup> Also some of the synthetic derivatives of *myo*-inositol, for example 1D-3-deoxy *myo*-inositol-1-phosphate, 1-phosphonate and some ether analogs have been shown to be inhibitors of cell proliferation and phosphatidylinositol-3-kinase signaling pathways.<sup>111</sup> Also it has been recently shown that D-3-azido-3-deoxy *myo*-inositol is a selective inhibitor for cancer cell growth.<sup>112</sup> These developments in biology and their consequences in medicine have necessitated simpler methods for the synthesis of various inositol derivatives. The key intermediate for the synthesis of the biologically important derivatives of inositols are the hydroxyl group protected derivatives (having the free hydroxyl derivatives at the desired position) that allow further modification or derivatization of *myo*-inositol to yield biologically important natural or unnatural products. There are many reports on the selective protection and deprotection of *myo*-inositol group in the literature.<sup>113</sup>

Orthoesters of the *myo*-inositol which obtained by the simultaneous protection of the three C1, C3 and C5 substituted hydroxyl groups of **1** (Scheme 2.1) are important intermediates for the preparation of biologically important phosphoinositols and their derivatives, glycosyl inositols and novel cyclitol based metal complexing agents. The formation of *myo*-inositol 1,3,5-orthoesters involves flipping of the carbocyclic ring (Scheme 2.1). Thus, *myo*-inositol orthoesters have one equatorial hydroxyl group and five axial hydroxyl groups. These *myo*-inositol orthoesters resemble adamantane in their

structure. Lee and Kishi<sup>114</sup> reported the preparation of *myo*-inositol 1,3,5-orthoformate (**2**) by reaction with triethyl orthoformate and *p*-toluenesulfonic acid. Billington et al<sup>115</sup> also prepared **2** by reaction with triethyl orthoformate in presence of *p*-toluenesulfonic acid and in DMF. This procedure gave better yield of the orthoformate **2** as compared to the procedure of Lee and Kishi, wherein DMSO was used as the solvent. Crystal structure of the *myo*-inositol 1,3,5-orthoformate (**2**) earlier reported by Vasella et al.<sup>116</sup> The three axial oxygen atoms attached to C1, C3 and C5 atoms are involved in the formation orthoformate bridge.

Scheme 2.1



We are engaged in the synthesis of several protected and deprotected *myo*-inositol derivatives for the last 10 years and found that many *myo*-inositol derivatives have a tendency to form inclusion complexes selectively with halogenated small organic molecules.<sup>117</sup>

Earlier, from this laboratory hexa-protected *myo*-inositol derivative racemic 1,2,3,4(6),5-penta-*O*-benzoyl,6(4)-*O*-tosyl-*myo*-inositol (**3**) was synthesized and serendipitously discovered that it was highly selective towards the encapsulation of dihalomethane in its crystal lattice. Compound **3** resisted crystallization from most of the common organic solvents but spontaneously crystallized in the presence of CH<sub>2</sub>X<sub>2</sub> (X

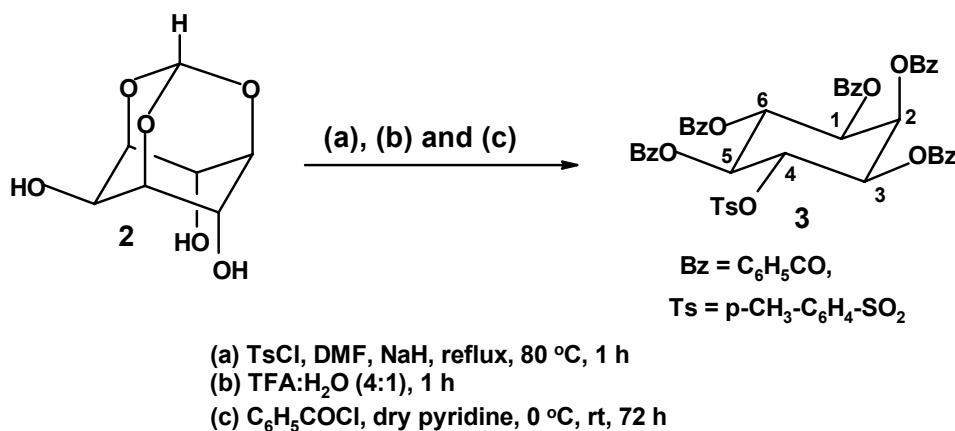
=Cl, Br) solvent as low as ~0.01% in other solvents to yield highly stable good quality single crystals. DSC, DTA/TGA studies showed that the solvent molecules are retained in the crystal lattice close to the melting point of the crystals suggesting a strong association of guest molecules with the host. Crystal structure of **3**<sup>118</sup> showed formation of open channels containing CH<sub>2</sub>X<sub>2</sub> (X = Cl, Br, I) guests, which makes two notable interactions with the host molecule, C-H...O and C-X...O, the later termed as ‘halogen bonding’. In order to explore its selectivity further, we have carried out a systematic study of its inclusion behaviour.<sup>117</sup> This chapter discusses the molecular recognition properties of **3** and its selectivity and specificity towards encapsulation of dihalomethane.

## 2.2 Experimental Section

### 2.2.1 Synthesis

Racemic 1,2,3,6,5-penta-*O*-benzoyl,4-*O*-tosyl-*myo*-inositol (**3**, m.p. 240-241 °C) was prepared in our laboratory (Scheme 2.2).<sup>117</sup>

**Scheme 2.2**



### 2.2.2 Crystallization

#### *Spontaneous Crystallization of 3 from Dihalomethane*

In order to probe the guest selectivity of this compound, crystallization of **3** was tried from various common organic solvents like chloroform, ethyl acetate, acetone, methanol, benzene, carbontetrachloride, dioxane, dibromoethane, dichloroethane and methyl iodide, but **3** resisted crystallization from most of these solvents. However, it readily crystallized from dichloromethane ( $\mathbf{3}\cdot\text{CH}_2\text{Cl}_2$ ). These observations suggested that the dichloromethane alone could induce the crystallization of **3** from solution. The crystallization of **3** is so much dependent on dichloromethane that even 0.01% (v/v) presence of  $\text{CH}_2\text{Cl}_2$  in chloroform showed formation of small shining crystals within 1h. Excellent quality plate shaped crystals grown is shown in **Figure 2.1**. This crystal form was obtained under varying crystallization conditions as seen over a wide range of concentration of solute as well as solvent (dichloromethane).

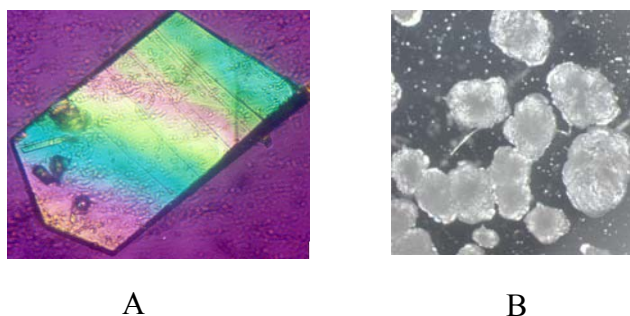


**Figure 2.1.** Photomicrographs of crystal of **3** with dichloromethane, A) single plate and B) crystals in the form of circular lumps

Crystallization of **3** in the presence of dihalomethanes, such as deuterated dichloromethane ( $\mathbf{3}\cdot\text{CD}_2\text{Cl}_2$ ), dibromomethane ( $\mathbf{3}\cdot\text{CH}_2\text{Br}_2$ ), diiodomethane, chlorobromomethane ( $\mathbf{3}\cdot\text{CH}_2\text{ClBr}$ ) and chloriodomethane ( $\mathbf{3}\cdot\text{CH}_2\text{ICl}$ ) were also tried.

All these dihalomethanes produced good quality single crystals with the exception of  $\text{CH}_2\text{I}_2$ , which yielded very thin crystals not suitable for single crystal X-ray analysis. Several trials to grow diiodomethane inclusion crystals of optimum dimensions for single crystal X-ray studies proved futile.

Experiments were carried out to study the preferences amongst dihalomethanes that are selected by the host system (**3**) during crystal formation. Crystallization of **3** from a mixture of  $\text{CH}_2\text{Cl}_2$  and  $\text{CH}_2\text{Br}_2$  (1:1 ratio) yielded crystals of **3** exclusively with  $\text{CH}_2\text{Br}_2$  (**3**· $\text{CH}_2\text{Br}_2$ ), clearly indicating the preference for Br over Cl. The selectivity of Br over Cl was seen in the other experiments too. For example, the crystals obtained from the mixture of solvents  $\text{CH}_2\text{Cl}_2$  and  $\text{CH}_2\text{ClBr}$  includes both the guests in crystal lattice, proportion of  $\text{CH}_2\text{ClBr}$  was slightly more. Similarly, crystallization of **3** from a mixture of  $\text{CH}_2\text{Br}_2$  and  $\text{CH}_2\text{ClBr}$  yielded crystals with higher proportion of the former. The amount of dihalomethanes present in these inclusion crystals was estimated by  $^1\text{H}$  NMR spectroscopy.<sup>26</sup> Proton NMR studies showed the presence of dichloromethane in the crystal lattice, methylene proton peak at  $\delta(\text{ppm}) = 5.30$  (s).  $^1\text{H}$  NMR spectra of the inclusion crystals in  $\text{CDCl}_3$  solution after heating at temperatures 50 °C, 100 °C, 150 °C, and 180 °C also showed the presence of dichloromethane.

### *Symmetry Requirement of the Guest*

It is noteworthy that all the solvents that lack  $\text{C}_2$  symmetry (for example, chloroform and methyl iodide) did not yield any crystals of **3** while  $\text{CH}_2\text{Cl}_2$ , and  $\text{CH}_2\text{Br}_2$  readily formed crystals with **3** possess  $\text{C}_2$  (two-fold) symmetry. The mixed

dihalomethanes such as  $\text{CH}_2\text{ClBr}$ , which lack  $\text{C}_2$  symmetry, also produced crystals but the X-ray structure showed that the inclusion crystals acquired two-fold symmetry by statistically distributing the two orientations of mixed dihalomethane molecules equally across the crystallographic 2-fold axis. However, the requirement of the  $\text{C}_2$  symmetry of the guest does not seem to be the sole criterion for the inclusion crystal formation but a restriction on the steric size of the guest molecule also. The larger dihaloalkane like 1,2-dichloroethane or 1,2-dibromoethane possessing 2-fold axis did not produce inclusion crystals of **3**.

### *Guest Induced Crystallization*

It is very interesting to note that crystallization of **3** from ethyl acetate yielded tiny but good quality crystals, later found to be due to the presence of traces of dichloromethane in ethyl acetate, triggered the crystallization of **3**. This suggests that even trace of dihalomethanes is sufficient to induce crystallization of **3**.

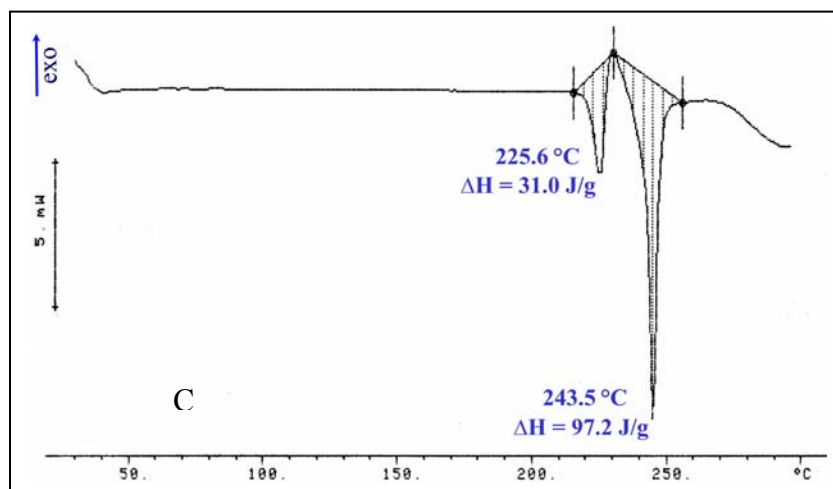
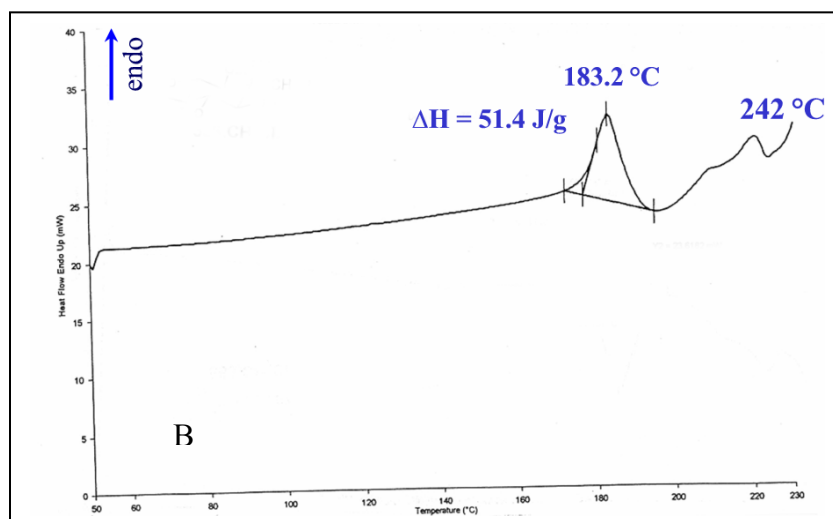
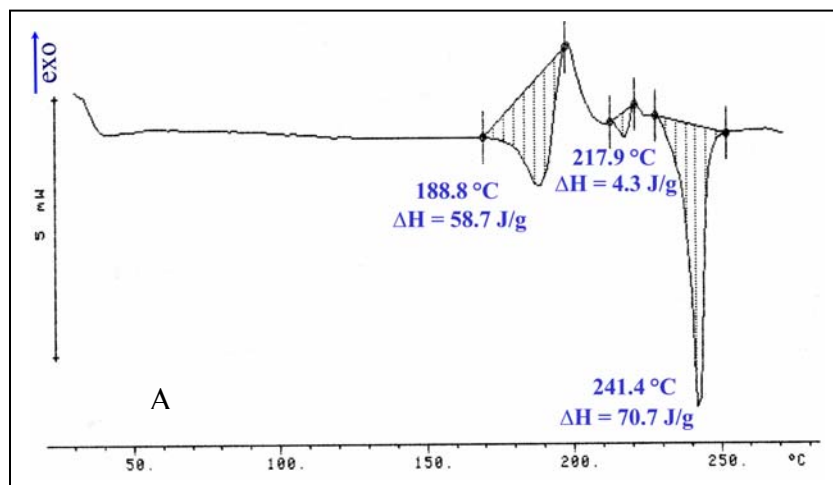
### **2.2.3 Thermal Analysis**

The Differential Scanning Calorimetry (DSC)<sup>119</sup> analysis of all the solvates of **3** (except crystals obtained from chloriodomethane) revealed the presence of dihalomethanes in the crystal lattice. The DSC study showed two endotherms; first endothermic peak (183-225 °C) indicated the escape of solvent from the crystal lattice and the second endotherm (241-243 °C) corresponded to the melting of crystals (**Table 2.1** and **Figure 2.2**). This suggested the included solvent remained in crystal lattice very close to the melting point of **3**, although different dihalomethane guests escaped at

different temperatures. The DSC studies of dichloromethane inclusion crystals of **3** at different time showed difference in the profiles. DSC of freshly grown inclusion crystals of **3** (**3**·CH<sub>2</sub>Cl<sub>2</sub>(F)), showed three endotherms, first one at ~189 °C (broad peak), second one at ~ 217 °C (small hump). The third endotherm at 243 °C associated with the melting of crystals whereas the DSC of two months old dichloromethane inclusion crystals of **3** (**3**·CH<sub>2</sub>Cl<sub>2</sub>(H)) showed only two endotherms (183 °C and 242 °C). This suggested that the guest molecules left the crystal lattice slightly at higher temperature from freshly grown dichloromethane inclusion crystals of **3** as compared to the two months old inclusion crystals. Further it is noteworthy that the final melting of the compound **3** does not vary much in all the solvates of **3**. Such interesting behavior of solvates of **3** suggests a strong association of the dihalomethane guest with the host molecules.

**Table 2.1:** DSC Data for Inclusion Crystals of **3**.

	1 <sup>st</sup> endotherm	2 <sup>nd</sup> endotherm
<b>3</b> ·CH <sub>2</sub> Cl <sub>2</sub> (Fresh crystals)	188.8 °C	241.4 °C
<b>3</b> ·CH <sub>2</sub> Cl <sub>2</sub> (two months old crystals)	183.2 °C	242 °C
<b>3</b> ·CD <sub>2</sub> Cl <sub>2</sub>	225°C	243.5°C
<b>3</b> ·CH <sub>2</sub> Br <sub>2</sub>	188.9 °C	240.6 °C
<b>3</b> ·CH <sub>2</sub> ClBr	192 °C	242.8 °C
<b>3</b> ·CH <sub>2</sub> ICI	Not observed	240.2 °C
<b>3</b> (Grown from Ethyl Acetate)	Not observed	241 °C





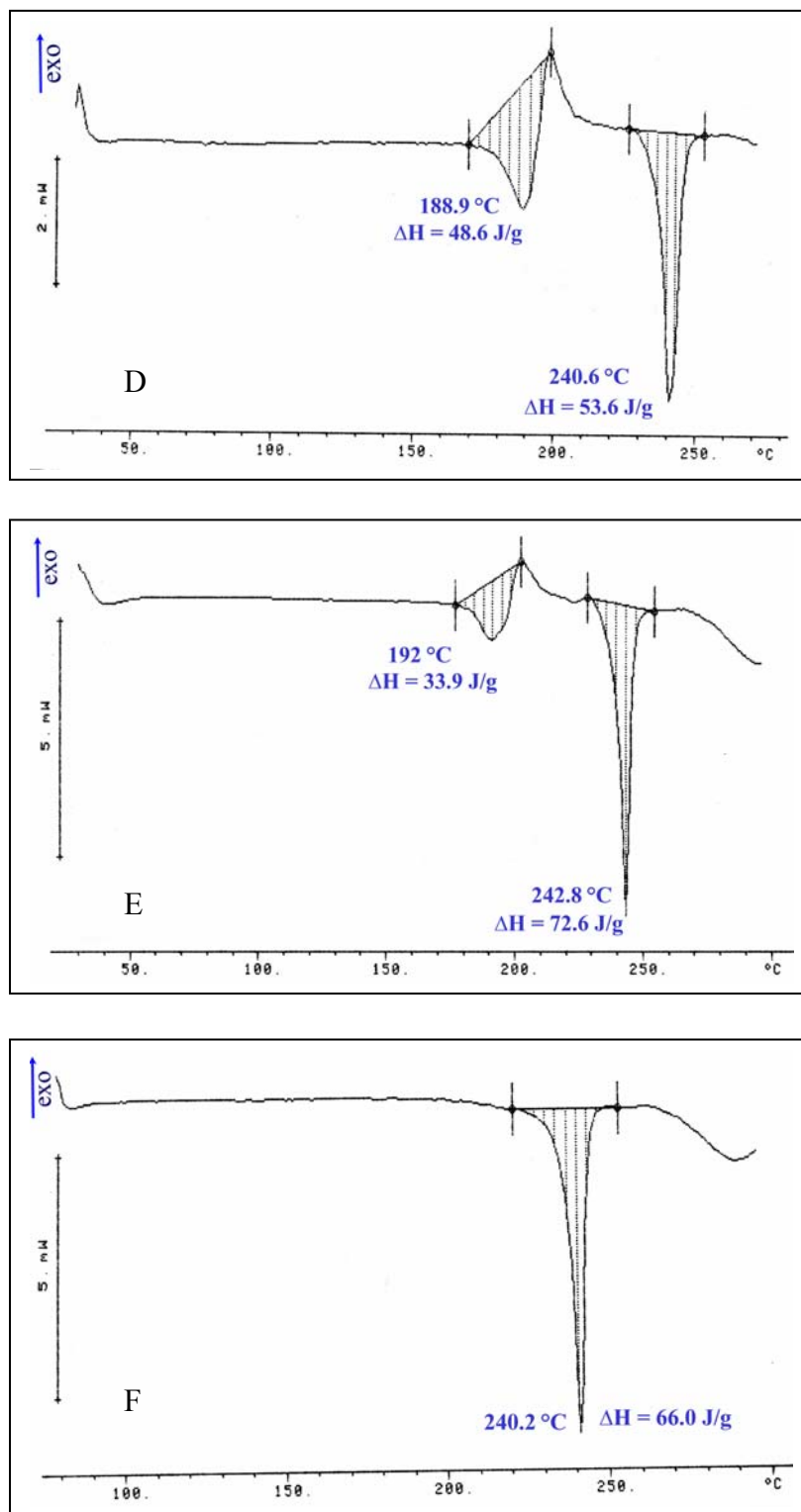


**Figure 2.2.** DSC profiles of solvates of **3**, A)  $3 \cdot \text{CH}_2\text{Cl}_2(\text{F})$ , B)  $3 \cdot \text{CH}_2\text{Cl}_2(\text{H})$ , C)  $3 \cdot \text{CD}_2\text{Cl}_2$ , D)  $3 \cdot \text{CH}_2\text{Br}_2$ , E)  $3 \cdot \text{CH}_2\text{ClBr}$  and F)  $3 \cdot \text{CH}_2\text{ICl}$ .

### 2.2.4 Heating Response of Crystals on Hot Stage Microscopy

Freshly grown dichloromethane inclusion crystals of **3** ( $3 \cdot \text{CH}_2\text{Cl}_2$ ) were heated on Leica polarizing microscope equipped with a heating stage P350. Crystals started losing transparency gradually around 160 °C, becoming completely opaque at ~185 °C and finally melted around 240 °C. This observation also confirms the presence of dichloromethane in the crystal lattice close to the melting of the crystals (**Figure 2.3**).

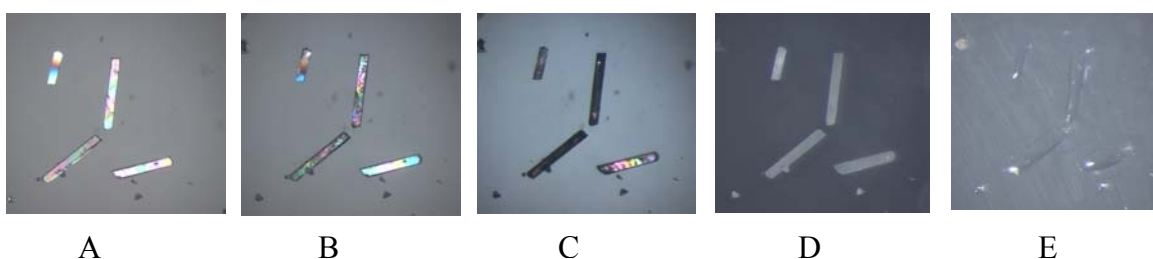


**Figure 2.3.** Photomicrographs of crystals of  $3 \cdot \text{CH}_2\text{Cl}_2$  subjected to heating. A) at room temperature, B) at 160 °C, C) at 180 °C, D) at 185 °C, E) at 240 °C.

### 2.2.5 X-ray Data Collection, Structure Solution and Refinement

In order to understand the remarkable specificity for the inclusion of dihalomethanes in crystals of **3**, single crystal X-ray structures were determined for seven dihalomethane solvates such as fresh dichloromethane inclusion crystals  $3 \cdot \text{CH}_2\text{Cl}_2(\text{F})$ , two month old dichloromethane inclusion crystals  $3 \cdot \text{CH}_2\text{Cl}_2(\text{H})$ ,  $3 \cdot \text{CD}_2\text{Cl}_2$ ,  $3 \cdot \text{CH}_2\text{Br}_2$ ,  $3 \cdot \text{CH}_2\text{CIBr}$ ,  $3 \cdot \text{CH}_2\text{ICI}$  and crystals obtained from ethyl acetate  $3 \cdot \text{CH}_2\text{Cl}_2(\text{T})$ . All the crystals were perfectly stable at room temperature and the intensity data measurements were carried out at room temperature (297K) on a Bruker SMART APEX CCD Diffractometer with graphite-monochromatized ( $\text{Mo K}_\alpha = 0.71073 \text{ \AA}$ ) radiation. The X-ray data collection was monitored by Bruker's SMART program.<sup>120</sup> All the data were

corrected for Lorentzian, polarisation and absorption effects using Bruker's SAINT<sup>121</sup> and SADABS<sup>121</sup> programs. SHELX-97<sup>122</sup> was used for structure solution and full matrix least squares refinement on  $F^2$ . Hydrogen atoms were included in the refinement as per the riding model. The summary of crystallographic experimental details for all the inclusion complexes is recorded in **Table 2.2**.

**Table 2.2.** Crystal data for solvate of **3**.

Crystal data	<b>3</b> ·CH <sub>2</sub> Cl <sub>2</sub> (F)	<b>3</b> ·CH <sub>2</sub> Cl <sub>2</sub> (H)	<b>3</b> ·CD <sub>2</sub> Cl <sub>2</sub>	<b>3</b> ·CH <sub>2</sub> Br <sub>2</sub>
Chemical formula	C <sub>48</sub> H <sub>38</sub> O <sub>13</sub> S· 0.5(CH <sub>2</sub> Cl <sub>2</sub> )· 1.63(O)	C <sub>48</sub> H <sub>38</sub> O <sub>13</sub> S· 0.25(CH <sub>2</sub> Cl <sub>2</sub> )	C <sub>48</sub> H <sub>38</sub> O <sub>13</sub> S· 0.5(CD <sub>2</sub> Cl <sub>2</sub> )· 0.5(O)	C <sub>48</sub> H <sub>38</sub> O <sub>13</sub> S· 0.5(CH <sub>2</sub> Br <sub>2</sub> )
$M_r$	923.31	876.08	897.31	941.77
Crystal system,	Monoclinic,	Monoclinic,	Monoclinic,	Monoclinic,
Space group	<i>C2/c</i>	<i>C2/c</i>	<i>C2/c</i>	<i>C2/c</i>
$a$ (Å)	26.344(9)	26.771(4)	26.892(4)	26.9267(17)
$b$ (Å)	11.544(4)	11.608(3)	11.6904(17)	11.7160(8)
$c$ (Å)	30.950(11)	30.783(6)	31.034(5)	30.874(2)
$\beta$ (°)	105.684(6)	105.176(6)	105.826(3)	105.998(1)
$V$ (Å <sup>3</sup> )	9062(5)	9232 (3)	9387 (2)	9362.7 (11)
$Z$ , $D_{\text{calc}}$ (g cm <sup>-3</sup> )	8, 1.353	8, 1.261	8, 1.270	8, 1.336
$\mu$ (mm <sup>-1</sup> )	0.20	0.16	0.19	0.99
$F(000)$	3840	3652	3736	3880
Crystal size, mm	0.77×0.18×0.10	0.20×0.19×0.11	0.39×0.23×0.04	0.24×0.22×0.16
Ab.correction	Multi-scan	Multi-scan	Multi-scan	Multi-scan
$T_{\text{min}}$	0.860	0.968	0.930	0.798
$T_{\text{max}}$	0.980	0.982	0.992	0.858
Reflns collected	47458	22898	22798	26695
Unique reflns	7961	6618	8243	6718
Observed reflns	5955	2756	3387	4006
$R_{\text{int}}$	0.072	0.087	0.084	0.036
$\theta_{\text{max}}$ (°)	25.0	23.3	25.0	23.3
$h, k, l$ (min, max)	(-31, 31), (-13, 13), (-36, 36)	(-26, 29), (-12, 12), (-32, 34)	(-31, 16), (-13, 13), (-36, 36)	(-29, 29), (-12, 13), (-34, 34)
No. of parameters	601	575	586	574
GoF	1.04	0.87	0.95	1.06
$R_1[I > 2\sigma(I)]$	0.0649	0.0556	0.0772	0.0666
$wR_2[I > 2\sigma(I)]$	0.1661	0.1611	0.1815	0.2329
$\Delta \rho_{\text{max}}, \Delta \rho_{\text{min}}$ (e Å <sup>-3</sup> )	0.88, -0.76	0.30, -0.22	0.50, -0.35	0.71, -1.16

	<b>3·CH<sub>2</sub>ClBr</b>	<b>3·CH<sub>2</sub>Cl</b>	<b>3 (from EA)</b>
Chemical formula	C <sub>48</sub> H <sub>38</sub> O <sub>13</sub> S1· 0.5(CH <sub>2</sub> ClBr)·O	C <sub>48</sub> H <sub>38</sub> O <sub>13</sub> S· 0.15(CH <sub>2</sub> Cl)· 0.10(CH <sub>2</sub> Cl <sub>2</sub> )	C <sub>48</sub> H <sub>38</sub> O <sub>13</sub> S· 0.05(CH <sub>2</sub> Cl <sub>2</sub> )
<i>M<sub>r</sub></i>	935.54	887.51	859.28
Crystal system,	Monoclinic,	Monoclinic,	Monoclinic,
Space group	<i>C2/c</i>	<i>C2/c</i>	<i>C2/c</i>
<i>a</i> (Å)	26.812(6)	26.831(5)	27.03 (3)
<i>b</i> (Å)	11.727(3)	11.612(2)	11.628 (11)
<i>c</i> (Å)	31.095(7)	30.705(6)	30.75 (3)
β (°)	106.049(5)	105.20(3)	104.789 (17)
<i>V</i> (Å <sup>3</sup> )	9396 (4)	9232 (3)	9343 (15)
<i>Z</i>	8	8	8
<i>D<sub>calc</sub></i> (g cm <sup>-3</sup> )	1.323	1.277	1.222
μ (mm <sup>-1</sup> )	0.59	0.24	0.14
<i>F</i> (000)	3872	3688	3585
Crystal size (mm)	0.32 × 0.16 × 0.04	0.23 × 0.15 × 0.04	0.19 × 0.08 × 0.03
Ab. correction	Multi-scan	Multi-scan	Multi-scan
<i>T<sub>min</sub></i>	0.832	0.947	0.974
<i>T<sub>max</sub></i>	0.980	0.990	0.996
Reflns collected	23335	22846	32595
Unique reflns	8287	8086	8200
Observed reflns	3336	2834	3239
<i>R<sub>int</sub></i>	0.059	0.109	0.179
θ <sub>max</sub> (°)	25.0	25.0	25.0
H, k, l (min, max)	(-31, 29), (-13, 7), (-36, 34)	(-31, 31), (-13, 13), (-36, 17)	(-32, 32), (-13, 13), (-36, 36)
No. of parameters	615	583	566
GoF	0.87	0.96	1.04
<i>R</i> <sub>1</sub> [ <i>I</i> > 2σ( <i>I</i> )]	0.050	0.080	0.128
w <i>R</i> <sub>2</sub> [ <i>I</i> > 2σ( <i>I</i> )]	0.126,	0.150,	0.272
Δ ρ <sub>max</sub> , Δ ρ <sub>min</sub> (eÅ <sup>-3</sup> )	0.46, -0.24	0.41, -0.21	0.40, -0.37

Single crystal X-ray structure determination showed that all the inclusion crystals were isomorphous. The expansion of the c-axis of  $\sim 1 \text{ \AA}$  was observed in dibromomethane inclusion crystals ( $3 \cdot \text{CH}_2\text{Br}_2$ ) compared to dichloromethane solvate ( $3 \cdot \text{CH}_2\text{Cl}_2$ ). This expansion is probably due to bigger size of the  $\text{CH}_2\text{Br}_2$ . The volume of the chlorobromomethane solvate ( $3 \cdot \text{CH}_2\text{ClBr}$ ) is in between  $3 \cdot \text{CH}_2\text{Cl}_2$  and  $3 \cdot \text{CH}_2\text{Br}_2$ .

### *Structure of $3 \cdot \text{CH}_2\text{Cl}_2(\text{F})$*

Crystal structure of  $3 \cdot \text{CH}_2\text{Cl}_2(\text{F})$  revealed the presence of dichloromethane solvent in the crystal lattice with full occupancy. The included dichloromethane molecule occupies a special position (crystallographic two-fold axis) passing through the carbon of the  $\text{CH}_2\text{Cl}_2$  molecule. Difference Fourier (apart from  $\text{CH}_2\text{Cl}_2$ ) contained some peaks with heights 6.99, 2.25 and 1.25  $e/\text{\AA}^3$  (O14, O15 and O16 respectively), which were assigned to water molecules with appropriate occupancies (1.0, 0.4 and 0.25 respectively).

### *Structure of $3 \cdot \text{CH}_2\text{Cl}_2(\text{H})$*

Crystal structure of the same crystals (same batch,  $3 \cdot \text{CH}_2\text{Cl}_2(\text{H})$ ) as above collected after 2 months, revealed the reduction in the occupancy of guest dichloromethane from full to half. Also, this crystal lattice did not contain any water molecules. The gradual decrease of the occupancy of  $\text{CH}_2\text{Cl}_2$  and water molecules was seen only in chloro dihalomethanes. It is interesting to note that the crystals, even after losing half of  $\text{CH}_2\text{Cl}_2$ , did not show any signs of degradation.

### *Structure of $3 \cdot \text{CD}_2\text{Cl}_2$*

Structure of freshly grown crystals of **3** from deuterated dichloromethane solvent ( $3 \cdot \text{CD}_2\text{Cl}_2$ ) contained  $\text{CD}_2\text{Cl}_2$  with occupancy of 0.8. As in  $3 \cdot \text{CH}_2\text{Cl}_2(\text{F})$ , traces of three

water molecules (O14, O15 and O16) were also picked up in the difference Fourier with lower occupancies (0.25, 0.20 and 0.1).

### *Structure of 3·CH<sub>2</sub>Br<sub>2</sub>*

Crystals of **3·CH<sub>2</sub>Br<sub>2</sub>** were grown as thick plates and were bigger than those of **3·CH<sub>2</sub>Cl<sub>2</sub>(H)** (crystals with half occupied CH<sub>2</sub>Cl<sub>2</sub> molecule). Unlike **3·CH<sub>2</sub>Cl<sub>2</sub>**, these crystals did not show decrease in the occupancy of dibromomethane molecules. Further, no water molecules were found in the crystal lattice of **3·CH<sub>2</sub>Br<sub>2</sub>**.

### *Structure of 3·CH<sub>2</sub>ClBr*

Crystals of **3** obtained from chlorobromomethane (CH<sub>2</sub>ClBr) were thin needles. Data collection on fresh crystals revealed the presence of chlorobromomethane with full occupancy. Further, some peaks with very low heights were observed which were then treated as oxygen atom of water molecule during refinement. Interestingly, CH<sub>2</sub>ClBr molecules also sit on the two-fold axis of the space group by statistically distributing chlorine and bromine around two-fold axis creating pseudo C<sub>2</sub> symmetry. During refinement they have been treated separately as dichloromethane and dibromomethane molecules sharing the same carbon atom sitting at two fold with equal occupancies.

### *Structure of 3·CH<sub>2</sub>ICl*

Crystals of **3** obtained from chloriodomethane (CH<sub>2</sub>ICl) were very thin needles. X-ray crystal structure determination of fresh crystals of **3E** revealed the presence of chloriodomethane (CH<sub>2</sub>ICl) with occupancy 0.15. Further the trace of CH<sub>2</sub>Cl<sub>2</sub> was also crystallized along with CH<sub>2</sub>ICl with occupancy 0.1 this could be due to the presence of

dichloromethane as an impurity in the  $\text{CH}_2\text{I}\text{Cl}$  used for crystallization. The dichloromethane molecule occupies the same position of  $\text{CH}_2\text{I}\text{Cl}$ , sharing the methylene carbon atom. Also  $\text{CH}_2\text{I}\text{Cl}$  molecule is statistically disordered around crystallographic two-fold axis possessed by the space group  $\text{C}2/\text{c}$ . Same refinement strategy was followed for treating this statistical disorder i.e. by separately refining the positions of dichloromethane and diiodomethane molecules sharing the same carbon atom sitting at two fold with different occupancies, chlorine has major occupancy compared to iodine, as iodine is bulkier than chlorine (occupancies for Cl and I were 0.35 and 0.15 respectively). Hence the dimensions of the cavity increase to accommodate the bulky dihalomethane.

***Structure of 3 grown from Ethyl Acetate ( $3 \cdot \text{CH}_2\text{Cl}_2(\text{T})$ )***

Interestingly crystals obtained from ethyl acetate also were very thin, tiny needles and diffracted very weakly. However, difference Fourier revealed two residual peaks of height 0.29 (Q1) and 0.19 (Q2)  $\text{e} \text{ \AA}^{-3}$  and the geometry of these peaks was almost like dichloromethane molecule. The peaks Q1 and Q2 were assigned to Cl and C atoms of the DCM molecule and were given occupancies 0.1 and 0.05 respectively.

## 2.3 Results and Discussion

### 2.3.1 Intramolecular Geometry

The ORTEP<sup>123</sup> view of **3**·CH<sub>2</sub>Cl<sub>2</sub>(F) is shown in **Figure 2.4**. The core inositol ring has the chair configuration. Out of the five benzoyl groups, the C2-O-benzoyl group is axial and remaining are at equatorial positions. Somewhat off centered intramolecular aromatic  $\pi\cdots\pi$  stacking<sup>14</sup> interactions (**Table 2.3**) between the phenyl rings of the C4-O-tosyl group (Cg4) and C5-O-benzoyl group (Cg5) were observed in all the solvates. It was observed that the geometry of the  $\pi\cdots\pi$  contacts is better in the crystals where occupancy of dihalomethanes is full as compared to the crystals where solvent occupancy is less. For example the dihedral angle between the two phenyl rings was  $\sim 7.66^\circ$  in **3**·CD<sub>2</sub>Cl<sub>2</sub> where the occupancy of CD<sub>2</sub>Cl<sub>2</sub> is one and  $\sim 12.31^\circ$  in **3**·CH<sub>2</sub>Cl<sub>2</sub>(T), where the occupancy of CH<sub>2</sub>Cl<sub>2</sub> was far less (**Table 2.3**).

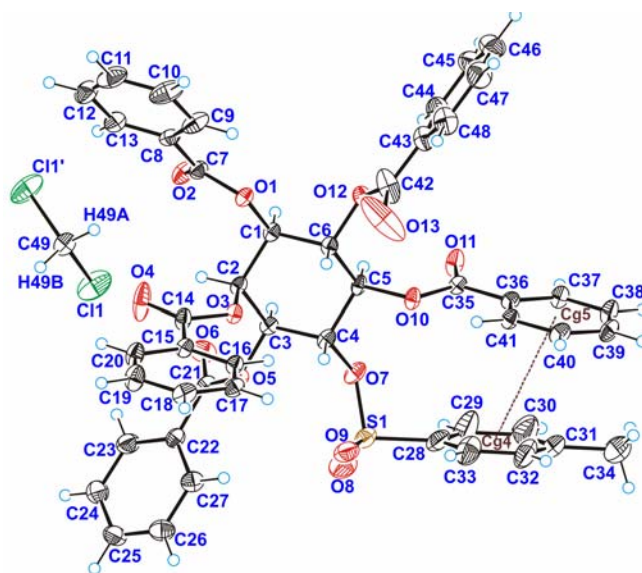


**Figure 2.4.** ORTEP view of **3**·CH<sub>2</sub>Cl<sub>2</sub>(F) showing intramolecular  $\pi\cdots\pi$  stacking interactions



**Table 2.3:** Intramolecular  $\pi\cdots\pi$  stacking contacts in solvates of **3**.

	Cg(4) $\cdots$ Cg(5) (Å)	Dihedral angle $\alpha$ (°)	CgI <sub>perp</sub> (Å)	CgJ <sub>perp</sub> (Å)	Occupancy
<b>3</b> ·CH <sub>2</sub> Cl <sub>2</sub> (F)	4.0283	8.16	3.726	3.484	1.0
<b>3</b> ·CH <sub>2</sub> Cl <sub>2</sub> (H)	4.1937	12.04	3.814	3.409	0.5
<b>3</b> ·CD <sub>2</sub> Cl <sub>2</sub>	4.1016	7.66	3.553	3.780	0.8
<b>3</b> ·CH <sub>2</sub> Br <sub>2</sub>	4.1723	9.96	3.800	3.472	1.0
<b>3</b> ·CH <sub>2</sub> ClBr	4.1099	7.15	3.762	3.545	1.0
<b>3</b> ·CH <sub>2</sub> ICl	4.1864	11.44	3.805	3.432	Trace
<b>3</b> ·CH <sub>2</sub> Cl <sub>2</sub> (T)	4.2024	12.31	3.826	3.435	Trace

The included dihalomethane molecule has C<sub>2</sub> symmetry; only one halogen atom is seen in the structure with one carbon and two hydrogen atoms. The other halogen atom of the dichloromethane is generated by two-fold symmetry by growing the fragment. So the occupancy of halogen is adjusted accordingly (**Figure 2.5**).

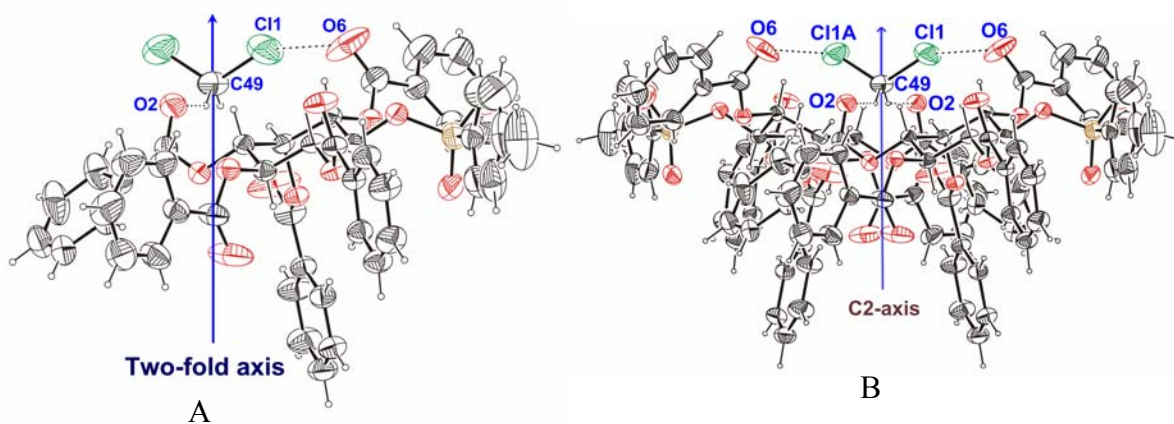


**Figure 2.5.** ORTEP view of **3**·CH<sub>2</sub>Cl<sub>2</sub>(F), showing crystallographic two-fold axis passing through the carbon atom of CH<sub>2</sub>Cl<sub>2</sub> molecule.

Conformation of host molecule in all the solvates is almost the same confirming their isostructurality (**Figure 2.6**). Orientation of the C3-O-benzoyl is slightly different in all the solvates perhaps because the carbonyl oxygen O6 is involved in halogen bonding contacts in these crystals.

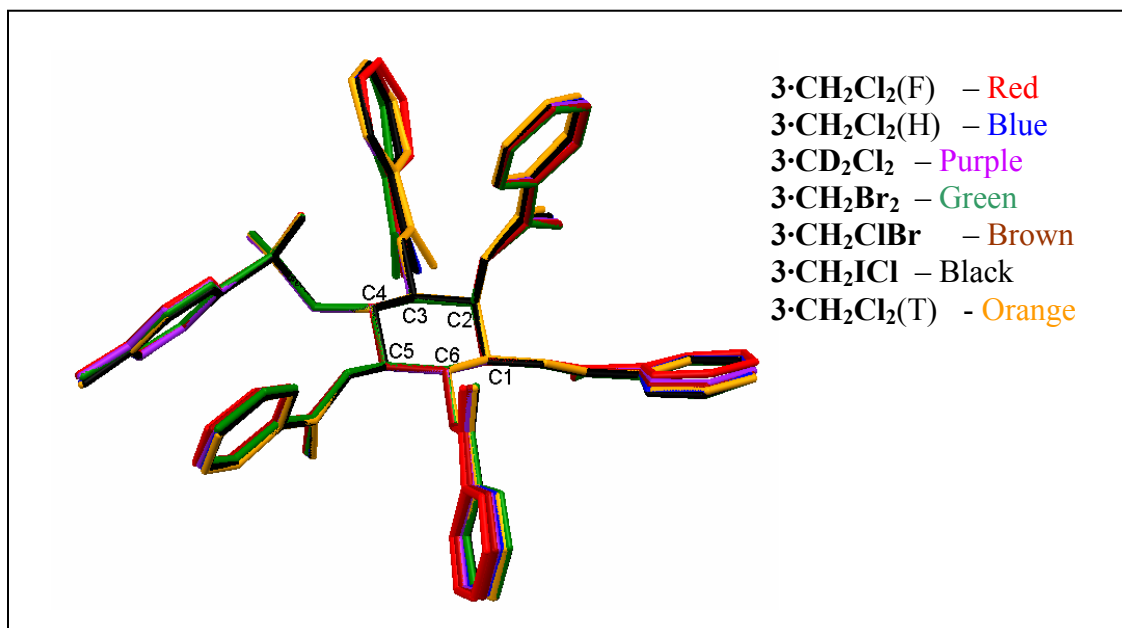


**Figure 2.6.** Overlap of the host molecule in all the solvates of **3**.

### 2.3.2 Host Organization

In crystals of all the solvates the host molecules form a centrosymmetric dimer via trifurcated C-H $\cdots$ O interactions.<sup>4</sup> The three axial H-atoms H1, H3 and H5 of the *myo*-inositol ring from each molecule make contacts with the carbonyl oxygen O11 of the other molecule. The host molecules also make centrosymmetric C-H $\cdots$ O=(S) interactions between the phenyl hydrogen atom H45 and sulphonyl oxygen O8 (C45-H45 $\cdots$ O8, not shown in the figure for clarity) and C37-H37 $\cdots$ O2 contacts holding the centrosymmetric dimer more strongly (Figure 2.7, Table 2.4). The geometries of C1-H1 $\cdots$ O11 and C5-H5 $\cdots$ O11 are better than the C3-H3 $\cdots$ O11 contact. The C37-H37 $\cdots$ O2 and C45-H45 $\cdots$ O8 contacts, which hold the dimers further, are weaker in strength compared to the C-H $\cdots$ O geometries of trifurcated assembly. The geometries of the C-H $\cdots$ O interactions (Figure 2.7) do not vary with the included guests.

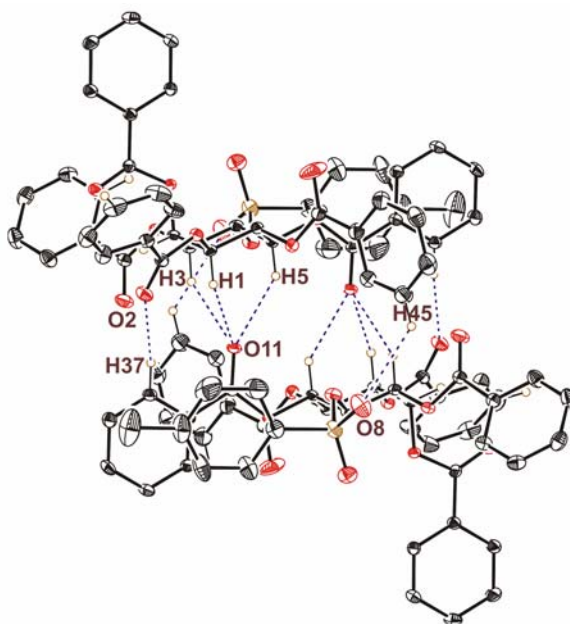


**Figure 2.7.** Closely interacting host molecules of  $3\cdot\text{CH}_2\text{Cl}_2(\text{F})$  linked via centrosymmetric trifurcated C-H $\cdots$ O assembly.

**Table 2.4:** Host-host C-H...O interactions across inversion center in all the solvates of **3**.

	D-H...A	D-H (Å)	H...A (Å)	D...A (Å)	D-H...A (°)
<b>3</b> ·CH <sub>2</sub> Cl <sub>2</sub> (F)	C(1)-H(1)...O(11)#1	0.98	2.35	3.233(4)	143
	C(3)-H(3)...O(11)#1	0.98	2.52	3.307(4)	137
	C(5)-H(5)...O(11)#1	0.98	2.41	3.190(4)	142
	C(37)-H(37)...O(2)#1	0.93	2.71	3.521(4)	146
	C(45)-H(45)...O(8)#1	0.93	2.70	3.411(5)	133
<b>3</b> ·CH <sub>2</sub> Cl <sub>2</sub> (H)	C(1)-H(1)...O(11)#2	0.98	2.35	3.206(5)	146
	C(3)-H(3)...O(11)#2	0.98	2.66	3.435(5)	136
	C(5)-H(5)...O(11)#2	0.98	2.44	3.275(5)	143
	C(37)-H(37)...O(2)#2	0.93	2.77	3.590(6)	148
	C(45)-H(45)...O(8)#2	0.93	2.67	3.434(7)	150
<b>3</b> ·CD <sub>2</sub> Cl <sub>2</sub>	C(1)-H(1)...O(11)#2	0.98	2.40	3.246(5)	144
	C(3)-H(3)...O(11)#2	0.98	2.60	3.393(6)	137
	C(5)-H(5)...O(11)#2	0.98	2.44	3.281(5)	143
	C(37)-H(37)...O(2)#2	0.93	2.80	3.618(6)	147
	C(45)-H(45)...O(8)#2	0.93	2.78	3.498(9)	135
<b>3</b> ·CH <sub>2</sub> Br <sub>2</sub>	C(1)-H(1)...O(11)#2	0.98	2.36	3.226(6)	146
	C(3)-H(3)...O(11)#2	0.98	2.60	3.395(6)	138
	C(5)-H(5)...O(11)#2	0.98	2.49	3.314(6)	141
	C(37)-H(37)...O(2)#2	0.93	2.82	3.646(7)	148
	C(45)-H(45)...O(8)#2	0.93	2.74	3.490(9)	138
<b>3</b> ·CH <sub>2</sub> ClBr	C(1)-H(1)...O(11)#3	0.98	2.38	3.234(5)	145
	C(3)-H(3)...O(11)#3	0.98	2.60	3.387(5)	138
	C(5)-H(5)...O(11)#3	0.98	2.45	3.283(6)	143
	C(37)-H(37)...O(2)#3	0.93	2.79	3.625(6)	149
	C(45)-H(45)...O(8)#3	0.93	2.78	3.497(7)	134
<b>3</b> ·CH <sub>2</sub> ICl	C(1)-H(1)...O(11)#2	0.98	2.33	3.199(6)	147
	C(3)-H(3)...O(11)#2	0.98	2.66	3.438(6)	136
	C(5)-H(5)...O(11)#2	0.98	2.47	3.297(5)	142
	C(37)-H(37)...O(2)#2	0.93	2.78	3.614(8)	150
	C(45)-H(45)...O(8)#2	0.93	2.65	3.437(9)	142
<b>3</b> ·CH <sub>2</sub> Cl <sub>2</sub> (T)	C(1)-H(1)...O(11)#2	0.98	2.39	3.244(8)	146
	C(3)-H(3)...O(11)#2	0.98	2.73	3.490(9)	135
	C(5)-H(5)...O(11)#2	0.98	2.43	3.270(8)	143
	C(37)-H(37)...O(2)#2	0.93	2.78	3.599(10)	147
	C(45)-H(45)...O(8)#2	0.93	2.66	3.444(13)	142

Symmetry codes: #1 -x,-y,-z; #2 -x,1-y,-z; #3 -x+1, -y+1, -z+2.

### 2.3.3 Role of Guest in the Assembly of Dimers

The two trifurcated C-H $\cdots$ O linked dimers are bridged along c-axis via dihalomethane molecule (**Figure 2.8**). These assemblies are linked via centrosymmetric C41-H41 $\cdots$ O13 interactions down b-axis forming pillars that are cemented by the guest molecule all along. A very significant role played by the guest by bridging the two dimers that lead to the formation of the entire supramolecular assembly perhaps explains the strong dependence of the dihalomethanes having a C<sub>2</sub> axis for crystal formation. Linking of centrosymmetric dimers via moderately good C41-H41 $\cdots$ O13 contacts (H41 $\cdots$ O13 = 2.31 $\cdots$ 2.36 Å,  $\angle$ C-H $\cdots$ O =  $\sim$  142°, **Table 2.5**) is seen in all the structures.

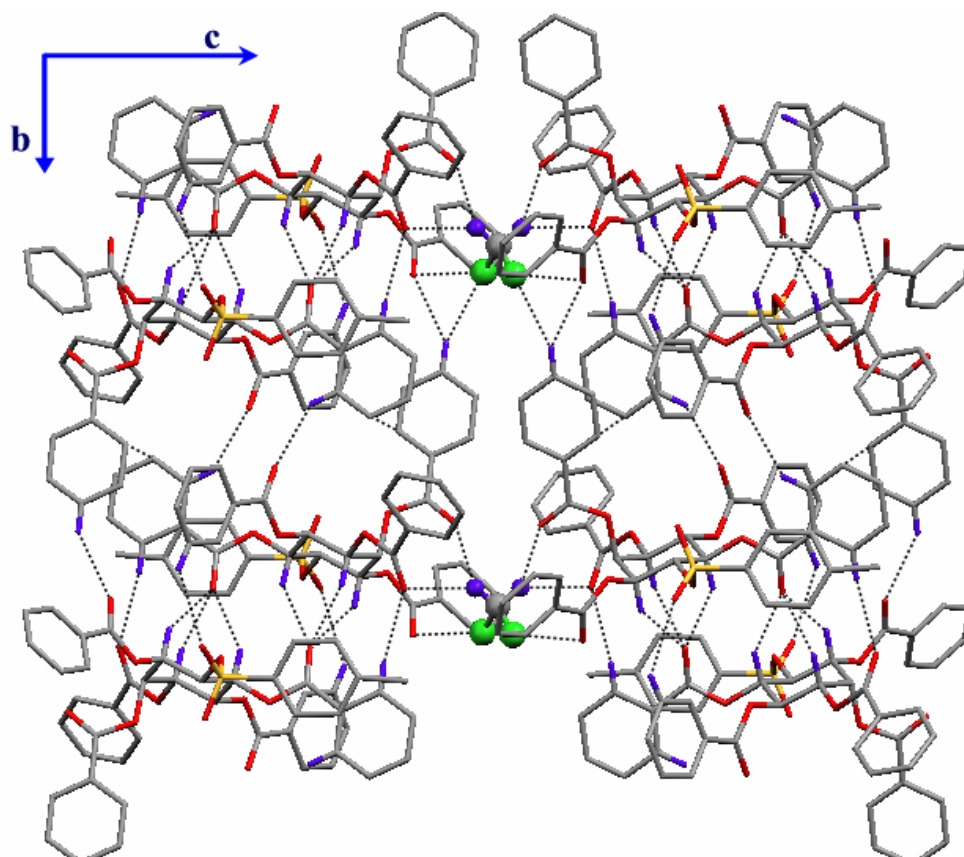


**Figure 2.8.** Linking of centrosymmetric trifurcated C-H $\cdots$ O assembly along b-axis and c-axis in crystals of **3**·CH<sub>2</sub>Cl<sub>2</sub>(F).

**Table 2.5:** C-H...O interactions involved in bridging of trifurcated dimeric assembly.

	D-H...A	D-H (Å)	H...A (Å)	D...A (Å)	D-H...A (°)
<b>3·CH<sub>2</sub>Cl<sub>2</sub>(F)</b>	C41-H41...O13#1	0.93	2.31	3.128(4)	146
<b>3·CH<sub>2</sub>Cl<sub>2</sub>(H)</b>	C41-H41...O13#2	0.93	2.35	3.145(6)	143
<b>3·CD<sub>2</sub>Cl<sub>2</sub></b>	C41-H41...O13#3	0.93	2.36	3.139(7)	142
<b>3·CH<sub>2</sub>Br<sub>2</sub></b>	C41-H41...O13#3	0.93	2.37	3.160(7)	143
<b>3·CH<sub>2</sub>ClBr</b>	C41-H41...O13#4	0.93	2.36	3.153(6)	143
<b>3·CH<sub>2</sub>ICl</b>	C41-H41...O13#2	0.93	2.35	3.149(8)	143
<b>3·CH<sub>2</sub>Cl<sub>2</sub>(T)</b>	C41-H41...O13#2	0.93	2.32	3.114(11)	144

Symmetry codes: #1 -x, -y+1, -z; #2 -x, -y+2, -z; #3 -x, -y, -z; #4 -x+1, -y+2, -z+2.

### 2.3.4 Significance of Halogen Bonding in Host-Guest Interactions

The included dihalomethane molecule makes short C-X...O (halogen bonding) contact with the carbonyl oxygen O6 of C3-*O*-benzoyl group and C-H...O interactions with the carbonyl oxygen atom O2 of C1-*O*-benzoyl group and somewhat weaker C-H...O interaction with O4 of C2-*O*-benzoyl group. Thus one C-X...O and two C-H...O interactions hold the dihalomethane molecule from one side and consequently the other side also by same interactions due to 2-fold symmetry of the dihalomethane molecule (Figure 2.9 and Table 2.6).

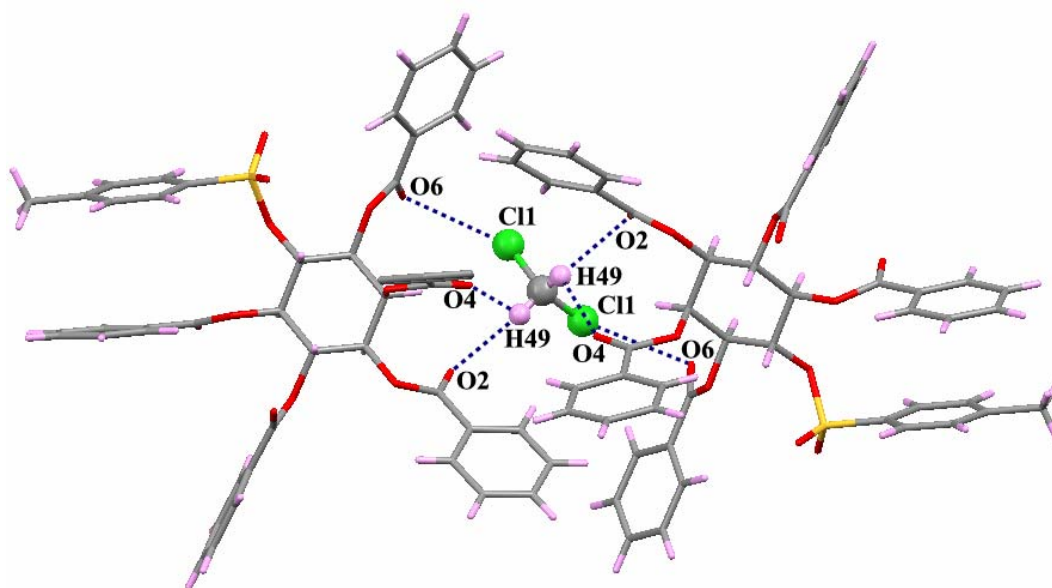


**Figure 2.9.** Host-guest association via symmetric C-Cl $\cdots$ O and C-H $\cdots$ O contacts in **3·CH<sub>2</sub>Cl<sub>2</sub>(F)**.

Thus a guest molecule makes a total of eight interactions with the host molecules as listed in **Table 2.5**. Amongst the various host-guest contacts, the ‘halogen bonding’ contact (Chapter 1 for details), C-X $\cdots$ O=C is a notable one. Although, geometrical parameters of this interaction varies with the included guest and in all the solvates halogen $\cdots$ oxygen distances are less than the sum of their van der Waals radii. Thus, halogen $\cdots$ oxygen distances are short, the  $\angle$ C-X $\cdots$ O deviate from the ideal value of 180° averaging to a value of  $\sim$ 140°. During the least-squares refinement of crystals containing mixed dihalomethanes, the identity of each halogen is maintained using PART option in SHELXL, which gives different halogen $\cdots$ O distances (e.g. in iodochloromethane solvate **3·CH<sub>2</sub>ICl**, the Cl $\cdots$ O and I $\cdots$ O contacts are 3.141 Å and 2.787 Å respectively).

**Table 2.6:** Geometrical parameters of host-guest interactions in solvates of **3**.

X = halogens	D-H(X)⋯A	H(X)⋯A (Å)	D⋯A (Å)	D-H(X)⋯A (°)
<b>3</b> ·CH <sub>2</sub> Cl <sub>2</sub> (F)	C(49)-Cl(1)⋯O(6)#1	3.180(3)		145(1)
	C(49)-H(49)⋯O(2)#1	2.54	3.145(4)	140
	C(49)-H(49)⋯O(4)#1	2.59	3.339(3)	116
	C(18)-H(18)⋯Cl(1)#2	2.97	3.696(3)	136
<b>3</b> ·CH <sub>2</sub> Cl <sub>2</sub> (H)	C(49)-Cl(1)⋯O(6)#1	2.968(2)		139(2)
	C(49)-H(49)⋯O(2)#1	2.52	3.353(4)	144
	C(49)-H(49)⋯O(4)#1	2.77	3.316(11)	116
	C(18)-H(18)⋯Cl(1)#2	3.05	3.764(6)	135
<b>3</b> ·CD <sub>2</sub> Cl <sub>2</sub>	C(49)-Cl(1)⋯O(6)#1	3.220(3)		140(1)
	C(49)-H(49)⋯O(2)#1	2.57	3.397(4)	144
	C(49)-H(49)⋯O(4)#1	2.70	3.291(8)	120
	C(18)-H(18)⋯Cl(1)#2	3.06	3.790(6)	136
<b>3</b> ·CH <sub>2</sub> Br <sub>2</sub>	C(49)-Br(1)⋯O(6)#1	3.336(7)		142(1)
	C(49)-H(49)⋯O(2)#1	2.53	3.348(4)	142
	C(49)-H(49)⋯O(4)#1	2.63	3.219(9)	119
	C(18)-H(18)⋯Br(1)#2	3.09	3.814(6)	136
<b>3</b> ·CH <sub>2</sub> ClBr	C(49)-Cl(1)⋯O(6)#1	3.209		146
	C(49)-Br(1)⋯O(6)#1	3.348		135
	C(49)-H(49)⋯O(2)#1	2.57	3.392(3)	143
	C(49)-H(49)⋯O(4)#1	2.72	3.268(7)	116
	C(18)-H(18)⋯Cl(1)#2	3.07	3.793(7)	136
	C(18)-H(18)⋯Br(1)#2	3.10	3.820(6)	136
<b>3</b> ·CH <sub>2</sub> ICl	C(49)-Cl(1)⋯O(6)#1	3.141		148
	C(49)-I(1)⋯O(6)#1	2.787		135
	C(49)-H(49)⋯O(2)#1	2.54	3.321(5)	138
	C(49)-H(49)⋯O(4)#1	2.60	3.178(16)	118
	C(18)-H(18)⋯Cl(1)#2	3.12	3.807(16)	132
	C(18)-H(18)⋯I(1)#2	2.98	3.749(13)	141

Symmetric code: #1 x, y, z; #2 x, 1+y, z.



### 2.3.5 Other Host...Guest (C-H...O and C-H...halogen) Interactions

The C-H...O interaction made by the hydrogen atom of the dihalomethane molecules (C49-H49...O2) do not vary much in all the crystal structures (**Table 2.6**). The H...O distances and angles are averages to 2.55 Å and 142° respectively. The same is true with the somewhat weaker C49-H49...O4 contacts; here the H...O distances are longer (ranging from 2.6-2.7 Å) and the angle also deviates from linearity (116-120°). The halogen atoms also make another weak interaction, C-H...halogen contact with the C18-H18 of C2-O-benzoyl group of the next translated molecule along the b-axis. Geometrical parameters of C-H...halogen are similar with H...halogen distances averaging to 3.06 Å and angles to 135.16°. It should be realized here that the strength of individual interactions discussed so far might not be judged by comparison with the ideal geometrical parameters, as the host-guest system has to attain maximum stability by optimizing several weak interactions. In this process, concertedly the strength of all the interactions is balanced in order to give the maximum stability to the host-guest assembly.

### 2.3.6 Channel Formation

A dihalomethane molecule induces the assembling process by bringing the two molecules of the host across two-fold axis forming half portion of the cavity (**Figure 2.5B**). Molecular packing viewed down c-axis shows the interactions made by the hemispherical cavity with its neighboring cavities. Each unit-translated half cavity is linked via C18-H18...halogen and C18-H18...O6 interactions along the b-axis whereas along the a-axis these are interacting via C10-H10...O8 interaction and C-H... $\pi$  contacts<sup>13</sup> between

the C25-H25 of C3-*O*-benzoyl group and phenyl ring of the axial benzoyl group (Cg2) and C11-H11 of C1-*O*-benzoyl group and phenyl ring of C3-*O*-benzoyl group (Cg3) forming open framework like structure down the *c*-axis with dihalomethane molecules situated at the center of each unit (**Figure 2.10**). The C11-H11 $\cdots\pi$  contact is better than C25-H25 $\cdots\pi$  contact (**Table 2.7**). Thus carbonyl oxygen O6 interacts with halogen and hydrogen via halogen $\cdots$ O6 and H18 $\cdots$ O6, halogen atoms make, halogen $\cdots$ O6 and H18 $\cdots$ halogen and H18 is involved in C18-H18 $\cdots$ O6 and C18-H18 $\cdots$ halogen contact forming triangular interacting geometry.

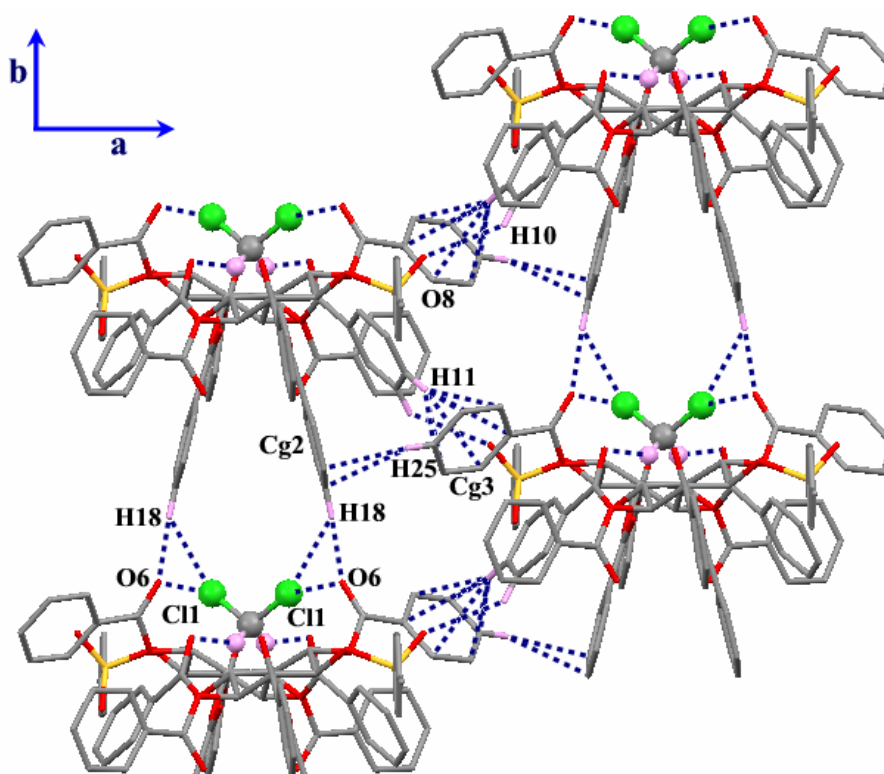


**Figure 2.10.** Linking of molecular capsule via C-H $\cdots$ O, C-H $\cdots$ X and C-H $\cdots\pi$  contacts.

Another assembly of the guest molecule with the two host molecules (**Figure 2.5B**) pointing downwards completes the other half of the cavity (**Figure 2.11A**) down

the c-axis to generate the thorough open channel (**Figure 2.11B**). The organization of the channels is quite interesting. All the hydrophobic phenyl groups point outwards while the hydrophilic carbonyl oxygens point towards the center of the cavity (**Figure 2.11C**). Only three rings bearing oxygens O2, O4 and O6 are involved in specific host-guest interactions (**Figure 2.9**). Thus, a total four-host molecules form a cavity containing two  $\text{CH}_2\text{X}_2$  ( $\text{X} = \text{halogens}$ ) molecules related by an inversion center (**Figure 2.11B**). Projection of molecular packing down c-axis depicts the two  $\text{CH}_2\text{X}_2$  molecules to be close to each other, but in fact the  $\text{CH}_2\text{X}_2$  molecules are 15 Å apart. View of the molecular packing down c-axis (**Figure 2.12**) clearly reveals the thorough open channels of dimension  $\sim 6.5 \times 4.5$  Å formed by the host containing the guest molecules.

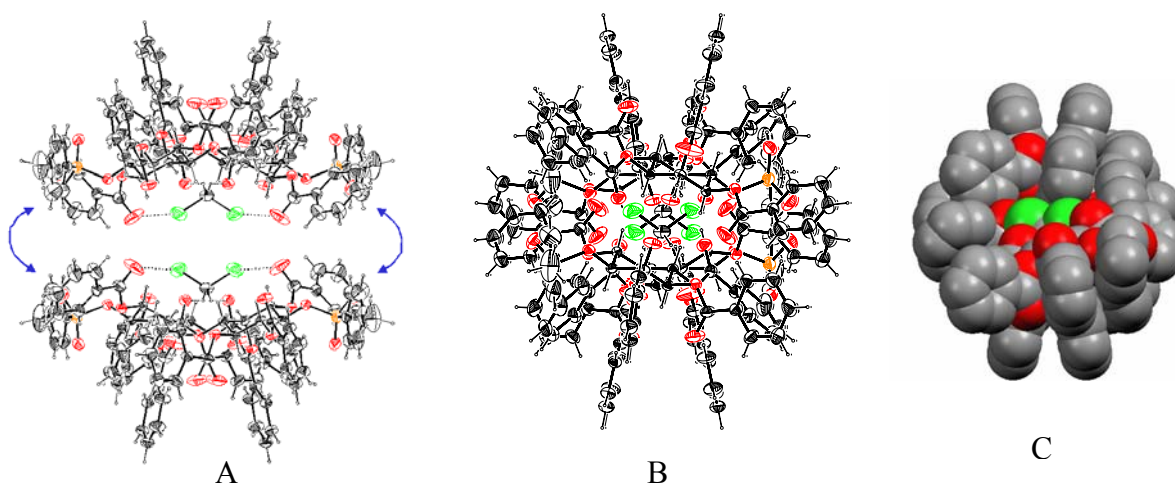


**Figure 2.11.** A) ORETP view shows capsule formation, B) ORTEP view of capsule viewed down c-axis and C) CPK view shows hydrophilic group pointing inside and hydrophobic groups pointing outside the cavity.

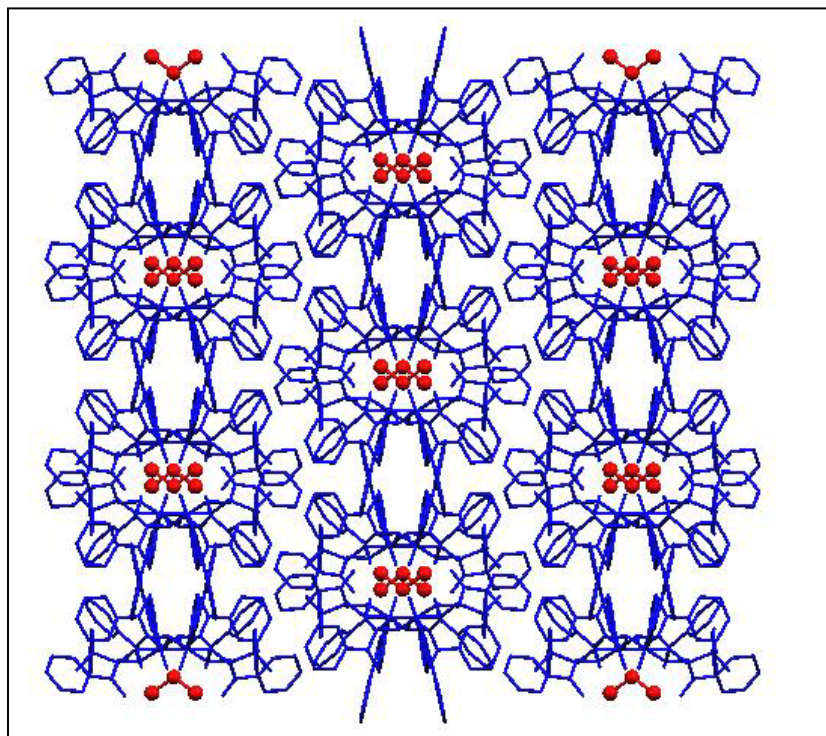


**Figure 2.12.** Molecular packing in crystals of  $3 \cdot \text{CH}_2\text{Cl}_2(\text{F})$  viewed down the *c*-axis showing thorough open channel formed by the host molecule accommodating the dihalomethane guest molecules.

### 2.3.7 Other Weak Interactions that Stabilize Molecular Packing

A view of molecular packing down *b*-axis is shown below (**Figure 2.13**). The centrosymmetric trifurcated  $\text{C-H} \cdots \text{O}$  bonded dimers are associated via good centrosymmetric  $\text{C-H} \cdots \pi$  ( $\text{C11-H11} \cdots \text{Cg4}$ ,  $\text{C46-H46} \cdots \text{Cg2}$ ) and  $\text{C10-H10} \cdots \text{O8(=S)}$  interactions along the *a*-axis forming a layered structure. The geometry of  $\text{C11-H11} \cdots \text{Cg4}$  is much better than the  $\text{C46-H46} \cdots \text{Cg2}$  contact (**Table 2.7**).

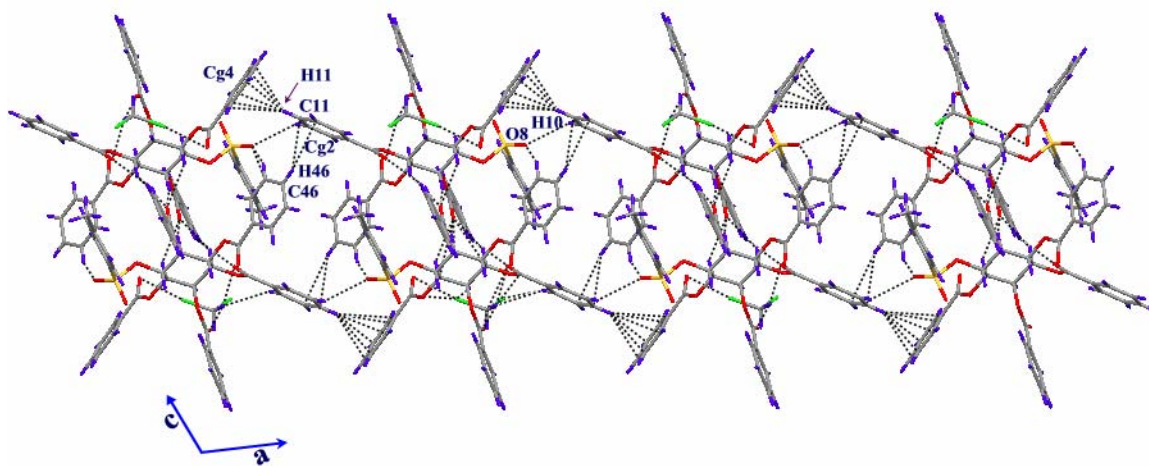


**Figure 2.13.** Centrosymmetric dimers linked via C-H $\cdots$ O and C-H $\cdots$  $\pi$  contacts forming molecular string down b-axis.

In inclusion crystals where occupancy of dihalomethanes is half, the geometries (distances and angles) of C10-H10 $\cdots$ O8 interactions are better as compared to crystals where occupancy of dihalomethanes is full. Further the geometry of the C11-H11 $\cdots$  $\pi$  contact is better in crystals fully occupied by dihalomethanes as compared to crystals with lesser occupancy ones. Similar trend was observed for other C-H $\cdots$  $\pi$  interactions (**Table 2.7**). Hence the occupancies of the guest molecules in crystals of **3** appear to influence geometries of the host-host interactions.

**Table 2.7:** C-H...O and C-H... $\pi$  interactions in host-host organization of solvates of **3**.

X = halogens	D-H(X)...A	H(X)...A (Å)	D...A (Å)	D-H(X)...A (°)
<b>3</b> ·CH <sub>2</sub> Cl <sub>2</sub> (F)	C(18)-H(18)...O(6)#1	2.53	3.281(4)	143
	C(10)-H(10)...O(8)#2	2.87	3.644(5)	141
	C(11)-H(11)...Cg(3)#2	2.65	3.574(4)	174
	C(17)-H(17)...Cg(6)#4	2.94	3.688(3)	139
	C(25)-H(25)...Cg(2)#3	2.89	3.645(4)	140
	C(46)-H(46)...Cg(1)#5	2.98	3.719(4)	137
<b>3</b> ·CH <sub>2</sub> Cl <sub>2</sub> (H)	C(18)-H(18)...O(6)#1	2.47	3.296(7)	148
	C(10)-H(10)...O(8)#2	2.62	3.405(8)	143
	C(11)-H(11)...Cg(3)#2	2.91	3.795(7)	159
	C(25)-H(25)...Cg(2)#3	2.90	3.675(8)	142
	C(46)-H(46)...Cg(1)#7	3.08	3.818(7)	138
<b>3</b> ·CD <sub>2</sub> Cl <sub>2</sub>	C(18)-H(18)...O(6)#8	2.60	3.368(7)	141
	C(10)-H(10)...O(8)#9	2.81	3.600(9)	143
	C(11)-H(11)...Cg(3)#9	2.82	3.738(9)	168
	C(25)-H(25)...Cg(2)#11	2.96	3.732(9)	141
	C(46)-H(46)...Cg(1)#5	3.17	3.889(7)	136
<b>3</b> ·CH <sub>2</sub> Br <sub>2</sub>	C(18)-H(18)...O(6)#8	2.57	3.339(7)	140
	C(10)-H(10)...O(8)#9	2.68	3.439(9)	140
	C(11)-H(11)...Cg(3)#9	2.90	3.768(8)	166
	C(25)-H(25)...Cg(2)#11	2.97	3.710(7)	137
	C(46)-H(46)...Cg(1)#5	3.18	3.878(7)	133
<b>3</b> ·CH <sub>2</sub> ClBr	C(18)-H(18)...O(6)#1	2.60	3.374(6)	141
	C(10)-H(10)...O(8)#12	2.78	3.554(7)	142
	C(11)-H(11)...Cg(3)#9	2.84	3.749(7)	142
	C(25)-H(25)...Cg(2)#11	2.98	3.736(7)	140
	C(46)-H(46)...Cg(1)#13	3.15	3.873(6)	136
<b>3</b> ·CH <sub>2</sub> ICl	C(18)-H(18)...O(6)#1	2.49	3.314(9)	148
	C(10)-H(10)...O(8)#2	2.64	3.41(1)	141
	C(11)-H(11)...Cg(3)#2	2.94	3.81(1)	157
	C(25)-H(25)...Cg(2)#3	2.89	3.68(1)	144
	C(46)-H(46)...Cg(1)#7	3.11	3.827(8)	136
<b>3</b> ·CH <sub>2</sub> Cl <sub>2</sub> (T)	C(18)-H(18)...O(6)#1	2.51	3.376(11)	155
	C(10)-H(10)...O(8)#2	2.69	3.459(12)	141
	C(11)-H(11)...Cg(3)#2	3.00	3.857(12)	153
	C(25)-H(25)...Cg(2)#3	2.90	3.707(14)	147
	C(46)-H(46)...Cg(1)#7	3.09	3.831(11)	138

Symmetric code: #1 x, 1+y, z; #2 -1/2+x, 1/2+y, z; #3 1/2-x, -1/2+y, 1/2-z; #4 -x, 1-y, -z; #5 -1/2-x, 1/2-y, -z; #6 -x, 2-y, -z; #7 -1/2-x, 1.5-y, -z; #8 x, -1+y, z; #9 -1/2+x, -1/2+y, z; #10 =-x, -y, -z; #11 =1/2-x, 1/2+y, 1/2-z; #12 1/2+x, 1/2+y, z; #13 1.5-x, 1.5-y, 2-z, Cg1, Cg2, Cg3 and Cg6 are the centroids of the phenyl ring of C1, C2, C3 and C6-benzoate group.

### 2.3.8 Spontaneous Crystallization of **3** Induced by $\text{CH}_2\text{X}_2$

It is thought that the centrosymmetric dimeric C-H...O assembly of host molecules may have been formed first in solution (**Figures 2.7A and B**). The dihalomethane molecule helps in assembling these C-H...O supramolecular synthon around crystallographic two-fold axis, thereby inducing the crystallization (**Figure 2.7C and D**). The geometrical parameters of the trifurcated dimeric C-H...O assembly, which do not vary with different guest inclusion further strengthens this thought. This also sheds light on the need of  $C_2$  symmetry guest to induce crystallization of **3**. There are very few cases of such guest induced inclusion phenomena.<sup>124</sup> Such ‘guest-induced’ crystallization with capsule formation is an interesting topic as it mimics the biological processes as well as dynamic combinatorial library of assemblies.<sup>125</sup> Although each centrosymmetric dimer comes with one-dihalomethane molecule across the two-fold axis, only one molecule of the dimer hold the guest molecule through one H and one Cl whereas the other H and Cl are held by another molecule of **3** of the other centrosymmetric dimer (**Figure 2.14**)

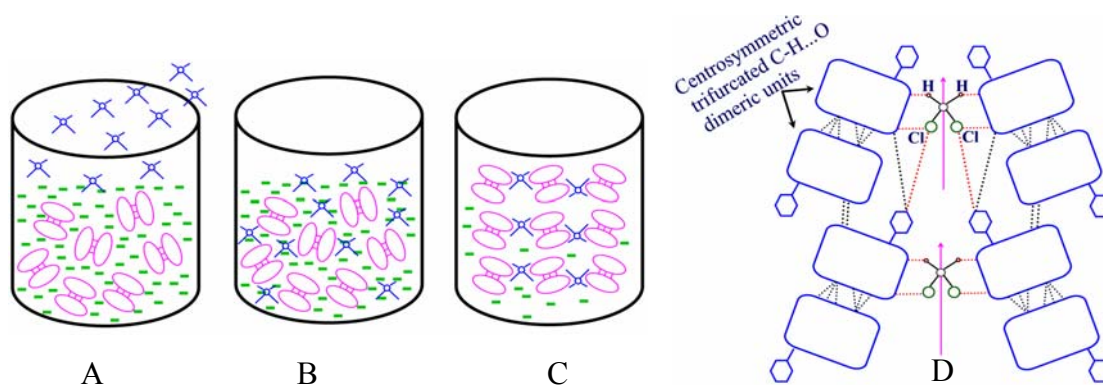


**Figure 2.14.** Cartoon representation of the nucleation process of **3** (magenta) with  $\text{CH}_2\text{Cl}_2$  (blue), A) **3** in solution, B) **3** and  $\text{CH}_2\text{Cl}_2$  in solution, C) Association of **3** and  $\text{CH}_2\text{Cl}_2$  in solution and D) zoom of association of **3** and  $\text{CH}_2\text{Cl}_2$  shown in C.



### 2.3.9 Trace of Dihalomethane Induces Self Assembly

X-ray structure determination of the crystals obtained from ethyl acetate revealed the presence of residual peaks (Q1 and Q2) of very low heights but having geometry similar to  $\text{CH}_2\text{Cl}_2$  molecule (**Figure 2.15**, for details see section 2.2.5). Assigning the Cl atom and C atom to the peak Q1 and Q2 respectively refined the structure with good R-value. This strongly suggests that even a trace of dichloromethane, triggers the nucleation process of **3**.

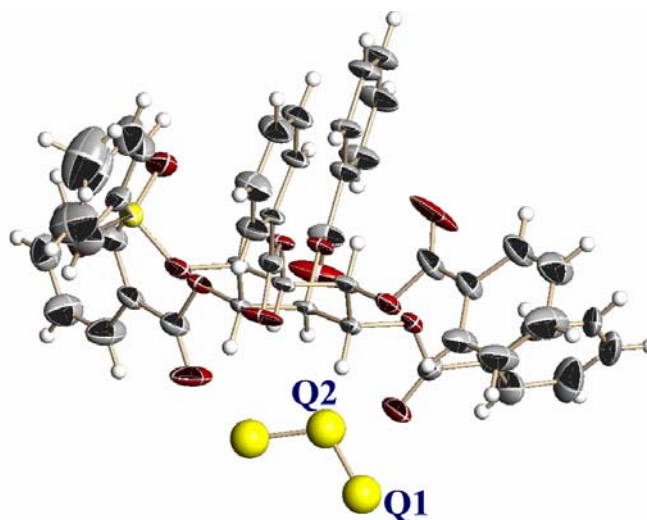


**Figure 2.15.** The geometry of the residual peaks (Q1 and Q2) in the inclusion crystals of  $\mathbf{3}\cdot\text{CH}_2\text{Cl}_2(\text{T})$ .

An interesting exercise, using squeeze option in PLATON program,<sup>126</sup> was carried out on all the crystals to see what percentage of the channels were occupied by the guest molecules. The results showed (**Table 2.8**) that only fully occupied guests in  $\mathbf{3}\cdot\text{CH}_2\text{Cl}_2(\text{F})$ ,  $\mathbf{3}\cdot\text{CD}_2\text{Cl}_2$  and  $\mathbf{3}\cdot\text{CH}_2\text{ClBr}$  contained no possibility of any residual electron density whereas  $\mathbf{3}\cdot\text{CH}_2\text{Cl}_2(\text{H})$ ,  $\mathbf{3}\cdot\text{CH}_2\text{Br}_2$ ,  $\mathbf{3}\cdot\text{CH}_2\text{ICl}$  and  $\mathbf{3}\cdot\text{CH}_2\text{Cl}_2(\text{T})$  leave voids, which



vary depending on the occupancies. Normally, the crystal structures do not leave any voids in achieving close packing of molecules, but these structures with varying guests provide an insight into the crystallization of the host, which strongly depend on the guest. Crystallization process was observed at various low guest concentrations; shining small crystals could be detected in ~ 2h at the lowest concentration of dichloromethane (0.01%) in chloroform.

**Table 2.8:** Squeeze analysis of pseudopolymorphs of **3**.

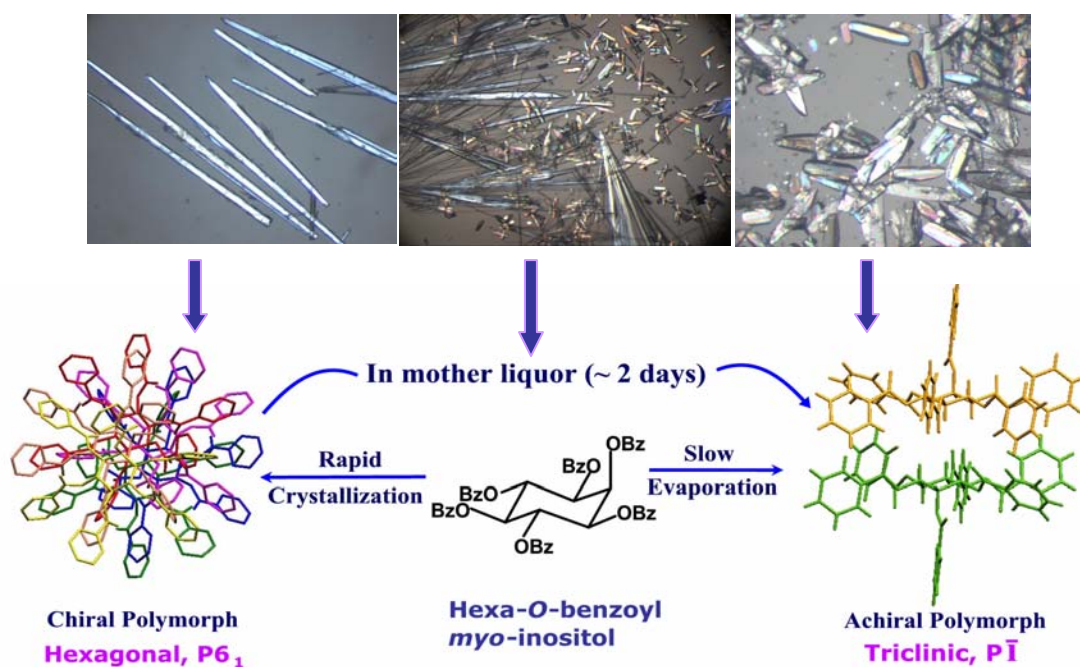
Inclusion complex	No. of electrons/unit cell Before assigning solvent peaks	No. of electrons/unit cell After assigning solvent peaks
<b>3</b> ·CH <sub>2</sub> Cl <sub>2</sub> (F)	260	0
<b>3</b> ·CH <sub>2</sub> Cl <sub>2</sub> (H)	115	20
<b>3</b> ·CD <sub>2</sub> Cl <sub>2</sub>	272	1
<b>3</b> ·CH <sub>2</sub> Br <sub>2</sub>	326	38
<b>3</b> ·CH <sub>2</sub> ClBr	349	0
<b>3</b> ·CH <sub>2</sub> ICl	184	25
<b>3</b> ·CH <sub>2</sub> Cl <sub>2</sub> (T)	71	29

## 2.4 Conclusions:

Spontaneous crystallization of **3**, only in the presence of dihalomethane solvents, suggests its role in the process of crystallization. Although, the guest occupancies are different, in all the solvates the C-H...O and C-H...halogen host guest interactions are well conserved, with some differences in their halogen bonding parameters. Crystals with lower occupancy of dihalomethanes show shorter halogen...oxygen contacts as compared to those with full occupancies. It appears that with the increasing occupancy of dihalomethane guests in the crystal cavity, 'halogen bonding' distances also increase to some extent. The selectivity experiments confirm the preference of dibromomethane over dichloromethane for inclusion in crystals. More inputs from charge distribution around halogen, oxygen and along halogen bond (halogen...oxygen) are essential in order to comment on their energies and the nature of their orbital interaction. In summary this compound provides a unique example of highly specific molecular recognition of dihalomethane and induced self-assembly of **3**.

# Chapter 3

## Polymorphic and Pseudopolymorphic Behaviour of hexa-*O*-benzoyl *myo*-inositol: Conversion of Chiral to Achiral Crystals, Gradual Escape of Guest from Inclusion Crystal Lattice



# Chapter 3

## 3.1 Introduction

Polymorphism is a physical phenomenon, as defined by McCrone,<sup>127</sup> “a solid crystalline phase of given compound resulting from the possibility of at least two crystalline arrangements of that compound in the solid state”. In simple words, polymorphism is the ability of any crystalline compound to exist in two or more forms in the solid state. Different polymorphs have different structures and hence, in effect, each is a unique material with its own physical and chemical properties. Therefore, polymorphism is an intensely researched topic of current interest having tremendous scientific and industrial importance.<sup>128</sup> The impact is evident by an outburst of publications, patents, conferences, special issues of journals and an analysis of all the entries in the Cambridge Structural Database (CSD) on this ‘enigmatic’ phenomenon.<sup>129</sup> In the pharmaceutical industries the phenomenon of polymorphism has prime importance because of the direct influence of this on the dissolution rate of the particular drug. In general, polymorphs are classified into three major categories based on the molecular packing in the crystal lattice. First one is *conformational polymorphism*, which involves changes at the molecular level (different molecular conformations) and occurs mainly in the flexible molecules. Second one is *packing polymorphism* in which molecule of the same conformation have different packing arrangement directed by the intermolecular interactions. This occurs mostly in the rigid molecules. The third category is a

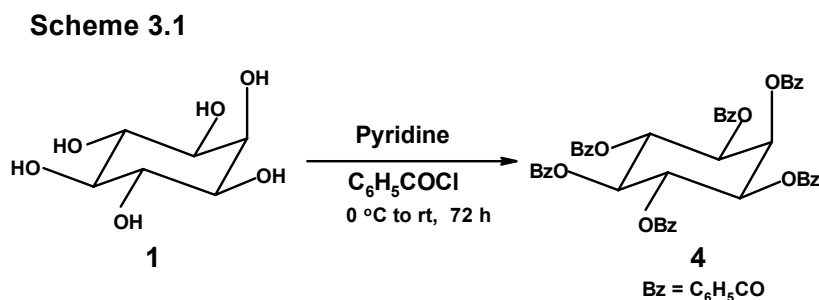
consequence of the presence of solvent molecules in the crystal lattice, referred to as *pseudopolymorphism or solvato-morphism*, which involves large changes in crystal density and packing. One of the main objectives in the study of polymorphism is to understand the effect of various parameters of crystallization experiment in controlling the ‘nucleation’ to obtain a desired polymorph.<sup>130</sup> Gay Lussac observed in 19<sup>th</sup> century that during crystallization, an unstable form is obtained first that subsequently transforms into second form. This statement then explained thermodynamically by Ostwald, known as ‘Ostwald step rule’ which states that, “*In all process, it is not the most stable state with the lowest amount of free energy that is initially formed, but the least stable state lying in the free energy to the original state.*”<sup>131</sup> The crystallization of a compound is still a poorly understood process, although, it is known to be a multi step process mostly governed by thermodynamic and kinetic conditions. The effect of solvent, an important parameter influencing nucleation, continues to be the subject of investigations. This highlights the importance of the kinetics and thermodynamics in solution rather than the formation of molecular assemblies.<sup>132</sup> Under the specific thermodynamic and similar rates in kinetics in a crystallization process, two or more domains overlap forcing the polymorphs to crystallize simultaneously from the same solvent and from the same crystallization flask under identical condition of crystal growth resulting in the formation of *concomitant polymorphism*.<sup>133</sup> The nearly equivalent crystal energetics involved in the generation of concomitant polymorphs provides excellent and demanding benchmarks for theoretical and computational models.<sup>134</sup>

This chapter reports interesting phenomena of polymorphic and pseudopolymorphic behaviour of a *myo*-inositol derivative. Selective encapsulation of

dihalomethane by **3** prompted us to synthesize analogs of **3** in order to explore the effect of any change in the molecular structure on its inclusion behaviour. Hexa-*O*-benzoyl *myo* inositol (**4**)<sup>135</sup> is symmetric and has *meso* configuration. The difference between **3** and **4** is the replacement of tosyl group at C4 position in **3** by a benzoyl group in **4**. The hexabenzoate **4** did not show highly specific inclusion behaviour as observed in **3**. But, the compound **4** exhibited interesting polymorphic behaviour, which is described in this chapter. The most fascinating polymorphic behaviour of **4** was the formation of chiral crystals (hexagonal, P6<sub>1</sub>) from ethyl acetate-ether solution, which upon standing in the mother liquor slowly dissolved to yield achiral crystals (Triclinic P-1), which did not contain any solvent molecules.<sup>136</sup> Compound **4** also formed inclusion crystals with dihalomethane, and with CHCl<sub>3</sub>, CHBr<sub>3</sub> and dioxane with varying stabilities. Although all the inclusion crystals belong to triclinic system, the host molecules have different packing arrangements depending on the nature of the guest molecules. This phenomenon known as ‘guest dependent polymorphism’.

## 3.2 Experimental Section

### 3.2.1 Synthesis



Hexa-*O*-benzoyl *myo*-inositol was prepared from *myo*-inositol as reported.<sup>135</sup> (m.p. 268-269 °C, Lit. m.p. 265-266 °C).

### 3.2.2 Crystallization

Crystallization of **4** was attempted from most of the common organic solvents. A number of trials made, methods of crystallization along with the results obtained are given in **Table 3.1**.

**Table 3.1:** Crystallization data of **4** from various solvents.

Trial No	Solvent Used	Method of Crystallization*	Result
1	Ethyl acetate	1	Plates (Form II) of <b>4</b>
2	Nitromethane	1	Plates (Form II) of <b>4</b>
3	Pyridine	1	Plates (Form II) of <b>4</b>
4	Tetrahydrofuran	1	Plates (Form II) of <b>4</b>
5	Toluene	1	Plates (Form II) of <b>4</b>
6	Acetonitrile	1	Plates (Form II) of <b>4</b>
7	Ethyl acetate (supersaturated)	2	Needles (Form I) of <b>4</b>
8	Benzene	2	Needles (Form I) of <b>4</b>
9	CCl <sub>4</sub>	2	Needles (Form I) of <b>4</b>
10	Acetone	2	Needles (Form I) of <b>4</b>
11	Diiodomethane	1	Needles (Form I) of <b>4</b>
12	Ethyl acetate	3	Plates (Form II) of <b>4</b>
13	Dichloromethane	3	Pseudopolymorph, <b>4</b> ·CH <sub>2</sub> Cl <sub>2</sub>
14	Dibromomethane	3	Pseudopolymorph, <b>4</b> ·CH <sub>2</sub> Br <sub>2</sub>
15	Chlorobromomethane	3	Pseudopolymorph, <b>4</b> ·CH <sub>2</sub> ClBr
16	Chloroform	3	Pseudopolymorph, <b>4</b> ·CHCl <sub>3</sub>
17	Bromoform	3	Pseudopolymorph, <b>4</b> ·CHBr <sub>3</sub>
18	Dioxane	3	Pseudopolymorph, <b>4</b> ·C <sub>4</sub> H <sub>8</sub> O <sub>2</sub>

\*1= slow evaporation, 2 = Fast evaporation, 3 = vapour diffusion

**Solvent Free Crystals (Form I and Form II)**

Crystallization of hexa-*O*-benzoyl-*myo*-inositol (**4**) from supersaturated solutions of ethyl acetate, yielded long needle like crystals (sharp at one end, Form I, **Figure 3.1A**). These crystals upon standing in the mother-liquor gradually disappeared with the simultaneous appearance of small plate like crystals (Form II, **Figure 3.1B**) in 1-2 days. The plate like crystals could also be obtained from a number of other solvents such as ethyl acetate, pyridine and nitromethane by slow evaporation (~ 2 days, **Figure 1C**). However, only the Form I crystals (sharp needles) could be reproducibly obtained from these solvents when nucleation was achieved very rapidly by cooling a supersaturated solution (~ 30 – 60 min.). The Form I crystals could also be obtained from a solvent where **4** is sparingly soluble viz, diiodomethane. Seeding the Form I crystals in a solution of **4** also produced Form I crystals initially but not exclusively. These results suggested that the formation of metastable Form I crystals was favoured under ‘kinetic’ conditions while that of Form II crystals under ‘thermodynamic’ conditions.<sup>131a</sup> Both Form I and Form II crystals were stable at room temperature and had almost the same melting point. (Form I, m.p. 268-269°C and Form II, m.p. 269-271 °C).

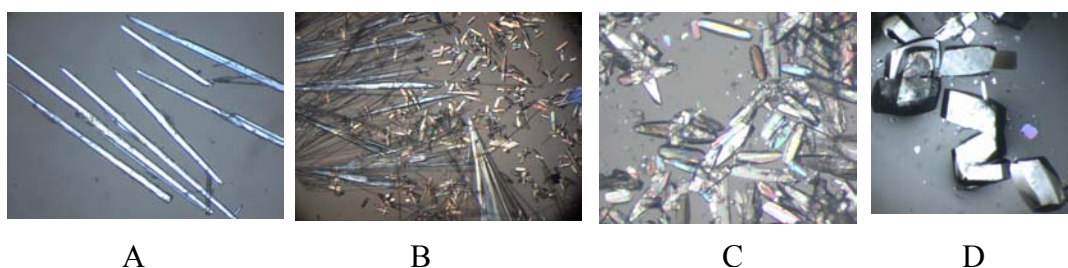


**Figure 3.1.** Photomicrographs of solvent free polymorphs of **4**. A) Form I crystals, B) Form I and Form II crystals in mother liquor, C) Form II crystals and D) crystals obtained from pyridine.



### *Crystallization from Dihalomethane*

Crystallization of **4** from dihalomethane such as dichloromethane ( $4 \cdot \text{CH}_2\text{Cl}_2$ ),<sup>136</sup> dibromomethane ( $4 \cdot \text{CH}_2\text{Br}_2$ ) and chlorobromomethane ( $4 \cdot \text{CH}_2\text{ClBr}$ ) by vapor diffusion method produced good quality crystals (**Figure 3.2A**). Unlike inclusion crystals of **3**, these were highly unstable when exposed to an open atmosphere. They lost the crystallinity and became opaque within 5-10 seconds (**Figure 3.2B**). However, in the mother liquor the crystals remained quite stable. Also, crystals could be stabilized for ~ 8 h in paraffin oil but beyond this time they started developing cracks, subsequently disintegrating completely.

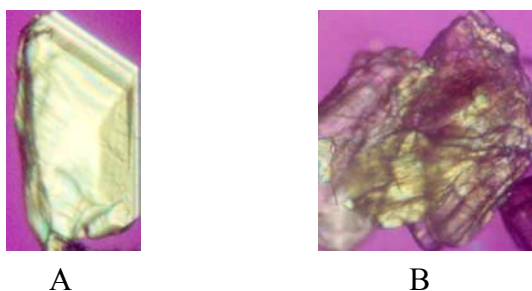


**Figure 3.2.** Photomicrographs of crystals of **4**, A) Crystals in  $\text{CH}_2\text{Cl}_2$  mother liquor, B) Crystal after taking out from the mother liquor

### *Crystallization from Chloroform, Bromoform and Dioxane*

Compound **4** could also be crystallized readily from chloroform, bromoform and dioxane. The thin plate like crystals containing chloroform (**Figure 3.3A**,  $4 \cdot \text{CHCl}_3$ ) were highly unstable in the open atmosphere and also in paraffin oil; they started crumbling within ~ 2 minutes. In comparison, bromoform inclusion crystals were stable upto ~ 1-3 minutes in an open atmosphere and they could be stabilized in paraffin oil for a 1-2 hours

(**Figure 3.3B**,  $4 \cdot \text{CHBr}_3$ ). Crystals from dioxane ( $4 \cdot \text{C}_4\text{H}_8\text{O}_2$ ) were also highly unstable, almost like those obtained from chloroform.

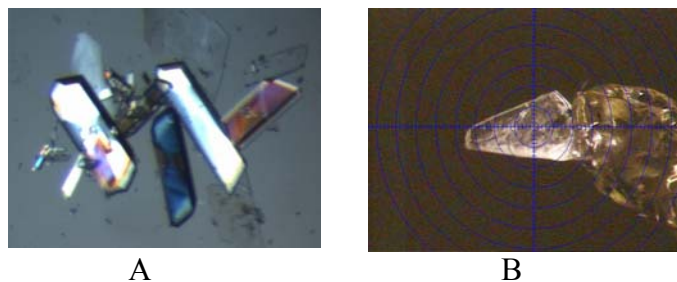


**Figure 3.3.** Photomicrographs of inclusion crystals of **4**, A) from chloroform, B) from bromoform.

### 3.2.3 Thermal Analysis

The DSC and TGA/DTA analysis of the solvent free polymorphs of **4** (Form I and Form II) was carried out in order to check the possibility of phase transformation between the two polymorphs. Form I crystals showed a single endotherm at 269 °C corresponding to the melting of the crystal (**Figure 3.4A**) whereas the DSC curve of Form II crystals showed two endotherms (**Figure 3.4B**). First endotherm at 234 °C was broad (onset temperature 221 °C, end temperature 246 °C) suggesting a possible phase change and the second endotherm at 271 °C (onset temperature 259 °C, end temperature 282 °C) due to the melting of the crystal. The DTA/TGA analysis also showed similar behaviour for Form I and Form II crystals of **4** (**Figure 3.5**). The DSC and DTA/TGA studies of the inclusion crystals of **4** could not be carried out because of the instability of the inclusion crystals at room temperature.

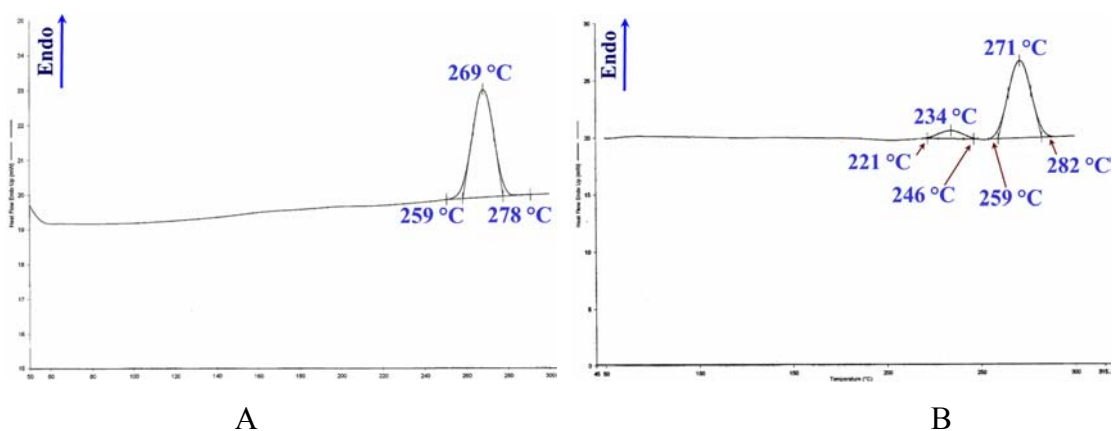


Figure 3.4. DSC profile of polymorphs of **4**, A) Form I and B) Form II.

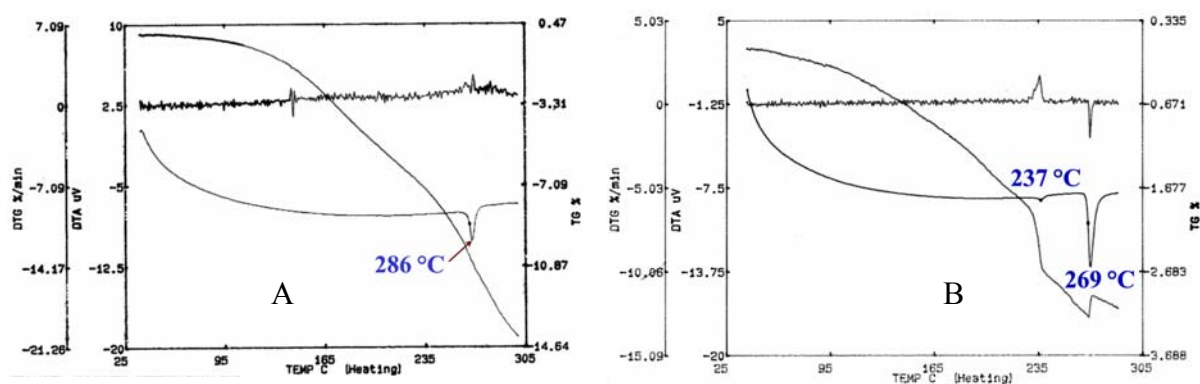


Figure 3.5. TGA / DTA profile of Form I and Form II crystals of **4**.

### 3.2.4 Data Collection, Structure Solution and Refinement

#### *Solvent Free Crystals*

X-ray diffraction data of the meta-stable Form I crystal was collected at 133 K using LN<sub>2</sub> Oxford 700 series Cryosystem, whereas data of Form II crystals was collected at room temperature. Form I crystals (kinetic form, needles) were chiral crystals belonging to hexagonal system with space group P6<sub>1</sub> or P6<sub>5</sub> with Z = 6 (The assignment of P6<sub>1</sub> or P6<sub>5</sub> for an organic molecule with no heavy atom scatterer cannot be established with Mo-K<sub>α</sub> radiation). Form II crystals belong to the triclinic system, space group P-1 with Z = 2.

### *Inclusion Crystals with Dihalomethane*

All dihalomethane inclusion crystals of **4** were highly unstable in an open atmosphere and were protected in paraffin oil. A crystal grown from dichloromethane was removed from the mother liquor and coated with the paraffin oil was cooled to 133 K with a stream of liquid nitrogen for the X-ray diffraction data collection.

Due to highly unstable nature of the crystals, the X-ray intensity measurements were carried out giving 5 sec exposure per frame to get the complete data before the crystal deteriorated. Structure solution revealed the presence of two molecules of  $\text{CH}_2\text{Cl}_2$  per one molecule of the host **4** [**4**· $\text{CH}_2\text{Cl}_2$ (**2**)]. Since, the structure did not refine to a low R-value (~9%), data was collected from another crystal which had been stored in paraffin oil for about ~ 6 h. The full sphere X-ray data collected with more exposure (10 s per frame) revealed the presence of only one of the guest molecules of  $\text{CH}_2\text{Cl}_2$  per one molecule of **4** in the crystal lattice [**4**· $\text{CH}_2\text{Cl}_2$ (**1**)]. This structure refined to a better R-value (6.6%). The kinetics of the guest escape monitored by determining the unit cell parameters after every 1h showed a gradual reduction in the unit cell volume. The X-ray diffraction data of fresh crystals and after ~ 6 h (stored in paraffin) were collected of other dihalomethane inclusion crystals ( $\text{CH}_2\text{Br}_2$  and  $\text{CH}_2\text{ClBr}$ ), which also behaved in the same manner. Crystallographic data (**Tables 3.3, 3.4 and 3.5**) indicate the reduction in the unit cell lengths after the escape of one guest molecule, resulting in overall decrease in the unit cell volume. A slight increase in unit cell volume from **4**· $\text{CH}_2\text{Cl}_2$  to **4**· $\text{CH}_2\text{Br}_2$  is probably due to bigger size of the  $\text{CH}_2\text{Br}_2$ . The volume of the chlorobromomethane solvate **4**· $\text{CH}_2\text{ClBr}$  was between those of **4**· $\text{CH}_2\text{Cl}_2$  and **4**· $\text{CH}_2\text{Br}_2$ .

---

*Inclusion crystals of 4 with Chloroform ( $4\cdot\text{CHCl}_3$ ), Bromoform ( $4\cdot\text{CHBr}_3$ ) and Dioxane ( $4\cdot\text{C}_4\text{H}_8\text{O}_2$ )*

The X-ray diffraction data of  $4\cdot\text{CHCl}_3$ ,  $4\cdot\text{CHBr}_3$  and  $4\cdot\text{C}_4\text{H}_8\text{O}_2$  was also collected after coating them with paraffin oil at 133 K using liquid nitrogen stream. All the inclusion complexes belong to triclinic P-1 system. The unit cell volume of the chloroform ( $4\cdot\text{CHCl}_3$ ) and dioxane ( $4\cdot\text{C}_4\text{H}_8\text{O}_2$ ) solvated crystals was about  $\sim 500 \text{ \AA}^3$  more compared to the bromoform inclusion crystals ( $4\cdot\text{CHBr}_3$ ).

The crystallographic data of polymorphs and all the pseudopolymorphs of **4** are summarized in **Tables 3.2, 3.3, 3.4, 3.5** and **3.6**.

**Table 3.2:** Crystal data of dimorphs of **4**.

	Form I (chiral form)	Form II (achiral form)
Chemical formula	C <sub>48</sub> H <sub>36</sub> O <sub>12</sub>	C <sub>48</sub> H <sub>36</sub> O <sub>12</sub>
M <sub>r</sub>	804.77	804.77
Temperature/K	133(2)	297(2)
Morphology	Thin needle	Plate
Crystal size	0.74 × 0.08 × 0.06	0.38 × 0.15 × 0.06
Crystal system	Hexagonal	Triclinic
Space group	<i>P</i> 6 <sub>1</sub>	<i>P</i> -1
<i>a</i> (Å)	13.9840(7)	11.931(3)
<i>b</i> (Å)	13.9840(7)	14.463(4)
<i>c</i> (Å)	36.504(3)	14.722(4)
$\alpha$ (°)	90	64.109(4)
$\beta$ (°)	90	71.642(5)
$\gamma$ (°)	120	67.851(6)
<i>V</i> (Å <sup>3</sup> )	6182.1(7)	2082.2(10)
<i>Z</i>	6	2
<i>D</i> <sub>calc</sub> (g cm <sup>-3</sup> )	1.297	1.284
$\mu$ (mm <sup>-1</sup> )	0.094	0.093
<i>F</i> (000)	2520	840
Ab. correction	Multi-scan	Multi-scan
<i>T</i> <sub>min</sub>	0.934	0.965
<i>T</i> <sub>max</sub>	0.994	0.995
$\theta$ <sub>max</sub> (°)	25	25.0
<i>h</i> , <i>k</i> , <i>l</i> (min, max)	(-16,10), (-15,16), (-43,42)	(-14,14), (-17,17), (-17,17)
Reflns collected	31322	15011
Unique reflns	7233	7285
Observed reflns	5192	3862
No. of parameters	583	541
GoF	1.069	0.981
R <sub>obs</sub>	0.0673	0.0541
wR <sub>2_obs</sub>	0.1265	0.1211
R <sub>all</sub>	0.0988	0.1159
wR <sub>2_all</sub>	0.1363	0.1474
$\Delta \rho_{\max}$ , $\Delta \rho_{\min}$ (eÅ <sup>-3</sup> )	0.30, -0.19	0.21, -0.22

Table 3.3: Crystal data of 4·CH<sub>2</sub>Cl<sub>2</sub>.

	4·CH <sub>2</sub> Cl <sub>2</sub> (2)	4·CH <sub>2</sub> Cl <sub>2</sub> (1)
Chemical formula	C <sub>48</sub> H <sub>36</sub> O <sub>12</sub> · 1.75(CH <sub>2</sub> Cl <sub>2</sub> ) · 0.25 H <sub>2</sub> O	C <sub>48</sub> H <sub>36</sub> O <sub>12</sub> · CH <sub>2</sub> Cl <sub>2</sub>
M <sub>r</sub>	950.89	889.69
Temperature/K	133(2)	133(2)
Morphology	Prism	Prism
Crystal size	0.66 × 0.58 × 0.38	0.55 × 0.42 × 0.21
Crystal system	Triclinic	Triclinic
Space group	<i>P</i> -1	<i>P</i> -1
<i>a</i> (Å)	13.961(2)	13.976(9)
<i>b</i> (Å)	14.214(2)	14.041(9)
<i>c</i> (Å)	15.134(2)	15.106(16)
$\alpha$ (°)	104.827(2)	102.291(16)
$\beta$ (°)	101.516(2)	106.104(16)
$\gamma$ (°)	117.970(2)	117.514(11)
<i>V</i> (Å <sup>3</sup> )	2377.7(6)	2315(3)
<i>Z</i>	2	2
<i>D</i> <sub>calc</sub> (g cm <sup>-3</sup> )	1.328	1.276
$\mu$ (mm <sup>-1</sup> )	0.282	0.202
<i>F</i> (000)	985	924
Ab. correction	Multi-scan	multi-scan
<i>T</i> <sub>min</sub>	0.836	0.897
<i>T</i> <sub>max</sub>	0.900	0.959
$\theta$ <sub>max</sub> (°)	25	25.0
<i>h</i> , <i>k</i> , <i>l</i> (min, max)	(-13,16), (-16,16), (-17,14)	(-9,16), (-16,16), (-17,14)
Reflns collected	11397	11063
Unique reflns	8203	7484
Observed reflns	6143	3777
No. of parameters	646	572
Restraints	6	0
GoF	1.053	0.840
R <sub>obs</sub>	0.0667	0.0557
wR <sub>2_obs</sub>	0.1866	0.1134
R <sub>all</sub>	0.0828	0.1173
wR <sub>2_all</sub>	0.2021	0.1321
$\Delta \rho_{max}$ , $\Delta \rho_{min}$ (eÅ <sup>-3</sup> )	0.64, -0.46	0.35, -0.37

Table 3.4: Crystal data of 4·CH<sub>2</sub>Br<sub>2</sub>.

	4·CH <sub>2</sub> Br <sub>2</sub> (2)	4·CH <sub>2</sub> Br <sub>2</sub> (1)
Chemical formula	C <sub>48</sub> H <sub>36</sub> O <sub>12</sub> · 2(CH <sub>2</sub> Br <sub>2</sub> ) · 0.125(H <sub>2</sub> O)	C <sub>48</sub> H <sub>36</sub> O <sub>12</sub> · CH <sub>2</sub> Br <sub>2</sub> · 0.125(H <sub>2</sub> O)
M <sub>r</sub>	1152.46	978.61
Temperature/K	133(2)	133(2)
Morphology	Prism	Prism
Crystal size	0.85 × 0.47 × 0.24	0.54 × 0.44 × 0.22
Crystal system	Triclinic	Triclinic
Space group	<i>P</i> -1	<i>P</i> -1
<i>a</i> (Å)	13.874(4)	13.9775(18)
<i>b</i> (Å)	14.218(4)	13.9867(18)
<i>c</i> (Å)	15.298(4)	15.0051(19)
$\alpha$ (°)	103.711(5)	105.867(2)
$\beta$ (°)	102.920(5)	102.299(2)
$\gamma$ (°)	117.361(4)	117.410(2)
<i>V</i> (Å <sup>3</sup> )	2402.6(12)	2299.2(5)
<i>Z</i>	2	2
<i>D</i> <sub>calc</sub> (g cm <sup>-3</sup> )	1.593	1.414
$\mu$ (mm <sup>-1</sup> )	3.412	1.825
<i>F</i> (000)	1152	996
Ab. correction	multi-scan	multi-scan
<i>T</i> <sub>min</sub>	0.159	0.437
<i>T</i> <sub>max</sub>	0.494	0.695
$\theta$ <sub>max</sub> (°)	25	25
<i>h</i> , <i>k</i> , <i>l</i> (min, max)	(-16,16), (-16,16), (-18,18)	(-16,16), (-16,16), (-17,17)
Reflns collected	22997	21494
Unique reflns	8362	8054
Observed reflns	5474	4706
No. of parameters	603	572
Restraints	0	0
GoF	0.939	1.016
R <sub>obs</sub>	0.0661	0.0630
WR <sub>2_obs</sub>	0.1781	0.1717
R <sub>all</sub>	0.0922	0.1059
WR <sub>2_all</sub>	0.1905	0.1857
$\Delta \rho_{max}$ , $\Delta \rho_{min}$ (eÅ <sup>-3</sup> )	1.28, -1.16	1.54, -1.18



Table 3.5: Crystal data of 4·CH<sub>2</sub>ClBr.

	4·CH <sub>2</sub> ClBr(2)	4·CH <sub>2</sub> ClBr(1)
Chemical formula	C <sub>48</sub> H <sub>36</sub> O <sub>12</sub> · 1.5(CH <sub>2</sub> ClBr)	C <sub>48</sub> H <sub>36</sub> O <sub>12</sub> · (CH <sub>2</sub> Br <sub>2</sub> ) · 0.5(H <sub>2</sub> O)
M <sub>r</sub>	998.85	942.15
Temperature/K	133(2)	133(2)
Morphology	prism	prism
Crystal size	0.77 × 0.45 × 0.38	0.65 × 0.35 × 0.19
Crystal system	Triclinic	Triclinic
Space group	<i>P</i> -1	<i>P</i> -1
<i>a</i> (Å)	13.953(6)	13.922(2)
<i>b</i> (Å)	14.206(6)	13.956(2)
<i>c</i> (Å)	15.232(7)	14.985(2)
$\alpha$ (°)	104.955(7)	102.313(2)
$\beta$ (°)	102.544(7)	105.932(2)
$\gamma$ (°)	117.477(6)	117.518(2)
<i>V</i> (Å <sup>3</sup> )	2380.6(19)	2277.0(6)
<i>Z</i>	2	2
<i>D</i> <sub>calc</sub> (g cm <sup>-3</sup> )	1.393	1.374
$\mu$ (mm <sup>-1</sup> )	1.428	1.025
<i>F</i> (000)	1020	968
Ab. correction	multi-scan	multi-scan
<i>T</i> <sub>min</sub>	0.406	0.554
<i>T</i> <sub>max</sub>	0.673	0.829
$\theta$ <sub>max</sub> (°)	25	25
<i>h</i> , <i>k</i> , <i>l</i> (min, max)	(-16,16), (-16,16), (-18,18)	(-16,16), (-16,16), (-17,17)
Reflns collected	21218	20999
Unique reflns	7989	7867
Observed reflns	4036	4257
No. of parameters	621	572
Restraints	10	0
GoF	0.973	0.935
R <sub>obs</sub>	0.0982	0.0708
WR <sub>2_obs</sub>	0.2482	0.1792
R <sub>all</sub>	0.1632	0.1318
WR <sub>2_all</sub>	0.2788	0.2048
$\Delta \rho_{max}$ , $\Delta \rho_{min}$ (eÅ <sup>-3</sup> )	0.72, -0.58	1.42, -0.87

**Table 3.6:** Crystallographic data of **4·CHCl<sub>3</sub>**, **4·CHBr<sub>3</sub>** and **4·C<sub>2</sub>H<sub>8</sub>O<sub>2</sub>**.

	<b>4·CHCl<sub>3</sub></b>	<b>4·CHBr<sub>3</sub></b>	<b>4·C<sub>2</sub>H<sub>8</sub>O<sub>2</sub></b>
Chemical formula	C <sub>48</sub> H <sub>36</sub> O <sub>12</sub> · 1.5(CHCl <sub>3</sub> )	C <sub>48</sub> H <sub>36</sub> O <sub>12</sub> · 1.5(CHBr <sub>3</sub> )	C <sub>48</sub> H <sub>36</sub> O <sub>12</sub> · 2.5(C <sub>4</sub> H <sub>8</sub> O <sub>2</sub> )
M <sub>r</sub>	965.09	1109.48	1026.04
Temperature/K	133(2)	133(2)	133(2)
Morphology	Prism	Prism	Prism
Crystal size	0.58 × 0.31 × 0.19	0.52 × 0.22 × 0.13	0.50 × 0.29 × 0.18
Crystal system	Triclinic	Triclinic	Triclinic
Space group	<i>P</i> -1	<i>P</i> -1	<i>P</i> -1
<i>a</i> (Å)	13.140(8)	12.803(3)	13.901(3)
<i>b</i> (Å)	14.435(8)	13.767(3)	14.949(3)
<i>c</i> (Å)	16.669(9)	15.592(3)	15.846(3)
$\alpha$ (°)	94.192(9)	75.588(4)	70.405(3)
$\beta$ (°)	103.051(9)	68.121(3)	76.841(3)
$\gamma$ (°)	115.856(9)	64.207(3)	63.965(3)
<i>V</i> (Å <sup>3</sup> )	2718(3)	2283.8(8)	2774.8(9)
<i>Z</i>	2	2	2
<i>D</i> <sub>calc</sub> (g cm <sup>-3</sup> )	1.179	1.613	1.228
$\mu$ (mm <sup>-1</sup> )	0.272	3.152	0.09
<i>F</i> (000)	995	1111	1082
Ab. correction	multi-scan	multi-scan	multi-scan
<i>T</i> <sub>min</sub>	0.857	0.291	0.957
<i>T</i> <sub>max</sub>	0.950	0.676	0.984
$\theta$ <sub>max</sub> (°)	23	25	25
<i>h</i> , <i>k</i> , <i>l</i> (min, max)	(-14,14), (-15,15), (-18,18)	(-15,15), (-16,16), (-18,18)	(-16,16), (-17,17), (-18,18)
Reflns collected	21836	21288	26397
Unique reflns	7543	7898	9696
Observed reflns	4101	5330	7097
No. of parameters	589	593	703
Restraints	329	0	22
GoF	1.755	0.999	1.190
R <sub>obs</sub>	0.1745	0.0638	0.1337
WR <sub>2_obs</sub>	0.4601	0.1532	0.3112
R <sub>all</sub>	0.2375	0.0997	0.1693
WR <sub>2_all</sub>	0.5006	0.1767	0.3333
$\Delta \rho$ <sub>max</sub> , $\Delta \rho$ <sub>min</sub> (eÅ <sup>-3</sup> )	0.97, -0.62	1.31, -1.27	0.94, -0.32

### 3.3 Results and Discussion

#### 3.3.1 Structure of Dimorphs of 4 (Form I and Form II)

In the structure Form I crystal (chiral) the benzoyl groups at equatorial positions C1, C3 and C4 have almost planar conformation whereas benzoyl groups at C5 and C6 equatorial positions deviate from planarity by about 24° and 19° respectively. The axial benzoyl group shows rotational disorder over two positions with the occupancies 0.6 and 0.4. The major component benzoyl group is slightly out of plane (9.73°) whereas the minor component benzoyl group is deviating from planarity by 22° (**Figure 3.6A**). All the benzoyl groups have planar geometry and show no sign of disorder in Form II crystals of **4**(**Figure 3.6B**).

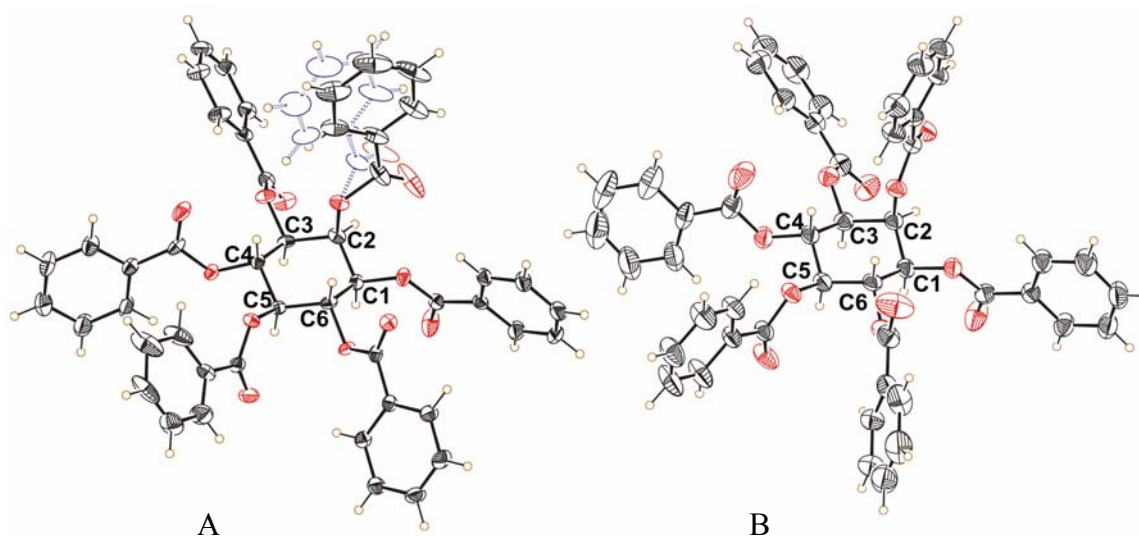


**Figure 3.6.** ORTEP views of **4**, A) Form I crystals, rotational disordered of the axial benzoyl group is shown in blue dotted lines and open ellipsoids and B) Form II crystals.

Crystal structure analysis of Form I (chiral) and Form II (achiral) crystals revealed the dominance of C-H...O interactions in both structures (**Table 3.7**). Closely interacting

pair of molecules in Form I and II is shown in **Figure 3.7**. In Form I chiral crystals, the neighbouring molecules make C-H $\cdots$ O interactions in such a way that the ‘helicity’ is spontaneously generated at the nucleation of this basic unit. The two C-H groups C4-H4 and C6-H6 of **molecule 1** make a bifurcated C-H $\cdots$ O interaction with O9 of **molecule 2**; in turn, oxygen O12 of **molecule 1** accepts protons from C3-H3 and C5-H5 belonging to **molecule 2**. In addition, C44-H44 of **molecule 1** makes C-H $\cdots$ O interaction with O11 of **molecule 2**; and oxygen O10 of **molecule 1** accepts proton from C27-H27 of **molecule 2** (**Figure 3.7A**). This continuous pattern gives each successive molecule a twist of 60°, coinciding with the crystallographic six-fold screw axis. In Form II crystals, the molecules are closely associated via centrosymmetric trifurcated C-H $\cdots$ O interactions as observed in all inclusion crystals of **3** (Chapter 2). The three axial H-atoms H1, H3 and H5 of the *myo*-inositol ring from each molecule make contacts with the carbonyl oxygen O11 of the other molecule across the inversion center. Hydrogen H5 also makes somewhat compromised intramolecular C-H $\cdots$ O interaction with O11. These two C-H $\cdots$ O interactions, doubly bridged the two centrosymmetrically related molecules (**Figure 3.7B**).

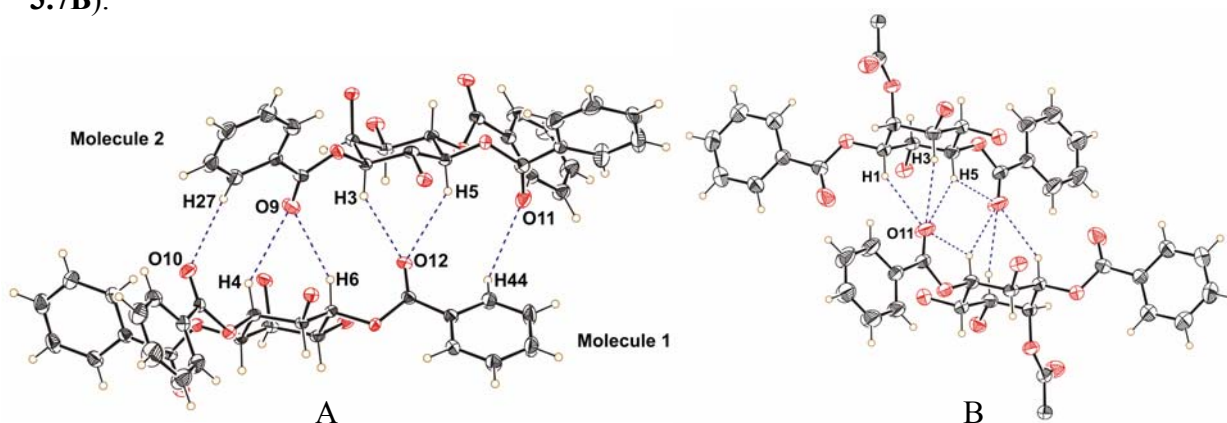


**Figure 3.7.** Closely interacting pairs of polymorphs of **4**, A) in Form I and B) in Form II.

**Table 3.7:** C-H $\cdots$ O interactions in closely interacting pairs of Form I and Form II crystals of **4**.

	D-H $\cdots$ A	D-H (Å)	H $\cdots$ A (Å)	D $\cdots$ A (Å)	D-H $\cdots$ A (°)
<b>Form I</b>	C(4)-H(4) $\cdots$ O(9)#1	0.98	2.67	3.491(5)	141
	C(6)-H(6) $\cdots$ O(9)#1	0.98	2.63	3.461(5)	143
	C(3)-H(3) $\cdots$ O(12)#2	0.98	2.40	3.259(4)	146
	C(5)-H(5) $\cdots$ O(12)#2	0.98	2.56	3.369(4)	139
	C(44)-H(44) $\cdots$ O(11)#1	0.93	2.69	3.376(5)	132
	C(27)-H(27) $\cdots$ O(10)#2	0.93	2.42	3.227(5)	145
<b>Form II</b>	C(1)-H(1) $\cdots$ O(11)#3	0.98	2.48	3.340(3)	147
	C(3)-H(3) $\cdots$ O(11)#3	0.98	2.70	3.514(3)	140
	C(5)-H(5) $\cdots$ O(11)#3	0.98	2.48	3.335(3)	145
	C(5)-H(5) $\cdots$ O(11)#4	0.98	2.24	2.686(3)	106

Symmetry codes: #1  $y, -x+y+1, z-1/6$ ; #2  $x-y+1, x, z+1/6$ ; #3  $-x+1, -y+1, -z$ ; #4  $x, y, z$ .

In the crystallization process, the formation of the ‘nuclei’ starting from the first interacting pair seems to be critical in deciding the outcome of the polymorph. The centrosymmetric pair produces stable Form II crystals, whereas helically related pair gives a metastable chiral Form I. The stability of Form II could arise due to the adamantane like geometry formed by the three C-H $\cdots$ O hydrogen bonds, a robust non-covalent ‘supramolecular synthon’.<sup>9</sup>

The centrosymmetric C-H $\cdots$ O dimers in Form II are associated via C41-H41 $\cdots$ O12 and form columnar assembly (**Figure 3.8A**). Furthermore, the C24-H24 $\cdots$ O10 and slightly offset C-H $\cdots$  $\pi$  contact between the C33-H33 group and phenyl ring of the axial C2-O-benzoyl group links the centrosymmetric C-H $\cdots$ O dimer in different fashion resulting in the formation of another type of columnar assembly diagonal to ab-plane

(**Figure 3.8B**, **Table 3.8**). The axial benzoyl group is tightly held by one more C-H $\cdots$ O interaction C18-H18 $\cdots$ O9 in Form II crystals (**Figure 3.9A**), thus giving more stability to this group. This is not observed in Form I crystals where the axial group shows rotational disorder. In Form I crystals, the hexagonal assembly down the c-axis (made by six molecules related by hexagonal symmetry) is held together by various C-H $\cdots$ O contacts such as C12-H12 $\cdots$ O10, C25-H25 $\cdots$ O11 and C39-H39 $\cdots$ O7 along a and b-axes (**Figure 3.9B**). Thus, in Form I crystals, molecule adapts a chiral confirmation and forms hexameric helical assemblies, whereas in Form II crystals, molecules formed centrosymmetric dimers which are further held by weak C-H $\cdots$ O and C-H $\cdots$  $\pi$  contacts (**Table 3.8**). Molecular packing in Form I crystals is more compact (**Figure 3.10A**) whereas in Form II the packing has channels or cavities but no inclusion was observed (**Figure 3.10B**).

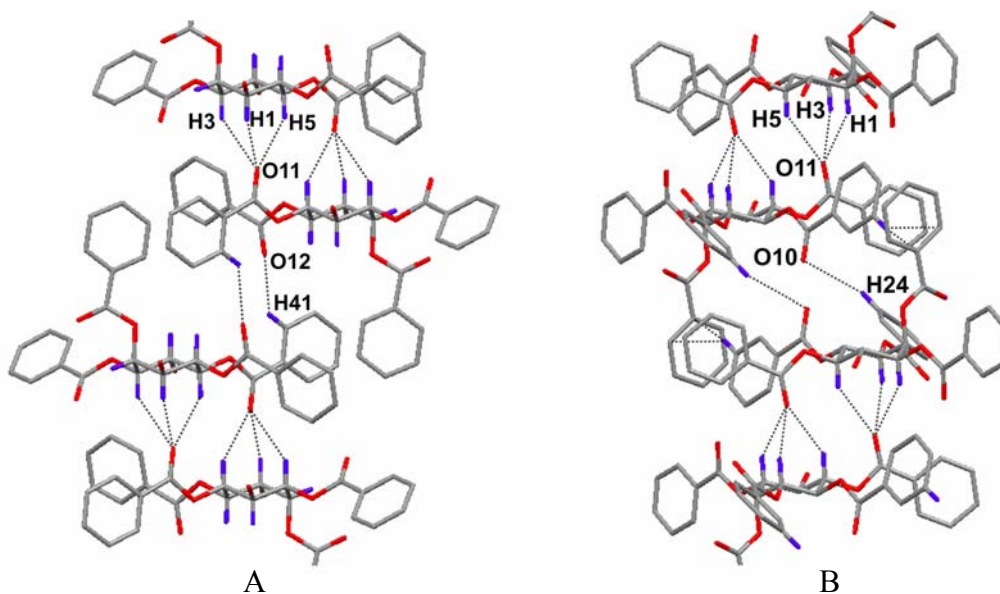


**Figure 3.8.** Different columnar assemblies formed by Form II crystals of **4**, A) via C41-H41 $\cdots$ O12 and B) via C24-H24 $\cdots$ O10 interactions.

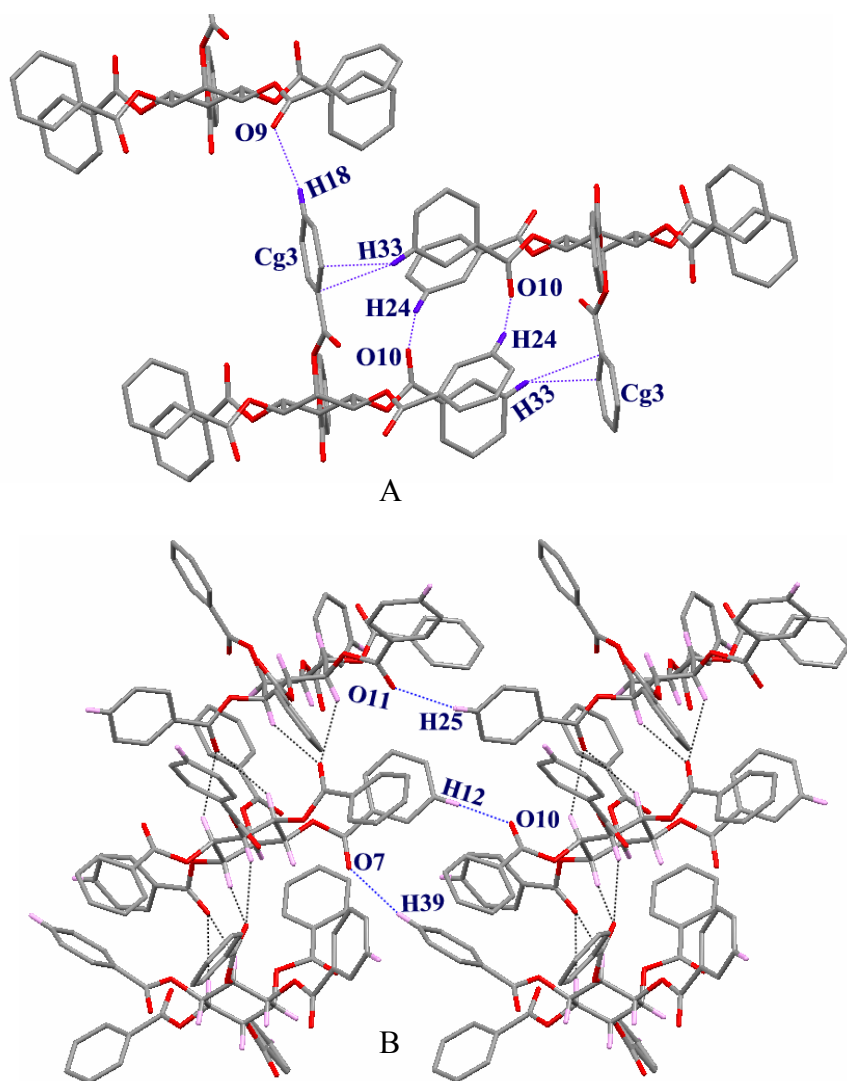


**Figure 3.9.** A) Intermolecular interactions made by the C2-axial benzoate group in Form II crystals of **4** and B) Interhelical C-H...O interactions in Form I crystals of **4**.

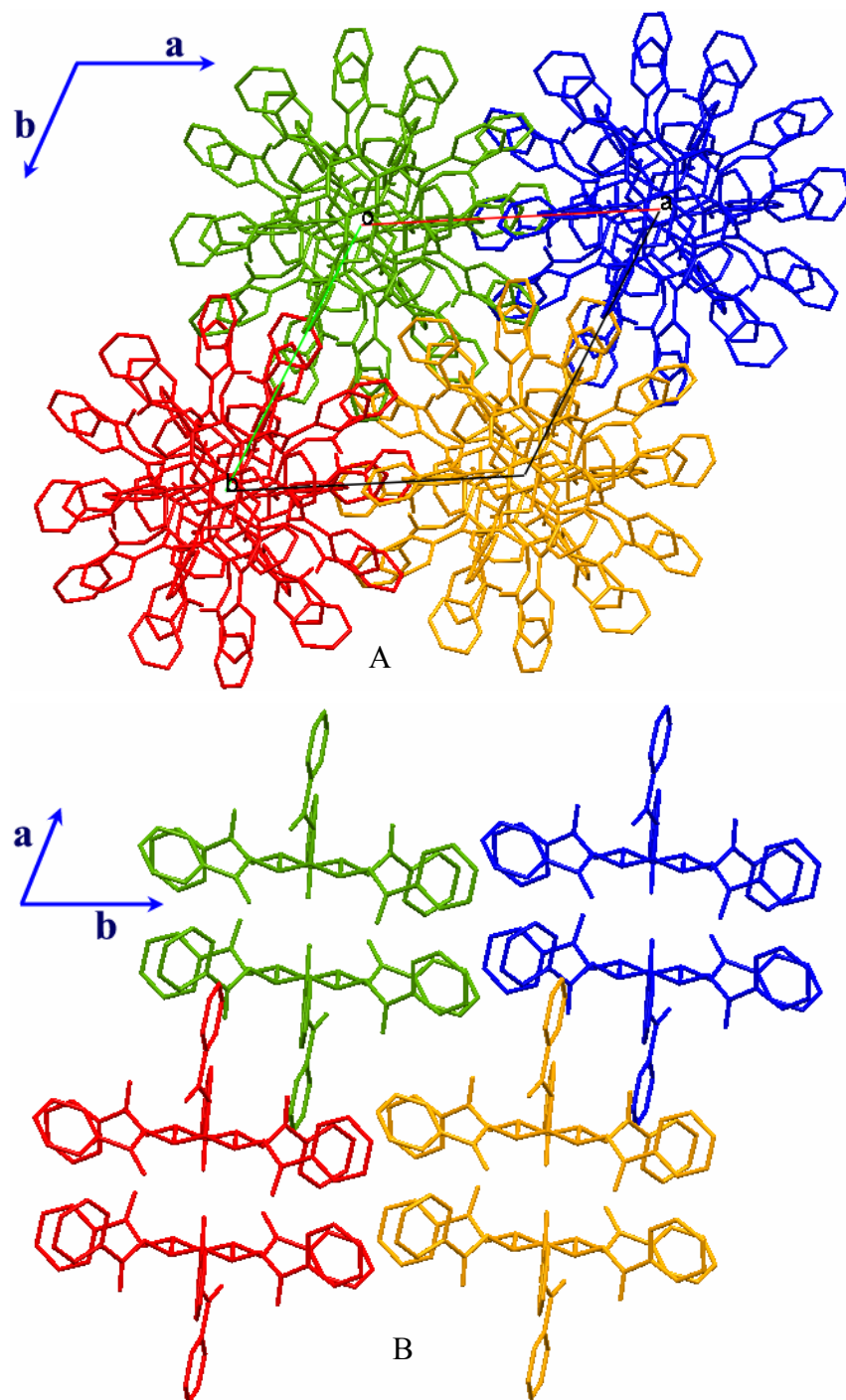


**Figure 3.10.** Molecular packing in, A) Form I crystals viewed down the c-axis and B) Form II crystals viewed down the a-axis.



**Table 3.8:** C-H $\cdots$ O interactions involved in assembling closely interacting pairs of Form I and Form II crystals of **4**.

	D-H $\cdots$ A	D-H (Å)	H $\cdots$ A (Å)	D $\cdots$ A (Å)	D-H $\cdots$ A (°)
<b>Form I</b>	C(12)-H(12) $\cdots$ O(10)#1	0.93	2.48	3.334(5)	152
	C(25)-H(25) $\cdots$ O(11)#2	0.93	2.52	3.322(5)	144
	C(39)-H(39) $\cdots$ O(7)#3	0.93	2.63	3.538(6)	165
<b>Form II</b>	C(41)-H(41) $\cdots$ O(12)#4	0.93	2.52	3.228(4)	133
	C(24)-H(24) $\cdots$ O(10)#5	0.93	2.77	3.613(4)	151
	C(18)-H(18) $\cdots$ O(9)#6	0.93	2.79	3.673(4)	158
	C(33)-H(33) $\cdots$ Cg(3)#7	0.93	2.95	2.833(5)	138
	C(26)-H(26) $\cdots$ Cg(2)#1	0.93	2.84	2.787(3)	146
	C(45)-H(45) $\cdots$ Cg(5)#8	0.93	3.00	2.772(2)	141
	C(10)-H(10) $\cdots$ Cg(4)#9	0.93	2.85	2.841(4)	141

Symmetry codes: #1  $x, 1+y, z$ ; #2  $1+x, y, z$ ; #3  $-1+y, -x+y, -1/6+z$ ; #4  $-x, 1-y, -z$ ; #5  $-x, 2-y, -z$ ; #6  $-1+x, y, z$ ; #7  $-x, 2-y, -z$ ; #8  $x, -1+y, z$ ; #9  $-x, 1-y, 1-z$ .

The polymorphic behaviour of **4** may be attributed to the conformational flexibility that generates different patterns of intermolecular weak interactions, e.g. C-H $\cdots$ O in the present case. Overlap of molecular conformations of **4** in two crystal forms (Form I and Form II, **Figure 3.11**) reveal differences in the orientation of all the benzoyl groups but the benzoate groups attached to C2 and C5 positions of the inositol ring show more difference. The axial benzoate at C2 exhibits rotational disorder in Form I, perhaps due to the non-involvement of these atoms in any significant intermolecular interactions.

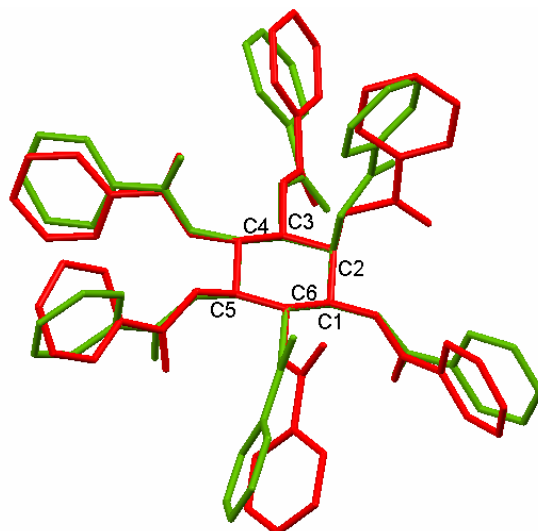


**Figure 3.11.** Molecular overlap of Form I (red) and Form II (green) crystals of **4**.

### 3.3.2 Structures of Dihalomethane Inclusion Crystals Before and After Guest

#### Escape

The inclusion complexes of dihalomethane solvents are categorized in to two groups. Group I, which consists of inclusion complexes with two molecules of dihalomethane i.e. **4**·CH<sub>2</sub>Cl<sub>2</sub>(2), **4**·CH<sub>2</sub>Br<sub>2</sub>(2) and **4**·CH<sub>2</sub>ClBr(2) and Group II, includes the inclusion complexes containing only one molecule of dihalomethane i.e. **4**·CH<sub>2</sub>Cl<sub>2</sub>(1), **4**·CH<sub>2</sub>Br<sub>2</sub>(1) and **4**·CH<sub>2</sub>ClBr(1).

#### *Structures of Dichloromethane Inclusion Crystals [4·CH<sub>2</sub>Cl<sub>2</sub>(2) and 4·CH<sub>2</sub>Cl<sub>2</sub>(1)]*

In inclusion crystals **4**·CH<sub>2</sub>Cl<sub>2</sub>(2), out of two CH<sub>2</sub>Cl<sub>2</sub> contained in the crystal lattice, one has full occupancy (DCM1) whereas the other (DCM2) has only 75% occupancy (it is this molecule DCM2 which diffuses out of the crystal lattice on storing at room temperature in paraffin). There was also one peak, which was assigned as a trace of water molecule (occupancy 0.25). The included guest molecules did not show any sign of disorder, but

the phenyl ring of the C5-*O*-benzoyl group of the host **4·CH<sub>2</sub>Cl<sub>2</sub>(2)** showed rotational disorder over two positions (**Figure 3.12**) with different occupancies (80 and 20%). The implication of these disordered sites in relation with the guest escape is discussed later (Section 3.3.3).

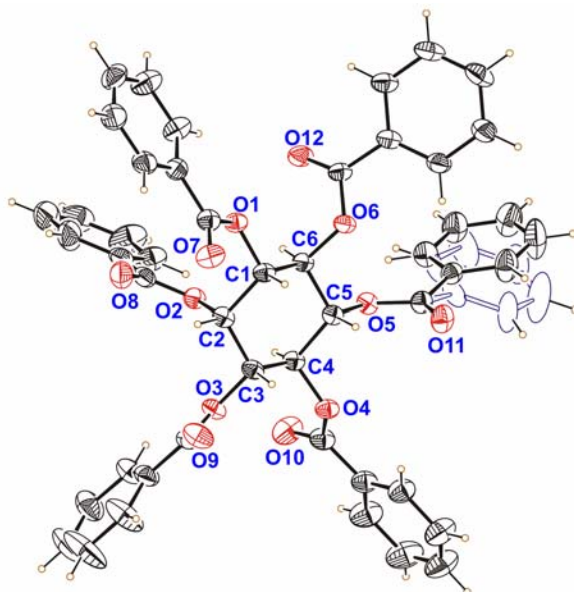


**Figure 3.12.** ORTEP view of the host molecule in crystals of **4·CH<sub>2</sub>Cl<sub>2</sub>(2)** showing rotational disorder (open ellipsoid connected with open bond, blue colour) of the phenyl ring at C5 position.

In crystals of **4·CH<sub>2</sub>Cl<sub>2</sub>(1)**, the molecule of CH<sub>2</sub>Cl<sub>2</sub> (DCM1) retained its full occupancy as in **4·CH<sub>2</sub>Cl<sub>2</sub>(2)**, whereas the other molecule DCM2 escaped from the crystal lattice completely. Also, the occupancy of the water was further reduced to 0.125 from 0.25 in **4·CH<sub>2</sub>Cl<sub>2</sub>(2)**. The disorder of the phenyl ring of the host observed in **4·CH<sub>2</sub>Cl<sub>2</sub>(2)** was not seen in this structure (**Figure 3.12**). The behaviour of inclusion crystals was almost similar with guests CH<sub>2</sub>Br<sub>2</sub> and CH<sub>2</sub>ClBr; with two molecules in the

fresh crystals and the escape of one of them upon standing in the paraffin oil for ~ 6-8 h. There are some small differences in the behaviour as detailed below.

***Structures of Dibromomethane Inclusion Crystals [4·CH<sub>2</sub>Br<sub>2</sub>(2) and 4·CH<sub>2</sub>Br<sub>2</sub>(1)]***

Two molecules of CH<sub>2</sub>Br<sub>2</sub> guests in the crystal lattice of **4·CH<sub>2</sub>Br<sub>2</sub>(2)** (DBM1 and DBM2) have full occupancy. Unlike in **4·CH<sub>2</sub>Cl<sub>2</sub>(2)**, the phenyl ring in the host molecule did not show any disorder. However in **4·CH<sub>2</sub>Br<sub>2</sub>(2)**, guest DBM1 exhibited disorder for the bromine atom Br1 that takes two positions with occupancies 0.9 and 0.1. The second molecule DBM2 did not show any such behaviour. These crystals [**4·CH<sub>2</sub>Br<sub>2</sub>(2)**] also contained a peak in the same position in the crystal lattice, which was assigned to a water molecule having the occupancy of 0.25.

In crystals structure of **4·CH<sub>2</sub>Br<sub>2</sub>(1)**, the molecule DBM1 maintained its full occupancy. As in **4·CH<sub>2</sub>Cl<sub>2</sub>(1)**, the occupancy of water molecule was reduced to 0.125 on conversion of **4·CH<sub>2</sub>Br<sub>2</sub>(2)** to **4·CH<sub>2</sub>Br<sub>2</sub>(1)**.

***Structures of Chlorobromomethane Inclusion Crystals [4·CH<sub>2</sub>ClBr(2) and 4·CH<sub>2</sub>ClBr(1)]***

The two guest molecules of CH<sub>2</sub>ClBr (BCM1 and BCM2) have occupancies of 1.0 and 0.5 respectively in **4·CH<sub>2</sub>ClBr(2)**. Here again, as in **4·CH<sub>2</sub>Cl<sub>2</sub>(2)**, the phenyl ring of C5-*O*-benzoyl group of the host molecule (**4**) showed rotational disorder over two positions with occupancies distributed over major (0.7) and minor (0.3) sites. In **4·CH<sub>2</sub>ClBr(2)**, BCM1 molecule showed statistical disorder with occupancies 0.8 at one

position and 0.2 for both bromine and chlorine atoms. Unlike  $4 \cdot \text{CH}_2\text{Cl}_2(2)$ , crystals of  $4 \cdot \text{CH}_2\text{ClBr}(2)$  did not contain any water molecule.

Again in crystals  $4 \cdot \text{CH}_2\text{ClBr}(1)$ , the guest BCM1 molecules which had full occupancy in  $4 \cdot \text{CH}_2\text{ClBr}(2)$ , remained in the crystal lattice whereas the half occupied BCM2 escaped from the crystal after  $\sim 6$  hours. In crystals of  $4 \cdot \text{CH}_2\text{ClBr}(1)$  the host molecule as well as the retained  $\text{CH}_2\text{ClBr}$  (BCM1) molecule did not show any sign of disorder as seen in  $4 \cdot \text{CH}_2\text{ClBr}(2)$ . Interestingly, in crystals of  $4 \cdot \text{CH}_2\text{ClBr}(1)$  the trace of water molecule was noticed which was given the 0.25 occupancy. It is to recall that the fresh crystal chosen [ $4 \cdot \text{CH}_2\text{ClBr}(2)$ ] did not contain water molecule but the crystal selected from the same batch stored in paraffin after  $\sim 6$  h contained water molecule.

### *Host Organization*

As in **3** (Chapter 2) and the Form II crystals of **4**, the host molecule in all its dihalomethane inclusion complexes of **4** formed centrosymmetric dimers via trifurcated C-H $\cdots$ O interactions. The three axial H-atoms H1, H3 and H5 of the *myo*-inositol ring from each molecule make contacts with the carbonyl oxygen O11 of the other molecule. In addition to the trifurcated C-H $\cdots$ O interactions, centrosymmetric C48-H48 $\cdots$ O4 contact also bridges these dimers (not shown in the figure for the sake of clarity). The geometrical parameters of all these four interactions are comparable in all dihalomethane inclusion crystals of **4** (Table 3.9). In Group I [ $4 \cdot \text{CH}_2\text{Cl}_2(2)$ ,  $4 \cdot \text{CH}_2\text{Br}_2(2)$  and  $4 \cdot \text{CH}_2\text{ClBr}(2)$ ] inclusion crystals, one more centrosymmetric interaction C37-H37 $\cdots$ O7 strengthens the dimer from either side of trifurcated C-H $\cdots$ O assembly (Figure 3.13A). But upon guest escape, in Group II inclusion crystals [ $4 \cdot \text{CH}_2\text{Cl}_2(1)$ ,  $4 \cdot \text{CH}_2\text{Br}_2(1)$  and  $4 \cdot \text{CH}_2\text{ClBr}(1)$ ], this additional C-H $\cdots$ O (C37-H37 $\cdots$ O7) contact is lost with the formation

of two new C37-H37...O9 and C31-H32...O7 contacts that take over strengthening of the dimers (**Figure 3.13B**). Interestingly in **4·CH<sub>2</sub>ClBr(2)**, C37'-H37'...O9 contact also exists in the minor occupied site of the disordered phenyl ring of C5-*O*-benzoyl group, which becomes the only site upon guest escape in **4·CH<sub>2</sub>ClBr(1)**.

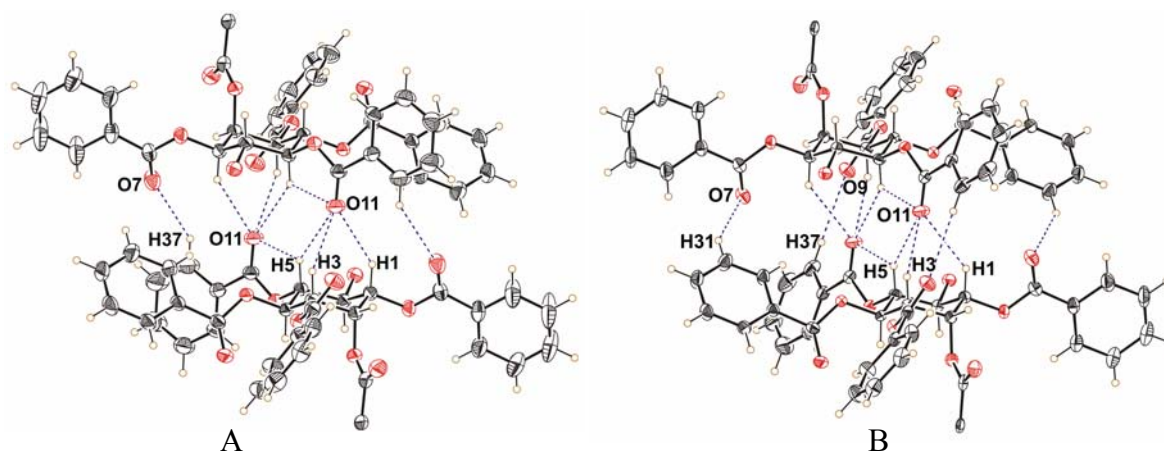


**Figure 3.13.** The centrosymmetric trifurcated C-H...O assembly is supported by other dimeric C-H...O interactions in A) **4·CH<sub>2</sub>Cl<sub>2</sub>(2)** and B) **4·CH<sub>2</sub>Cl<sub>2</sub>(1)**. Some benzoyl groups are omitted for clarity.

**Table 3.9:** Intermolecular C-H...O interactions involved in centrosymmetric assembly formation in dihalomethane inclusion crystals of **4**.

	D-H...A	D-H (Å)	H...A (Å)	D...A (Å)	D-H...A (°)
<b>4·CH<sub>2</sub>Cl<sub>2</sub>(2)</b>	C(1)-H(1)···O(11)#1	0.98	2.40	3.249(3)	144
	C(3)-H(3)···O(11)#1	0.98	2.51	3.335(3)	142
	C(5)-H(5)···O(11)#1	0.98	2.67	3.444(3)	136
	C(37)-H(37)···O(7)#1	0.93	2.61	3.402(5)	143
	C(48)-H(48)···O(4)#1	0.93	2.71	3.516(3)	146
<b>4·CH<sub>2</sub>Cl<sub>2</sub>(1)</b>	C(1)-H(1)···O(11)#2	0.98	2.40	3.258(4)	146
	C(3)-H(3)···O(11)#2	0.98	2.56	3.366(4)	139
	C(5)-H(5)···O(11)#2	0.98	2.61	3.410(4)	139
	C(48)-H(48)···O(4)#2	0.93	2.72	3.518(5)	144
	C(37)-H(37)···O(9)#2	0.93	2.67	3.581(5)	165
	C(31)-H(31)···O(7)#2	0.93	2.55	3.343(5)	143
<b>4·CH<sub>2</sub>Br<sub>2</sub>(2)</b>	C(1)-H(1)···O(11)#3	0.98	2.50	3.327(5)	141
	C(3)-H(3)···O(11)#3	0.98	2.44	3.269(6)	142
	C(5)-H(5)···O(11)#3	0.98	2.56	3.358(5)	139
	C(37)-H(37)···O(7)#3	0.93	2.52	3.313(8)	143
	C(48)-H(48)···O(4)#3	0.93	2.70	3.489(6)	143
<b>4·CH<sub>2</sub>Br<sub>2</sub>(1)</b>	C(1)-H(1)···O(11)#4	0.98	2.37	3.224(5)	146
	C(3)-H(3)···O(11)#4	0.98	2.57	3.365(5)	138
	C(5)-H(5)···O(11)#4	0.98	2.58	3.379(5)	139
	C(37)-H(37)···O(9)#4	0.93	2.60	3.500(6)	164
	C(31)-H(31)···O(7)#4	0.93	2.55	3.336(6)	143
	C(48)-H(48)···O(4)#4	0.93	2.70	3.484(6)	143
<b>4·CH<sub>2</sub>ClBr(2)</b>	C(1)-H(1)···O(11)#3	0.98	2.48	3.312(8)	141
	C(3)-H(3)···O(11)#3	0.98	2.42	3.266(8)	144
	C(5)-H(5)···O(11)#3	0.98	2.65	3.431(8)	137
	C(37)-H(37)···O(7)#3	0.93	2.55	3.382(13)	149
	C(37')-H(37')···O(9)#3	0.93	2.51	3.433(18)	170
	C(48)-H(48)···O(4)#3	0.93	2.69	3.497(9)	146
<b>4·CH<sub>2</sub>ClBr(1)</b>	C(1)-H(1)···O(11)#5	0.98	2.54	3.335(6)	139
	C(3)-H(3)···O(11)#5	0.98	2.36	3.215(5)	146
	C(5)-H(5)···O(11)#5	0.98	2.57	3.367(5)	138
	C(31)-H(31)···O(7)#5	0.93	2.52	3.310(7)	143
	C(37)-H(37)···O(9)#5	0.93	2.62	3.523(7)	165
	C(48)-H(48)···O(4)#5	0.93	2.71	3.502(6)	144

Symmetry code: #1 -x+2,-y+2,-z+1; #2 -x+1,-y+2,-z+1; #3 -x+1,-y,-z+1;

#4 -x+1,-y+1,2-z; #5 -x+2,-y+2,-z.

Although the nucleation process cannot be visualized, we propose a possible mechanism of nucleation in all the solvates. The dimeric trifurcated C-H $\cdots$ O assembly, which exists in all the pseudopolymorphs, is most likely to have formed first with subsequent crystal growth taking place depending upon the solvent of crystallization. It has already been mentioned that all the pseudopolymorphs of **4** with dihalomethane are isomorphous, implying similar association of dimeric assemblies in their inclusion crystals. The association of these trifurcated centrosymmetric assemblies creates two different types of supramolecular architecture in two different directions (**Figures 3.14** and **3.15**). The representative packing of molecules in **4**·CH<sub>2</sub>Cl<sub>2</sub>(**2**) is shown below (**Figure 3.14A**). The dimeric assemblies are linked along the b-axis via C34-H34 $\cdots$ O10 contact forming columnar structure whereas along ac-plane these columns are bridged via centrosymmetric C11-H11 $\cdots$ O8 interaction and  $\pi\cdots\pi$  contacts (Cg1 $\cdots$ Cg1) between phenyl rings of the C1-O-benzoyl group (**Tables 3.10** and **3.11**) creating hydrophobic layer between the columns (**Figure 3.14A**). These hydrophobic regions consist of the voids, which accommodate the guest molecules (**Figure 3.14A**). The C34-H34 $\cdots$ O10 linked pillars are bridged along c-axis in another way via weaker C27-H27 $\cdots$ O8 interactions forming different molecular architecture (**Figure 3.14B**).



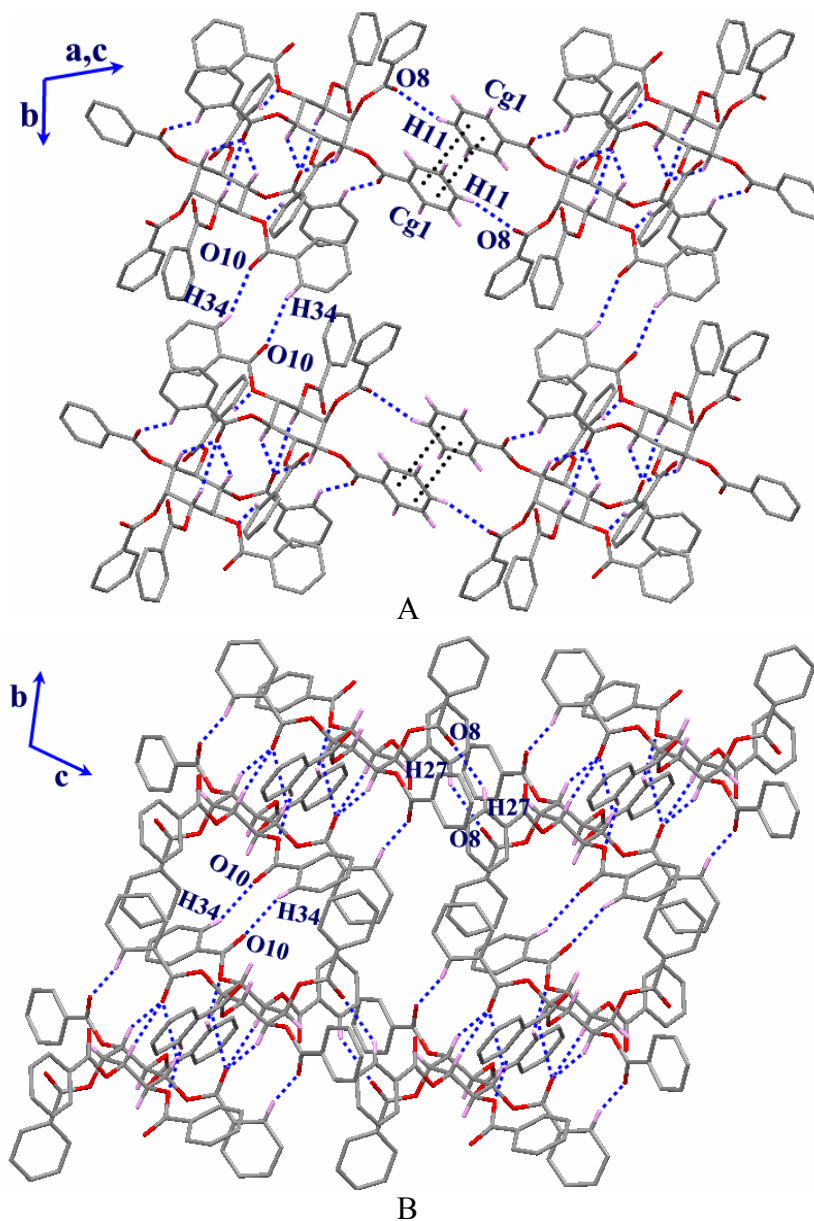


**Figure 3.14.** Molecular packing viewed down (A) ac-plane and (B) a-axis showing association of dimeric assemblies in  $4 \cdot \text{CH}_2\text{Cl}_2(2)$ .

These centrosymmetric C-H $\cdots$ O assemblies are further linked via C17-H17 $\cdots$ O12 contacts along b-axis forming different types of columnar structure. These columns are bridged via similar interactions as in **Figure 3.14** forming two different molecular

networks. The dimeric C11-H11...O8 interaction and  $\pi\cdots\pi$  contacts between phenyl rings of the C1-O-benzoyl group link these columns along c-axis (**Figure 3.5A**) whereas along ac-plane they are connected via C27-H27...O8 contact (**Figure 3.5B**). The association of the dimeric assemblies is almost the same in all the other dihalomethane inclusion crystals of **4** with a slight change in the geometrical parameters of the intermolecular interactions (**Table 3.10**).

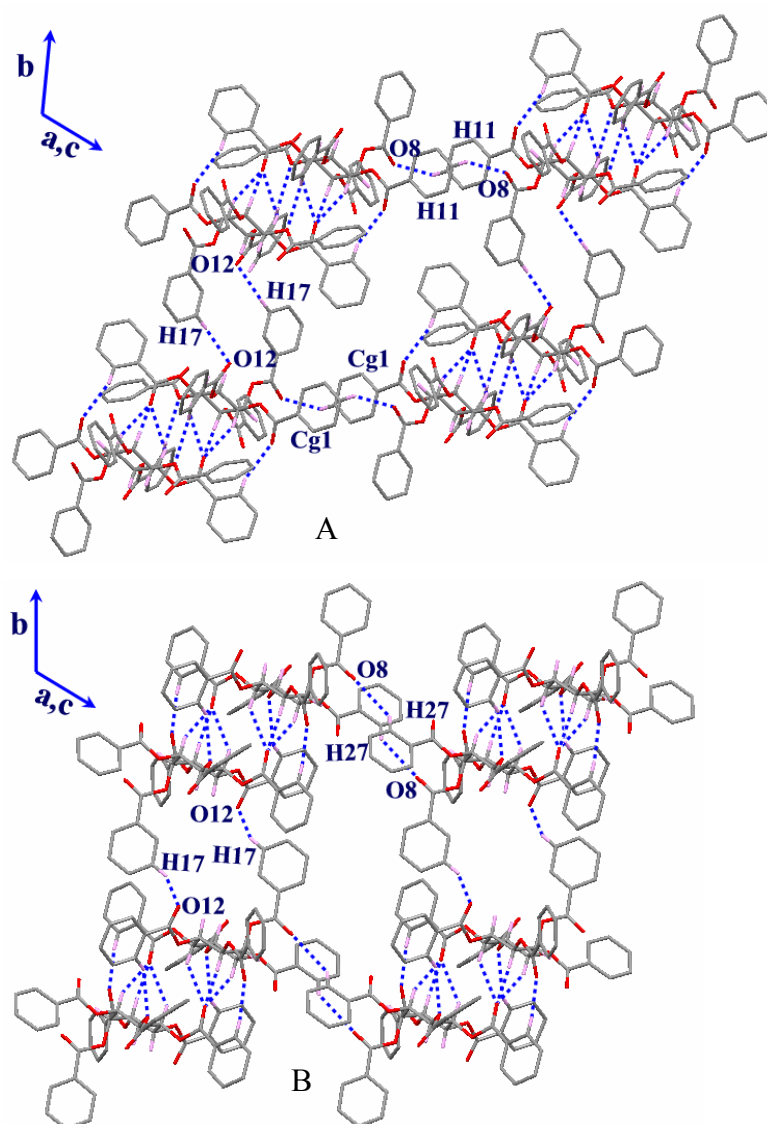


**Figure 3.15.** Interlinking of centrosymmetric assemblies in  $4\cdot\text{CH}_2\text{Cl}_2(2)$ , A) along a-axis, and B) ac-plane (dotted lines in blue represents  $\pi\cdots\pi$  contact).

**Table 3.10:** Intermolecular C-H...O interactions involved in bridging the dimeric assemblies in dihalomethane inclusion crystals of **4**.

	D-H...A	D-H (Å)	H...A (Å)	D...A (Å)	D-H...A (°)
<b>4</b> ·CH <sub>2</sub> Cl <sub>2</sub> (2)	C(11)-H(11)...O(8)#1	0.93	2.52	3.365(4)	151
	C(17)-H(17)...O(12)#2	0.93	2.50	3.231(6)	135
	C(27)-H(27)...O(8)#3	0.93	2.82	3.489(4)	130
	C(34)-H(34)...O(10)#4	0.93	2.53	3.400(4)	156
<b>4</b> ·CH <sub>2</sub> Cl <sub>2</sub> (1)	C(26)-H(26)...O(7)#5	0.93	2.54	3.336(5)	144
	C(27)-H(27)...O(8)#5	0.93	2.77	3.594(5)	148
	C(17)-H(17)...O(12)#6	0.93	2.70	3.373(6)	130
	C(11)-H(11)...O(8)#7	0.93	2.55	3.387(5)	150
	C(34)-H(34)...O(10)#8	0.93	2.45	3.311(4)	155
<b>4</b> ·CH <sub>2</sub> Br <sub>2</sub> (2)	C(27)-H(27)...O(8)#9	0.93	2.80	3.444(7)	128
	C(17)-H(17)...O(12)#10	0.93	2.44	3.205(7)	140
	C(11)-H(11)...O(8)#11	0.93	2.54	3.401(7)	154
	C(34)-H(34)...O(10)#12	0.93	2.54	3.367(6)	149
<b>4</b> ·CH <sub>2</sub> Br <sub>2</sub> (1)	C(26)-H(26)...O(7)#13	0.93	2.54	3.342(6)	145
	C(27)-H(27)...O(8)#13	0.93	2.68	3.514(6)	150
	C(17)-H(17)...O(12)#14	0.93	2.65	3.402(8)	139
	C(11)-H(11)...O(8)#15	0.93	2.52	3.375(6)	153
	C(34)-H(34)...O(10)#16	0.93	2.45	3.290(5)	151
<b>4</b> ·CH <sub>2</sub> ClBr(2)	C(27)-H(27)...O(8)#17	0.93	2.76	3.445(9)	132
	C(26)-H(26)...O(7)#17	0.93	2.87	3.601(11)	137
	C(17)-H(17)...O(12)#18	0.93	2.47	3.209(13)	137
	C(11)-H(11)...O(8)#19	0.93	2.52	3.372(11)	152
	C(34)-H(34)...O(10)#20	0.93	2.52	3.367(9)	151
<b>4</b> ·CH <sub>2</sub> ClBr(1)	C(11)-H(11)...O(8)#21	0.93	2.51	3.354(7)	151
	C(17)-H(17)...O(12)#21	0.93	2.66	3.361(7)	133
	C(27)-H(27)...O(8)#22	0.93	2.71	3.533(6)	148
	C(26)-H(26)...O(7)#22	0.93	2.51	3.314(6)	144
	C(34)-H(34)...O(10)#23	0.93	2.42	3.276(6)	153

Symmetry codes: #1 -x+2,-y+3,-z+2; #2 -x+2,-y+3,-z+1; #3 -x+3,-y+3,-z+2;  
 #4 -x+3,-y+3,-z+1; #5 -x+1,-y+2,-z+2; #6 -x+1,-y+1,-z+1; #7 -x+2,-y+2,-z+2;  
 #8 -x,-y+1,-z+1; #9 -x+2,-y+1,-z+2; #10 -x+1,-y+1,-z+1; #11 -x+1,-y+1,-z+2;  
 #12 -x+2,-y+1,-z+1; #13 -x+1,-y+1,-z+1; #14 -x+2,-y+1,-z+2; #15 -x+1,-y,-z+1;  
 #16 -x+2,-y+2,-z+2; #17 -x+2,-y+1,-z+2; #18 -x+1,-y+1,-z+1; #19 -x+1,-y+1,-z+2;  
 #20 -x+2,-y+1,-z+1; #21 -x+3,-y+2,-z+1; #22 -x+2,-y+2,-z+1; #23 -x+1,-y+1,-z.

**Table 3.11:** Geometry of the  $\pi\cdots\pi$  stacking contacts engaged in connecting dimeric assemblies in the dihalomethane inclusion crystals of **4**.

	Cg $\cdots$ Cg (Å)	Alpha (dihedral angle) (°)	CgI_Perp (Å)	CgJ_Perp (Å)
<b>4</b> ·CH <sub>2</sub> Cl <sub>2</sub> ( <b>2</b> ), Cg(1) $\cdots$ Cg(1)#1	3.876	0.02	3.835	3.835
<b>4</b> ·CH <sub>2</sub> Cl <sub>2</sub> ( <b>1</b> ), Cg(1) $\cdots$ Cg(1)#2	3.833	0.03	3.701	3.701
<b>4</b> ·CH <sub>2</sub> Br <sub>2</sub> ( <b>2</b> ), Cg(1) $\cdots$ Cg(1)#3	3.899	0.02	3.732	3.732
<b>4</b> ·CH <sub>2</sub> Br <sub>2</sub> ( <b>1</b> ), Cg(1) $\cdots$ Cg(1)#4	3.809	0.00	3.650	3.650
<b>4</b> ·CH <sub>2</sub> ClBr( <b>2</b> ), Cg(1) $\cdots$ Cg(1)#5	3.902	0.02	3.788	3.788
<b>4</b> ·CH <sub>2</sub> ClBr( <b>1</b> ), Cg(1) $\cdots$ Cg(1)#6	3.804	0.00	3.666	3.666

(Cg(1) centroid of phenyl rings C8-C13), Symmetry codes: #1 -x, 1-y, 2-z; #2 -x,-y,-z; #3 1-x,1-y,-z; #4 1-x,2-y,1-z; #5 1-x,1-y, 2-z; #6 3-x, 2-y, 1-z.

### **Cavity Formation**

The association of these centrosymmetric C-H $\cdots$ O assemblies (**Figure 3.13**) creates two different types of guest inclusion sites in the crystal lattice. Site A (**Figure 3.16**), is generated by the linking of centrosymmetric C-H $\cdots$ O dimeric assembly along b-axis and the site B is in the hydrophobic region created by the arrangement of four such assemblies in their center along the c-axis (Site B, **Figure 3.16**).

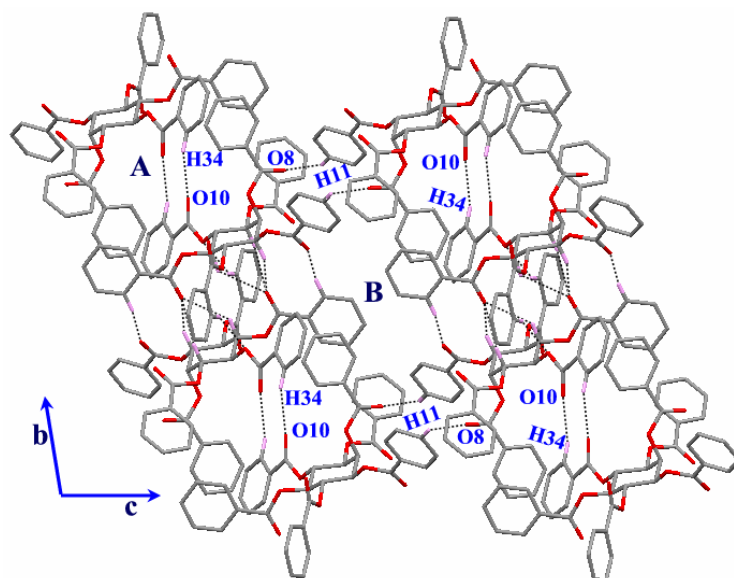


**Figure 3.16.** Molecular packing viewed down a-axis showing two different guest inclusion sites in  $4 \cdot \text{CH}_2\text{Cl}_2(2)$ .

### *Guest Inclusion in the Channel*

The host-guest assemblies of the dichloromethane inclusion crystals of **4** before and after the guest escape are shown in **Figure 3.17**. The guest molecules occupy the sites in the crystal lattice as indicated in **Figure 3.16**. In Group I [ $4 \cdot \text{CH}_2\text{Cl}_2(2)$ ,  $4 \cdot \text{CH}_2\text{Br}_2(2)$  and  $4 \cdot \text{CH}_2\text{ClBr}(2)$ ] inclusion crystals and corresponding crystals left in the paraffin oil for  $\sim 6$  h [Group II inclusion crystals,  $4 \cdot \text{CH}_2\text{Cl}_2(1)$ ,  $4 \cdot \text{CH}_2\text{Br}_2(1)$  and  $4 \cdot \text{CH}_2\text{ClBr}(1)$ ] revealed that the two dihalomethane guests in the fresh crystals had different binding environments. In Group I inclusion crystals, the site A accommodates one of the dihalomethane guest molecules (DCM1 or DBM1 or BCM1, **Figure 3.17A**), whereas the site B encompasses other molecule of dihalomethane (DCM2 or DBM2 or BCM2, **Figure 3.17A**). In Group II inclusion crystals, the retained dihalomethane molecule (DCM1 or DBM1 or BCM1) occupies site A (**Figure 3.17B**). Thus the

dihalomethane molecule, which occupies site A, is intact whereas the dihalomethane molecule, which is present in the hydrophobic site B, escapes. Due to this guest dynamics the cavities that were well separated in Group I inclusion crystals (**Figure 3.17A**) are ‘closed in’ in Group II inclusion crystals resulting in the shortening of the c-axis (**Figure 3.17B**).

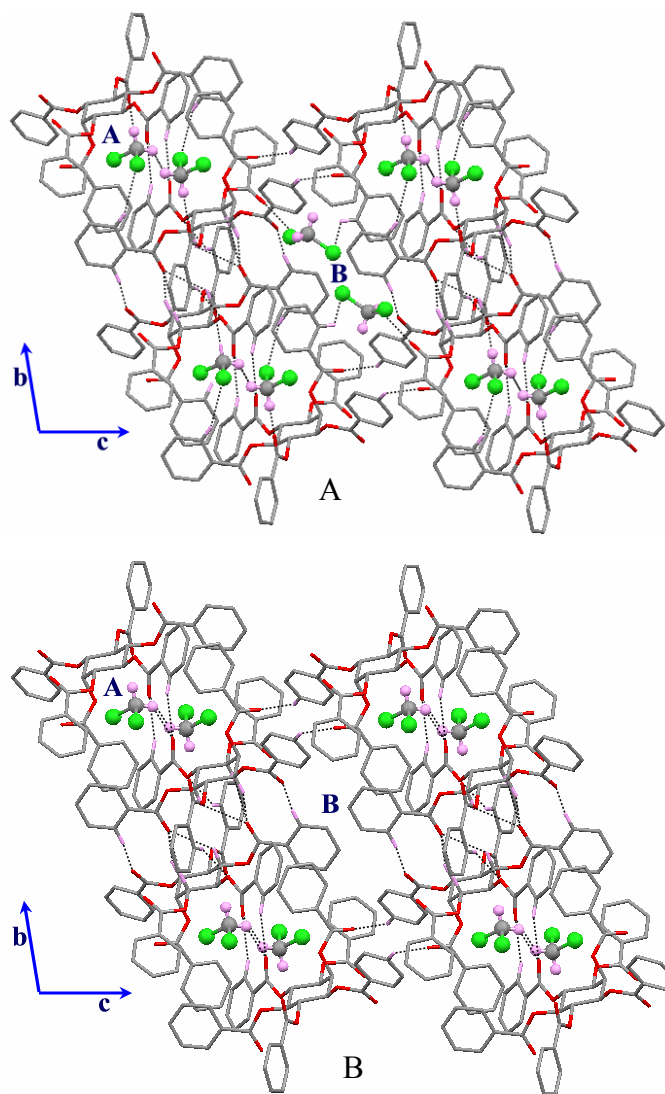


**Figure 3.17.** Host-guest assembly of dihalomethane inclusion crystals, A) guest molecules occupying both sites in  $4\cdot\text{CH}_2\text{Cl}_2(2)$  and B) guest molecule occupying site A whereas site B is empty in  $4\cdot\text{CH}_2\text{Cl}_2(1)$ .

### *Host-Guest Interactions*

In all dihalomethane solvates of **4**, the guest molecule which occupies site A makes more number of interactions as compared to the guest molecules which are present in site B. Although, escape of guest molecules from site B did not produce much effect on the host-guest assembly, the crystal lattice collapses after the escape of guest at site A. The dihalomethane molecules in site A (DCM1, DBM1, and BCM1 = DHM1) in Group I and Group II inclusion crystals makes similar contacts with the host. Similarly the dihalomethane molecule at site B (DCM2, DBM2 and BCM2 = DHM2) in Group I inclusion crystals also makes identical contacts with the host (**Figure 3.17A**). The H-atoms of the dihalomethane molecule in site A make two C-H $\cdots$ O contacts such as C49-H49A $\cdots$ O10 and C49-H49B $\cdots$ O12 with the carbonyl oxygen of the host (**Figure 3.18A**, **Table 3.12**). One of the halogens Cl1 (Br1) of the DHM1 interacts with the host via C-H $\cdots$ halogen contacts [C16-H16 $\cdots$ Cl1 (Br1) and C41-H41 $\cdots$ Cl1 (Br1)]. The other halogen Cl2 (Br2) is involved in almost linear halogen $\cdots$  $\pi$  contact with the phenyl ring of the C3-*O*-benzoyl group (Cg3) of the host (**Table 3.13**). Thus the DHM1 molecules, which occupies, site A makes total five contacts with the host. Further, the halogen of the DHM1 molecule makes marginal halogen bonding contacts with oxygen of the host. The dihalomethane molecules at site B makes very weak C50-H50B $\cdots$ O9, almost linear C20-H20 $\cdots$ Cl3(Br3) and somewhat compromised C50-Cl3(Br3) $\cdots$  $\pi$ (C43-C48, Cg6) interactions with the host (**Figure 3.18A**, **Tables 3.12** and **3.13**). In Group II inclusion complexes the dihalomethane guest molecule (DCM1, DBM1, and BCM1) occupies site A and make similar contacts with the host as in Group I inclusion crystals (**Figure 3.18B**). Further it was observed that the strength of the C-H $\cdots$ O contacts between the

guest and the host molecules enhances after the escape of the dihalomethane from site B in the crystal lattice (Table 3.12).

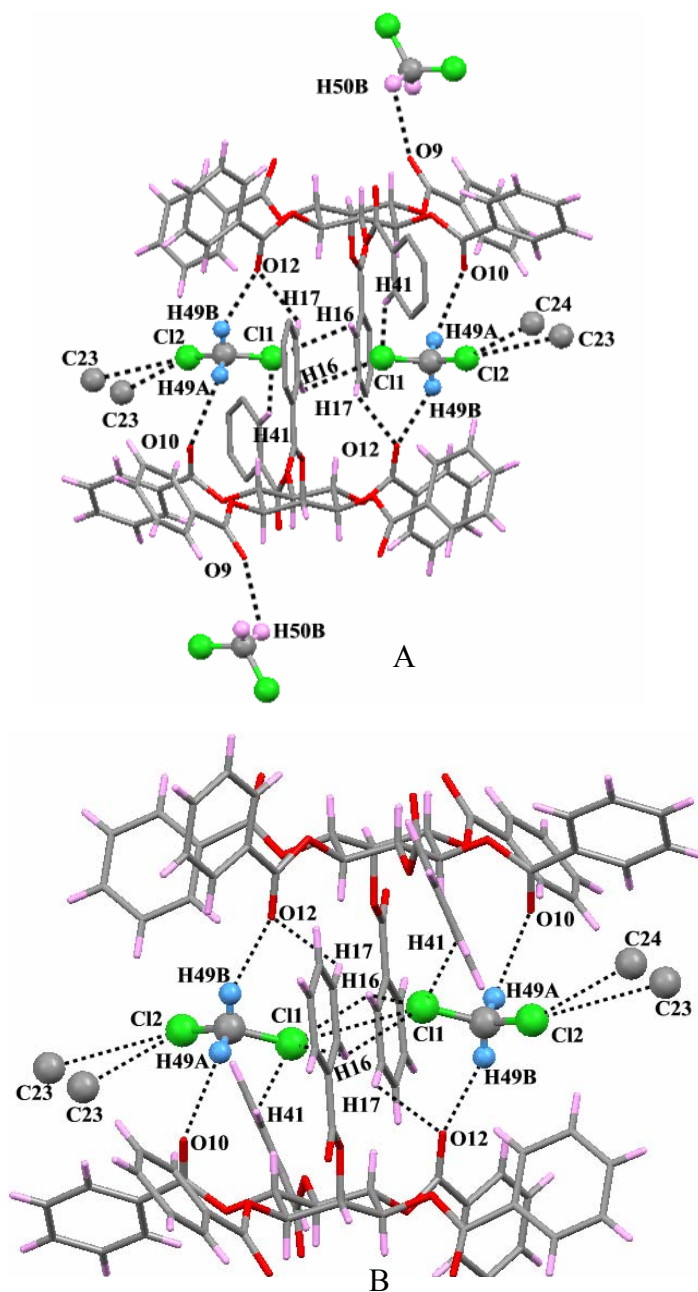


**Figure 3.18.** Representative close view of the host-guest interactions in dihalomethane inclusion complexes, A) host-guest interactions in  $4 \cdot \text{CH}_2\text{Cl}_2(2)$  and B) host-guest interactions in  $4 \cdot \text{CH}_2\text{Cl}_2(1)$ .



**Table 3.12:** Host –guest interactions in dihalomethane inclusion complexes of **4**.

	D-H...A	D-H (Å)	H...A (Å)	D...A (Å)	D-H...A (°)
<b>4•CH<sub>2</sub>Cl<sub>2</sub>(2)</b>	C(49)-H(49A)...O(10)#1	0.97	2.64	3.376(5)	133
	C(49)-H(49B)...O(12)#2	0.97	2.40	3.232(4)	143
	C(50)-H(50B)...O(9)#3	0.97	2.59	3.104(3)	113
	C(16)-H(16)...Cl(1)#4	0.93	3.07	3.681(5)	125
	C(41)-H(41)...Cl(1)#4	0.93	2.86	3.729(6)	155
	C(20)-H(20)...Cl(3)#5	0.93	3.01	3.919(5)	167
<b>4•CH<sub>2</sub>Cl<sub>2</sub>(1)</b>	C(49)-H(49A)...O(10)#7	0.97	2.47	3.250(5)	137
	C(49)-H(49B)...O(12)#6	0.97	2.27	3.148(5)	149
	C(16)-H(16)...Cl(1)#7	0.93	3.04	3.704(6)	129
	C(41)-H(41)...Cl(1)#7	0.93	3.06	3.896(6)	151
<b>4•CH<sub>2</sub>Br<sub>2</sub>(2)</b>	C(49)-H(49A)...O(10)#7	0.97	2.67	3.406(8)	133
	C(49)-H(49B)...O(12)#6	0.97	2.46	3.247(7)	138
	C(50)-H(50B)...O(9)#6	0.97	2.59	3.174(10)	119
	C(17)-H(17)...Br(1)#7	0.93	3.17	3.843(7)	131
	C(41)-H(41)...Br(1)#7	0.93	2.94	3.755(6)	147
	C(20)-H(20)...Br(3)#8	0.93	3.16	4.068(7)	165
<b>4•CH<sub>2</sub>Br<sub>2</sub>(1)</b>	C(49)-H(49A)...O(10)#8	0.97	2.54	3.264(7)	132
	C(49)-H(49B)...O(12)#6	0.97	2.30	3.130(6)	144
	C(16)-H(16)...Br(1)#6	0.93	3.10	3.675(5)	121
	C(16)-H(16)...Br(1)#8	0.93	3.10	3.775(6)	131
	C(41)-H(41)...Br(1)#8	0.93	3.05	3.869(5)	147
<b>4•CH<sub>2</sub>ClBr(2)</b>	C(49)-H(49A)...O(10)#7	0.97	2.62	3.371(11)	134
	C(49)-H(49B)...O(12)#6	0.97	2.44	3.215(10)	136
	C(50)-H(50B)...O(9)#1	0.97	2.56	3.121(14)	117
	C(50)-H(50A)...O(8)#9	0.97	2.77	3.639(18)	150
	C(41)-H(41)...Cl(1)#7	0.93	2.97	3.752(19)	143
	C(20)-H(20)...Br(2)#9	0.93	3.07	3.985(11)	168
<b>4•CH<sub>2</sub>ClBr(1)</b>	C(49)-H(49A)...O(10)#10	0.97	2.49	3.241(7)	134
	C(49)-H(49B)...O(12)#11	0.97	2.27	3.134(7)	147
	C(16)-H(16)...Cl(1)#10	0.93	3.04	3.694(6)	129
	C(41)-H(41)...Cl(1)#10	0.93	3.03	3.871(6)	151

Symmetry codes: #1 x-1,y-1,z; #2 -x+1,-y+2,-z+1; #3 -x+1,-y+1,-z+1; #4 1+x, 1+y, z;  
#5 1+x, 1+y, 1+z; #6 x,y,z; #7 1-x,1-y,1-z ; #8 -x+2,-y+1,-z+2; #9 x-1,y-1,z-1;  
#10 -x+1,-y+1,-z; #11 x-1,y,z.

**Table 3.13:** C-halogen $\cdots\pi$  interactions between guest molecule and the host in all dihalomethane inclusion complexes of **4**.

X = Cl, Br	C-X $\cdots$ Cg	X $\cdots$ Cg (Å)	C $\cdots$ Cg (Å)	C-X $\cdots$ Cg (°)
<b>4</b> •CH <sub>2</sub> Cl <sub>2</sub> ( <b>2</b> )	C(49)-Cl(2) $\cdots$ Cg(3)#1	3.845	5.570	174
	C(50)-Cl(3) $\cdots$ Cg(6)#2	3.888	5.250	143
<b>4</b> •CH <sub>2</sub> Cl <sub>2</sub> ( <b>1</b> )	C(49)-Cl(2) $\cdots$ Cg(3)#3	3.930	5.632	163
<b>4</b> •CH <sub>2</sub> Br <sub>2</sub> ( <b>2</b> )	C(49)-Br(2) $\cdots$ Cg(3)#4	3.730	5.637	168
	C(50)-Br(3) $\cdots$ Cg(6)#5	3.819	5.582	148
<b>4</b> •CH <sub>2</sub> Br <sub>2</sub> ( <b>1</b> )	C(49)-Br(2) $\cdots$ Cg(3)#6	3.729	5.604	168
<b>4</b> •CH <sub>2</sub> ClBr( <b>2</b> )	C(49)-Br(1) $\cdots$ Cg(3)#7	3.785	5.630	148
	C(50)-Br(2) $\cdots$ Cg(6)#2	3.781	5.716	148
<b>4</b> •CH <sub>2</sub> ClBr( <b>1</b> )	C(49)-Br(1) $\cdots$ Cg(3)#2	3.841	5.641	167

Cg3 = C22-C27, Cg6 = C43-C48, Symmetry codes: #1 2-x, 2-y, 1-z; #2 x, y, z;

#3 -1+x, y, z; #4 -x, 1-y, 1-z; #5 1-x, 2-y, 1-z; #6 x, 1+y, z; #7 1+x, y, z.

### 3.3.3 Structural Changes Upon Guest escape in Dihalomethane Inclusion Crystals of **4**

The superimposition of the host molecules of Group I and Group II inclusion crystals (**Figure 3.19**) reveal differences in conformation of the benzoyl groups at C1 and C5 positions. Interestingly, the conformation of the minor component C5-*O*-benzoyl group (green dots) in **4**·CH<sub>2</sub>Cl<sub>2</sub>(**2**) and **4**·CH<sub>2</sub>ClBr(**2**) is almost same as that of the C5-*O*-benzoyl group in **4**·CH<sub>2</sub>Cl<sub>2</sub>(**1**) and **4**·CH<sub>2</sub>ClBr(**1**).

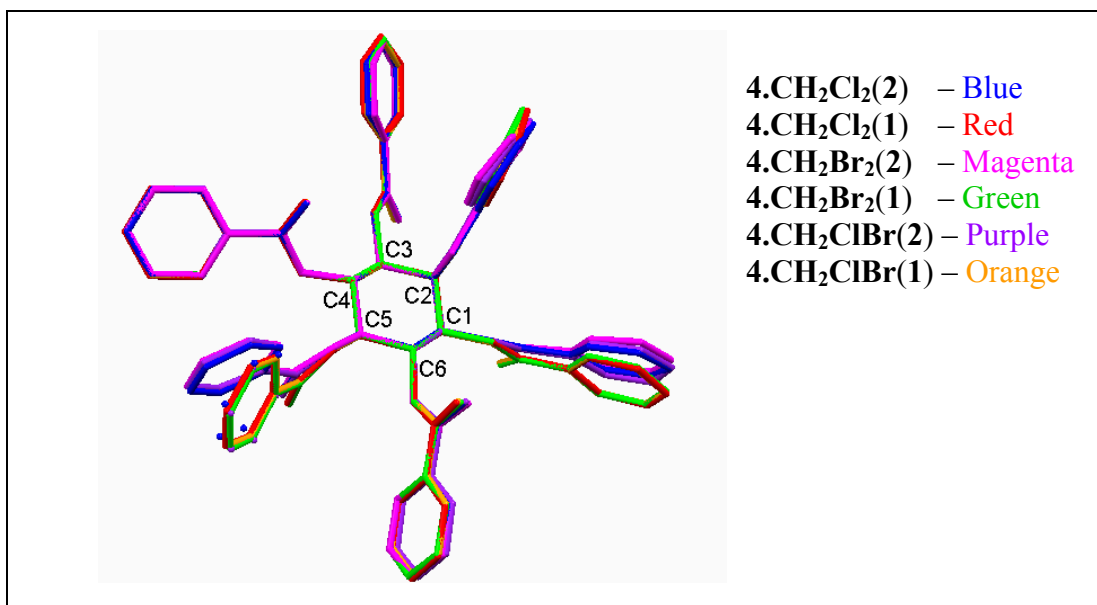


**Figure 3.19.** Molecular overlap of the host molecules in Group I and Group II inclusion crystals of **4**. Blue and purple dots represent the conformation of the minor component C5-*O*-benzoyl group in **4**·CH<sub>2</sub>Cl<sub>2</sub>(**2**) and **4**·CH<sub>2</sub>Br<sub>2</sub>(**2**) respectively.

However, the overall arrangement of the host guest assembly in Group I and Group II inclusion crystals does not differ much. In Group I inclusion crystals, the hosts molecules are linked by dimeric C27-H27···O8 contact along the *c*-axis, whereas along *a*-axis they are associated via dimeric C11-H11···O8 contact and  $\pi$ ··· $\pi$  interaction between

the phenyl ring (Cg1) of C1-*O*-benzoyl group (**Figure 3.18A**). The DHM2 (DHM2 = DCM2, DBM2 and BCM2) molecule occupies the space between the two dimeric C3-*O*-benzoyl groups, which are linked by centrosymmetric C27-H27 $\cdots$ O8 contact along the *c*-axis (**Figure 3.20A**). The DHM1 (DHM1 = DCM1, DBM1 and BCM1) molecule is located on either side of the C1-*O*-benzoyl groups, the phenyl ring of which is engaged in dimeric  $\pi\cdots\pi$  interactions along the *b*-axis. DHM1 molecule is interacting via two C-H $\cdots$ O interactions, two C-H $\cdots$ halogen contacts and one C-halogen $\cdots\pi$  contacts. The DHM2 molecule makes less number of interactions (C50-H50B $\cdots$ O9 and C20-H20 $\cdots$ Cl3(Br3), C20-H20 $\cdots$ Br2 in **4-CH<sub>2</sub>ClBr**) with the host molecule (**Figure 3.20A**). In Group II inclusion crystals due to the absence of DHM2 molecule, the arrangement of the host molecules in the lattice is slightly altered to adjust the effect after escape.

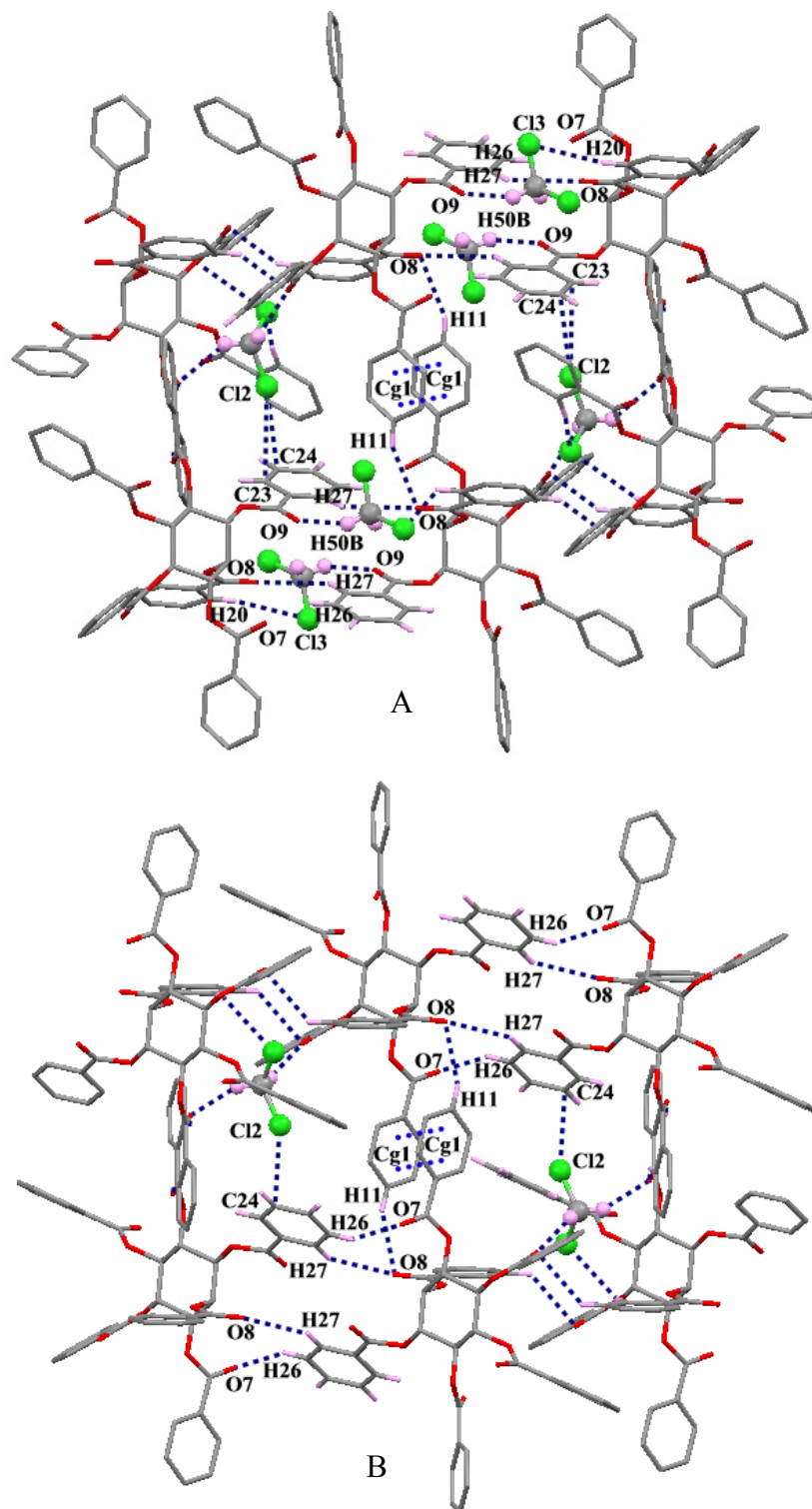


**Figure 3.20.** Molecular packing viewed down b-axis showing structural changes due to guest escape, A) in 4·CH<sub>2</sub>Cl<sub>2</sub>(2) and B) in 4·CH<sub>2</sub>Cl<sub>2</sub>(1).

The geometry of the dimeric C27-H27···O8 contact is slightly improved in Group II inclusion crystals compared to Group I inclusion crystals with the formation of one more short C26-H26···O7 interaction, the geometry of latter is better than the former (**Table 3.10** and **Figure 3.20B**). This suggests that due to the escape of the DHM2 molecule from the space between the C3-*O*-benzoyl groups, the benzoyl groups move towards each other resulting in the shortening of C27-H27···O8 contact. The formation of C26-H26···O7 contact is a consequence of molecular movement along the *c*-axis. Furthermore, due to the escape of DHM2 molecule, the geometry of the C49-H49B···O12 and C49-H49A···O10 interactions made by the hydrogen atoms of dichloromethane molecule has significantly improved (**Table 3.2**). Another notable feature is the development of new halogen···halogen contact across the inversion center between the DHM1 molecules upon escape of DHM2 molecule. The Cl1 atoms of DCM1 molecules, which are 4.053 Å away from each other in **4·CH<sub>2</sub>Cl<sub>2</sub>(2)**, came closer (3.568 Å) in **4·CH<sub>2</sub>Cl<sub>2</sub>(1)**, the Br1 atoms of DBM1 molecules, which are 4.497 Å away from each other in **4·CH<sub>2</sub>Br<sub>2</sub>(2)**, came closer to 3.641 Å in **4·CH<sub>2</sub>Br<sub>2</sub>(1)** and the Cl1 atom of BCM1 molecules in **4·CH<sub>2</sub>ClBr(2)**, which are 4.309 Å away from each other, came closer to 3.552 Å in **4·CH<sub>2</sub>ClBr(1)**.

### 3.3.4 Structures of Chloroform and Bromoform Inclusion Crystals of 4

#### *Structure of Inclusion Crystal of 4 with CHCl<sub>3</sub>*

In the chloroform inclusion complex (**4**·CHCl<sub>3</sub>), three molecules of chloroform were present in the crystal lattice. One of the included CHCl<sub>3</sub> (now onwards CLO1) has a regular geometry, whereas the other two (CLO2 and CLO3) are highly disordered. The host molecule also showed more thermal liberation for benzoyl groups at C1, C2 and C3 positions. The geometries of the phenyl rings were fixed using the AFIX 66 option in the SHELXL97 and Uij's of the phenyl rings were restrained using DELU and SIMU treatment. The structure refined to very high R-value (17%) due to the highly disordered chloroform as well as the host molecule. Two chloroform molecules (CLO1 and CLO2) were half occupied and the third one CLO3, which is highly disordered, had 0.125 occupancy. The squeeze option in the PLATON did not show any electron count in the solvent accessible area after taking into account all the three chloroform molecules in refinement.

#### *Structure of Inclusion Crystal of 4 with CHBr<sub>3</sub>*

In the bromoform inclusion complex, two molecules of the bromoform were present in the crystal lattice (BRO1 and BRO2); out of which BRO2 was disordered over two positions across the inversion center. Two bromine atoms of BRO2 commonly share the positions. The other bromoform molecule (BRO1) did not show any sign of disorder but all the three bromine atoms were having more residual density around it. The ordered bromoform molecule had full occupancy whereas the disordered one had half occupancy.

In comparison with chloroform inclusion crystals, the benzoyl groups of the host molecule in bromoform inclusion crystals did not show any disorder.

### Host Organization

The chloroform and bromoform inclusion complex are not isomorphous even though they belong to same space group (**Table 3.6**) Host molecules in chloroform ( $4\cdot\text{CHCl}_3$ ) and bromoform inclusion crystals ( $4\cdot\text{CHBr}_3$ ) formed centrosymmetric trifurcated C-H $\cdots$ O bonding assembly like dihalomethane inclusion crystals of **4** (**Figure 3.13**). The three axial H-atoms H1, H3 and H5 of the *myo*-inositol ring from each molecule make contacts with the carbonyl oxygen O11 of the other molecule. In  $4\cdot\text{CHCl}_3$ , addition to the trifurcated C-H $\cdots$ O interactions, centrosymmetric C37-H37 $\cdots$ O9 interaction also bridges these dimers thus strengthening the dimeric trifurcated C-H $\cdots$ O assemblies whereas in  $4\cdot\text{CHBr}_3$  no such supporting C-H $\cdots$ O contacts are present (**Table 3.14**).

**Table 3.14:** Intermolecular C-H $\cdots$ O interactions involved in linking of dimeric assembly in crystals of  $4\cdot\text{CHCl}_3$  and  $4\cdot\text{CHBr}_3$ .

	D-H $\cdots$ A	D-H (Å)	H $\cdots$ A (Å)	D $\cdots$ A (Å)	D-H $\cdots$ A (°)
$4\cdot\text{CHCl}_3$	C(1)-H(1) $\cdots$ O(11)#1	0.98	2.60	3.402(10)	139
	C(3)-H(3) $\cdots$ O(11)#1	0.98	2.37	3.246(10)	148
	C(5)-H(5) $\cdots$ O(11)#1	0.98	2.55	3.381(10)	143
	C(37)-H(37) $\cdots$ O(9)#1	0.93	2.74	3.532(13)	144
$4\cdot\text{CHBr}_3$	C(1)-H(1) $\cdots$ O(11)#2	0.98	2.55	3.356(6)	140
	C(3)-H(3) $\cdots$ O(11)#2	0.98	2.46	3.297(6)	143
	C(5)-H(5) $\cdots$ O(11)#2	0.98	2.41	3.278(7)	147

Symmetry codes: #1 -x+1,-y,-z; #2 -x+2,-y+1,-z+1.



### Identical Molecular String Formation

Although, overall organization of the host molecules is different in  $4 \cdot \text{CHCl}_3$  and  $4 \cdot \text{CHBr}_3$ , the C-H $\cdots$ O linked centrosymmetric assemblies formed identical polymeric molecular string<sup>137</sup> via dimeric C40-H40 $\cdots$ O7 contact [H40 $\cdots$ O7 = 2.55 Å, C40 $\cdots$ O7 = 3.320(9) Å,  $\angle$ C40-H40 $\cdots$ O7 = 140° in  $4 \cdot \text{CHCl}_3$  and H40 $\cdots$ O7 = 2.77 Å, C40 $\cdots$ O7 = 3.579(8) Å,  $\angle$ C40-H40 $\cdots$ O7 = 146° in  $4 \cdot \text{CHBr}_3$ ] and  $\pi \cdots \pi$  stacking interaction between phenyl ring (Cg5) of C5-O-benzoyl group (Cg5 $\cdots$ Cg5 = 3.993 Å in  $4 \cdot \text{CHCl}_3$  and 3.729 Å in  $4 \cdot \text{CHBr}_3$ ) along the a-axis in both solvates (**Figure 3.21**). It is important to mention here that in dihalomethane inclusion complexes of **4**, the carbonyl oxygen O7 was engaged in centrosymmetric C-H $\cdots$ O synthon formation but in trihalomethane inclusion crystals they are involved in bridging dimeric trifurcated C-H $\cdots$ O assemblies.

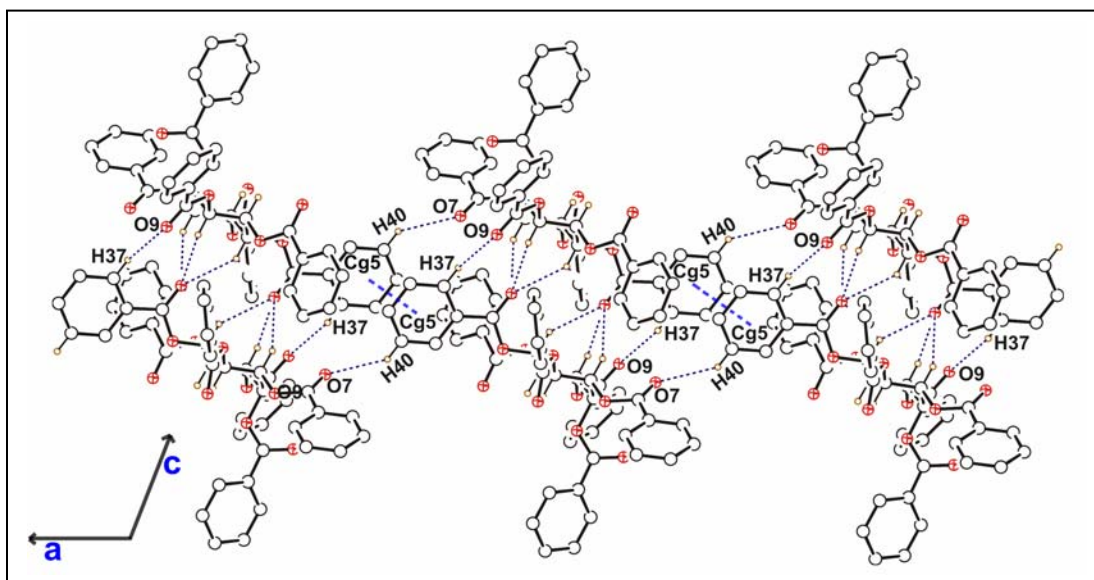


**Figure 3.21.** Interlinking of centrosymmetric C-H $\cdots$ O assemblies via C-H $\cdots$ O and  $\pi \cdots \pi$  interactions along a-axis in  $4 \cdot \text{CHCl}_3$ .

***Differences in Association of Identical Molecular String***

These identical molecular strings are bridged differently along other two directions leading to different molecular framework in **4·CHCl<sub>3</sub>** and **4·CHBr<sub>3</sub>**. In **4·CHCl<sub>3</sub>**, they are linked via centrosymmetric C11-H11···O8 contact [H11···O8 = 2.75 Å, C11···O8 = 3.653(19), ∠C11-H11···O8 = 163°] and π···π stacking interaction between phenyl ring (Cg1···Cg1 = 3.971 Å) of C1-*O*-benzoyl group along the *c*-axis, forming two dimensional open framework structures (**Figure 3.22A**), whereas in **4·CHBr<sub>3</sub>**, these identical molecular strings are connected via C19-H19···O9 contact [H19···O9 = 2.64 Å, C19···O9 = 3.449(8) Å, ∠C19-H19···O9 = 146°] along the *c*-axis forming another type of open framework structure (**Figure 3.22B**).

Packing of the host molecules in **4·CHCl<sub>3</sub>** and **4·CHBr<sub>3</sub>** is also different down the *c*-axis. The identical molecular string are linked diversely along *b*-axis in **4·CHCl<sub>3</sub>** and **4·CHBr<sub>3</sub>** forming different two-dimensional molecular network. In **4·CHCl<sub>3</sub>**, they are linked via dimeric C32-H32···π [H32···Cg3 = 3.30 Å, C32···Cg3 = 3.866(10) Å, ∠C32-H32···Cg3 = 121°] interactions (**Figure 3.23A**) whereas in **4·CHBr<sub>3</sub>**, they are associated via C26-H26···O12 [H26···O12 = 2.80 Å, C26···O12 = 3.574(9) Å, ∠C26-H26···O12 = 141°] and good C12-H12···π [H12···Cg3 = 2.63 Å, C32···Cg3 = 3.422(7) Å, ∠C32-H32···Cg3 = 144°] interactions (**Figure 3.23B**).

Further, the molecular packing down *a*-axis is different in **4·CHCl<sub>3</sub>** and **4·CHBr<sub>3</sub>**. The centrosymmetric C-H···O assemblies are linked via dimeric C11-H11···O8 and π···π contact (Cg1···Cg1) along the *c*-axis and along *b*-axis these assemblies are not involved in any significant contacts (**Figure 3.24A**) in **4·CHCl<sub>3</sub>**, whereas in **4·CHBr<sub>3</sub>**, they are

associated via C19-H19...O9 along c-axis and C26-H26...O12 contact along b-axis (Figure 3.24B).

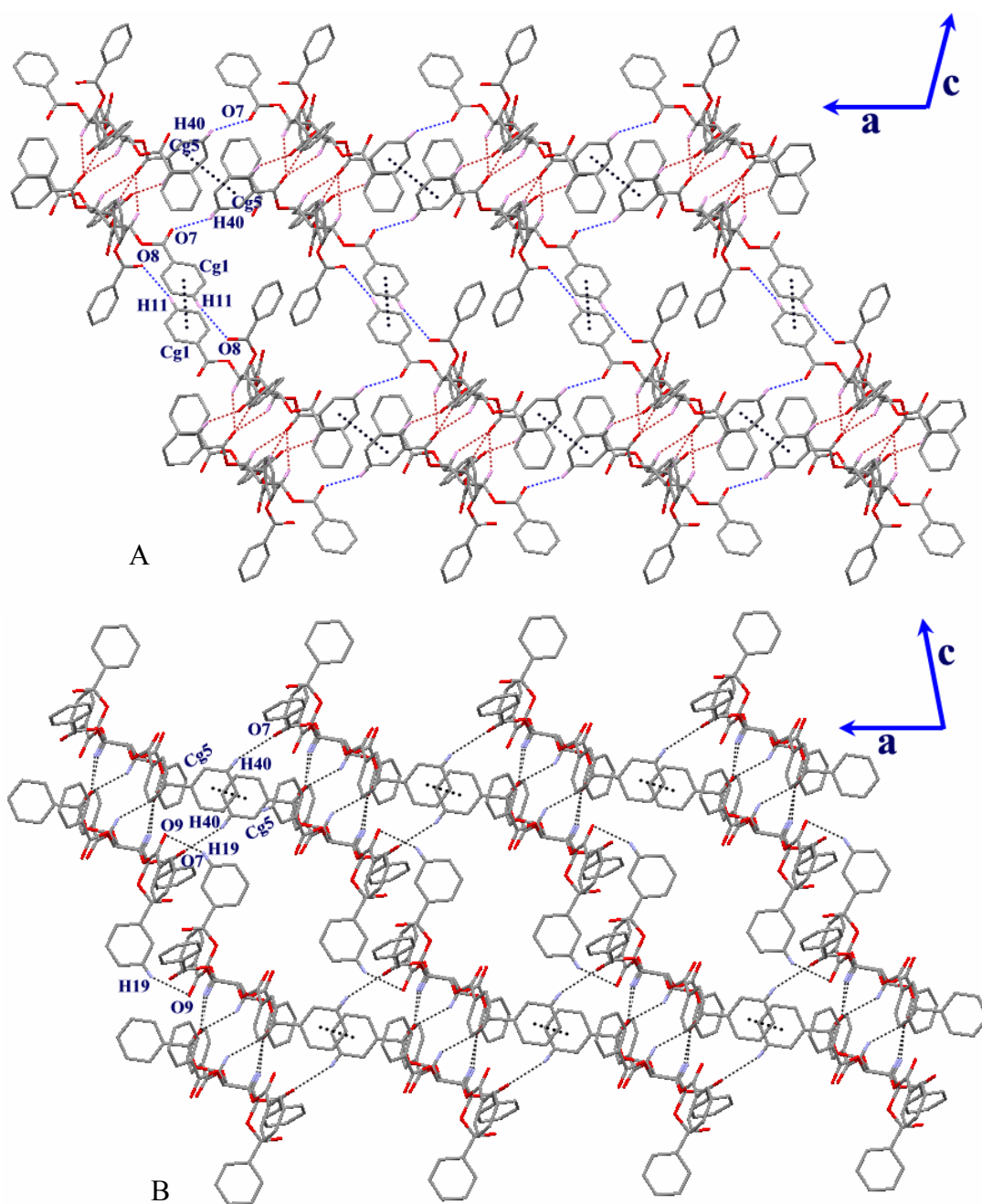


**Figure 3.22.** Association of the identical molecular strings along c-axis, A) via C11-H11...O and  $\pi \cdots \pi$  interactions in  $4 \cdot \text{CHCl}_3$  and B) via C19-H19...O9 interactions in  $4 \cdot \text{CHBr}_3$ .

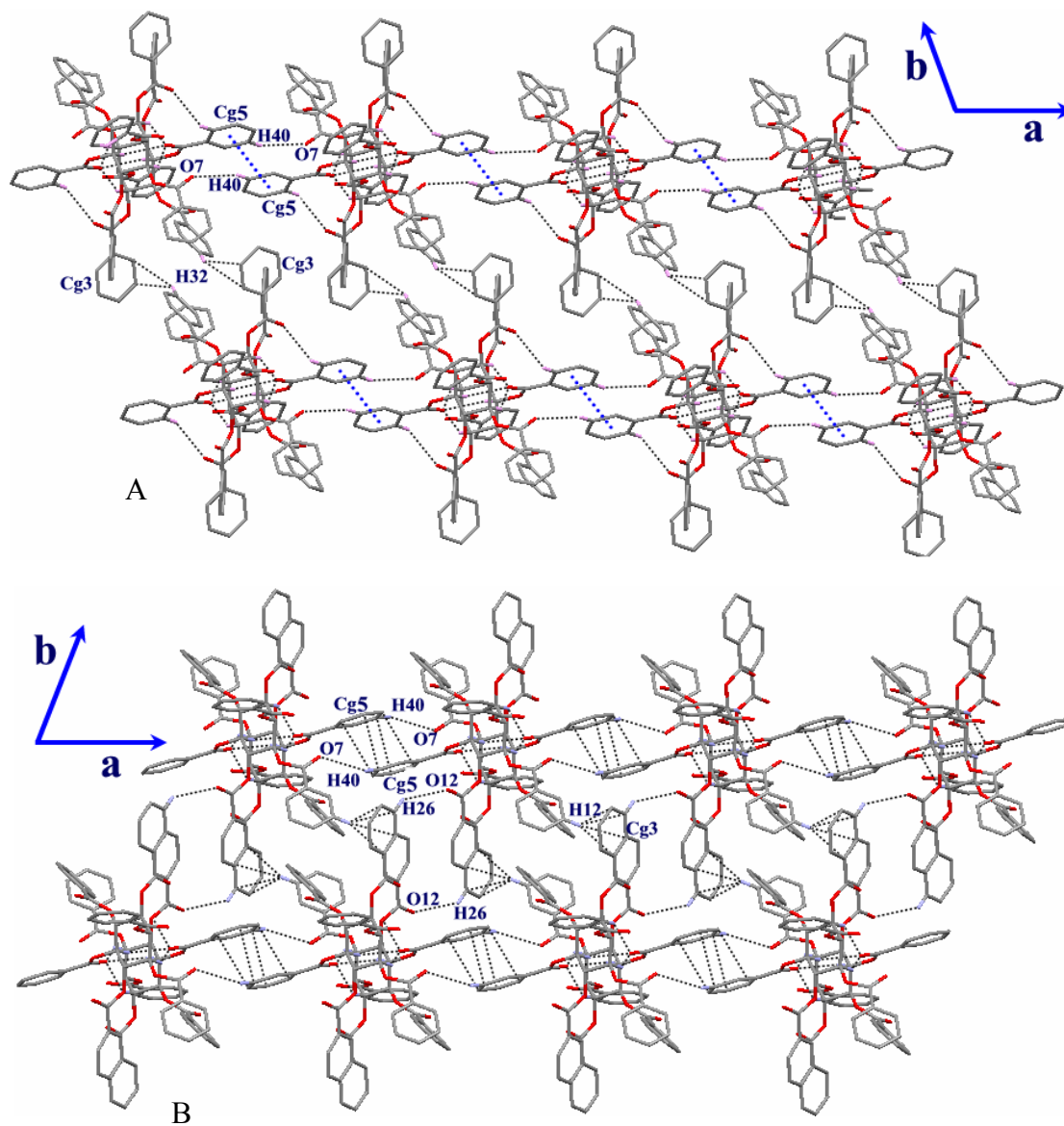


**Figure 3.23.** Association of identical molecular strings along b-axis, A) via C32-H32 $\cdots\pi$  interactions in  $4 \cdot \text{CHCl}_3$  and B) via C26-H26 $\cdots\text{O12}$  and C12-H12 $\cdots\pi$  interactions in  $4 \cdot \text{CHBr}_3$ .

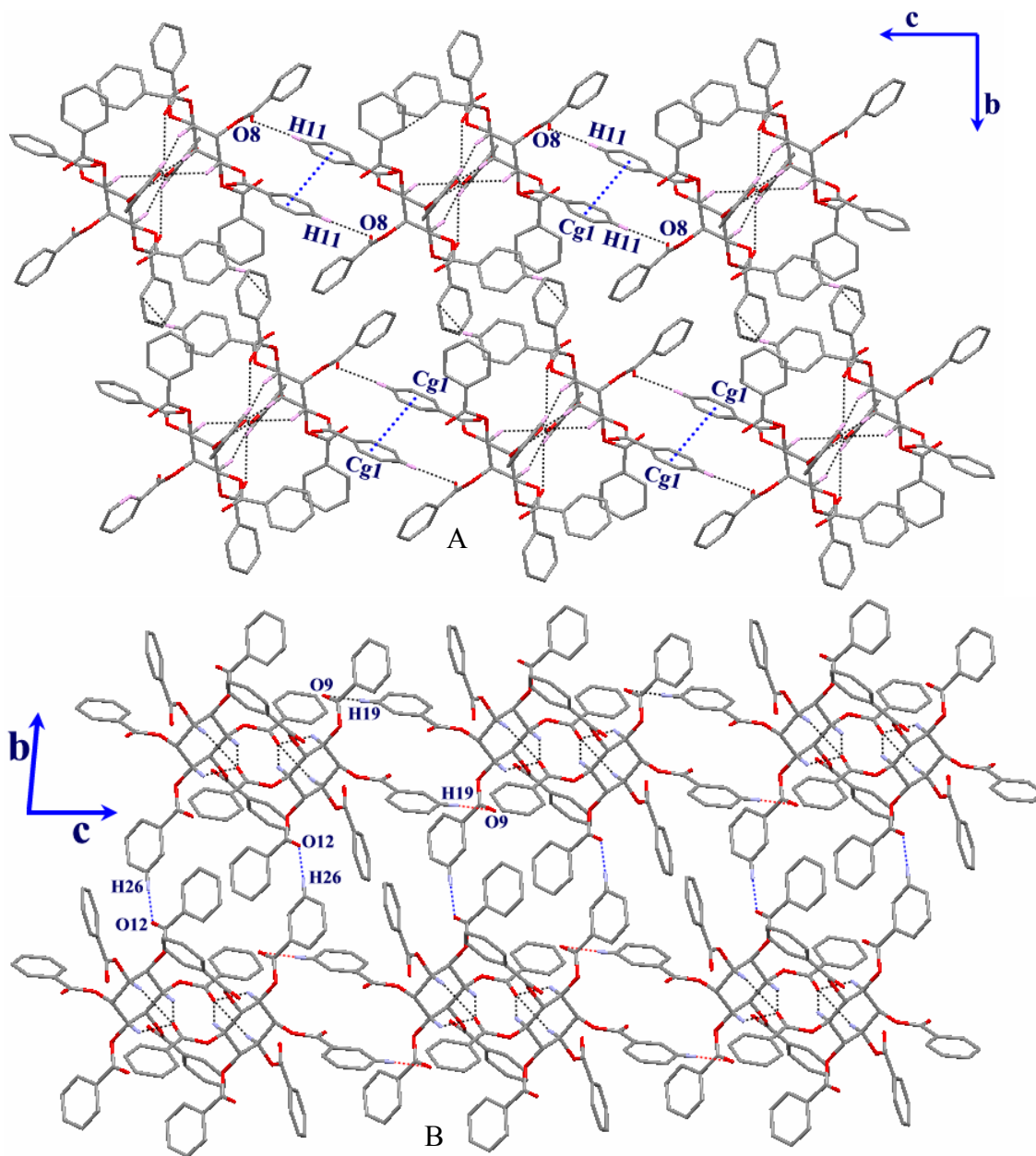


**Figure 3.24.** Bridging of centrosymmetric C-H...O assembly down a-axis in A)  $4 \cdot \text{CHCl}_3$  and B)  $4 \cdot \text{CHBr}_3$ .

### *Host-Guest Association and Interactions in 4·CHCl<sub>3</sub>*

Molecular packing roughly viewed down the a-axis shows (**Figure 3.25**) the host-guest association in **4·CHCl<sub>3</sub>**. The centrosymmetric trifurcated assemblies along the c-axis bridge by the guest chloroform molecules via C-H···O and halogen-oxygen short contact, whereas along the b-axis no significant interactions observed. Due to the bigger size of the guest molecules (compared to dihalomethane), the host dimeric assemblies, which have direct link in dihalomethane inclusion crystals via C34-H34···O10 and C17-H17···O12 interactions, expand breaking up these host-host interactions (**Figure 3.26**). The guest molecules are accommodated in two different channels. The chloroform molecules having regular geometry, bridge the dimeric units along the c-axis whereas the two disordered chloroform molecules occupy the channel created by four centrosymmetric assemblies in their center.

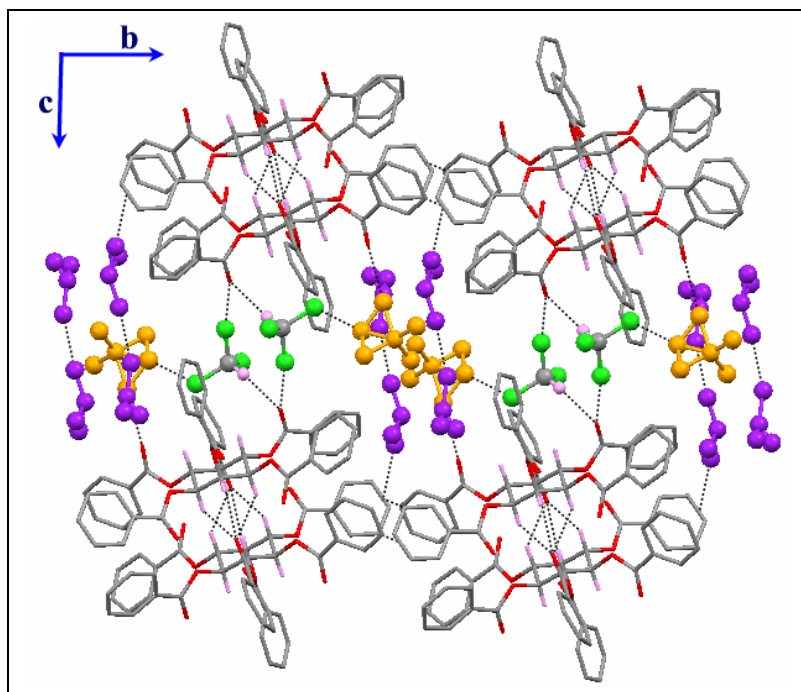


**Figure 3.25.** Host-guest association in **4·CHCl<sub>3</sub>**.

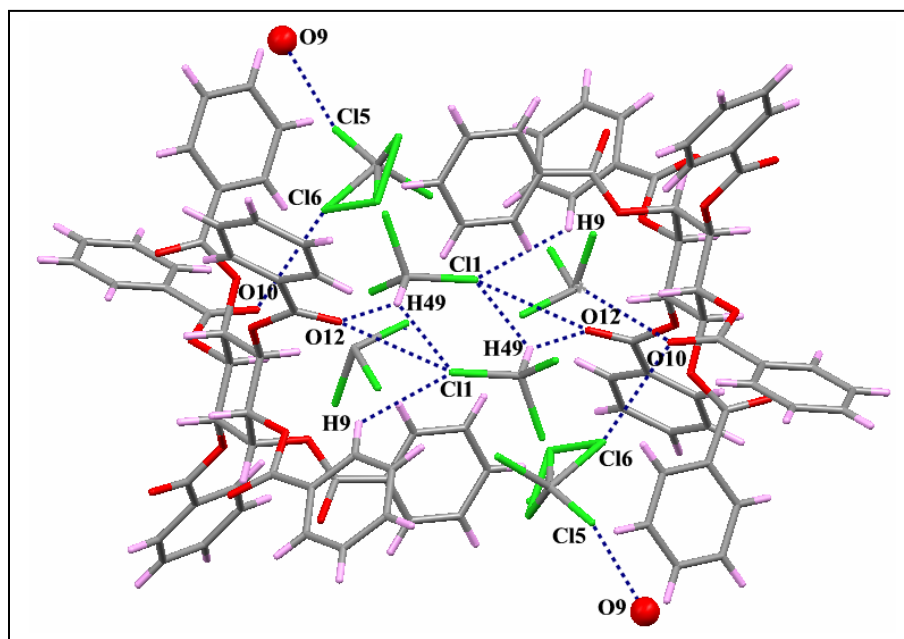


**Figure 3.26.** Bridging of host molecules via guest chloroform molecules in inclusion crystals of  $4 \cdot \text{CHCl}_3$ .

The ordered chloroform molecule (CLO1) makes various contacts with the host, the notable one are the C-H...O interaction between the H-atom (H49) of the chloroform molecules with carbonyl oxygen O12 and the ‘halogen bonding’ contacts between the chlorine atom Cl1 of CLO1 with carbonyl oxygen O12 of the host molecule. The halogen bonding (halogen-oxygen) contact is almost linear and the distance Cl1...O12 is much less than the sum of van der Waals radii (**Table 3.15**). Thus the carbonyl oxygen O12 is involved in bifurcated interactions. Amongst other interactions, three C-H...Cl interactions such as C25-H25...Cl3, C49-H49...Cl1 and C9-H9...Cl1 also link the CLO1 molecule with the host. The angles of all these interactions average to around  $143^\circ$ . The Cl2 of CLO1 molecule also makes short Cl...Cl contact with the chlorine of the disordered chloroform molecule (CLO2). The chloroform molecule CLO2, which shows

rotational disorder has two of its chlorine atoms (Cl4 and Cl6) disordered over two positions whereas the third one is ordered (Cl5). The ordered chlorine atom Cl5 makes short and linear halogen bonding contact C50-Cl5...O9 and C2-H2...Cl5 contact with the host, whereas the disordered ones are involved in C-H...Cl and Cl...Cl short contacts (**Table 3.15**). Furthermore the disordered chlorine atom (Cl6) is involved in a linear halogen bonding contact C50-Cl6...O10 with the host molecule. It is noteworthy that those chlorine atoms, which are involved in halogen bonding contacts are have more occupancies. The third chloroform molecule CLO3 that is highly disordered over two positions is also involved in Cl...Cl contacts.

**Table 3.15:** Various host-guest interactions in **4·CHCl<sub>3</sub>**.

D-H/Cl...A	D-H/Cl (Å)	H/Cl...A (Å)	D...A (Å)	D-H/Cl...A (°)
C(49)-H(49)...O(12)#1	0.98	2.36	3.205(16)	143
C(49)-H(49)...Cl(1)#2	0.98	2.90	3.678(15)	137
C(9)-H(9)...Cl(1)#2	0.93	2.92	3.601(7)	139
C(25)-H(25)...Cl(3)#3	0.93	2.78	3.422(10)	127
C(40)-H(40)...Cl(4')#1	0.93	2.93	3.826(17)	161
C(2)-H(2)...Cl(5)#4	0.98	2.78	3.724(10)	161
C(49)-Cl(1)...O(12)#2	1.735(10)	3.174(9)		158.0
C(50)-Cl(5)...O(9)#5	1.683(13)	3.083(14)		165.0
C(50)-Cl(6)...O(10)#1	1.832(13)	3.178(8)		164.8

Symmetry codes: #1 x,y,z; #2 -x+1,-y,-z+1; #3 x+1,y+1,z; #4 x+1,y,z; #5 x-1,y,z.



Although chloroform molecules in  $4\cdot\text{CHCl}_3$  make good halogen bonding contacts, the host guest assembly is highly unstable. This may be because of the bigger size of the guest molecules in  $4\cdot\text{CHCl}_3$  compared to dihalomethane inclusion crystals of **4** resulting in the breaking of host-host contacts (**Figures 3.16** and **3.26**). Therefore as soon as the guest escapes from the lattice, the crystal collapses completely.

#### *Host-Guest Association and Interactions in $4\cdot\text{CHBr}_3$*

The host-guest assembly in  $4\cdot\text{CHBr}_3$  is interesting. Both bromoform molecules occupy different sites in the crystal lattice. Bromoform (BRO1) molecule having regular geometry, occupy the channel formed by the dimeric trifurcated C-H $\cdots$ O assembly via C40-H40 $\cdots$ O7, C19-H19 $\cdots$ O9 and  $\pi\cdots\pi$  interactions down the b-axis (**Figure 3.27A**) whereas the disordered BRO2 guest molecule is located at the inversion center (disordered across the inversion center) in voids created by C19-H19 $\cdots$ O9 and C26-H26 $\cdots$ O12 interactions down the a-axis (**Figure 3.27B**). Due to bigger size of the guest molecule compared to dihalomethane, the host assembly expands along the c-axis breaking up host-host interactions (**Figure 3.16** and **3.28A**). The BRO1 guest bridges the host molecules via various host-guest interactions notably by C-Br $\cdots$ O halogen bonding interactions (**Figure 3.28A**). The bromine atoms Br1, Br2 and Br3 of the BRO1 molecule make three excellent halogen-bonding interactions (C49-Br1 $\cdots$ O7, C49-Br2 $\cdots$ O10 and C40-Br3 $\cdots$ O12) with carbonyl oxygens O7, O10 and O12 of the host (**Table 3.16**). Further, the bromines of BRO1 are engaged in four C-H $\cdots$ Br (C17-H17 $\cdots$ Br2, C23-H23 $\cdots$ Br2, C26-H26 $\cdots$ Br3 and C41-H41 $\cdots$ Br3) interactions with the host and among these interactions, C41-H41 $\cdots$ Br3 is almost linear (**Table 3.16**). The disordered BRO2

molecule makes three C-H $\cdots$ Br contacts with the host (C10-H10 $\cdots$ Br4, C9-H9 $\cdots$ Br4) along with marginal C-Br $\cdots$ O (C50-Br4 $\cdots$ O12, Br4 $\cdots$ O12 = 3.360,  $\angle$ C50-Br4 $\cdots$ O12 = 130 $^\circ$ ) and C-Br $\cdots$  $\pi$  (Cg2) contacts (**Figure 3.28B**). Interestingly, the H-atom of the BRO1 molecule did not involved in any significant interaction with the host.

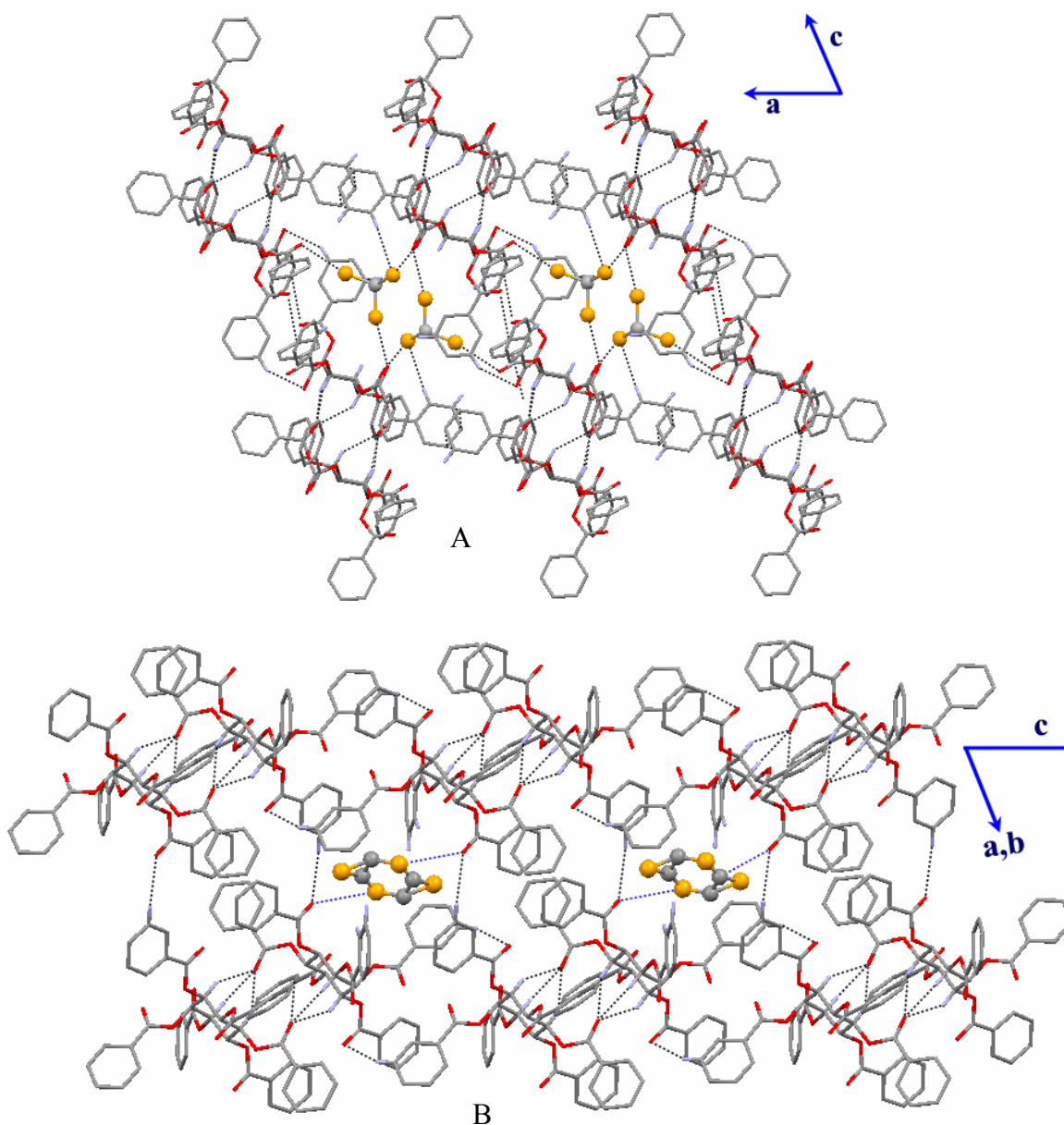


**Figure 3.27.** Guest molecules occupy different channels in 4-CHBr<sub>3</sub>, A) BRO1 and B) BRO2.

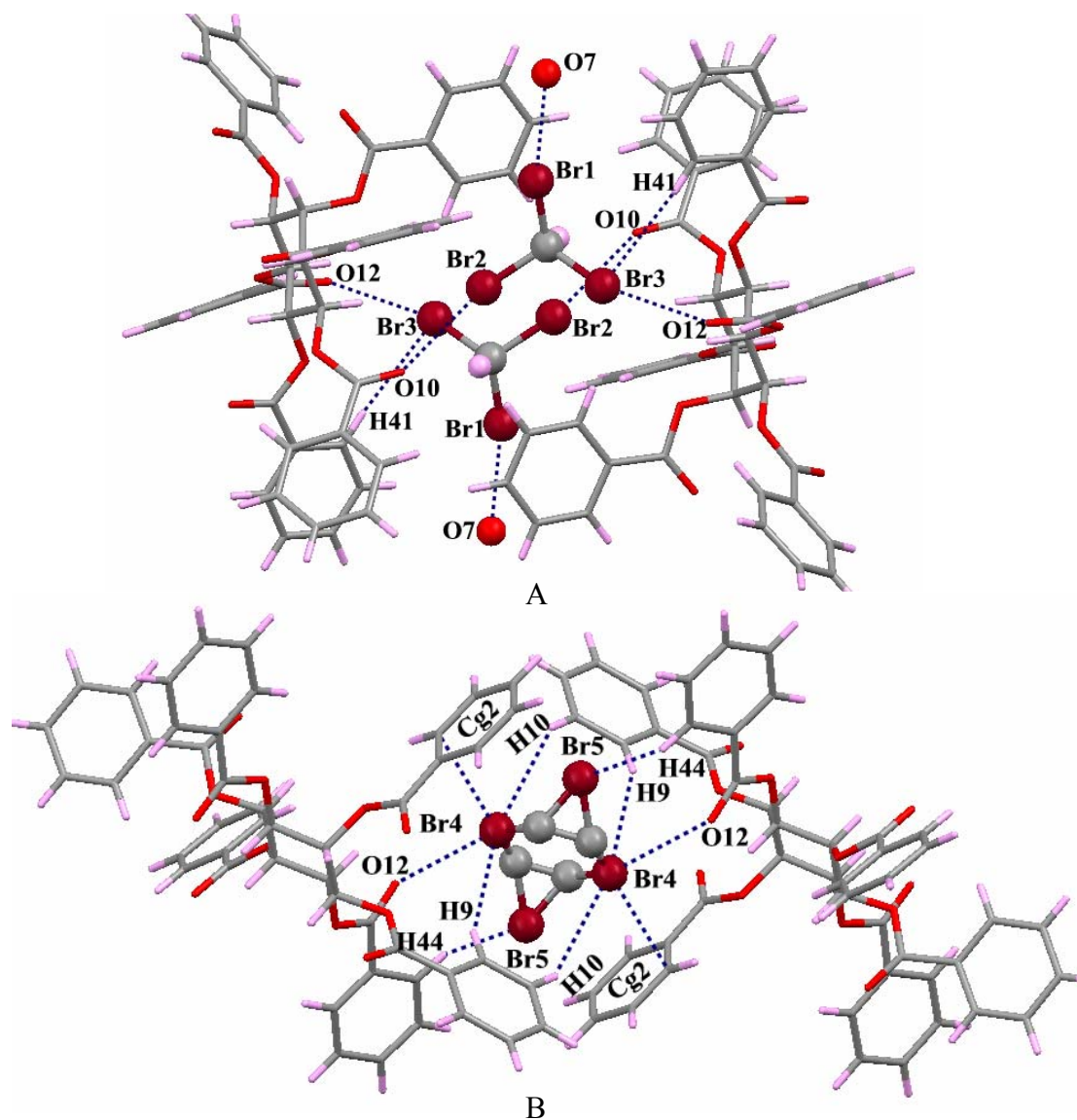


**Figure 3.28.** Host-guest interactions in 4-CHBr<sub>3</sub>, A) with ordered bromoform molecule (BRO1) and B) with disordered bromoform molecule (BRO2).

**Table 3.16:** Host-guest interactions in inclusion crystals of **4·CHBr<sub>3</sub>**.

D-H/Br...A	D-H/Br (Å)	H/Br...A (Å)	D...A (Å)	D-H/Br...A (°)
C(9)-H(9)···Br(4)#2	0.93	2.90	3.732(7)	149
C(10)-H(10)···Br(4)#3	0.93	3.09	3.809(8)	135
C(44)-H(44)···Br(5)#3	0.93	2.71	3.461(7)	138
C(17)-H(17)···Br(2)#1	0.93	3.07	3.892(6)	149
C(23)-H(23)···Br(2)#4	0.93	3.11	3.850(7)	138
C(26)-H(26)···Br(3)#5	0.98	3.12	3.951(8)	150
C(41)-H(41)···Br(3)#1	0.93	3.03	3.956(6)	174
C(49)-Br(1)···O(7)#6	1.904(5)	3.188(4)		166.4
C(49)-Br(2)···O(10)#4	1.918(6)	3.012(4)		166.7
C(49)-Br(3)···O(12)#1	1.912(6)	3.209(5)		165.1

Symmetry codes: #1  $x,y,z$ ; #2  $x,y,z+1$ ; #3  $-x+2,-y,-z+1$ ; #4  $-x+1,-y+1,-z+2$ ;  
#5  $x,y+1,z$ ; #6  $-1+x,y,z$ .

Although the included bromoform molecules in **4·CHBr<sub>3</sub>** are involved in excellent halogen bonding contacts with the host, these inclusion crystals are unstable in open atmosphere. The breaking of host-host contacts in accommodating the bulkier guest may be the reason for its instability.

### 3.3.5 Crystal Structure of Dioxane Solvated Crystals ( $4 \cdot C_4H_8O_2$ )

The dioxane inclusion crystals ( $4 \cdot C_4H_8O_2$ ) are isomorphous with dihalomethane inclusion crystals (Tables 3.3 and 3.6). Crystal structure determination revealed three molecules of dioxane are present in the crystal lattice per one molecule of the host. Two dioxane molecules had full occupancy. The third is only half occupied. For the third dioxane molecule, which was disordered, restrained refinement was carried out to keep the geometry stereochemically reasonable throughout the least-squares cycles of refinement.

#### *Host Organization in $4 \cdot C_4H_8O_2$*

Host molecules in  $4 \cdot C_4H_8O_2$  also formed centrosymmetric trifurcated C-H $\cdots$ O assembly like dihalomethane inclusion crystals of **4** (Figure 3.13). The three axial H-atoms H1, H3 and H5 of the *myo*-inositol ring from each molecule make contacts with the carbonyl oxygen O11 of the other molecule. In addition to the trifurcated C-H $\cdots$ O interactions; centrosymmetric C37-H37 $\cdots$ O7 interaction also bridges these dimers thereby strengthening the dimeric trifurcated C-H $\cdots$ O assemblies (Table 3.17).

**Table 3.17:** Intermolecular C-H $\cdots$ O interactions involved in the formation of dimeric assembly in  $4 \cdot C_4H_8O_2$ .

D-H $\cdots$ A	D-H (Å)	H $\cdots$ A (Å)	D $\cdots$ A (Å)	D-H $\cdots$ A (°)
C(1)-H(1) $\cdots$ O(11)#1	0.98	2.35	3.202(5)	146
C(3)-H(3) $\cdots$ O(11)#1	0.98	2.62	3.394(6)	136
C(5)-H(5) $\cdots$ O(11)#1	0.98	2.52	3.343(6)	141
C(37)-H(37) $\cdots$ O(7)#1	0.93	2.55	3.446(6)	161
C(17)-H(17) $\cdots$ O(12)#2	0.93	2.68	3.604(8)	170
C(34)-H(34) $\cdots$ O(10)#3	0.93	2.73	3.646(7)	169

Symmetry codes: #1 -x+1,-y,-z+1; #2 -x,-y+1,-z+1; #3 -x,-y,-z+1.

The trifurcated C-H $\cdots$ O linked centrosymmetric assemblies (**Figure 3.13**) are linked via centrosymmetric C34-H34 $\cdots$ O10 interaction forming discrete pillars along the a-axis as observed in dihalomethane inclusion crystals of **4** (**Figure 3.29A**). The neighbouring pillars are bridged via guest dioxane molecules along the c-axis. Unlike dihalomethane inclusion crystals of **4**, there is no direct interaction between the pillars in **4**·C<sub>4</sub>H<sub>8</sub>O<sub>2</sub>. The C17-H17 $\cdots$ O12 interaction also links the centrosymmetric C-H $\cdots$ O dimers in different fashion forming another type of distinct columnar assembly (**Figure 3.29B**). Both type of assemblies create thorough open channel between them, which is filled by the guest dioxane molecules. The geometrical parameters of C34-H34 $\cdots$ O10 and C17-H17 $\cdots$ O12 interactions are much better than the trifurcated C-H $\cdots$ O assembly (**Table 3.18**).

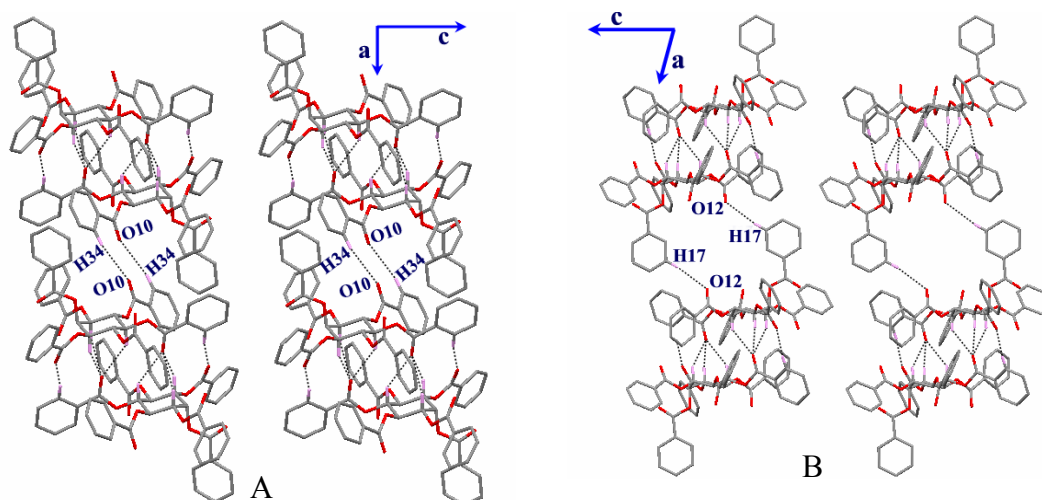


**Figure 3.29.** Different columnar assemblies formed by host molecules of **4**·C<sub>4</sub>H<sub>8</sub>O<sub>2</sub>, linking of centrosymmetric C-H $\cdots$ O dimers A) via C34-H34 $\cdots$ O10 and B) via C17-H17 $\cdots$ O12 contacts.

*Host-Guest Association in  $4 \cdot C_4H_8O_2$* 

The host-guest assembly of  $4 \cdot C_4H_8O_2$  is somewhat different than halogen containing inclusion crystals of **4**. Packing diagram shows the presence of three molecules of dioxane in the crystal lattice. One of the dioxane molecules (DIOX1 (brown), **Figure 3.30**) occupies the void created by centrosymmetric C-H $\cdots$ O dimeric assembly whereas the other two dioxane molecules [DIOX 2 (purple) and DIOX 3 (red)] are located in the open channel created by the pillars.

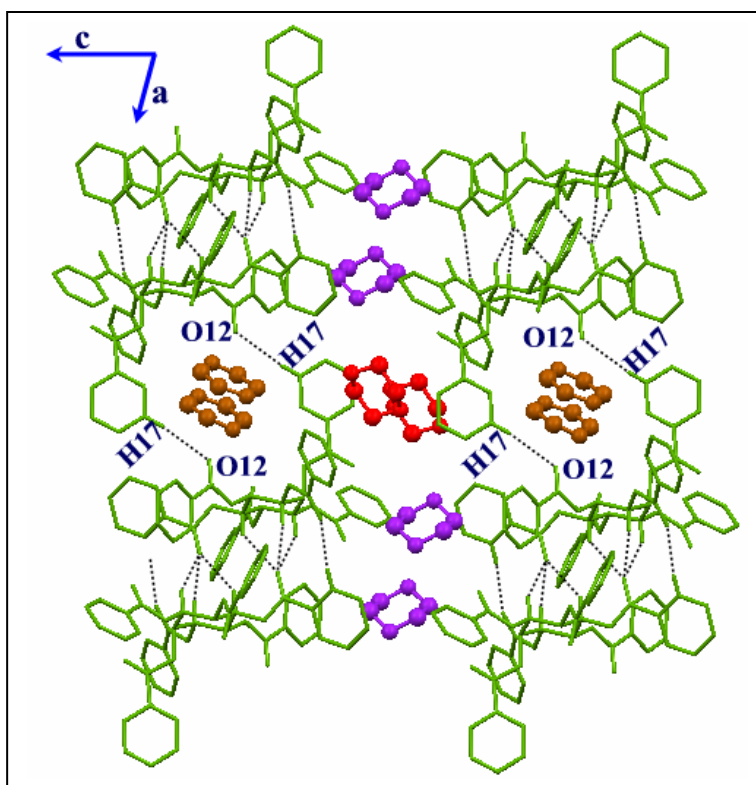


**Figure 3.30.** Host-guest assembly viewed down the b-axis in  $4 \cdot C_4H_8O_2$ .

*Host-Guest Interactions in 4·C<sub>4</sub>H<sub>8</sub>O<sub>2</sub>*

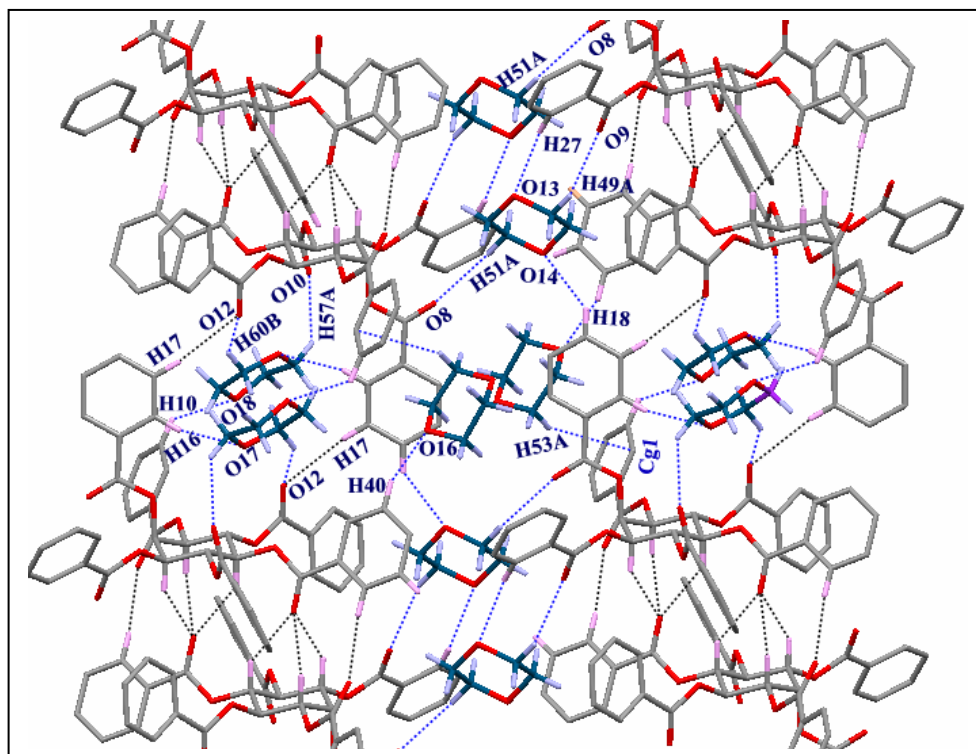
In inclusion crystals  $4\cdot\text{C}_4\text{H}_8\text{O}_2$ , voids created by C17-H17...O12 interaction accommodates half occupied dioxane molecule (DIOX1) whereas the open channel created by columnar assemblies along the a-axis contains two molecules of dioxane (DIOX2 and DIOX3). DIOX1 molecule makes a number of C-H...O interactions with the host. The C57 and C60 of the dioxane molecule donate their methylene hydrogen H57A and H60B to the carbonyl oxygen O10 and O12 of the host respectively. On the other hand, the ether oxygens O17 and O18 of the same dioxane molecule accept protons from C16-H16 and C17-H16 of the host respectively. Remaining two dioxane molecules (DIOX2 and DIOX3) bridge the two pillars via several C-H...O contacts. The dioxane molecule DIOX2 (purple in **Figure 3.30**) stitches the two trifurcated C-H...O assemblies along the c-axis whereas DIOX 3 (red) occupies the space created by four such trifurcated C-H...O associations in their center. The dioxane molecule DIOX2 makes five C-H...O interactions with the host (**Table 3.18**). The ether oxygens O13 and O14 of DIOX2 accepts proton from C11-H11, C18-H18 and C27-H27 of the host whereas it donates two of its protons H49A and H51A to the carbonyl oxygens O9 and O8 respectively of the host. The dioxane molecule DIOX3 makes one C-H...O (C40-H40...O16) contact and almost linear C-H... $\pi$  (C53-H53A...Cg1) interaction with phenyl ring of the C1-O-benzoyl group of the host (**Table 3.18** and **Figure 3.31**).



**Table 3.18:** Host-guest interactions in  $4 \cdot C_4H_8O_2$ .

D-H...A	D-H (Å)	H...A (Å)	D...A (Å)	D-H...A (°)
C(49)-H(49A)...O(9)#7	0.97	2.75	3.380(8)	123
C(51)-H(51A)...O(8)#1	0.97	2.66	3.417(8)	135
C(57)-H(57A)...O(10)#2	0.97	2.56	3.498(17)	161
C(60)-H(60B)...O(12)#2	0.97	2.67	3.412(7)	134
C(11)-H(11)...O(13)#3	0.93	2.53	3.307(7)	141
C(27)-H(27)...O(13)#4	0.93	2.59	3.474(6)	160
C(16)-H(16)...O(17)#5	0.93	2.64	3.415(9)	142
C(18)-H(18)...O(14)#5	0.93	2.64	3.335(7)	132
C(40)-H(40)...O(16)#6	0.93	2.77	3.465(7)	132
C(10)-H(10)...O(18)#8	0.93	2.77	3.368(6)	123
C(53)-H(53A)...Cg(1)#1	0.97	2.82	3.757(7)	162

Symmetry codes: #1  $-x+1, -y+1, -z$ ; #2  $x+1, y, z$ ; #3  $x, y, z$ ; #4  $x, y-1, z$ ; #5  $x-1, y, z$ ; #6  $-x, -y+1, -z+2$ ; #7  $x, y+1, z$ ; #8  $-x+1, -y+1, -z+1$ .

**Figure 3.31.** Host-guest interactions in  $4 \cdot C_4H_8O_2$ .

### 3.4 Conclusions

Hexa-*O*-benzoyl *myo*-inositol showed polymorphic and pseudopolymorphic behaviour. *myo*-Inositol hexabenzoate (**4**) having *meso* configuration produces chiral polymorph when crystallized rapidly but yields achiral polymorph when allowed to crystallize slowly. In the mother liquor the chiral polymorph slowly but completely converts to give achiral polymorph. The spontaneous generation of chirality (formation of the chiral crystals of an achiral compound) is quite unusual and an enigmatic phenomenon which has fascinated chemists and biologists.<sup>138</sup> The chiral crystals capable of showing optical activity can be compared with a class of crystals where the activity is due to the helical arrangement of the molecules in the entire lattice (e.g. quartz) rather than configurational or conformational<sup>139</sup> chirality of individual molecules.

Compound **4** also formed the highly unstable inclusion crystals, which could be stabilized by coating with paraffin oil. Inclusion crystals with dihalomethane solvents showed guest dynamics when kept in paraffin oil; of the two molecules of dihalomethane present in crystals of **4**, one molecule was able to escape while standing in the paraffin for ~ 6 h, but the crystal collapsed when retained dihalomethane molecule left the crystal lattice. The inclusion crystals with haloform solvents were also unstable. Although the guest molecule made excellent halogen bonding contact with the host, it could not hold the host-guest assembly firmly. This could be because of a compromise in host-host interactions. Although, the included dioxane molecules in crystals of **4** made several C-H...O interactions with the host, they could not stabilize the host-guest assembly. From this observation it seems that C-H...O contacts alone are not sufficient to stabilize the

inclusion crystals in the absence of halogen bonding interactions. In all the inclusion crystals of **4**, the host molecules formed centrosymmetric trifurcated C-H...O assembly similar to inclusion complexes of **3** (Chapter 2). But the associations of these dimeric units differ in **4** as compared to **3**. In **3**, the included dihalomethane molecule bridges these dimeric units across the two-fold axis, whereas in **4** the dimeric units are associated via weak C-H...O contacts creating voids to accommodate the guest molecules.

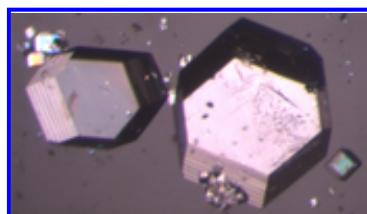
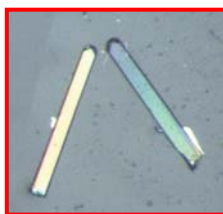
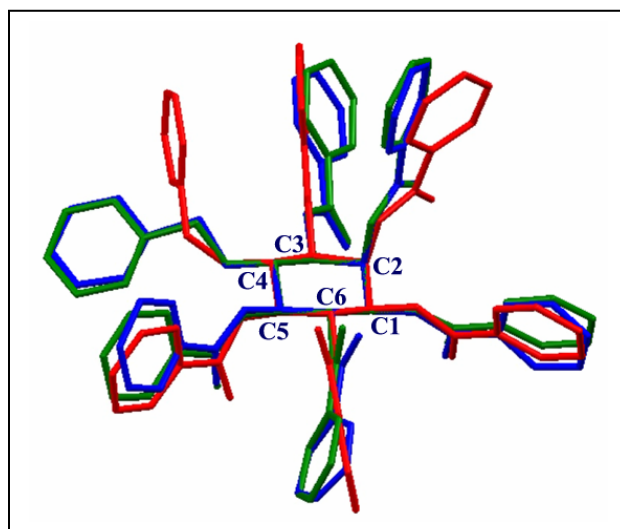
# Chapter 4

**Pseudopolymorphic Behaviour of Racemic 1, 2, 3,**

**5, 6-penta-*O*-benzoyl-4-*O*-benzyl-*myo*-inositol:**

**Synthesis, Crystallization and X-ray**

**Crystallographic Studies**



# Chapter 4

## 4.1 Introduction

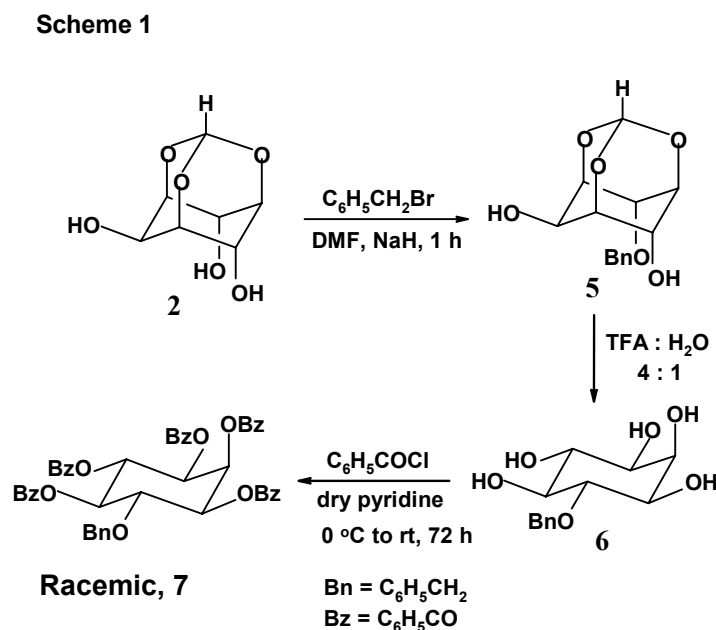
In continuation with the investigation of inclusion behaviour of hexa-*O*-substituted-*myo*-inositol derivatives, racemic 1, 2, 3, 5, 6-penta-*O*-benzoyl-4-*O*-benzyl-*myo*-inositol (**7**) was synthesized. This derivative is obtained by replacing the tosyl group in **3** by a benzyl group (Chapter 2). Interestingly, with a very close similarity to **3**, compound **7** yielded highly unstable inclusion crystals with the halogenated solvents. The molecular organization in **7** was similar to compound **4** (Chapter 3) and even the inclusion tendency towards halogenated solvents was similar. A detail study of structures of the solvent free form and the solvates of **7** are discussed in this chapter.

## 4.2 Experimental Section

### 4.2.1 Synthesis:

Racemic **7** was prepared from *myo*-inositol-1,3,5-orthoformate (**2**) in three steps (**Scheme 4.1**). Benzyl bromide (0.360 g, 2.1 mmol) was added to a stirred solution of *myo*-inositol 1,3,5-orthoformate (**2**) (0.360 g, 2 mmol) and sodium hydride (0.08, 2 mmol) in DMF (5 ml). Stirring of the reaction mixture at room temperature was continued for one hour. TLC confirmed the completeness of the reaction. After usual

work up and evaporation of the solvent, racemic 4-*O*-benzyl *myo*-inositol 1,3,5-orthoformate (**5**) obtained as a gum. The orthoformate bridge in **5** was then cleaved by stirring with trifluoroacetic acid (TFA) and water mixture (4:1) for 3 to 4 hours at room temperature. Excess of TFA was evaporated under reduced pressure and the residue washed 2 to 3 times with toluene when racemic 4-*O*-benzyl-*myo*-inositol (**6**) was obtained as solid. To a stirred cooled solution (in ice bath) of **6** (0.411 g, 1.51 mmol) in dry pyridine (10 mL), benzoyl chloride (3.8 g, 27 mmol) was added drop wise and the reaction mixture was allowed to come to room temperature. Stirring was continued for ~72 h. TLC confirmed the completeness of the reaction. Pyridine was removed under reduced pressure and the residue obtained was dissolved in chloroform and washed successively with water, dilute HCl, sodium bicarbonate solution, brine and finally dried over anhydrous sodium sulphate. The organic layer was evaporated under reduced pressure and the white solid (**7**) obtained (0.872 g, 66%) was purified by crystallization from ethyl acetate.



**Data for 7:**

**mp** 200-201 °C; **IR** (CHCl<sub>3</sub>)  $\nu$  = 1745, 1737, 1731, 1714, cm<sup>-1</sup>; **<sup>1</sup>H NMR** (CDCl<sub>3</sub>, 200 MHz):  $\delta$  4.47-4.56 (m, 2H), 4.65-4.69 (m, 1H), 5.71-5.78 (m, 2H), 5.84-5.94 (t, 1H), 6.19-6.29 (t, 2H), 6.98-7.09 (m, 5H), 7.21-7.31 (m, 5H), 7.36-7.46 (m, 5H), 7.50-7.66 (m, 4H), 7.66-7.70 (m, 2H), 7.79-7.91 (m, 5H), 7.96-8.10 (m, 4H); **Elemental analysis** calcd for C<sub>48</sub>H<sub>38</sub>O<sub>11</sub>; C 72.83%, H 4.61%; found C 72.41%, H 4.51%.

**4.2.2 Crystallization**

Crystallization of **7** was attempted from common organic solvents (**Table 4.1**) by vapour diffusion method (vapour of petroleum ether was diffused). The solvent free crystals were thin needles (**Figure 4.1A**) and stable at room temperature, whereas the inclusion crystals were highly unstable in the open atmosphere. The inclusion crystals obtained from chloroform were hexagonal in shape (**Figure 4.1B**) but lost crystallinity in 2-5 seconds (**Figure 4.1C**).

**Table 4.1:** Crystallization data of **7** from various solvents.

Entry No	Solvent Used	Method of Crystallization*	Result
1	Ethyl acetate	1	Solvent free crystals, <b>7</b>
2	Acetone	1	Solvent free crystals, <b>7</b>
3	Nitromethane	1	Solvent free crystals, <b>7</b>
4	Pyridine	1	Solvent free crystals, <b>7</b>
5	Acetonitrile	1	Solvent free crystals, <b>7</b>
6	Dioxane	2	Solvent free crystals, <b>7</b>
7	Tetrahydrofuran	1	Solvent free crystals, <b>7</b>
8	Dichloromethane	2	Pseudopolymorph, <b>7</b> ·CH <sub>2</sub> Cl <sub>2</sub>
9	Dibromomethane	2	Pseudopolymorph, <b>7</b> ·CH <sub>2</sub> Br <sub>2</sub>
10	Chloroform	2	Pseudopolymorph, <b>7</b> ·CHCl <sub>3</sub>
11	Bromoform	2	Solvent free crystals, <b>7</b>
12	Dichlorobromomethane	2	Pseudopolymorph, <b>7</b> ·CHCl <sub>2</sub> Br

\*1= slow evaporation, 2 = vapour diffusion

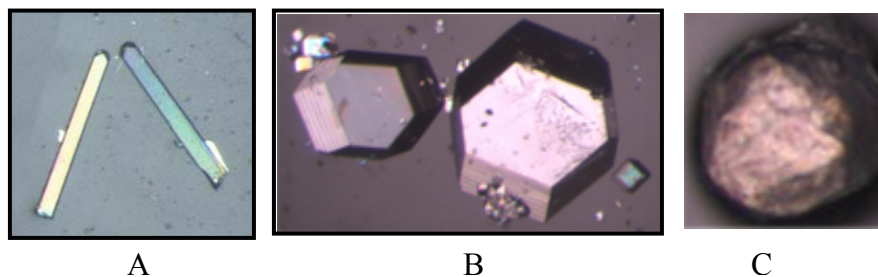


**Figure 4.1.** Photomicrographs of crystals of **7**, A) solvent free crystals obtained from ethyl acetate, B) inclusion crystals with chloroform ( $7 \cdot \text{CHCl}_3$ ) and C) crystals with chloroform left in open atmosphere ( $\sim 2$ -5 sec).

#### 4.2.3 Differential Scanning Calorimetric Analysis (DSC)

DSC studies of the solvent free crystals of **7** showed two sharp endothermic peaks (**Figure 4.2**), the first one at  $186^\circ\text{C}$  ( $\Delta H = 8.7 \text{ J/g}$ ) suggesting a possible phase transition and the second one at  $203^\circ\text{C}$  corresponding to the melting of the crystal ( $\Delta H = 36.0 \text{ J/g}$ ). The DSC studies of the inclusion crystals of **7** could not be carried out because of the high instability.

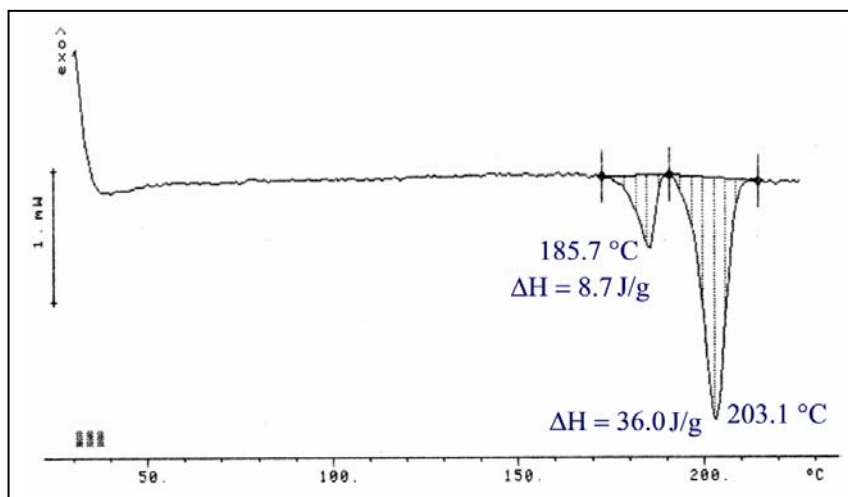


**Figure 4.2.** DSC profile of solvent free crystals of **7**.



#### 4.2.4 Data Collection, Structure Solution and Refinement

X-ray diffraction data of solvent free crystal (**7**) were collected at room temperature, whereas data of pseudopolymorphs (coated in paraffin oil) **7**·**CH<sub>2</sub>Cl<sub>2</sub>**, **7**·**CH<sub>2</sub>Br<sub>2</sub>**, **7**·**CHCl<sub>3</sub>** and **7**·**CHCl<sub>2</sub>Br** were collected at 133(2) K using SMART APEX CCD diffractometer with graphite monochromated MoK<sub>α</sub> radiation ( $\lambda = 0.71073 \text{ \AA}$ ). The solvent free crystal of **7** diffracted very weakly, whereas inclusion crystals diffracted moderately. The solvent free crystal of **7** was monoclinic *C2/c* and all the solvates were triclinic P-1. Due to weak diffracted intensities, the least-squares refinement of **7** could not be carried out using high angles data as some of the atoms were non-positive definite when allowed to go anisotropic. Therefore, this structure was refined to  $\theta = 23^\circ$  whereas, all other structure were refined to  $\theta = 25^\circ$ . SHELX-97 was used for structure solution and full matrix least squares refinement was carried out on  $F^2$ . Hydrogen atoms were included in the refinement as per the riding model. In all the inclusion crystals, the guest molecules had full occupancy. However, the stoichiometry of host to guest was 1:1 in **7**·**CH<sub>2</sub>Cl<sub>2</sub>** and **7**·**CH<sub>2</sub>Br<sub>2</sub>**, whereas 2:1 in **7**·**CHCl<sub>3</sub>** and **7**·**CHCl<sub>2</sub>Br** crystals. In **7**·**CH<sub>2</sub>Cl<sub>2</sub>** and **7**·**CHCl<sub>3</sub>** the difference Fourier also contained single peak with low height, which was included as a trace of water molecule with the occupancy of 0.2. In **7**·**CH<sub>2</sub>Br<sub>2</sub>** and **7**·**CHCl<sub>2</sub>Br** no such peak was observed. Crystallographic details are summarized in **Table 4.2**.

**Table 4.2:** Crystal data table for solvent free and solvates of 7.

	7	7·CH <sub>2</sub> Cl <sub>2</sub>	7·CH <sub>2</sub> Br <sub>2</sub>	7·CHCl <sub>3</sub>	7·CHCl <sub>2</sub> Br
Chemical formula	C <sub>48</sub> H <sub>38</sub> O <sub>11</sub>	C <sub>48</sub> H <sub>38</sub> O <sub>11</sub> · CH <sub>2</sub> Cl <sub>2</sub> · 0.2(H <sub>2</sub> O)	C <sub>48</sub> H <sub>38</sub> O <sub>11</sub> · CH <sub>2</sub> Br <sub>2</sub>	C <sub>48</sub> H <sub>38</sub> O <sub>11</sub> · 0.5(CHCl <sub>3</sub> )· 0.2(H <sub>2</sub> O)	C <sub>48</sub> H <sub>38</sub> O <sub>11</sub> · 0.5(CHCl <sub>2</sub> Br)
M <sub>r</sub>	790.78	875.71	964.63	850.47	872.19
Temperature/K	297(2)	133(2)	133(2)	133(2)	133(2)
Morphology	Thin needle	Prism	Plate	Hexagonal	Needle
Crystal size	0.53×0.07× 0.05	0.77×0.25× 0.21	0.51×0.45× 0.08	0.38×0.23× 0.20	0.18×0.15× 0.10
Crystal system	Monoclinic	Triclinic	Triclinic	Triclinic	Triclinic
Space group	<i>C2/c</i>	<i>P-1</i>	<i>P-1</i>	<i>P-1</i>	<i>P-1</i>
<i>a</i> (Å)	27.171(12)	13.617(11)	13.72(2)	13.853(8)	13.760(3)
<i>b</i> (Å)	6.580(3)	13.983(13)	13.93(2)	15.642(9)	15.566(4)
<i>c</i> (Å)	47.16(2)	14.829(13)	14.89(3)	22.301(13)	22.388(6)
$\alpha$ (°)	90	75.22(2)	75.06(3)	107.681(12)	108.009(4)
$\beta$ (°)	100.107(9)	63.15(2)	62.61(2)	91.857(13)	91.611(5)
$\gamma$ (°)	90	61.394(17)	61.03(2)	104.255(12)	104.322(5)
<i>V</i> (Å <sup>3</sup> )	8301(6)	2209(3)	2209(7)	4432(4)	4389.9(19)
<i>Z</i>	8	2	2	4	4
<i>D</i> <sub>calc</sub> (g cm <sup>-3</sup> )	1.266	1.317	1.450	1.275	1.320
$\mu$ (mm <sup>-1</sup> )	0.090	0.208	1.896	0.177	0.603
<i>F</i> (000)	3312	912	984	1772	1806
Ab.Correction	Multi-scan	Multi-scan	Multi-scan	Multi-scan	Multi-scan
<i>T</i> <sub>min</sub>	0.954	0.856	0.445	0.937	0.901
<i>T</i> <sub>max</sub>	0.995	0.957	0.869	0.965	0.940
$\theta$ <sub>max</sub> (°)	23	25	25	25	25
<i>h</i> , <i>k</i> , <i>l</i> (min, max)	(-29,29), (-7,7), (-51,30)	(-16,16), (-16,16), (-17,17)	(-16,16), (-16,16), (-17,17)	(-16,16), (-18,18), (-26,26)	(-16,16), (-18,18), (-26,26)
Reflns collected	13415	46216	19837	42756	40267
Unique reflns	5768	7738	7689	15565	15396
Observed reflns	2115	4433	2384	9080	4960
No. of paramet.	560	580	571	1188	1138
Restraints	0	0	4	12	10
GoF	0.890	1.047	0.940	1.031	0.914
R <sub>1</sub> [ <i>I</i> > 2σ( <i>I</i> )]	0.0864	0.1117	0.0986	0.0897	0.0852
wR <sub>2</sub> [ <i>I</i> > 2σ( <i>I</i> )]	0.1064	0.2764	0.2511	0.2186	0.1596
R <sub>1</sub> _all data	0.2387	0.1739	0.2610	0.1486	0.2719
wR <sub>2</sub> _all data	0.1432	0.3128	0.3455	0.2516	0.2264
Δ ρ <sub>max</sub> , Δ ρ <sub>min</sub> (eÅ <sup>-3</sup> )	0.19, -0.23	0.69, -0.57	0.64, -0.47	0.90, -0.30	0.638, -0.308

#### 4.2.5 Thermal Response on Hot Stage Microscopy

Observations in DSC prompted us to carry out Hot Stage Microscopy of solvent free crystals of **7**. Solvent free crystals of **7** were heated on Leica polarizing microscope equipped with a heating stage P350. Around 175 °C, the upper surface of the needles began shining with a change in colour (**Figure 4.3**) from orange (at room temperature) to magenta (~185 °C) and to blue (~195 °C). Each of the crystals retained their single crystalline nature even at 195 °C when observed under polarizer. However, the unit cell parameters of these needle like crystals after heating revealed them to belong to the same crystalline form as of those prior to heating. The reason for the appearance of the first endotherm, therefore, remains to be explained.

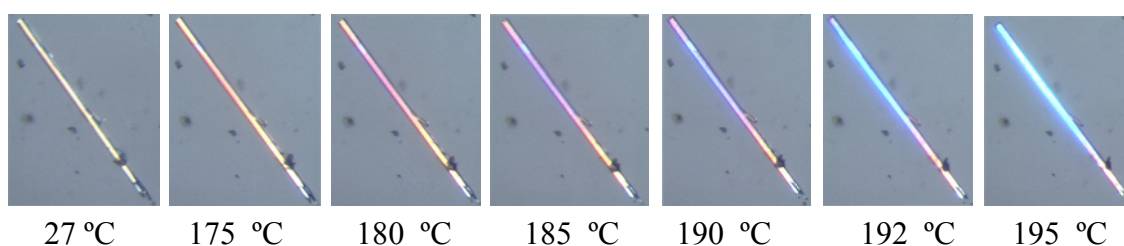


**Figure 4.3.** Photomicrographs of crystals of solvent free form of **7**.

### 4.3 Results and Discussion

The dihalomethane inclusion crystals of **7** ( $7 \cdot \text{CH}_2\text{Cl}_2$  and  $7 \cdot \text{CH}_2\text{Br}_2$ ) are isomorphs and the same is true for the trihalomethane inclusion crystals ( $7 \cdot \text{CHCl}_3$  and  $7 \cdot \text{CHCl}_2\text{Br}$ ). However, the unit cell parameters clearly revealed that the structure of the solvent free crystals (**7**) do not match with the pseudopolymorphs of **7**. Therefore, the solvent free crystals, dihalomethane inclusion crystals and trihalomethane inclusion crystals are categorized as Form I, Form II and Form III crystals respectively and are discussed separately in the following sections.

### 4.3.1 Structure of Solvent Free Crystals of 7 (Form I)

The compound **3** has a benzyl group at the C4-*O*-position of the inositol ring and benzoates occupy rest of the positions. In solvent free crystals (**7**), phenyl rings of the C3 and C4-*O*-benzyl group are involved in intramolecular aromatic  $\pi\cdots\pi$  stacking interactions ( $Cg3\cdots Cg4 = 4.341 \text{ \AA}$ , dihedral angle,  $\alpha = 11.31^\circ$ , **Figure 4.4**).

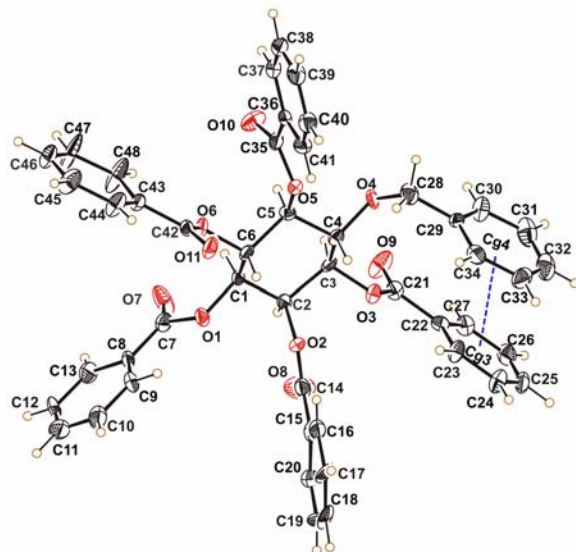


**Figure 4.4.** ORTEP view of the solvent free crystals of **7** (30% ellipsoid probability level). Intramolecular  $\pi\cdots\pi$  ( $Cg3\cdots Cg4$ ) stacking interactions shown with blue dotted line.

#### *Molecular Organization*

The neighboring molecules in Form I crystals of **7** related by unit-translation along b-axis make bifurcated C-H $\cdots$ O interactions as shown in **Figure 4.5**. The two C-H groups, C4-H4 and C6-H6 of *molecule 1* make close contact with carbonyl oxygen O9 of the translated *molecule 2*. Further C41-H41 and C40-H40 of *molecule 1* also make a bifurcated but longer C-H $\cdots$ O interaction with O4 of *molecule 2* and C16-H16 of *molecule 1* make C-H $\cdots$ O interaction with O9 of *molecule 2* (omitted in the figure for

clarity). In turn oxygen O11 of *molecule 1* accepts protons from C1-H1 and C3-H3 of *molecule 2* (**Figure 4.5**). In continuing this pattern, each successive translated molecule gets assembled forming a layered structure along b-axis (**Table 4.3**). It may be recalled that this type of non-centrosymmetric association in contrast with the centrosymmetric trifurcated dimers was seen only in the chiral polymorph of **7** (Chapter 3).<sup>136</sup>

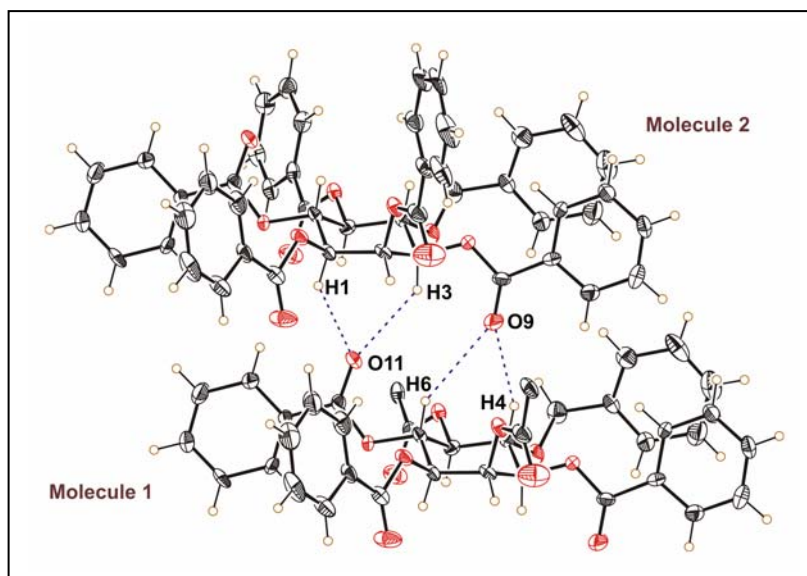


**Figure 4.5.** ORTEP view of closely interacting pairs of **7**.

**Table 4.3:** Intermolecular C-H $\cdots$ O and C-H $\cdots$  $\pi$  interactions in **7**.

D-H $\cdots$ A	D-H (Å)	H $\cdots$ A (Å)	D $\cdots$ A (Å)	D-H $\cdots$ A (°)
C(1)-H(1) $\cdots$ O(11)#1	0.98	2.37	3.188(9)	140
C(3)-H(3) $\cdots$ O(11)#1	0.98	2.54	3.293(7)	134
C(4)-H(4) $\cdots$ O(9)#2	0.98	2.42	3.341(9)	156
C(6)-H(6) $\cdots$ O(9)#2	0.98	2.82	3.650(9)	140
C(11)-H(11) $\cdots$ O(8)#3	0.93	2.71	3.404(12)	132
C(16)-H(16) $\cdots$ O(9)#2	0.93	2.91	3.817(11)	163
C(17)-H(17) $\cdots$ O(8)#2	0.93	2.60	3.107(11)	114
C(18)-H(18) $\cdots$ O(10)#4	0.93	2.44	3.302(10)	155
C(41)-H(41) $\cdots$ O(4)#2	0.93	2.76	3.391(4)	126
C(40)-H(40) $\cdots$ O(4)#2	0.93	2.81	3.407(10)	123
C(46)-H(46) $\cdots$ O(7)#5	0.93	2.60	3.449(10)	153
C(28)-H(28A) $\cdots$ Cg(4)#6	0.93	2.75	3.592(10)	146

Symmetry codes: #1  $x, -1+y, z$ ; #2  $x, 1+y, z$ ; #3  $1/2-x, 1/2+y, 1/2-z$ ; #4  $1/2+x, 1/2+y, z$ ; #5  $-x, 1+y, 1/2-z$  #6  $-x, -y, -z$ .

Molecular packing down a-axis shows the linking of centrosymmetrically related molecular layers via C-H $\cdots$  $\pi$  interactions between the methylene proton H28A and the phenyl ring (Cg4) of the same C4-O-benzyl group (**Figure 4.6**).

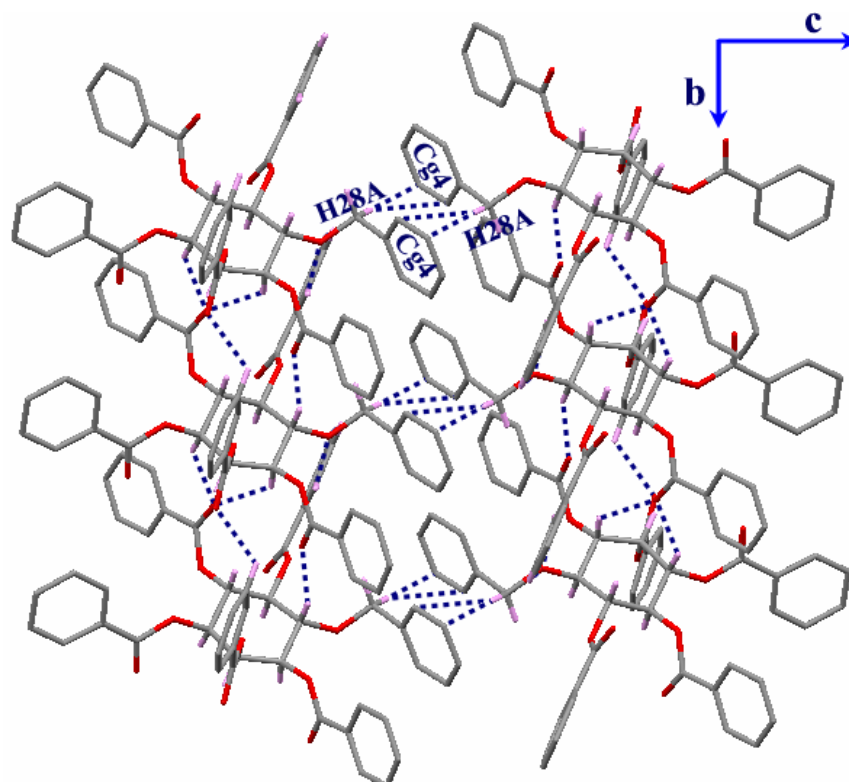


**Figure 4.6.** Bilayer formation via C-H $\cdots$  $\pi$  interaction in **7** viewed down the a-axis.

### ***Bilayer Formation and its Association***

These molecular rows are linked via different interactions along a, b and c-axes. Along c-axis, the successive dimeric bilayers are associated via centrosymmetric C46-H46 $\cdots$ O7 contacts between c-glide related molecules (**Figure 4.7A**). The dimeric layers, along b-axis, are associated via C11-H11 $\cdots$ O8 contacts having two-fold screw axis relationship (**Figure 4.7B**). The C-H $\cdots$  $\pi$  linked dimers are connected via C18-H18 $\cdots$ O10 interaction along a-axis (**Figure 4.7C**).

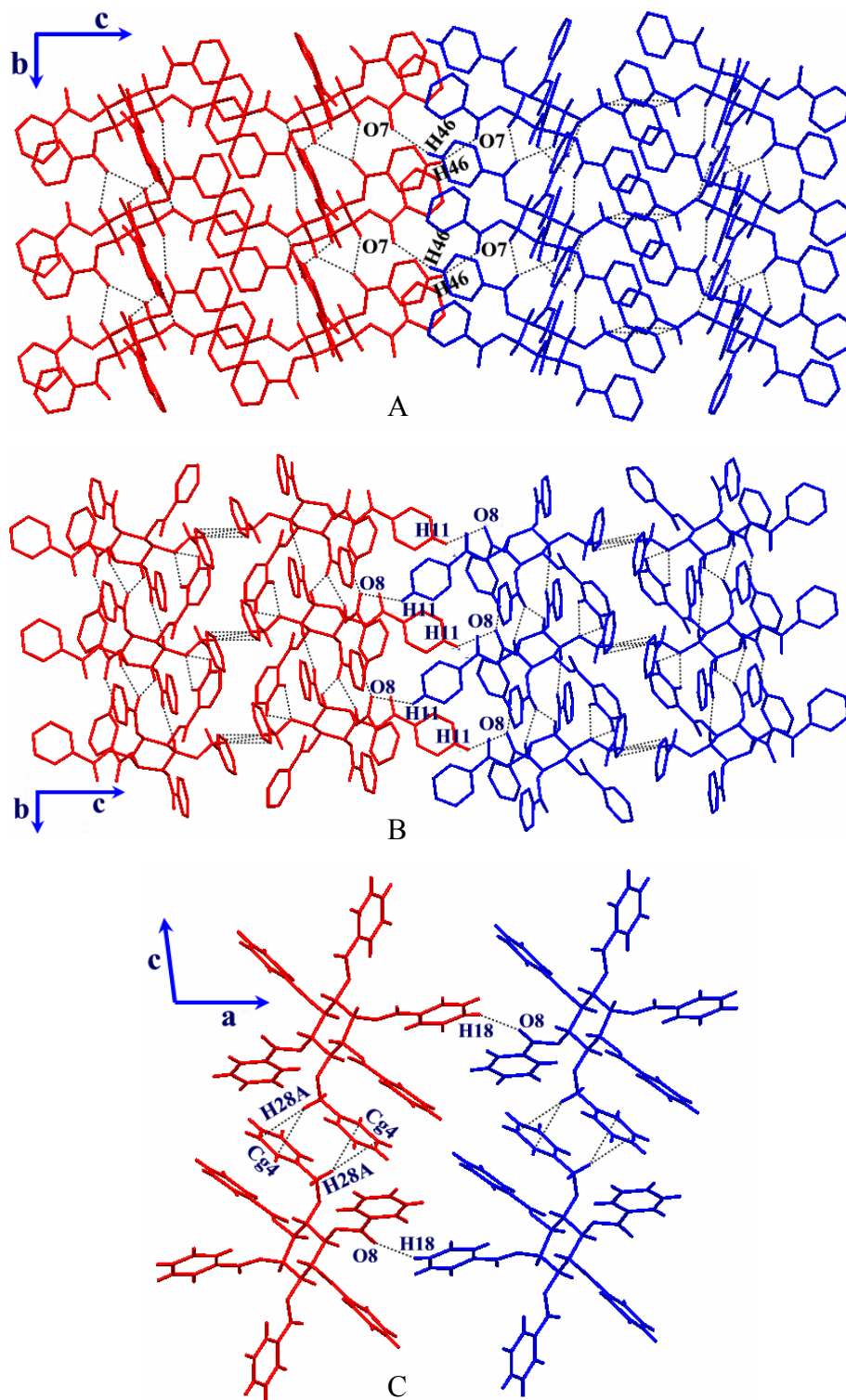


**Figure 4.7.** Association of bilayers in solvent free crystals of 7, A) along the c-axis, B) along the b-axis and C) Molecular packing down the b-axis.

Thus, molecules in solvent free crystals of **7** are so closely packed due to various C-H $\cdots$ O and C-H $\cdots$  $\pi$  interactions that it does not leave any room for the inclusion of solvent molecules.

#### ***Overlap of Molecules of Solvent Free Crystals of 7 and Dichloromethane Inclusion Crystals of 3***

The crystals structure of **3** and solvent free crystal of **7** showed intramolecular aromatic  $\pi\cdots\pi$  stacking interactions. Therefore the difference in the conformation of molecules of **3** and **7** were compared (**Figure 4.8**). In inclusion crystals of **3**, the intramolecular  $\pi\cdots\pi$  stacking interaction is present between the phenyl rings of C4-*O*-tosyl group and C5-*O*-benzoyl group. However, in solvent free crystals of **7**,  $\pi\cdots\pi$  stacking interaction is between the phenyl rings of C4-*O*-benzyl group and C3-*O*-benzoyl group. Although C4-*O*-acyl group in both molecules have different orientations, they are involved in intramolecular  $\pi\cdots\pi$  stacking interactions and did not lead to cavity formation as in the inclusion crystals of **4**.

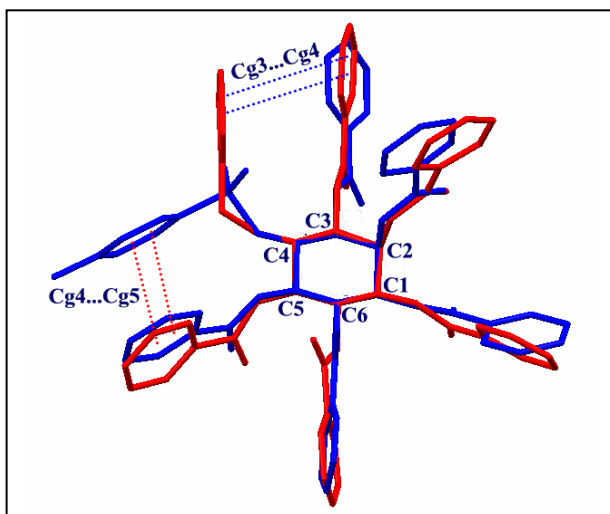


**Figure 4.8.** Overlap of molecules of dichloromethane inclusion crystals of **3** (blue) and solvent free form of **7** (red).



### 4.3.2 Structures of Form II Inclusion Crystals of 7 ( $7 \cdot \text{CH}_2\text{Cl}_2$ and $7 \cdot \text{CH}_2\text{Br}_2$ )

The conformations of the host molecule in  $7 \cdot \text{CH}_2\text{Cl}_2$  and  $7 \cdot \text{CH}_2\text{Br}_2$  crystals are different as compared with solvent free crystals of 7. All the *O*-substituents in  $7 \cdot \text{CH}_2\text{Cl}_2$  and  $7 \cdot \text{CH}_2\text{Br}_2$  have extended conformation and there is no intramolecular  $\pi \cdots \pi$  contact as was seen in solvent free crystals of 7 (**Figure 4.4**). Structure of  $7 \cdot \text{CH}_2\text{Cl}_2$  exhibits interesting two-fold enantiomeric disorder<sup>141</sup> about the possible symmetry plane bisecting the inositol ring passing through C2 and C5. Thus the benzyl group at C4 and the benzoyl group at C6 swap their positions; each one having the major occupancy of 80% with the minor occupancy (20%) of the other as shown in **Figure 4.9**. In  $7 \cdot \text{CH}_2\text{Cl}_2$ , one of the chlorine atoms of  $\text{CH}_2\text{Cl}_2$  showed disorder over two positions with occupancies 0.8 and 0.2. None of these disorders was noticed in the crystals  $7 \cdot \text{CH}_2\text{Br}_2$ . The conformations of the host molecules in  $7 \cdot \text{CH}_2\text{Cl}_2$  and  $7 \cdot \text{CH}_2\text{Br}_2$  were almost the same, the isostructurality also reflected in their unit cell parameters (**Table 4.2**).

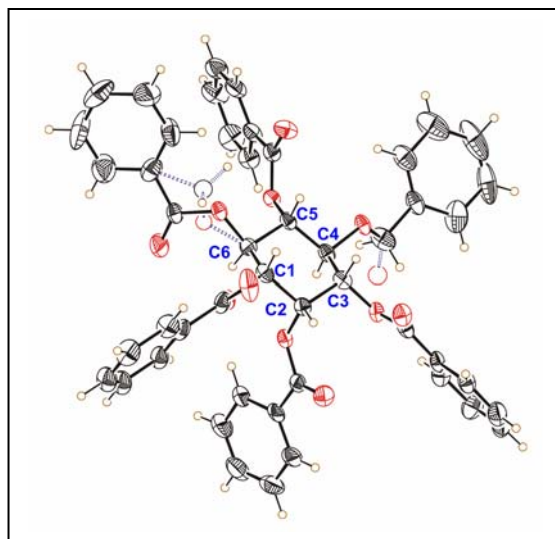


**Figure 4.9.** ORTEP view of the host molecule in  $7 \cdot \text{CH}_2\text{Cl}_2$ , showing statistical disorder of benzyl and benzoyl group (open circles and blue dotted lines).

### Host Organization

Interestingly, host molecules in dihalomethane inclusion crystals formed a well recognized centrosymmetric dimer associated via trifurcated C-H $\cdots$ O contacts, as seen in structures of **3** (Chapter 2) and **4** (Chapter 3). Here again, the H-atoms of C1, C3 and C5 of inositol from either of the molecules make centrosymmetric C-H $\cdots$ O hydrogen bonding interactions with the carbonyl oxygen O10 of the C5-O-benzoyl group. The geometrical parameters of three C-H $\cdots$ O contacts in **7**·CH<sub>2</sub>Cl<sub>2</sub> and **7**·CH<sub>2</sub>Br<sub>2</sub> are comparable (Table 4.4). Further, three more centrosymmetric C-H $\cdots$ O interactions, C31-H31 $\cdots$ O7, C37-H37 $\cdots$ O9 and C48-H48 $\cdots$ O4 (omitted in the figure for clarity) also support the dimeric assembly (Figure 4.10).

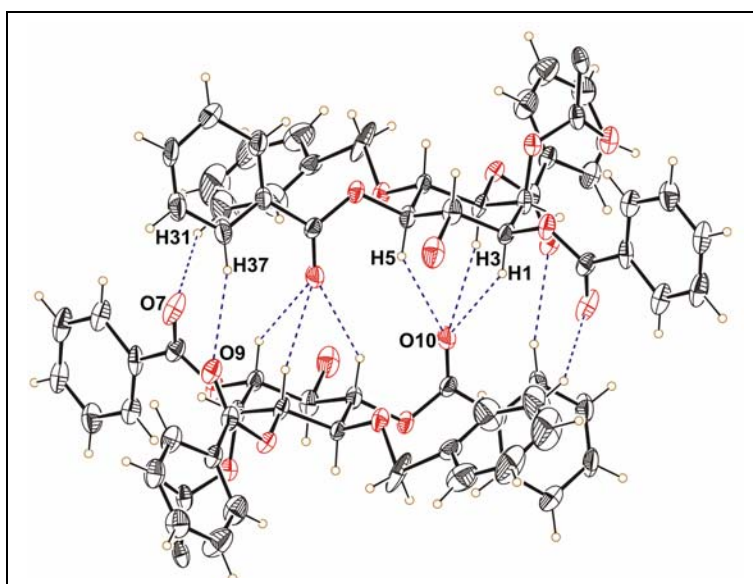


**Figure 4.10.** Dimeric assembly of host molecules in **7**·CH<sub>2</sub>Cl<sub>2</sub>.

**Table 4.4:** Intermolecular C-H $\cdots$ O interactions involved in the formation of centrosymmetric dimeric assembly.

	D-H $\cdots$ A	D-H (Å)	H $\cdots$ A (Å)	D $\cdots$ A (Å)	D-H $\cdots$ A (°)
<b>7·CH<sub>2</sub>Cl<sub>2</sub></b>	C(1)-H(1) $\cdots$ O(10)#1	0.98	2.63	3.420(8)	138
	C(3)-H(3) $\cdots$ O(10)#1	0.98	2.42	3.262(8)	144
	C(5)-H(5) $\cdots$ O(10)#1	0.98	2.49	3.319(7)	142
	C(31)-H(31) $\cdots$ O(7)#1	0.93	2.47	3.286(15)	146
	C(37)-H(37) $\cdots$ O(9)#1	0.93	2.54	3.421(9)	159
	C(48)-H(48) $\cdots$ O(4)#1	0.93	2.68	3.460(10)	142
<b>7·CH<sub>2</sub>Br<sub>2</sub></b>	C(1)-H(1) $\cdots$ O(10)#2	0.98	2.64	3.443(13)	139
	C(3)-H(3) $\cdots$ O(10)#2	0.98	2.45	3.287(13)	144
	C(5)-H(5) $\cdots$ O(10)#2	0.98	2.48	3.313(13)	143
	C(31)-H(31) $\cdots$ O(7)#2	0.93	2.49	3.320(18)	148
	C(37)-H(37) $\cdots$ O(9)#2	0.93	2.56	3.440(15)	159
	C(48)-H(48) $\cdots$ O(4)#2	0.93	2.75	3.554(18)	145

Symmetry codes: #1 -x+2,-y+2,-z+1; #2 -x+1,-y+2,-z.

These centrosymmetric dimers are linked via different interactions along a, b and c-axes. These dimers associate along the b-axis via C17-H17 $\cdots$ O11 interaction forming columnar assembly creating cavities to accommodate guest molecules, as observed in dihalomethane inclusion crystals of **4** (Chapter 3). Along the c-axis, the dimers are associated via centrosymmetric C11-H11 $\cdots$ O8 and  $\pi\cdots\pi$  stacking interactions (Cg1 $\cdots$ Cg1) between the phenyl ring of the C1-O-benzoyl group (**Figure 4.11A**), whereas C26-H26 $\cdots$ O7 contacts bridge them along the a-axis (**Figure 4.11B**).

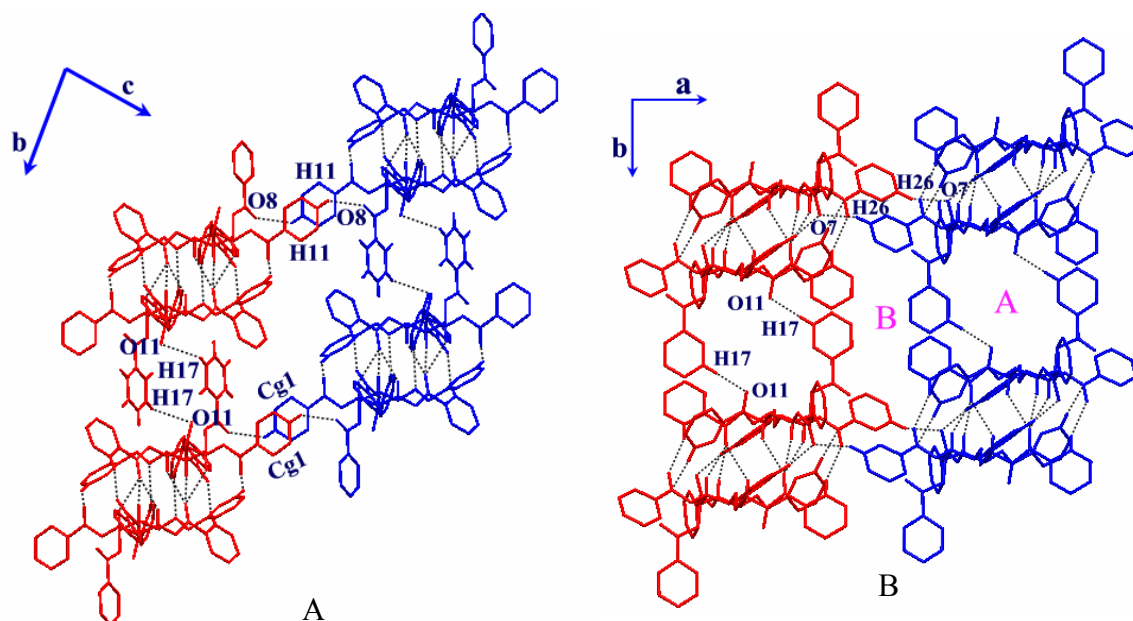


**Figure 4.11.** Association of the pillars formed via C17-H17 $\cdots$ O11 interactions in inclusion crystals  $7\cdot\text{CH}_2\text{Cl}_2$ , A) along c-axis via C11-H11 $\cdots$ O8 and  $\pi\cdots\pi$  stacking interactions and B) along a-axis via C26-H26 $\cdots$ O7 contact.

When viewed down b-axis, the molecular packing did not show any void for the guest inclusion. The dimers are associated via C11-H11 $\cdots$ O8 and  $\pi\cdots\pi$  ( $Cg\cdots Cg = 3.711$  Å in  $7\cdot\text{CH}_2\text{Cl}_2$  and  $3.709$  Å in  $7\cdot\text{CH}_2\text{Br}_2$ ) stacking interactions along c-axis and C26-H26 $\cdots$ O7 and C-H $\cdots\pi$  interactions between C46-H46 and phenyl ring of C1-O-benzoyl group along the a-axis (**Figure 4.11, Tables 4.5**).

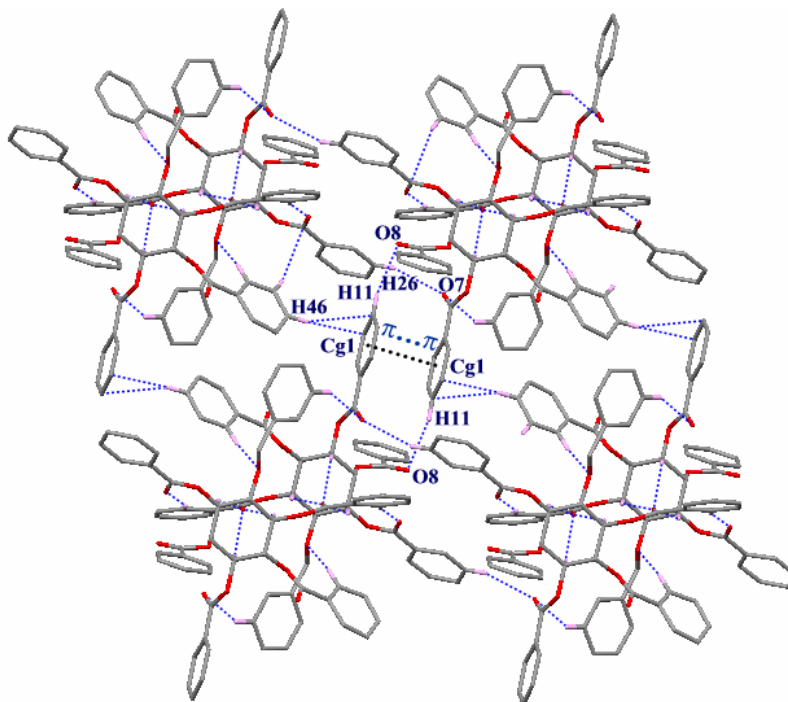


**Figure 4.12.** View of molecular packing down b-axis in inclusion crystals  $7 \cdot \text{CH}_2\text{Cl}_2$ .

**Table 4.5:** Intermolecular host-host C-H $\cdots$ O and C-H $\cdots$  $\pi$  interactions involved in the association of dimeric assembly in  $7 \cdot \text{CH}_2\text{Cl}_2$  and  $7 \cdot \text{CH}_2\text{Br}_2$ .

	D-H $\cdots$ A	D-H (Å)	H $\cdots$ A (Å)	D $\cdots$ A (Å)	D-H $\cdots$ A (°)
$7 \cdot \text{CH}_2\text{Cl}_2$	C(11)-H(11) $\cdots$ O(8)#1	0.93	2.61	3.393(9)	142
	C(17)-H(17) $\cdots$ O(11)#2	0.93	2.71	3.331(13)	125
	C(20)-H(20) $\cdots$ O(12)#3	0.93	2.68	3.520(20)	151
	C(26)-H(26) $\cdots$ O(7)#4	0.93	2.50	3.325(10)	147
	C(46)-H(46) $\cdots$ Cg(1)#5	0.93	2.96	3.712(12)	139
$7 \cdot \text{CH}_2\text{Br}_2$	C(11)-H(11) $\cdots$ O(8)#6	0.93	2.58	3.397(13)	146
	C(17)-H(17) $\cdots$ O(11)#7	0.93	2.70	3.370(12)	129
	C(26)-H(26) $\cdots$ O(7)#8	0.93	2.49	3.303(14)	147
	C(46)-H(46) $\cdots$ Cg(1)#9	0.93	2.87	3.726(13)	153
	C(33)-H(33) $\cdots$ Cg(2)#10	0.93	3.00	3.725(11)	136

Symmetry codes: #1 -x+2,-y+1,-z+2; #2 -x+2,-y+1,-z+1; #3 x,y,z+1;

#4 -x+1,-y+2,-z+2; #5 -1-x,1-y,1-z; #6 -x+1,-y+1,-z+1; #7 -x+1,-y+1,-z;

#8 -x,-y+2,-z+1; #9 2-x,1-y,-z; #10 -x,2-y,-z.

### Host-Guest Assembly and Interactions

The host-guest assembly in  $7 \cdot \text{CH}_2\text{Cl}_2$  and  $7 \cdot \text{CH}_2\text{Br}_2$  is identical with that of dihalomethane inclusion crystals of **4** (Chapter 2). The dihalomethane guest molecules occupy the channels created by linking of dimers via C17-H17 $\cdots$ O11 contact (Site A in **Figure 4.11B** and **Figure 4.13**). This is the only channel that includes the guest molecules. The second channel formed here (Site B in **Figures 4.11B** and **4.13**) could not accommodate guest molecule as was included in dihalomethane inclusion crystals of **4**.

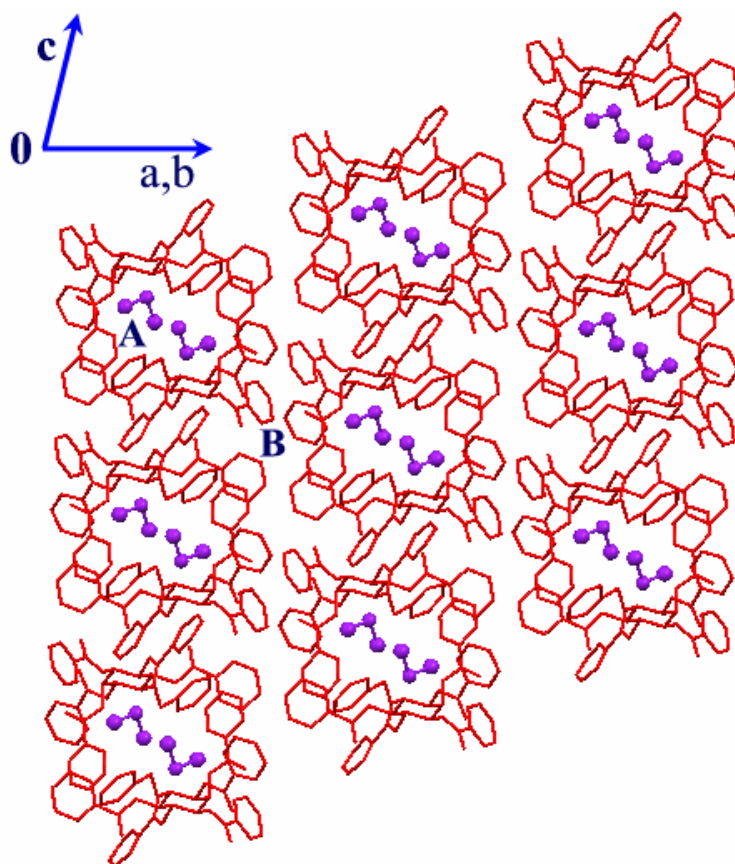


**Figure 4.13.** Host-guest assembly in inclusion crystals  $7 \cdot \text{CH}_2\text{Cl}_2$ .

The included guest makes various weak interactions with the host molecules that surround them (**Figure 4.14**). The methylene hydrogen H49A of the guest molecule

makes somewhat weaker C-H $\cdots$ O interaction with the carbonyl oxygen O11, whereas the halogens (X = Cl, Br) make C-H $\cdots$ X and C-X $\cdots$  $\pi$  contacts with the host, similar to that observed in inclusion crystals of **3**. The Cl1 (Br1) of the guest makes bifurcated interactions, C28-H28A $\cdots$ Cl1(Br1) and C41-H41 $\cdots$ Cl1(Br1) and is also involved in an almost linear C-Cl(Br) $\cdots$  $\pi$  [ $\pi$  cloud of phenyl of C3-*O*-benzoyl group, Cg(3)] interaction. The other halogen Cl2(Br2) makes trifurcated C-H $\cdots$ Cl(Br) interactions, C4-H4 $\cdots$ Cl2(Br2), C16-H16 $\cdots$ Cl2(Br2) and C41-H41 $\cdots$ Cl2(Br2) (**Figure 4.14**). The geometrical parameters of all the C-H $\cdots$ Cl (Br) interactions are of comparable strength (**Table 4.6**).

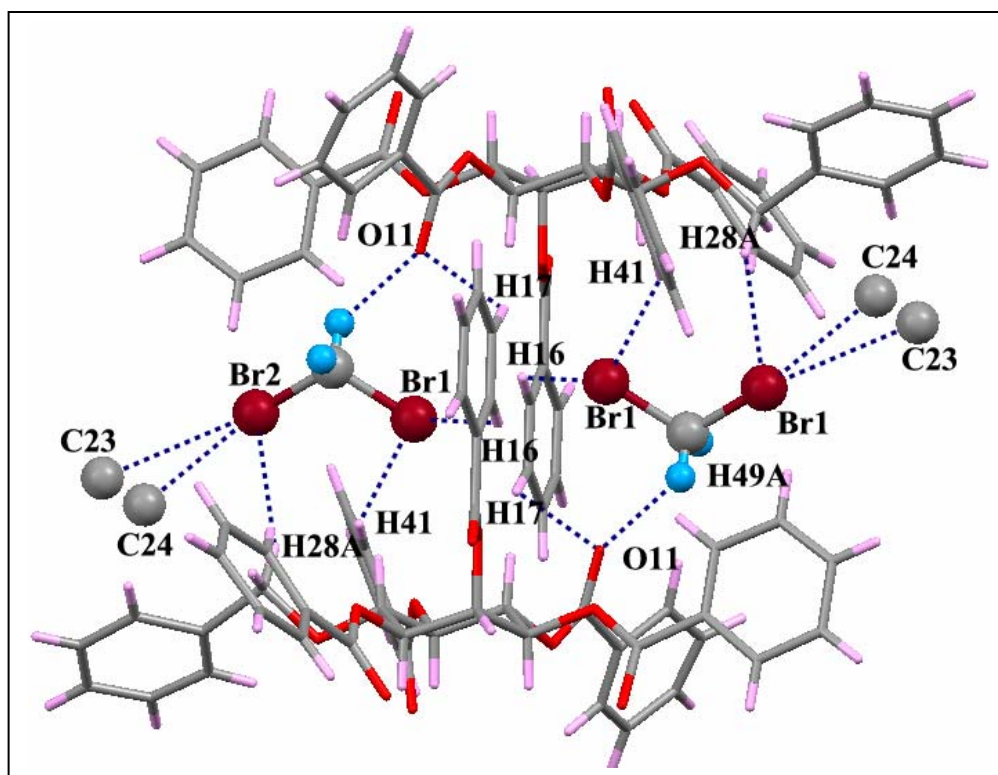


**Figure 4.14.** Host-guest association via various intermolecular interactions in **7**·CH<sub>2</sub>Br<sub>2</sub>.

**Table 4.6:** Host-guest interactions in  $7 \cdot \text{CH}_2\text{Cl}_2$  and  $7 \cdot \text{CH}_2\text{Br}_2$ .

	D-H/X...A	D-H/X (Å)	H/X...A (Å)	D...A (Å)	D-H/X...A (°)
$7 \cdot \text{CH}_2\text{Cl}_2$	C(49)-H(49A)...O(11)#1	0.97	2.38	2.858(15)	110
	C(28)-H(28A)...Cl(1)#2	0.97	3.12	4.093(13)	167
	C(41)-H(41)...Cl(1)#2	0.93	3.10	3.881(14)	144
	C(4)-H(4)...Cl(2)#2	0.98	3.14	3.979(15)	145
	C(16)-H(16)...Cl(2)#2	0.93	3.06	3.679(15)	126
	C(41)-H(41)...Cl(2)#2	0.93	3.12	3.972(11)	153
	C(49)-Cl(1)...Cg(3)#3	1.718	3.68	5.335(12)	161
$7 \cdot \text{CH}_2\text{Br}_2$	C(49)-H(49A)...O(11)#2	0.97	2.35	2.910(2)	116
	C(28)-H(28A)...Br(1)#4	0.97	3.03	3.947(14)	159
	C(16)-H(16)...Br(2A)#3	0.93	2.96	3.654(17)	132
	C(16)-H(16)...Br(2)#4	0.93	3.08	3.723(13)	128
	C(41)-H(41)...Br(2)#4	0.93	3.14	3.972(12)	149
	C(49)-Br(1)...Cg(3)#5	1.913	3.547	5.411(15)	164

Symmetry codes: #1 -x+2,-y+1,-z+1; #2 x,y,z; #3 1-x,-y,1-z; #4 -x+1,-y+1,-z;  
#5 1+x,-1+y,z.

### ***Difference Between Host-Guest Interactions in Dihalomethane Inclusion Crystals of 4 and 7***

Dihalomethane inclusion crystals of both **4** and **7** were highly unstable, but the crystals of **4** were relatively more stable than crystals of **7**. In the dihalomethane inclusion crystals of compounds **4** and **7**, the host molecules have similar packing arrangement with guest molecules occupying the same sites in the crystal lattice. The guest molecules in crystals of **4** and **7** make almost similar interactions with the host molecules. The main difference in molecular structure between *myo*-inositol derivatives **4**



and **7** is that the substituent at C4 position in **4** is benzoate while in **7** the substituent is a benzyloxy group. The presence of an additional carbonyl group in **4** brings in extra C-H $\cdots$ O contacts. For example, both the hydrogen atoms H49A and H49B of dichloromethane in **4** are involved in C-H $\cdots$ O hydrogen bonding with the carbonyl oxygen atoms O10 and O12 respectively (**Figure 4.15A**), but in **7**·CH<sub>2</sub>Cl<sub>2</sub> and **7**·CH<sub>2</sub>Br<sub>2</sub>, only H49A make a contact with O11 and H49B is not involved in any interaction. However, in **7**·CH<sub>2</sub>Cl<sub>2</sub> and **7**·CH<sub>2</sub>Br<sub>2</sub> a C-H $\cdots$ X interaction (C28-H28A $\cdots$ Br1(Cl1)) exists between the CH<sub>2</sub> hydrogen (benzyloxy group) and the halogen atom of the guest (**Figure 4.15B**). Hence, a change in the substitution at C4 does not alter the cavities in **4** and **7** but result in different weak interactions that hold the guest molecules in the crystal lattice.

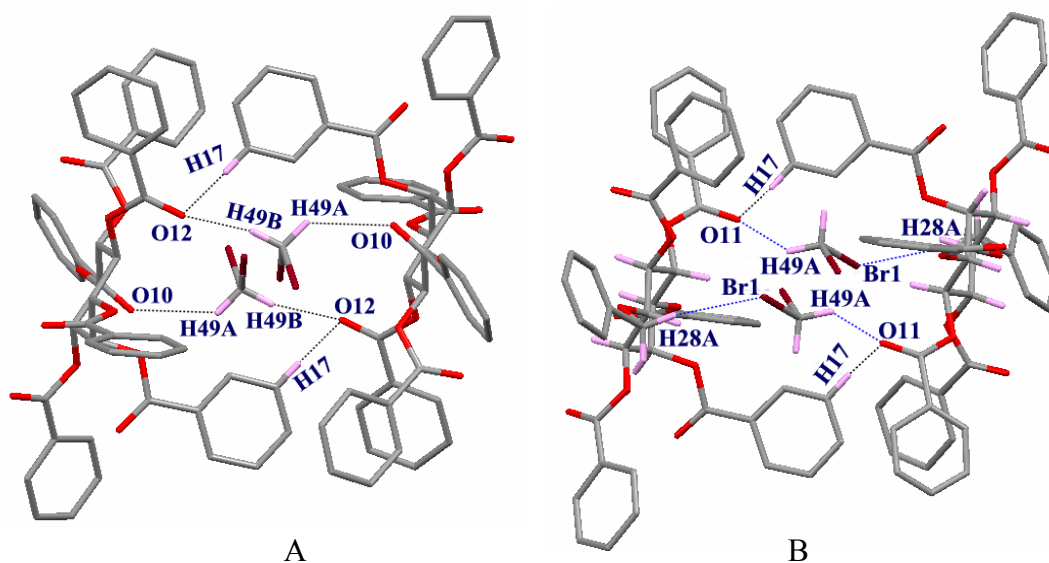


**Figure 4.15.** Host-guest interactions in A) **4**·CH<sub>2</sub>Br<sub>2</sub> and B) **7**·CH<sub>2</sub>Br<sub>2</sub>.

### 4.3.3 Structures of Form III Inclusion Crystals ( $7 \cdot \text{CHCl}_3$ and $7 \cdot \text{CHCl}_2\text{Br}$ )

As described earlier (section 4.6), the crystals of inclusion complexes of **7** with  $\text{CHCl}_3$  ( $7 \cdot \text{CHCl}_3$ ) and  $\text{CHCl}_2\text{Br}$  ( $7 \cdot \text{CHCl}_2\text{Br}$ ) are isostructural. In both  $7 \cdot \text{CHCl}_3$  and  $7 \cdot \text{CHCl}_2\text{Br}$ , asymmetric unit contains two molecules of host **7** and one molecule of the guest. Interestingly, the two independent molecules in the asymmetric unit are enantiomers i.e. in one molecule have the benzyl group at C4 position and the other having the benzyl group at the C6 position. The phenyl rings of the C5 and C6- benzoates of one of the isomers (with benzyl group at C4, now onwards *molecule D3*) in  $7 \cdot \text{CHCl}_3$  show rotational disorder over two positions having equal occupancies (**Figure 4.16A**) whereas in the other isomer (with benzyl group at C6, now onwards *molecule L3*) no such disorder is observed (**Figure 4.16B**). In crystals  $7 \cdot \text{CHCl}_2\text{Br}$ , the phenyl rings at C5 and C6 benzoates of *molecule D3* show large thermal vibrations but not to the extent seen in  $7 \cdot \text{CHCl}_3$ . All the three halogen atoms of the guest molecule in  $7 \cdot \text{CHCl}_3$  and  $7 \cdot \text{CHCl}_2\text{Br}$  show rotational disorder along the C-H bond. A total four orientations of three chlorine atoms were obtained by keeping the position of C-H bond fixed in  $7 \cdot \text{CHCl}_3$ . The occupancies of chlorines in  $7 \cdot \text{CHCl}_3$  at four different positions were 0.4, 0.3, 0.15 and 0.15. Only the halogen atoms having occupancies 0.4 were refined anisotropically, the rest were kept isotropic during the least-squares refinement. In crystals of  $7 \cdot \text{CHCl}_2\text{Br}$  also the  $\text{CHCl}_2\text{Br}$  molecule exhibited similar rotational disorder but over three different orientations having occupancies 0.5, 0.4 and 0.1. Again here, only the higher occupancy halogen atoms 0.5 and 0.4 were refined anisotropically.

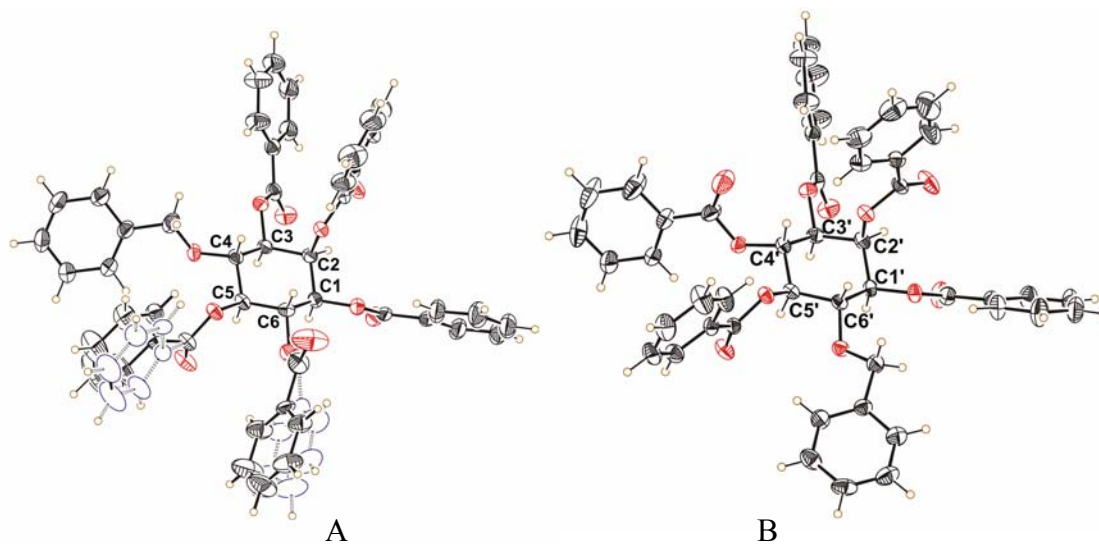


**Figure 4.16.** ORTEP view of A) *molecule* D3 (the open ellipsoids with dotted lines in blue at C5 and C6 represent the disordered part of the phenyl rings) and B) *molecule* L3 in  $7 \cdot \text{CHCl}_3$ .

### Host Organization

In the inclusion crystals of  $7 \cdot \text{CHCl}_3$  and  $7 \cdot \text{CCl}_2\text{Br}$ , the host molecules assemble in a strikingly similar fashion via ‘trifurcated C-H $\cdots$ O interactions’ as was observed in several pseudopolymorphs [**3** (Chapter 2), **4** (Chapter 3),  $7 \cdot \text{CH}_2\text{Cl}_2$  and  $7 \cdot \text{CH}_2\text{Br}_2$ , **section 4.7.2**] discussed in this chapter. However, two molecules in the asymmetric unit having different chirality (*molecule* D3 and *molecule* L3) form this well noted dimer via non-crystallographic center of symmetry. The three axial H-atoms H1, H3 and H5 of the *myo*-inositol ring of isomer D3 make C-H $\cdots$ O contacts with the carbonyl oxygen O11’ of the other enantiomer L3 whereas the three axial H-atoms H1’, H3’ and H5’ of the *myo*-inositol ring of L3 make C-H $\cdots$ O contacts with the carbonyl oxygen O10 of molecule D3 (**Figure 4.17**). Among these, *molecule* D3  $\rightarrow$  *molecule* L3 contacts, interactions C1-

H1...O11' and C3-H3...O11' are shorter compared to the C5-H5...O11' (Table 4.7), whereas in other trifurcated C-H...O assembly (*molecule L3* → *molecule D3*), all the C-H...O contacts are of comparable strengths (C1'-H1'...O10, C3'-H3'...O10 and C5'-H5'...O10, Table 4.7).

**Table 4.7:** C-H...O interactions in *pseudo*-centrosymmetric dimeric assembly formation in 7·CHCl<sub>3</sub> and 7·CHCl<sub>2</sub>Br.

	D-H...A	D-H (Å)	H...A (Å)	D...A (Å)	D-H...A (°)
<b>7·CHCl<sub>3</sub></b>	C(1)-H(1)...O(11')#1	0.98	2.34	3.178 (5)	143
	C(3)-H(3)...O(11')#1	0.98	2.31	3.141(5)	142
	C(5)-H(5)...O(11')#1	0.98	2.61	3.393(5)	137
	C(1')-H(1')...O(10)#1	0.98	2.49	3.296(5)	139
	C(3')-H(3')...O(10)#1	0.98	2.54	3.356(5)	141
	C(5')-H(5')...O(10)#1	0.98	2.51	3.273(5)	135
	C(31)-H(31)...O(9')#1	0.93	2.62	3.471(7)	152
	C(48)-H(48)...O(6')#1	0.93	2.86	3.643(6)	143
	C(30')-H(30')...O(4)#1	0.93	2.54	3.330(6)	142
	C(47')-H(47')...O(7)#1	0.93	2.74	3.454(7)	134
<b>7·CHCl<sub>2</sub>Br</b>	C(1)-H(1)...O(11')#2	0.98	2.34	3.174(8)	142
	C(3)-H(3)...O(11')#2	0.98	2.30	3.136(8)	142
	C(5)-H(5)...O(11')#2	0.98	2.60	3.388(8)	138
	C(1')-H(1')...O(10)#3	0.98	2.42	3.236(8)	141
	C(3')-H(3')...O(10)#3	0.98	2.53	3.344(8)	140
	C(5')-H(5')...O(10)#3	0.98	2.50	3.254(8)	134
	C(31)-H(31)...O(9')#2	0.93	2.55	3.393(9)	151
	C(48)-H(48)...O(6')#2	0.93	2.81	3.627(10)	148
	C(30')-H(30')...O(4)#3	0.93	2.55	3.342(9)	143
	C(47')-H(47')...O(7)#3	0.93	2.70	3.416(8)	135

Symmetry codes: #1 x,y,z; #2 x,y+1,z; #3 x,y-1,z.

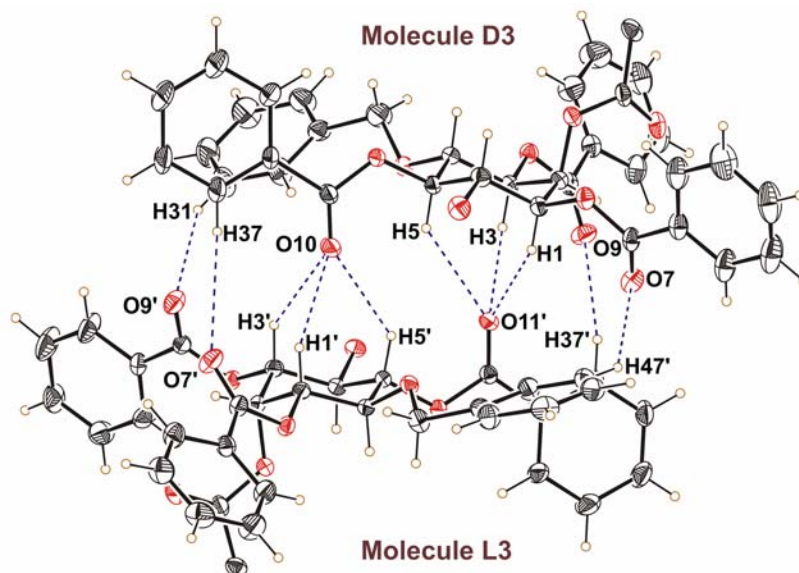


**Figure 4.17.** ORTEP view of closely interacting pair of molecules in inclusion crystals  $7 \cdot \text{CHCl}_3$ .

As observed in these dimeric assemblies, further support to these dimeric assemblies also comes from other C-H $\cdots$ O interactions (**Figure 4.17**). The H-atoms of the phenyl ring of *molecule* D3, H31, H37 and H48 (not shown in the figure for the sake of clarity) form C-H $\cdots$ O interactions with the carbonyl oxygens O9' and O7' and ether oxygen O6' of *molecule* L3 respectively. Further the H-atoms H30', H37' and H47' of *molecule* L3 make C-H $\cdots$ O contacts with the ether oxygen O4 and carbonyl oxygen atoms O9 and O7 of *molecule* D3 respectively. Thus, twelve C-H $\cdots$ O interactions hold these two molecules together in the asymmetric unit.

***Packing of Dimers in the Unit Cell and Formation of the Cavity in Crystals of 7·CHCl<sub>3</sub> and 7·CHCl<sub>2</sub>Br***

The dimeric units (**Figure 4.17**) formed by enantiomers D3 and L3 make different cohesions along each of the axes during the formation of the inclusion crystal. The molecular packing of these dimers creates two types of thorough open channels when viewed down a-axis. The association of *molecule* D3 forms a large cavity (~ 9 x 7 Å, red in **Figure 4.18**), whereas *molecule* L3 associates to produce narrow elliptical cavity (~12 x 3 Å, blue in **Figure 4.18**). Both of these cavities are arranged alternately as shown in **Figure 4.18**.

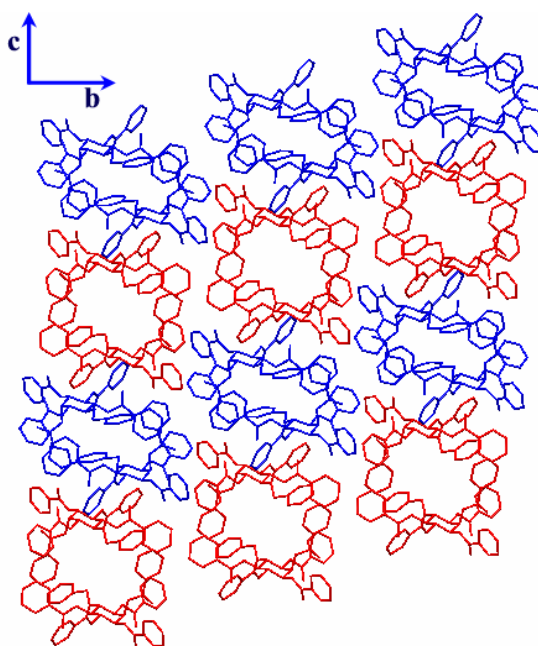


**Figure 4.18.** Molecular packing down a-axis showing two different types of cavities in 7·CHCl<sub>3</sub>.

While forming the larger cavity (site A in **Figure 4.19A**), *molecule* D3 makes C17-H17···O11 interaction with its centrosymmetrically related counterpart, whereas

*molecule* L3 associates with its centrosymmetrically related molecule via C-H $\cdots\pi$  interactions that creates smaller cavity (site B in **Figure 4.19A**); the CH<sub>2</sub> H-atom (H42') of the C6-*O*-benzyl group (Cg6') forms centrosymmetric C-H $\cdots\pi$  interactions with the phenyl ring (Cg 6) of C6-*O*-benzyl group (**Figure 4.19A**). In turn, the H-atom (H46') of the phenyl ring (Cg6) of C6-*O*-benzyl group makes C-H $\cdots\pi$  contact with the phenyl ring (Cg2) of the axial C2-*O*-benzoyl group (**Figure 4.19B**).

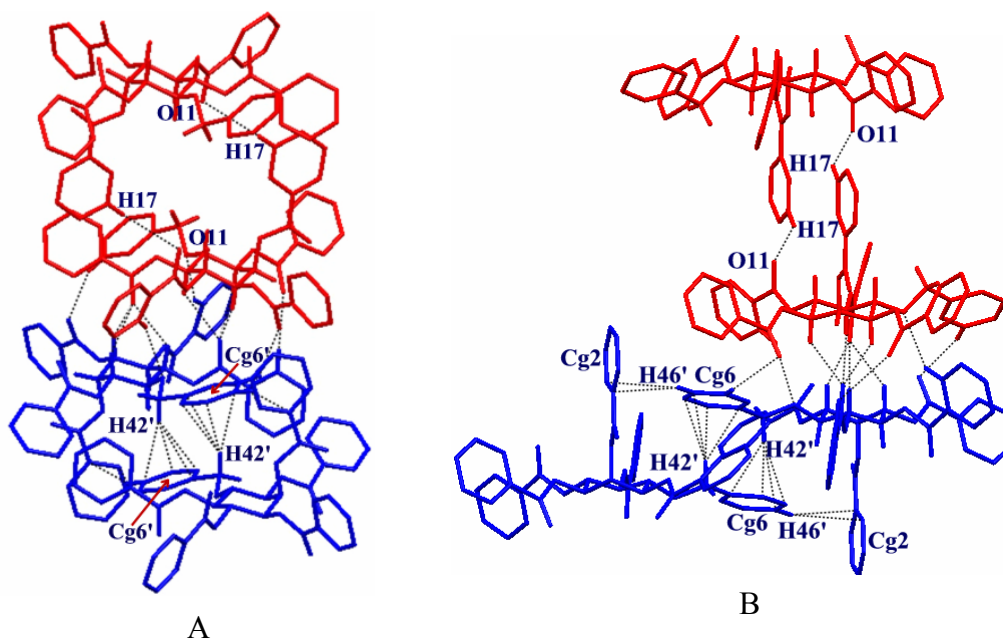


**Figure 4.19.** Different types of cavity formation in  $7\cdot\text{CHCl}_3$ , A) view down a-axis and B) same association down b-axis.

The dimers (**Figure 4.17**) are linked via C-H $\cdots$ O and  $\pi\cdots\pi$  stacking interactions along b-axis via C10'-H10' $\cdots$ O7, C9'-H9' $\cdots$ O8 and C26-H26 $\cdots$ O9', whereas via C11-H11 $\cdots$ O8', C18'-H18' $\cdots$ O9, C25'-H25' $\cdots$ O8 (**Table 4.8**) and  $\pi\cdots\pi$  stacking interactions between the phenyl rings of C1-*O*-benzoyl group of *molecule* D3 (Cg1) and C3-*O*-benzoyl group of *molecule* L3 (Cg3') along a-axis ( $\text{Cg1}\cdots\text{Cg3}' = 3.960 \text{ \AA}$  in  $7\cdot\text{CHCl}_3$  and

$Cg1 \cdots Cg3' = 3.930 \text{ \AA}$  in  $7 \cdot \text{CHCl}_2\text{Br}$ , **Figure 4.20A**). Molecular packing down b-axis also shows involvement of C-H $\cdots\pi$  interactions along c-axis during molecular aggregation (**Figure 4.20B**). *Molecule D3* forms dimeric C-H $\cdots\pi$  contact by donating H-atom (H33) to the phenyl ring (Cg2) of the axial C2-*O*-benzoyl group. In addition, one more C-H $\cdots\pi$  interaction exists between enantiomers D3 and L3. The H-atom of C6-*O*-benzoyl group (H46) of *molecule D3* makes C-H $\cdots\pi$  contact with phenyl ring (Cg3') of the C3-*O*-benzoyl group of molecule L3 (**Figure 4.20B**).

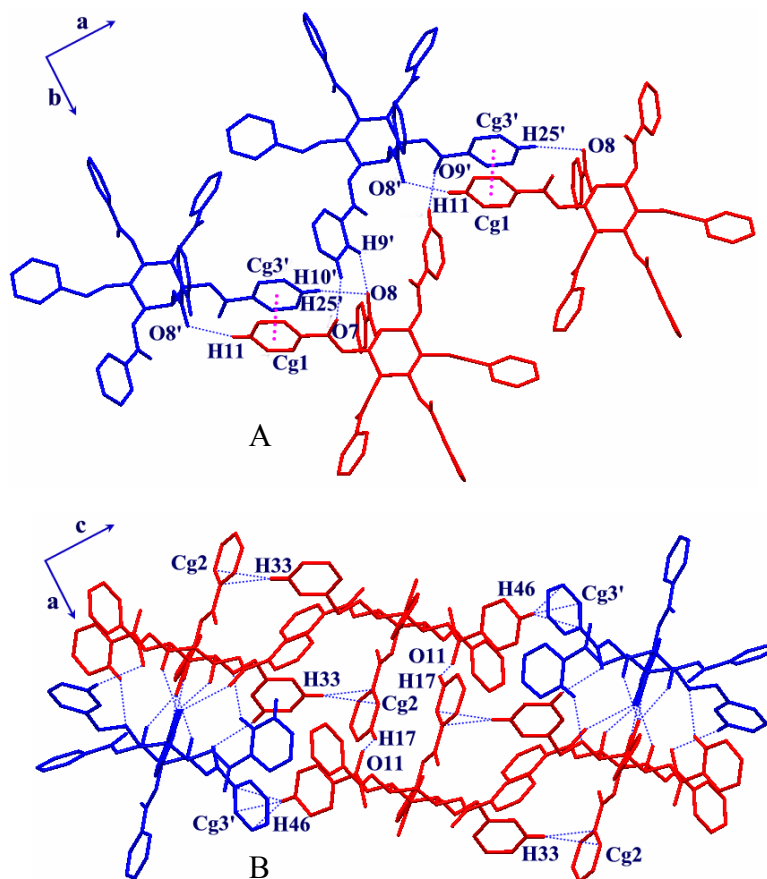


**Figure 4.20.** Association of host molecules in crystals of  $7 \cdot \text{CHCl}_3$  A) viewed down c-axis (dotted line in magenta shows  $\pi \cdots \pi$  stacking interactions) and B) viewed roughly down b-axis.



**Table 4.8:** C-H...O and C-H... $\pi$  interactions involved in bridging the dimeric assembly in crystals of  $7\cdot\text{CHCl}_3$  and  $7\cdot\text{CHCl}_2\text{Br}$ .

	D-H...A	D-H (Å)	H...A (Å)	D...A (Å)	D-H...A (°)
<b><math>7\cdot\text{CHCl}_3</math></b>	C(17)-H(17)...O(11)#1	0.93	2.95	3.775(11)	148
	C(25)-H(25)...O(9')#2	0.93	2.83	3.439(7)	124
	C(26)-H(26)...O(9')#2	0.93	2.86	3.643(6)	126
	C(11)-H(11)...O(8')#3	0.93	2.53	3.415(8)	160
	C(9')-H(9')...O(8)#4	0.93	2.49	3.226(7)	136
	C(10')-H(10')...O(7)#4	0.93	2.63	3.481(6)	153
	C(18')-H(18')...O(9)#5	0.93	2.76	3.611(7)	152
	C(25')-H(25')...O(8)#6	0.93	2.65	3.553(6)	164
	C(33)-H(33)...Cg(2)#7	0.93	2.84	3.663(6)	148
	C(42')-H(42')...Cg(6')#8	0.93	2.65	3.588(8)	163
C(46)-H(46)...Cg(3')#9	0.93	2.79	3.687(6)	164	
<b><math>7\cdot\text{CHCl}_2\text{Br}</math></b>	C(17)-H(17)...O(11)#10	0.93	2.86	3.676(13)	147
	C(25)-H(25)...O(9')#11	0.93	2.83	3.430(7)	123
	C(26)-H(26)...O(9')#11	0.93	2.72	3.376(9)	128
	C(11)-H(11)...O(8')#12	0.93	2.51	3.386(10)	157
	C(9')-H(9')...O(8)#11	0.93	2.45	3.197(7)	137
	C(10')-H(10')...O(7)#11	0.93	2.59	3.429(8)	150
	C(18')-H(18')...O(9)#13	0.93	2.75	3.605(11)	153
	C(25')-H(25')...O(8)#14	0.93	2.61	3.521(8)	166
	C(33)-H(33)...Cg(2)#15	0.93	2.81	3.621(7)	146
	C(42')-H(42')...Cg(6')#16	0.93	2.65	3.594(9)	164
C(46)-H(46)...Cg(3')#17	0.93	2.78	3.687(8)	164	

Symmetry codes: #1 -x+1,-y,-z+1; #2 x,y-1,z; #3 x-1,y-1,z; #4 x,y+1,z; #5 -x+2,-y,-z;  
 #6 x+1,y+1,z; #7 -x,-y,1-z; #8 1-x,-y,-z; #9 2-x,-y,1-z; #10 -x,-y+2,-z+1; #11 x,y,z;  
 #12 x-1,y,z; #13 -x+1,-y+1,-z; #14 x+1,y,z; #15 1-x,2-y,1-z; #16 -x,-y,-z;  
 #17 -1+x,1+y,z.

### *Host-Guest Assembly and Interactions in 7·CHCl<sub>3</sub> and 7·CHCl<sub>2</sub>Br*

The inclusion of guests in **7·CHCl<sub>3</sub>** and **7·CHCl<sub>2</sub>Br** crystals is interesting. The guest molecules are located only in the larger cavities, whereas smaller cavities are vacant (**Figure 4.21**). Therefore, guest molecules are associated and essentially interact with *molecule D3* and not with *molecule L3*.

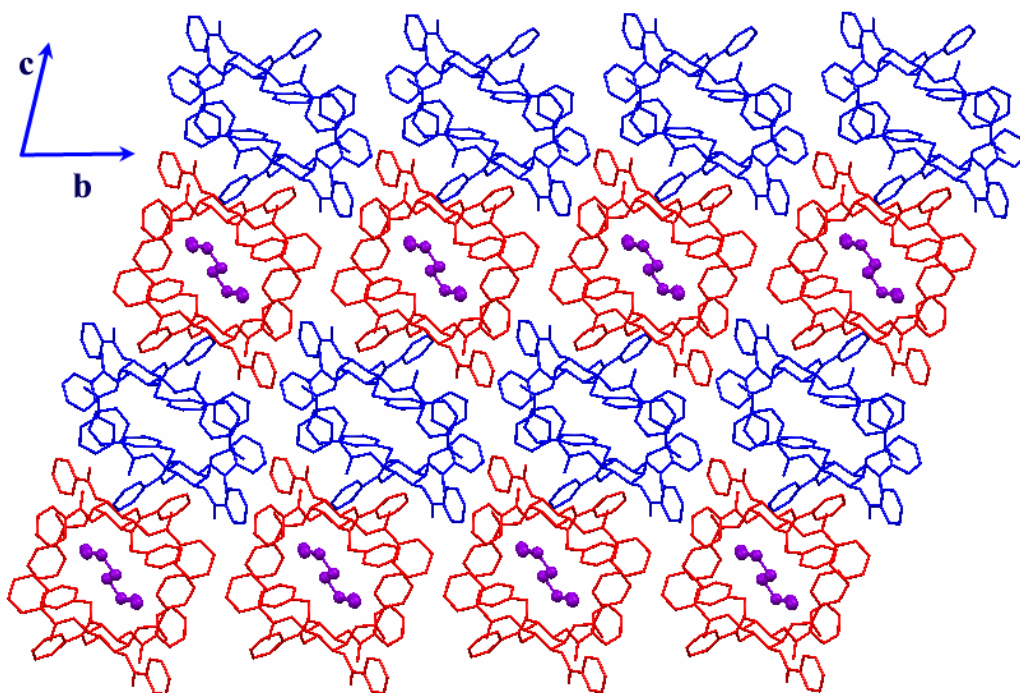


**Figure 4.21.** Molecular packing viewed down a-axis showing alternate arrangement of the cavities in **7·CHCl<sub>3</sub>**.

### *Host-Guest Interactions in 7·CHCl<sub>3</sub>*

The hydrogen H49 of chloroform molecule makes C-H···O contact with the carbonyl oxygen O11 of the host *molecule D3*. Although, the chloroform molecule shows

rotational disorder over four positions, chlorine atoms in each of the positions make C-H $\cdots$ Cl interactions with the host. The chlorine atoms Cl1, Cl2 and Cl3 of major occupancy chloroform molecule make stronger interactions with the host molecules; Cl2 and Cl3 make very short and almost linear C-H $\cdots$ Cl contacts with the *molecule* D3 (C4-H4 $\cdots$ Cl3 and C13-H13 $\cdots$ Cl2), whereas Cl1 makes a good C-Cl $\cdots$  $\pi$  interaction with phenyl ring of C3-*O*-benzoyl group of *molecule* D3. Other chlorine atoms make somewhat weaker C-H $\cdots$ Cl interactions with the host *molecule* D3 (Table 4.9).

**Table 4.9:** Host-guest interactions in 7·CHCl<sub>3</sub>.

D-H $\cdots$ A	D-H (Å)	H $\cdots$ A (Å)	D $\cdots$ A (Å)	D-H $\cdots$ A (°)
C(49)-H(49) $\cdots$ O(11)#2	0.97	2.28	3.027(9)	133
C(4)-H(4) $\cdots$ Cl(3)#1	0.98	2.86	3.814(7)	164
C(13)-H(13) $\cdots$ Cl(2)#2	0.93	3.01	3.902(10)	160
C(41)-H(41) $\cdots$ Cl(4)#1	0.93	2.79	3.411(9)	138
C(41)-H(41) $\cdots$ Cl(5)#1	0.93	3.02	3.900(14)	158
C(41)-H(41) $\cdots$ Cl(11)#1	0.93	2.86	3.746(14)	160
C(13)-H(13) $\cdots$ Cl(12)#2	0.93	2.54	3.34(2)	146
C49-Cl1 $\cdots$ Cg (3)#3	1.923	3.726	5.533(8)	156

Symmetry codes: #1 x,y,z; #2 -x+1,-y,-z+1; #3-x+2,-y,-z+1.

#### ***Host-Guest Interactions in 7·CHCl<sub>2</sub>Br***

The host-guest (having major occupancy) contacts in 7·CHCl<sub>2</sub>Br are similar to those observed in 7·CHCl<sub>3</sub>. The methyl hydrogen H49 of CHCl<sub>2</sub>Br makes weaker C-H $\cdots$ O contact with the carbonyl oxygen O11. The two chlorine atoms Cl1 and Cl2 are involved in short and almost linear C-H $\cdots$ Cl contact (C4-H4 $\cdots$ Cl2 and C13-H13 $\cdots$ Cl2) whereas the bromine Br1 makes good C-H $\cdots$ Br (C41-H41 $\cdots$ Br1) and C-Br $\cdots$  $\pi$  contacts with the phenyl

ring of the C3-*O*-benzoyl group. The other guest molecule with occupancy (0.4) also makes somewhat weaker C-H $\cdots$ Cl and C-H $\cdots$ Br interactions with the host *molecule* D3 (Table 4.10, Figure 4.22).

**Table 4.10:** Host-guest interactions in 7·CHCl<sub>2</sub>Br.

D-H $\cdots$ A	D-H/X (Å)	H $\cdots$ A/X (Å)	D $\cdots$ A (Å)	D-H/X $\cdots$ A (°)
C(49)-H(49) $\cdots$ O(11)#1	0.98	2.38	3.098(10)	129
C(4)-H(4) $\cdots$ Cl(2) #2	0.98	2.86	3.816(8)	164
C(13)-H(13) $\cdots$ Cl(1)#1	0.93	3.02	3.917(9)	163
C(49)-Br(1) $\cdots$ Cg(3)#3	1.975	3.586	5.469	158
C(41)-H(41) $\cdots$ Cl(3)#4	0.93	2.88	3.543(9)	129
C(34)-H(34) $\cdots$ Cl(4)#2	0.93	2.47	2.997(9)	116
C(41)-H(41) $\cdots$ Br(2)#2	0.93	3.03	3.894(8)	155
C(49)-Br(1) $\cdots$ Cg (3)#3	1.975	3.586	5.469	158

Symmetry codes: #1  $x, y, z$ ; #2  $x+1, y, z$ ; #3  $-1+x, y, z$ ; #4  $-x, 2-y, 1-z$ .

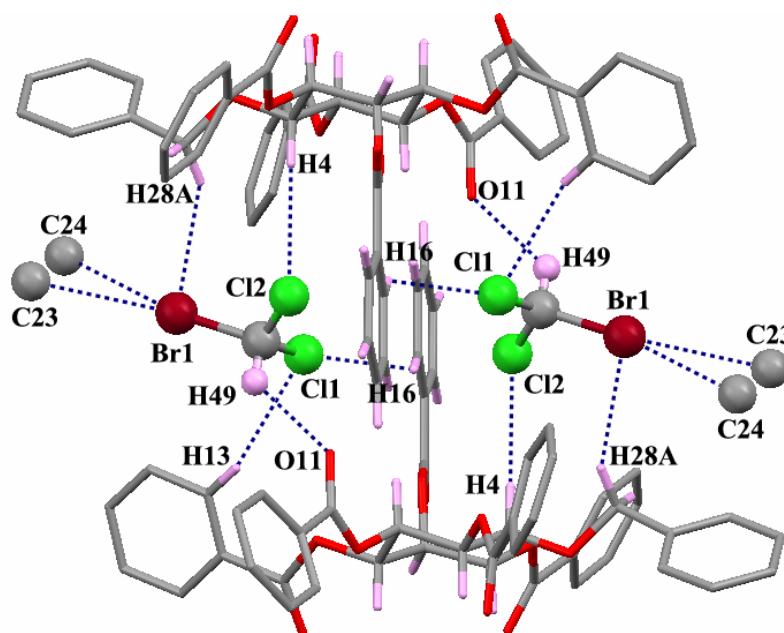


**Figure 4.22.** Significant host-guest interactions in 7·CHCl<sub>2</sub>Br, the host-guest interactions in 7·CHCl<sub>3</sub> are similar.

#### 4.3.4 Comparison of Conformations of Molecules of **7** in its Crystals **7**, **7**·**CH<sub>2</sub>Br<sub>2</sub>** and **7**·**CHCl<sub>3</sub>**

The overlap of the conformations of the benzoyl groups as well as benzyl group in host molecule of **7**·**CH<sub>2</sub>Br<sub>2</sub>** (blue) and **7**·**CHCl<sub>3</sub>** (green) are very similar in both. But the superimposing the host molecules of these with the solvent free crystals of **3** revealed an interesting feature; the orientation of the benzyl group in **7**·**CHCl<sub>3</sub>** (**7**·**CH<sub>2</sub>Br<sub>2</sub>**) and solvent free crystals of **3** (red) showed significant orientational change of about 61° (**Figure 4.23**). There are also differences in the conformations of all the benzoyl groups as well in the solvent free and **7**·**CHCl<sub>3</sub>** (**7**·**CH<sub>2</sub>Br<sub>2</sub>**).

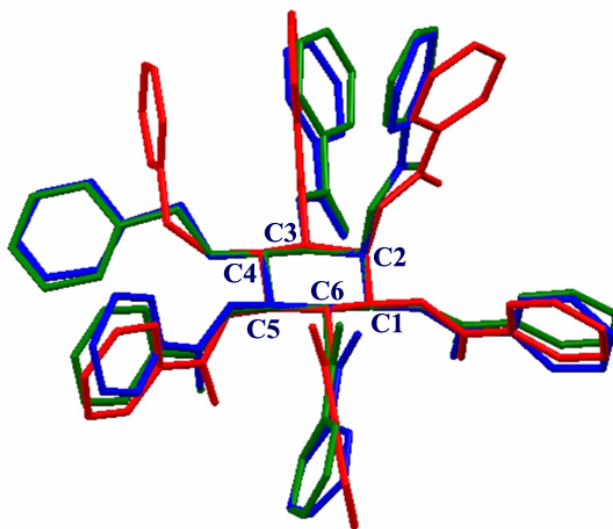


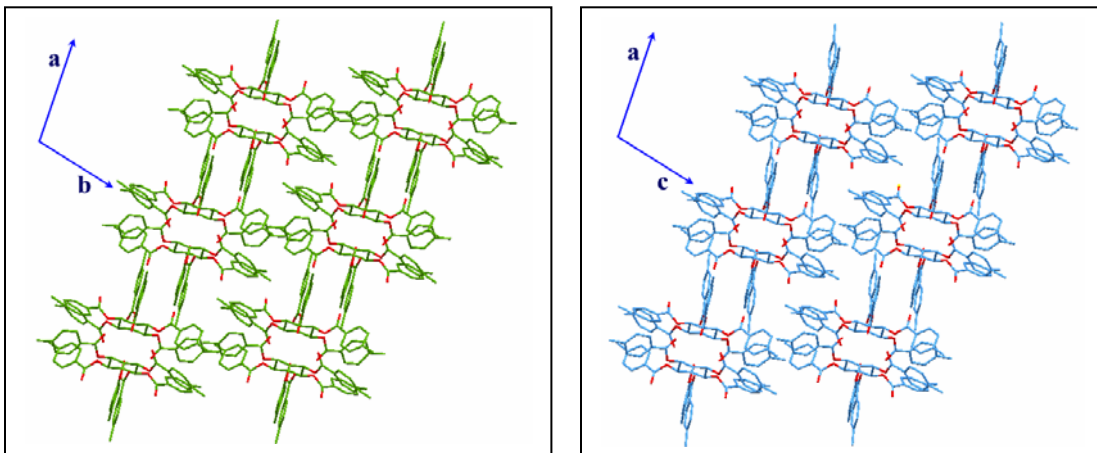
**Figure 4.23.** Molecular overlap of solvent free crystals (**7**, red), dibromomethane inclusion crystals (**7**·**CH<sub>2</sub>Br<sub>2</sub>**, blue) and chloroform inclusion crystals (**7**·**CHCl<sub>3</sub>**, green).

#### 4.4 Conclusions

Racemic 1,2,3,5,6-penta-*O*-benzoyl-4-*O*-benzyl-*myo*-inositol (**7**) formed inclusion complexes exclusively with halogenated solvents, whereas other solvents gave solvent free stable crystals. All the pseudopolymorphs were highly unstable in the open atmosphere. The host molecules formed centrosymmetric C-H $\cdots$ O assembly similar to the pseudopolymorphs of **3** and **4**. Two different types of packing modes were observed; in dihalomethane inclusion complexes (Form II) guest molecules occupied all the cavities generated by the host, whereas in the trihalomethane inclusion crystals (Form III), the guest molecules fill up only larger cavities (alternate cavities). Overall molecular packing of Form II inclusion complexes of **7** is similar to the dihalomethane inclusion complexes of **4** (Chapter 3). Thus, replacing the tosyl group at C4 position in **3** by a benzyloxy group maintained the pseudopolymorphic behavior but lost the specificity and stability of inclusion complexes.

# Chapter 5

## Single Crystal to Single Crystal Phase Transition of Room Temperature Form to High Temperature Form and Solvatomorphism in Hexa-*O*-*p*-toluoyl- *myo*-inositol: Synthesis, Crystallization and X-ray Studies



# Chapter 5

## 5.1 Introduction

In continuation with the exploration of clathration behaviour of symmetric hexa-*O*-substituted *myo*-inositol derivatives, one more analog of **4**, symmetric (meso) hexa-*O*-*p*-toluoyl-*myo*-inositol (**8**) was synthesized (Scheme 1). Crystallization from most of the solvents, **8** produced solvent free crystals (Form I). Interestingly, this form showed single crystal to single crystal phase transition upon heating to ~ 260 °C giving crystals of a new form (Form II). The Form II crystals could also be obtained by cooling the melt of **8**. Also crystallization of **8** from dioxane produced highly unstable inclusion complex (Form III). As mentioned earlier, this compound did not exhibit the inclusion tendency towards halogenated solvents. The X-ray structures of the three Forms I, II and III of **8** are discussed in this chapter.

## 5.2 Experimental Section

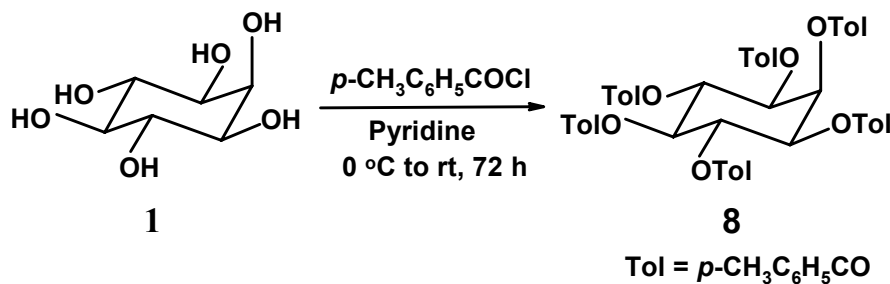
### 5.2.1 Synthesis

Hexa-*O*-*p*-toluoyl-*myo*-inositol was prepared by adding toluoyl chloride (20 mmol, ~3 g) drop wise to a mixture of *myo*-inositol (1.12 mmol, 0.2 g) in pyridine (5 mL) at 0 °C (Scheme 1). This was followed by a constant stirring of the reaction mixture at



room temperature for ~72 hrs. After usual work up and evaporation of the solvent, compound **8** separated as a white solid mass (0.62 g, 70%).

Scheme 1

**Data for 8:**

mp 263-264 °C; IR (CHCl<sub>3</sub>)  $\nu = 1722, 1724, 1722 \text{ cm}^{-1}$ ; <sup>1</sup>H NMR (CDCl<sub>3</sub>, 200 MHz):  $\delta$  2.29 (s, 15H), 2.49 (s, 3H), 5.75-5.85 (m, 2H), 5.94-6.04 (t, 1H), 6.28-6.37 (t, 3H), 7.04-7.10 (m, 10H), 7.26-7.39 (m, 2H), 7.69-7.79 (m, 10H), 8.02-8.07 (d, 2H); **Elemental analysis** calcd for C<sub>48</sub>H<sub>38</sub>O<sub>11</sub>; C 72.83%, H 4.61%; found C 72.42 %, H 4.33 %.

**5.2.2 Crystallization**

Crystallization of **8** was attempted by diffusing vapours of petroleum ether into the solution of **8** with almost all the common organic solvents like, acetone, ethyl acetate, dichloromethane, chloroform, benzene, dioxane, nitromethane etc. All the solvents gave solvent free crystals (Form I) (**Figure 5.1**) except dioxane, which produced highly unstable inclusion crystals (Form III).

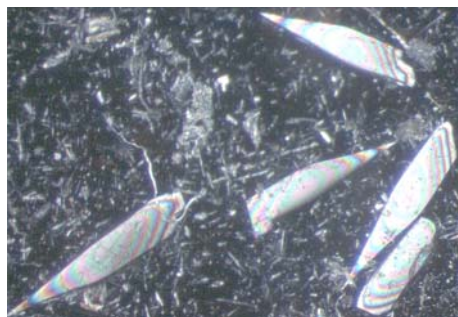


**Figure 5.1:** Solvent free crystals (Form I) of **8**.

### 5.2.3 DSC of Solvent Free Crystals

The DSC profile revealed a small endotherm at 261 °C ( $\Delta H = 4.0$  J/g) just before the onset of melting endotherm ( $\Delta H = 13.2$  J/g) at 274 °C suggesting a possible structural phase transition before melting (**Figure 5.2**). The DSC studies of the dioxane inclusion crystals (Form II) of **8** could not be carried out because of the instability of the crystals at room temperature.

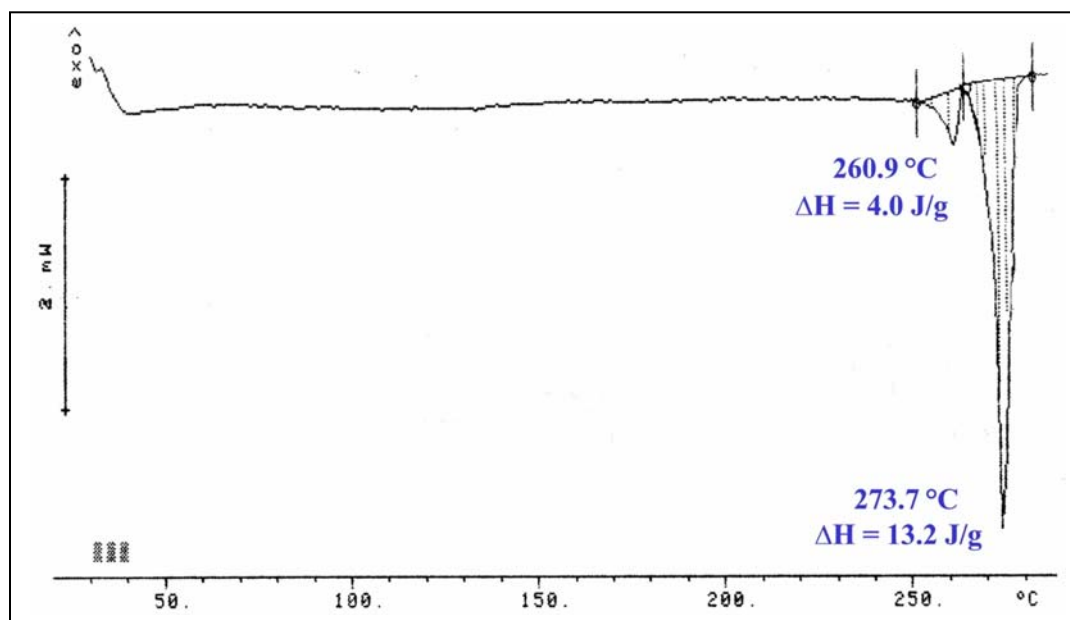


**Figure 5.2.** DSC of solvent free (Form I) crystals of **8**.

### 5.2.4 Thermal Response on Hot Stage Microscopy

Form I crystals were heated on a Leica polarizing microscope equipped with a heating stage P350. Around 190 °C, the upper surface of the crystals started becoming somewhat opaque but regained their transparency at ~265 °C, just before the melting at 272 °C (**Figure 5.3**). On continuing the heating further, the crystals melted ~ 274 °C and on cooling the melt crystallized immediately giving bigger crystals of good single crystalline nature as confirmed from the polarizing microscope.

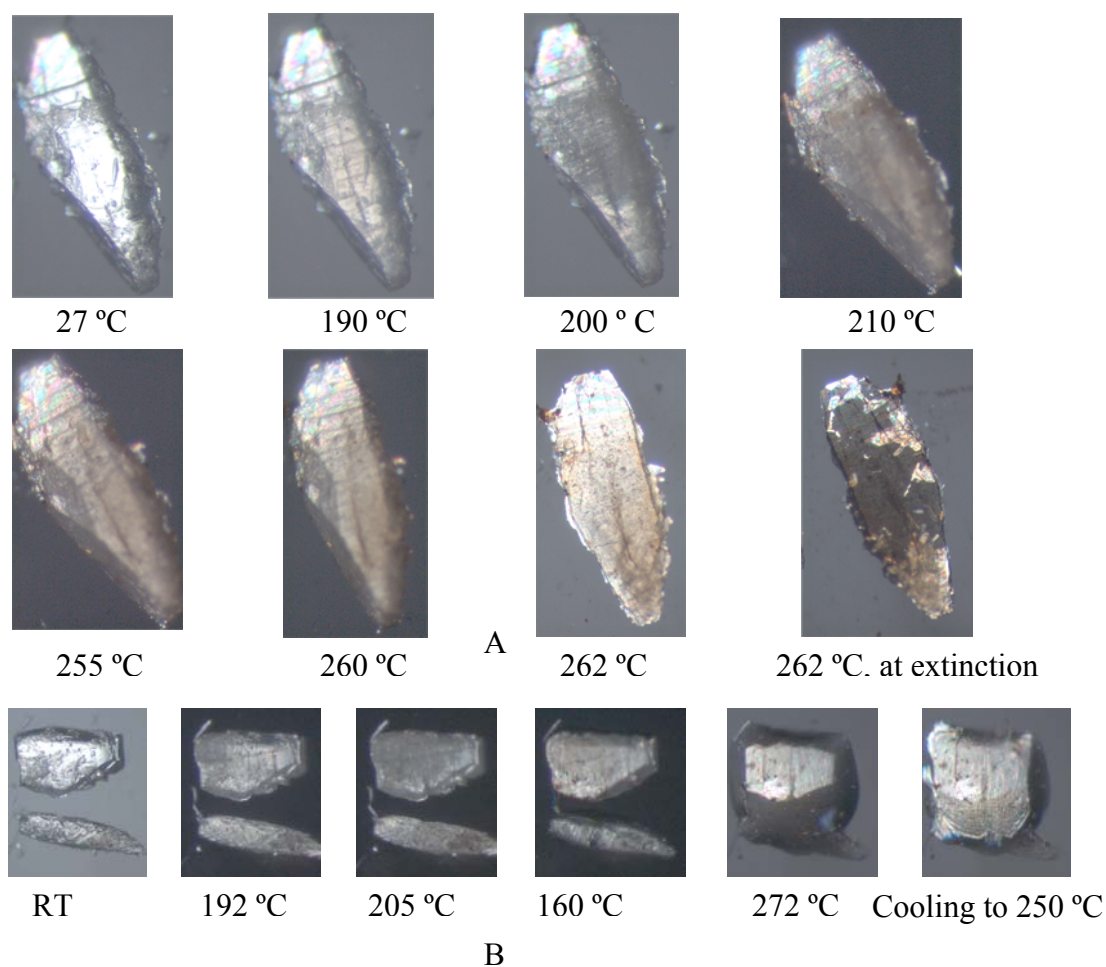


**Figure 5.3.** Photomicrographs of the thermal response of the Form I crystal of **8** heated under polarizing microscope, A) crystal-to-crystal phase transformation and B) melt crystallization.

### 5.2.5 X-Ray Data Collection, Structure Solution and Refinement

Diffraction data of Form I crystals of **8** (room temperature form) was collected at room temperature. The X-ray diffraction studies of the Form I crystals heated to 265 °C and cooled to room temperature revealed that the Form I had undergone crystal to crystal phase transition<sup>142</sup> giving rise to a new form of **8**, called Form II. Furthermore, the unit cell parameters of the crystals obtained from the melt of **8** were identical to the high temperature form, Form II. The crystal that started turning opaque (~ 210 °C, **Figure 5.3A**) was put on the diffractometer to check its crystallinity during the transition. Interestingly, the diffraction spots confirmed its single crystalline nature belonging to the Form I phase, but the high mosaicity and the bad least squares of the orientation matrix suggested that the phase transition had begun. Thus, it appears that the phase transformation starts around 190 °C and goes to completion between 255 °C-260 °C just before the melting. Reproducibility of this irreversible crystal-to-crystal transition<sup>35g</sup> was confirmed by repeating this experiment on several solvent free Form I crystals of **8**.

The X-ray data for Form III crystals (dioxane solvate, protected by paraffin oil coating) were collected at 133(2) K. Hydrogen atoms in all the structures were included in the refinement as per the riding model. Structures of both solvent free crystals Form I and Form II were refined to good R-value whereas the structure of dioxane inclusion crystals was refined to high R-value. The highly unstable nature of Form III inclusion crystals could be the reason for its high R-value (13%). Crystallographic data are summarized in **Table 5.1**.

**Table 5.1:** Crystal Data Table for Form I, Form II and Form III crystals of **8**.

	Form I	Form II	Form III
Chemical formula	C <sub>54</sub> H <sub>48</sub> O <sub>12</sub>	C <sub>54</sub> H <sub>48</sub> O <sub>12</sub>	C <sub>54</sub> H <sub>48</sub> O <sub>12</sub> · 1.25(C <sub>4</sub> H <sub>8</sub> O <sub>2</sub> )
M <sub>r</sub>	888.92	888.92	999.05
temperature/K	297(2)	297(2)	133(2)
Morphology	Plate	Plate	Prism
Crystal size	0.59 × 0.28 × 0.09	0.28 × 0.14 × 0.11	0.70 × 0.64 × 0.54
Crystal system	Triclinic	Monoclinic	Triclinic
Space group	<i>P</i> -1	<i>P</i> 2 <sub>1</sub> / <i>n</i>	<i>P</i> -1
<i>a</i> (Å)	12.150(8)	12.130(5)	14.173(3)
<i>b</i> (Å)	14.363(7)	30.223(11)	15.185(4)
<i>c</i> (Å)	16.451(11)	14.383(5)	16.475(4)
$\alpha$ (°)	99.374(15)	90	74.586(3)
$\beta$ (°)	106.419(12)	110.068(7)	77.393(4)
$\gamma$ (°)	111.167(14)	90	64.500(3)
<i>V</i> (Å <sup>3</sup> )	2453(3)	4953(3)	3063.3(13)
<i>Z</i>	2	4	2
<i>D</i> <sub>calc</sub> (g cm <sup>-3</sup> )	1.204	1.192	1.083
<i>F</i> (000)	936	1872	1056
$\mu$ (mm <sup>-1</sup> )	0.085	0.084	0.077
Ab. correction	Multi-scan	Multi-scan	Multi-scan
<i>T</i> <sub>min</sub>	0.952	0.977	0.948
<i>T</i> <sub>max</sub>	0.992	0.991	0.959
$\theta$ <sub>max</sub> (°)	25	25.0	25.0
<i>h</i> , <i>k</i> , <i>l</i> (min, max)	(-14,14), (-17,17), (-19,19)	(-14,14), (-35,35), (-16,17)	(-16,16), (-18,18), (-19,19)
Reflns collected	23496	35458	29021
Unique reflns	8569	8719	10681
Observed reflns	4648	3524	5398
No. of parameters	601	602	727
Restraints	0	0	122
GoF	1.024	0.964	1.356
R <sub>obs</sub>	0.0793	0.0628	0.1321
wR <sub>2_obs</sub>	0.1982	0.1334	0.3586
R <sub>all</sub>	0.1427	0.1838	0.2039
wR <sub>2_all</sub>	0.2366	0.1847	0.4073
$\Delta \rho_{\max}$ , $\Delta \rho_{\min}$ (eÅ <sup>-3</sup> )	0.33, -0.24	0.18, -0.18	1.02, -0.36

Form I and Form III crystals of **8** are triclinic P-1, whereas Form II crystals are monoclinic P2<sub>1</sub>/n. Unit cell lengths of Form I and II crystals before and after phase transition, bear some relationship. The length of a-axis (~12.15 Å) is almost the same in both the forms, b-axis length in Form I crystals matches with the c-axis length in Form II crystals and c-axis length of Form I crystals is about half of the b-axis length in Form II crystals (**Table 5.1**). There is some correspondence in the unit cell lengths of Forms I and III crystals too, but the inclusion of dioxane has obviously increased the unit cell volume in Form III crystals. But the c-axis length is almost the same in both the forms and lengthening of a-axis (by ~ 2 Å) and b-axis (~ 0.8 Å) is seen in Form III crystals compared to Form I crystals.

In Form III crystals of **8**, three molecules of dioxane occupy three different sites in crystal lattice, of which two have half occupancy and the third has 0.25 occupancy. One of the half occupied dioxane molecules showed rotational disorder over two positions with 0.25 occupancy at each position. Hence, a total of 1.25 molecules of dioxane are present in the crystal lattice per one molecule of the host **8**. The geometries of all the three-dioxane molecules were kept to an ideal chair confirmation by using restrain least-squares refinement keeping 1-2, 1-3 and 1-4 distances equal using DFIX instruction in the SHELXL97 program.<sup>122</sup>

## 5.3 Results and Discussion

### 5.3.1 Structures of Forms I and II Crystals of **8**

A perspective (ORTEP) view of the molecule is shown in **Figure 5.4**. All the benzoyl groups have extended conformation and there is no intramolecular interaction of any kind present in both forms.

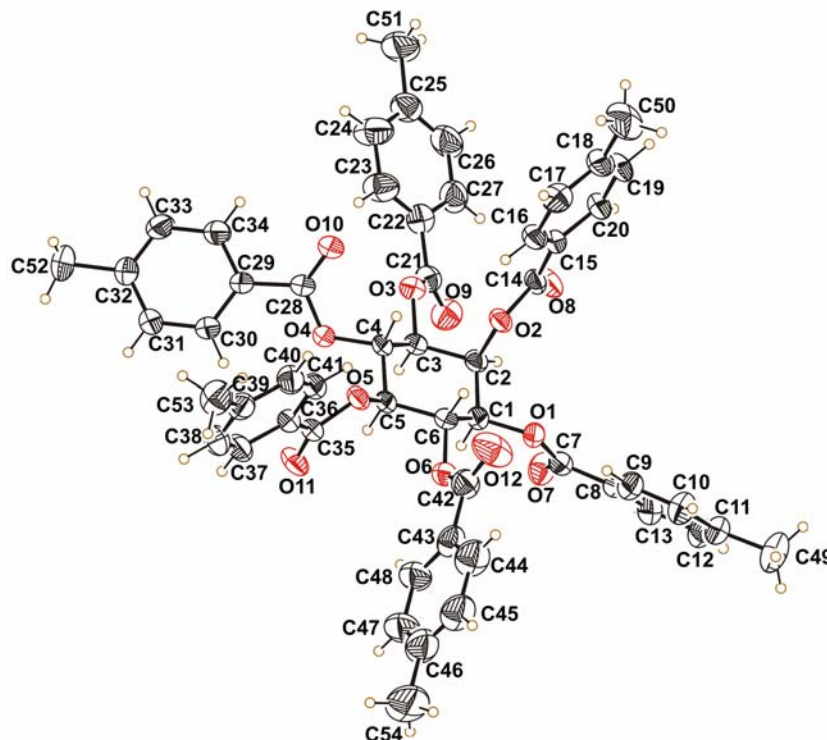


**Figure 5.4.** ORTEP view of Form I crystals of **8** (Form III crystals of **8** has similar view).

Molecules in Form I and Form II crystals of **8** make almost similar centrosymmetric trifurcated C-H $\cdots$ O assembly (**Figure 5.5**) as observed in all the earlier cases of *myo*-inositol derivatives [**3** (Chapter 2), **4** (Chapter 3) and **7**(Chapter 4)]. Two C-H $\cdots$ O contacts, namely C1-H1 $\cdots$ O11 and C3-H3 $\cdots$ O11 have better geometrical parameters than the third one (C5-H5 $\cdots$ O11, **Table 5.2**). In this ‘off centered’ trifurcation,

O11 points more towards the center of C1 and C3 atoms rather than being at the center of all the three atoms C1, C3 and C5 which was the case in structures of **3**, **4** and **7**. In both the forms centrosymmetric C48-H48 $\cdots$ O4 interaction (not shown in the **Figure 5.5** for clarity) provides additional support to stabilize centrosymmetric trifurcated C-H $\cdots$ O assembly (**Figure 5.5**). There are more weak interactions to add support; two centrosymmetric C-H $\cdots$  $\pi$  contacts made by methyl hydrogen H52B of C4-*O*-toluoyl group with phenyl ring of C1-*O*-toluoyl group and C31-H31 with the carbonyl group (C7=O7) and part of the phenyl (C8-C13) of C1-*O*-toluoyl group (**Table 5.2**). It is remarkable to note that the dimeric assembly is conserved even after the transformation of Form I crystals to Form II crystals upon heating, implying the robustness of this centrosymmetric assembly.

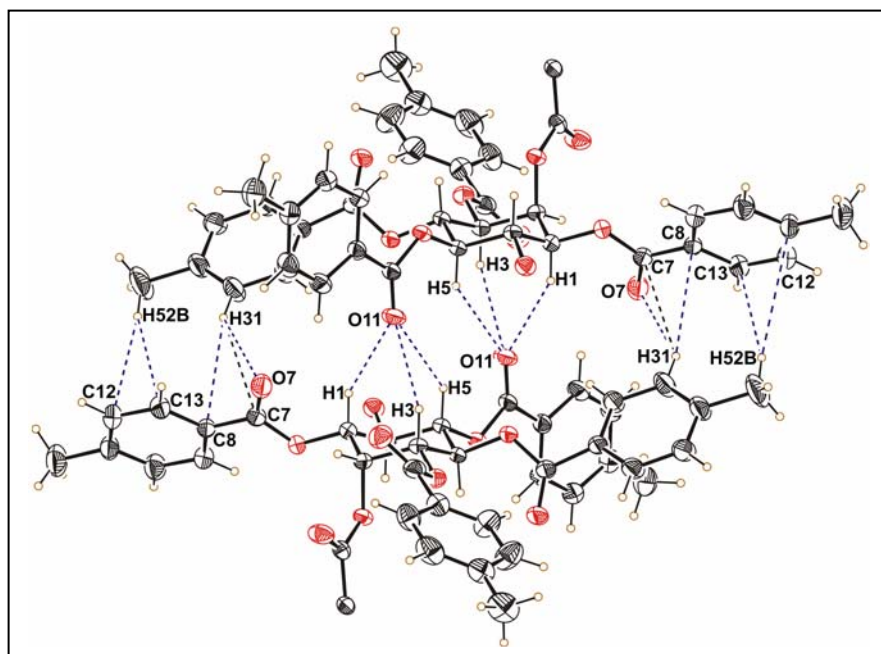


**Figure 5.5.** Closely interacting pair of molecules of Form I crystals of **8** (Form II crystals have similar molecular association).



**Table 5.2:** C-H $\cdots$ O and C-H $\cdots$  $\pi$  interactions in dimeric assembly formation in Form I and Form II crystals of **8**.

	D-H $\cdots$ A	D-H (Å)	H $\cdots$ A (Å)	D $\cdots$ A (Å)	D-H $\cdots$ A (°)
<b>Form I</b>	C(1)-H(1) $\cdots$ O(11)#1	0.98	2.48	3.361(4)	149
	C(3)-H(3) $\cdots$ O(11)#1	0.98	2.54	3.378(4)	144
	C(5)-H(5) $\cdots$ O(11)#1	0.98	2.84	3.598(4)	135
	C(31)-H(31) $\cdots$ O(7)#1	0.93	2.79	3.557(6)	140
	C(48)-H(48) $\cdots$ O(4)#1	0.93	2.88	3.690(7)	147
	C(52)-H(52B) $\cdots$ Cg(1)#1	0.96	3.21	4.123	159
<b>Form II</b>	C(1)-H(1) $\cdots$ O(11)#2	0.98	2.48	3.341(5)	147
	C(3)-H(3) $\cdots$ O(11)#2	0.98	2.49	3.369(5)	149
	C(5)-H(5) $\cdots$ O(11)#2	0.98	2.85	3.608(5)	135
	C(31)-H(31) $\cdots$ O(7)#2	0.93	2.84	3.609(6)	141
	C(48)-H(48) $\cdots$ O(4)#2	0.93	2.84	3.666(6)	148

Symmetry codes: #1 1-x, -y, -z; #2 2-x, 2-y, -z.

**Two Dimensional Isostructurality in Forms I and II Crystals of 8**

Molecular packing down the c-axis in Form I crystals (**Figure 5.6A**) and down the b-axis in Form II crystals (**Figure 5.6B**) reveal a two-dimensional isostructurality,<sup>137e</sup> as suggested by the similarity of the two unit cell parameters (**Table 5.1**). At the molecular level also the interactions within this layer are identical. Centrosymmetric dimers in Form I and Form II crystals are linked via dimeric C41-H41 $\cdots$ O12 contacts and centrosymmetric  $\pi\cdots\pi$  stacking interaction (**Tables 5.3** and **5.4**) between phenyl rings of axial C2-O-toluoyl group (Cg2) and equatorial C5-O-toluoyl group (Cg5) along the a-axis. Dimeric C34-H34 $\cdots$ O10 contacts along the b-axis in Form I crystals and along the c-

axis in Form III crystals (**Figure 5.6C**) are also seen. However, C-H $\cdots$ O contact in Form II crystals are marginally weaker than in Form I crystals.

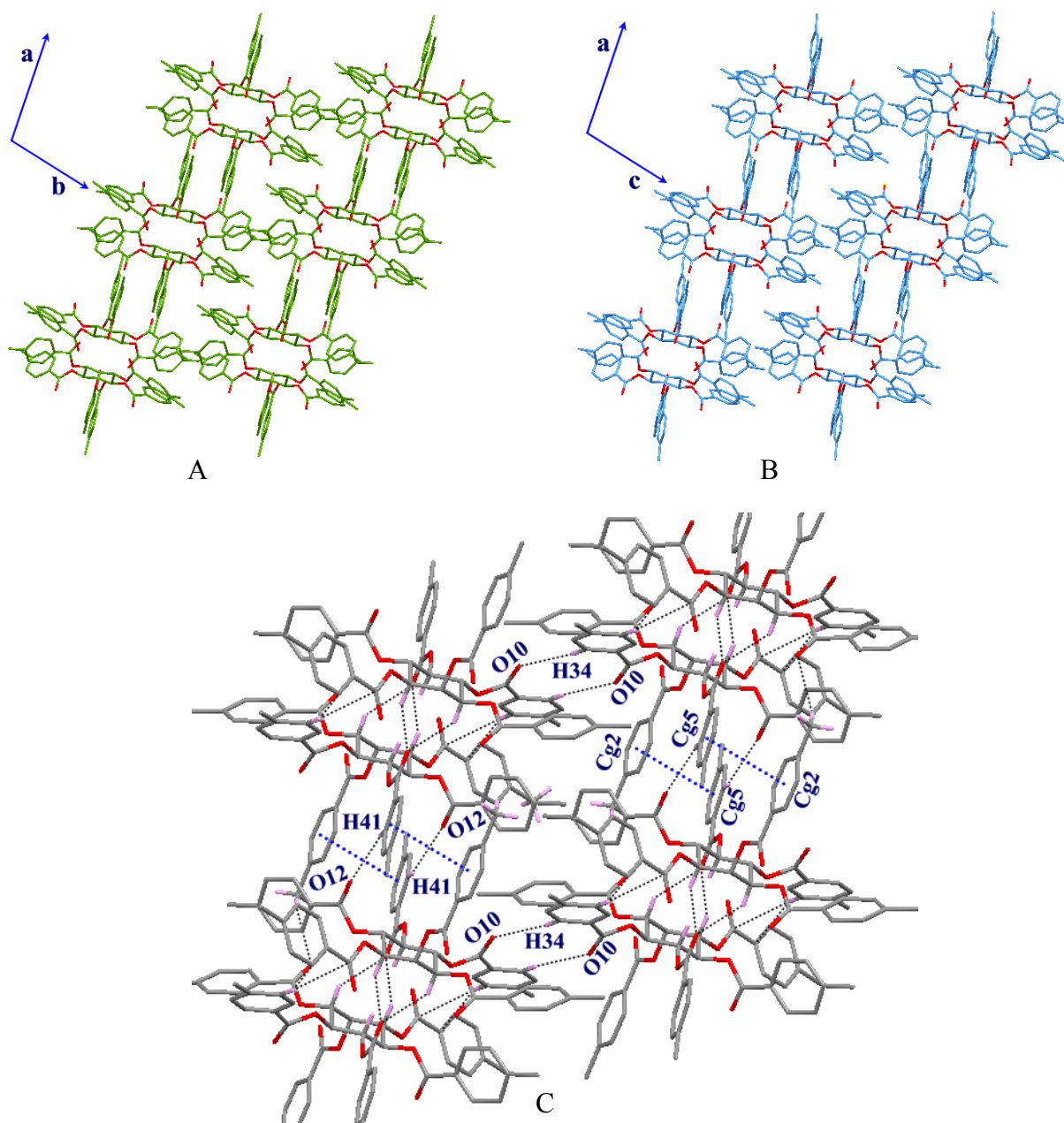


**Figure 5.6.** Identical association of the centrosymmetric synthons in A) Form I crystals, B) Form II crystals and C) close view in Form I crystals of **8**, blue dotted lines indicate  $\pi \cdots \pi$  stacking interaction.

**Table 5.3:** Intermolecular C-H $\cdots$ O and C-H $\cdots$  $\pi$  interactions involved in linking dimeric assembly in Form I and Form II crystals of **8**.

	D-H $\cdots$ A	D-H (Å)	H $\cdots$ A (Å)	D $\cdots$ A (Å)	D-H $\cdots$ A (°)
<b>Form I</b>	C(12)-H(12) $\cdots$ O(8)#2	0.93	2.68	3.494(5)	146
	C(34)-H(34) $\cdots$ O(10)#3	0.93	2.47	3.218(5)	137
	C(41)-H(41) $\cdots$ O(12)#4	0.93	2.71	3.399(5)	131
	C(49)-H(49B) $\cdots$ O(8)#2	0.96	2.65	3.398(6)	135
	C(52)-H(52C) $\cdots$ Cg(2)#3	0.96	2.94	3.685	135
<b>Form II</b>	C(34)-H(34) $\cdots$ O(10)#6	0.93	2.58	3.246(5)	129
	C(41)-H(41) $\cdots$ O(12)#5	0.93	2.84	3.571(6)	136
	C(50)-H(50C) $\cdots$ O(9)#7	0.96	2.57	3.296(6)	133
	C(49)-H(49C) $\cdots$ O(7)#8	0.96	2.73	3.268(5)	116
	C(49)-H(49B) $\cdots$ O(8)#8	0.96	2.49	3.411(6)	160
	C(52)-H(52C) $\cdots$ Cg(2)#9	0.96	2.98	3.861	153

Symmetry codes: #1 -x+1,-y,-z; #2 -x+1,-y,-z+1; #3 -x+1,-y+1,-z; #4 -x+2,-y+2,-z;  
#5 -x+1,-y+2,-z; #6 -x+2,-y+2,-z+1; #7 x-1,y,z; #8 x-1/2,-y+3/2,z-1/2; #9 -x,-y,1-z.

**Table 5.4:** Intermolecular  $\pi\cdots\pi$  stacking interactions in Form I and Form II crystals of **8**.

	Cg $\cdots$ Cg	Cg $\cdots$ Cg (Å)	Alpha (°)	CgI_Perp (Å)	CgJ_Perp (Å)
<b>Form I</b>	Cg(1) $\cdots$ Cg(1)#1	4.596	0.02	3.177	3.177
	Cg(2) $\cdots$ Cg(5)#2	4.041	10.42	3.687	3.687
<b>Form II</b>	Cg(2) $\cdots$ Cg(5)#3	4.059	15.20	3.586	3.857

Symmetry codes: #1 1-x,-y,1-z; #2 -x,-1-y,-z; #3 1-x,-y,2-z, Cg1 = C8-C13,  
Cg2 = C15-C20, Cg5 centroid of the phenyl ring, C36 -C41.

***Different Pathways of Associations in Form I and Form II Crystals of 8***

The difference in the two forms is best seen along the third dimension. Molecular packing down the a-axis clearly reveals the differences in the mode of association of the dimeric units in both polymorphs (**Figure 5.7**). The almost doubling of the unit cell length of Form I crystals after phase transition to Form II crystals can be seen. Bridging of the centrosymmetric assemblies (**Figure 5.5**) along the c-axis in Form I crystals and along the b-axis in Form II crystals is different. In Form I crystals, they are linked via dimeric C12-H12 $\cdots$ O8, C49B-H49B $\cdots$ O8 contacts (**Table 5.3**) as well as via centrosymmetric  $\pi\cdots\pi$  stacking interaction between phenyl rings of C1-*O*-toluoyl group (**Figure 5.7A**, **Table 5.4**), whereas in Form II crystals, they have catameric (two-fold screw) association along the b-axis via C49B-H49B $\cdots$ O8 interaction (**Figure 5.7B**, **Table 5.3**).

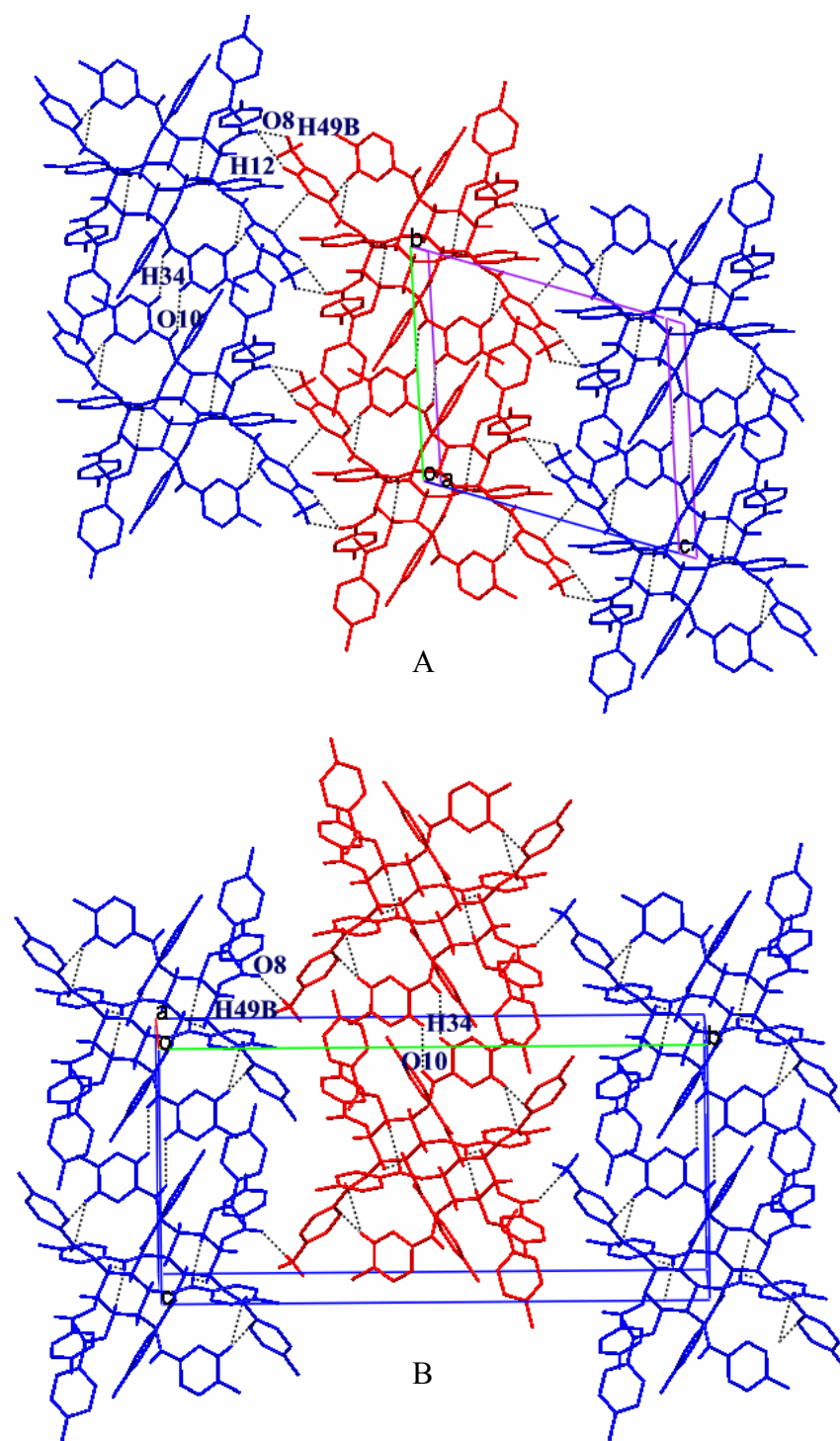


**Figure 5.7.** View of molecular packing down the a-axis in, A) Form I and B) Form II crystals of **8**.

### 5.3.2 Structure of Dioxane Inclusion Crystals (Form III) of **8**

The host molecules in Form III crystals of **8** also form trifurcated C-H $\cdots$ O assembly (**Figure 5.8**). The centrosymmetric interactions C1-H1 $\cdots$ O11, C3-H3 $\cdots$ O11 and C5-H5 $\cdots$ O11 are of comparable strength to each other (**Table 5.5**). The carbonyl oxygen O11 is in the center of the C1, C3 and C5 atoms unlike in Form I and Form III crystals of **8** (see **section 5.7.1**). Two more C-H $\cdots$ O interactions C48-H48 $\cdots$ O4 (not shown in **Figure 5.8** for the sake of clarity) and C37-H37 $\cdots$ O7 give additional support to this bimolecular association.

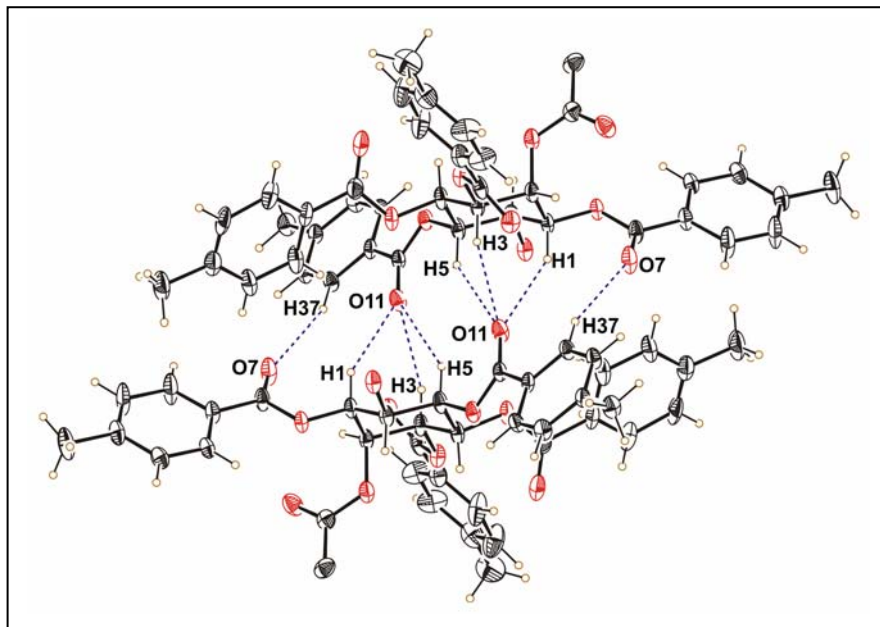


**Figure 5.8.** ORTEP view of closely interacting pair of molecules of dioxane inclusion crystals (Form III) of **8**.

**Table 5.5:** Intermolecular C-H $\cdots$ O interactions in dimeric assembly formation in Form III crystals of **8**.

D-H $\cdots$ A	D-H (Å)	H $\cdots$ A (Å)	D $\cdots$ A (Å)	D-H $\cdots$ A (°)
C(1)-H(1) $\cdots$ O(11)#1	0.98	2.34	3.214(7)	148
C(3)-H(3) $\cdots$ O(11)#1	0.98	2.62	3.419(8)	139
C(5)-H(5) $\cdots$ O(11)#1	0.98	2.49	3.321(7)	142
C(37)-H(37) $\cdots$ O(7)#1	0.93	2.58	3.460(7)	159
C(48)-H(48) $\cdots$ O(4)#1	0.93	2.83	3.595(7)	140

Symmetry codes: #1 -x+2,-y,-z+1.

These trifurcated C-H $\cdots$ O centrosymmetric dimers (**Figure 5.8**) are linked via marginal C-H $\cdots$  $\pi$  interaction along the b-axis forming one-dimensional molecular string (**Figure 5.9A** and **Table 5.6**). The C49-H49A of the methyl group of the C1-O-toluoyl group makes off centered C-H $\cdots$  $\pi$  interaction with the phenyl ring of the C5-O-toluoyl group. There are no other notable contacts between the dimeric assemblies along this string. Along the c-axis, these assemblies make dimeric  $\pi\cdots\pi$  contacts (*between the phenyl rings of C3-O- toluoyl group*,  $Cg3\cdots Cg3 = 4.241 \text{ \AA}$  and dihedral angle ( $\alpha$ ) =  $0.02^\circ$ ) as well as dimeric C-H $\cdots$  $\pi$  contacts between the methyl hydrogen H51A and phenyl ring of C3-O- toluoyl group (**Table 5.6**). Thus, the dimers make weak cohesions along the b and c-axes to form rectangular open-framework structure when viewed down the a-axis (**Figure 5.9B**) with open channels ( $\sim 10 \times 12 \text{ \AA}$ ) that include dioxane. This open framework structure formed purely by organic molecule<sup>143</sup> resembles nanoporous

framework created by metal-organic hybrid structures.<sup>144</sup> These have potential applications in selective inclusions used for molecular separations.

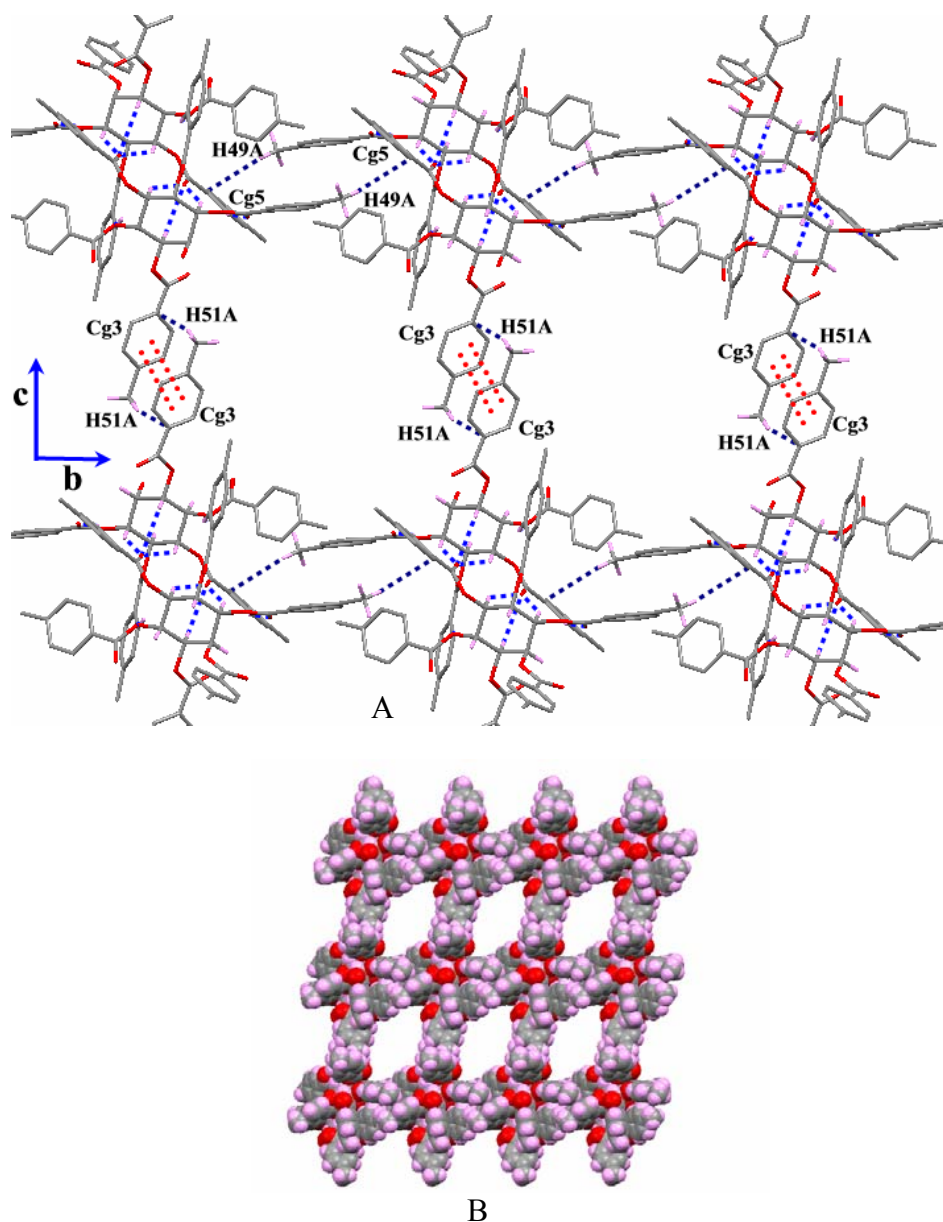


**Figure 5.9.** A) Molecular packing viewed roughly down the a-axis showing association of the host molecules via C-H... $\pi$  and  $\pi$ ... $\pi$  (red dotted lines) contacts forming open framework structure and B) CPK view of the same assembly (dioxane guest is omitted to show porosity).



**Table 5.6:** Intermolecular C-H $\cdots$ O and C-H $\cdots$  $\pi$  interactions involved in linking dimeric assembly in Form III of **8**.

D-H $\cdots$ A	D-H ( $\text{\AA}$ )	H $\cdots$ A ( $\text{\AA}$ )	D $\cdots$ A ( $\text{\AA}$ )	D-H $\cdots$ A ( $^\circ$ )
C(55)-H(55B) $\cdots$ O(9)#1	0.93	2.74	3.452(13)	131
C(49)-H(49A) $\cdots$ Cg(5)#2	0.96	2.97	3.730(11)	137
C(53)-H(53A) $\cdots$ Cg(6)#3	0.96	2.98	3.636(14)	127
C(53)-H(53C) $\cdots$ Cg(5)#3	0.96	2.85	3.680(11)	145

Symmetry codes: # 1  $x-1, y, z$ ; #2  $x, 1+y, z$ ; #3  $1-x, -y+1, -z$ . Cg5 and Cg6 – centroid of the phenyl rings C36-C41 and C43-C48 respectively.

### *Molecular Association Down c-axis*

Molecular packing down the c-axis shows the linking of the dimers via weak C-H $\cdots$  $\pi$  interactions along the a and b-axes forming a two-dimensional sheet (**Figure 5.10**). The C49-H49A $\cdots$  $\pi$  (Cg5, phenyl ring of C5-O-toluoyl group) interaction joins them along the b-axis, whereas along the a-axis they are associated via C53-H53C $\cdots$  $\pi$  (Cg5) interaction.

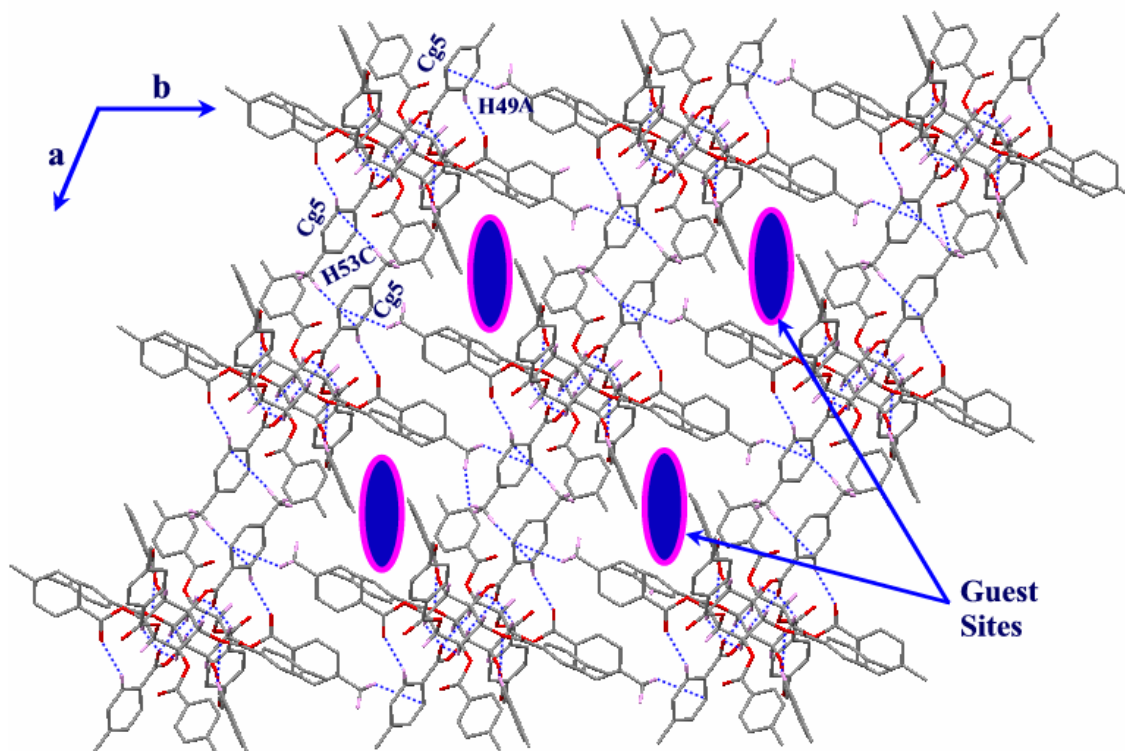


**Figure 5.10.** Associations of the centrosymmetric dimeric assemblies down c-axis in Form II crystals of **8**. Oval shape (blue with magenta border) represents guest molecules.

The open framework structure formed by the centrosymmetric C-H $\cdots$ O assemblies (**Figure 5.9**) down the a-axis accommodates two molecules of dioxane (green and red in **Figure 5.11** and sites A and B in **Figure 5.12**), whereas the disordered dioxane molecules (purple in **Figure 5.11** and site C in **5.12**) are located above and below the plane of molecular sheet (**Figure 5.12**).

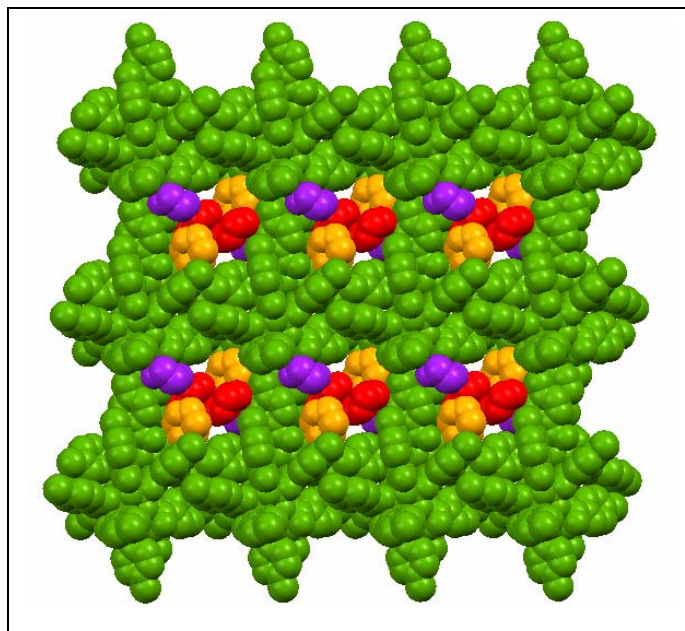


**Figure 5.11.** CPK view of host-guest assembly viewed down the a-axis in Form III crystals of **8**.

### *Host-Guest and Guest-Guest Interactions*

The dioxane molecules in the open channel are engaged in C-H $\cdots$ O contacts with the host (**Figure 5.12**, **Table 5.7**). Dioxane molecules with 0.5 occupancy (A) make seven C-H $\cdots$ O interactions. It accepts three protons from the host molecules and donates four of its hydrogen atoms. The oxygen O13 of dioxane (A) molecule makes bifurcated C-H $\cdots$ O contacts by accepting protons bonded to C33, C52 (C33-H33 $\cdots$ O13 and C52-H52B $\cdots$ O13, former has better geometry as compared with the latter) and oxygen O14 makes another weak C-H $\cdots$ O contact with H27 of the host (C27-H27 $\cdots$ O14). Methylene H-atoms H55A and H55B of the dioxane molecule make weak C-H $\cdots$ O interactions with the carbonyl oxygen O8 and O9 respectively of the host, whereas two protons H56B and H58A of dioxane are involved in guest-guest weak C-H $\cdots$ O interactions with the ether

oxygens O16 and O15 of the other dioxane molecule (B, 0.25 occupancy) in the same channel (C56-H56B···O16 and C58-H58A···O15). The dioxane molecule B does not make any contacts with the host molecule but its ether oxygens O15 and O16 are involved in accepting H-atoms from the half occupied dioxane molecule (A) as discussed above. The dioxane molecule (C), which is disordered over two positions, also makes C-H···O interactions with the host (only one position is shown for clarity in **Figure 5.12**). At one position its ether oxygen O18 makes bifurcated good C-H···O hydrogen bond with C26-H26 and C49-H49C groups of the host (C26-H26···O18 and C49-H49C···O18) and on other position, the ether oxygen O19 accepts protons from C4-H4 and C16-H16 groups of the host to form weak C4-H4···O19 and C16-H16···O19 contacts (not shown in the **Figure 5.12**) whereas other ether oxygens O17 and O20 (dioxane not shown in the **Figure 5.12**) did not take part in any interactions.

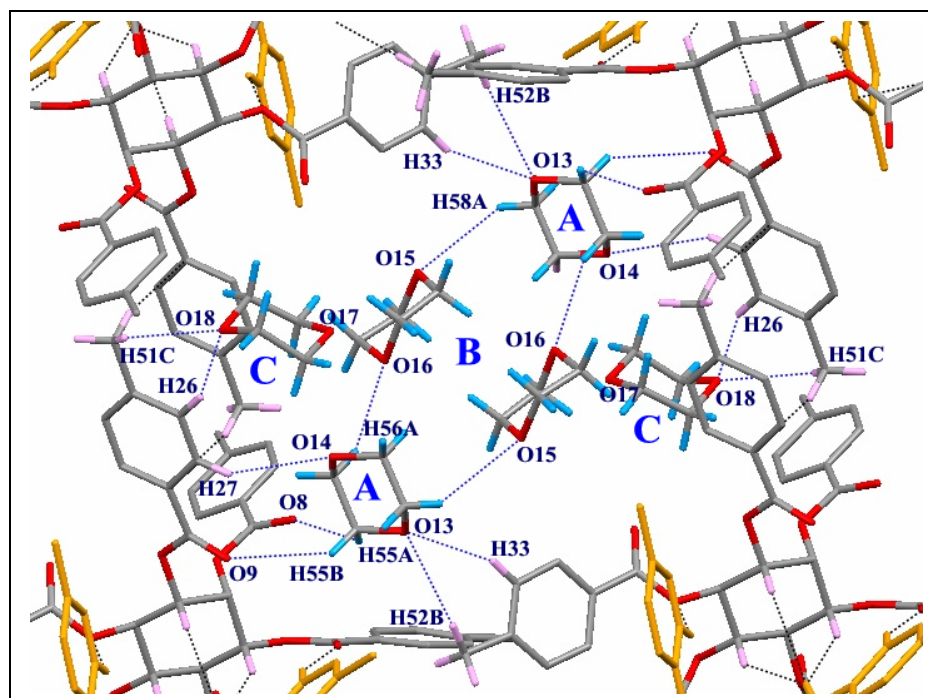


**Figure 5.12.** Host-guest interactions in Form III (dioxane inclusion) crystals of **8**.

**Table 5.7:** Intermolecular host-guest and guest-guest (C-H $\cdots$ O and C-H $\cdots\pi$ ) interactions in Form III crystals of **8**.

D-H $\cdots$ A	D-H (Å)	H $\cdots$ A (Å)	D $\cdots$ A (Å)	D-H $\cdots$ A (°)
C(33)-H(33) $\cdots$ O(13)#1	0.93	2.54	3.409(9)	156
C(52)-H(52B) $\cdots$ O(13)#1	0.96	2.74	3.525(13)	139
C(27)-H(27) $\cdots$ O(14)#2	0.93	2.75	3.503(13)	139
C(55)-H(55A) $\cdots$ O(8)#3	0.97	2.90	3.604(12)	130
C(55)-H(55B) $\cdots$ O(9)#3	0.97	2.74	3.452(15)	131
C(56)-H(56B) $\cdots$ O(16)#4	0.97	2.67	3.570(18)	155
C(58)-H(58A) $\cdots$ O(15)#5	0.97	2.83	3.529(17)	130
C(26)-H(26) $\cdots$ O(18)#1	0.93	2.56	3.434(15)	157
C(49)-H(49C) $\cdots$ O(18)#5	0.96	2.40	3.352(17)	171
C(4)-H(4) $\cdots$ O(19)#6	0.98	2.81	3.751(12)	162
C(16)-H(16) $\cdots$ O(19)#6	0.93	2.81	3.083(17)	140
C(58)-H(58A) $\cdots$ O12#5	0.97	2.72	3.423(11)	130

Symmetry codes: #1  $x+1, y-1, z$ ; #2  $x+1, y, z$ ; #3  $x-1, y, z$ ; #4  $-x+1, -y+1, -z$ ; #5  $x, y, z$ ; #6  $x, y-1, z$ .

### 5.3.3 Difference Between Structures of Form I and Form III Crystals of **8**

Molecular packing viewed down the  $c$ -axis in Form I crystals (**Figure 5.13A**) and down the  $b$ -axis in Form III crystals (**Figure 5.13B**) of **8** clearly showed the difference in molecular organization upon inclusion of dioxane molecules. The elongation of  $a$ -axis by  $\sim 2$  Å in Form III compared to Form I is due to the inclusion of solvent along this axis. The centrosymmetric C-H $\cdots$ O assemblies (**Figure 5.8**) are moved further away along this axis breaking C41-H41 $\cdots$ O12 contact and generating in its place a weak C-H $\cdots\pi$  (C53-H53C $\cdots$ Cg5, not shown in the **Figure 5.13A**) interaction. The oxygen O12, left free from the host interaction, makes a bifurcated C62-H62B $\cdots$ O12 and C58-H58A $\cdots$ O12

interactions with the methylene H-atoms of the dioxane guest (**Figure 5.13B**). Another change upon inclusion of dioxane is the loss of C34-H34 $\cdots$ O10 contact linking dimers in Form I crystals along the b-axis (the involvement of O10 in C67-H67B $\cdots$ O10 contact instead of C34-H34 $\cdots$ O10 as seen in Form I crystals).

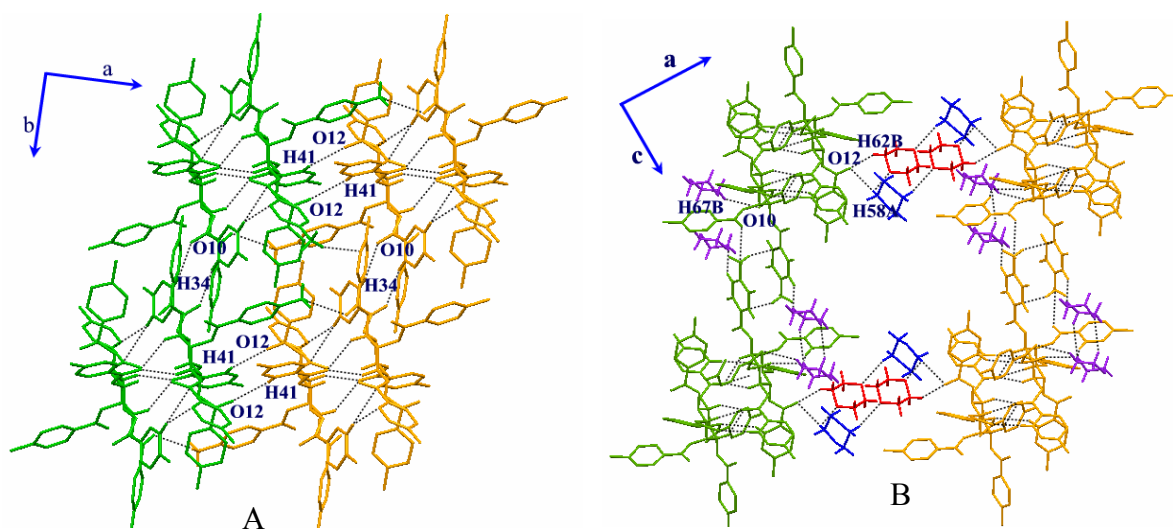


**Figure 5.13.** Molecular packing, A) down the c-axis in Form I crystals and B) down the b-axis in Form II crystals of **8**.

### 5.3.4 Conformational Difference in Molecules of Form I, Form II and Form III of **8**

The superposition of the molecules of Form I and Form II crystals of **8** revealed slight difference in the conformations of C1, C2, C3 and C6-*O*-toluoyl groups, whereas the conformations of C4 and C5-*O*-toluoyl groups are similar (**Figure 5.14**). This clearly shows that the structural phase transition upon heating from Form I to Form II is accompanied by very little conformational change in the molecule. But the molecule of Form III showed a marked difference in the orientations of toluoyl groups at C2, C3 and C5 positions as compared to the Form I and Form II crystals of **8** (**Figure 5.14**).

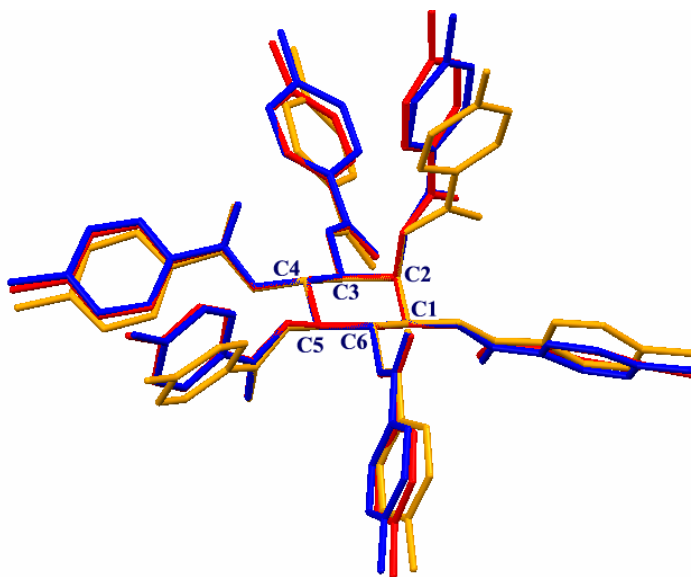


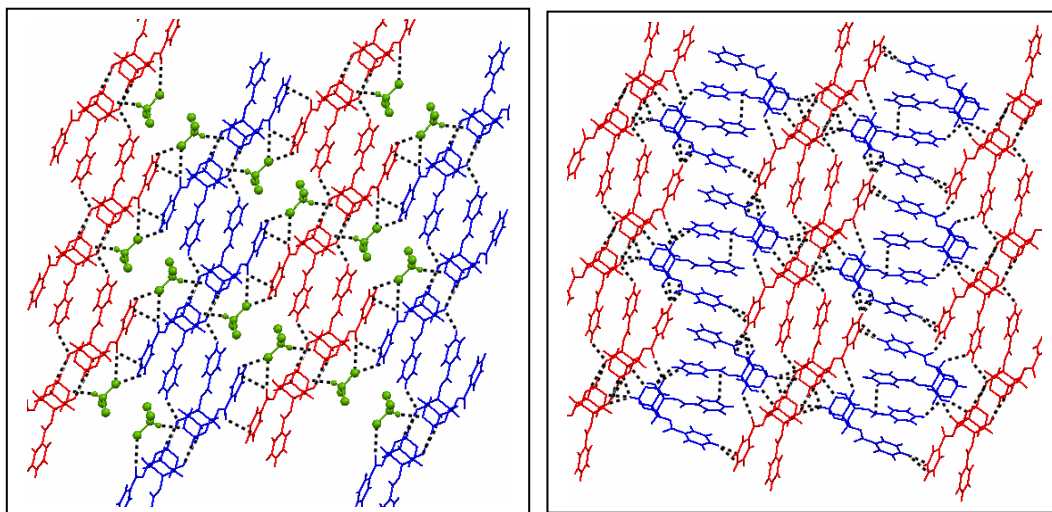
**Figure 5.14.** View of Molecular overlap of Form I (blue), Form II (red) and Form III (orange) crystals of **8**.

#### 5.4 Conclusions

Hexa-*O*-toluoyl-*myo*-inositol (**8**) gave stable solvent free crystals (Form I) from most of the organic solvents except dioxane, which produced highly unstable inclusion crystals (Form III). Form I crystals undergo crystal-to-crystal phase transition to produce Form II crystals upon heating, which can also be obtained from cooling the melt. The molecular packing in the two forms show two-dimensional isostructurality,<sup>137e</sup> the difference comes from their organization along the third dimension. Similar to all other hexa-*O*-acyl derivatives of *myo*-inositol, molecules in all the forms of **8** also associated via centrosymmetric trifurcated C-H $\cdots$ O contacts. In solvent free forms (Form I and Form II crystals), these assemblies are packed in a very compact way leaving no room for the solvent inclusion, whereas in Form III crystals the dimers have weaker cohesion thereby creating an open framework that includes dioxane molecules in the crystal lattice.

# Chapter 6

## Exploring the Inclusion Behaviour of 4,6-di-*O*- benzoyl-*myo*-inositol-1, 3, 5 - orthoformate and its orthoacetate Analog: Isostructurality in Host Organization and Self-Inclusion Phenomena





# Chapter 6

## 6.1 Introduction

As seen in earlier chapters, the hexa-*O*-acyl-*myo*-inositol derivatives have a tendency to form the inclusion complexes with small organic solvent molecules as guests. It was decided worthwhile to explore the inclusion behavior of C1, C3 and C5 protected *myo*-inositol 1,3,5-orthoesters. To perform these studies various *myo*-inositol 1,3,5-orthoesters derivatives were prepared in our laboratory. This chapter discusses the inclusion behaviour of 4,6-di-*O*-benzoyl-*myo*-inositol-1,3,5-orthoformate (**9**) and its orthoacetate derivative (**10**, Figure 6.1).

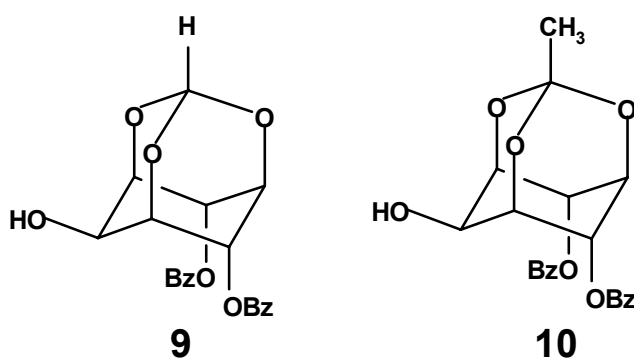


**Figure 6.1.** Structure of **9** and **10**

The dibenzoate **9** produced inclusion complexes exclusively with halogenated solvent molecules, whereas non-halogenated solvents produced solvent free crystals.

Stability of these inclusion crystals was seen to depend largely on the presence of the halogen bonding interactions between the host and the guest. Solvent free crystals of compound **9**, present an interesting structure where molecules of **9** play the role of host as well as guest ('self inclusion'). Detailed structural analysis of crystals of **9**, its solvates and the crystal structure of orthoacetate derivative **10** are reported in the following sections.

## 6.2 Experimental Section

### 6.2.1 Synthesis

The dibenzoates **9** (Lit. m.p. 205-207 °C)<sup>117,145</sup> and **10** (Lit. m.p. 160-162 °C)<sup>146</sup> were prepared as reported earlier.

### 6.2.2 Crystallization

Crystallization of **9** was attempted from most of the common organic solvents by slow evaporation as well as vapour diffusion method (petroleum ether was used for diffusion). The crystal growth experiments and the results obtained are listed in **Table 6.1**.

**Table 6.1:** Crystallization data of **9** from various solvents.

Trial No	Solvent Used	Method of Crystallization*	Result
1	Dichloromethane	1	Pseudopolymorph, <b>9</b> ·CH <sub>2</sub> Cl <sub>2</sub>
2	Chlorobromomethane	1	Pseudopolymorph, <b>9</b> ·CH <sub>2</sub> ClBr
3	Dibromomethane	1	No crystals were obtained
4	Chloroform	1	Pseudopolymorph, <b>9</b> ·CHCl <sub>3</sub>
5	Bromoform	1	Pseudopolymorph, <b>9</b> ·CHBr <sub>3</sub>
6	Dichlorobromomethane	1	Pseudopolymorph, <b>9</b> ·CHCl <sub>2</sub> Br
7	Ethyl acetate/Pet. ether	1, 2	Very thin needles (Whiskers)
8	Nitromethane	2	Very thin needles
9	Tetrahydrofuran	2	Very thin needles
10	Toluene	2	Very thin needles
11	Acetonitrile	2	Very thin needles
12	Benzene	2	Very thin needles
13	Methanol	2	Very thin needles
14	Acetone	1, 2	Very thin needles
15	Dioxane	1	Very thin needles

\*1= Vapour diffusion; 2 = Slow evaporation

Amongst the inclusion crystals of **9**, those containing CH<sub>2</sub>Cl<sub>2</sub> and CH<sub>2</sub>ClBr were highly unstable in the open atmosphere, whereas those from CHCl<sub>3</sub> (**Figure 6.1A**), CHBr<sub>3</sub> (**Figure 6.1B**) and CH<sub>2</sub>ClBr were stable up to two-three days. Observation of the latter crystals under the polarizing microscope revealed the crystals going opaque from one end of the crystal to the other end, which was later understood in terms of the solvent escape along channels in the direction [100] (**Figure 6.1C**). Solvent free crystals were very thin needles (whiskers) and attempt to grow bigger crystals of **9** were unsuccessful. However, relatively larger crystals could be grown from ethyl acetate-petroleum ether mixture (4:1) (Trial 7 (1) in **Table 6.1** and **Figure 6.1D**). It was interesting that the orthoacetate substitution (**10**) produced only solvent free plate like crystals in most of the trials (trials same as 1,4,7,8,9,11,13,14 in **Table 6.1**).

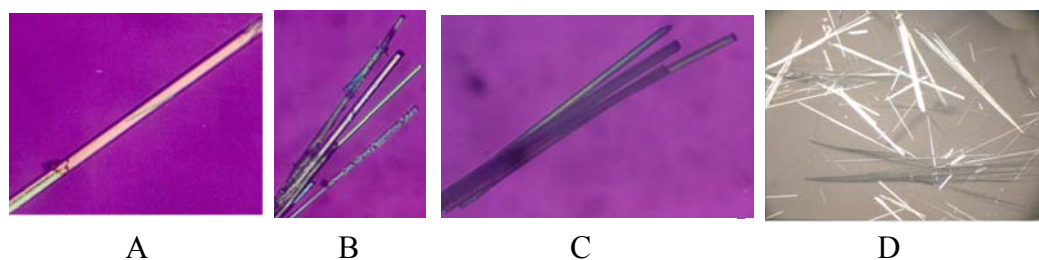


**Figure 6.1.** Photomicrographs of crystals of **9** from, A) chloroform, B) bromoform, C) chloroform crystals after one day in open atmosphere and D) solvent free crystals from trail 7 in **Table 6.1**.

### 6.2.3 Thermal Analysis of Inclusion Crystals of **9**

The DSC of **9**·CHCl<sub>3</sub> chloroform crystals showed an endothermic peaks ~ 75 °C followed by exothermic peak ~ 85 °C, probably indicating the escape of chloroform molecules followed by an exothermic phase transition between 85 °C and 122 °C and the endothermic peak at 208 °C associated with the melting of the crystals (**Figure 6.2A**). The DSC of **9**·CHBr<sub>3</sub> crystals also showed two endothermic peaks, first one at 103 °C and the second one corresponding to the melting at 206 °C (**Figure 6.2B**). The DSC of **9**·CHCl<sub>2</sub>Br also exhibited the pattern as **9**·CHBr<sub>3</sub>, but the first endotherm was at a lower temperature (69 °C), and the second one a melting endotherm (209 °C). Since all the three solvates have comparable melting points, it is highly possible that the first endotherm (**Figure 6.2**) is due to escape of solvent molecules. Broad endotherms prior to melting suggest a gradual release of the guest molecules from the crystal lattice.

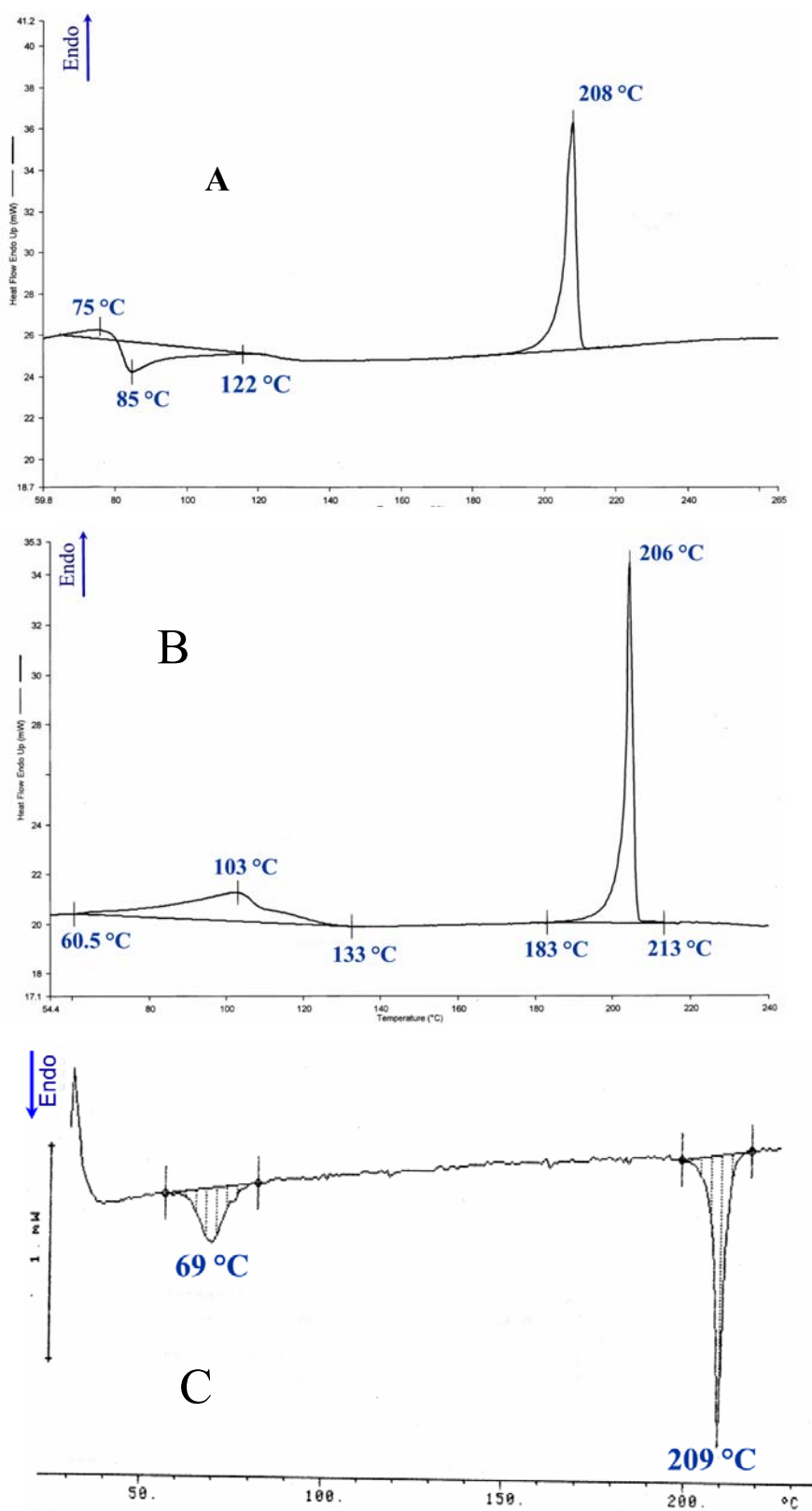


**Figure 6.2.** DSC profiles of inclusion crystals of **9** obtained from A) chloroform, B) bromoform and C) dichlorobromomethane.

### 6.2.4 Hot Stage Microscopy

Inclusion crystals  $\mathbf{9}\cdot\text{CHCl}_3$  and  $\mathbf{9}\cdot\text{CHBr}_3$  were heated on the Leica polarizing microscope (5 °C/minute). Crystals of  $\mathbf{9}\cdot\text{CHCl}_3$  became opaque  $\sim 60$  °C (**Figure 6.3A**), whereas those obtained from bromoform ( $\mathbf{9}\cdot\text{CHBr}_3$ ) lost their crystallinity at  $\sim 100$ -103 °C (**Figure 6.3B**) before both finally melted between 210-213 °C.

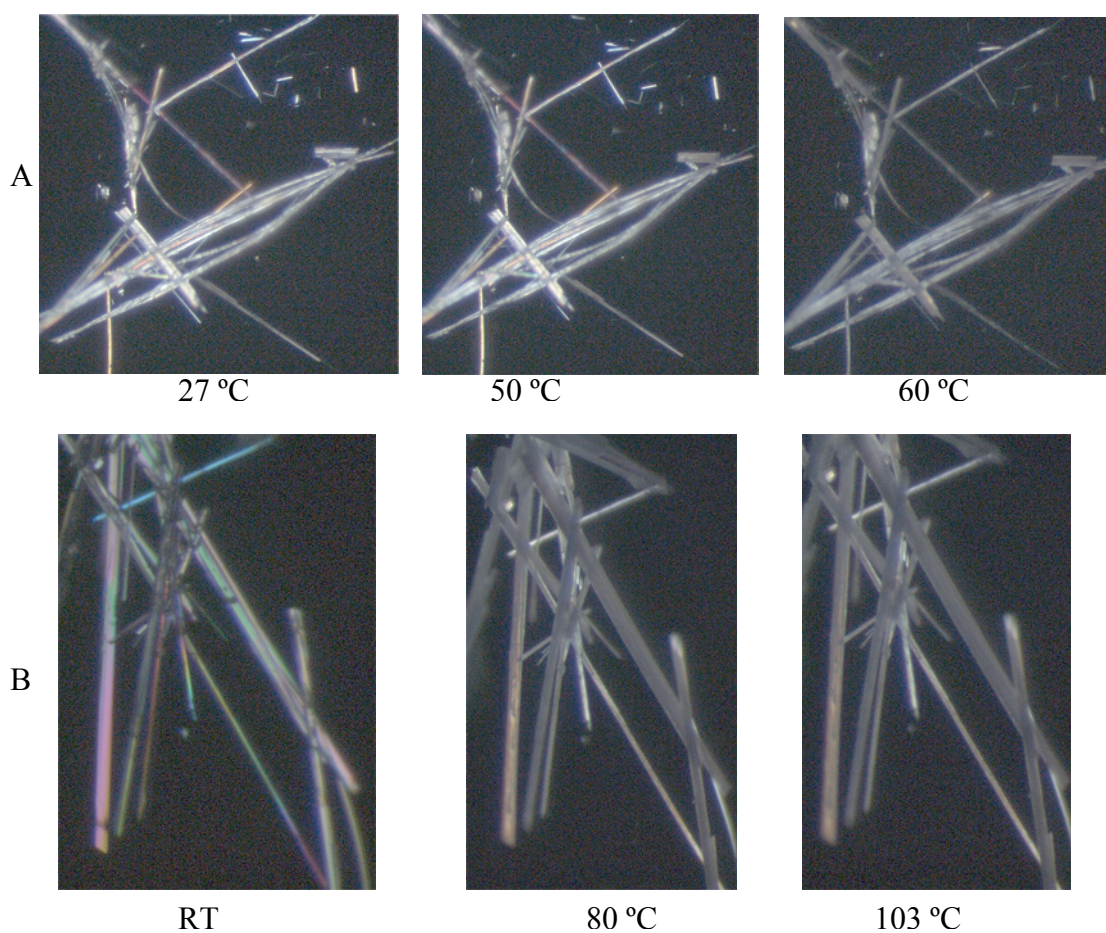


**Figure 6.3.** Photomicrographs of inclusion crystals of  $\mathbf{9}$  obtained from A) chloroform ( $\mathbf{9}\cdot\text{CHCl}_3$ ) and B) bromoform ( $\mathbf{9}\cdot\text{CHBr}_3$ ) while heating.

### 6.2.5 X-ray Data Collection, Structure Determination and Refinement

Single crystal X-ray data measurements were carried out on five solvates and solvent free crystals of **9** and solvent free crystals of **10**. Inclusion crystals **9·CH<sub>2</sub>Cl<sub>2</sub>** and **9·CH<sub>2</sub>ClBr** were soaked in paraffin oil in order to protect them from exposure to the open atmosphere. Suitable single crystals were selected using Leica polarizing microscope and mounted on the glass fibre with epoxy cement and immediately taken into the liquid nitrogen stream maintained at 133K (OXFORD 700 series LN2 open-flow cryostat.). The crystals were allowed to stabilize for half an hour at 133K before proceeding for data collection. The X-ray data for inclusion crystals **9·CHCl<sub>3</sub>**, **9·CHBr<sub>3</sub>** and **9·CHCl<sub>2</sub>Br** and solvent free crystals **9** and **10** were collected at room temperature (297K). Crystallographic data for all the crystals are summarized in **Table 6.2**. In all the solvates of **9**, the host:guest ratio was 1:1.

Both **9·CH<sub>2</sub>Cl<sub>2</sub>** and **9·CH<sub>2</sub>ClBr** are isostructural (**Table 6.2**) and the structures were refined to a rather higher R-value (0.08%) because of the highly unstable nature of these inclusion crystals. The included CH<sub>2</sub>ClBr molecule in **9·CH<sub>2</sub>ClBr** showed statistical disorder over two positions with bromine and chlorine atoms sharing positions with half occupancy each at the same site with CH<sub>2</sub> group being common in both the orientations. The bond lengths of the C-Cl and C-Br of CH<sub>2</sub>ClBr were restrained using DFIX option in SHELXTL. Unit cell parameters of **9·CHCl<sub>3</sub>** revealed similarity to **9·CH<sub>2</sub>Cl<sub>2</sub>** and **9·CH<sub>2</sub>ClBr** except the c-axis length was increased by ~ 1.4 Å. The crystals **9·CHBr<sub>3</sub>** and **9·CHCl<sub>2</sub>Br** are isomorphous. Interestingly, the space group of these two inclusion crystals is different (P-1) than its predecessors (P2<sub>1</sub>/n), although, unit cell axes bear some relations. The length of a and b-axes in **9·CHBr<sub>3</sub>** and **9·CHCl<sub>2</sub>Br** are very

close to those of  $\mathbf{9}\cdot\text{CH}_2\text{Cl}_2$ ,  $\mathbf{9}\cdot\text{CH}_2\text{ClBr}$  and  $\mathbf{9}\cdot\text{CHCl}_3$ , whereas the c-axis is reduced to half the length compared to crystals  $\mathbf{9}\cdot\text{CH}_2\text{Cl}_2$ ,  $\mathbf{9}\cdot\text{CH}_2\text{ClBr}$  and  $\mathbf{9}\cdot\text{CHCl}_3$ . Asymmetric unit of solvent free crystals of  $\mathbf{9}$  contained two symmetry independent molecules, whereas that of  $\mathbf{10}$  contained only one molecule. A curious relationship between the unit cell parameters of the solvent free crystals of  $\mathbf{9}$  and inclusion crystals of  $\mathbf{9}$  was observed. The a and b axes are of the same magnitude but with the transformation of  $a \rightarrow b$  and  $b \rightarrow a$  axis. The c-axis length is elongated by  $\sim 14 \text{ \AA}$  in  $\mathbf{9}$  as compared to  $\mathbf{9}\cdot\text{CH}_2\text{Cl}_2$  and  $\mathbf{9}\cdot\text{CH}_2\text{ClBr}$ . All the hydrogen atoms in  $\mathbf{9}\cdot\text{CH}_2\text{Cl}_2$ ,  $\mathbf{9}\cdot\text{CH}_2\text{ClBr}$ ,  $\mathbf{9}\cdot\text{CHCl}_2\text{Br}$  and solvent free crystals of  $\mathbf{9}$  and  $\mathbf{10}$  included in the refinement as per the riding model except for  $\mathbf{9}\cdot\text{CHCl}_3$  and  $\mathbf{9}\cdot\text{CHBr}_3$  in which the H-atoms were located from a difference Fourier map and were refined isotropically. The inclusion complexes of  $\mathbf{9}$  are categorized into two groups, Group I ( $\mathbf{9}\cdot\text{CH}_2\text{Cl}_2$ ,  $\mathbf{9}\cdot\text{CH}_2\text{ClBr}$  and  $\mathbf{9}\cdot\text{CHCl}_3$ ) and Group II ( $\mathbf{9}\cdot\text{CHBr}_3$  and  $\mathbf{9}\cdot\text{CHCl}_2\text{Br}$ ).



**Table 6.2:** Crystal Data of Solvates **9** and Solvent free Crystals of **9** and **10**.

	<b>9·CH<sub>2</sub>Cl<sub>2</sub></b>	<b>9·CH<sub>2</sub>ClBr</b>	<b>9·CHCl<sub>3</sub></b>
Chemical formula	C <sub>21</sub> H <sub>18</sub> O <sub>8</sub> · CH <sub>2</sub> Cl <sub>2</sub>	C <sub>21</sub> H <sub>18</sub> O <sub>8</sub> · CH <sub>2</sub> ClBr	C <sub>21</sub> H <sub>18</sub> O <sub>8</sub> · CHCl <sub>3</sub>
M <sub>r</sub>	483.28	527.74	517.72
Temperature/K	133(2)	133(2)	297(2)
Morphology	Thin needle	Thin needle	Needle
Crystal size	0.71×0.07×0.024	0.77×0.11×0.03	0.77×0.07×0.03
Crystal system	Monoclinic	Monoclinic	Monoclinic
Space group	<i>P</i> 2 <sub>1</sub> / <i>n</i>	<i>P</i> 2 <sub>1</sub> / <i>n</i>	<i>P</i> 2 <sub>1</sub> / <i>n</i>
<i>a</i> (Å)	6.316(3)	6.420(6)	6.2775(10)
<i>b</i> (Å)	13.408(6)	13.679(13)	12.993(2)
<i>c</i> (Å)	25.382(13)	25.96(3)	26.789(4)
$\beta$ (°)	91.566(10)	90.73(4)	92.771(3)
<i>V</i> (Å <sup>3</sup> )	2148.6(18)	2280(4)	2182.5(6)
<i>Z</i>	4	4	4
<i>D</i> <sub>calc</sub> (g cm <sup>-3</sup> )	1.494	1.538	1.576
$\mu$ (mm <sup>-1</sup> )	0.350	1.966	0.469
<i>F</i> (000)	1000	1072	1064
Ab.Correction	Multi-scan	Multi-scan	Multi-scan
<i>T</i> <sub>min</sub>	0.789	0.313	0.714
<i>T</i> <sub>max</sub>	0.992	0.953	0.986
$\theta$ <sub>max</sub> (°)	25	25	25
<i>h</i> , <i>k</i> , <i>l</i> (min, max)	(-7,7), (-15,15), (-30,30)	(-5,6), (-13,13), (-24,24)	(-6,7), (-15,15), (-25,31)
Reflns collected	19057	6552	10840
Unique reflns	3783	2084	3851
Observed reflns	2594	1305	2940
R <sub>int</sub>	0.0969	0.1184	0.0416
No. of parameters	293	313	374
Restraints	0	4	0
GoF	1.127	1.139	1.015
R <sub>1</sub> [ <i>I</i> > 2σ( <i>I</i> )]	0.0835	0.0878	0.0440
wR <sub>2</sub> [ <i>I</i> > 2σ( <i>I</i> )]	0.1524	0.1835	0.1045
R <sub>1</sub> _all data	0.1287	0.1424	0.0600
wR <sub>2</sub> _all data	0.1684	0.2061	0.1115
$\Delta \rho_{\max}$ , $\Delta \rho_{\min}$ (eÅ <sup>-3</sup> )	0.72, -0.55	0.29, -0.27	0.73, -0.60

	<b>9.CHBr<sub>3</sub></b>	<b>9.CHCl<sub>2</sub>Br</b>	<b>9</b>	<b>10</b>
Chemical formula	C <sub>21</sub> H <sub>18</sub> O <sub>8</sub> · CHBr <sub>3</sub>	C <sub>21</sub> H <sub>18</sub> O <sub>8</sub> · CHCl <sub>2</sub> Br	C <sub>21</sub> H <sub>18</sub> O <sub>8</sub>	C <sub>22</sub> H <sub>20</sub> O <sub>8</sub>
M <sub>r</sub>	651.10	562.18	398.35	412.38
Temperature/K	297(2)	133(2)	297(2)	297(2)
Morphology	Needle	Needle	Thin needle	Thin plate
Crystal size	0.82×0.06×0.02	0.82×0.05×0.03	1.00×0.09×0.03	0.65×0.13×0.13
Crystal system	Triclinic	Triclinic	Monoclinic	Orthorhombic
Space group	<i>P</i> -1	<i>P</i> -1	<i>P</i> 2 <sub>1</sub> / <i>c</i>	<i>P</i> na2 <sub>1</sub>
<i>a</i> (Å)	6.3686(7)	6.3499(8)	14.570(5)	11.646(3)
<i>b</i> (Å)	12.9056(13)	12.9978(17)	6.261(2)	11.101(2)
<i>c</i> (Å)	14.7324(15)	14.6720(19)	39.927(13)	14.949(3)
$\alpha$ (°)	67.374(2)	66.898(2)	90	90
$\beta$ (°)	85.408(2)	86.114(2)	91.493(6)	90
$\gamma$ (°)	87.943(2)	89.020(2)	90	90
<i>V</i> (Å <sup>3</sup> )	1114.1(2)	1111.2(2)	3641(2)	1932.7(7)
<i>Z</i>	2	2	8	4
<i>D</i> <sub>calc</sub> (g cm <sup>-3</sup> )	1.941	1.680	1.453	1.417
$\mu$ (mm <sup>-1</sup> )	5.480	2.138	0.113	0.109
<i>F</i> (000)	640	568	1664	864
Ab.Correction	Multi-scan	Multi-scan	Multi-scan	Multi-scan
<i>T</i> <sub>min</sub>	0.094	0.273	0.895	0.932,
<i>T</i> <sub>max</sub>	0.880	0.948	0.997	0.986
$\theta$ <sub>max</sub> (°)	25	25	25	25
<i>h</i> , <i>k</i> , <i>l</i> (min, max)	(-7,7),(-15,15), (-17,17)	(-7,7),(-15,15), (-17,17)	(-17,17),(-7,7), (-47,47)	(-13,13),(- 10,13), (-17,17)
Reflns collected	10878	10591	33400	9116
Unique reflns	3923	3869	6417	3374
Observed reflns	2893	2902	3707	3026
R <sub>int</sub>	0.0428	0.0357	0.1044	0.0220
No. of parameters	374	299	526	351
GoF	0.894	1.049	1.034	1.060
R <sub>1</sub> [ <i>I</i> > 2σ( <i>I</i> )]	0.0326	0.0692	0.0612	0.0297
wR <sub>2</sub> [ <i>I</i> > 2σ( <i>I</i> )]	0.0612	0.1889	0.1050	0.0630
R <sub>1</sub> _all data	0.0496	0.0944	0.1243	0.0353
wR <sub>2</sub> _all data	0.0647	0.2095	0.1267	0.0651
$\Delta \rho_{\max}$ , $\Delta \rho_{\min}$ (eÅ <sup>-3</sup> )	0.94, -0.53	1.60, -1.117	0.20, -0.21	0.09, -0.13

## 6.3 Results and Discussion

### 6.3.1 Intramolecular Geometry in Solvates and Solvent Free Crystals of **9**

Molecules in crystals of **9** make identical intramolecular contacts in all the solvates as they have similar conformation<sup>147</sup> (**Figure 6.4A** and **6.4B**). The two symmetry independent molecules in solvent free crystals of **9** superpose quite well except for minor conformational difference between the axial benzoyl groups ( $\sim 3\text{-}6^\circ$ , cyan and dark green in **Figure 6.4B**). It is interesting to note that the conformation of these two symmetry independent molecules is almost the same with respect to the to the host molecule of all the inclusion complexes of **9** (**Figure 6.4B**). There are a total of six intramolecular interactions of type O-H $\cdots$ O and C-H $\cdots$ O in all the crystals of **9**. The equatorial hydroxyl group O2-H2A makes bifurcated O-H $\cdots$ O contacts with the orthoformate bridge oxygens O1 and O3. Another bifurcated contact of C-H $\cdots$ O is made by C2-H2 of the inositol ring with ether oxygens O4 and O6 (**Table 6.3**). The two axial benzoate groups are away from each other and do not make any interaction. The two molecules in the asymmetric unit of **9** (solvent free crystals) also interact with each other via C-H $\cdots$ O contacts. The orthoformate bridge oxygen O3 and carbonyl oxygen O7 of unprimed molecule (now onwards molecule 1) accepts H-atom from the orthoformate carbon (H7') and *myo*-inositol C1'(H1') of the primed molecule (now onwards molecule 2) to form C-H $\cdots$ O contacts. Further the *myo*-inositol ring H-atom (H3) of molecule 1 makes C-H $\cdots$ O contact with orthoformate bridge oxygen O1' of molecule 2 (**Figure 6.4C** and **Table 6.3**).

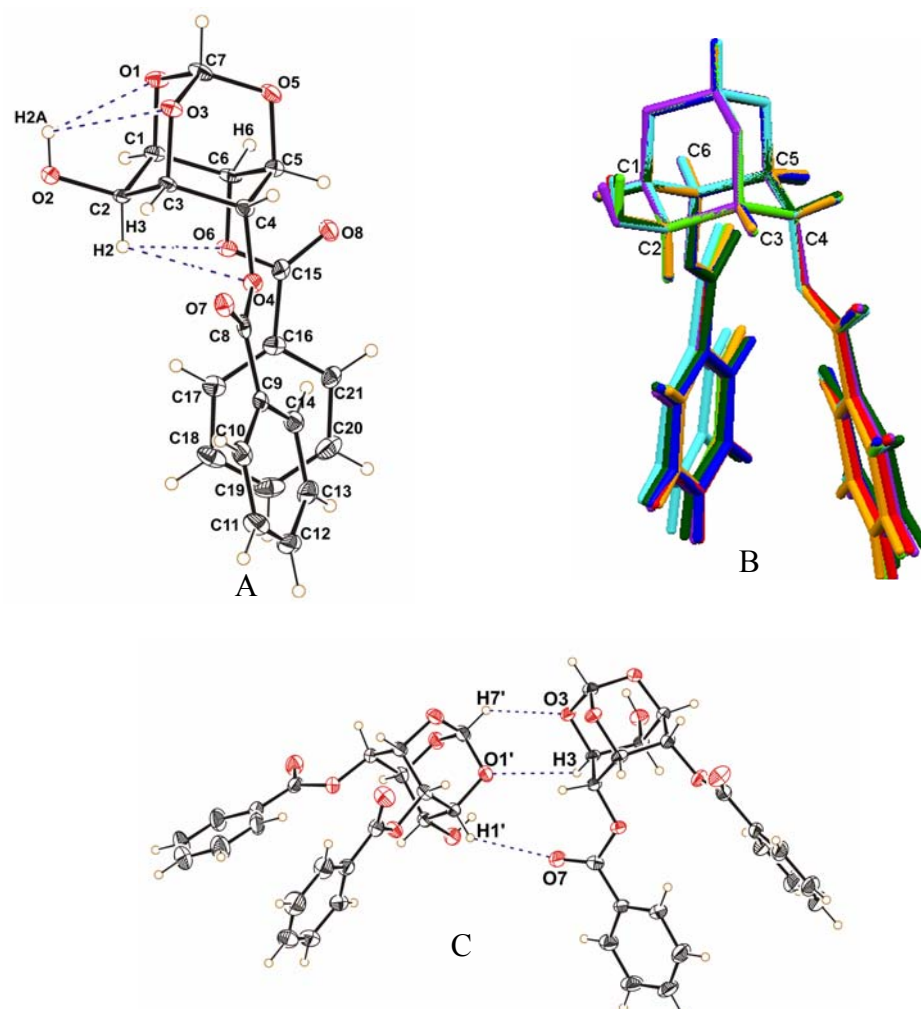


**Figure 6.4.** A) ORTEP view (30% probability displacement ellipsoids) depicting intramolecular interactions in  $\mathbf{9} \cdot \text{CH}_2\text{Cl}_2$  (Intramolecular interactions in all the solvates and solvent free crystals of  $\mathbf{9}$  are similar), B) overlap of the host molecules in crystals  $\mathbf{9} \cdot \text{CH}_2\text{Cl}_2$  (red),  $\mathbf{9} \cdot \text{CH}_2\text{ClBr}$  (purple),  $\mathbf{9} \cdot \text{CHCl}_3$  (blue),  $\mathbf{9} \cdot \text{CHBr}_3$  (orange),  $\mathbf{9} \cdot \text{CHCl}_2\text{Br}$  (light green) and two symmetry independent molecules of  $\mathbf{9}$ , (cyan and dark green) and C) ORTEP view showing C-H $\cdots$ O interactions between the two independent molecules in the asymmetric unit of  $\mathbf{9}$ .

**Table 6.3:** Intramolecular hydrogen bond geometry in all the solvates and solvent free crystals of **9**.

	D-H...A	D-H (Å°)	H...A (Å)	D...A (Å)	D-H...A (°)
<b>9</b> ·CH <sub>2</sub> Cl <sub>2</sub>	O(2)-H(2A)...O(1)	0.82	2.50	2.873(4)	109
	O(2)-H(2A)...O(3)	0.82	2.66	2.907(4)	99
	C(2)-H(2)...O(4)	0.98	2.74	3.063(5)	100
	C(2)-H(2)...O(6)	0.98	2.61	2.949(5)	101
<b>9</b> ·CH <sub>2</sub> ClBr	O(2)-H(2A)...O(1)	0.82	2.49	2.893(8)	111
	O(2)-H(2A)...O(3)	0.82	2.75	2.921(9)	94
	C(2)-H(2)...O(4)	0.98	2.75	3.092(12)	101
	C(2)-H(2)...O(6)	0.98	2.64	2.993(13)	102
<b>9</b> ·CHCl <sub>3</sub>	O(2)-H(2A)...O(1)	0.76(3)	2.44(3)	2.823(2)	113(2)
	O(2)-H(2A)...O(3)	0.76(3)	2.60(3)	2.867(2)	111(2)
	C(2)-H(2)...O(4)	0.94(2)	2.74(2)	3.040(3)	100(1)
	C(2)-H(2)...O(6)	0.94(2)	2.64 (2)	2.930(3)	98(1)
<b>9</b> ·CHBr <sub>3</sub>	O(2)-H(2A)...O(1)	0.74(3)	2.46(3)	2.824(3)	113(3)
	O(2)-H(2A)...O(3)	0.74(3)	2.58(4)	2.861(3)	105(3)
	C(2)-H(2)...O(4)	0.89(3)	2.73(3)	3.024(4)	101(2)
	C(2)-H(2)...O(6)	0.89(3)	2.70(3)	2.953(4)	98(2)
<b>9</b> ·CHCl <sub>2</sub> Br	O(2)-H(2A)...O(1)	0.82	2.56	2.840(5)	102
	O(2)-H(2A)...O(3)	0.82	2.52	2.880(6)	108
	C(2)-H(2)...O(4)	0.98	2.73	3.042(7)	99
	C(2)-H(2)...O(6)	0.98	2.64	2.959(7)	99
Molecule 1 of <b>9</b>	O(2)-H(2A)...O(1)	0.82	2.53	2.877(3)	107
	O(2)-H(2A)...O(3)	0.82	2.60	2.887(3)	102
	C(2)-H(2)...O(4)	0.98	2.68	3.012(4)	101
	C(2)-H(2)...O(6)	0.98	2.58	2.923(4)	101
Molecule 2 of <b>9</b>	O(2')-H(2'A)...O(1')	0.82	2.55	2.858(3)	104
	O(2')-H(2'A)...O(3')	0.82	2.53	2.861(3)	106
	C(2')-H(2')...O(4')	0.98	2.73	3.042(4)	99
	C(2')-H(2')...O(6')	0.98	2.58	2.916(4)	100
Between molecule 1 and 2 of <b>9</b>	C(3)-H(3)...O(1')	0.98	2.70	3.160(4)	109
	C(1')-H(1')...O(7)	0.98	2.62	3.335(4)	130
	C(7')-H(7')...O(3)	0.98	2.61	3.228(4)	121

### 6.3.2 Dimer Formation

The host molecules in all the inclusion complexes of **9** and molecule 1 in solvent free crystals of **9** form centrosymmetric dimers through intermolecular O2-H2A...O3 and C7-H7...O2 contacts bringing orthoformate bridge-heads together with the benzoyl groups of the two molecules pointing away (**Figure 6.5A**). In addition, the host molecules in all the inclusion complexes of **9** and molecule 1 in solvent free crystals of **9** are also engaged in another dimer formation via C7-H7...O1 contact (**Figure 6.5B**). Thus, the orthoformate H-atom makes bifurcated C-H...O contacts C7-H7...O2 and C7-H7...O1. These two dimers intersect each other resulting in the formation of bilayers when viewed perpendicularly down the b-axis. Molecules in the bilayers are linked with unit-translated molecule via various C-H...O contacts C2-H2...O8, C3-H3...O5, C5-H5...O7 and C6-H6...O2 providing extra stability. In the bilayer formation, the hydrophilic groups are clustered together while the phenyl rings of the benzoyl groups protrude outwards. (**Figure 6.5C** and **Tables 6.4** and **6.5**). All these observations reveal that molecule 1 in solvent free crystals of **9** behaves exactly like the host molecule in solvates of **9**. Molecule 2 of solvent free crystals of **9** did not form such dimeric assembly. Molecule 2 of **9** forms sheet like structure by weaving the unit translated molecule via three C-H...O interactions, C5'-H5'...O7', C6'-H6'...O2' and C2'-H2'...O8' (**Figure 6.6**, **Table 6.5**).

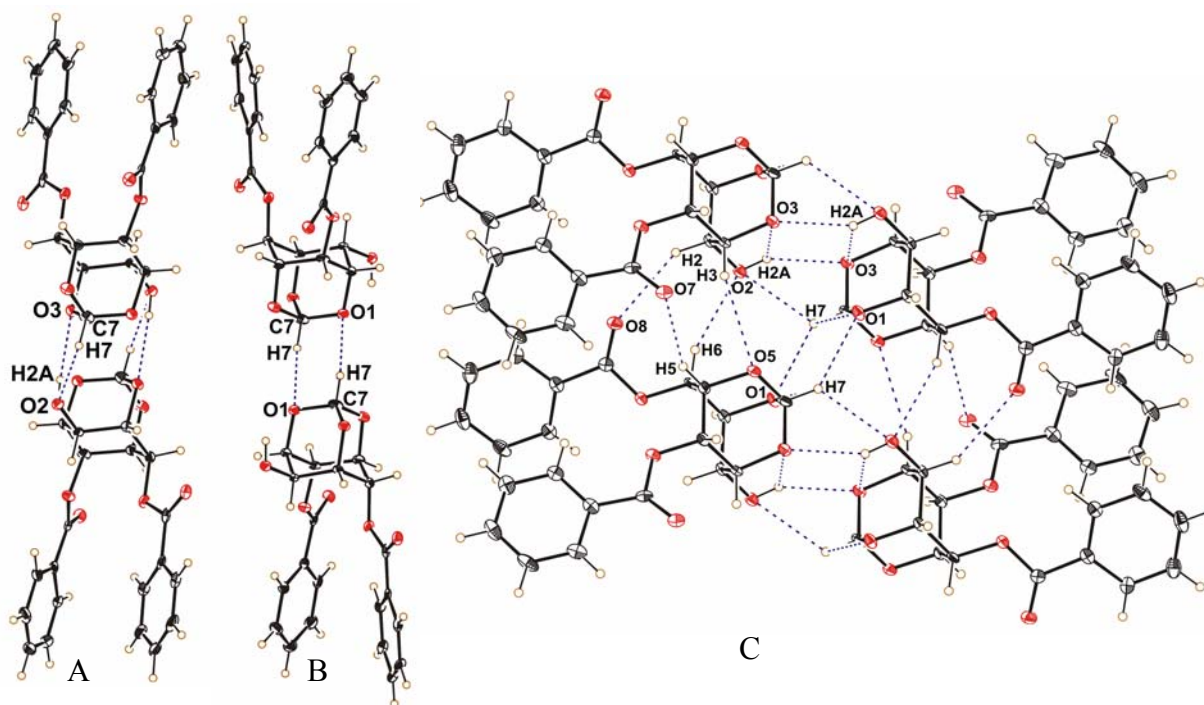


**Figure 6.5.** ORTEP view showing the head-to-head dimer formation via A) O2-H2A...O3 and C7-H7...O2, B) C7-H7...O1 contacts and C) linking of these dimers to form bilayers through O-H...O and C-H...O contacts in inclusion crystals of  $\mathbf{9} \cdot \text{CH}_2\text{Cl}_2$  (head-to-head dimer formation is identical in all solvates of  $\mathbf{9}$  and molecule 1 of solvent free crystals of  $\mathbf{9}$ ).

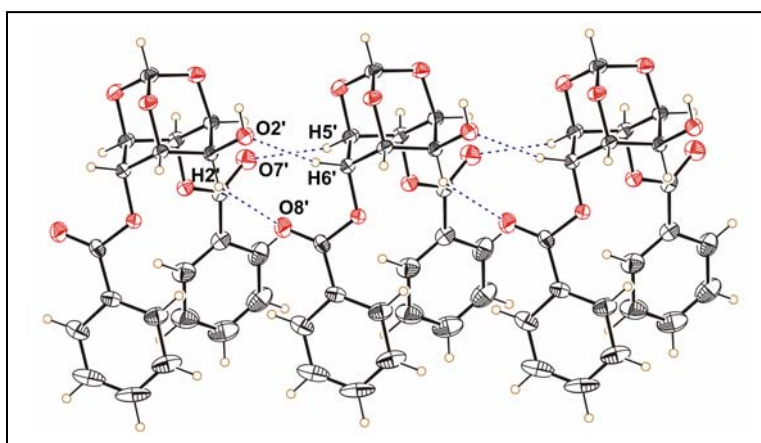


**Figure 6.6.** ORTEP view of the sheet formed by the molecule 2 of solvent free crystals of  $\mathbf{9}$ .

**Table 6.4:** Intermolecular O-H...O and C-H...O contacts involved in the formation of bilayers in all the inclusion complexes of **9**.

	D-H...A	D-H (Å)	H...A (Å)	D...A (Å)	D-H...A (°)
<b>9·CH<sub>2</sub>Cl<sub>2</sub></b>	O(2)-H(2A)...O(3)#1	0.82	2.22	2.974(4)	153
	C(2)-H(2)...O(8)#2	0.98	2.64	3.491(5)	145
	C(3)-H(3)...O(5)#2	0.98	2.76	3.682(5)	156
	C(5)-H(5)...O(7)#3	0.98	2.47	3.377(5)	154
	C(6)-H(6)...O(2)#3	0.93	2.63	3.564(5)	159
	C(7)-H(7)...O(1)#4	0.93	2.38	3.173(5)	137
	C(7)-H(7)...O(2)#1	0.93	2.53	3.186(6)	124
<b>9·CH<sub>2</sub>ClBr</b>	O(2)-H(2A)...O(3)#2	0.82	2.34	3.040(10)	144
	C(2)-H(2)...O(8)#3	0.98	2.70	3.544(12)	145
	C(3)-H(3)...O(5)#5	0.98	2.84	3.768(12)	157
	C(5)-H(5)...O(7)#2	0.98	2.57	3.472(12)	153
	C(6)-H(6)...O(2)#2	0.98	2.68	3.615(11)	160
	C(7)-H(7)...O(1)#5	0.98	2.43	3.216(12)	137
	C(7)-H(7)...O(2)#6	0.98	2.62	3.273(13)	125
<b>9·CHCl<sub>3</sub></b>	O(2)-H(2A)...O(3)#7	0.76(3)	2.39(3)	3.083(2)	152(3)
	C(2)-H(2)...O(8)#3	0.94(2)	2.51(2)	3.311(3)	143(2)
	C(3)-H(3)...O(5)#8	0.93(2)	2.85(2)	3.714(3)	156(2)
	C(5)-H(5)...O(7)#8	0.97(2)	2.53(2)	3.464(3)	162(2)
	C(6)-H(6)...O(2)#2	0.89(2)	2.60(2)	3.467(3)	164(2)
	C(7)-H(7)...O(1)#9	1.01(2)	2.37(2)	3.161(3)	134(1)
	C(7)-H(7)...O(2)#7	1.01(2)	2.561(2)	3.266(3)	127(2)
<b>9·CHBr<sub>3</sub></b>	O(2)-H(2A)...O(3)#10	0.74(3)	2.36(3)	3.026(3)	151(4)
	C(2)-H(2)...O(8)#3	0.89(3)	2.51(3)	3.269(4)	144(2)
	C(3)-H(3)...O(5)#3	0.98(3)	2.87(3)	3.806(4)	157(2)
	C(6)-H(6)...O(2)#2	0.95(3)	2.62(3)	3.546(4)	167(2)
	C(5)-H(5)...O(7)#2	0.97(3)	2.59(3)	3.537(4)	166(2)
	C(7)-H(7)...O(2)#10	0.93(3)	2.60(3)	3.239(4)	127(2)
	C(7)-H(7)...O(1)#11	0.93(3)	2.40(3)	3.098(4)	132(2)
<b>9·CHCl<sub>2</sub>Br</b>	O(2)-H(2A)...O(3)#5	0.82	2.27	3.016(5)	152
	C(2)-H(2)...O(8)#3	0.98	2.48	3.296(7)	140
	C(3)-H(3)...O(5)#3	0.98	2.86	3.762(7)	153
	C(5)-H(5)...O(7)#2	0.98	2.55	3.486(7)	161
	C(6)-H(6)...O(2)#2	0.98	2.59	3.546(7)	164
	C(7)-H(7)...O(1)#12	0.98	2.37	3.109(7)	131
	C(7)-H(7)...O(2)#5	0.98	2.55	3.198(7)	124

Symmetry codes: #1 -x,-y,-z+1; #2 x-1,y,z; #3 x+1,y,z; #4 -x+1,-y,-z+1; #5 -x+1,-y+1,-z+1; #6 -x+2,-y+1,-z+1; #7 -x+2,-y+1,-z; #8 -x+5/2,y-1/2,-z+1/2; #9 -x+1,-y+1,-z; #10 -x+1,-y,-z+2; #11 -x,-y,-z+2; #12 -x,-y,-z.



**Table 6.5:** Intermolecular O-H...O and C-H...O contacts involved in the formation of bilayers by molecule 1 and sheet by molecule 2 in solvent free crystals of **9**.

D-H...A	H...A (Å)	D...A (Å)	D-H...A (Å)	D-H...A (°)
C-H...O interactions involved in the formation of bilayers by molecule 1				
O(2)-H(2A)...O(3)#2	0.82	2.31	3.052(3)	151
C(2)-H(2)...O(8)#1	0.98	2.62	3.472(4)	146
C(3)-H(3)...O(5)#1	0.98	2.72	3.650(4)	159
C(5)-H(5)...O(7)#4	0.98	2.55	3.464(4)	154
C(6)-H(6)...O(2)#4	0.98	2.67	3.598(4)	158
C(7)-H(7)...O(1)#7	0.98	2.39	3.178(4)	138
C(7)-H(7)...O(2)#1	0.98	2.64	3.262(4)	121
C(19)-H(19)...O(2)#3	0.93	2.80	3.521(5)	135
C(11)-H(11)...O(7)#5	0.93	2.86	3.610(8)	138
C-H...O interactions involved in the formation of sheets by molecule 2				
C(2')-H(2')...O(8')#1	0.98	2.54	3.315(4)	136
C(5')-H(5')...O(7')#4	0.98	2.68	3.625(4)	163
C(6')-H(6')...O(2')#4	0.98	2.44	3.399(4)	166
C(19')-H(19'')...O(2')#5	0.93	2.57	3.252(5)	130

Symmetry codes: #1  $x, y+1, z$ ; #2  $-x+1, -y+1, -z$ ; #3  $-x, -y+1, -z$ ; #4  $x, y-1, z$ ;  
 #5  $-x+1, y-1/2, -z+1/2$ ; #6  $x-1, y-1, z$ ; #7  $-x+1, -y, -z$ ; #8  $x, y, z$ .

### 6.3.3 Difference in Association of Dimers in the Inclusion Crystals of **9**

The head-to-head (**Figures 6.5A**) linked O-H $\cdots$ O dimers form identical looking two-dimensional sheets in ab-plane in all the inclusion crystals of **9** (head-to-head dimers coloured in red, **Figure 6.7**). But, the sheets are woven differently for Group I (**9**·CH<sub>2</sub>Cl<sub>2</sub>, **9**·CH<sub>2</sub>ClBr and **9**·CHCl<sub>3</sub>) and Group II (**9**·CHBr<sub>3</sub> and **9**·CHCl<sub>2</sub>Br) inclusion complexes. In Group I, the head-to-head dimers are ‘zip locked’ via 2<sub>1</sub>-screw axis making C-H $\cdots$  $\pi$  and  $\pi\cdots\pi$  contacts along b-axis (**Figure 6.7A**). The C1-H1 and C4-H4 groups of the inositol ring make C-H $\cdots$  $\pi$  contacts with the edge of the (2<sub>1</sub>- screw related) axial phenyl rings at C4 and C6 respectively. The  $\pi\cdots\pi$  contact is between the carbonyl groups C15=O8 and C8=O7 involving again the same phenyl rings. In Group II crystals, the head-to-head dimers are zip locked via centrosymmetric C19-H19 $\cdots$ O2 and  $\pi\cdots\pi$  contacts between the C8=O7 carbonyl and the phenyl ring at C4 (**Figure 6.7C**). However, both these sheets create open framework architecture (**Figures 6.7B** and **6.7D**), which includes guest molecules (triangles in magenta).

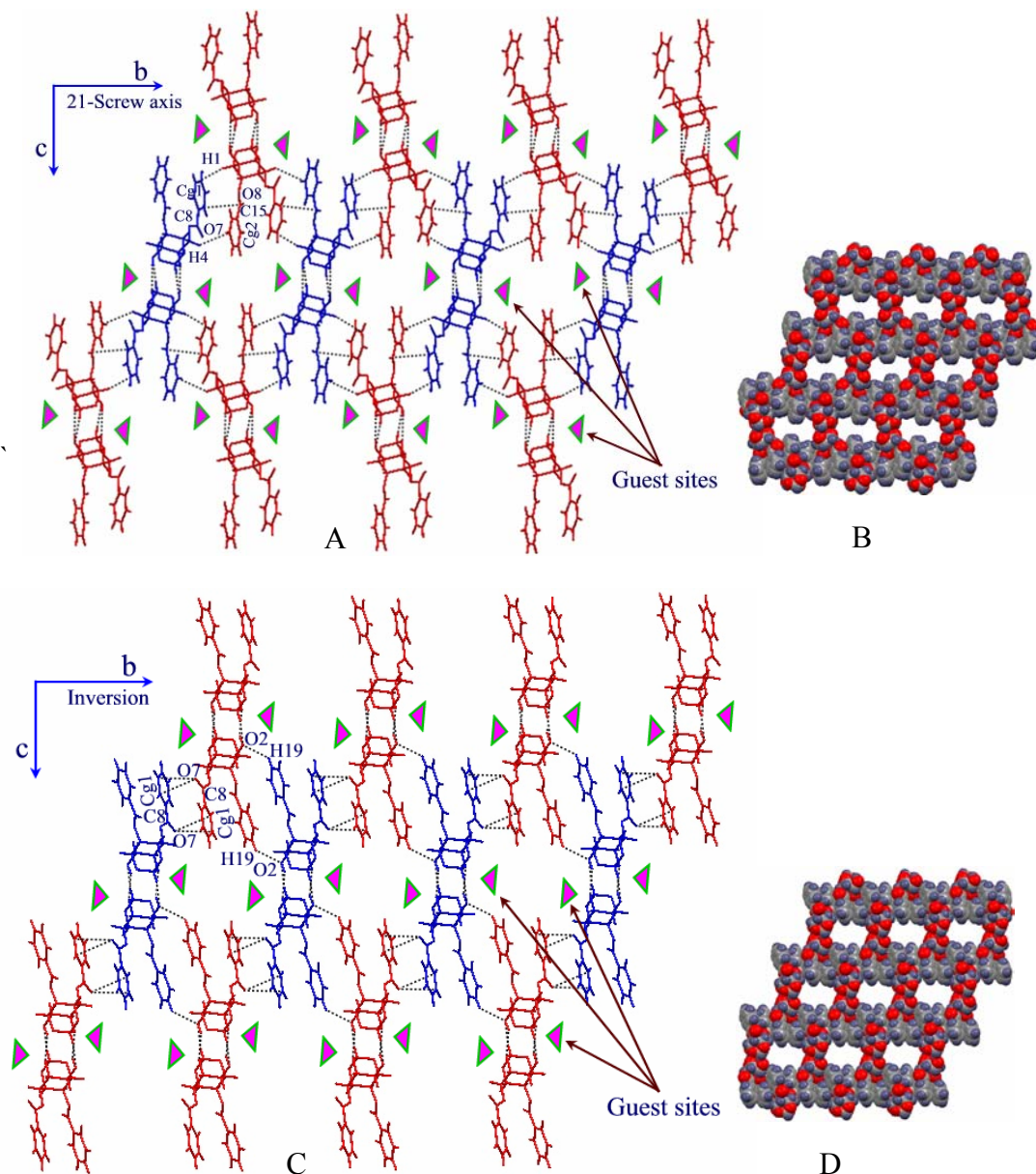


**Figure 6.7.** Difference in association of dimeric units forming identical open framework structure, A) linked via C-H... $\pi$  and  $\pi$ ... $\pi$  contacts having  $2_1$ -screw axis relation in inclusion crystals of **9-CH<sub>2</sub>Cl<sub>2</sub>** (similar association in **9-CH<sub>2</sub>CIBr** and **9-CHCl<sub>3</sub>**), B) CPK view of the same, C) linked via C-H...O and  $\pi$ ... $\pi$  having inversion symmetry in inclusion crystals of **9-CHBr<sub>3</sub>** (similar association in **9-CHCl<sub>2</sub>Br**) and D) CPK view of the same, location of the guest molecules in the crystal lattice is represented by triangles.

The two-dimensional sheet of head-to-head dimers (red in **Figure 6.7**) is stitched from the layer beneath the layer of blue dimers down a-axis by C-H $\cdots$ O interactions in both Group I and II inclusion crystals. In Group I, they are linked by weak C-H $\cdots$ O interactions via  $2_1$ -screw symmetry forming rectangular cavities (**Figure 6.8A**) that accommodate guest molecules. The C12-H12 $\cdots$ O2 and C13-H13 $\cdots$ O2 contact links  $2_1$ -screw symmetry related dimers in **9**·CH<sub>2</sub>Cl<sub>2</sub> and **9**·CH<sub>2</sub>CIBr, whereas in **9**·CHCl<sub>3</sub> the dimers are associated via C12-H12 $\cdots$ O2 and C20-H20 $\cdots$ O7 interactions (**Figure 6.8A**). In inclusion crystals of **9**·CHCl<sub>3</sub>, the C13-H13 $\cdots$ O2 contact is taken over by the new C20-H20 $\cdots$ O7 contact (**Table 6.6**) due to a slight shift of the dimeric units along the c-axis. As a result, the H $\cdots$ A distances between the C20 $\cdots$ O7 of 3.28 Å (**9**·CH<sub>2</sub>Cl<sub>2</sub>) and 3.36 Å (**9**·CH<sub>2</sub>CIBr) are reduced to 2.71 Å in **9**·CHCl<sub>3</sub>, whereas distance H13 $\cdots$ O2 is increased from 2.81 Å in **9**·CH<sub>2</sub>Cl<sub>2</sub>, 2.91 Å in **9**·CH<sub>2</sub>CIBr to 3.10 Å in **9**·CHCl<sub>3</sub>. In Group II inclusion crystals, the dimeric units are linked via centrosymmetric C19-H19 $\cdots$ O2 and C13-H13 $\cdots$ O7 interactions forming rectangular cavities down the a-axis (**Figure 6.8B**).

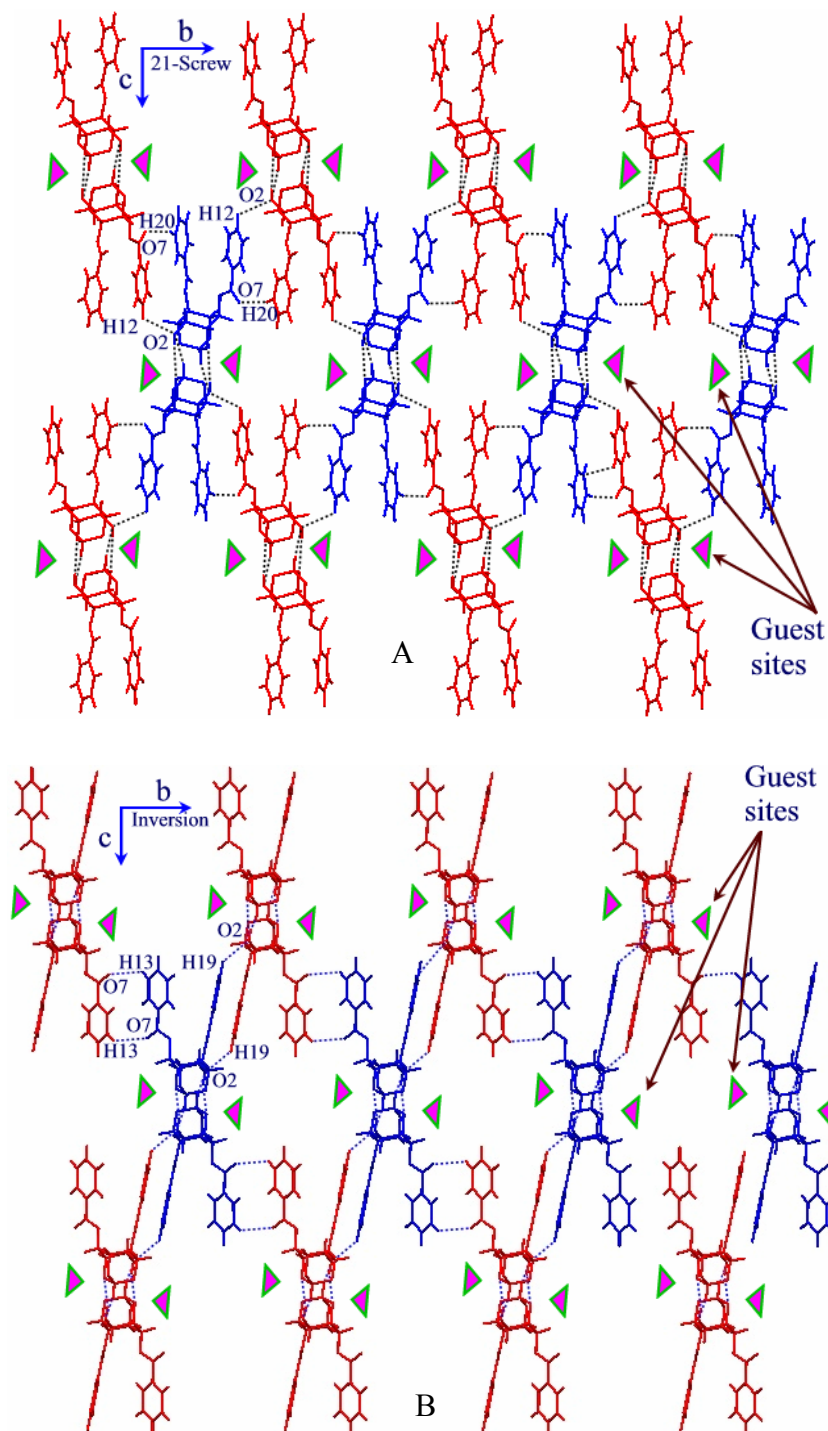


**Figure 6.8.** Association of the dimeric units via C-H...O interactions along the b-axis, A) having 2<sub>1</sub>- screw in **9·CHCl<sub>3</sub>** (similar association in **9·CH<sub>2</sub>Cl<sub>2</sub>** and **9·CH<sub>2</sub>ClBr**) and B) having inversion relation in **9·CHBr<sub>3</sub>** (similar association in **9·CHCl<sub>2</sub>Br**).

**Table 6.6:** C-H...O interactions involved in the association of head-to-head dimers in solvates of **9**.

	D-H...A	D-H (Å)	H...A (Å)	D...A (Å)	D-H...A (°)
<b>9·CH<sub>2</sub>Cl<sub>2</sub></b>	C(13)-H(13)...O(2)#1	0.93	2.81	3.317(6)	116
	C(12)-H(12)...O(2)#1	0.93	2.89	3.359(6)	113
<b>9·CH<sub>2</sub>ClBr</b>	C(13)-H(13)...O(2)#2	0.93	2.91	3.425(16)	116
<b>9·CHCl<sub>3</sub></b>	C(20)-H(20)...O(7)#3	0.93(3)	2.75(3)	3.643(3)	161(2)
	C(12)-H(12)...O(2)#4	0.99(3)	2.74(3)	3.316(3)	116(2)
<b>9·CHBr<sub>3</sub></b>	C(19)-H(19)...O(2)#5	0.88(3)	2.54(4)	3.291(5)	144(3)
	C(13)-H(13)...O(7)#6	0.92(3)	2.88(3)	3.683(5)	147(3)
<b>9·CHCl<sub>2</sub>Br</b>	C(19)-H(19)...O(2)#7	0.93	2.54	3.298(7)	139
	C(13)-H(13)...O(7)#8	0.93	2.86	3.610(8)	138

Symmetry codes: #1  $-1/2-x, 1/2+y, 1.5-z$ ; #2  $-x+3/2, y-1/2, -z+1/2$ ; #3  $-x+5/2, y+1/2, -z+1/2$ ; #4  $-x+5/2, y-1/2, -z+1/2$ ; #5  $-x+1, -y, -z+1$ ; #6  $-x+2, -y+1, -z+1$ ; #7  $1-x, 1-y, 1-z$ ; #8  $-x+2, -y+1, -z$ .

### 6.3.4 Host-Guest Association in **9·CH<sub>2</sub>Cl<sub>2</sub>** and **9·CH<sub>2</sub>ClBr**

Cavities formed in packing of the head-to-head dimers<sup>30,148</sup> with two axial phenyl rings accommodate the guest molecules (**Figures 6.7A, 6.8A**, triangles in magenta). The dihalomethane guest molecules interact via two C-H...O and one C-H...Cl(Br) contact with the host (**Table 7.7**). The dimeric units (**Figure 6.5A**) hold dihalomethane molecules on either side making centrosymmetric C22-H22A...O1 and C22-H22A...O5 (not shown in **Figure 6.5A**) interactions. Thus, one of the methylene H-atoms (H22A) is involved in bifurcated C-H...O contacts (**Figure 6.9**), although the latter contact is weak as compared to the former (**Table 7.7**). The other H-atom (H22B) is engaged in making

C-H $\cdots$ O interaction with the carbonyl oxygen O7. In **9**·CH<sub>2</sub>Cl<sub>2</sub>, C22-H22A $\cdots$ O1 and C22-H22B $\cdots$ O7 contacts have better geometry as compared to the crystals **9**·CH<sub>2</sub>ClBr (**Table 6.6**). The halogen atom Cl (Br) of dihalomethane molecule is involved in C-H $\cdots$ Cl (Br) interaction with the host (C19-H19 $\cdots$ Cl2, **Figure 6.9**, C19-H19 $\cdots$ Br1A in crystals **9**·CH<sub>2</sub>ClBr) related by 2<sub>1</sub>-screw axis with comparable geometries. To sum up, each guest molecule makes three C-H $\cdots$ O and one C-H $\cdots$ Cl(Br) interaction with the host holding the dihalomethane molecule firmly (**Figure 6.9**). The halogens of the guest molecules are not involved in any halogen bonding (halogen $\cdots$ oxygen contact) with the host.

**Table 7.7:** Host-guest interactions in **9**·CH<sub>2</sub>Cl<sub>2</sub> and **9**·CH<sub>2</sub>ClBr.

	D-H $\cdots$ A	D-H (Å)	H $\cdots$ A (Å)	D $\cdots$ A (Å)	D-H $\cdots$ A (°)
<b>9</b> ·CH <sub>2</sub> Cl <sub>2</sub>	C(22)-H(22A) $\cdots$ O(5)	0.97	2.66	3.262(6)	121
	C(22)-H(22A) $\cdots$ O(1)#1	0.97	2.70	3.621(6)	158
	C(22)-H(22B) $\cdots$ O(7)#2	0.97	2.77	3.690(6)	159
	C(19)-H(19) $\cdots$ Cl(2)#3	0.93	2.98	3.772(5)	144
	C(22)-Cl(1) $\cdots$ Cl(2)	1.756	3.693 (5)	4.989 (6)	129
<b>9</b> ·CH <sub>2</sub> ClBr	C(22)-H(22A) $\cdots$ O(5)	0.97	2.73	3.275(13)	116
	C(22)-H(22A) $\cdots$ O(1)#4	0.97	2.81	3.658(15)	146
	C(22)-H(22B) $\cdots$ O(7)#5	0.97	2.85	3.718(13)	149
	C(19)-H(19) $\cdots$ Br(1A)#6	0.93	3.06	3.860(16)	145
	C(22)-Cl(1) $\cdots$ Br(1)	1.834(5)	3.504(6)	5.384(9)	163
	C(22)-Cl(1) $\cdots$ Cl(1A)	1.834(5)	3.354(6)	5.105(8)	159

Symmetry codes: #1 -x+1,-y,-z+1; #2 x+1,y,z; #3 -x+1/2,y-1/2,-z+3/2;

#4 -x+1,-y+1,-z+1; #5 x-1, y, z; #6 -x+3/2,y-1/2,-z+1/2.

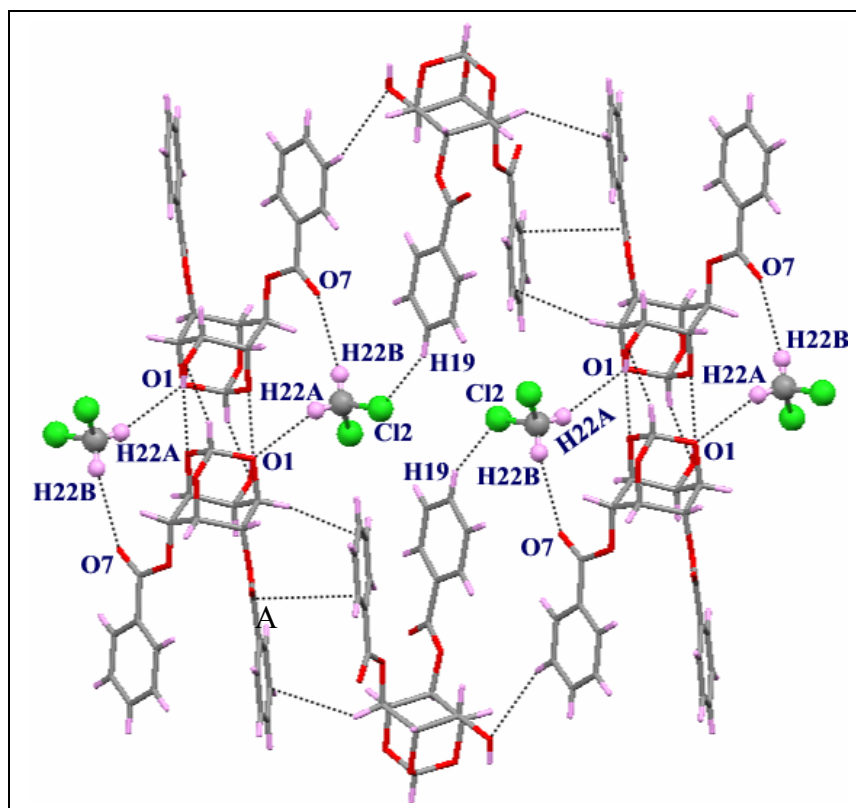


**Figure 6.9.** Association of the guest and the host molecules via C-H...O and one C-H...Cl interactions in inclusion crystals of  $9 \cdot \text{CH}_2\text{Cl}_2$ .

Host-guest association down b-axis revealed that the guest molecules occupy the sites above and below the plane of head-to-head bilayers (**Figures 6.10A**). Along with the guest-host interactions, the guest molecules also interact among themselves via X...X contacts (**Figure 6.10A**). There are Cl2...Cl1 contacts in  $9 \cdot \text{CH}_2\text{Cl}_2$  crystals (**Figure 6.10**), but in  $9 \cdot \text{CH}_2\text{ClBr}$  crystals with the orientational disorder of  $\text{CH}_2\text{ClBr}$ , Cl1 is involved in Cl1...Cl1A as well as Cl1...Br1 short contacts. It is noteworthy that only Br1(A) is preferred for the C-H...X interaction over Cl1 atom (**Table 6.6**). The X...X contact is of



the type I category<sup>44</sup> where the angles at both the halogens is almost the same. The directionality of the halogen...halogen contact is much better in  $9\cdot\text{CH}_2\text{ClBr}$  crystals as compared to  $9\cdot\text{CH}_2\text{Cl}_2$  crystals (Table 7.7). The packing viewed in a perpendicular direction to the view shown in Figure 6.10A (Figure 6.10B) clearly shows the channel along the a-axis through which included guest molecules can easily diffuse out of the crystal lattice. As mentioned earlier, the direction of crystal becoming opaque can now be well correlated with guest molecules escape along the needle axis i.e. a-axis.

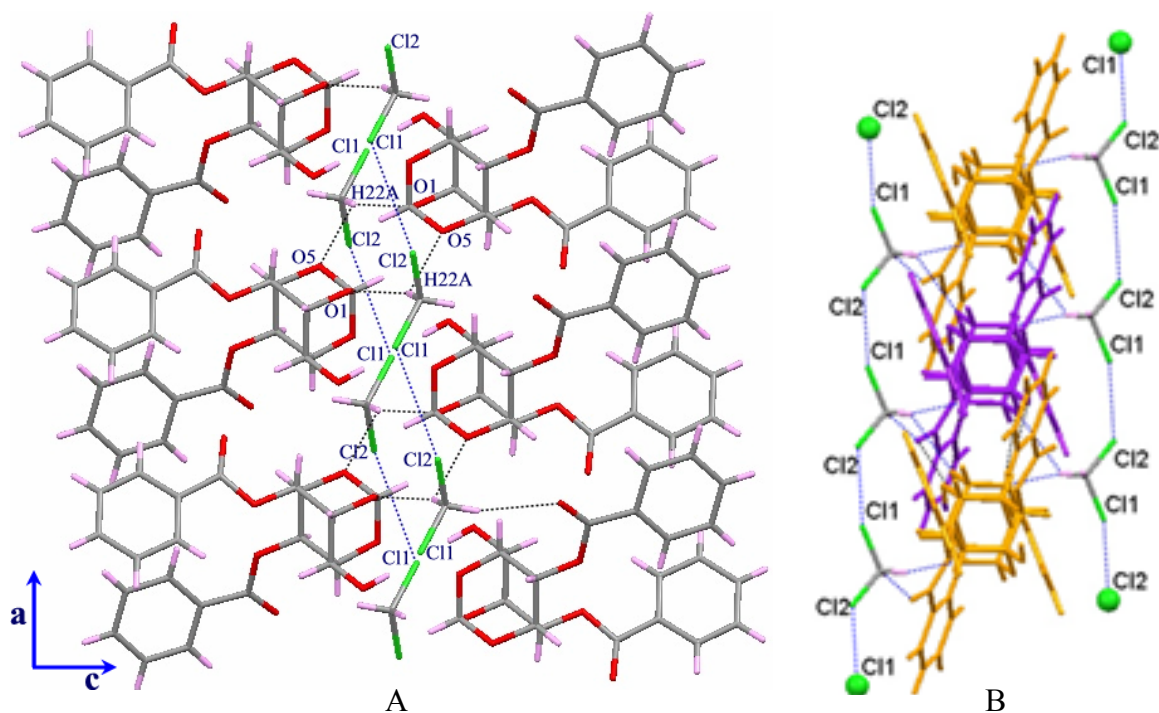


**Figure 6.10.** Host-guest assembly A) down the b-axis and B) same view down the c-axis in inclusion crystals of  $9\cdot\text{CH}_2\text{Cl}_2$  (different colour code represents O-H...O linked head-to-head dimeric units)

### 6.3.5 Host-Guest and Guest-Guest Interactions in $9\cdot\text{CHCl}_3$ , $9\cdot\text{CHBr}_3$ and $9\cdot\text{CHCl}_2\text{Br}$

The host-guest interactions in trihalomethane inclusion crystals ( $9\cdot\text{CHCl}_3$ ,  $9\cdot\text{CHBr}_3$  and  $9\cdot\text{CHCl}_2\text{Br}$ ) are different as compared with dihalomethane inclusion complexes  $9\cdot\text{CH}_2\text{Cl}_2$  and  $9\cdot\text{CH}_2\text{ClBr}$ . The fact that the  $9\cdot\text{CHCl}_3$ ,  $9\cdot\text{CHBr}_3$  and  $9\cdot\text{CHCl}_2\text{Br}$  inclusion crystals are more stable compared to  $9\cdot\text{CH}_2\text{Cl}_2$  and  $9\cdot\text{CH}_2\text{ClBr}$  inclusion crystals, suggests stronger binding of the guest molecules to the host. Among trihalomethane inclusion crystals, although the association of the head-to-head dimeric unit (Figures 6.7 and 6.8) down the a-axis in  $9\cdot\text{CHCl}_3$  is different than  $9\cdot\text{CHBr}_3$  and  $9\cdot\text{CHCl}_2\text{Br}$  due to different space group symmetry, the host-guest interactions are quite similar. The guest molecule makes C-H $\cdots$ O, C-H $\cdots$ X and short X $\cdots$ X interactions (Figure 6.11) with the host but the notable one is the good halogen bonding contact, C-X $\cdots$ O(=C) (Table 6.8).

The H-atom of trihalomethane molecule makes bifurcated C-H $\cdots$ O intermolecular interactions with the orthoformate bridge oxygens O1 and O5 of the host molecules (C22-H22 $\cdots$ O1 and C22-H22 $\cdots$ O5), similar to crystals  $9\cdot\text{CH}_2\text{Cl}_2$  and  $9\cdot\text{CH}_2\text{ClBr}$ . The former C-H $\cdots$ O contact is stronger than the latter (Table 6.8). Here also, halogen atoms in  $9\cdot\text{CHCl}_3$ ,  $9\cdot\text{CHBr}_3$  and  $9\cdot\text{CHCl}_2\text{Br}$  are engaged in C-H $\cdots$ X type interactions with the host (Figure 6.11). Four C-H $\cdots$ Cl interactions, C1-H1 $\cdots$ Cl1, C11-H11 $\cdots$ Cl1, C18-H18 $\cdots$ Cl2 and C12-H12 $\cdots$ Cl3 bind chloroform molecules in  $9\cdot\text{CHCl}_3$  (Figure 6.11A), whereas in  $9\cdot\text{CHBr}_3$  ( $9\cdot\text{CHCl}_2\text{Br}$ ) interactions C1-H1 $\cdots$ Br1 (Cl1), C11-H11 $\cdots$ Br2(Cl2), C13-H13 $\cdots$ Br2(Cl2) and C18-H18 $\cdots$ Br1(Cl1) hold the guest molecules (Figure 6.11B). All the C-H $\cdots$ Cl interactions in  $9\cdot\text{CHCl}_3$  have comparable geometries except C18-H18 $\cdots$ Cl2 for which the angle of approach is close to 120°. In  $9\cdot\text{CHBr}_3$  and  $9\cdot\text{CHCl}_2\text{Br}$

also three C-H...X interactions have good strength (C18-H18...Br1(Cl1) interactions is almost linear) except C11-H11...Br2(Cl2) the angle of approach of which is close to tetrahedral value (**Table 6.8**). Another notable interaction is the presence of X...X short contact<sup>3</sup> (guest-guest) in **9·CHBr<sub>3</sub>** ( $Br1...Br3 = 3.6277(7) \text{ \AA}$ ) and **9·CHCl<sub>2</sub>Br** ( $Br1...Cl1 = 3.627(2) \text{ \AA}$ ) whereas in **9·CHCl<sub>3</sub>** this contact is somewhat longer ( $Cl3...Cl1 = 3.729(2) \text{ \AA}$ ,  $C22-Cl3...Cl1 = 163^\circ$ ).

**Table 6.8:** Host-guest interactions in **9·CHCl<sub>3</sub>**, **9·CHBr<sub>3</sub>** and **9·CHCl<sub>2</sub>Br**.

X = Cl, Br	D-H/X...A	D-H/X (\AA)	H/X...A (\AA)	D...A (\AA)	D-H/X...A (^\circ)
<b>9·CHCl<sub>3</sub></b>	C(22)-H(22)...O(1)#1	0.90(3)	2.52(3)	3.363(4)	157(2)
	C(22)-H(22)...O(5)#2	0.90(3)	2.58(3)	3.206(3)	127(2)
	C(1)-H(1)...Cl(1)#3	0.95(2)	3.11(2)	3.850(3)	136(2)
	C(11)-H(11)...Cl(1)	0.92(3)	3.09(3)	3.939(3)	154(2)
	C(12)-H(12)...Cl(3)	0.99(3)	3.04(3)	3.959(3)	155(2)
	C(18)-H(18)...Cl(2)#3	1.00(2)	3.00(2)	3.618(3)	121(3)
	C(22)-Cl(2)...O(7)#4	1.740(3)	3.051(2)	4.752(2)	142 (2)
<b>9·CHBr<sub>3</sub></b>	C(22)-H(22)...O(1)#5	0.91(4)	2.56(4)	3.436(5)	162(3)
	C(22)-H(22)...O(5)#6	0.91(4)	2.89(4)	3.394(5)	116(3)
	C(1)-H(1)...Br(1)#5	0.93(3)	3.23(4)	4.062(5)	147(3)
	C(11)-H(11)...Br(2)#3	0.91(4)	3.14(4)	3.617(4)	114(3)
	C(13)-H(13)...Br(2)#7	0.91(4)	3.15(4)	3.931(4)	144(3)
	C(18)-H(18)...Br(1)#8	0.93(3)	3.22(3)	4.144(4)	172(3)
	C(22)-Br(3)...Br(1)#6	1.913(4)	3.628(2)	5.521(5)	170(2)
C(22)-Br(2)...O(7)	1.909 (4)	3.195(2)	4.808(4)	139(2)	
<b>9·CHCl<sub>2</sub>Br</b>	C(22)-H(22)...O(1)#3	0.98	2.59	3.504(8)	156
	C(22)-H(22)...O(5)#6	0.98	2.87	3.364(8)	112
	C(1)-H(1)...Cl(1)#3	0.93	3.26	4.057(8)	140
	C(11)-H(11)...Cl(2)#9	0.93	3.04	3.874(7)	114
	C(13)-H(13)...Cl(2)#10	1.766	3.03	3.506(6)	149
	C(18)-H(18)...Cl(1)#8	0.93	3.210	4.137(8)	174
	C(22)-Br(1)...Cl(1)#6	1.892	3.627(2)	5.501(7)	170(3)
C(22)-Cl(2)...O(7)	1.892	3.312(5)	4.752(7)	136(4)	

Symmetry codes: #1 1-x,1-y,-z; #2 1/2+x, 1/2-y,1/2+z; #3 -x+1, -y+1, -z+1;

#4 -1/2+x, 1/2-y, 1/2+z; #5 -x+1,-y,-z+2; #6 x+1,y,z; #7 -x+2,-y+1,-z+1; #8 x-1,y,z-1;

#9 -x+1,-y+2,-z; #10 -x+2,-y+2,-z.

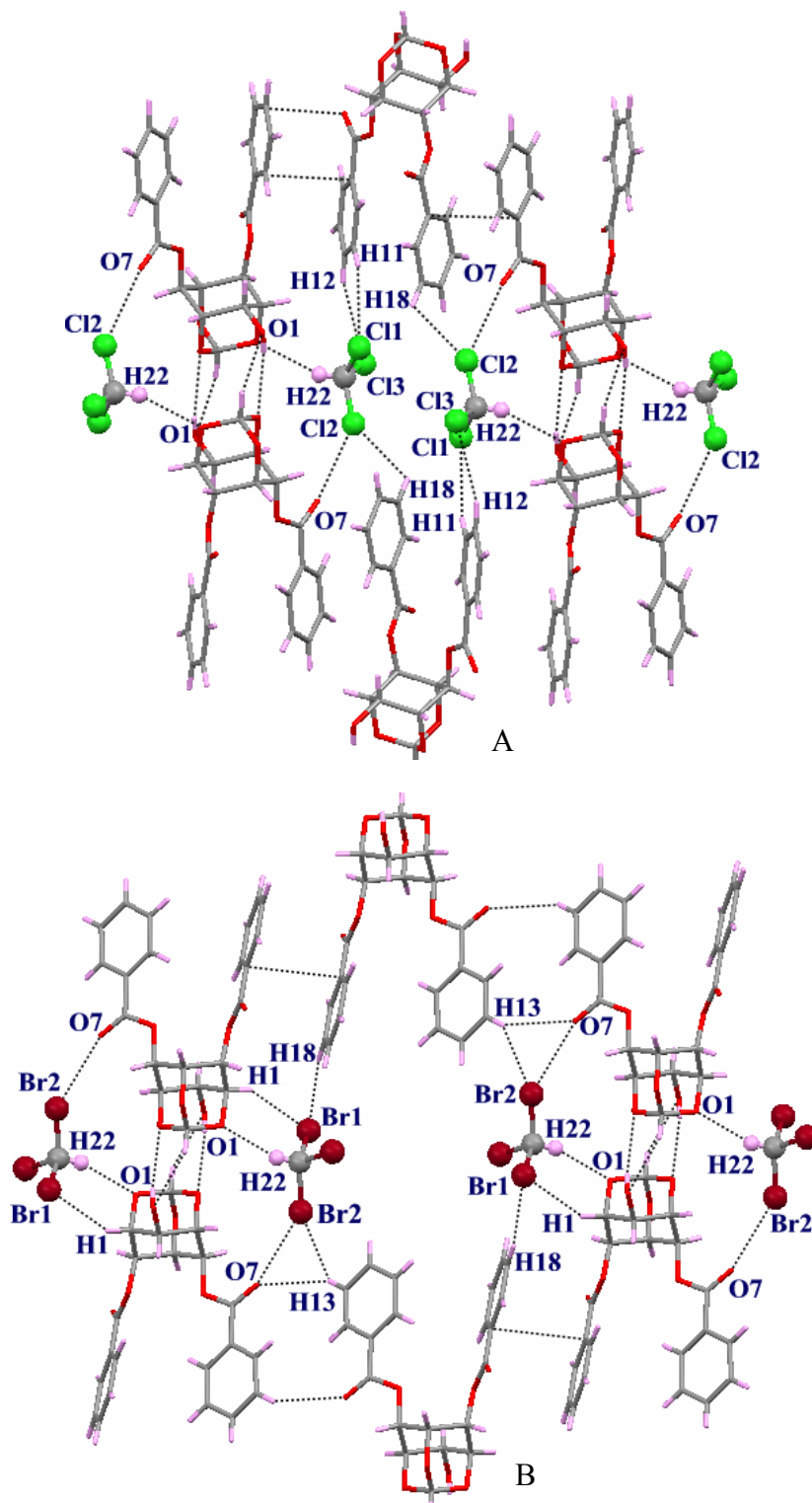


**Figure 6.11.** Host-guest interactions in inclusion crystals A)  $9 \cdot \text{CHCl}_3$  and B)  $9 \cdot \text{CHBr}_3$ .

Host guest interactions in  $9 \cdot \text{CHCl}_2\text{Br}$  are same as  $9 \cdot \text{CHBr}_3$ .

### *Association via Halogen Bonding Contact*

Amongst all the host-guest interactions in **9·CHCl<sub>3</sub>**, **9·CHBr<sub>3</sub>** and **9·CHCl<sub>2</sub>Br**, the halogen-bonding contact between halogen of the guest and carbonyl oxygen O7 of the host (**Figure 6.11**, **Table 6.8**) molecule is noteworthy. The Cl2(Br2)···O7 distance is less than the sum of van der Waals radii for the two atoms in **9·CHCl<sub>3</sub>** and **9·CHBr<sub>3</sub>** crystals ( $Cl2\cdots O7 = 3.0512(18) \text{ \AA}$  in **9·CHCl<sub>3</sub>** and  $Br2\cdots O7 = 3.195(2) \text{ \AA}$  in **9·CHBr<sub>3</sub>**), but the angle of approach deviates from linearity ( $C22-Cl2\cdots O7 = 142.3(20)^\circ$  in **9·CHCl<sub>3</sub>** and  $C22-Br2\cdots O7 = 139(2)^\circ$  in **9·CHBr<sub>3</sub>**, **Table 6.8**). In **9·CHCl<sub>2</sub>Br**, the distance between the Cl2 and O7 is slightly more than the sum of van der Waal's radii of the two atoms ( $Cl2\cdots O7 = 3.312(5) \text{ \AA}$ , *sum of van der Waals radii for Cl and O = 3.27 \AA*) with the angle  $C22-Cl2\cdots O7$  again deviating from the linearity ( $C22-Cl2\cdots O7 = 136^\circ$ ). It is noteworthy that the carbonyl oxygen O7 that was involved in C-H···O interactions in **9·CH<sub>2</sub>Cl<sub>2</sub>** and **9·CH<sub>2</sub>ClBr** is now engaged in halogen bonding interactions. There is a remarkable similarity in the host-guest assembly of crystals containing trihalomethanes and dihalomethanes, as viewed down the b and c-axis (host-guest assembly of trihalomethanes inclusion crystals is same as **Figure 6.10** except the difference in the guest molecule).

### 6.3.6 Stability of Dihalomethane and Trihalomethane Inclusion Crystals of **9**

The stability of the two-type inclusion complexes can be examined on the basis of host-guest associations. In crystals of **9**·CH<sub>2</sub>Cl<sub>2</sub> and **9**·CH<sub>2</sub>ClBr, the dihalomethane guest molecules make C-H···O and C-H···Cl contacts with the host (**Figure 6.9**), whereas in **9**·CHCl<sub>3</sub>, **9**·CHBr<sub>3</sub> and **9**·CHCl<sub>2</sub>Br, the guest molecules in addition to C-H···O and C-H···Cl(Br) interactions, make halogen bonding (C-Cl(Br)···O) contacts<sup>118c</sup> with the host (**Figure 6.11**). Relatively higher stability of **9**·CHCl<sub>3</sub>, **9**·CHBr<sub>3</sub> and **9**·CHCl<sub>2</sub>Br inclusion crystals therefore can be attributed to this extra halogen bonding contact arising due to the presence of an extra halogen on the carbon atom. As observed in *myo*-inositol derivative **1** (Chapter 2), the association of the guest molecules via C-X···O and C-H···O gave the most stable inclusion complexes.

### 6.3.7 Association of Dimers in Solvent Free Crystals of **9**: When Host Becomes Guest

The head-to-head dimeric assembly (**Figure 6.5A**) formed by molecule **1** in solvent free crystals of **9** creates one-dimensional molecular string along the a-axis linked by centrosymmetric C19-H19...O2 interactions (shown by red colour in **Figure 6.12A**) similar to Group II inclusion crystals of **9** (**Figure 6.12C**). But there are no direct contacts between these head-to-head dimers along the c-axis as observed in Group II inclusion crystals (**Figure 6.12C**). The association of the dimers produced thorough open channel (not the cavities as seen in solvates of **9**, **Figures 6.12C**) along the a-axis, which accommodates the layers of molecule **2**. Thus, the molecule **2** occupies the channel (occupied by the guest molecules in solvates of **9**) and bridge the head-to-head dimeric molecular string formed by molecule **1** along the c-axis. The orthoformate bridge of the molecule **2** occupies the same position as that occupied by solvent molecules in inclusion crystals of **9** and interacts with the head-to-head dimeric units at their bridging point on either side of it (**Figure 6.12A**). The other part of the molecule **2** i.e. the benzoyl groups acts like a spacer between the two head-to-head dimeric molecular strings resulting in the elongation of the c-axis of about 14 Å compared to solvates of **9**. This suggested that molecule **1** accommodates molecule **2** forming self host-guest type complex (**Figure 6.12A**) and can be called as 'self-inclusion' phenomenon. These observations indicate that molecules of **9** which form head-to-head dimeric units can in principle organize themselves to accommodate other *myo*-inositol orthoformate derivatives that have axially substituted acyl groups.

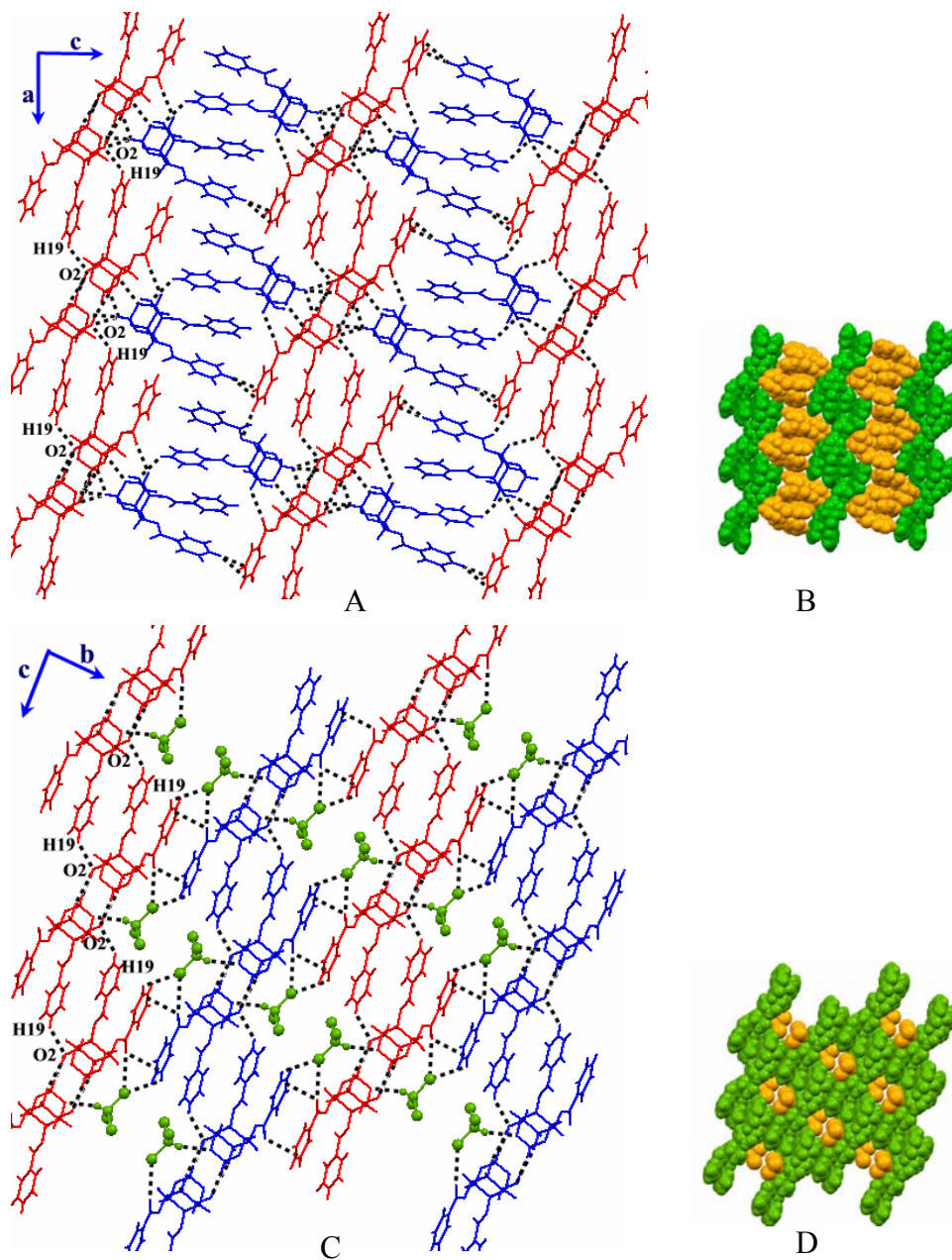


**Figure 6.12.** A) View of molecular packing of solvent free crystals **9** down the b-axis showing self-inclusion type pattern (The molecule 1 (red as host) includes the molecule 2 (blue as guest), B) CPK view of **9**, C) Similar view of molecular packing in **9·CHBr<sub>3</sub>** down the a-axis and D) CPK inlay of **9·CHBr<sub>3</sub>**.



Such self-inclusion type phenomena are very rare in the literature<sup>149</sup> and need some explanation. Usually the host and the guest, in host-guest complexes are different molecular entities as observed in solvates of **9**, but in solvent free crystals of **9**, the molecules of **9** act as host and guest due to different packing arrangements. Two molecules of molecule 2 bridge the head-to-head dimeric assembly of molecule 1 by C-H $\cdots$ O and C-H $\cdots$  $\pi$  interactions along the c-axis (**Figure 6.13** and **Table 6.9**). Molecule 2 donates its hydroxyl hydrogen H2'A to the orthoformate bridge oxygen O5 of molecule 1 (O2'-H2'A $\cdots$ O5). The hydroxyl oxygen (O2') also accepts proton from the *myo*-inositol ring of molecule 1 to form C4-H4 $\cdots$ O2' contact. The orthoformate bridge oxygen O1' and carbonyl oxygen O7' of molecule 2 accepts H-atom from C3-H3 and C11-H11 (of next head-to-head dimer of molecule 1) to form C3-H3 $\cdots$ O1' and C11-H11 $\cdots$ O7'. The orthoformate hydrogen (H7') of molecule 2 makes trifurcated C-H $\cdots$ O contacts with the hydroxyl oxygen (O2) and orthoformate bridge oxygens (O1 and O3) of molecule 1 forming C7'-H7' $\cdots$ O2, C7'-H7' $\cdots$ O1 and C7'-H7' $\cdots$ O3 interactions (**Figure 6.13** and **Table 6.9**). Further the included molecule 2 makes C-H $\cdots$  $\pi$  contact with the molecule 1; the phenyl H-atom (H12') of C4-O-benzoyl group of molecule 2 makes C-H $\cdots$  $\pi$  contact with the phenyl ring of the C4-O-benzoyl group of molecule 1 [C12'-H12' $\cdots$ Cg ( $\pi$  cloud of C9-C14 ring)]. Molecules 2 in the channel are related by c-glide symmetry and interact with each other via C19'-H19' $\cdots$ O2' contact and are positioned one over the other.

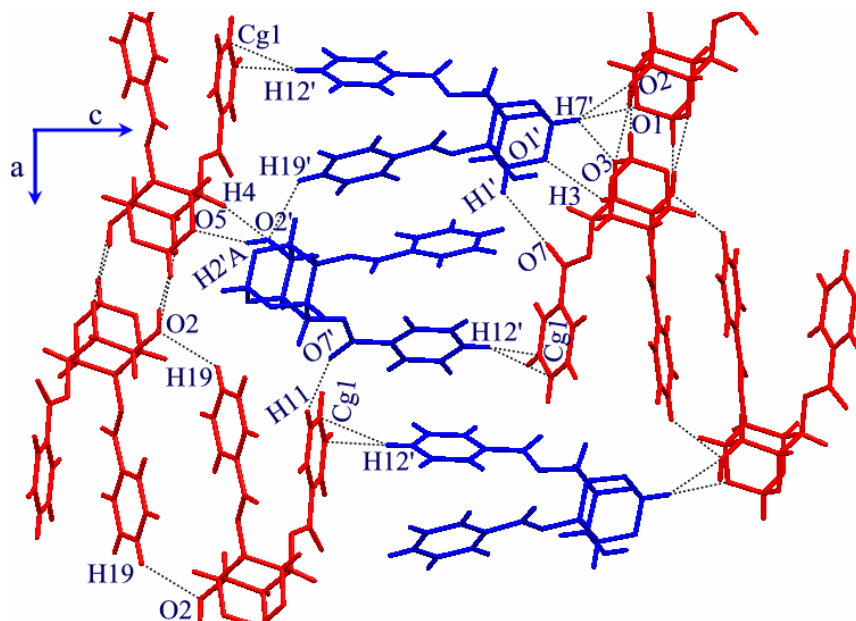


**Figure 6.13.** Close view of the channel showing interactions between molecules of molecule 1 and molecule 2.

**Table 6.9:** Intermolecular H-bonding interactions in **9**.

D-H...A	H...A (Å)	D...A (Å)	D-H...A (Å)	D-H...A (°)
C-H...O interactions made by the molecule 1 with molecule 2				
C(4)-H(4) ...O(2')#4	0.98	2.58	3.362(4)	137
C(3)-H(3) ...O(1')	0.98	2.70	3.160(4)	109
C(11)-H(11) ...O(7')#6	0.93	2.51	3.330(5)	147
C-H...O and C-H... $\pi$ interactions made by molecule 2 with molecule 1				
O(2')-H(2'A)...O(5)#1	0.82	2.16	2.932(3)	157
C(7')-H(7')...O(1)#2	0.98	2.76	3.567(4)	140
C(7')-H(7')...O(2)#2	0.98	2.74	3.614(4)	148
C(1')-H(1')...O(7)	0.98	2.62	3.335(4)	130
C(7')-H(7')...O(3)	0.98	2.61	3.228(4)	121
C12'-H12'...Cg	0.93	2.73	3.648	168

Symmetry codes: #1  $x, y+1, z$ ; #2  $-x+1, -y+1, -z$ ; #3  $-x, -y+1, -z$ ; #4  $x, y-1, z$ ;

#5  $-x+1, y-1/2, -z+1/2$ ; #6  $x-1, y-1, z$ ; #7  $-x+1, -y, -z$ ,

Cg - centroid of the phenyl ring C9-C14.

### 6.3.8 Crystal Structure of 10

Molecules in **10** show intramolecular interactions involving OH group and H2 at C2 position similar to those seen in **9** (**Figures 6.4A**) but the interactions involving phenyl rings are different (**Figure. 6.14A** and **Table 6.10**). Superimposing the molecules of **9** and **10** reveal significant difference in the orientation of both the axial benzoyl groups due to free rotation around O...C bond, whereas the conformation of the orthoesters and equatorial – OH group is almost the same, due to rigidity of the orthoester moiety (**Figure 6.14B**). The conformation of C6-*O*-benzoyl group in both the structure differs by about 22° and that of C4-*O*-benzoyl group by about 34°. In crystals of **10** almost perpendicular orientation of the two phenyl rings (dihedral angle between the planes of the ring 83.07°) facilitates good C-H...O interaction between the phenyl hydrogen H14 and ester oxygen O6 of the benzoyl group<sup>147</sup> [(H14...O6 = 2.80(2) Å, C14...O6 = 3.744(2) Å and ∠C14-H14...O6 = 164.0(15)°] but somewhat off centered C14-H14...π interaction (H14...C16 = 2.90 Å and H14...C21 = 2.81 Å) between the phenyl rings.

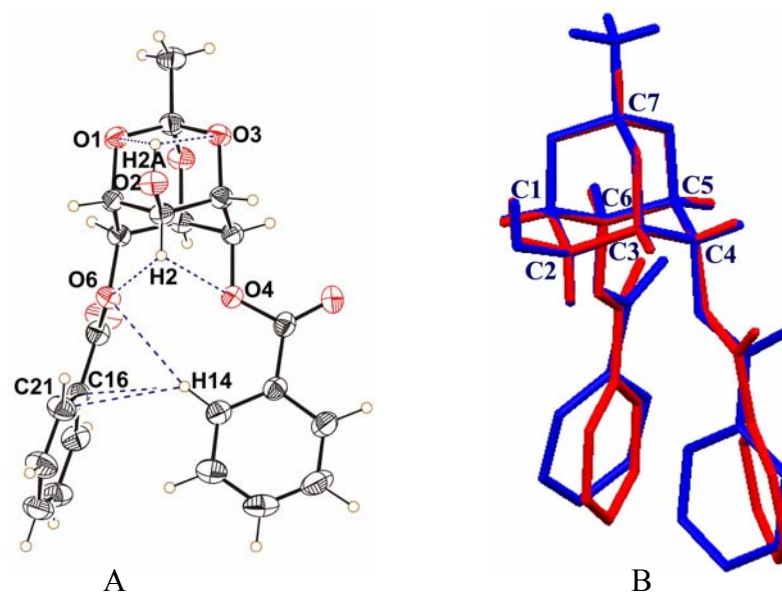


**Figure 6.14.** A) ORTEP view of **10** showing various intramolecular interactions and B) overlap of molecule of **10** (blue) and molecule **1** of solvent free crystals of **9** (red).

**Table 6.10:** Intramolecular hydrogen bond geometry in **10**.

D-H...A	D-H (Å)	H...A (Å)	D...A (Å)	D-H...A (°)
O(2)-H(2A)...O(1)	0.88(2)	2.62(2)	2.902(2)	100(2)
O(2)-H(2A)...O(3)	0.88(2)	2.59(2)	2.910(2)	103(2)
C(2)-H(2)...O(4)	0.96(2)	2.59(2)	2.915(2)	100(1)
C(2)-H(2)...O(6)	0.96(2)	2.70(27)	2.996(2)	99(1)
C(14)-H(14)...O(6)	0.98(2)	2.80(2)	3.744(2)	164(1)

In crystals of **10**, the molecules do not bridge in head-to-head fashion due to the presence of bulky methyl group at orthoester carbon (C7) position. Also the methyl group does not take part in any type of non-bonded interaction with its neighboring molecules. In crystals of **10**, the molecules are arranged helically around crystallographic two-fold screw axis (along c-axis) via conventional O-H...O and C-H...O hydrogen bonding

interactions (**Figure 6.15**). The OH-group (O2-H2A) at C2 position donates its H-atom to the carbonyl oxygen O7 of the C4-*O*-benzoyl group (O2-H2A $\cdots$ O7) and orthoformate oxygen O3 accepts H-atom from the phenyl carbon C10 of the same benzoyl group forming helical assembly along *c*-axis (C10-H10 $\cdots$ O3). The distances H2A $\cdots$ O7 and H10 $\cdots$ O3 are less than the sum of the van der Waals radii but the contacts are not so linear (**Table 6.11**).

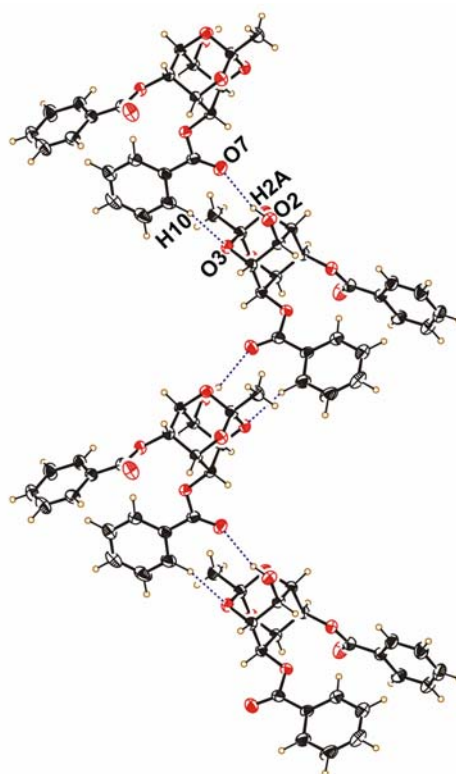


**Figure 6.15.** Helical self-assembly of molecules via O-H $\cdots$ O and C-H $\cdots$ O hydrogen bonding in crystals of **10**.

These helical assemblies are linked along the *b*-axis via two weak C-H $\cdots$ O contacts. The C18-H18 and C19-H19 groups bridge the neighboring helices by donating

their respective protons to hydroxyl oxygen O2 and carbonyl oxygen O7 to form C18-H18 $\cdots$ O2 ( $2_1$ - symmetry) and C19-H19 $\cdots$ O7 (unit translation) interactions (**Figure 6.16**).

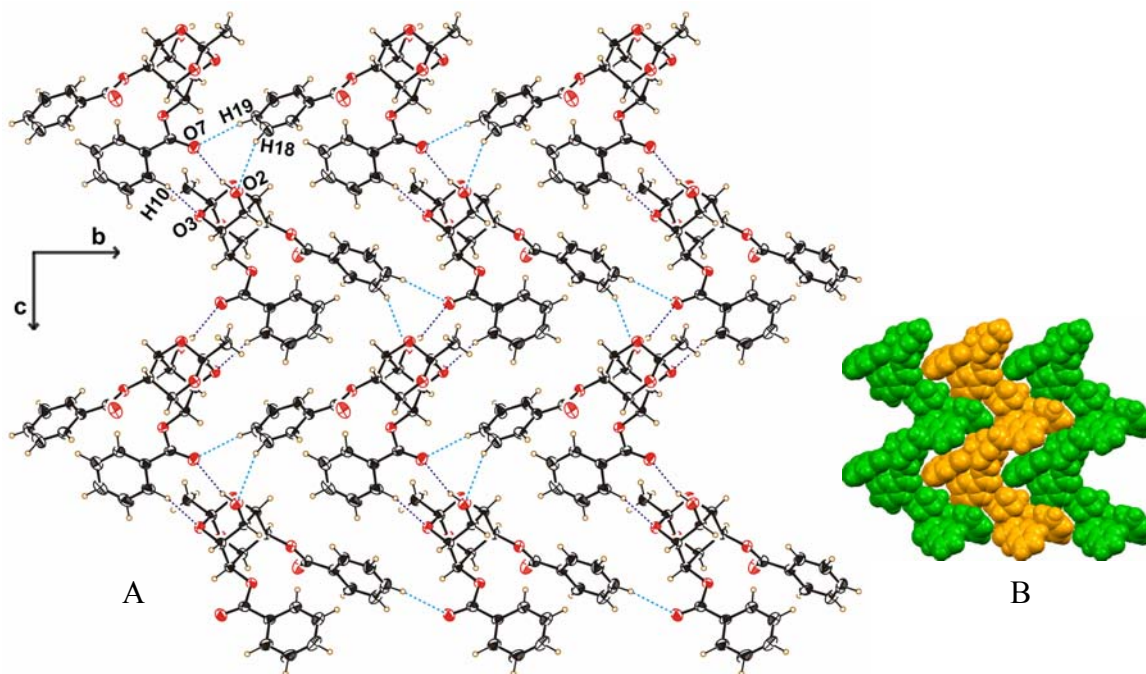


**Figure 6.16.** A) Interlinking of helices along b-axis via C-H $\cdots$ O interaction and B) CPK view of the neighbouring helices.

This helical assembly is stitched to other helical assembly beneath, down a-axis by C-H $\cdots$ O interactions to form the dancing pair like arrangement extended along b-axis (**Figure 6.17**). Molecules in a dancing pair are related by crystallographic a-glide symmetry, which interact with each other via four C-H $\cdots$ O interactions.

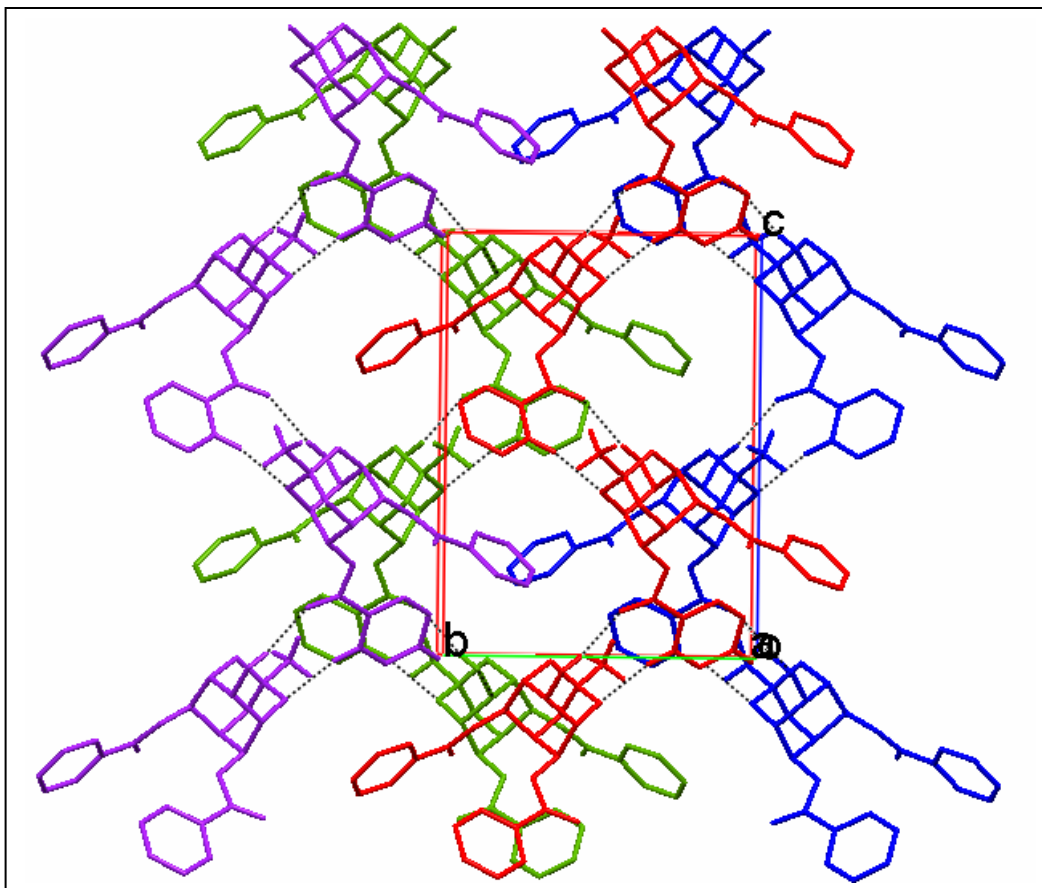


**Figure 6.17.** Molecular packing showing endless chain of dancing pair along b-axis.

Molecular packing in **Figure 6.17** when viewed down the b-axis, revealed helices, which are separated beneath, and they are stitched via four C-H $\cdots$ O a-glide related contacts along a-axis forming helical pattern along the c-axis (**Figure 6.18**). The orthoformate oxygen O5 makes bifurcated C-H $\cdots$ O contacts by accepting proton from C2 and C14 of the a-glide related molecule (C2-H2 $\cdots$ O5 and C21-H21 $\cdots$ O5). The carbonyl oxygen O7 and hydroxyl oxygen O2 accepts proton from the C1 and C4 of the *myo*-inositol ring. All these C-H $\cdots$ O interactions bind the molecules of **10** tightly leaving no void in the crystal lattice for solvent inclusion.

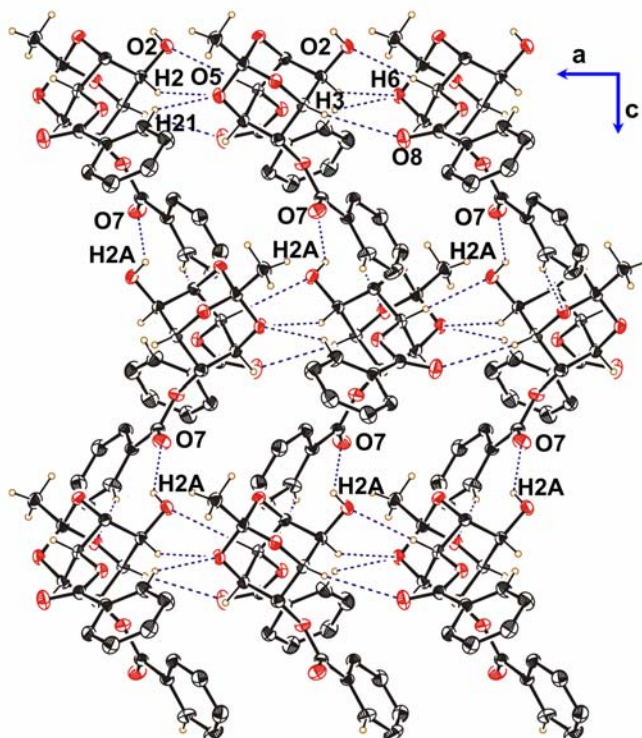


**Figure 6.18.** Helical assembly viewed down the b-axis in **10** showing interhelical contacts.

**Table 6.11:** Intermolecular hydrogen bond geometry in **10**.

D-H...A	D...A (Å)	H...A (Å)	D...A (Å)	D-H...A(°)
O(2)-H(2A)...O(7)#1	0.88(2)	2.23(3)	2.971(2)	142(2)
C(3)-H(3)...O(8)#2	0.95(2)	2.68(2)	3.296(7)	138(1)
C(2)-H(2)...O(5)#2	0.96(2)	2.64(2)	3.501(2)	150(1)
C(6)-H(6)...O(2)#3	0.95(2)	2.46(2)	3.399(2)	172(1)
C(18)-H(18)...O(2)#4	0.91(2)	2.73(2)	3.370(3)	128(2)
C(19)-H(19)...O(7)#5	0.92(2)	2.80(2)	3.469(3)	130(2)
C(12)-H(12)...O(2)#6	0.96(3)	2.82(3)	3.719(3)	157(2)
C(10)-H(10)...O(3)#7	1.02(3)	2.31(3)	3.251(3)	153(2)
C(21)-H(21)...O(5)#2	0.93(2)	2.80(2)	3.598(3)	145(2)

Symmetry codes: #1  $-x, -y+1, z+1/2$ ; #2  $x-1/2, -y+3/2, z$ ; #3  $x+1/2, -y+3/2, z$ ;  
 #4  $-x, -y+2, z-1/2$ ; #5  $x, y+1, z$ ; #6  $-x-1/2, y+1/2, z-1/2$ ; #7  $-x, -y+1, z-1/2$ .

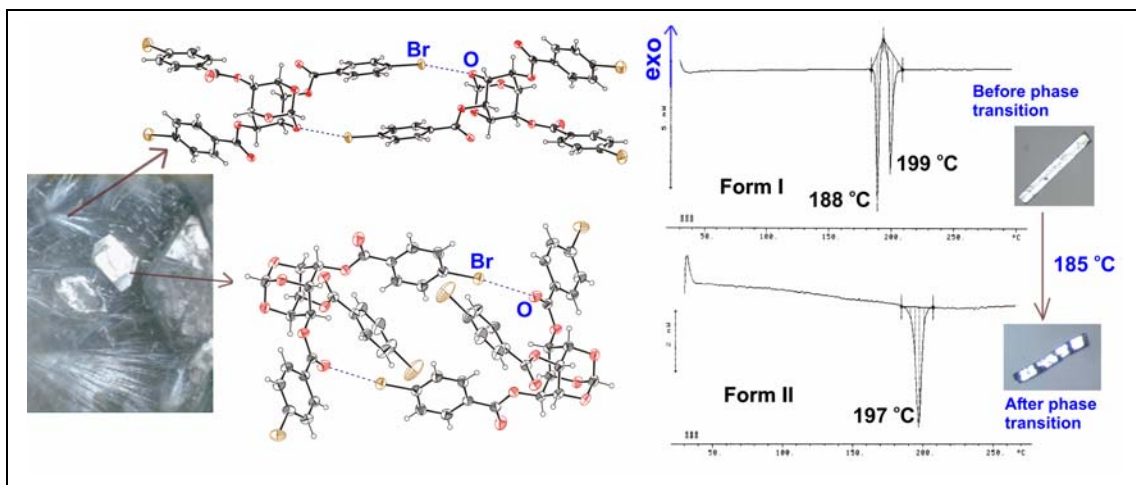


## 6.4 Conclusions

Ortho-bridged compound **9** formed inclusion crystals exclusively with halogen containing solvents. In all the inclusion complexes and in solvent free crystal, the head-to-head dimeric association of the host molecules is well conserved leading to the formation of one-dimensional isostructural molecular string.<sup>137</sup> This head-to-head association with two axial phenyl rings protruding out, to create open framework that encompasses the solvent molecules. The dihalomethane inclusion crystals were highly unstable, whereas those with trihalomethane were relatively more stable. The higher stability of latter can be attributed to the ‘halogen bonding interaction’ between the guest and the host, which is missing in the former. In dihalomethane inclusion crystals, halogen bonding is overwhelmed by C-H $\cdots$ O interactions. Solvent free crystals of **9**, showed a self-inclusion type phenomena, the well conserved head-to-head dimeric assembly created thorough open channel that accommodated another symmetry independent molecules of **9**. The orthoacetate analog, **10** did not associate in head-to-head fashion, probably due to bulky methyl group at carbon C7, but formed helical assemblies, which did not leave any void for guest inclusion.

# Chapter 7

## Concomitant Dimorphs of tri-*O*-[*p*-halobenzoyl]-*myo*-inositol 1,3,5-orthoformates with Different Halogen Bonding Contacts: First Order Crystal-to-Crystal Thermal Phase Transition of Kinetic Form to the Thermodynamic Form



# Chapter 7

## 7.1 Introduction

The *myo*-inositol derivatives reported so far showed a strong tendency to form inclusion crystals with halogenated solvents like  $\text{CH}_2\text{Cl}_2$ ,  $\text{CH}_2\text{Br}_2$ ,  $\text{CH}_2\text{ClBr}$ ,  $\text{CHCl}_3$ ,  $\text{CHBr}_3$  etc. It was also observed consistently that the stability of inclusion crystals largely depended on the strength of the halogen-oxygen interactions. Further, to explore the possibility of studying molecular association via halogen bonding contacts, it was planned to substitute halogen atoms on the *myo*-inositol derivative itself. Accordingly, the halo substituted derivatives of *myo*-inositol (**11** and **12**, **Figure 7.1**) were synthesized.

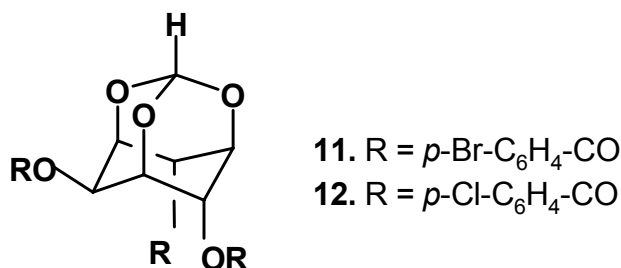


**Figure 7.1.** Structures of halogenated derivatives of *myo*-inositol, **11** and **12**.

Compounds **11** and **12** did not produce any inclusion crystals but molecules associated using  $\text{C-X}\cdots\text{O}$  ( $\text{X} = \text{Cl}, \text{Br}$ ) contacts producing concomitant polymorphs.<sup>133</sup> The kinetic crystals (needles, Form I) appeared within few hours, whereas thermodynamic crystals (octahedral blocks, Form II) were obtained during slow evaporation after  $\sim 2$

days. DSC studies suggested an irreversible first order crystal-to-crystal phase transition<sup>35g</sup> of Form I crystals to Form II crystals at 185-186 °C, which was confirmed by X-ray analysis. Crystal structures revealed two types of ‘halogen bonding’ contacts; C-Br...O-C (ether oxygen) in Form I and C-Br...O=C (carbonyl oxygen) in Form II. These results gave some more insight into the preferred types of halogen bonding contacts and its manifestation in crystal growth.

## 7.2 Experimental Section

### 7.2.1 Synthesis

#### *Preparation of 2,4,6-tri-O-(p-bromobenzoyl) myo-inositol 1,3,5-orthoformate (11)*

A solution of *myo*-inositol 1,3,5-orthoformate (**2**) (0.100 g, 0.525 mmol) in dry pyridine (3 mL) was cooled (ice bath) and a solution of *p*-bromobenzoyl chloride (0.635 g, 2.893 mmol) in pyridine (1 mL) was added dropwise. The reaction mixture was stirred at room temperature for about 48 hours. Completion of the reaction was confirmed by checking TLC of the reaction mixture, which showed two spots. About 2 mL water was then added into the reaction mixture and stirring continued for about two hours. Solvent was evaporated under reduced pressure to obtain a solid. It was dissolved in sodium bicarbonate solution and usual work up of the residue gave a gum.. The products were separated by column chromatography to obtain **11** (upper major spot, 0.238 g, 60%) as white solids (lower spot also was separated, which will be discussed in next chapter).

**Data for 11:**

**mp** 199-200 °C; **IR** (CHCl<sub>3</sub>)  $\nu$  = 1728 and 1704 cm<sup>-1</sup>; **<sup>1</sup>H NMR** (CDCl<sub>3</sub>, 200 MHz):  $\delta$  4.64 (s, 2H), 5.03 (m, 1H), 5.65 (m, 1H), 5.73 (s, 1H), 5.80 (t, 2H), 7.26-7.36 (m, 4H), 7.61-7.65 (m, 6H), 8.03-8.04 (m, 2H); **<sup>13</sup>C NMR** (CDCl<sub>3</sub>, 75 MHz):  $\delta$  27.0, 39.0, 63.0, 67.0, 68.4, 69.3, 103.3, 128.3, 128.6, 129.8, 133.4, 165.1, and 178.2; **Elemental analysis** calcd for C<sub>28</sub>H<sub>19</sub>O<sub>9</sub>Br<sub>3</sub>; C 45.50%, H 2.58%; found C 45.37%, H 2.25%.

### ***Preparation of 2,4,6-tri-O-(p-chlorobenzoyl) -myo-inositol 1,3,5-orthoformate (12)***

The *p*-chloro derivative **12** was prepared as above using *myo*-Inositol 1,3,5-orthoformate (0.380 g, 2 mmol in 15 mL dry pyridine) and *p*-chlorobenzoyl chloride (1.575 g, 9 mmol) as above to obtain 0.883 g of **12** (73%).

#### **Data for 12:**

**mp** 195-196 °C; **IR** (CHCl<sub>3</sub>)  $\nu$  = 1735 cm<sup>-1</sup> and 1704 cm<sup>-1</sup>; **<sup>1</sup>H NMR** (CDCl<sub>3</sub>, 200 MHz):  $\delta$  4.65-4.67 (m, 2H), 5.02-5.06 (m, 1H), 5.65 (m, 1H), 5.66-5.83 (m, 3H), 7.17-7.33 (m, 4H), 7.46-7.50 (m, 2H), 7.64-7.74 (m, 4H), 7.92-8.14 (m, 2H); **<sup>13</sup>C NMR** (CDCl<sub>3</sub>, 75 MHz):  $\delta$  63.9, 66.4, 68.5, 69.1, 77.0, 103.2, 123.3, 126.7, 127.6, 128.6, 130.9, 140.2, 164.0, and 165.2; **Elemental analysis** calcd for C<sub>28</sub>H<sub>19</sub>O<sub>9</sub>Cl<sub>3</sub>; C 55.42%, H 3.16%; found C 54.95%, H 2.94%.

## **7.2.2 Crystallization**

Crystallization of **11** and **12** was attempted from various common organic solvents by fast evaporation, slow evaporation and vapour diffusion method (Petroleum ether vapours used for diffusion). The number of trials made along with the results obtained is given in **Table 7.1**.

**Table 7.1:** Crystallization data of **11** and **12** from various solvents.

Trial No	Solvent Used	Method of Crystallization*	Result
1	Ethyl acetate	1,2	Block crystals
2	Ethyl acetate and Petroleum ether	1	Concomitant dimorphs (thin needles and blocks)**
3	Ethyl acetate and Petroleum ether	3	Very thin needles appeared first and block crystals latter
4	Acetone	1	Concomitant dimorphs (thin needles and blocks)
5	Dichloromethane	2	block crystals
6	Dichloromethane	1,3	Concomitant dimorphs (thin needles and blocks)
7	Chloroform	2	block crystals
8	Chloroform	1,3	Concomitant dimorphs (thin needles and blocks)
9	Toluene	1,3	Concomitant dimorphs (thin needles and blocks)

\*1- slow evaporation, 2 - vapour diffusion and 3 - fast evaporation

\*\* In case of **12**, the needles obtained were like very thin whiskers and the quantity obtained was also very less

The compounds **11** and **12** gave concomitant dimorphs, Form I needles (**Figure 7.2A**, whiskers in case of **12**, **Figure 7.2C**) and Form II blocks (**Figure 7.2B**) when crystallized from ethyl acetate/petroleum ether mixture. Needles appeared from the solution within first few hours, while the blocks were obtained after two days from the same flask (by slow evaporation). The majority of the crystals belonged to Form II, whereas the Form I was a minor product. On standing in the mother liquor some of the needles gradually disappeared with the simultaneous appearance block crystals appeared.<sup>136</sup> Needles of Form I could also be obtained by achieving rapid nucleation by cooling a saturated solution of **11** or **12** (in ethyl acetate, chloroform, dichloromethane or

acetone). In case of **12**, the needles were very thin whiskers and the quantity obtained was also very less.

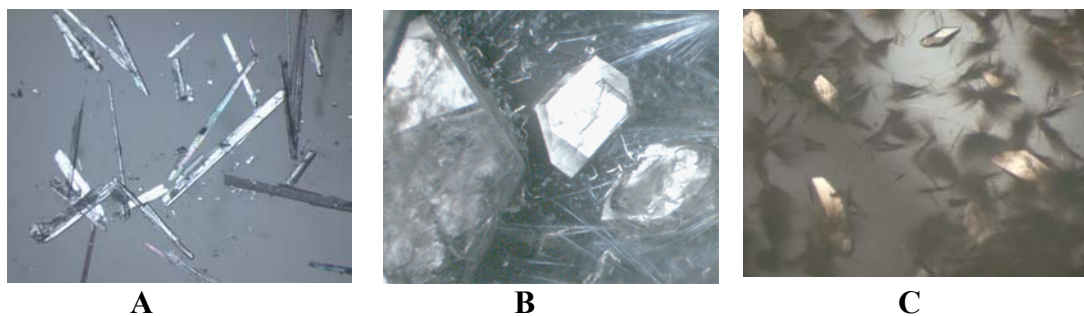


**Figure 7.2.** Photomicrographs of crystals of **11** and **12**, A) Form I crystals of **11**, B) Form II crystals of **11** and C) Form I and Form II crystals of **12**.

### 7.2.3 Thermal Analysis (DSC Study)

The thermal behaviour of polymorphs of **11** and **12** was studied by measuring enthalpy with a Differential Scanning Calorimeter (DSC). The DSC of Form I crystals of **11** (**Figure 7.3A**) showed two sharp endotherms, the first one at 188.1 °C suggesting a first order phase transition<sup>142</sup> and the second one at 198.7 °C corresponding to the melting of the crystal. Interestingly, a repeat of the DSC for the Form I crystals of **11** (cooled after heating up to the transition temperature 198 °C) contained only a melting endotherm at 198 °C suggesting an irreversible phase transition of Form I. The DSC of Form II crystals of **11** showed a single peak representing melting of the crystal (**Figure 7.3B**). As evident from **Figure 7.3** both the crystals forms have similar melting points.

DSC studies of Form I crystals of **12**, could not be carried out, as the quantity of these crystals was very less (less than 1 mg obtained from many crystallization trials).

The DSC of the Form II crystals of **12** showed only one endothermic peak at 196.3 °C corresponding to the melting of the crystals (**Figure 7.3C**).

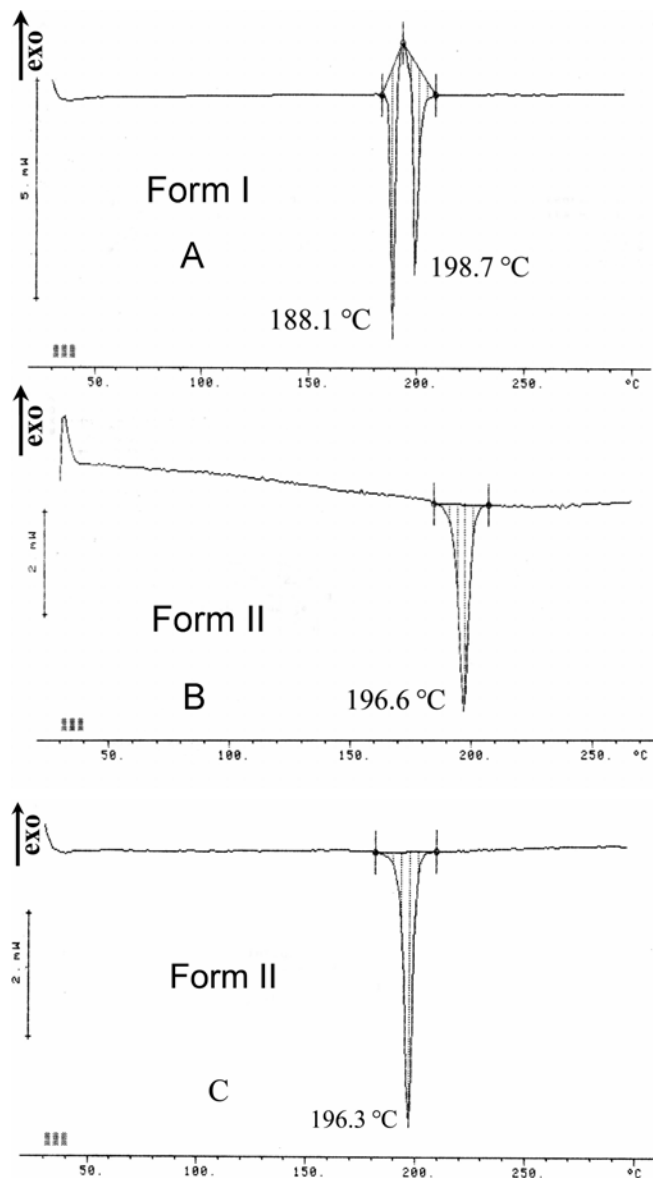


**Figure 7.3.** DSC profiles of, A) Form I crystals of **11**, B) Form II crystals of **11** and C) Form II crystals of **12**.



#### 7.2.4 Data Collection, Structure Solution and Refinement of Crystals of **11** and **12**

Single crystal X-ray studies were carried out on both the polymorphs of **11** (Form I and Form II) and Form II crystals of **12**. The needles of **12** (Form I) were too thin and the yield was too low to allow single crystal or X-ray powder diffraction measurements. Single crystal structure analysis revealed that the Form I crystals of **11** belong to monoclinic C2/c, whereas Form II crystals of **11** and **12** are triclinic P-1. Unit cell parameters of Form II crystals of **11** and **12** are almost the same, indicating their isostructurality. The summary of crystallographic data is given in **Table 7.2**. The higher density of the crystals ( $1.862 \text{ g cm}^{-3}$  in Form I and  $1.758 \text{ g cm}^{-3}$  in Form II crystals of **11** and  $1.515 \text{ g cm}^{-3}$  in Form II crystals of **12**) indicates the close packing of molecules in the crystal lattice in both the forms.

**Table 7.2:** Crystallographic Data of **11** and **12**.

	<b>11 (Form I)</b>	<b>11 (Form II)</b>	<b>12 (Form II)</b>
Chemical formula	C <sub>28</sub> H <sub>19</sub> Br <sub>3</sub> O <sub>9</sub>	C <sub>28</sub> H <sub>19</sub> Br <sub>3</sub> O <sub>9</sub>	C <sub>28</sub> H <sub>19</sub> Cl <sub>3</sub> O <sub>9</sub>
M <sub>r</sub>	739.16	739.16	605.78
Temperature/K	297(2)	297(2)	297(2)
Morphology	Thin needle	Octahedral	Octahedral
Crystal size	0.44×0.08×0.02	0.64×0.57×0.30	0.48×0.41×0.12
Crystal system	Monoclinic	Triclinic	Triclinic
Space group	<i>C</i> 2/ <i>c</i>	<i>P</i> -1	<i>P</i> -1
<i>a</i> (Å)	57.945(13)	10.002(2)	10.2740(17)
<i>b</i> (Å)	6.0511(13)	12.126(2)	11.2899(18)
<i>c</i> (Å)	15.465(3)	13.146(3)	12.717(2)
$\alpha$ (°)	90	70.536(3)	75.582(3)
$\beta$ (°)	103.469(4)	80.100(3)	86.976(3)
$\gamma$ (°)	90	68.503(3)	68.503(3)
<i>V</i> (Å <sup>3</sup> )	5273(2)	1396.5(5)	1328.0(4)
<b>Z</b>	8	2	2
<i>D</i> <sub>calc</sub> (g cm <sup>-3</sup> )	1.862	1.758	1.515
$\mu$ (mm <sup>-1</sup> )	4.646	4.386	0.401
<i>F</i> (000)	2912	728	620
Ab.Correction	Multi-scan	Multi-scan	Multi-scan
<i>T</i> <sub>min</sub>	0.236	0.166	0.832
<i>T</i> <sub>max</sub>	0.909	0.353	0.953
$\theta$ <sub>max</sub> (°)	25	25	25
<i>h</i> , <i>k</i> , <i>l</i> (min, max)	(-68,68),(-7,7), (-18,18)	(-11,11),(-14,14), (-15,15)	(-12,12),(-13,12), (-15,15)
Reflns collected	18012	13350	9709
Unique reflns	4623	4893	4648
Observed reflns	3261	4105	3362
R <sub>int</sub>	0.0708	0.0276	0.0212
No. of parameters	361	380	361
GoF	1.010	1.031	1.038
R <sub>1</sub> [ <i>I</i> > 2σ( <i>I</i> )]	0.0485	0.0417	0.0525
wR <sub>2</sub> [ <i>I</i> > 2σ( <i>I</i> )]	0.0972	0.1055	0.1374
R <sub>1</sub> _all data	0.0787	0.0505	0.0737
wR <sub>2</sub> _all data	0.1074	0.1113	0.1495
$\Delta \rho_{\max}$ , $\Delta \rho_{\min}$ (eÅ <sup>-3</sup> )	0.85, -0.48	1.21, -1.05	0.49, -0.22

### 7.2.5 Thermal Response on Hot Stage Microscopy

As mentioned earlier, DSC had indicated first order phase transition in Form I crystals of **11** just before the melting endotherm (**Figure 7.3**). The transition was so sharp that the energy absorbed during transition is more than the energy needed for melting. In order to observe the phase transition visually, the crystals of Form I were heated on Leica hot stage polarizing microscope MZ 75 and the photomicrographs were captured using Leica DC 300 CCD camera attached. Form I crystals of **11** (**Figure 7.4A**) upon heating to  $\sim 185$ - $186$  °C showed a transition front moving quickly along the needle axis (**Figure 7.4B** and **7.4C**) from one end to the other within a second subsequently fragmenting the crystal transverse to the length of the needle (**Figure 7.4D**). Each of the fragments observed under optical polarizing microscope showed extinction which confirmed their single crystalline nature. It also appeared that the thickness of the fragments obtained after transition (**Figure 7.4D**) had increased compared to their state before transition (**Figure 7.4A**).<sup>142 a,e</sup>

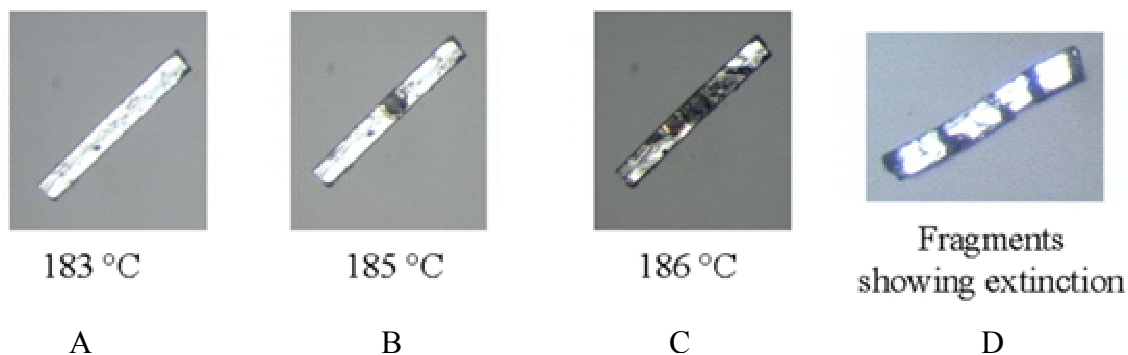


**Figure 7.4.** Photomicrographs of Form I crystal of **11** during heating experiment, A) before transition, B) transition in progress, C) transition completed and D) crystal fragmented after transition.

The unit cell parameters of one of the fragments mounted on the diffractometer revealed that it was the crystal of Form II of **11**. Reproducibility of this irreversible crystal-to-crystal transition was confirmed by repeating this experiment on several Form I crystals of **11** which always yielded Form II crystals.

### 7.3 Results and Discussion

#### 7.3.1 Intramolecular Geometry

Three axial positions at C1, C3 and C5 constitute the orthoformate bridge, whereas two remaining axial positions C4 and C6 and one equatorial position are occupied by *p*-halobenzoyl groups (**Figure. 7.5**). The conformation of the molecule as observed in the crystal shows that the *p*-halo benzoyl groups do not involve in any intramolecular interactions.

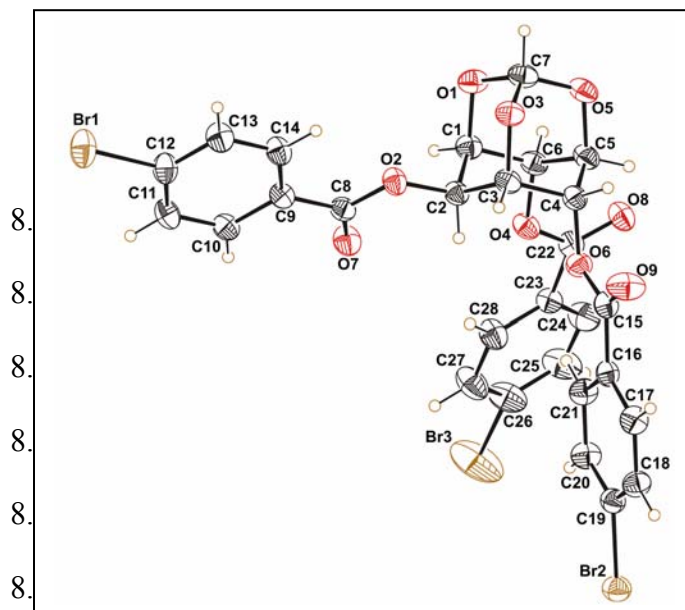


**Figure 7.5.** ORTEP view of molecule in Form II crystals of **11**. Form II of **12** is almost same.

### 7.3.2 Dimer Formation via Halogen Bonding Contacts

The molecules in Form I and Form II crystals of **11** form centrosymmetric dimers via halogen bonding contacts, but with a difference in the nature of the acceptor oxygen atom.<sup>50a</sup> In Form I crystals of **11**, the halogen bonding is between the C12-Br1 (of the C2-equatorial benzoyl group) and orthoformate bridge oxygen O1 (**Figure 7.6A**), whereas in Form II crystals of **11** the halogen bonding is between the C19-Br2 (of the C4-axial benzoyl group) and the carbonyl oxygen O7 (of the C2-equatorial benzoyl group, **Figure 7.6B**). The Br $\cdots$ O distance is slightly shorter in Form I crystals [3.027(3) Å] than in Form II crystals [3.174(3) Å], but the  $\angle$ C-Br $\cdots$ O shows more linearity in Form II crystals [173.8(3) $^\circ$ ] in as compared to Form I crystals [163.4(5) $^\circ$ ].

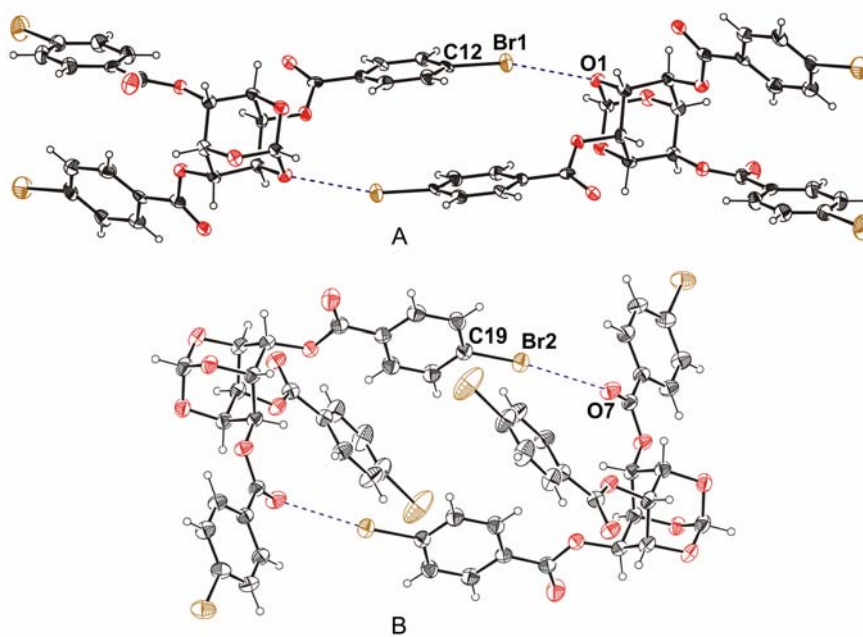


**Figure 7.6.** Halogen bonded dimeric assembly in crystals of **11**, A) with ether oxygen in Form I crystals and B) with carbonyl oxygen in Form II crystals.

### 7.3.3 Association of Dimers

The halogen bonded dimeric unit in Form I crystals is linked via centrosymmetric Br2⋯Br3 short contacts [3.404 (1) Å] with the neighbouring dimeric unit forming ribbon like structure (**Figure 7.7A**), whereas in Form II crystals these units are linked by C7-H7⋯O9 [H7⋯O9 = 2.71 Å, C7⋯O9 = 3.373(5) Å, ∠C7-H7⋯O9 = 125.2°] in Form II crystals of **11** (**Figure 7.7B**, and **Table 7.3**).

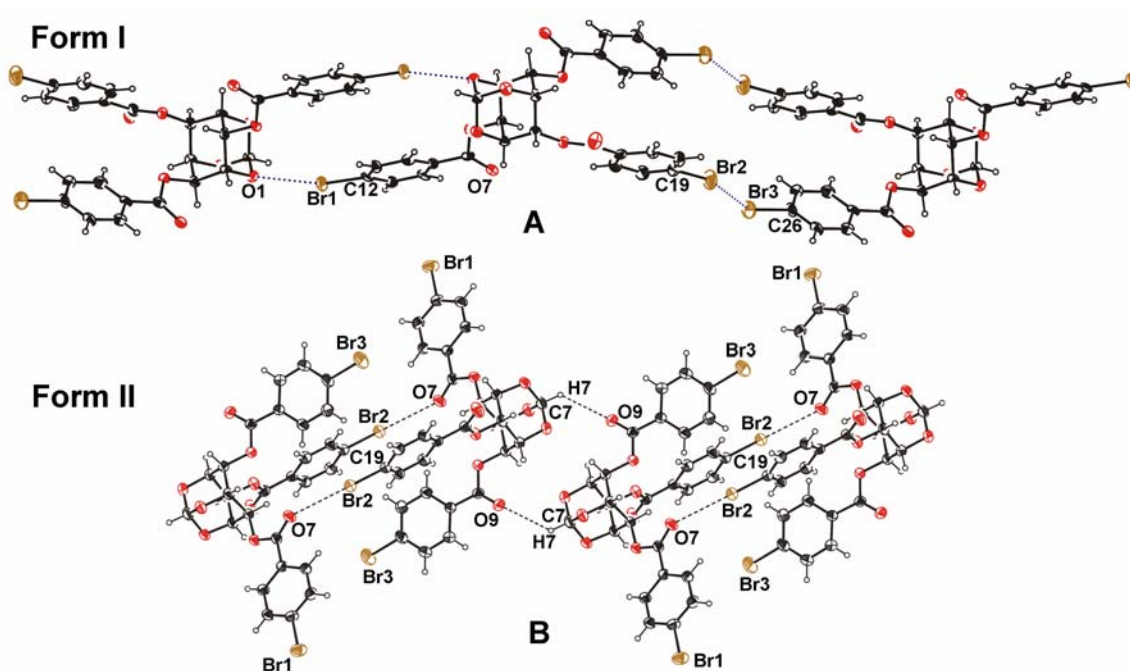


**Figure 7.7.** Bridging of halogen bonded dimeric units in crystals of **11**, A) via Br⋯Br contact and B) via C-H⋯O contact.

**Table 7.3:** Intermolecular C-H...O, C-H...halogen and C-halogen... $\pi$  interactions.

X =Cl, Br	D-H/X...A	H/X...A (Å)	D...A (Å)	D-H/X...A (°)
Form I of <b>11</b>	C(1)-H(1)...O(5)#1	2.38	3.248(6)	147
	C(3)-H(3)...O(9)#2	2.39	3.339(6)	164
	C(4)-H(4)...O(7)#3	2.48	3.278(6)	138
	C(5)-H(5)...O(9)#3	2.76	3.413(6)	124
	C(6)-H(6)...O(7)#4	2.53	3.370(6)	144
	C(10)-H(10)...O(9)#5	2.55	3.450(6)	163
	C(24)-H(24)...O(7)#6	2.73	3.646(6)	168
	C(12)-Br(1)...O(1)#7	3.027(3)		163
	C(19)-Br(2)...Br(3)#8	3.404 (1)		157
	C(26)-Br(3)...Br(2)#8	3.404 (1)		140
Form II of <b>11</b>	C(5)-H(5)...Br(2)#8	3.03	3.715(4)	128
	C(6)-H(6)...O(5)#9	2.77	3.495(4)	131
	C(7)-H(7)...O(9)#9	2.71	3.373(5)	125
	C(10)-H(10)...O(5)#10	2.82	3.610(4)	144
	C(11)-H(11)...O(3)#10	2.60	3.374(5)	141
	C(13)-H(13)...O(8)#11	2.78	3.445(5)	130
	C(18)-H(18)...O(9)#8	2.55	3.351(5)	145
	C(12)-Br(1)...Cg(2)#12	3.926	5.818	170
	C(19)-Br(2)...O(7)#13	3.174(3)		174
	C(26)-Br(3)...Br(3)#14	3.444(2)		154
Form II of <b>12</b>	C(1)-H(1)...O(7)#15	2.75	3.483(3)	132
	C(3)-H(3)...O(3)#16	2.71	3.560(3)	145
	C(5)-H(5)...Cl(2)#17	3.20	3.958(3)	136
	C(6)-H(6)...O(5)#16	2.46	3.256(3)	139
	C(7)-H(7)...O(9)#18	2.66	3.363(3)	129
	C(10)-H(10)...O(5)#19	2.83	3.525(3)	133
	C(11)-H(11)...O(3)#19	2.57	3.432(3)	153
	C(13)-H(13)...O(8)#16	2.77	3.381(4)	124
	C(14)-H(14)...O(8)#16	2.77	3.384(4)	125
	C(18)-H(18)...O(9)#17	2.43	3.240(4)	145
	C(27)-H(27)...O(1)#15	2.64	3.360(4)	135
	C(12)-Cl(1)...Cg(2)#13	4.491	6.184(4)	165
	C(19)-Cl(2)...O(7)#20	3.102(2)		167
	C(26)-Cl(3)...Cl(3)#21	3.423 (2)		150

Symmetry codes: #1  $x, y+1, z$ ; #2  $x, -y+1, z+1/2$ ; #3  $x, y-1, z$ ; #4  $x, -y+1, z-1/2$ ;  
#5  $x, -y+2, z+1/2$ ; #6  $x, -y+2, z-1/2$ ; #7  $-x+1.5, -y+1.5, -z+1$ ; #8  $-x+1, -y+2, -z$ ;  
#9  $-x+1, -y+2, -z+1$ ; #10  $x-1, y, z$ ; #11  $-x+1, -y+1, -z+1$ ; #12  $x, y-1, z+1$ ;  
#13  $-x, -y+2, -z$ ; #14  $-x-1, -y+3, -z$ ; #15  $-x, -y+2, -z+2$ ; #16  $-x+1, -y+1, -z+2$ ;  
#17  $-x+1, -y+2, -z+1$ ; #18  $-x+1, -y+2, -z+2$ ; #19  $x-1, y, z$ ; #20  $-x, -y+2, -z+1$ ;  
#21  $-x-1, -y+3, 1-z$ , Cg2- centroid of the phenyl ring C16-C21

In Form I crystals of **11** the Br1···O1 and Br2···Br3 bonded ribbons are linked via two C-H···O contacts (C1-H1···O5 and C4-H4···O7, **Table 7.3**) along b-axis forming bilayer (**Figure 7.8A**). In Form II crystals the halogen bonded (Br2···O7) dimeric units are linked by Br3···Br3 [3.444(2) Å] short contacts along b-axis forming chains of dimers. Further these dimeric units are associated via C7-H7···O9 contacts along c-axis (**Figure 7.8B**). Other halogen atom Br1 of **11** in Form II crystals is involved in the Br··· $\pi$  contact. Thus all the bromine atoms are involved in intermolecular interactions in Form I and Form II crystals of **11**. The Br···Br contact in both forms is of the type I category<sup>44</sup> (angles at both bromine atoms are similar) and is less than the sum of van der Waals radii (3.72 Å).<sup>15</sup> Further, the Cl3···Cl3 [3.423 (2) Å] distance in Form II crystals of **12** is also less than the sum of van der Waal radii (3.56 Å).

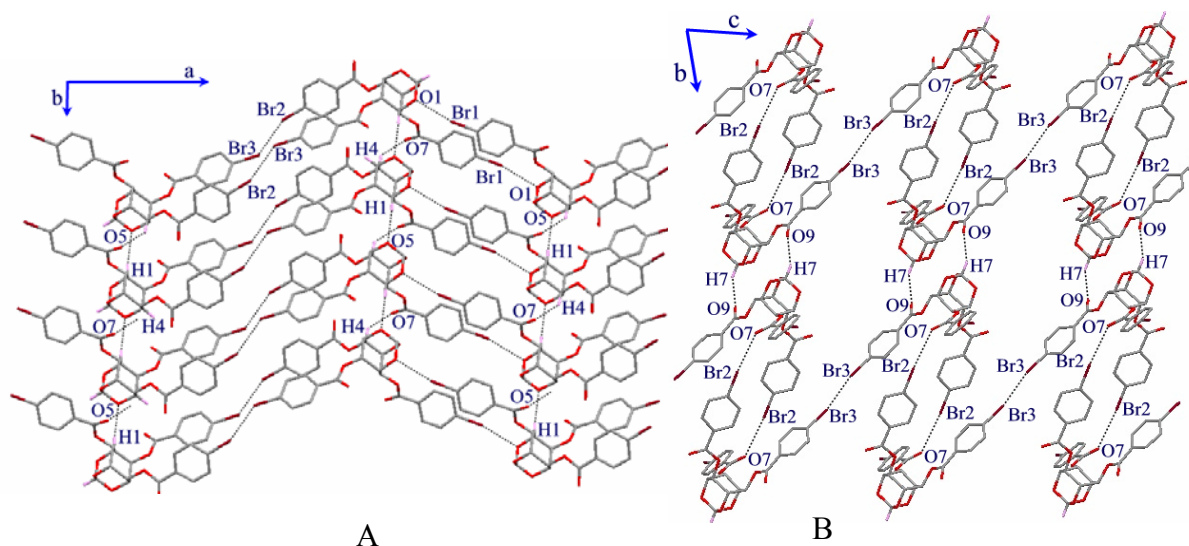


**Figure 7.8.** A) Bilayer formation in Form I crystals of **11** and B) halogen bonded dimers linked by Br···Br contact forming chain in Form II crystals of **11**.



Molecular packing in Form I crystals of **11** viewed down the b-axis show that the Br1...O1 bridged centrosymmetric dimers are linked via C3-H3...O9 contact along the c-axis forming another type of bilayer assembly (**Figure 7.9A**). In Form II crystals of **11** the centrosymmetric dimers are associated via (i) almost linear dimeric C12-Br1... $\pi$  (phenyl ring of C4-O-benzoyl group, Cg2, **Table 7.3**), (ii) off centered dimeric  $\pi$ ... $\pi$  stacking interactions (Cg1...Cg1 = 3.878 Å in Form II crystals of **11** and 3.993 Å in Form II of **12**, Cg1 – centroid of phenyl ring C9-C14) between the phenyl ring of the equatorial C2-O-benzoyl group along the bc plane and (iii) three C-H...O (C10-H10...O5, C11-H11...O3 and C13-H13...O9) contacts along the a-axis (**Figure 7.9B**, **Table 7.3**). Thus the molecules of **11** in Form I and Form II crystals are closely packed by various weak interactions described above (**Table 7.3**).

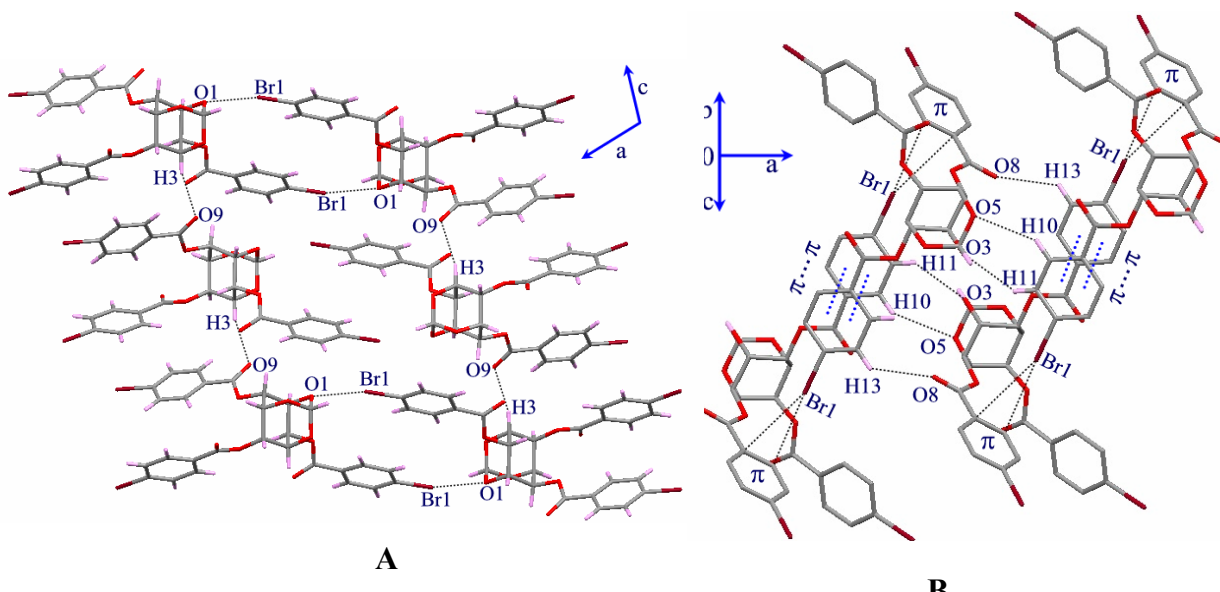


**Figure 7.9.** Association of centrosymmetric dimers in A) Form I and B) Form II crystals of **11**.

### 7.3.4 Conformational Differences

The overlap of molecule in Form II crystals of **11** and **12** revealed a slight difference in the orientation of the axial C4 and C6-*O-p*-halobenzoyl groups. Orientation of C4-*O*-benzoyl groups vary by  $\sim 21^\circ$  and that of C6-*O*-benzoyl group by  $\sim 32^\circ$ , but the orientation of the equatorial C2-*O-p*-halobenzoyl group showed lesser difference ( $10^\circ$ , **Figure 7.10A**). The overlap of molecules in Form I and Form II crystals of **11** showed significant difference in the conformation of all the three *p*-bromobenzoyl groups. The difference in orientation between C4-*O-p*-bromobenzoyl group in Form I and Form II crystals of **11** is  $70^\circ$  and that between C6-*O-p*-bromobenzoyl group in Form I and Form II crystals of **11** is about  $75^\circ$ . Carbonyl groups of the C6-*O-p*-bromobenzoyl group in the two molecules point in opposite directions. The difference in conformation of C2-*O-p*-bromobenzoyl groups in Form I and Form II crystals of **11** is about  $27^\circ$  (**Figure 7.10B**).

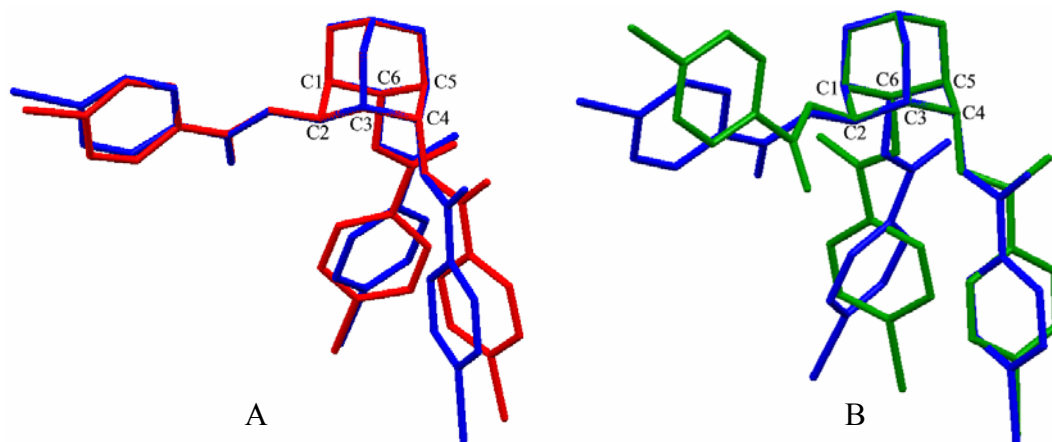
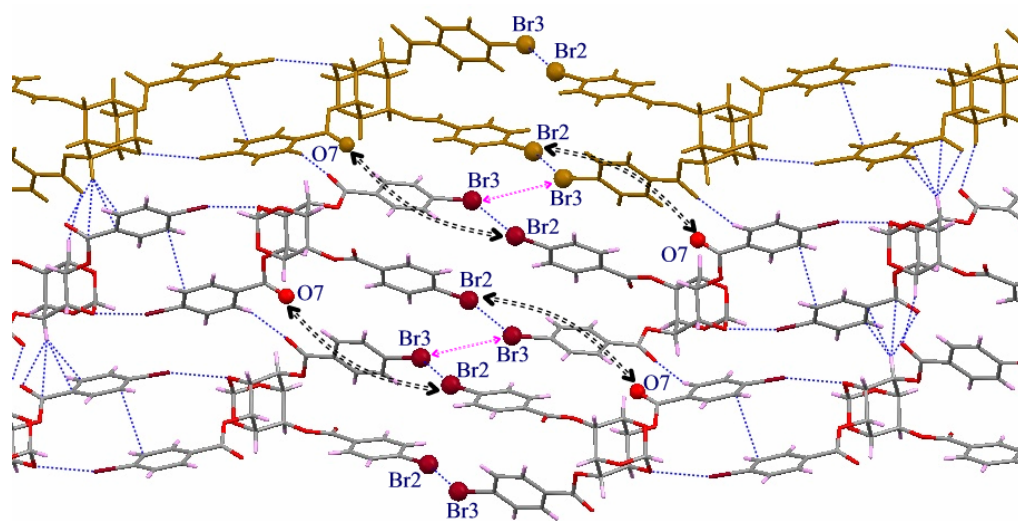


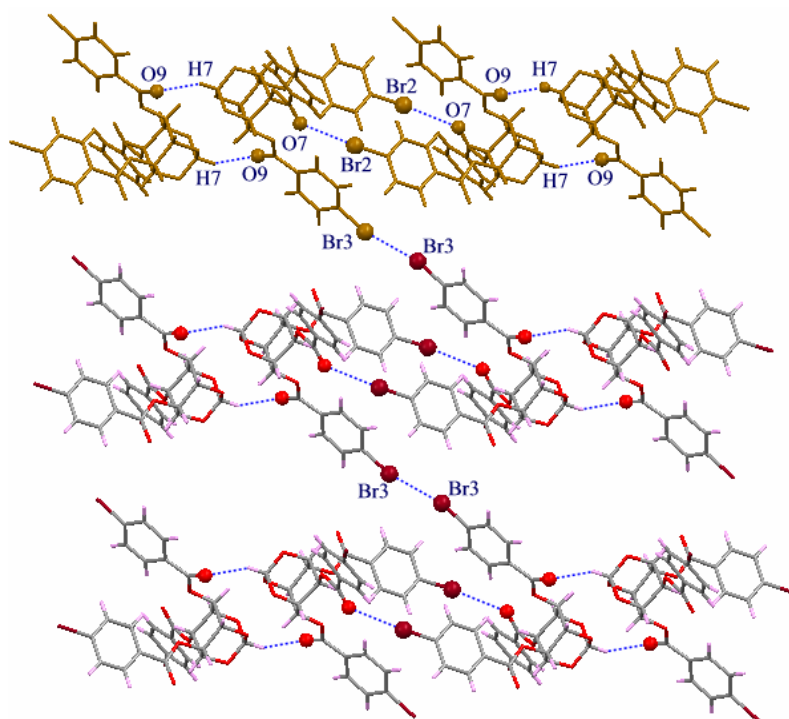
**Figure 7.10.** Overlap of molecules from polymorphs of **11** and **12**, A) Form II crystals of **11** (blue) and **12** (red) and B) Form I (green) and Form II (blue) crystals of **11**.

### 7.3.5 Proposed Mechanism of Transition from Form I to Form II Crystals of **11**

For the conversion of Form I to Form II crystals of **11**, the molecules linked via centrosymmetric Br2...Br3 contacts (orange ribbon in **Figure 7.11A**) in Form I crystals have to rearrange to make C19-Br2...O7 and Br3...Br3 short contacts as in Form II crystals (**Figure 7.11B**). We propose that this involves relative movement of molecules from the two ribbons (brown and elemental colour) towards each other by  $\sim 3 \text{ \AA}$  (blue dotted arrows in **Figure 7.11A**) accompanied by conformational changes in aromatic rings. The spontaneous fragmentation of the crystal could be a consequence of these large molecular movements resulting in new interactions C19-Br2...O7(=C8) and Br3...Br3 while sacrificing Br2...Br3, C12-Br1...O1(-C1) and inter ribbon C-H...O interactions.



A



B

**Figure 7.11.** A) The proposed molecular displacement is marked by blue arrows in Form I crystals of **11** and B) contact Br2...O7 and Br3...Br3 to be formed after transition are shown in Form II crystals of **11**.

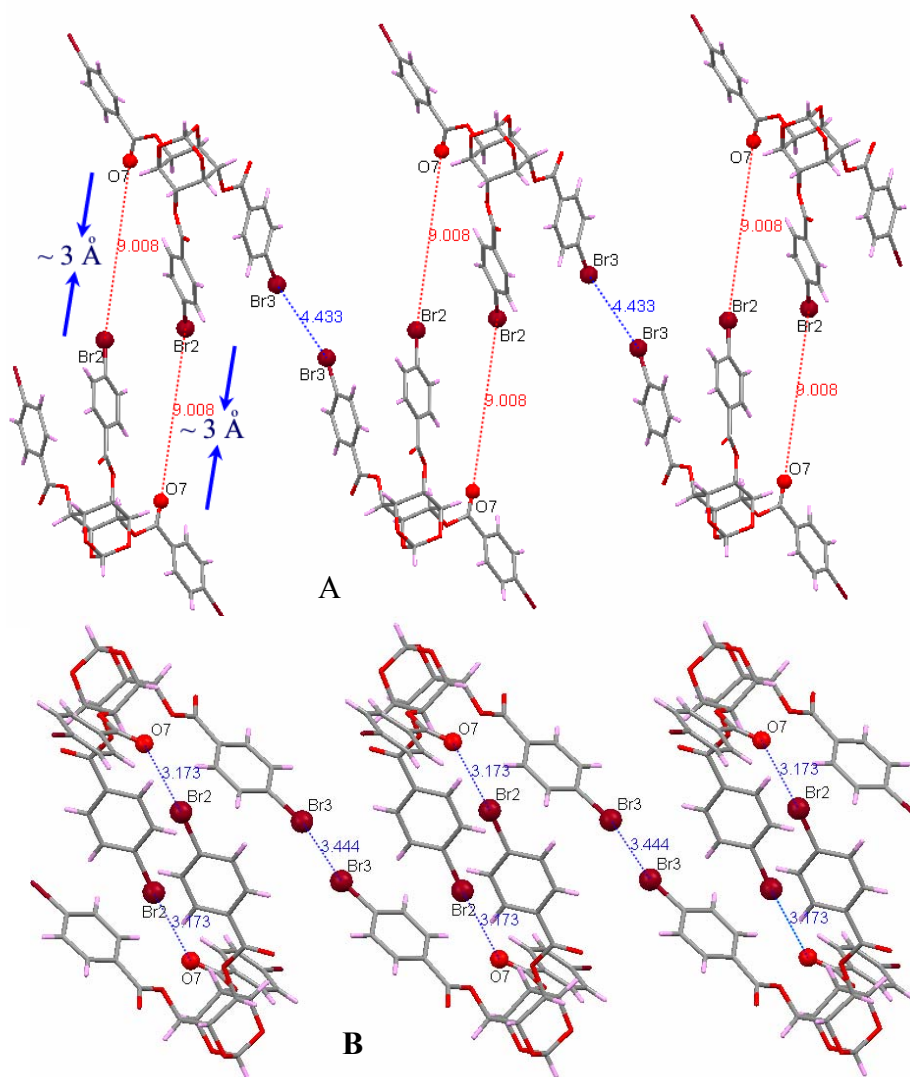


**Figure 7.12.** View of association of dimers via Br3...Br3 contacts in A) Form I crystals and B) Form II crystals of **11**. Blue arrows in A indicate the molecule movement necessary to bring in the phase transition.

The possible mechanism of transformation can be seen more clearly in **Figure 7.12**. Upon heating the crystals of Form I crystals, a ‘closing in’ of Br2...O7 contacts are thought to give rise to halogen-bonded dimers as in Form II crystals. It is remarkable that these structural changes occur without loss of single crystalline nature. This is in contrast

to the molecular movements in reversible phase transformations, which involve minimum molecular movement and hence are restorable.<sup>142</sup> The changes in the present transition are far too large and hence molecules cannot regain their original position in the crystal lattice.

### 7.3.6 Lattice Energy Calculations\*

In order to calculate reliable lattice energies of Form I and Form II crystals of **11**, first lattice energy optimisation of the crystal structure (starting from the experimental structure) was carried out in which the unit cell parameters and the atomic coordinates are optimized (optimization of the molecular geometry). During the optimisation the molecular geometries as well as the crystal structures changed only slightly, but the unit cell volume of the Form I crystals of **11** obtained from single crystal X-ray study increased by 7 %, as a result the crystal density of the Form II crystals of **11** became more than that of Form I crystals (**Table 7.4**). Lattice energies were derived by calculating the total energy (including the intramolecular energy) and subtracting the energy of a single molecule. The methodology followed for the lattice energy calculations is given in detail in Appendix I.

The resulting lattice energies are:

Form I: -168.33 KJ/mol

Form II: -179.41 KJ/mol

According to these calculations, Form II crystals should be considerably more stable than Form I crystals.

---

\*Courtesy - Prof. Dr. Martin Schmidt, Institut für Anorganische und Analytische Chemie der Universität Frankfurt, Germany.

**Table 7.4:** Experimental and optimized crystal data of Form I and Form II crystals of **11** obtained during lattice energy calculation.

	Parameters	Experimental	Optimized
Form I (C2/c)	a / Å	57.945(13)	58.759
	b / Å	6.0511(13)	6.3154
	c / Å	15.465(3)	15.885
	$\alpha$ /°	90	90
	$\beta$ /°	103.469(4)	106.858
	$\gamma$ /°	90	90
	V /Å <sup>3</sup>	5273(2)	5641.3
	Density /g cm <sup>-3</sup>	1.8621	1.7430
Form II (P-1)	a / Å	10.002(2)	9.888
	b / Å	12.126(2)	12.384
	c / Å	13.146(3)	13.036
	$\alpha$ /°	70.536(3)	70.777
	$\beta$ /°	80.100(3)	78.397
	$\gamma$ /°	68.503(3)	67.067
	V /Å <sup>3</sup>	1396.5(5)	1383.3
	Density /g cm <sup>-3</sup>	1.7579	1.7746

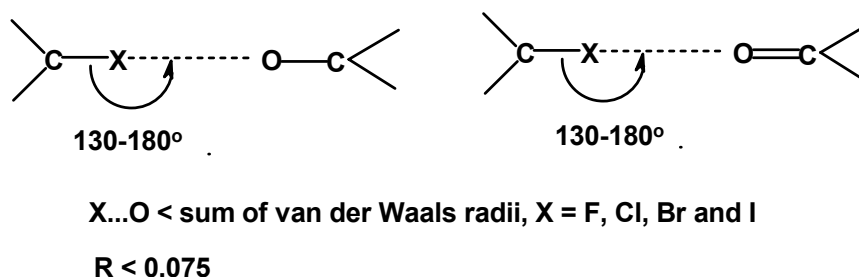
The experimental results indicate that the volume associated with a single molecule of Form I crystals of **11** is  $\sim 659 \text{ \AA}^3$  (unit cell volume / Z), whereas it is about  $40 \text{ \AA}^3$  higher in Form II crystals of **11** ( $\sim 698 \text{ \AA}^3$ ). This is also translated in their calculated densities obtained from the experiment; the crystals density of Form I is  $1.8621 \text{ g cm}^{-3}$  whereas that of Form II is  $1.7579 \text{ g cm}^{-3}$ . It is interesting that the lattice energy minimization of Form I crystals of **11** gave higher unit cell volume and unit cell parameters (**Table 7.4**) compared to the parameters obtained from the experiment for Form I crystals of **11**. These optimized parameters have almost the same volume

associated per molecule ( $\sim 700 \text{ \AA}^3$ ) and crystal density ( $1.7430 \text{ g cm}^{-3}$ ) as in Form II crystals of **11** obtained from the experiment. The unit cell parameters obtained in the lattice energy minimization procedure for Form II crystals of **11** do not show such deviation from the experimentally observed values (**Table 7.4**). Therefore, it is quite tempting to hypothesize that heating the crystals of Form I of **11** can bring them the phase obtained by lattice energy minimization before the molecular movement takes place to convert them into Form II.

### 7.3.7 CSD Survey on Different Types of Halogen Bonding

CSD<sup>150</sup> search was carried out on different types of halogen bonding. The constraints applied were  $R < 0.075$ , distances  $\leq$  sum of van der Waals radii and angles in the range  $130\text{-}180^\circ$  (**Scheme 7.1**). The CSD search included halogen atoms X (X=F, Cl, Br, I) and differently hybridized oxygen atoms (carbonyl and ether).

**Scheme 7.1**



Combined as well as separate searches were performed for organic and organometallic compounds. Combined search resulted in 1045 hits for the halogen bonding between X atom and carbonyl oxygen atom and 411 between X atom and ether



oxygen atom. Separate CSD search gave 893 hits for the organic compounds and 152 hits for the organometallic compounds for halogen bonding involving carbonyl oxygen. For halogen bonding involving ether oxygen, 344 hits for organic compounds and 67 hits for organometallic compounds was obtained. In both types of halogen bonding, the number of organic compounds is significantly more than that of number of organometallic ones. The scatter plot revealed better directionality in halogen bonds involving C=O oxygens (**Figure 7.13B**) compared to C- O oxygens (**Figure 7.13A**). The search clearly shows the preference of halogen bonding involving O=C (carbonyl oxygen) over that of O-C (ether oxygen). The scatter plots for organometallic and organic compounds are shown differently for C-X $\cdots$ O(=C) and C-X $\cdots$ O(-C) (X = F, Cl, Br, I) in **Figures 7.14** and **7.15** respectively. Distribution of hits found in C-X $\cdots$ O=C and C-X $\cdots$ O-C for each halogen atoms are listed in **Table 7.5**.

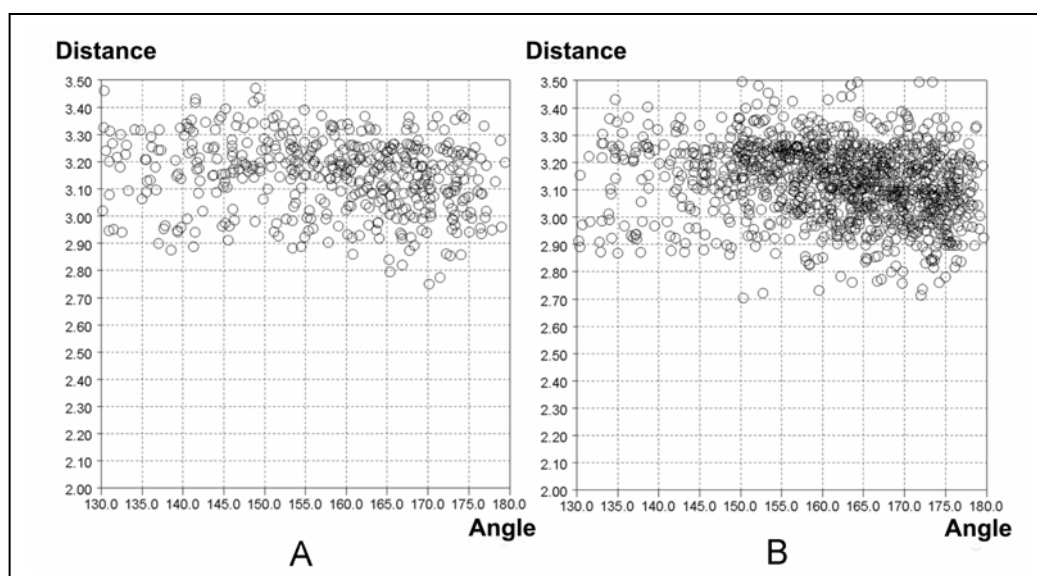


**Figure 7.13.** Scatter plots of distance X $\cdots$ O (Å) vs. angle C-X $\cdots$ O(°) for A) C-X $\cdots$ O-C and B) C-X $\cdots$ O=C.

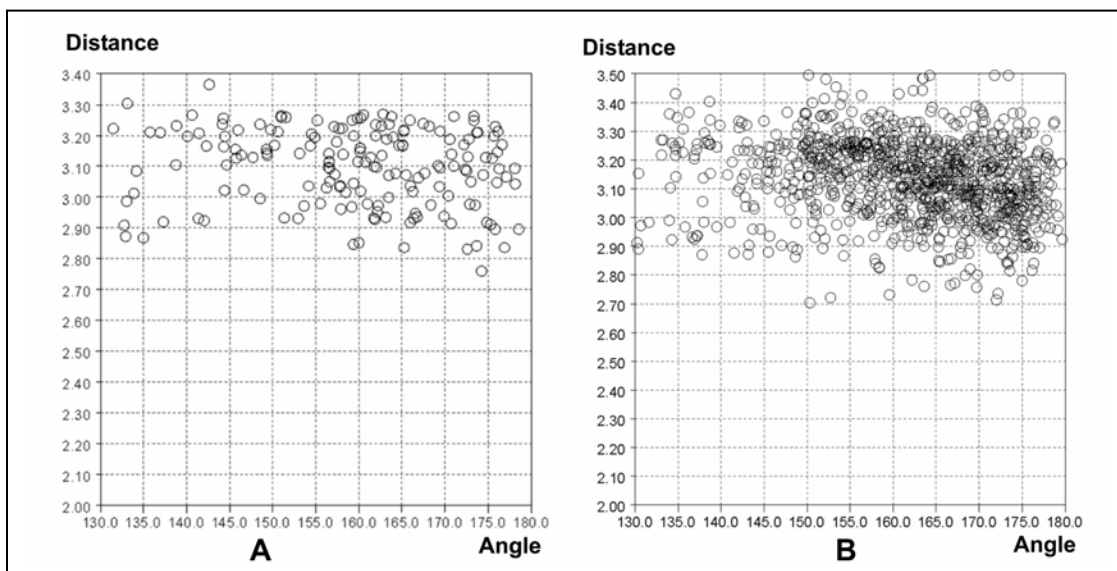


**Figure 7.14.** Scatter plots of distance  $X\cdots O$  (Å) vs. angle  $C-X\cdots O$  (°) for A) organometallic and B) organic compounds for  $C-X\cdots O=C$ .

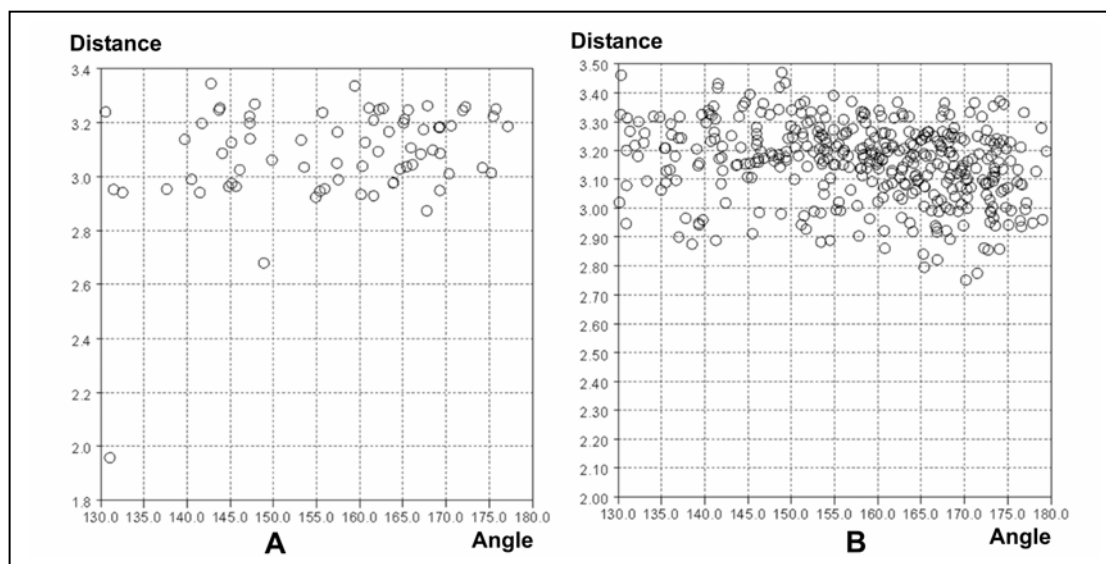


**Figure 7.15.** Scatter plots of distance  $X\cdots O$  (Å) vs. angle  $C-X\cdots O$  (°) for A) organometallic and B) organic compounds for  $C-X\cdots O-C$ .

**Table 7.5:** Distribution of hits in CSD for various categories included in **Figures 7.13 - 7.15.**

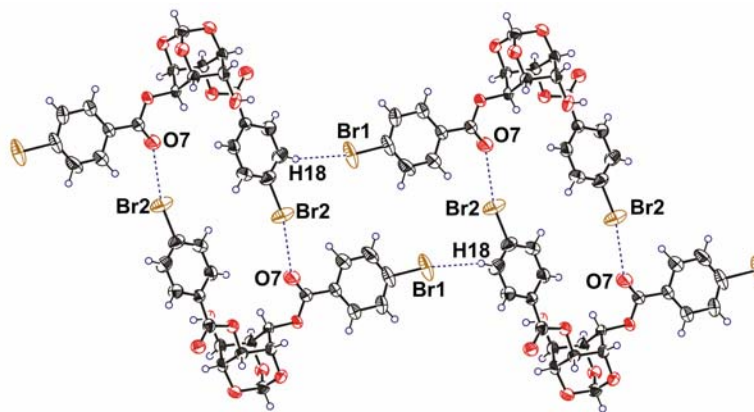
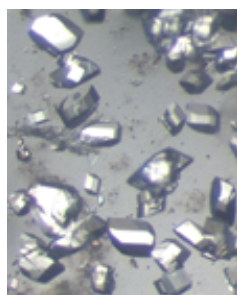
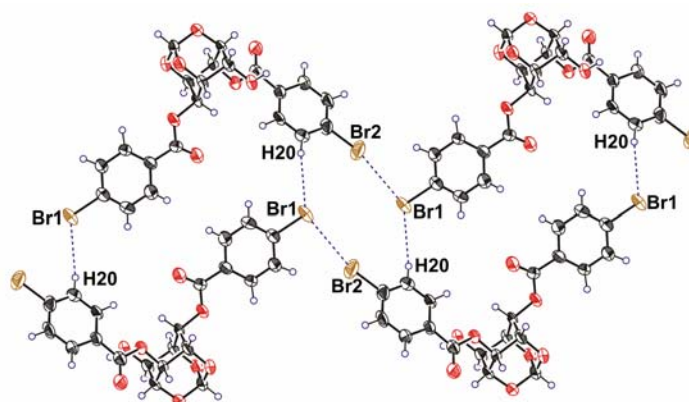
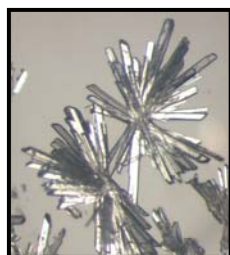
		Organic compounds	Organometallic compounds
For Carbonyl Oxygen Atom (C-X...O=C, X = F, Cl, Br, I)	X = F	42	14
	X = Cl	429	115
	X = Br	312	17
	X = I	114	6
For Ether Oxygen Atom (C-X...O-C)	X = F	22	14
	X = Cl	174	44
	X = Br	111	7
	X = I	38	2

#### 7.4 Conclusions

Formation of stable large octahedral crystals (Form II) of **11** with greater yield of this form compared to thin long needles (Form I) suggests clearly the preference of molecular association in nucleation via C-Br...O=C contacts over C-Br...O-C contacts. The higher preference (and occurrence) for halogen bonding involving O=C over O-C was overwhelmingly evident in a survey conducted of CSD. Thermal conversion of crystals of **11** containing C-Br...O-C bridges (Form I) to those containing C-Br...O=C bridges (Form II) further endorses this view. Temperature induced crystal-to-crystal phase transitions<sup>142b</sup> are of interest as they provide uncommon cases in which the crystal lattice can accommodate the molecular reorganization within the same lattice.<sup>151</sup> Theoretical crystal lattice energies computed showed higher stability for Form II crystals compared to Form I crystals, which transform to Form II upon heating.

# Chapter 8

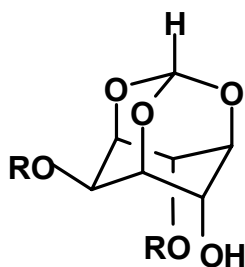
## Polymorphic and Pseudopolymorphic Behaviour of Racemic 2,6-di-*O*- (*p*-halobenzoyl)-*myo*-inositol 1,3,5-orthoformates: Different Halogen Bonding Contacts in Molecular Associations and Crystal-to-Crystal Phase Transition



# Chapter 8

## 8.1 Introduction

Continuing with the investigation of the possibility of halogen bonding interactions as well as (pseudo) polymorphism in *myo*-inositol derivatives, racemic 2,6-di-*O*-(*p*-halobenzoyl)-1,3,5-orthoformates (both bromo (**13**) and chloro (**14**) derivatives) were prepared (**Figure 8.1**). This chapter discusses the results on crystallization and crystal structures of these two derivatives of *myo*-inositol containing halogen atoms.



**13.** R = *p*-Br-C<sub>6</sub>H<sub>4</sub>-CO

**14.** R = *p*-Cl-C<sub>6</sub>H<sub>4</sub>-CO

**Figure 8.1.** Structures of **13** and **14**.

Since the two derivatives **13** and **14** have one hydroxyl group at C4 position, it is interesting to see the role of this free hydroxyl group in the molecular packing arrangement in the presence of *p*-halobenzoyl group. It would be appropriate to mention here that the non-halo analog of **13** and **14** (i.e. racemic 2,6-di-*O*-benzoyl-1,3,5-

orthoformate) in its crystals adopted the formation of helical molecular assembly across the crystallographic two fold axis via strong O-H...O hydrogen bond.<sup>1</sup> Thus it is interesting to see whether the presence of halogens at the para position of the 2,6 benzoyl groups in **13** and **14**, would lead to the formation of polymorphs similar to those discussed in the previous chapter or to the helical arrangement as reported earlier.<sup>1</sup>

## 8.2 Experimental Section

### 8.2.1 Synthesis:

#### Preparation of racemic 2,6-di-O-(p-bromobenzoyl)-myo-inositol-1,3,5-orthoformate (**13**)

Compound **13** was obtained from the purification of compound **11** by column chromatography as by product (discussed in previous chapter, which showed two spots on TLC, lower spot was compound **13**, 0.080 g, 20%).

#### Data for **13**:

**mp** 240-242 °C; **IR** (CHCl<sub>3</sub>)  $\nu$  = 1731 and 3345 cm<sup>-1</sup>; **<sup>1</sup>H NMR** (CDCl<sub>3</sub>, 200 MHz):  $\delta$  2.25-2.45 (br s 1H), 4.46-4.75 (m, 4H), 5.64 (s, 2H), 5.82 (m, 1H), 7.58-7.64 (m, 4H), 7.89-8.03 (m, 4H), **Elemental analysis** calcd for C<sub>21</sub>H<sub>16</sub>Br<sub>2</sub>O<sub>8</sub>; C 45.352%, H 2.90%; found C 46.83%, H 2.91%.

### Preparation of racemic 2,6-di-O-(p-chlorobenzoyl)-myo-inositol-1,3,5-orthoformate (14)

A solution of *myo*-inositol 1,3,5-orthoformate (**2**, 0.380 g, 2 mmol) in dry pyridine (5 mL) was cooled (ice bath) and a solution of 4-chlorobenzoyl chloride (0.796 g, 4.548 mmol) in pyridine (5 mL) was added drop wise. After the completion of the addition, the ice bath was removed. The reaction mixture was stirred at room temperature for about 24 hours. Completion of the reaction was confirmed by checking TLC of the reaction mixture. About 2 mL water was then added into the reaction mixture and stirring continued for about half an hours. Solvent was evaporated under reduced pressure to obtain a solid. It was dissolved in ethyl acetate, washed with sodium bicarbonate solution and worked up as usual. The required product was isolated by column chromatography (yield 0.562 g, 60%).

#### Data for 14:

**mp** 204-206 °C; **IR** (CHCl<sub>3</sub>)  $\nu$  = 1728 and 3394 cm<sup>-1</sup>. **<sup>1</sup>H NMR** (CDCl<sub>3</sub>, 500 MHz):  $\delta$  2.29-2.50 (br s, 1H), 4.45-4.80 (m, 4H), 5.60-5.70 (s, 2H), 5.85-5.85 (m, 1H), 7.42-7.55 (m, 4H), 7.95-8.13 (m, 4H), **Elemental analysis** calcd for C<sub>21</sub>H<sub>16</sub>Cl<sub>2</sub>O<sub>8</sub>; C 59.93%, H 3.42%; found C 60.41%, H 3.49%.

### 8.2.2 Crystallization of 13 and 14

Crystallization of compounds **13** and **14** was attempted from common organic solvents (Tables 8.1 and 8.2) by slow evaporation (1) and vapour diffusion (2) method (light petroleum ether was used for diffusing). Crystallization of **13** and **14** from

methanol gave thin needle type crystals, Form I (**Figure 8.2A** and **8.2D**) whereas crystallization from ethyl acetate gave small rectangular crystals Form II (**Figure 8.2B** and **8.2E**). Both **13** and **14** produced concomitant polymorphs, small needles (Form I) and blocks (Form II), when crystallized from ethyl acetate-petroleum ether mixture (v/v: 4/1). The needles appeared within 4 to 5 hours whereas small rectangular blocks started to appear after one two days. The amount of needles obtained was very less compared to the block crystals of **13** and **14**, indicating the preference for the crystallization of rectangular crystals. The fact that Form I crystals could be obtained by rapid crystallization showed that these were kinetic crystals while Form II crystals were thermodynamic.<sup>131a</sup> Crystallization of **13** and **14** from chloroform (**Figure 8.2C**), acetone yielded inclusion crystals. Chloroform inclusion crystals of **13** and **14** were thin plates (**Figure 8.2C**) but crystals of **14** obtained from acetone were robust square plates (**Figure 8.2F**). Acetone inclusion crystals of **13** were similar in shape to those of chloroform inclusion crystals of **13**. Crystallization of **14** from other common solvents also produced inclusion crystals, which were stable in the open atmosphere but crystals of **14** obtained from benzene were highly unstable.

**Table 8.1:** Crystallization data of **13** from various solvents.

Entry	Solvent used	Method of crystallization*	Results
1	Methanol	1	Thin needles (Form I)
2	Ethyl acetate	1	Rectangular crystals (Form II)
3	Ethyl acetate-petroleum ether	1	Both Form I and Form II crystals appeared concomitantly
4	Chloroform	2	Plates, $13 \cdot \text{CHCl}_3$
5	Acetone	2	Plates, $13 \cdot \text{CH}_3\text{COCH}_3$

\*1 = slow evaporation method, 2 = vapour diffusion method



**Table 8.2:** Crystallization data of **14** from various solvents.

Entry No	Solvent Used	Method of Crystallization*	Results
1	Methanol	1	Thin needles (Form I)
2	Ethyl acetate	1	Rectangular crystals (Form II)
3	Ethyl acetate/ light petroleum	2	Both Form I and Form II crystals appeared concomitantly
4	Chloroform	1	Inclusion crystals (plates), $14 \cdot \text{CHCl}_3$
5	Acetone	2	Inclusion crystals (plates), $14 \cdot \text{CH}_3\text{COCH}_3$
6	Dichloromethane	2	Inclusion crystals (plates), $14 \cdot \text{CH}_2\text{Cl}_2$
7	Acetonitrile	1	Inclusion crystals (plates), $14 \cdot \text{CH}_3\text{CN}$
8	THF	1	Inclusion crystals (plates), $14 \cdot \text{C}_4\text{H}_8\text{O}$
9	Nitromethane	1	Inclusion crystals (plates), $14 \cdot \text{CH}_3\text{NO}_2$
10	Dioxane	1	Inclusion crystals (plates), $14 \cdot \text{C}_4\text{H}_8\text{O}_2$
11	Benzene	1	Inclusion crystals (plates), $14 \cdot \text{C}_6\text{H}_6$
12	$\text{CCl}_4$	1	Inclusion crystals (plates), $14 \cdot \text{CCl}_4$
13	Dichloroethane	1	Inclusion crystals (plates), $14 \cdot \text{ClC}_2\text{H}_4\text{Cl}_2$
14	<i>p</i> -xylene	1	Inclusion crystals (needles), $14 \cdot \text{C}_6\text{H}_4(\text{CHO})_2^*$

\* = slow evaporation method, 2 = vapour diffusion method and \*\* inclusion crystals obtained from *p*-xylene contained 1,4-terephthalaldehyde in the crystal lattice.

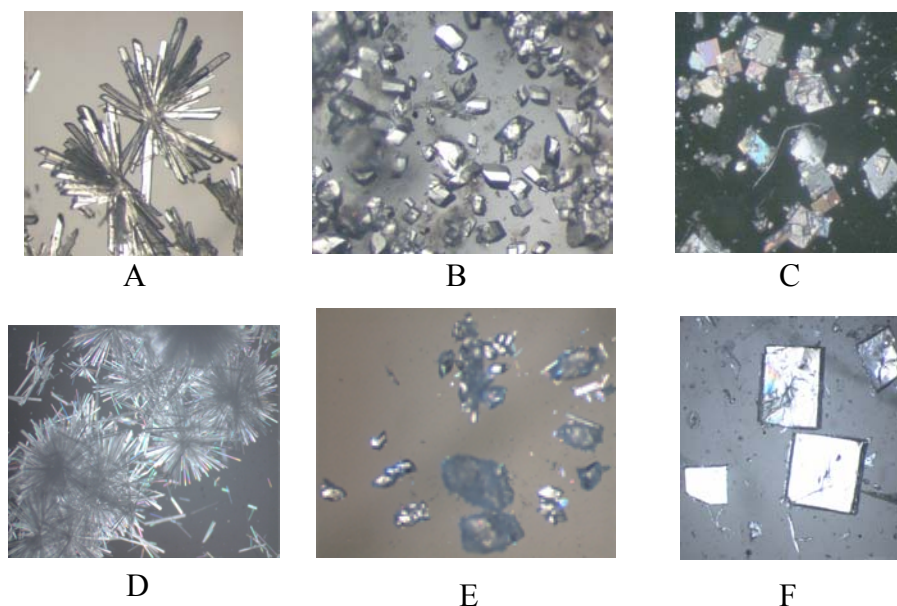


**Figure 8.2.** Photomicrographs of crystals of **13** and **14**, A) Form I crystals of **13**, B) Form II crystals of **13**, C) Inclusion crystals of **13** from chloroform, D) Form I crystals of **14**, E) Form II crystals of **14** and F) Inclusion crystals of **14** from acetone.

### 8.2.3 DSC Studies of **13** and **14**

The thermal behaviour of polymorphs of **13** and **14** was investigated by measuring enthalpy change with a Differential Scanning Calorimeter. The DSC of Form I crystals of **13** (**Figure 8.3A**) showed two endotherms, the first one at 224 °C suggesting possible structural phase transition and the second one at 241 °C corresponding to the melting of the crystal. Interestingly, a repeat of the DSC for the Form I crystals of **13** (cooled after heating up to the transition temperature 224 °C) contained only the melting endotherm at 241 °C. A comparison of the DSC profiles of Form I and Form II crystals of **13** suggests an irreversible phase transition of Form I crystals to Form II crystals of **13** (**Figure 8.3B**).

The DSC of Form I crystals of **14**, showed only one endotherm at 201°C, corresponding to the melting of the crystals (**Figure 8.3C**). Similarly, Form II crystals of **14** also showed a single endotherm at 212 °C, which is corresponding to the melting of the crystals (**Figure 8.3D**). It is noteworthy that the Form I and Form II crystals of **14** showed a difference of 11 °C in melting whereas Form I and Form II crystals of **13** have almost the same melting point.

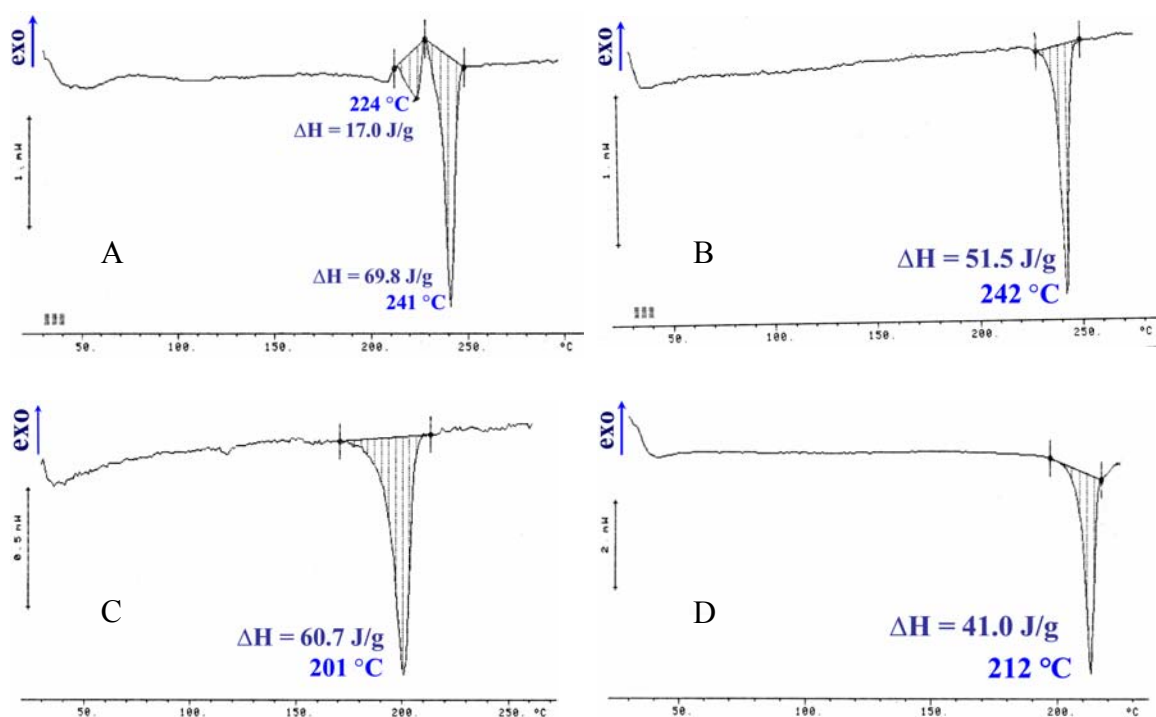


**Figure 8.3.** DSC profiles of, A) Form I crystals of **13**, B) Form II crystals of **13**, C) Form I crystals of **14** and D) Form II crystals of **14**.

DSC study of chloroform inclusion crystals of **13** showed two endotherms; one at 112 °C and the other at 242 °C (**Figure 8.4A**). The DSC of the acetone inclusion crystals of **13** also showed two endotherms, one at 128 °C and the other at 236 °C (**Figure 8.4B**). In both inclusion crystals the first endotherm, which was observed much before melting endotherm, could be because of the escape of solvent molecule from the crystal lattice and the second endotherm due to the melting of the solvent free crystals. This is suggested by a comparison of DSC plots of Form II crystals (**Figure 8.3B**) and pseudopolymorphs (**Figure 8.4A and B**) of **13**.

The chloroform and acetone inclusion crystals of **14** also showed similar behaviour as observed for **13** above when subjected to DSC analysis. Chloroform

inclusion crystals of **14** showed two endotherms, one at 121 °C and the other at 217 °C (**Figure 8.4C**), whereas for acetone inclusion crystals of **14** the first endotherm was at 129 °C and the second endotherm was at 211 °C (**Figure 8.4D**). In the DSC profile of **14**·CH<sub>3</sub>COCH<sub>3</sub>, the first endotherm was very broad (ΔH = 89.1 J/g), this could be due to the robust and big square plate like crystals as compared to other inclusion crystals. The first peak in both solvates of **14** could be because of the escape of solvent molecule from the crystal lattice and the second endotherm corresponding to the melting of the crystals. Since the endotherms for acetone inclusion crystals of **14** are quite broad, it is likely that phase transition occur before melting of crystals. A comparison of **Figures 8.3C**, **8.3D** and **8.4D** supports this view.

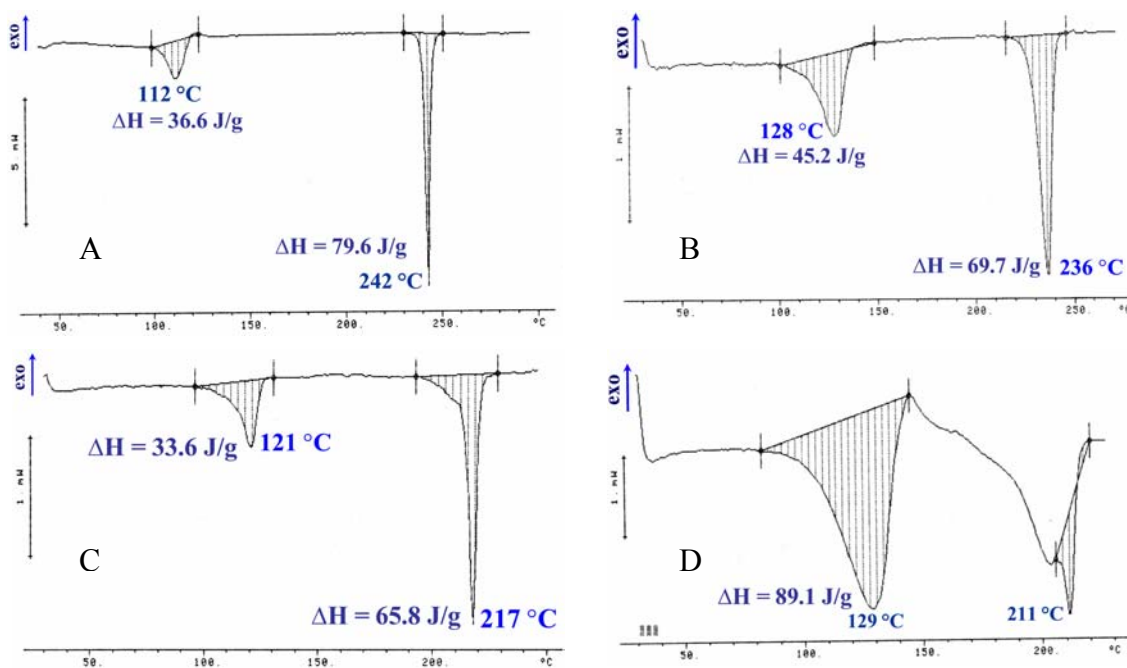


**Figure 8.4.** DSC profiles of A) **13**·CHCl<sub>3</sub>, B) **13**·CH<sub>3</sub>COCH<sub>3</sub>, C) **14**·CHCl<sub>3</sub> and D) **14**·CH<sub>3</sub>COCH<sub>3</sub>.

### 8.2.4 Thermal Response on Hot Stage Microscopy

Form I (needles) crystals of **13** showed possible structural phase transition just before melting, as suggested from the DSC study. Needles of Form I crystals when heated on the hot stage polarizing microscope appeared to lose their transparency at one end and the other end became clearer (**Figure 8.5**). However, major changes were not observed near the transition temperature of 224 °C.

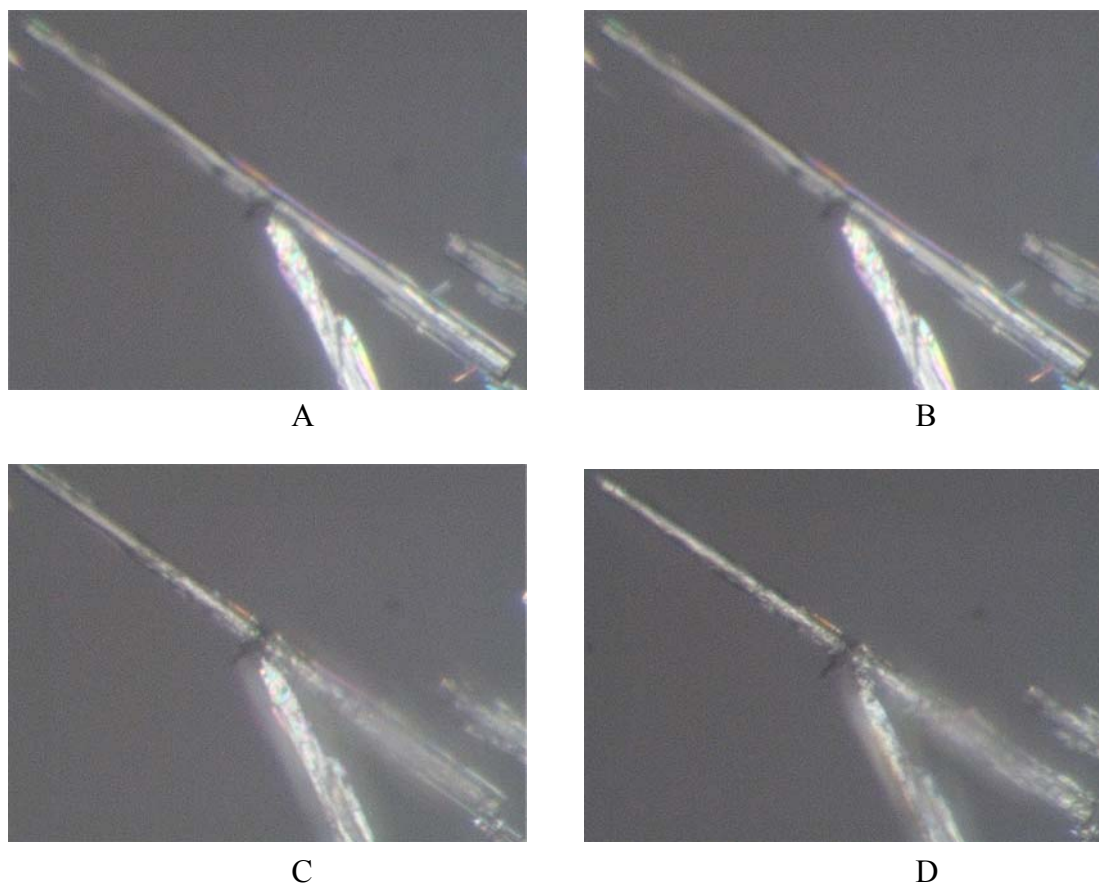


**Figure 8.5.** Photomicrographs of Form I crystals of **13** during hot stage microscopy, A) at room temperature, B) at 200 °C, C) at 210 °C and D) at 224 °C.

Chloroform inclusion crystals of **13** when heated, lost their crystallinity around 110 °C and became completely opaque at 112 °C (**Figure 8.6**). The loss of crystalline character at ~110 °C could be due to the escape of the chloroform molecules resulting in the collapse of the crystal lattice.

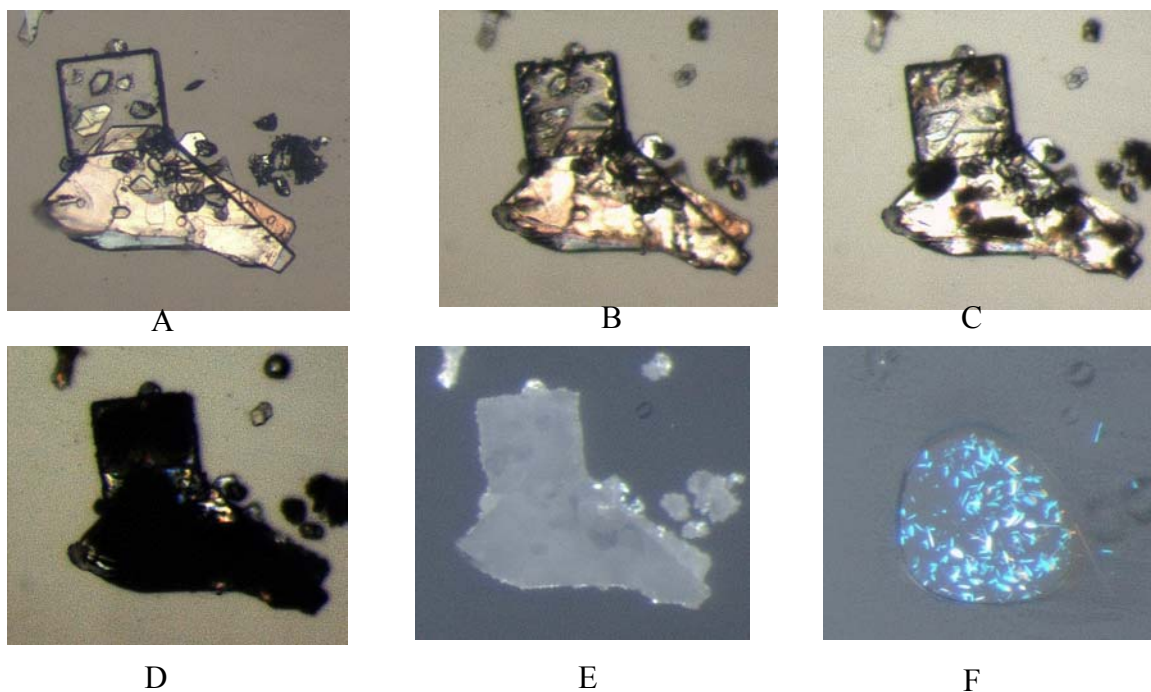


**Figure 8.6.** Photomicrographs of **13**·CHCl<sub>3</sub>, during hot stage microscopy at, A) room temperature, B) 107 °C, C) 109 °C, D) 111 °C, E) 112 °C and F) 243 °C.

### 8.2.5 X-ray Data Collection, Structure Solution and Refinement

Single crystal X-ray studies were carried out on both the polymorphs (Form I and Form II) of **13** and **14** at room temperature. Structure analysis revealed that both forms of **13** and **14** belong to triclinic system with centrosymmetric space group  $P\bar{1}$ . Form I crystals of **13** and **14** and Form II crystals of **13** and **14** are isomorphous (**Table 8.3**).

The unit cell parameters of the Form I crystal (needles) of **13** mounted on the diffractometer, after heating the needles at the transition temperature, revealed them to be Form II crystals of **13**. This suggested that the Form I crystals are transformed to Form II crystals upon heating. Reproducibility of this irreversible crystal-to-crystal transitions<sup>35g</sup> confirmed by repeating this process with several Form I crystals of **13**.

Crystal structure of chloroform and acetone inclusion crystals of **13** and chloroform, acetone, THF inclusion crystals of **14** were determined at room temperature. The X-ray data of other inclusion crystals of **14** obtained from dichloromethane ( $\mathbf{14}\cdot\mathbf{CH}_2\mathbf{Cl}_2$ ), dioxane ( $\mathbf{14}\cdot\mathbf{C}_4\mathbf{H}_8\mathbf{O}_2$ ), acetonitrile ( $\mathbf{14}\cdot\mathbf{CH}_3\mathbf{CN}$ ), benzene ( $\mathbf{14}\cdot\mathbf{C}_6\mathbf{H}_6$ ), *p*-xylene (latter found to contained terephthaldehyde,  $\mathbf{14}\cdot\mathbf{C}_6\mathbf{H}_4(\mathbf{CHO})_2$ ), dichloroethane ( $\mathbf{14}\cdot\mathbf{ClCH}_2\mathbf{CH}_2\mathbf{Cl}$ ), carbon tetra chloride ( $\mathbf{14}\cdot\mathbf{CCl}_4$ ,  $\mathbf{14}\cdot\mathbf{CH}_3\mathbf{NO}_2$ ) were collected at 133 K. For inclusion crystals obtained from benzene ( $\mathbf{14}\cdot\mathbf{C}_6\mathbf{H}_6$ ) paraffin oil coat was applied before data collection, as they were highly unstable in the open atmosphere. Chloroform and acetone inclusion crystals of **13** belong to monoclinic  $P2_1/n$  system (**Table 8.4**), but inclusion crystals of **14** revealed different modification (**Tables 8.3** and **8.4**). Chloroform, acetone, dichloromethane, dioxane,  $\text{CCl}_4$  and nitromethane inclusion crystals of **14** are monoclinic  $P2_1/n$ ; acetonitrile and dichloroethane are monoclinic  $P2_1/c$  whereas the inclusion crystals obtained from benzene and *p*-xylene are monoclinic  $C2/c$ . Solvates

belonging to monoclinic  $P2_1/n$  system of **13** and **14** are isomorphous and same is true with other solvates belonging to  $P2_1/c$  and  $C2/c$  systems. The a-axis length in all the pseudopolymorphs belonging to space groups  $P2_1/n$  and  $P2_1/c$  is almost identical (12-13 Å), whereas in the solvates having space group  $C2/c$ , the a-axis length increased by about ~18 Å. Interestingly in all the pseudopolymorphs of **13** and **14**, the b-axis length is strikingly similar except in solvates belonging to monoclinic  $P2_1/c$  and  $C2/c$  where slight reduction is observed (0.2-0.3 Å and 0.5-0.6 Å respectively). Similarly the c-axis length in all the inclusion crystals belonging to monoclinic  $P2_1/n$  system is almost the same (~18 Å), whereas in  $P2_1/c$  and  $C2/c$  inclusion crystals the c-axis length is elongated by about 2 Å. The relevant crystallographic data for the pseudopolymorphs of the diesters **13** and **14** are recorded in **Table 8.4**. In all the solvates of **13** and **14** the crystal lattice contained one molecule of host per one molecule of the guest except in **14**·**C<sub>6</sub>H<sub>6</sub>** where two molecules of benzene (with 0.75 and 0.50 occupancy) were present per one molecule of the guest. Thus the host guest ratio is 1:1.25.



**Table 8.3:** Crystallographic Data of solvent free polymorphs of **13** and **14**.

	<b>13 (Form I)</b>	<b>13(Form II)</b>	<b>14 (Form I)</b>	<b>14 (Form II)</b>
Chemical formula	C <sub>21</sub> H <sub>16</sub> Br <sub>2</sub> O <sub>8</sub>	C <sub>21</sub> H <sub>16</sub> Br <sub>2</sub> O <sub>8</sub>	C <sub>21</sub> H <sub>16</sub> Cl <sub>2</sub> O <sub>8</sub>	C <sub>21</sub> H <sub>16</sub> Cl <sub>2</sub> O <sub>8</sub>
M <sub>r</sub>	556.16	556.16	467.24	467.24
Temperature/K	297(2)	297(2)	297(2)	297(2)
Morphology	Thin needle	Block	Thin needle	Block
Crystal size	0.50×0.06×0.02	0.20×0.20×0.14	0.61×0.08×0.05	0.32×0.27×0.16
Crystal system	Triclinic	Triclinic	Triclinic	Triclinic
Space group	<i>P</i> -1	<i>P</i> -1	<i>P</i> -1	<i>P</i> -1
<i>a</i> (Å)	6.825(3)	6.8481(14)	6.815(3)	6.794(5)
<i>b</i> (Å)	8.330(4)	11.662(2)	8.325(3)	11.545(9)
<i>c</i> (Å)	18.181(9)	13.675(3)	17.887(7)	13.565(10)
$\alpha$ (°)	80.744(9)	107.123(4)	80.140(7)	106.843(11)
$\beta$ (°)	88.609(9)	99.175(4)	87.493(8)	98.733(12)
$\gamma$ (°)	83.038(10)	90.909(3)	83.024(8)	91.059(12)
<i>V</i> (Å <sup>3</sup> )	1012.5(9)	1028.1(4)	992.0(7)	1004.4(13)
<i>Z</i> , <i>D</i> <sub>calc</sub> (g cm <sup>-3</sup> )	2, 1.824	2, 1.797	2, 1.564	2, 1.545
$\mu$ (mm <sup>-1</sup> ), F(000)	4.052, 552	3.990, 552	0.377, 480	0.372, 480
Ab.correction	Multi-scan	Multi-scan	Multi-scan	Multi-scan
<i>T</i> <sub>min</sub>	0.239	0.502	0.804	0.891
<i>T</i> <sub>max</sub>	0.909	0.595	0.983	0.943
<i>h</i> , <i>k</i> , <i>l</i> (min, max)	(-8,8),(-9,9), (-21,21)	(-8,8),(-12,13), (-16,16)	(-8,8),(-9,9), (-21,21)	(-8,8),(-13,13), (-16,16)
Reflns collected	9754	7440	9248	9304
Unique reflns	3529	3580	3463	3506
Observed reflns	1982	2567	2322	3152
R <sub>int</sub>	0.0886	0.0235	0.0384	0.0241
No. of parameters	344	344	344	344
GoF	0.965	1.023	1.046	1.078
R <sub>1</sub> [ <i>I</i> > 2σ( <i>I</i> )]	0.0663	0.0405	0.0602	0.0474
wR <sub>2</sub> [ <i>I</i> > 2σ( <i>I</i> )]	0.1489	0.0860	0.1213	0.1206
R <sub>1</sub> _all data	0.1264	0.0652	0.0954	0.0520
wR <sub>2</sub> _all data	0.1757	0.0946	0.1359	0.1241
Δ ρ <sub>max</sub> , Δ ρ <sub>min</sub> (eÅ <sup>-3</sup> )	0.88, -0.74	0.60, -0.45	0.41, -0.27	0.48, -0.17

**Table 8.4:** Crystallographic data of inclusion crystals of **13** and **14**.

	<b>13·CHCl<sub>3</sub></b>	<b>13·CH<sub>3</sub>COCH<sub>3</sub></b>	<b>14·CHCl<sub>3</sub></b>	<b>14·CH<sub>3</sub>COCH<sub>3</sub></b>
Chemical formula	C <sub>21</sub> H <sub>16</sub> Br <sub>2</sub> O <sub>8</sub> · CHCl <sub>3</sub>	C <sub>21</sub> H <sub>16</sub> Br <sub>2</sub> O <sub>8</sub> · C <sub>3</sub> H <sub>6</sub> O	C <sub>21</sub> H <sub>16</sub> Cl <sub>2</sub> O <sub>8</sub> · CHCl <sub>3</sub>	C <sub>21</sub> H <sub>16</sub> Cl <sub>2</sub> O <sub>8</sub> · C <sub>3</sub> H <sub>6</sub> O
M <sub>r</sub>	675.53	614.24	586.61	525.32
Temperature/K	297(2)	297(2)	297(2)	297(2)
Morphology	Thin square plates	Thin square plates	Thin square plates	Thick square plate
Crystal size	0.28×0.26×0.02	0.31×0.16×0.04	0.22×0.19×0.04	0.34×0.18×0.05
Crystal system	Monoclinic	Monoclinic	Monoclinic	Monoclinic
Space group	<i>P</i> 2 <sub>1</sub> / <i>n</i>	<i>P</i> 2 <sub>1</sub> / <i>n</i>	<i>P</i> 2 <sub>1</sub> / <i>n</i>	<i>P</i> 2 <sub>1</sub> / <i>n</i>
<i>a</i> (Å)	13.139(6)	12.65(2)	13.142(2)	12.938(4)
<i>b</i> (Å)	10.292(4)	10.133(19)	10.2530(19)	10.180(3)
<i>c</i> (Å)	18.836(8)	18.64(2)	18.350(3)	18.564(6)
$\beta$ (°)	102.368(8)	104.19(4)	101.372(4)	102.327(5)
<i>V</i> (Å <sup>3</sup> )	2488.1(18)	2316(7)	2424.0(8)	2388.6(12)
<i>Z</i>	4	4	4	4
<i>D</i> <sub>calc</sub> (g cm <sup>-3</sup> )	1.803	1.762	1.607	1.461
$\mu$ (mm <sup>-1</sup> )	3.626	3.555	0.646	0.325
<i>F</i> (000)	1336	1232	1192	1088
Ab.correction	Multi-scan	Multi-scan	Multi-scan	Multi-scan
<i>T</i> <sub>min</sub>	0.421	0.401	0.870	0.898
<i>T</i> <sub>max</sub>	0.918	0.877	0.972	0.985
$\theta$ <sub>max</sub> (°)	25	25	25	25
<i>h</i> , <i>k</i> , <i>l</i> (min, max)	(-14,15),(-12,9), (-22,19)	(-14,15),(-12,9), (-22,21)	(-15,15),(-12,12), (-21,21)	(-15,15),(- 12,12), (-22,22)
Reflns collected	12223	12240	16884	16704
Unique reflns	4357	3950	4218	4198
Observed reflns	2805	2460	2913	3277
R <sub>int</sub>	0.0483	0.1819	0.0483	0.0646
No. of parameters	333	319	339	382
GoF	1.025	0.993	1.038	1.294
R <sub>1</sub> [ <i>I</i> > 2σ( <i>I</i> )]	0.0583	0.1125	0.0771	0.1106
wR <sub>2</sub> [ <i>I</i> > 2σ( <i>I</i> )]	0.1395	0.2614	0.1809	0.2141
R <sub>1</sub> _all data	0.0972	0.1605	0.1097	0.1412
wR <sub>2</sub> _all data	0.1577	0.2985	0.2025	0.2279
$\Delta \rho$ <sub>max</sub> , $\Delta \rho$ <sub>min</sub> (eÅ <sup>-3</sup> )	0.66, -0.56	1.17, -1.85	0.91, -0.44	0.64, -0.26

	<b>14·CH<sub>2</sub>Cl<sub>2</sub></b>	<b>14·dioxane</b>	<b>14·THF</b>	<b>14·CCl<sub>4</sub></b>	<b>14·CH<sub>3</sub>NO<sub>2</sub></b>
Chemical formula	C <sub>21</sub> H <sub>16</sub> Cl <sub>2</sub> O <sub>8</sub> ·0.05(CH <sub>2</sub> Cl <sub>2</sub> )	C <sub>21</sub> H <sub>16</sub> Cl <sub>2</sub> O <sub>8</sub> ·0.5(C <sub>4</sub> H <sub>8</sub> O <sub>2</sub> )	C <sub>21</sub> H <sub>16</sub> Cl <sub>2</sub> O <sub>8</sub> ·0.5(C <sub>4</sub> H <sub>8</sub> O)	C <sub>21</sub> H <sub>16</sub> Cl <sub>2</sub> O <sub>8</sub> ·0.5(CCl <sub>4</sub> )	C <sub>21</sub> H <sub>16</sub> Cl <sub>2</sub> O <sub>8</sub> ·0.75(CH <sub>3</sub> NO <sub>2</sub> )
M <sub>r</sub>	467.24	511.29	503.29	544.14	513.02
Temperature/K	133(2)	133(2)	297(2)	133(2)	133(2)
Morphology	Thick Plate	Square plate	Square plate	Square plate	Square plate
Crystal size	0.33×0.33×0.13	0.16×0.15×0.06	0.64×0.22×0.14	0.35×0.25×0.07	0.44×0.39×0.1
Crystal system	Monoclinic	Monoclinic	Monoclinic	Monoclinic	Monoclinic
Space group	<i>P</i> 2 <sub>1</sub> / <i>n</i>	<i>P</i> 2 <sub>1</sub> / <i>n</i>	<i>P</i> 2 <sub>1</sub> / <i>n</i>	<i>P</i> 2 <sub>1</sub> / <i>n</i>	<i>P</i> 2 <sub>1</sub> / <i>n</i>
<i>a</i> (Å)	12.962(2)	13.086(8)	13.1528(15)	12.822(3)	12.754(10)
<i>b</i> (Å)	10.1406(17)	10.181(6)	10.1844(12)	10.180(2)	10.055(8)
<i>c</i> (Å)	18.391(3)	18.718(9)	18.582(2)	18.405(4)	18.289(14)
$\beta$ (°)	102.627(3)	103.795(16)	101.853(2)	102.195(4)	103.031(13)
<i>V</i> (Å <sup>3</sup> )	2358.8(7)	2422(2)	2436.0(5)	2348.2(9)	2285(3)
<i>Z</i>	4	4	4	4	4
<i>D</i> <sub>calc</sub> (g cm <sup>-3</sup> )	1.316	1.402	1.372	1.539	1.491
$\mu$ (mm <sup>-1</sup> )	0.317	0.318	0.313	0.550	0.340
<i>F</i> (000)	960	1056	1040	1108	1056
Ab. Correction	Multi-scan	Multi-scan	Multi-scan	Multi-scan	Multi-scan
<i>T</i> <sub>min</sub>	0.902	0.951	0.825	0.831	0.864
<i>T</i> <sub>max</sub>	0.960	0.980	0.957	0.964	0.961
$\theta$ <sub>max</sub> (°)	25	25	25	25	25
<i>h</i> , <i>k</i> , <i>l</i> (min, max)	(-15,15), (-12,8), (-21,21)	(-15,15), (-12,12), (-22,22)	(-15,15), (-12,12), (-22,22)	(-15,15), (-12,12), (-21,21)	(-14,15), (-11,11), (-21,16)
Reflns collected	11455	16939	17106	16402	10605
Unique reflns	4141	4229	4270	4120	3947
Observed reflns	2915	2217	3636	3366	3170
R <sub>int</sub>	0.0284	0.1070	0.0183	0.0600	0.0709
No. of parameters	364	335	350	338	381
GoF	1.035	1.050	1.062	1.070	1.098
R <sub>1</sub> [ <i>I</i> > 2σ( <i>I</i> )]	0.0602	0.0939	0.0735	0.0866	0.0702
WR <sub>2</sub> [ <i>I</i> > 2σ( <i>I</i> )]	0.1672	0.2122	0.2176	0.2314	0.1710
R <sub>1</sub> _all data	0.0840	0.1749	0.0802	0.1011	0.0859
WR <sub>2</sub> _all data	0.1885	0.2278	0.2274	0.2428	0.1820
$\Delta \rho$ <sub>max</sub> , $\Delta \rho$ <sub>min</sub> (e Å <sup>-3</sup> )	0.41, -0.46	0.41, -0.43	0.78, -0.71	1.18, -0.79	0.86, -0.57

	<b>14·CH<sub>3</sub>CN</b>	<b>14·C<sub>2</sub>H<sub>4</sub>Cl<sub>2</sub></b>	<b>14·C<sub>6</sub>H<sub>6</sub></b>	<b>14·C<sub>6</sub>H<sub>4</sub>(CHO)<sub>2</sub></b>
Chemical formula	C <sub>21</sub> H <sub>16</sub> Cl <sub>2</sub> O <sub>8</sub> · CH <sub>3</sub> CN	C <sub>21</sub> H <sub>16</sub> Cl <sub>2</sub> O <sub>8</sub> · 0.75(C <sub>2</sub> H <sub>4</sub> Cl <sub>2</sub> )	C <sub>21</sub> H <sub>16</sub> Cl <sub>2</sub> O <sub>8</sub> · 1.25(C <sub>6</sub> H <sub>6</sub> )	C <sub>21</sub> H <sub>16</sub> Cl <sub>2</sub> O <sub>8</sub> · 0.5(C <sub>6</sub> H <sub>4</sub> (CHO) <sub>2</sub> )
M <sub>r</sub>	508.29	538.43	532.56	533.29
Temperature/K	133(2)	133(2)	133(2)	133(2)
Morphology	Square plate	Plate	Plate	Needle
Crystal size	0.72×0.68×0.19	0.18×0.16×0.12	0.51×0.23×0.12	0.45×0.16×0.11
Crystal system	Monoclinic	Monoclinic	Monoclinic	Monoclinic
Space group	<i>P</i> 2 <sub>1</sub> / <i>c</i>	<i>P</i> 2 <sub>1</sub> / <i>c</i>	<i>C</i> 2/ <i>c</i>	<i>C</i> 2/ <i>c</i>
<i>a</i> (Å)	12.074(10)	12.076(6)	32.22(3)	30.181(12)
<i>b</i> (Å)	9.861(8)	9.906(5)	9.584(8)	9.568(4)
<i>c</i> (Å)	20.003(16)	20.239(10)	21.386(19)	20.472(8)
$\beta$ (°)	94.894(13))	92.339(8)	129.72(3)	125.584(5)
<i>V</i> (Å <sup>3</sup> )	2373(3)	2419(2)	5080(8)	4808(3)
<i>Z</i>	4	4	8	8
<i>D</i> <sub>calc</sub> (g cm <sup>-3</sup> )	1.423	1.478	1.393	1.474
$\mu$ (mm <sup>-1</sup> )	0.322	0.480	0.304	0.324
<i>F</i> (000)	1048	1098	2190	2192
Ab. Correction	Multi-scan	Multi-scan	Multi-scan	Multi-scan
<i>T</i> <sub>min</sub>	0.800	0.919	0.859	0.868
<i>T</i> <sub>max</sub>	0.942	0.944	0.964	0.966
$\theta$ <sub>max</sub> (°)	25	25	25	25
<i>h</i> , <i>k</i> , <i>l</i> (min, max)	(-14,14), (-11,11), (-23,23)	(-14,14), (-11,11), (-24,24)	(-36,38), (-11,11), (-25,25)	(-35,35), (-11,11), (-24,24)
Reflns collected	21364	16841	15066	15494
Unique reflns	4178	4263	4470	4229
Observed reflns	3590	3551	2805	3119
R <sub>int</sub>	0.0628	0.0635	0.1232	0.0608
No. of paramtr	372	339	350	339
GoF	1.077	1.125	1.145	1.057
R <sub>1</sub> [ <i>I</i> > 2σ( <i>I</i> )]	0.0518	0.0770	0.1158	0.0522
WR <sub>2</sub> [ <i>I</i> > 2σ( <i>I</i> )]	0.1277	0.2117	0.2567	0.1131
R <sub>1</sub> _all data	0.0597	0.0906	0.1795	0.0777
WR <sub>2</sub> _all data	0.1340	0.22264	0.2918	0.1258
$\Delta \rho$ <sub>max</sub> , $\Delta \rho$ <sub>min</sub> (e Å <sup>-3</sup> )	0.42 -0.51	1.08 -0.66	1.02, -0.58	0.47, -0.69

Chloroform molecule in **13·CHCl<sub>3</sub>** and **14·CHCl<sub>3</sub>**, showed rotational disorder over two positions. In **13·CHCl<sub>3</sub>**, the occupancies of chloroform at the two positions were 0.75 and 0.25 whereas in **14·CHCl<sub>3</sub>** the occupancies were 0.85 and 0.15. It is very interesting to note that the occupancies of the chloroform molecules at the two sites are exactly reversed in **13·CHCl<sub>3</sub>** and **14·CHCl<sub>3</sub>**. In **13·CHCl<sub>3</sub>**, the location of the major occupancy site contained less occupied chloroform molecule in **14·CHCl<sub>3</sub>**. The occupancy of dichloromethane in **14·CH<sub>2</sub>Cl<sub>2</sub>** was just a trace (0.05), dichloroethane in **14·ClCH<sub>2</sub>CH<sub>2</sub>Cl** was 0.75, nitromethane in **14·CH<sub>3</sub>NO<sub>2</sub>** was 0.75, benzene in **14·C<sub>6</sub>H<sub>6</sub>** were 0.75 and 0.5, and in all other solvate it was 0.5. Chloroform molecule in **13·CHCl<sub>3</sub>** was refined anisotropically with restrain applied on C-Cl distances using DFIX command in SHELXL, whereas in **14·CHCl<sub>3</sub>**, the major occupancy chloroform molecule refined anisotropically with restrain applied on C-Cl distances and other minor occupancy chloroform molecule refined isotropically. The solvent molecule in **13·CH<sub>3</sub>COCH<sub>3</sub>**, **14·CH<sub>3</sub>COCH<sub>3</sub>**, **14·C<sub>4</sub>H<sub>8</sub>O<sub>2</sub>**, **14·CH<sub>3</sub>CN**, **14·CH<sub>3</sub>NO<sub>2</sub>** and **14·C<sub>4</sub>H<sub>8</sub>O** had regular geometry whereas in other solvates **14·CH<sub>2</sub>Cl<sub>2</sub>**, **14·ClCH<sub>2</sub>CH<sub>2</sub>Cl**, **14·C<sub>6</sub>H<sub>6</sub>** and **14·CCl<sub>4</sub>**, the solvent molecule showed rotational disorder. In **14·CH<sub>2</sub>Cl<sub>2</sub>**, both chlorine atoms of CH<sub>2</sub>Cl<sub>2</sub> showed rotational disorder over two positions of 0.025 occupancies at each position and they commonly share the carbon atom. In **14·ClCH<sub>2</sub>CH<sub>2</sub>Cl** the dichloroethane molecule also showed disorder over two positions (occupancies 0.50 and 0.25) keeping the position of one of the chlorine atoms common (occupancy 0.75). In CCl<sub>4</sub> inclusion crystals of **14**, one of the chlorine atoms showed disorder over two positions with equal occupancies (0.25). In **14·C<sub>6</sub>H<sub>6</sub>**, two molecules of benzene are present in the crystal lattice having different occupancies (0.75 and 0.5). Both benzene

molecules occupy the crystallographic 2-fold axis (similar to the dihalomethane guest molecule in **3**, Chapter 2); the benzene molecule with occupancy 0.5 showed statistical disorder across the two-fold axis. Interestingly, structure solution of crystals obtained from *p*-xylene revealed the presence of terephthaldehyde (1,4-diformylbenzene) instead of *p*-xylene in crystals of **14**. This could be due to the presence of terephthaldehyde in *p*-xylene that we used (*p*-xylene might have got oxidized to terephthaldehyde during storage). The included terephthaldehyde molecule occupies a special position (crystallographic two-fold axis) passing through the 1,4 carbon atom of the terephthaldehyde molecule. The C=O and C-H group of aldehyde group (CHO) are statistically distributed itself over two equally occupied orientations across the two-fold axis. Thus, the O and the H atoms have only half the occupancies. Inclusion complexes of **13** and **14** can be categorized into three groups, Group I contained solvates belonging to monoclinic  $P2_1/n$ , Group II contained monoclinic  $P2_1/c$  and Group III comprises monoclinic  $C2/c$ .

### 8.3. Results and Discussion

#### 8.3.1 Structures of Polymorphs of **13** and **14**

In both polymorphs of **13** and **14** the conformation of the molecule as observed in the crystal shows that both the *p*-halobenzoyl groups at C2 and C6 positions and OH group at C4 position are not involved in any intramolecular interactions (**Figure 8.7**).

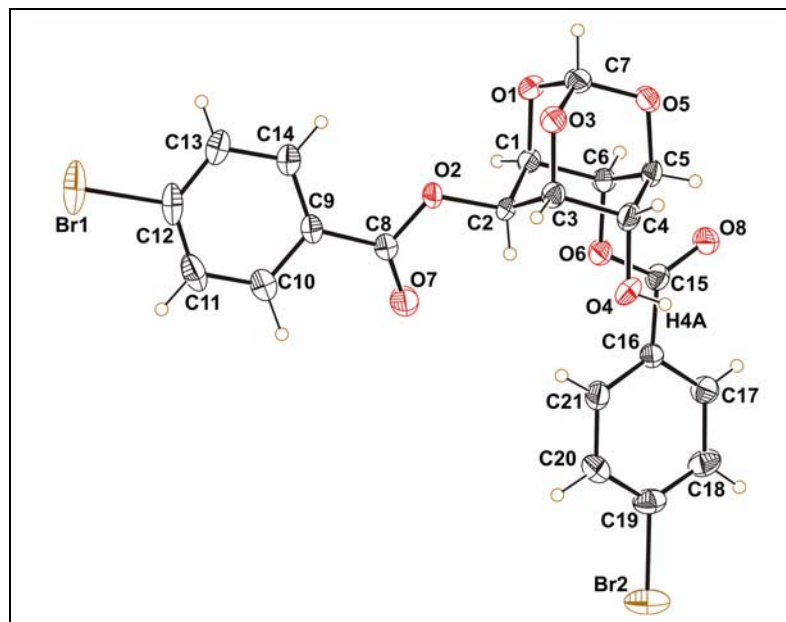


**Figure 8.7.** Representative ORTEP view of the molecule in Form II crystals of **13**.

### 8.3.1.1 One-Dimensional Isostructurality

The common significant feature in both the structures is linking of the molecules via strong intermolecular O4-H4A $\cdots$ O1 hydrogen bond along with good C14-H14 $\cdots$ O4 and C-H $\cdots$  $\pi$  (C1-H1 of *myo*-inositol ring interacts with phenyl ring of C6-O-*p*-bromobenzoyl group) contacts resulting in the formation of a one-dimensional H-bonded polymeric string (**Figure 8.8**).<sup>137f</sup> The geometry of O-H $\cdots$ O bond is almost the same in both polymorphs of **13** and **14** but variations were observed in C-H $\cdots$ O and C-H $\cdots$  $\pi$  interactions (**Table 8.5**). In Form I crystals of **13** and **14** the C14-H14 $\cdots$ O4 contact is short [H14 $\cdots$ O4 = 2.39(7) Å in **13** and 2.48(3) Å in **14** [compared to Form II crystals of **13** and **14** [H14 $\cdots$ O4 = 2.63(4) Å in **13** and 2.57(3) Å in **14**] but not so linear compared to the latter [ $\angle$ C14-H14 $\cdots$ O4 = 151(5) $^\circ$  and 147(2) $^\circ$  in Form I crystals of **13** and **14** and 166(3) $^\circ$  and 166(3) $^\circ$  in Form II crystals of **13** and **14**]. In Form I crystals of **13** and **14**, the

C-H $\cdots\pi$  contact is somewhat weaker as compared to Form II crystals. Thus, the gain in the strength of C-H $\cdots$ O contact in Form I crystals, appears to have compromised with C-H $\cdots\pi$  interaction. In short, in Form I crystals of **13**, the C-H $\cdots$ O is stronger but C-H $\cdots\pi$  is weaker and vice versa for Form II. The alignment of molecular string along a-axis in both forms explains the near equality of these axes in dimorphs of **9** and **14**(Figure 8.8).

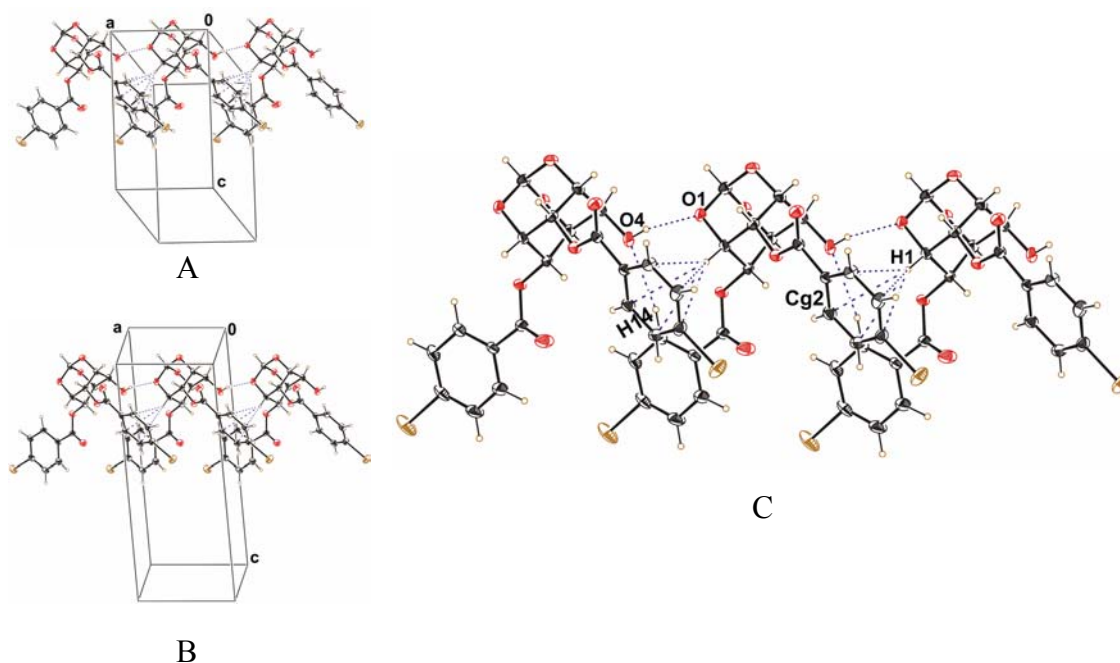


**Figure 8.8.** ORTEP view of identical molecular string linked via O4-H4A $\cdots$ O1, C14-H14 $\cdots$ O4 and C1-H1 $\cdots\pi$  (Cg2) contacts showing one-dimensional isostructurality in Form I and Form II crystals of **13** and **14** along the a-axis, A) in Form I crystals, B) in Form II crystals and C) a close view of the string in Form I crystals of **13**.



**Table 8.5:** Geometrical parameters of O-H $\cdots$ O, C-H $\cdots$ O and C-H $\cdots$  $\pi$  contacts involved in identical molecular string formation as shown in Figure 8.8.

	D-H $\cdots$ A	D-H (Å)	H $\cdots$ A (Å)	D $\cdots$ A (Å)	D-H $\cdots$ A (°)
Form I of <b>13</b>	O(4)-H(4A) $\cdots$ O(1)#1	0.82	2.07	2.867(7)	163
	C(14)-H(14) $\cdots$ O(4)#2	0.96(7)	2.39(7)	3.264(10)	151(5)
	C(1)-H(1) $\cdots$ Cg(2)#1	0.86(6)	2.67	3.506	165
Form II of <b>13</b>	O(4)-H(4A) $\cdots$ O(1)#1	0.73(4)	2.18(4)	2.894(4)	165(4)
	C(14)-H(14) $\cdots$ O(4)#2	0.94(4)	2.63(4)	3.551(5)	166(3)
	C(1)-H(1) $\cdots$ Cg(2)#1	0.96(3)	2.61	3.564	173
Form I of <b>14</b>	O(4)-H(4A) $\cdots$ O(1)#1	0.83(5)	2.03(5)	2.844(3)	170(5)
	C(14)-H(14) $\cdots$ O(4)#2	0.87(3)	2.48(3)	3.245(5)	147(2)
	C(1)-H(1) $\cdots$ Cg(2)#1	0.96(3)	2.55	3.482	165
Form II of <b>14</b>	O(4)-H(4A) $\cdots$ O(1)#1	0.82(3)	2.06(3)	2.866(3)	168(3)
	C(14)-H(14) $\cdots$ O(4)#2	0.91(3)	2.57(3)	3.466(4)	166(2)
	C(1)-H(1) $\cdots$ Cg(2)#1	0.92(2)	2.61	3.524	172

Symmetry codes: #1 x+1,y,z; #2 x-1,y,z. Cg2 - centroid of the phenyl ring C16-C21

These isostructural molecular strings (**Figure 8.8**) are weaved centrosymmetrically via four C-H $\cdots$ O interactions, C7-H7 $\cdots$ O8, C5-H5 $\cdots$ O8, C6-H6 $\cdots$ O5 and C17-H17 $\cdots$ O5 to form bilayer along the a-axis (**Figure 8.9A**, **Table 8.6**), in dimorphs of **13** and **14**. Former three C-H $\cdots$ O interactions have similar geometrical parameters in dimorphs of **13** and **14**, but, the geometry of the C17-H17 $\cdots$ O5 contact is not so good in both forms of **13** and **14**. The orthoformate oxygen O5 and carbonyl oxygen O8 are involved in bifurcated C-H $\cdots$ O contacts. The molecular association shown in **Figure 8.9A** when viewed down the a-axis revealed the formation of dimeric units (**Figure 8.9B**).

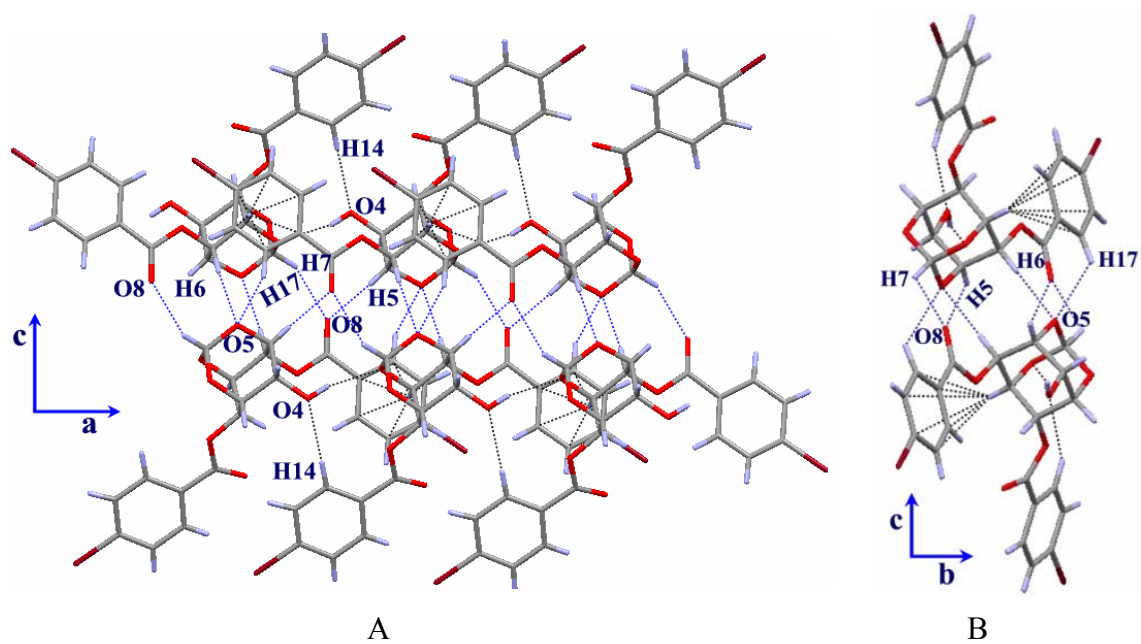


**Figure 8.9.** A) View of bilayer formed via bridging of one-dimensional string centrosymmetrically along the a-axis in Form I crystals of **13** and B) same view down the a-axis.

**Table 8.6:** Intermolecular C-H...O interactions involved in bilayer formation.

	D-H...A	D-H (Å)	H...A (Å)	D...A (Å)	D-H...A (°)
Form I of <b>13</b>	C(5)-H(5)...O(8)#1	0.85(8)	2.55(8)	3.322(9)	152(6)
	C(7)-H(7)...O(8)#2	1.02(6)	2.58(6)	3.250(10)	123(4)
	C(6)-H(6)...O(5)#2	1.01(6)	2.47(6)	3.480(10)	175(5)
	C(17)-H(17)...O(5)#1	0.97(6)	2.78(6)	3.362(9)	119(4)
Form II of <b>13</b>	C(5)-H(5)...O(8)#1	0.85(3)	2.55(3)	3.324(4)	151(3)
	C(7)-H(7)...O(8)#2	0.97(3)	2.54(3)	3.239(4)	129(2)
	C(6)-H(6)...O(5)#2	0.91(3)	2.48(3)	3.392(4)	173(2)
	C(17)-H(17)...O(5)#1	0.84(3)	2.94(3)	3.511(5)	127(3)
Form I of <b>14</b>	C(5)-H(5)...O(8)#3	0.94(3)	2.52(3)	3.342(4)	147(2)
	C(7)-H(7)...O(8)#4	0.88(3)	2.59(3)	3.262(4)	134(2)
	C(6)-H(6)...O(5)#4	0.99(3)	2.50(3)	3.484(4)	175(2)
	C(17)-H(17)...O(5)#3	0.89(3)	2.71(3)	3.353(4)	130(2)
Form II of <b>14</b>	C(5)-H(5)...O(8)#5	0.91(2)	2.50(2)	3.305(3)	148(2)
	C(7)-H(7)...O(8)#6	0.98(2)	2.51(2)	3.248(3)	132(2)
	C(6)-H(6)...O(5)#6	0.90(2)	2.49(2)	3.380(3)	174(2)
	C(17)-H(17)...O(5)#5	0.91(3)	2.83(3)	3.480(3)	129(2)

Symmetry codes: #1 -x+2,-y+2,-z+2; #2 -x+1,-y+2,-z+2; #3 -x+1,-y+1,-z+2;

#4 -x,-y+1,-z+2; #5 -x+2,-y+2,-z+1; #6 -x+1,-y+2,-z+1.

### 8.3.1.2 Differences in Dimer Formation

Although, the molecules of Form I and Form II crystals of **13** and **14** are isostructural in one-dimension<sup>137</sup> (**Figure 8.9**), they weave differently in other dimensions leading to two different path of nucleation. It is thought that during the process of crystallization, the one-dimensional layer formed by conventional O-H...O bonding, C-H... $\pi$  and C-H...O interactions (**Figure 8.8**) probably formed first and these strings were stitched subsequently via C-H...O interactions leading to bilayer formation (**Figure 8.9A**). These bilayers are linked differently in Form I and Form II crystals along the c-axis. In Form I, the bilayers are associated via C20-H20...Br1(Cl1) contact (**Figure 8.14A** for Form I of **13**) whereas in Form II they are linked via C19-Br2(Cl2)...O7 halogen bonding contact (**Figure 8.14B** for Form II of **13**).

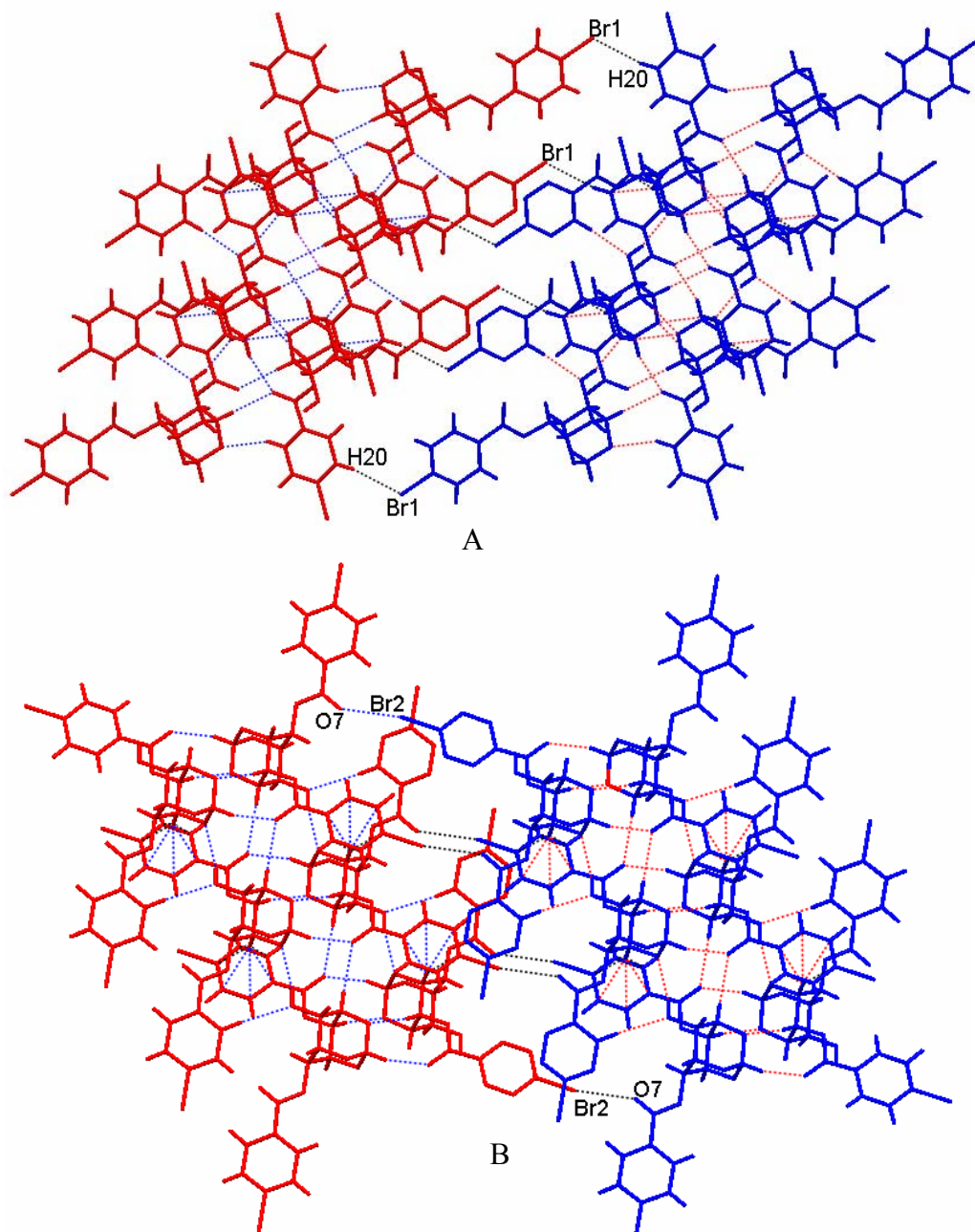


**Figure 8.14.** Bridging of bilayers in dimorphs of **13**, via A) C-H...Br(Cl) contact in Form I crystals and B) C-Br(Cl)...O contact in Form II crystals.

Association of the dimers (**Figure 8.9B**) viewed along the a-axis gives a clear picture of the difference in bridging of bilayers. In Form I crystals, the dimers are linked via

centrosymmetric C7-H7 $\cdots$ O3 and C18-H18 $\cdots$ O3 contacts along the b-axis and via C20-H20 $\cdots$ Br1 contact along the c-axis (**Figure 8.11A**, via C20-H20 $\cdots$ Cl1 in Form I crystals of 14), whereas in Form II crystals the dimers are linked via centrosymmetric weak C-H $\cdots$  $\pi$  contact between the C4-H4 and phenyl ring of the C2-O-benzoyl group along the b-axis and via short C19-Br2 $\cdots$ O7 halogen bond contact along the c-axis (**Figure 8.11B**, **Table 8.7**, via C19-Cl2 $\cdots$ O7 in Form I crystals of 14). The lengthening of the b-axis by  $\sim 3$  Å and shortening of c-axis by  $\sim 5$  Å in Form II crystals of 13 and 14 could be explained on the basis of these dimeric association (**Figure 8.11**).

**Table 8.7:** Intermolecular C-H $\cdots$ O, C-H $\cdots$  $\pi$ , C-H $\cdots$ X and C-X $\cdots$ O contacts in dimorphs of 13 and 14.

	D-H/X $\cdots$ A	D-H/X (Å)	H/X $\cdots$ A (Å)	D $\cdots$ A (Å)	D-H/X $\cdots$ A (°)
Form I of 13	C(7)-H(7) $\cdots$ O(3)#1	1.02(6)	2.65(6)	3.441(9)	134(4)
	C(18)-H(18) $\cdots$ O(3)#2	0.91(7)	2.67(7)	3.479(10)	148(5)
	C(20)-H(20) $\cdots$ Br(1)#3	0.90(8)	2.96(8)	3.724(9)	144(6)
Form II of 13	C(19)-Br(2) $\cdots$ O(7)#4	1.890(3)	3.131(3)	3.693(5)	161(3)
	C(4)-H(4) $\cdots$ Cg(1) #1	0.94(8)	3.039	3.959	166
Form I of 14	C(7)-H(7) $\cdots$ O(8)#5	0.88(3)	2.78(3)	3.438(4)	132(2)
	C(18)-H(18) $\cdots$ O(3)#2	0.90(4)	2.67(4)	3.476(5)	149(3)
	C(20)-H(20) $\cdots$ Cl(1)#6	0.88(4)	2.84(4)	3.615(4)	148(3)
Form II of 14	C(19)-Cl(2) $\cdots$ O(7)#7	1.731(2)	3.100(3)	3.898(4)	164(2)
	C(4)-H(4) $\cdots$ Cg(1)#8	0.971(4)	3.046	3.996	167

Symmetry codes: #1 -x+1,-y+1,-z+2; #2 x+1,y+1,z; #3 -x+1,-y+2,-z+1; #4 2-x, 1-y, 1-z;

#5 -x,-y+1,-z+2; #6 -x,-y+1,-z+1; #7 2-x, 1-y, -z; #8 -x+1,-y+1,-z+1,

Cg1 – Centroid of the C9-C14 phenyl ring.

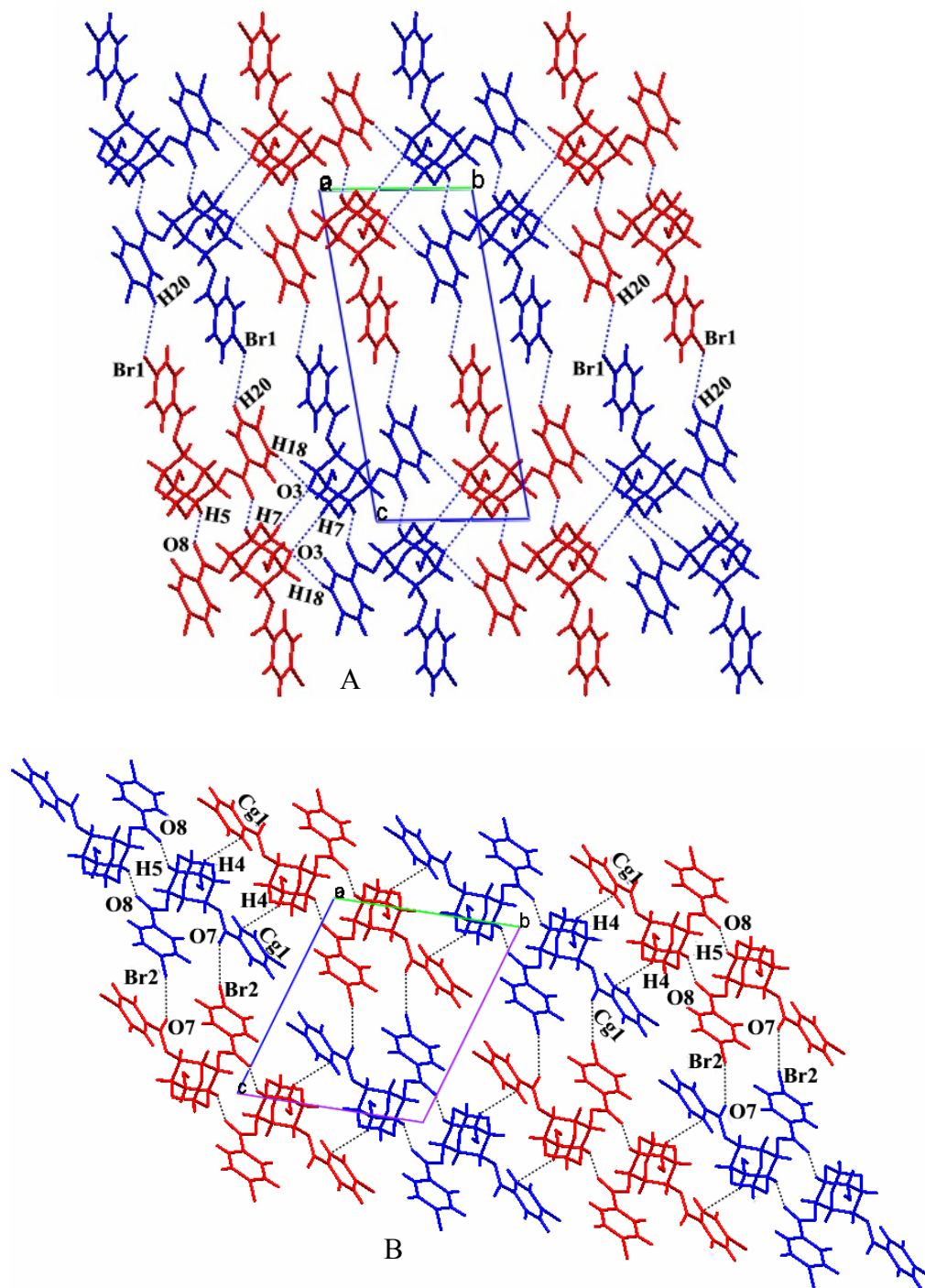


**Figure 8.11.** Association of dimers in A) Form I and B) Form II crystals of **13**.

### 8.3.1.3 Dimeric Association via C-H...X and C-X...O Contact

The notable difference in the dimorphs of **13** and **14** is the involvement of halogens in molecular association. In Form I crystals, the halogen atoms (X) are engaged in C-H...X and X...X interactions forming centrosymmetric dimers (**Figure 8.12A**), whereas in Form II crystals the halogen atoms take part in halogen bonding as well as C-H...X interaction forming another type of dimer (**Figure 8.12B**).

In Form I crystals of **13** and **14**, the halogen atom Br1(Cl1) is makes C-H...X contact with the C20-H20 of the axial *p*-halo-*O*-benzoyl group (**Table 8.7**). The same halogen atom is also engaged in the formation of Br1...Br2 [3.766(3) Å] in Form I crystals of **13** and Cl1...Cl2 [3.725 (4) Å] in Form I crystal of **14**. This X...X contact is of type II category as described by Desiraju et al.<sup>44</sup> In Form I crystals of **13**, the angle at Br1 is 100.3° and angle at Br2 is 153.6°, similarly in Form I crystals of **14**, the angle at Cl1 is 102.6° and the angle at Cl2 is 153.1°.

In Form II crystals of **13** and **14**, the halogen atom Br2(Cl2) is engaged in X...O short contact with the carbonyl oxygen O7 of the C2-equatorial *p*-halo-benzoyl group. The geometry of the halogen bonding contact in Form II crystals of both **13** and **14** is good, as the X...O distance is much less than the sum of van der Waals radii and the angle of approach is close to linearity (**Table 8.7**). The other halogen atom Br1(Cl1) is engaged in C-H...X type interaction. The C18-H18 of the C6-axial *p*-halobenzoyl group makes short and linear C-H...X interaction with Br1(Cl1). No X...X short contacts (as seen in Form I crystals of **13** and **14**) are present in Form II crystals of **13** and **14**.

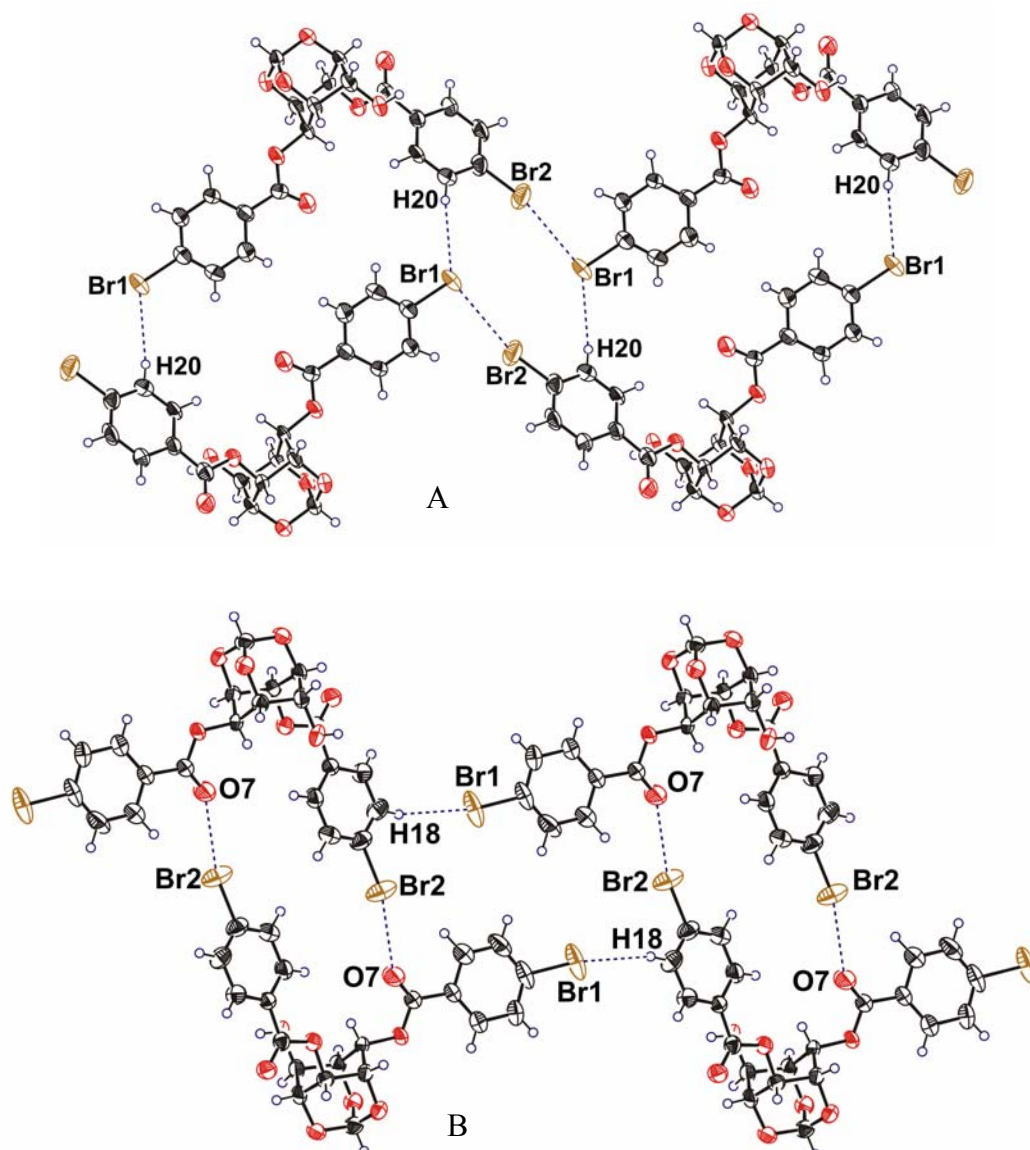


**Figure 8.12.** A) C-H...Br bonded dimers are linked via Br...Br short contact in Form I and B) the C-Br...O bonded dimers are associated via C-H...Br contact in Form II crystals of **13** respectively.



From the foregoing, it is clear that the conventional H-bonding contacts, which are involved in the isostructural bilayer formation in polymorphic crystals of **13** and **14**, are not involved in polymorphic modification. The interplay of the weak interactions such as C-H $\cdots$ O, C-H $\cdots$ Br(Cl) and C-Br(Cl) $\cdots$ O plays a vital role in the polymorphic behaviour of **13** and **14**. Further it is interesting to note that, in non-halogenated derivatives racemic 2,4-di-*O*-benzoyl-*myo*-inositol 1,3,5-orthoesters, the hydroxyl group at the C4 position makes O-H $\cdots$ O hydrogen bonding with crystallographic two-fold screw axis related carbonyl oxygen of the C2-equatorial benzoyl group forming helical assemblies.<sup>152</sup> Although both racemic **13** and **14** have hydroxyl group at the C4 position, these molecules do not assemble helically by forming intermolecular O-H $\cdots$ O hydrogen bond with O=C of the C2-benzoyl group. Instead a common molecular string linked via O-H $\cdots$ O interaction (**Figure 8.8A**) forms dimeric assembly via halogen bonding and C-H $\cdots$ X contacts. This could be due to the presence of halogen atom at para position.

#### 8.3.1.4 Possible Pathways of Nucleation

From the isostructurality in one dimension, intermolecular interactions ‘weave’ the common strings differently leading to two different paths of nucleation.<sup>137f</sup> Although the nucleation process cannot be visualized, we propose a possible sequence of events in the form of a cartoon (**Figure 8.13**) inferred from the final observed structures that emerge out of a dynamic equilibrium between various strong and weak interactions in solution. The sequence of crystallization events is proposed to start from the formation of one dimensional O-H $\cdots$ O bonded string (**step 1**), their similar C-H $\cdots$ O adhesions to form bilayers (**step 2A**) which can also be visualized to consist of dimers (**step 2B**), different

cohesion between these dimers via C-H $\cdots$ X and X $\cdots$ O contacts that extends the growth of the crystals in the third dimension (**steps 3A and 3B**).

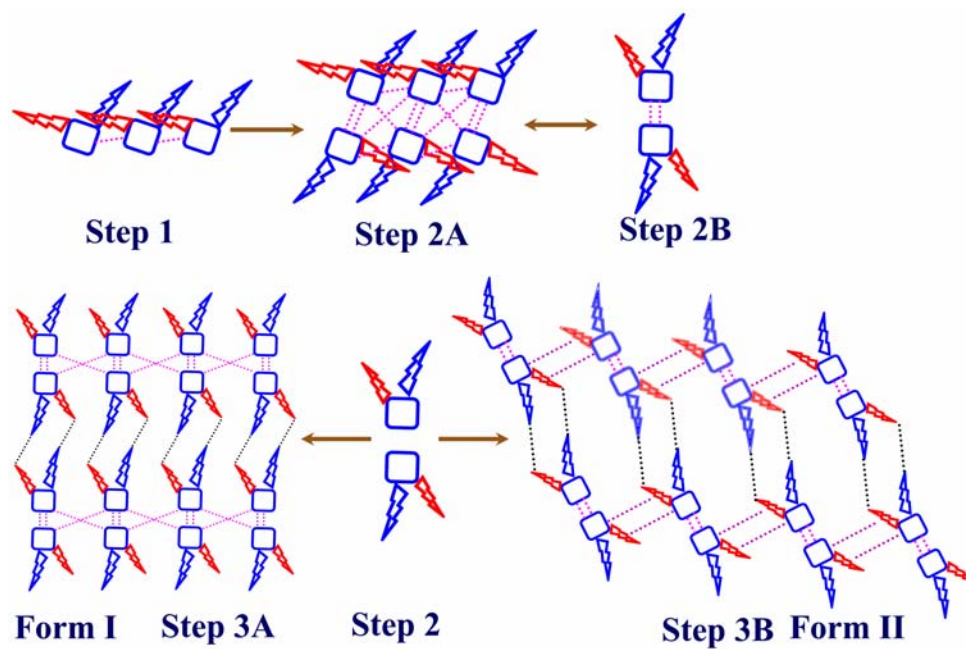


**Figure 8.13.** Cartoon representation of the proposed pathways of dimorph formation in crystals of **13** and **14**.

### 8.3.1.5 Conformational Differences

The molecules in Form I as well as Form II crystals of **13** and **14** have almost the same conformation. They superpose quite well except for the conformation of the C2-*O*-(*p*-halo-benzoyl) groups, which shows orientational difference of about 15° (**Figure 8.14**). The conformation of the molecules of Form I crystals of **13** and **14** have almost the same conformation.

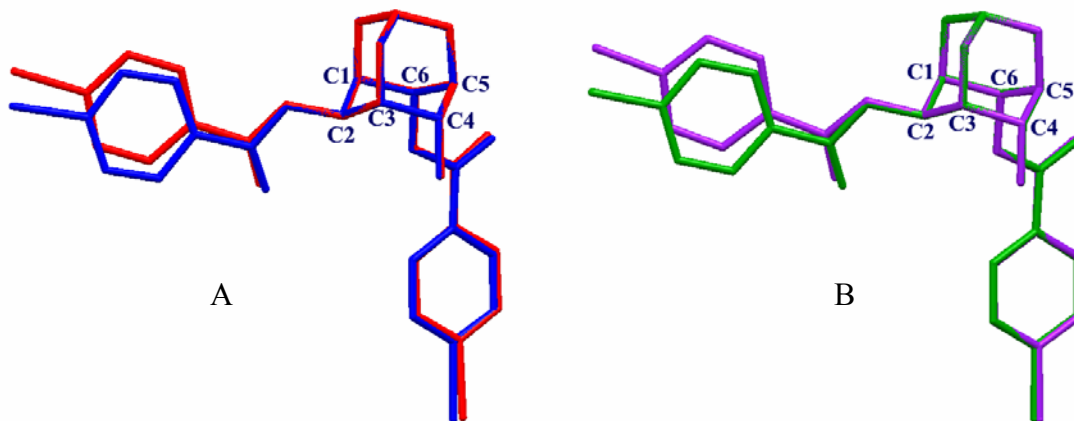


**Figure 8.14.** Molecular overlap of A) Form I (red) and Form II (blue) crystals of **13** and B) Form I (purple) and Form II (green) molecules of **14**.

### 8.3.1.6 Proposed Mechanism for Transition from Form I Crystals to Form II

#### Crystals of **13**

Form I crystals of **13** upon heating to 224 °C underwent transformation into the Form II crystals of **13**. For the conversion of Form I to Form II crystals of **13**, the molecules linked via centrosymmetric C20-H20···Br1 contacts (orange molecules in **Figure 8.15A**) in Form I crystals have to rearrange to make C19-Br2···O7 short contact as in Form II crystals (**Figure 8.15B**). We propose that this involves ‘closing in’ of the two O4-H4A···O1 linked molecular rows towards each other by  $\sim 1.8$  Å (red dotted arrows in **Figure 8.15A**). This relative movement of the molecules generate new C-Br···O=C interactions while sacrificing C20-H20···Br1 interactions (**Figure 8.15A**). This further endorses the view that Form II crystal in which halogen bonding interaction is predominant are more stable compared to their respective Form I crystals. No drastic changes were noticed at the crystal surface during heating; this could be because of the small movement of the molecules during crystal-to-crystal transformation as compared to the Form I crystal of **11**.

The crystal-to-crystal transformation observed in Form I crystals of **13** was similar to the Form I crystals of **11** (Chapter 7).<sup>35g</sup> But in Form I crystals of **13** the transition was not sharp as observed in Form I crystals of **11**. The relative movement of the molecules movements in Form I crystals of **13** was  $\sim 1.8$  Å to result in Form II crystals which is small, as compared to the Form I crystals of **11** where the molecules moved by  $\sim 3$  Å to convert into Form II crystals of **11**. Further, it is remarkable that both Form I crystals of **11** and **13** underwent crystal-to-crystal phase transition to yield the Form II crystals where the association of the molecules is mainly via X···O short contact.

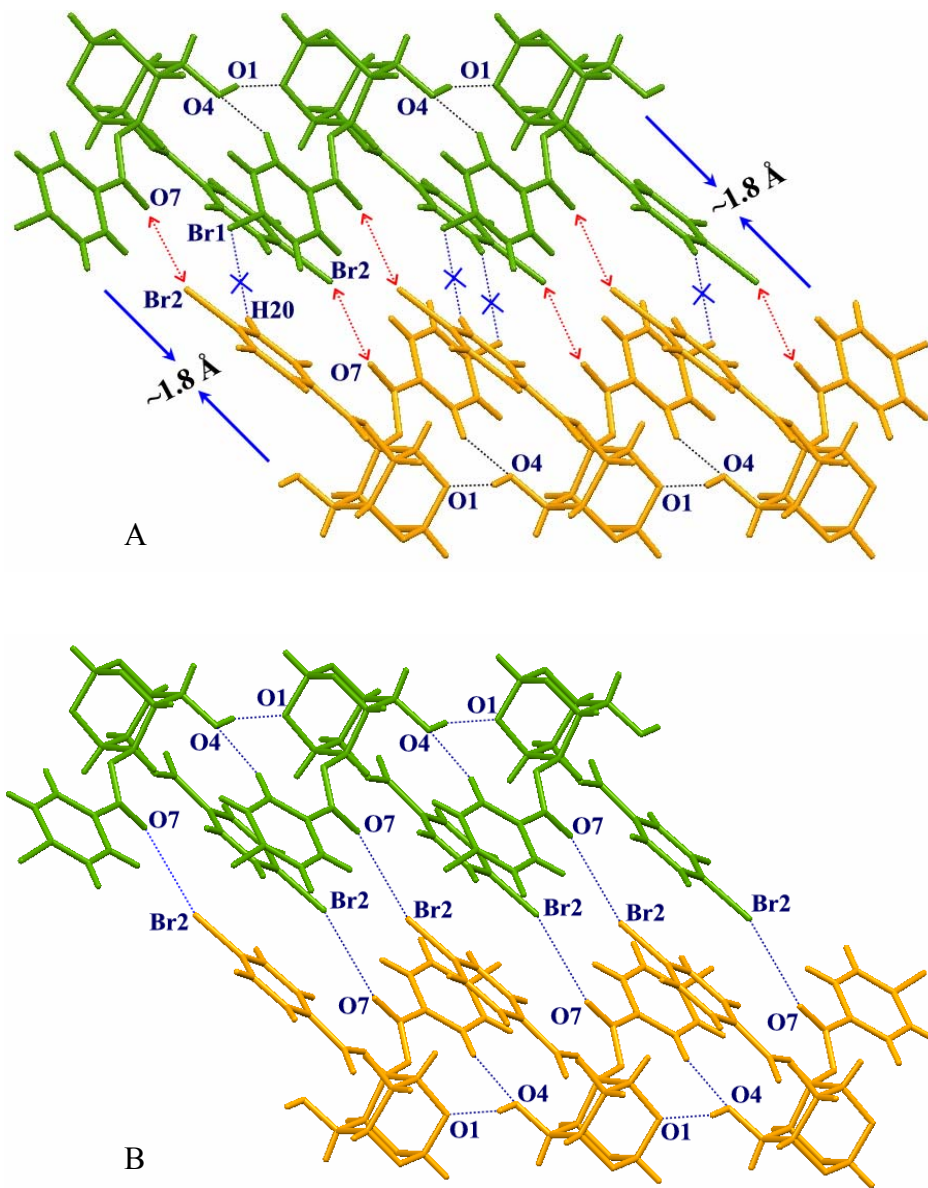


**Figure 8.15.** View of molecular packing in, A) Form I and B) Form II crystals of **13** down the a-axis. The proposed molecular displacement is marked by blue arrows in (A), and the contacts Br2...O7 to be formed (in Form II) are also shown by red double-headed arrows.

### 8.3.2 Structures of Solvates of **13** and **14**

#### 8.3.2.1 Conformational Difference

The conformation of the host molecule in **13**·CHCl<sub>3</sub> and **13**·CH<sub>3</sub>COCH<sub>3</sub> is similar, except for slight difference in the orientation of the C2 and C6-*O-p*-halobenzoyl groups. The conformation of the C2 and C6-*O-(p*-halobenzoyl) group in solvates of **14** showed difference (**Figure 8.16A**). Infact, the orientations of C6-*O-(p*-halobenzoyl) group differ by about 30° in **14**·CHCl<sub>3</sub>, **14**·CH<sub>3</sub>COCH<sub>3</sub> as compared to other solvates of **14**. Although, chloroform, acetone, dichloromethane, nitromethane, THF, dioxane and CCl<sub>4</sub> inclusion crystals of **14** belong to monoclinic P2<sub>1</sub>/n, the conformation of both C2 and C6-*O-(p*-chlorobenzoyl) groups showed difference of 30°. Further the conformation of the C6-*O-(p*-chlorobenzoyl) groups in nitromethane, THF, dioxane and CCl<sub>4</sub> (monoclinic P2<sub>1</sub>/n), acetonitrile, dichloroethane (monoclinic P2<sub>1</sub>/c) and terephthaldehyde (1,4-diformylbenzene), benzene (monoclinic C2/c) inclusion crystals of **14** showed conformational difference of about 6-14°. The conformation of the C2-*(p*-chlorobenzoyl) group in all the solvates of **14** showed slight difference in orientation (~2-5°) except in **14**·C<sub>6</sub>H<sub>6</sub>, the C2-*p*-chloro-benzoyl group of which showed difference of about 20°.

Superposing the molecules of the solvent free crystals of **14** (Form I and Form II) and host molecules of solvated crystals showed marked difference in relative movement of the C2 and C6-*O*-benzoyl groups due to free rotation about O-C bond (**Figure 8.16B**). The C6-*O-(p*-halobenzoyl) group of host molecules in inclusion crystals of **13** and **14** moved away from the axial OH-group in anticlockwise direction while the C2-*O-(p*-halobenzoyl) group moved closer to the -OH group. The C6-*O-(p*-halobenzoyl) group of

**14** in solvent free crystal showed difference of about  $42^\circ$  with C6-*O*-(*p*-halobenzoyl) group of **14**·CHCl<sub>3</sub> and about  $65$ - $68^\circ$  with C6-*O*-(*p*-halobenzoyl) group of other solvates of **14**. Similarly, the difference in the orientation of the C2-*O*-benzoyl group of **14** in its solvates as compared with C2-*O*-(*p*-halobenzoyl) group of solvent free crystals of **14** was about  $25$ - $28^\circ$ .

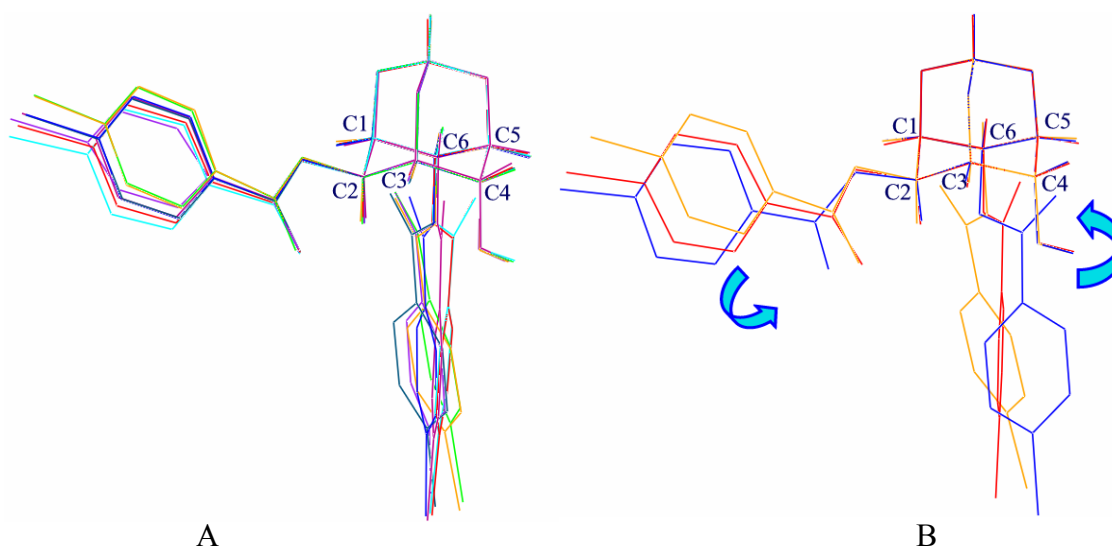


**Figure 8.16.** Molecular overlap of A) host molecules in inclusion crystals of **14**, **14**·CH<sub>3</sub>COCH<sub>3</sub> (red), **14**·CH<sub>3</sub>NO<sub>2</sub> (blue), **14**·CH<sub>3</sub>CN (orange), **14**·C<sub>6</sub>H<sub>6</sub> (purple), **14**·C<sub>6</sub>H<sub>4</sub>(CHO)<sub>2</sub> (green), **14**·CHCl<sub>3</sub> (cyan), **14**·CH<sub>2</sub>Cl<sub>2</sub> (brown), **14**·ClCH<sub>2</sub>CH<sub>2</sub>Cl (navy blue) and B) overlap of Form II molecule of **14** in Form II crystals (blue) and host molecules in **14**·CHCl<sub>3</sub> (red) and **14**·CH<sub>3</sub>CN (orange) showing relative movement of molecules.

### 8.3.2.2 Host Organization

Host molecules in all the solvates of **13** and **14** assemble around the crystallographic two-fold screw axis to form a helix (**Figure 8.17A**).<sup>152</sup> The successive molecules along the helix (b-axis) are linked by conventional O-H $\cdots$ O hydrogen bonding; the OH group at the C-4 position donates its H atom to the carbonyl oxygen O7 of the C2-*O-p*-halo-benzoyl group. The geometry of this conventional O-H $\cdots$ O bonding interaction is better in Group II (monoclinic P2<sub>1</sub>/c) and Group III (monoclinic C2/c) inclusion crystals as compared to Group I inclusion crystals (**Table 8.8**). H $\cdots$ O distances in all the pseudopolymorphs of **13** and **14** are in the range 1.95-2.04 Å but the angle of approach varies. The O-H $\cdots$ O angle is more linear in Group II and Group III (monoclinic C2/c) compared to the Group I solvates (**Table 8.8**). Along with O-H $\cdots$ O, some weak C-H $\cdots$ O contacts also hold the molecule along the helix. The C5-H5 of the inositol ring makes bifurcated C-H $\cdots$ O contacts with the hydroxyl oxygen O4 and carbonyl oxygen O7 (C5-H5 $\cdots$ O4 and C5-H5 $\cdots$ O7) of the neighboring 2<sub>1</sub>-screw related molecules along the helix, thereby supporting the tight binding of the helix. Thus each of the interacting atoms O4, O7 and C5-H5 make bifurcated contacts. The hydroxyl oxygen O4 donates its proton to carbonyl oxygen O7 and accepts H-atom from C5 of the inositol ring. Similarly the carbonyl oxygen O7 accepts H4A and H5 from O4 and C5 respectively and C5 donates its proton H5 to hydroxyl oxygen O4 and carbonyl oxygen O7. The orthoformate oxygen O5 also makes bifurcated weaker C-H $\cdots$ O contacts with the H-atoms of C20 and C21 of the axial C6-*O-p*-halo-benzoyl group. Two more weak C-H $\cdots$ O (C10-H10 $\cdots$ O5 and C11-H11 $\cdots$ O1) contacts link the unit-translated molecule along the helix (**Table 8.8**). Thus, the molecules in the helical assembly, predominantly linked by O4-H4A $\cdots$ O7



contacts are supported by C-H...O contacts, holding the molecules of the helix in the preorganized geometry.<sup>152</sup>

**Table 8.8:** Intermolecular hydrogen bonding interactions along helical assembly in solvates of **13** and **14**.

	D-H...A	D-H (Å)	H...A (Å)	D...A (Å)	D-H...A (°)
<b>13</b> ·CHCl <sub>3</sub>	O(4)-H(4A)...O(7)#1	0.82	2.00	2.812(5)	169
	C(5)-H(5)...O(4)#1	0.98	2.61	3.344(7)	132
	C(5)-H(5)...O(7)#1	0.98	2.72	3.401(6)	127
	C(11)-H(11)...O(1)#2	0.93	2.73	3.555(7)	148
	C(20)-H(20)...O(5)#3	0.93	2.78	3.395(8)	125
	C(21)-H(21)...O(5)#3	0.93	2.77	3.393(7)	125
<b>13</b> ·CH <sub>3</sub> COCH <sub>3</sub>	O(4)-H(4A)...O(7)#4	0.82	2.00	2.744(11)	151
	C(5)-H(5)...O(4)#4	0.98	2.48	3.204(14)	130
	C(5)-H(5)...O(7)#4	0.98	2.60	3.271(14)	126
	C(11)-H(11)...O(1)#2	0.93	2.66	3.488(14)	148
	C(20)-H(20)...O(5)#5	0.93	2.71	3.300(16)	122
	C(21)-H(21)...O(5)#5	0.93	2.63	3.263(14)	125
<b>14</b> ·CHCl <sub>3</sub>	O(4)-H(4A)...O(7)#4	0.82	2.04	2.824(4)	160
	C(5)-H(5)...O(4)#4	0.98	2.60	3.348(5)	133
	C(5)-H(5)...O(7)#4	0.98	2.73	3.411(5)	127
	C(11)-H(11)...O(1)#2	0.93	2.61	3.455(6)	152
	C(20)-H(20)...O(5)#5	0.93	2.83	3.421(6)	122
	C(21)-H(21)...O(5)#5	0.93	2.73	3.375(6)	127
<b>14</b> ·CH <sub>3</sub> COCH <sub>3</sub>	O(4)-H(4A)...O(7)#4	0.76(7)	2.04(7)	2.795(6)	169(7)
	C(5)-H(5)...O(4)#4	0.89(5)	2.60(5)	3.259(7)	131(4)
	C(5)-H(5)...O(7)#4	0.89(5)	2.74(5)	3.356(6)	127(4)
	C(11)-H(11)...O(1)#2	0.95(6)	2.67(6)	3.531(7)	152(5)
	C(20)-H(20)...O(5)#5	0.88(6)	2.81(6)	3.431(8)	130(5)
	C(21)-H(21)...O(5)#5	0.91(5)	2.67(5)	3.347(7)	132(3)

	D-H...A	D-H (Å)	H...A (Å)	D...A (Å)	D-H...A (°)
<b>14·CH<sub>2</sub>Cl<sub>2</sub></b>	O(4)-H(4A)...O(7)#6	0.84(4)	1.96(4)	2.786(3)	166(4)
	C(5)-H(5)...O(4)#6	0.93(3)	2.60(3)	3.331(4)	136(2)
	C(5)-H(5)...O(7)#6	0.93(3)	2.83(3)	3.422(4)	122(2)
	C(10)-H(10)...O(5)#2	0.95(4)	2.82(4)	3.584(4)	138(3)
	C(11)-H(11)...O(1)#2	0.97(4)	2.61(4)	3.438(4)	143(3)
	C(20)-H(20)...O(5)#7	0.97(4)	2.60(4)	3.313(5)	130(3)
	C(21)-H(21)...O(5)#7	0.89(4)	2.79(4)	3.360(4)	123(3)
<b>14·C<sub>4</sub>H<sub>8</sub>O<sub>2</sub></b>	O(4)-H(4A)...O(7)#1	0.82	2.03	2.841(6)	169
	C(5)-H(5)...O(4)#1	0.98	2.64	3.341(8)	128
	C(5)-H(5)...O(7)#1	0.98	2.70	3.384(7)	128
	C(10)-H(10)...O(5)#2	0.93	2.84	3.629(8)	143
	C(11)-H(11)...O(1)#2	0.93	2.72	3.542(8)	148
	C(20)-H(20)...O(5)#3	0.93	2.98	3.465(9)	114
	C(21)-H(21)...O(5)#3	0.93	2.83	3.396(9)	120
<b>14·C<sub>4</sub>H<sub>8</sub>O</b>	O(4)-H(4A)...O(7)#8	0.90(5)	1.94(5)	2.814(3)	165(4)
	C(5)-H(5)...O(4)#8	1.03(4)	2.52(4)	3.323(4)	135(3)
	C(5)-H(5)...O(7)#8	1.03(4)	2.78(4)	3.429(4)	121(3)
	C(10)-H(10)...O(5)#2	0.93	2.82	3.601(4)	142
	C(11)-H(11)...O(1)#2	0.93	2.65	3.469(4)	147
	C(20)-H(20)...O(5)#9	0.93	2.86	3.462(5)	123
	C(21)-H(21)...O(5)#9	0.93	2.78	3.424(4)	127
<b>14·CCl<sub>4</sub></b>	O(4)-H(4A)...O(7)#4	0.87(5)	1.96(5)	2.817(4)	165(4)
	C(5)-H(5)...O(4)#4	0.98	2.58	3.322(5)	132
	C(5)-H(5)...O(7)#4	0.98	2.73	3.414(5)	127
	C(10)-H(10)...O(5)#2	0.93	2.81	3.579(5)	141
	C(11)-H(11)...O(1)#2	0.93	2.66	3.492(5)	149
	C(20)-H(20)...O(5)#5	0.93	2.79	3.389(6)	123
	C(21)-H(21)...O(5)#5	0.93	2.72	3.358(5)	126
<b>14·CH<sub>3</sub>NO<sub>2</sub></b>	O(4)-H(4A)...O(7)#6	0.82	2.01	2.805(4)	165
	C(5)-H(5)...O(4)#6	0.98	2.59	3.308(5)	130
	C(5)-H(5)...O(7)#6	0.98	2.74	3.413(5)	126
	C(10)-H(10)...O(5)#2	0.93	2.81	3.574(5)	141
	C(11)-H(11)...O(1)#2	0.93	2.63	3.442(5)	146
	C(20)-H(20)...O(5)#7	0.93	2.72	3.325(5)	123
	C(21)-H(21)...O(5)#7	0.93	2.72	3.326(5)	123

	D-H...A	D-H (Å)	H...A (Å)	D...A (Å)	D-H...A (°)
<b>14·CH<sub>3</sub>CN</b>	O(4)-H(4A)...O(7)#10	0.79(3)	2.02(3)	2.813(3)	175(3)
	C(5)-H(5)...O(4)#10	0.94(3)	2.61(3)	3.332(3)	134(2)
	C(5)-H(5)...O(7)#10	0.94(3)	3.02(2)	3.536(3)	116(2)
	C(10)-H(10)...O(5)#2	0.86(3)	2.81(3)	3.537(3)	144(2)
	C(11)-H(11)...O(1)#2	0.95(3)	2.53(3)	3.306(3)	139(2)
	C(20)-H(20)...O(5)#11	0.88(3)	3.00(3)	3.428(4)	112(2)
	C(21)-H(21)...O(5)#11	0.93(3)	2.91(3)	3.383(4)	113(2)
<b>14·ClCH<sub>2</sub>CH<sub>2</sub>Cl</b>	O(4)-H(4A)...O(7)#10	0.82	2.00	2.822(4)	176
	C(5)-H(5)...O(4)#10	0.98	2.59	3.281(5)	128
	C(5)-H(5)...O(7)#10	0.98	2.81	3.464(5)	125
	C(10)-H(10)...O(5)#2	0.93	2.72	3.520(5)	144
	C(11)-H(11)...O(1)#2	0.93	2.51	3.293(5)	142
	C(20)-H(20)...O(5)#11	0.93	3.00	3.475(6)	113
	C(21)-H(21)...O(5)#11	0.93	2.80	3.371(5)	121
<b>14·C<sub>6</sub>H<sub>6</sub></b>	O(4)-H(4A)...O(7)#6	0.82	2.00	2.817(6)	173
	C(5)-H(5)...O(4)#6	0.98	2.74	3.374(8)	123
	C(5)-H(5)...O(7)#6	0.98	3.07	3.660(8)	120
	C(10)-H(10)...O(5)#2	0.93	2.91	3.762(9)	152
	C(11)-H(11)...O(1)#2	0.93	2.50	3.226(8)	135
	C(20)-H(20)...O(5)#7	0.93	2.91	3.459(9)	119
	C(21)-H(21)...O(5)#7	0.93	2.92	3.462(9)	119
<b>14·C<sub>6</sub>H<sub>4</sub>(CHO)<sub>2</sub></b>	O(4)-H(4A)...O(7)#3	0.84	1.98	2.815(3)	175
	C(5)-H(5)...O(4)#3	1.00	2.69	3.341(3)	123
	C(5)-H(5)...O(7)#3	1.00	3.05	3.660(3)	120
	C(10)-H(10)...O(5)#12	0.95	2.82	3.617(3)	142
	C(11)-H(11)...O(1)#12	0.95	2.45	3.174(3)	134
	C(20)-H(20)...O(5)#1	0.95	2.90	3.424(4)	116
	C(21)-H(21)...O(5)#1	0.95	2.84	3.401(4)	119

Symmetry codes: #1 -x+1/2, y-1/2, -z+1.5; #2 x, y+1, z; #3 -x+1/2, y+1/2, -z+1.5;

#4 -x+1.5, y-1/2, -z+1.5; #5 -x+1.5, y+1/2, -z+1.5; #6 -x+1/2, y-1/2, -z+1/2;

#7 -x+1/2, y+1/2, -z+1/2; #8 -x+1.5, y-1/2, -z+1/2; #9 -x+1.5, y+1/2, -z+1/2;

#10 -x+2, y-1/2, -z+1/2; #11 -x+2, y+1/2, -z+1/2; #12 x, -y+1, z.

The helical assembly across crystallographic two-fold axis via O-H $\cdots$ O bonding appears to be a consistent feature in the organization of the host molecules in all the solvates of **13** and **14**. The perpendicular view of the helix down b-axis shows dancing pair like organization of the molecules (**Figure 8.17B**).

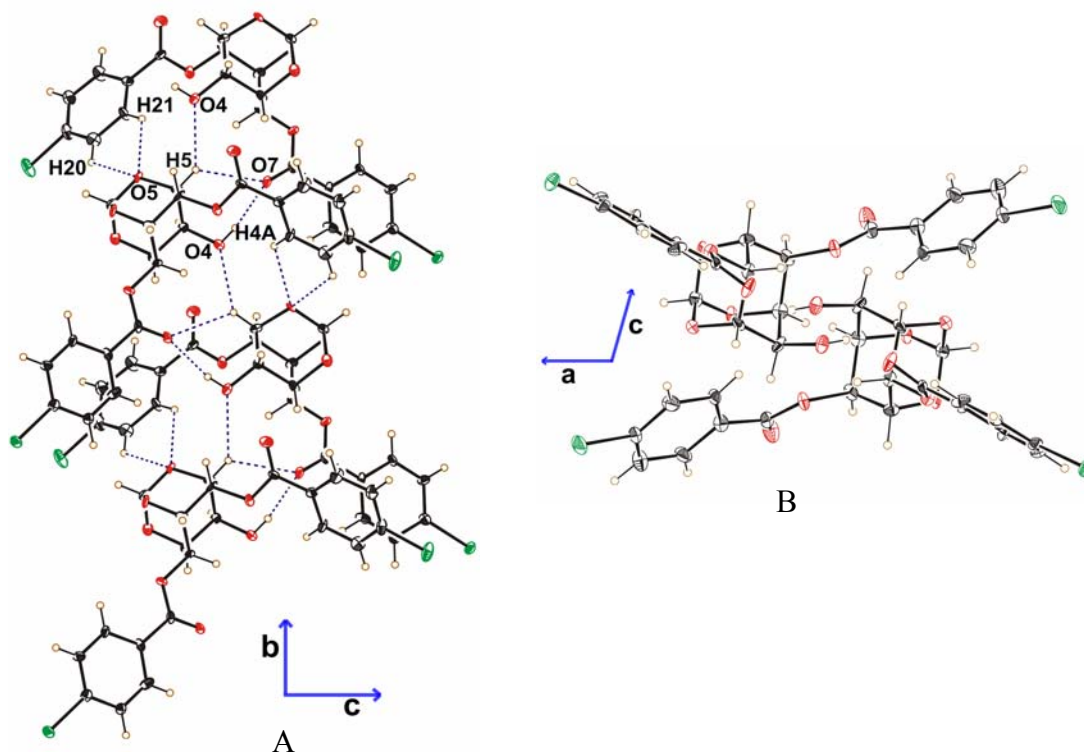


**Figure 8.17.** A) Helical assembly across crystallographic  $2_1$  axis via O-H $\cdots$ O and C-H $\cdots$ O interactions in  $14 \cdot \text{CH}_3\text{CN}$ , B) Dancing pair like association of host molecules viewed down the b-axis in  $14 \cdot \text{CH}_3\text{CN}$ .

The O-H...O linked helices in all the solvates of **13** and **14** are packed much more discretely providing a well guided tunnel throughout the crystal as observed in case of 2,6-di-*O*-benzoyl *myo*-inositol 1,3,5- orthoformate.<sup>152</sup> The neighboring helices have different chirality and are linked differently in three crystal forms. Helices in Group I solvates are linked via halogen bonding (C19-Cl2...O3) contact (via C19-Br2...O3 in inclusion crystals of **13**) along the ac plane (**Figure 8.18A**), in Group II solvates, the neighbouring helices are associated via C13-H13...Cl2 contact (**Figure 8.18B**) and in Group III solvates, the neighbouring helices are linked via short Cl2...Cl1 (**Figure 8.18C**) contact.

In Group I inclusion crystals, the halogen (Cl2 or Br2) atom of the axial C6-*O*-(*p*-halobenzoyl) group makes somewhat longer contact with the orthoformate bridge oxygen O3, but the angle of approach is more directional. In **13**·CH<sub>3</sub>COCH<sub>3</sub>, the Br2...O3 [3.170(9) Å] contact is much less than sum of van der Waals radii and it is more linear (C19-Br2...O3 = 163.4°) compared to **13**·CHCl<sub>3</sub> and other solvates of **14**. The halogen bonding contact in **13**·CHCl<sub>3</sub> is very close to the sum of van der Waals radii [Br2...O3 = 3.332(4)] and the C19-Br2...O3 angle is 158.8°. The halogen bonding interactions in the pseudopolymorphs of **14** are somewhat weaker as compared to those in inclusion crystals of **13**. The Cl...O contacts in Group I solvates of **14** are more than the sum of van der Waals radii (**Table 8.9**) and not so linear as compared to inclusion crystals of **13**. Thus, the neighbouring helices in Group I inclusion crystals of **13** and **14** are associated via halogen bonding contacts, which create the voids in between the helices to accommodate the guest solvents (**Figure 8.18B**).<sup>153</sup> In Group II solvates of **14** (**14**·CH<sub>3</sub>CN and **14**·ClCH<sub>2</sub>CH<sub>2</sub>Cl), the C-H...Cl contacts which link the neighbouring helices are close to

sum of van der Waals radii but not much linear. In Group III solvates of **14** (**14**·**C<sub>6</sub>H<sub>6</sub>** and **14**·**C<sub>6</sub>H<sub>4</sub>(CHO)<sub>2</sub>**), the Cl··Cl contacts that link the neighbouring helices are of type II category and the Cl2··Cl1 distance is much less than the sum of van der Waals radii (3.52 Å, **Table 8.9**).

**Table 8.9:** Interactions involved in the association of neighbouring helices.

X = Cl, Br	D-H/X··A	D-H/X (Å)	H/X··A (Å)	D··A (Å)	D-H/X··A (°)
<b>13</b> · <b>CHCl<sub>3</sub></b>	C(19)-Br(2)··O(3)#1	1.902(6)	3.332(4)	5.142(8)	159
<b>13</b> · <b>CH<sub>3</sub>COCH<sub>3</sub></b>	C(19)-Br(2)··O(3)#2	1.867(9)	3.170(9)	4.987	163
<b>14</b> · <b>CHCl<sub>3</sub></b>	C(19)-Cl(2)··O(3)#2	1.756(5)	3.390(4)	5.004(6)	152
<b>14</b> · <b>CH<sub>3</sub>COCH<sub>3</sub></b>	C(19)-Cl(2)··O(3)#3	1.725(7)	3.306(4)	4.931(8)	156
<b>14</b> · <b>CH<sub>2</sub>Cl<sub>2</sub></b>	C(19)-Cl(2)··O(3)#4	1.733(4)	3.230(3)	4.849(5)	154
<b>14</b> · <b>C<sub>4</sub>H<sub>8</sub>O<sub>2</sub></b>	C(19)-Cl(2)··O(3)#4	1.727(8)	3.451(5)	4.948(9)	144
<b>14</b> · <b>C<sub>4</sub>H<sub>8</sub>O</b>	C(19)-Cl(2)··O(3)#5	1.739(4)	3.431(3)	4.994(4)	148
<b>14</b> · <b>CCl<sub>4</sub></b>	C(19)-Cl(2)··O(3)#1	1.733(5)	3.365(3)	4.974(6)	153
<b>14</b> · <b>CH<sub>3</sub>NO<sub>2</sub></b>	C(19)-Cl(2)··O(3)#5	1.738(4)	3.338(3)	4.862(5)	145
<b>14</b> · <b>CH<sub>3</sub>CN</b>	C(13)-H(13)··Cl(2)#6	0.95(3)	2.83(3)	3.539(3)	132
<b>14</b> · <b>ClCH<sub>2</sub>CH<sub>2</sub>Cl</b>	C1(3)-H(13)··Cl(2)#7	0.93	2.91	3.658(4)	138
<b>14</b> · <b>C<sub>6</sub>H<sub>6</sub></b>	C(19)-Cl(2)··Cl(1)#8	1.730(9)	3.379(4)	5.093(9)	170
<b>14</b> · <b>C<sub>6</sub>H<sub>4</sub>(CHO)<sub>2</sub></b>	C(19)-Cl(2)··Cl(1)#9	1.743(3)	3.390(2)	5.086(4)	164

Symmetry codes: #1 x+1/2, -y+1/2, z-1/2; #2 x+1/2, -y+1.5, z-1/2;

#3 1/2+x, -y+1/2, x-1/2; #4 x-1/2, -y+1/2, z+1/2; #5 x-1/2, -y+1/2, z+1/2;

#6 x+1, -y+1.5, z-1/2; #7 x+1, -y+1/2, z-1/2; #8 x+1/2, y-1/2, z; #9 x+1/2, y+1/2, z+1.

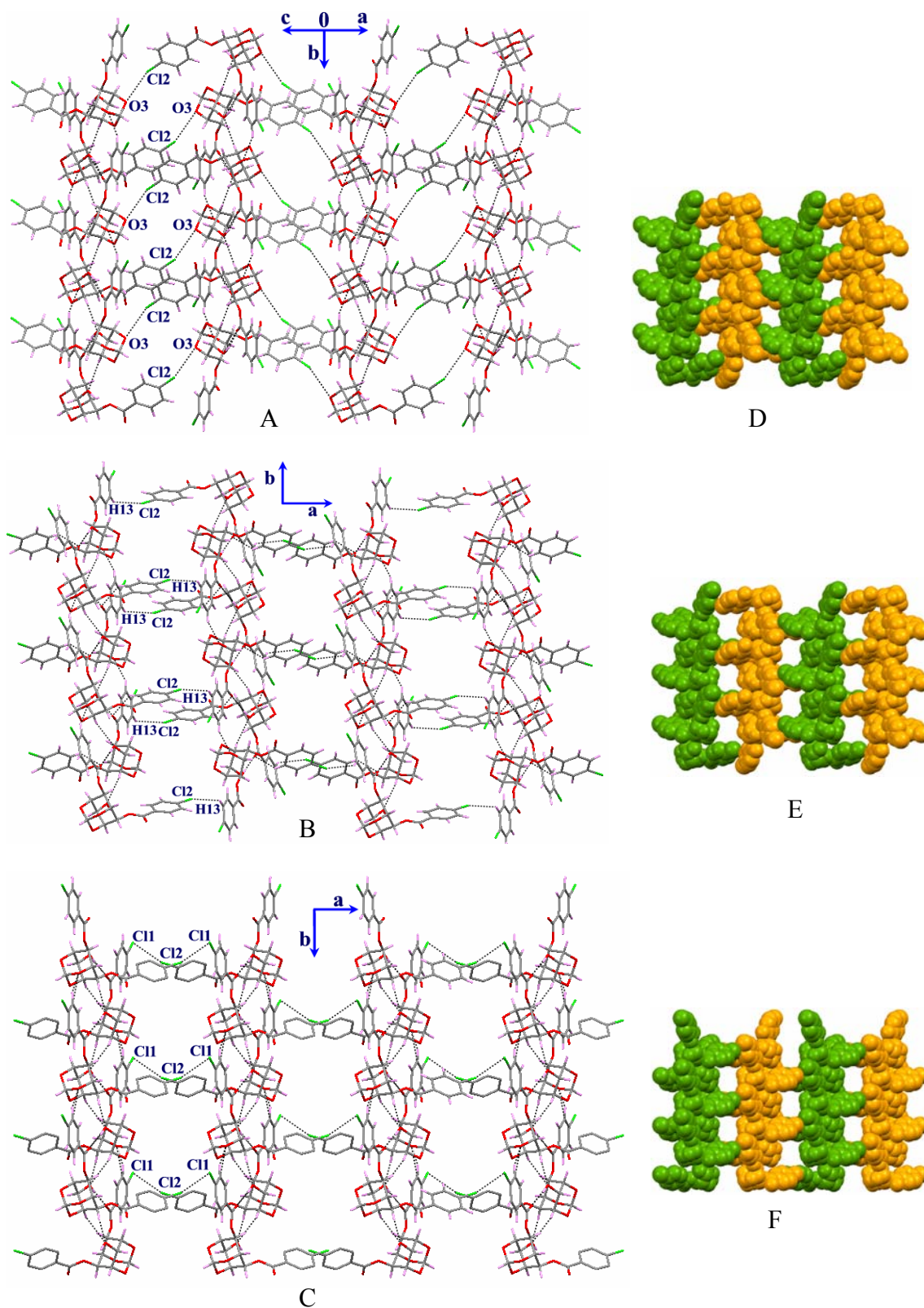
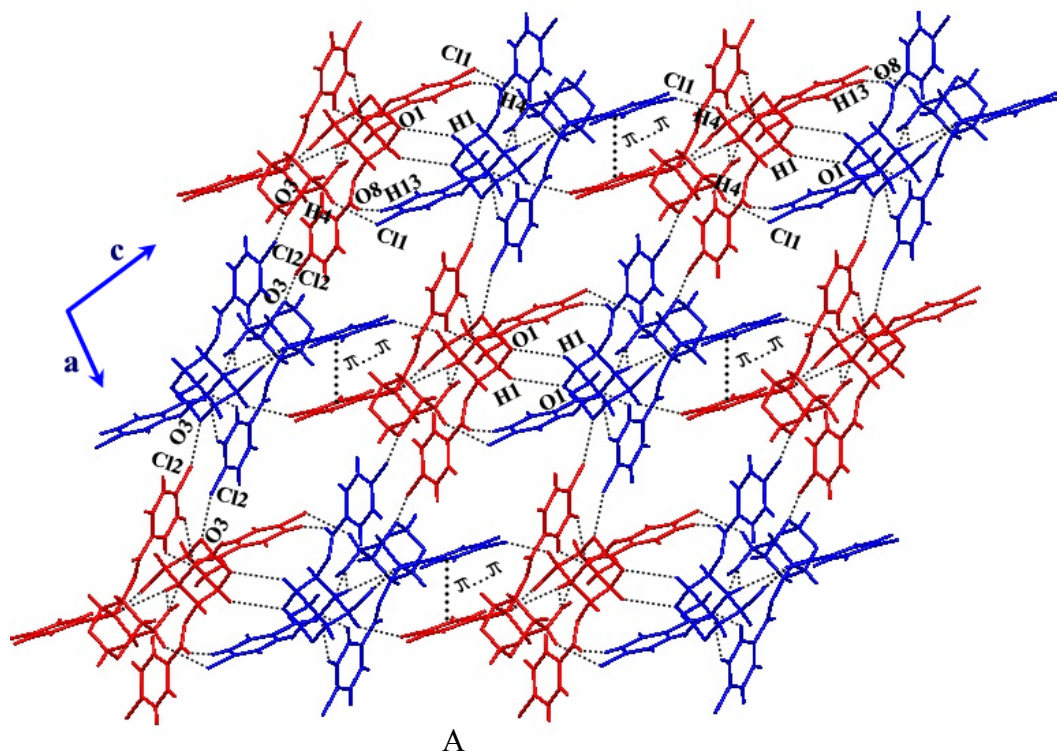


**Figure 8.18.** Association of the helices in A)  $14 \cdot \text{CH}_2\text{Cl}_2$ , B)  $14 \cdot \text{CH}_3\text{CN}$  and C)  $14 \cdot \text{C}_6\text{H}_4(\text{CHO})_2$  and D), E) and F) show the CPK view in respective modifications.

The arrangement of dancing pairs (**Figure 8.17B**) down the b-axis formed voids that accommodate the guest molecules. The overall packing of dancing pairs is different in all the three modifications (**Figure 8.18**). The association of the dancing pairs in Group I and Group II inclusion crystals look similar with slight change in the orientation. In Group I and Group II inclusion crystals, the dancing pairs form almost identical dimers (red-blue, **Figure 8.19A and B**) along the c-axis linked via C1-H1...O1 and C4-H4...Cl1(Br1) contacts. Two more C-H...O interactions C13-H13...O8 in Group I and C14...H14...O8 in Group II inclusion crystals link the dancing pairs along the c-axis. The crossover from C13-H13...O8 in Group I to C14-H14...O8 in Group II inclusion crystals is due to change in orientation of dancing pairs. In turn, these dimeric units (red-blue) are further linked to other dimeric units (red-blue) in the same direction via centrosymmetric C4-H4...Cl1(Br1) and  $\pi$ ... $\pi$  contact between the phenyl rings of the C2-O-*p*-halobenzoyl group thus forming identical molecular string of these dimers (**Figure 8.19A and B**). Bridging of these dancing pairs along the a-axis is also similar in both Group I and Group II inclusion crystals but they are associated via different types of interactions. In Group I inclusion crystals, the dancing pairs are linked via C19-Cl2...O3 (C19-Br2...O3 contact in solvates of **13**) contact whereas in Group II inclusion crystals they are bridged via C18-H18...O3 contacts (**Figure 8.19A and B, Table 8.10**). There are no contacts between diagonal dancing pairs (blue-blue) in Group I inclusion crystals whereas in Group II inclusion crystals, they are interacting diagonally via C13-H13...Cl2 interactions (these two atoms were about 6.2 Å apart in Group I inclusion crystals). Thus, the dancing pairs in Group II inclusion crystals are 'close in' by about 1.5 Å diagonally. In Group III inclusion crystals, the dancing pairs are linked via C14-H14...O8 contacts along the c-



axis forming molecular strings. The dancing pairs moved away slightly along the c-axis by breaking C1-H1...O1 and C4-H4...C11 interactions (as observed in Group I and Group II inclusion crystals) with the formation of new C14-H14...O8 contact. But along the a-axis they are bridged via C18-H18...O3 contact similar to the Group II inclusion crystals (**Figure 8.19C**, **Table 8.10**). The relative movements of the dancing pairs along the c-axis bring the diagonal dancing pairs close to each other (blue-blue) via C11...C12 contact. The expansion of the c-axis in both Group I and Group II inclusion crystals could be due to these relative movements of the dancing pairs.



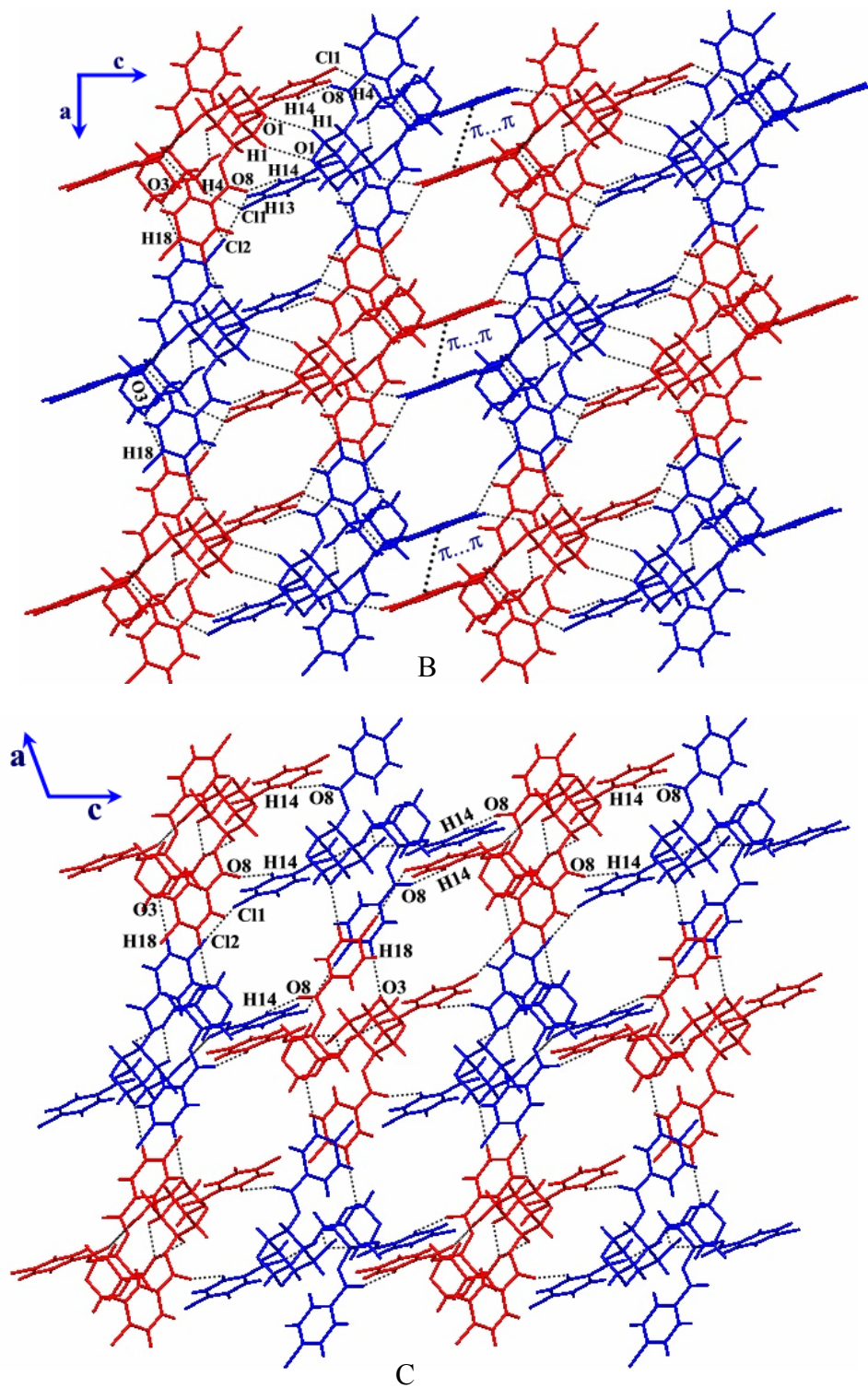


**Figure 8.19.** Association of dancing pairs, A) Group I, B) Group II and C) Group III inclusion crystals of **14**.

**Table 8.10:** Interactions involved in linking of dancing pairs in solvates of **13** and **14**.

$\alpha$ = dihedral angle	D-H...A	D-H (Å)	H...A (Å)	D...A (Å)	D-H...A/ $\alpha$ (°)
<b>13·CHCl<sub>3</sub></b>	C(1)-H(1)···O(1)#1	0.98	2.92	3.757(6)	144
	C(4)-H(4)···Br(1)#2	0.98	3.04	3.866(6)	143
	C(13)-H(13)···O(8)#1	0.93	2.58	3.391(7)	146
	$\pi$ ··· $\pi$ #3			3.847	0
<b>13·CH<sub>3</sub>COCH<sub>3</sub></b>	C(1)-H(1)···O(1)#4	0.98	2.66	3.471(12)	140
	C(4)-H(4)···Br(1)#5	0.98	2.95	3.793(11)	144
	C(13)-H(13)···O(8)#6	0.93	2.53	3.347(10)	147
	$\pi$ ··· $\pi$ #7			3.866	0
<b>14·CHCl<sub>3</sub></b>	C(1)-H(1)···O(1)#4	0.98	2.82	3.678(5)	147
	C(4)-H(4)···Cl(1)#5	0.98	2.89	3.707(5)	142
	C(13)-H(13)···O(8)#4	0.93	2.52	3.311(6)	143
	$\pi$ ··· $\pi$ #7			3.822	0.03
<b>14·CH<sub>3</sub>COCH<sub>3</sub></b>	C(1)-H(1)···O(1)#6	0.92(4)	2.81(4)	3.593(7)	143(3)
	C(4)-H(4)···Cl(1)#8	0.97(5)	2.97(5)	3.790(6)	142(3)
	C(13)-H(13)···O(8)#6	0.98(6)	2.58(6)	3.374(8)	138(5)
	$\pi$ ··· $\pi$ #9			3.898	0.02
<b>14·CH<sub>2</sub>Cl<sub>2</sub></b>	C(1)-H(1)···O(1)#10	0.88(4)	2.835(3)	3.613(5)	147(3)
	C(4)-H(4)···Cl(1)#11	0.96(3)	3.062(4)	3.613(4)	140(3)
	C(13)-H(13)···O(8)#10	0.90(4)	2.57(4)	3.233(5)	130(4)
	$\pi$ ··· $\pi$ #12			4.025	0
<b>14·C<sub>4</sub>H<sub>8</sub>O<sub>2</sub></b>	C(1)-H(1)···O(1) #1	0.98	2.885	3.716(6)	143
	C(4)-H(4)···Cl(1)#8	0.98	2.96	3.738(7)	137
	C(14)-H(14)···O(8)#1	0.93	2.90	3.614(7)	135
	$\pi$ ··· $\pi$ #3			3.889	0
<b>14·C<sub>4</sub>H<sub>8</sub>O</b>	C(1)-H(1)···O(1)#13	0.98	2.92	3.776(4)	146
	C(4)-H(4)···Cl(1)#14	1.00(4)	3.01(4)	3.798(3)	137(3)
	C(13)-H(13)···O(8)#13	0.93	2.55	3.263(4)	134
	$\pi$ ··· $\pi$ #3			3.872	0.02

$\alpha$ = dihedral angle	D-H...A	D-H (Å)	H...A (Å)	D...A (Å)	D-H...A/ $\alpha$ (°)
<b>14·CCl<sub>4</sub></b>	C(1)-H(1)...O(1)#6	0.98	2.82	3.668(7)	145
	C(4)-H(4)...Cl(1)#8	0.98	2.92	3.747(4)	142
	C(13)-H(13)...O(8)#6	0.93	2.54	3.330(6)	143
	$\pi$ ... $\pi$ #9			3.868	0
<b>14·CH<sub>3</sub>NO<sub>2</sub></b>	C(1)-H(1)...O(1)#7	0.98	2.77	3.609(5)	144
	C(4)-H(4)...Cl(1)#14	0.98	2.96	3.767(4)	141
	C(13)-H(13)...O(8)#7	0.93	2.84	3.409(7)	121
	C(14)-H(14)...O(8)#7	0.93	2.67	3.330(6)	129
	$\pi$ ... $\pi$ #15			4.016	0
<b>14·CH<sub>3</sub>CN</b>	C(1)-H(1)...O(1)#16	0.97(2)	2.78(2)	3.669(4)	153(2)
	C(4)-H(4)...Cl(1)#17	0.94(2)	3.04(2)	3.748(3)	133(2)
	C(13)-H(13)...O(8)#18	0.95(3)	2.83(3)	3.539(3)	132(2)
	C(14)-H(14)...O(8)#16	0.94(3)	2.58(3)	3.281(3)	132(2)
	C(18)-H(18)...O(3)#16	0.96(4)	2.71(4)	3.472(5)	137(3)
	$\pi$ ... $\pi$ #15			4.152	0.03
<b>14·ClCH<sub>2</sub>CH<sub>2</sub>Cl</b>	C(1)-H(1)...O(1)#18	0.98	2.91	3.770(4)	146
	C(4)-H(4)...Cl(1)#19	0.98	2.92	3.674(4)	134
	C(14)-H(14)...O(8)#18	0.93	2.60	3.306(5)	133
	C(18)-H(18)...O(3)#20	0.93	2.47	3.366(6)	162
	$\pi$ ... $\pi$ #21			3.914	0
<b>14·C<sub>6</sub>H<sub>6</sub></b>	C(18)-H(18)...O(3)#14	0.93	2.80	3.645(9)	152
	C(14)-H(14)...O(8)#22	0.93	2.61	3.239(8)	126
<b>14·C<sub>6</sub>H<sub>4</sub>(CHO)<sub>2</sub></b>	C(18)-H(18)...O(3)#14	0.95	2.66	3.503(4)	148
	C(14)-H(14)...O(8)#23	0.95	2.47	3.161(3)	129

Symmetry code: #1 -x+1, -y,-z+2; #2 x-1/2, y+1/2,z-1/2; #3 -x+1, -y+1,-z;

#4 -x+2,-y+1,-z+2; #5 x-1/2, -y+1.5, z-1/2; #6 -x+2,-y,-z+2; #7 -x,-y,-z;

#8 x-1/2, -y+1/2,z-1/2; #9 -x+1,-y,-z+1; #10 -x,-y+1,-z; #11 x+1/2,-y+1.5,z+1/2;

#12 -x,-y+2,-z; #13 -x+1,-y,-z; #14 x+1/2,-y+1/2,z+1/2; #15 -x, -y+1,-z;

#16 -x+2,-y+1,-z; #17 x, -y+1.5,z+1/2; #18 -x+2,-y,-z; #19 x, -y+1.2,z+1/2; #20 x-1,y,z;

#21 -x,-y+2,1-z; #22 -x+1/2,-y+1/2,-z+1; #23 -x+1/2, -y+1/2,z-1.

### 8.3.2.3 Host-Guest Assembly and Intermolecular Interactions in Solvates of 13 and 14

Voids created by the association of the neighbouring helices along the ac plane (**Figure 8.20A**) and the dancing pairs down the b-axis (**Figure 8.20B**) accommodate the guest molecules.

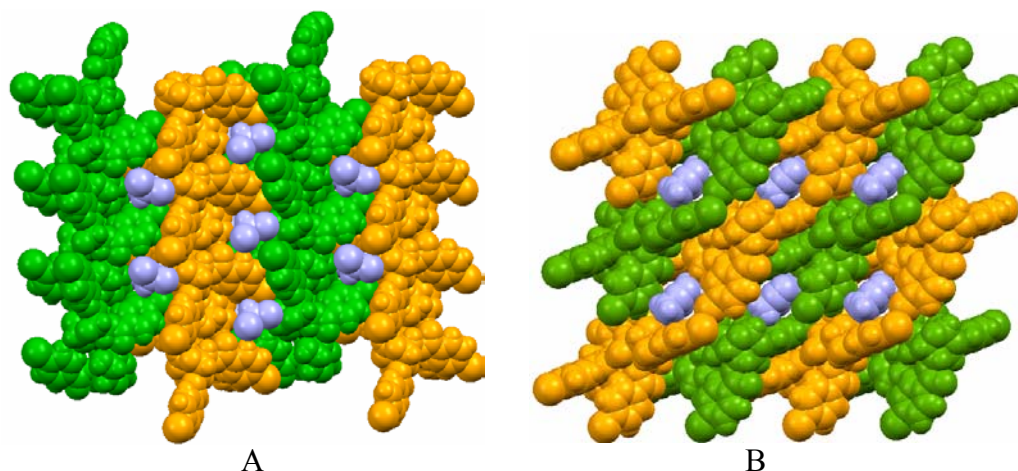


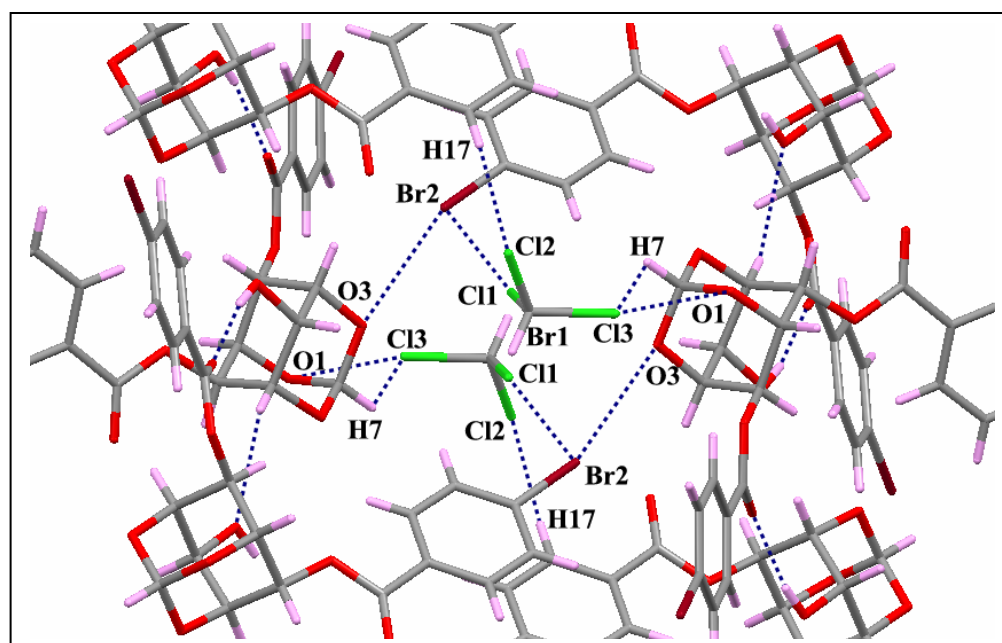
**Figure 8.20.** Representative CPK view of the host-guest assembly in  $14 \cdot \text{CHCl}_3$  and  $14 \cdot \text{CH}_3\text{CN}$ .

#### *Host Guest Interactions $13 \cdot \text{CHCl}_3$ and $14 \cdot \text{CHCl}_3$*

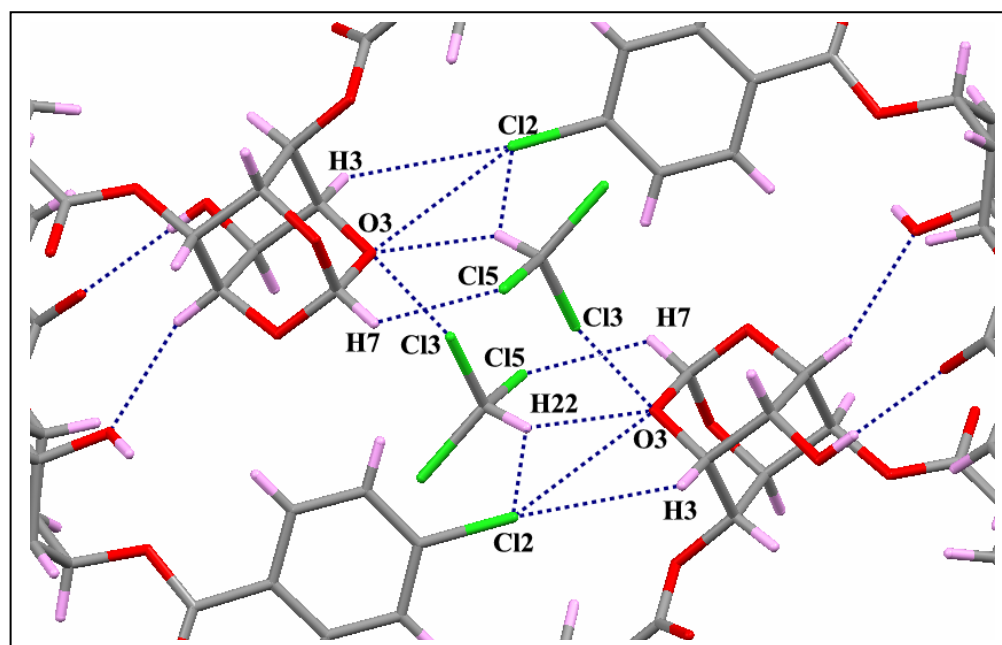
The included chloroform molecules interact via C-H $\cdots$ O and C-H $\cdots$ X interactions in  $13 \cdot \text{CHCl}_3$  and  $14 \cdot \text{CHCl}_3$ . The C22A-H22A of the minor constituents chloroform molecule (*section 8.2.5*) makes dimeric C-H $\cdots$ O contact with the orthoformate bridge oxygen O3 in  $13 \cdot \text{CHCl}_3$  [ $\text{H22A} \cdots \text{O3} = 2.68 \text{ \AA}$ ,  $\angle \text{C22A-H22A} \cdots \text{O3} = 161^\circ$ ] whereas in  $14 \cdot \text{CHCl}_3$  this C-H $\cdots$ O interaction is with the major component chloroform molecules [ $\text{H22} \cdots \text{O3} = 2.68(10) \text{ \AA}$ ,  $\angle \text{C22-H22} \cdots \text{O3} = 138(8)^\circ$ ], **Figure 8.21**]. The orthoformate hydrogen H7 and C17-H17 interact with the guest molecules via two C-H $\cdots$ Cl

interactions, C7-H7...Cl6 [H7...Cl6 = 3.04 Å, C7...Cl6 = 3.816(15) Å  $\angle$ C7-H7...Cl6 = 137°, chlorine atom Cl6 is of the minor occupancy chloroform molecule which is not shown in the Figure] and C17-H17...Cl2 [H17...Cl2 = 3.13 Å, C17...Cl2 = 4.059(8) Å  $\angle$ C17-H17...Cl2 = 174°] in **13·CHCl<sub>3</sub>** (**Figure 8.21A**). The guest chloroform molecule is also involved in short Cl...Br and Cl...O contacts with the host. The Cl...O contact is longer than sum of van der Waals radii and  $\angle$ C-Cl...O deviates from linearity [Cl3...O1 = 3.45 Å and  $\angle$ C22-Cl3...O1 = 136.3°] To sum up the chloroform molecule in **13·CHCl<sub>3</sub>**, makes one C-H...O, two C-H...Cl, Cl...Br and Cl...O contact with the host.

In **14·CHCl<sub>3</sub>**, the chloroform molecule is also involved in C-H...Cl, Cl...Cl and Cl...O contacts other than C-H...O interaction (**Figure 8.21B**). Two C-H...Cl interactions, C7-H7...Cl5 [H7...Cl5 = 3.05 Å, C7...Cl5 = 3.753(6) Å,  $\angle$ C7-H7...Cl5 = 130°] and C22-H22...Cl2 [H22...Cl2 = 2.95 Å, C22...Cl2 = 3.608(11) Å,  $\angle$ C22-H22...Cl2 = 120°] are weaker compared to the C-H...Cl interaction found in **13·CHCl<sub>3</sub>**. The Cl...O contact is longer than the sum of van der Waals radii and  $\angle$ C-Cl...O is close to linearity [Cl3...O3 = 3.441 Å and  $\angle$ C22-Cl3...O3 = 159.5°].



A



B

**Figure 8.21.** Host-guest interactions in A)  $13 \cdot \text{CHCl}_3$  and B)  $14 \cdot \text{CHCl}_3$ .



*Host-Guest Interactions in 13·CH<sub>3</sub>COCH<sub>3</sub> and 14·CH<sub>3</sub>COCH<sub>3</sub>*

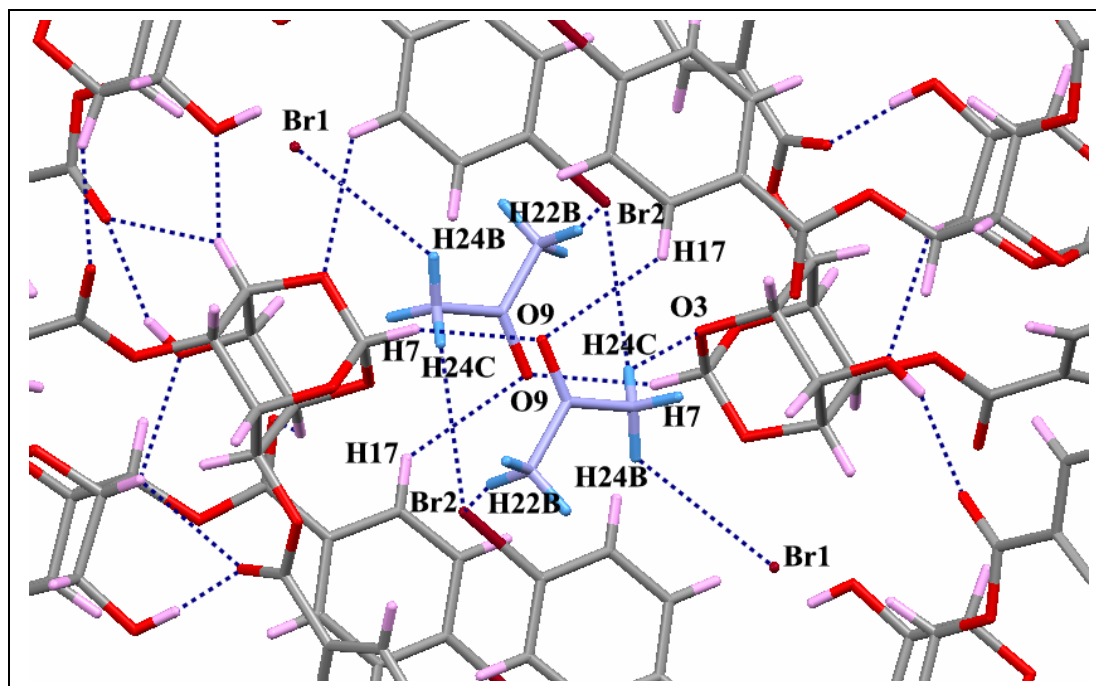
In **13·CH<sub>3</sub>COCH<sub>3</sub>** and **14·CH<sub>3</sub>COCH<sub>3</sub>** the included acetone molecule is involved in C-H···O and C-H···X interactions (**Table 8.11**). The carbonyl oxygen O9 of acetone is involved in bifurcated H-bonding interactions, C7-H7···O9 and C17-H17···O9 with the host. The former contact is short and close to linearity whereas the latter contact is somewhat compromised. The methyl groups of the acetone in **13·CH<sub>3</sub>COCH<sub>3</sub>** are also involved in C-H···O (C24-H24A···O8 and C24-H24C···O3) and C-H···X (C22-H22B···Br2, C24-H24C···Br2 and C24-H24B···Br1) interactions with the host. In **14·CH<sub>3</sub>COCH<sub>3</sub>**, the methyl groups of acetone are not involved in any C-H···O interaction but form C-H···X interactions C22-H22B···Cl2 and C24-H24C··· Cl2 (**Figure 8.22 B**)

**Table 8.11:** Host-guest interactions in acetone inclusion crystals of **13** and **14**

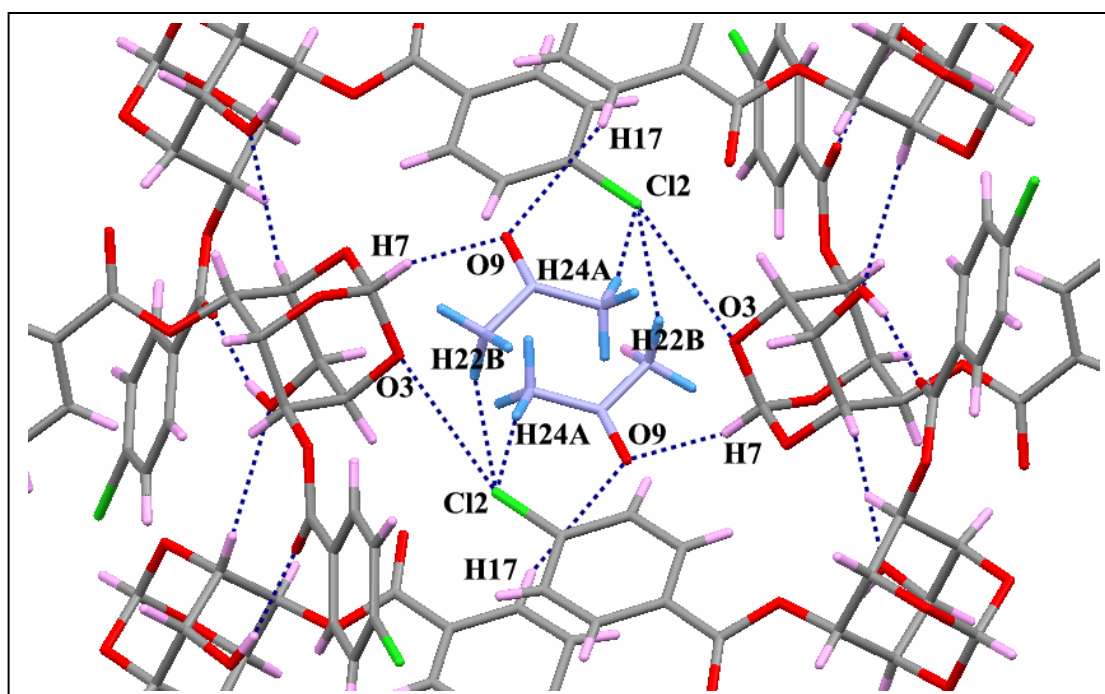
	D-H···A	D-H (Å)	H···A (Å)	D···A (Å)	D-H···A (°)
<b>13· CH<sub>3</sub>COCH<sub>3</sub></b>	C(24)-(24C)···O(3)#1	0.96	2.76	3.550(17)	140
	C(24)-H(24A)···O(8)#2	0.96	2.80	3.632(19)	145
	C(7)-H(7)···O(9)#3	0.98	2.30	3.243(19)	160
	C(17)-H(17)···O(9)#4	0.93	2.72	3.381(20)	129
	C(22)-H(22B)···Br(2)#4	0.93	2.94	3.755(20)	143
	C(24)-H(24C)···Br(2)#5	0.96	3.15	4.012(16)	150
	C(24)-H(24B)···Br(1)#6	0.96	3.13	3.822(20)	130
<b>14· CH<sub>3</sub>COCH<sub>3</sub></b>	C(7)-H(7)···O(9)#7	0.92(4)	2.38(4)	3.265(9)	160
	C(17)-H(17)···O(9)#4	0.82(6)	2.80(6)	3.473(11)	140
	C(22)-H(22B)···Cl(2)#4	0.96	3.00	3.905(17)	159
	C(24)-H(24A)···Cl(2)#8	0.96	3.08	4.032(19)	171

Symmetry codes: #1 x,y,x; #2 3/2-x,1/2+y, 3/2-z; #3 1-x,1-y,2-z; #4 3/2-x, -1/2+y, 3/2-z; #5 -1/2+x,3/2-y,1/2+z; #6 -1/2+x,3/2-y,-1/2+z; #7 1-x,-y,2-z; #8 -1/2+x, 1/2-y, 1/2+z.





A



B

Figure 8.22. Host-guest interactions in A)  $13 \cdot \text{CH}_3\text{COCH}_3$  and B)  $14 \cdot \text{CH}_3\text{COCH}_3$ .

*Host-Guest Interactions in 14·CH<sub>2</sub>Cl<sub>2</sub>*

The included CH<sub>2</sub>Cl<sub>2</sub> molecule interacts via weak C-H···Cl and C-Cl···O contact C7-H7···Cl4 [H7···Cl4 = 3.10 Å, C7···Cl4 = 3.677 Å, ∠C7-H7···Cl4 = 122°], C17-H17···Cl3 [H17···Cl3 = 2.94 Å, C17···Cl3 = 3.569 Å, ∠C17-H17···Cl3 = 126°] and C22-Cl3'···O3 [Cl3'···O33 = 3.296 Å, ∠C22-Cl3'···O3 = 146.8°], C22-Cl4'···O1 [Cl4'···O1 = 3.425 Å, ∠C22-Cl4'···O1 = 138.9°] halogen bond contact with the host (**Figure 8.23**). Both C-H···Cl contacts (C7-H7···Cl4 and C17-H17···Cl3) are shorter than the van der Waals radii sum but deviate from linearity whereas both halogen bonding contacts are longer than the sum of van der Waals radii and also not so linear.

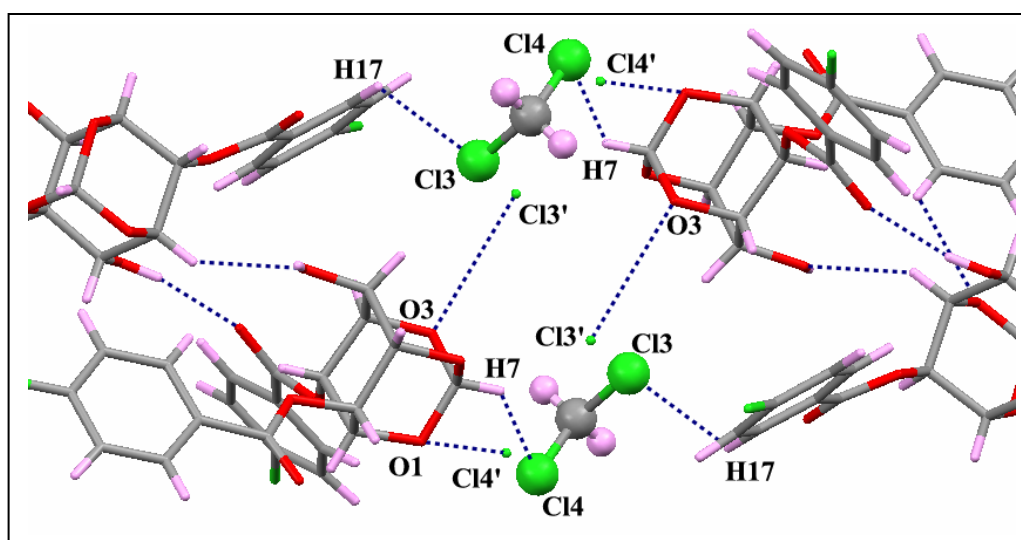


**Figure 8.23.** Host-guest interactions in 14·CH<sub>2</sub>Cl<sub>2</sub>, some atoms of the host are omitted for the sake of clarity.

*Host-Guest Interactions in 14·C<sub>4</sub>H<sub>8</sub>O<sub>2</sub>*

The dioxane molecule in 14·C<sub>4</sub>H<sub>8</sub>O<sub>2</sub> is engaged in C-H···O and C-H···Cl interactions with the host (**Figure 8.24**). The orthoformate hydrogen H7 of the host

makes short and linear C-H $\cdots$ O contact with the ether oxygen O10 of the dioxane [H7 $\cdots$ O10 = 2.22 Å, C7 $\cdots$ O10 = 3.128(3) Å,  $\angle$ C7-H7 $\cdots$ O10 = 153°]. Other ether oxygen O9 of dioxane interacts with the host via weak C13-H13 $\cdots$ O9 [H13 $\cdots$ O9 = 2.76 Å, C13 $\cdots$ O9 = 3.348(3) Å,  $\angle$ C13-H13 $\cdots$ O9 = 122°] contact. The methylene protons make weak C-H $\cdots$ O and C-H $\cdots$ Cl interactions C23-H23A $\cdots$ O8 [H23A $\cdots$ O8 = 2.69 Å, C23 $\cdots$ O8 = 3.421(3) Å,  $\angle$ C23-H23A $\cdots$ O8 = 132°], C25-H25B $\cdots$ O3 [H25B $\cdots$ O3 = 2.55 Å, C25 $\cdots$ O3 = 3.305(2) Å,  $\angle$ C25-H25B $\cdots$ O3 = 134°], C25-H25A $\cdots$ O8 [H25A $\cdots$ O8 = 2.87 Å, C25 $\cdots$ O8 = 3.828(2) Å,  $\angle$ C25-H25A $\cdots$ O8 = 172°], and C25-H25B $\cdots$ Cl2 [H25B $\cdots$ Cl2 = 2.89 Å, C25 $\cdots$ Cl2 = 3.716(2) Å,  $\angle$ C25-H25B $\cdots$ Cl2 = 143°] with the host. Thus, the dioxane makes total six interactions with the host four C-H $\cdots$ O and two C-H $\cdots$ Cl contacts, thereby stabilizing the host-guest assembly.

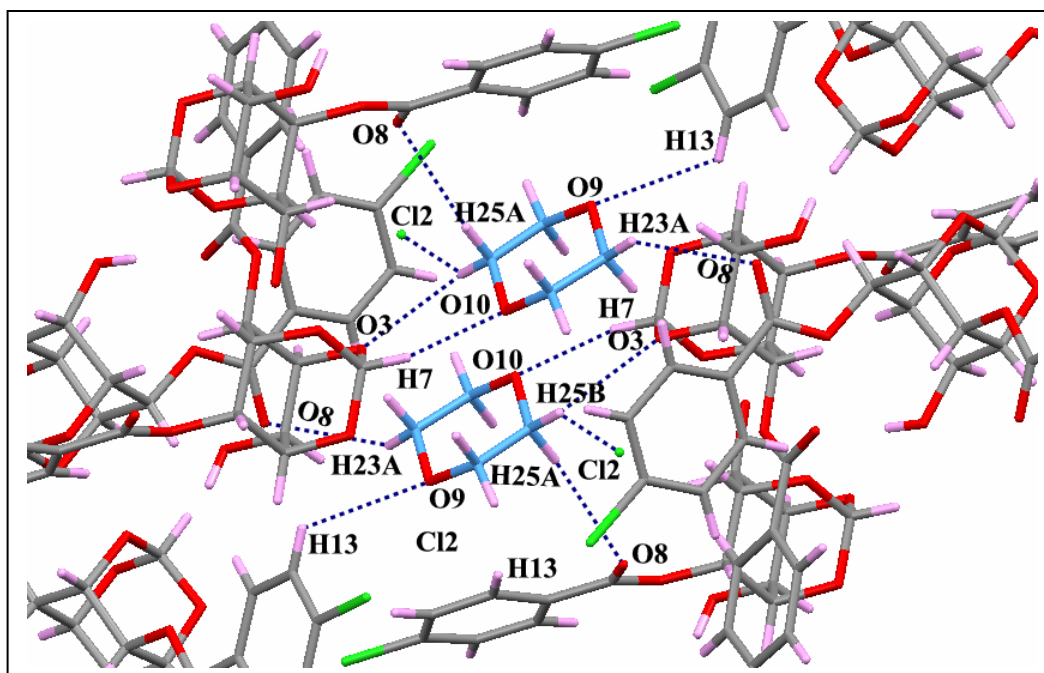


**Figure 8.24.** Host-guest interactions in  $14 \cdot C_4H_8O_2$ .

*Host-Guest Interactions in 14·C<sub>4</sub>H<sub>8</sub>O*

THF molecule in **14·C<sub>4</sub>H<sub>8</sub>O** inclusion crystals makes notably three interactions with the host (**Figure 8.25**), one C-H···O [C7-H7···O9, H7···O9 = 2.40 Å, C7···O9 = 3.310(3) Å, ∠ C7-H7···O9 = 155°] and two C-H···Cl [C22-H22A···Cl2, H22A···Cl2 = 3.10 Å, C22···Cl2 = 4.195(4) Å, ∠ C22-H22A···Cl2 = 123° and C25-H25A···Cl1, H25A···Cl1 = 3.11 Å, C25···Cl1 = 3.730(3) Å, ∠ C25-H25A···Cl1 = 124°]. The geometry of the C-H···O contact is short and linear compared to the C-H···Cl interactions.

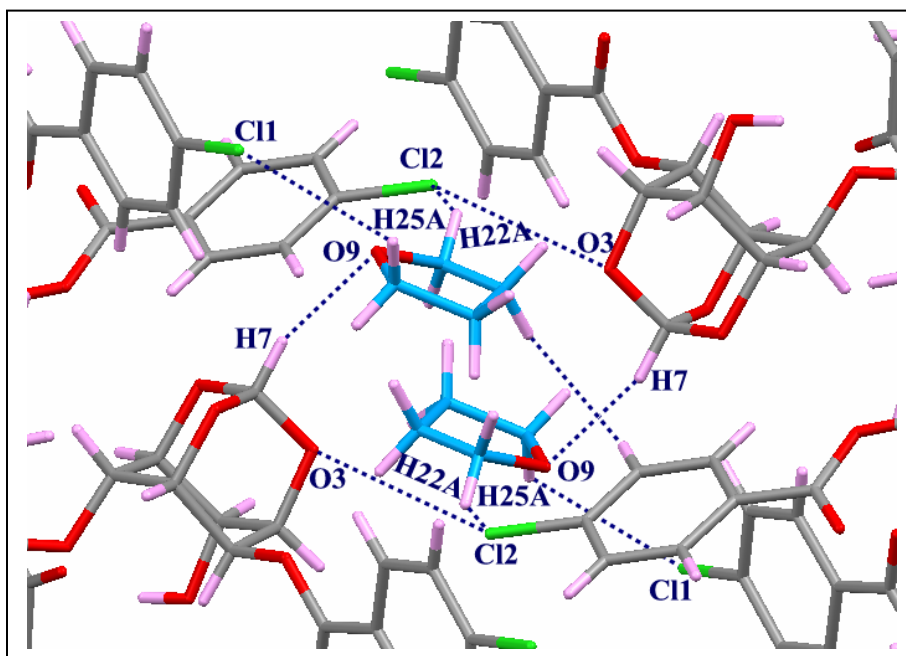


**Figure 8.25.** Host-guest interactions in **14·C<sub>4</sub>H<sub>8</sub>O**.

*Host-Guest and Guest-Guest Interactions in 14·CCl<sub>4</sub>*

In **14·CCl<sub>4</sub>** inclusion crystals, the CCl<sub>4</sub> molecule makes weak C-H···Cl, short C-X···O and Cl···Cl contacts with the host molecule (**Figure 8.26**). The C17-H17···Cl5 contact is shorter than the sum of the van der Waals radii but the angle deviates too much

from the linearity. The two halogen bonding contacts namely C22-Cl6 $\cdots$ O1 [Cl6 $\cdots$ O1 = 3.143 Å  $\angle$ C22-Cl6 $\cdots$ O1 = 140.4°] and C22-Cl4 $\cdots$ O3 [Cl4 $\cdots$ O3 = 3.268 Å,  $\angle$ C22-Cl4 $\cdots$ O3 = 154°] differ in geometrical parameters, former contact is much shorter than the sum of van der Waals radii but the angle is not so linear, whereas the latter contact is almost equal to the sum of van der Waals radii and angle of approach is better than the former one. It is important to mention here that the halogen atoms Cl4 and Cl6 that are involved in halogen bonding contact are not disordered whereas the other two halogens Cl5 and Cl7 (not involved in halogen bonding) show more thermal vibrations and are disordered. The CCl<sub>4</sub> molecule also makes Cl5 $\cdots$ Cl11 (3.234 Å) contact of type II (angle at both halogen atom is almost the same) with the host. The halogens of the CCl<sub>4</sub> molecule are also involved in guest-guest short X $\cdots$ X (Cl5 $\cdots$ Cl3 = 2.561 Å) interaction of type I category, i.e. the angle at both halogens is almost the same and close to linearity (angle at Cl5 = 172.7° and angle at Cl3 = 154.5°).

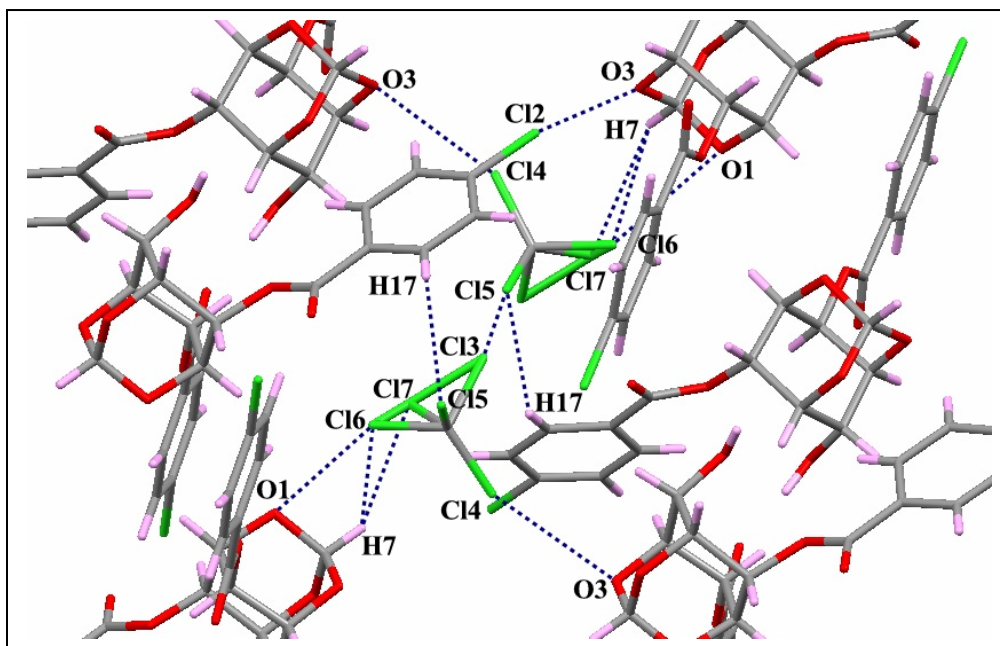


**Figure 8.26.** Host-guest and guest-guest interactions in 14·CCl<sub>4</sub>.

*Host-Guest Interactions in 14·CH<sub>3</sub>NO<sub>2</sub>*

The oxygen atoms of the nitro groups in **14·CH<sub>3</sub>NO<sub>2</sub>** make two short and linear C-H···O interactions with the host (**Figure 8.27**). The O9 of the nitromethane molecules accepts proton from the orthoformate H7 and the other oxygen O10 accepts H-atom from C13-H13 of the C2-*O-p*-chloro-benzoyl group. Both these interactions have comparable geometries [C7-H7···O9, H7···O9 = 2.53 Å, C7···O9 = 3.365 Å, ∠ C7-H7···O9 = 161° and C13-H13···O10, H13···O10 = 2.61 Å, C13···O10 = 3.463 Å, ∠ C13-H13···O10 = 152°].

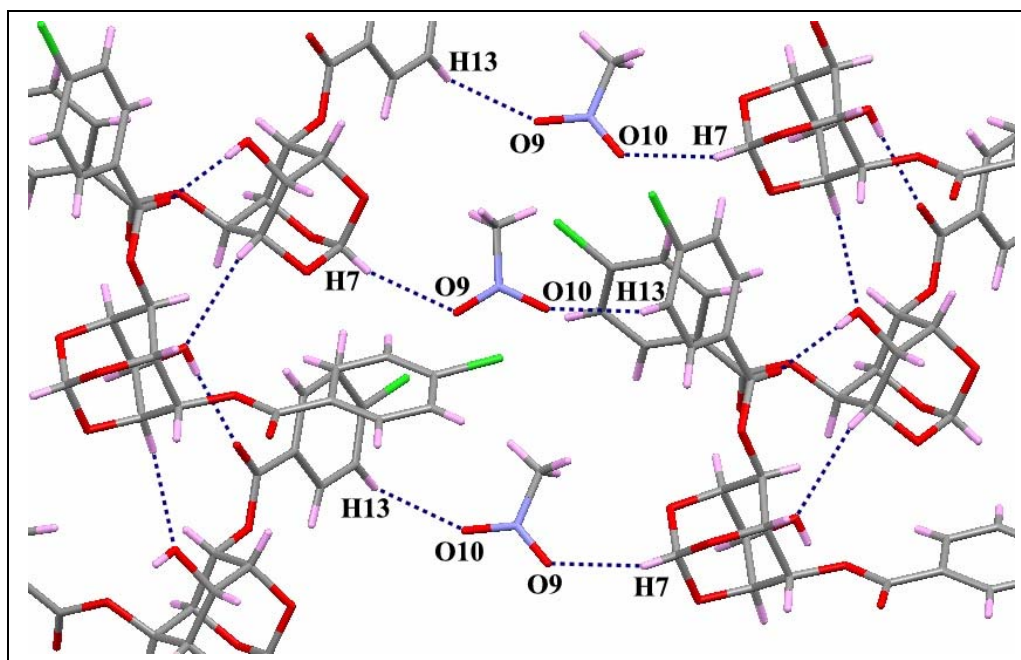


**Figure 8.27.** Host···guest interactions in **14·CH<sub>3</sub>NO<sub>2</sub>**.

*Host-Guest Interactions in 14·CH<sub>3</sub>CN*

Acetonitrile molecule in **14·CH<sub>3</sub>CN** makes two C-H···N contacts (**Figure 8.28**), such as C7-H7···N1 [C7-H7···N1, H7···N1 = 2.56 Å, C7···N1 = 3.450 Å, ∠ C7-H7···N1 =



167°] and C17-H17...N1 [H17...N1 = 2.78 Å, C17...N1 = 3.656 Å,  $\angle$ C17-H17...N1 = 151°] with the host. The former contact is very short and more linear compared to the latter. The methyl group of the acetonitrile molecule is not involved in any contact.

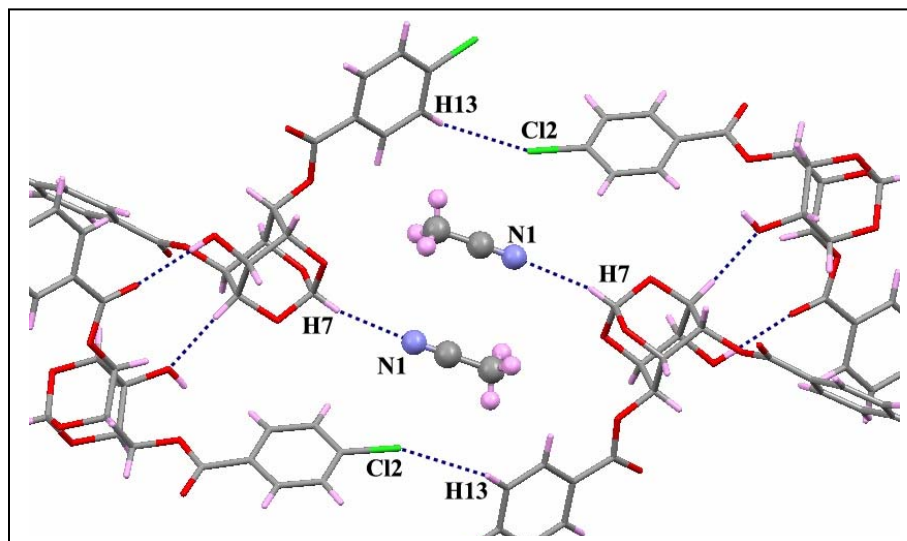


**Figure 8.28.** Host-guest interactions in **14**·CH<sub>3</sub>CN.

#### *Host-Guest Interactions in 14·ClCH<sub>2</sub>CH<sub>2</sub>Cl*

In **14**·ClCH<sub>2</sub>CH<sub>2</sub>Cl, methylene group of dichloroethane molecule and one of the Cl atoms are disordered over two positions. The ordered chlorine atom Cl3 makes short and linear Cl... $\pi$  contact<sup>40</sup> with the phenyl ring of the axial C6-*O*-*p*-chloro-benzoyl group [Cl3...Cg = 3.612 Å,  $\angle$ C22-Cl3...Cg = 164.4°, Cg -centroid of the phenyl ring C16-C21 **Figure 8.29**), whereas both the positions of the disordered chlorine atom Cl4 and Cl4' are involved in C-H...Cl interactions with the orthoformate H-atom, C7-H7...Cl4 [H7...Cl4 = 2.74 Å, C7...Cl4 = 3.674 Å,  $\angle$ C7-H7...Cl4 = 159°] and C7-H7...Cl4' [H7...Cl4' = 3.00 Å, C7...Cl4' = 3.983 Å,  $\angle$ C7-H7...Cl4' = 179°]. The methylene groups are not involved in any significant interactions with the host.

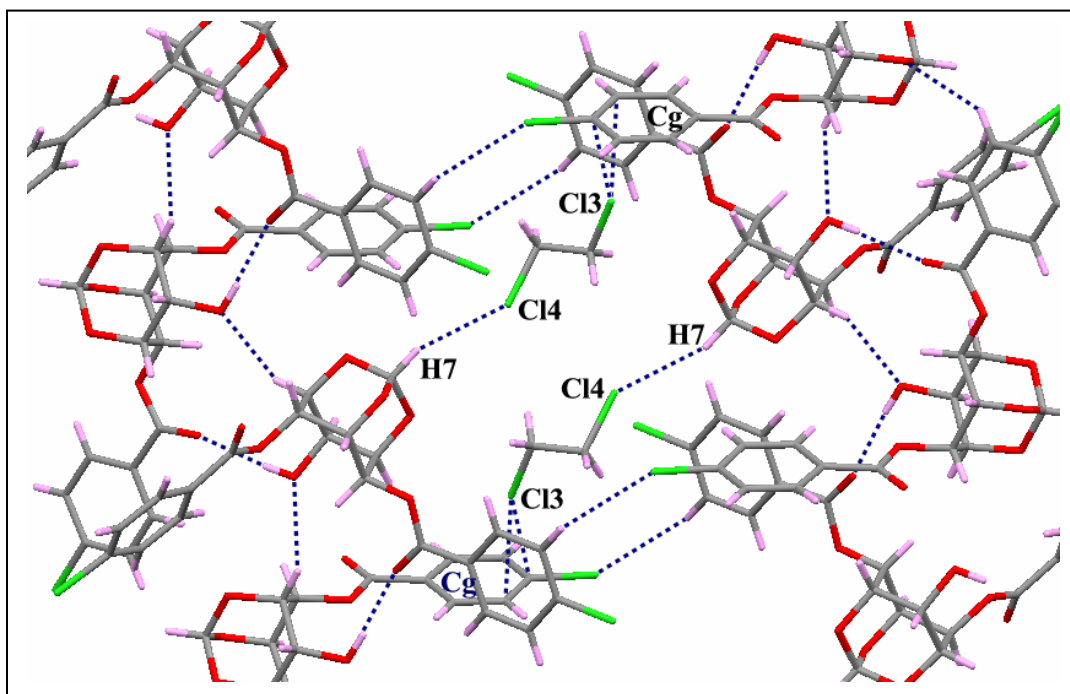


**Figure 8.29.** Host-guest interactions in  $14 \cdot \text{ClCH}_2\text{CH}_2\text{Cl}$ .

### *Host-Guest and Guest-Guest Interactions in $14 \cdot \text{C}_6\text{H}_6$*

The non-involvement of the both benzene molecules in any significant host-guest interactions in  $14 \cdot \text{C}_6\text{H}_6$  could be the reason for the instability of the inclusion crystals. The orthoformate H-atom (H7) makes marginal C-H $\cdots$  $\pi$  interactions with the edge of the disordered benzene molecule and the benzene molecule which occupies two fold-axis makes marginal C-H $\cdots$ O (interaction with the ester oxygen O2 of the host [C22-H22 $\cdots$ O2, H22 $\cdots$ O2 = 2.99 Å, C22 $\cdots$ O2 = 3.895 Å,  $\angle$ C22-H22 $\cdots$ O2 = 166°]). Both benzene molecules in  $14 \cdot \text{C}_6\text{H}_6$  are interacting with each other via weak C-H $\cdots$  $\pi$  contacts forming T-shape<sup>14a</sup> extended polymeric chain in the channel created by the host molecules (**Figure 8.30**).



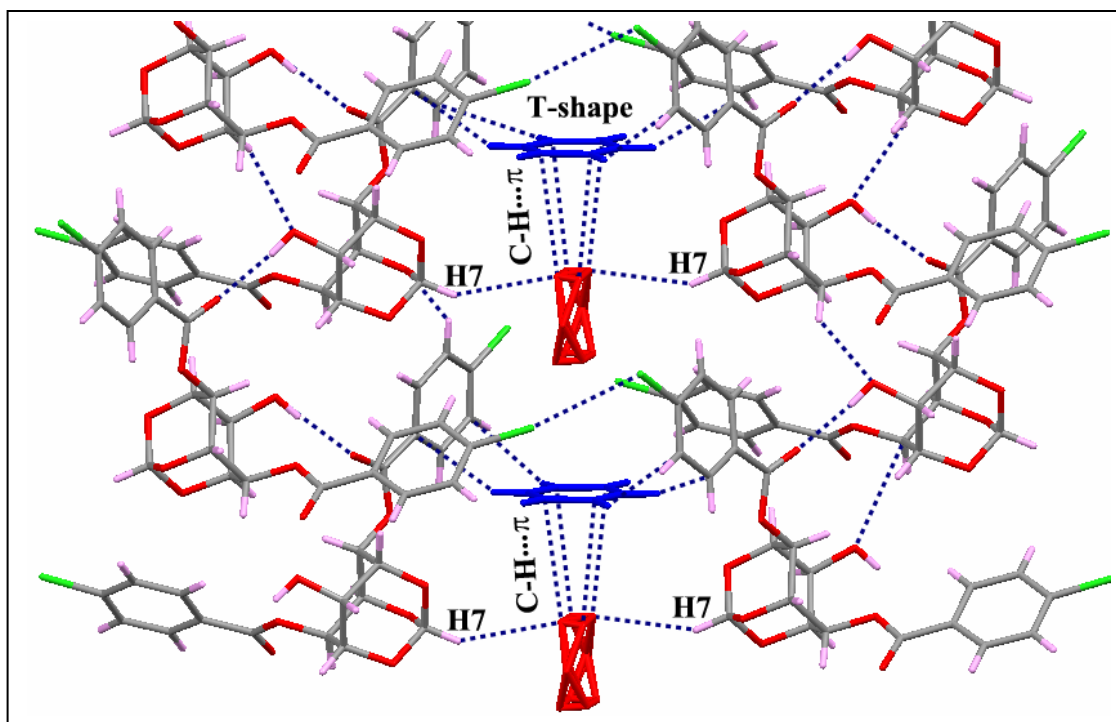


**Figure 8.30.** Host-guest and guest-guest interactions in  $14 \cdot C_6H_6$ .

***Host-Guest and Guest-Guest Interactions in  $14 \cdot C_6H_4(CHO)_2$***

The terephthalaldehyde [ $C_6H_4(CHO)_2$ ] molecule in  $14 \cdot C_6H_4(CHO)_2$  occupies the channel formed by the dancing pairs down the b-axis. The terephthalaldehyde molecule is engaged in the C-H...O interactions with the orthoformate H atom of the host molecule across the two-fold axis [ $C7-H7 \cdots O9$  and  $C7-H7 \cdots O10$ ,  $H7 \cdots O9(O10) = 2.711 \text{ \AA}$ ,  $C7 \cdots O9(O10) = 3.646 \text{ \AA}$ ,  $\angle C7-H7 \cdots O9(O10) = 156^\circ$ ]. In the channel the terephthalaldehyde molecules, which are on the C2-axis by forming extended linear polymeric chain link to each other via short  $O \cdots O$  ( $2.644 \text{ \AA}$ ) contacts (**Figure 8.31**).

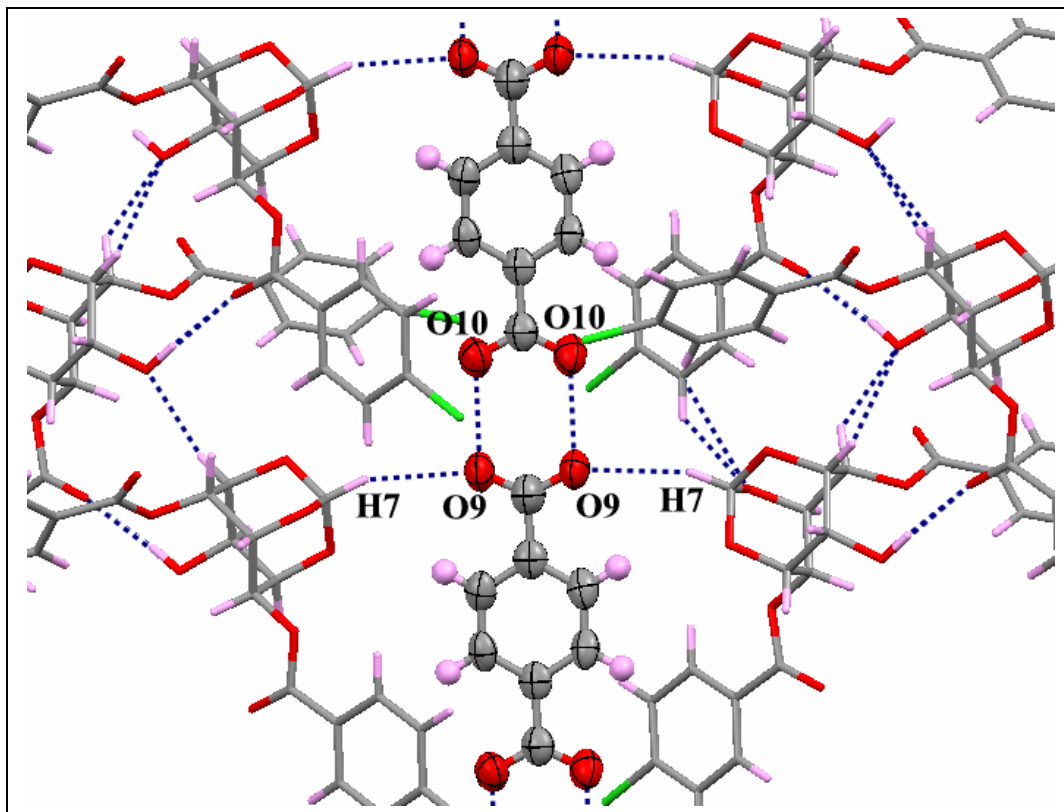


**Figure 8.31.** Host-guest interactions in  $14 \cdot \text{C}_6\text{H}_4(\text{CHO})_2$ .

#### 8.3.2.4 Difference in Association of Molecules in Polymorphs and Solvates of **13** and **14**

In polymorphs of **13** and **14** (Form I and Form II crystals) molecules do not assemble by forming intermolecular  $\text{O}-\text{H} \cdots \text{O}$  hydrogen bond with the  $\text{O}=\text{C}$  of the  $\text{C}2$ - $\text{O}$ - $p$ -halo-benzoyl group molecules but they are linked via  $\text{O}4-\text{H}4\text{A} \cdots \text{O}3$  contact to form one-dimensional molecular string and these strings are associated centrosymmetrically in head-to-head fashion leaving no room for solvent inclusion (**Figure 8.10**). It is thought

that during nucleation of the inclusion complexes, the included solvent molecule could be interacting with the orthoformate bridge in solution preventing the host molecules to associate in head to head fashion as observed in the dimorphs of **13** and **14** (**Figure 8.10**). Hence, host molecules associate via O-H...O contact to form helical assemblies resulting in the formation inclusion crystals (**Figure 8.32**). The three different modifications of inclusion crystals of **14** could be due to the bridging of the helices via diverse guest molecules having different size and shapes.

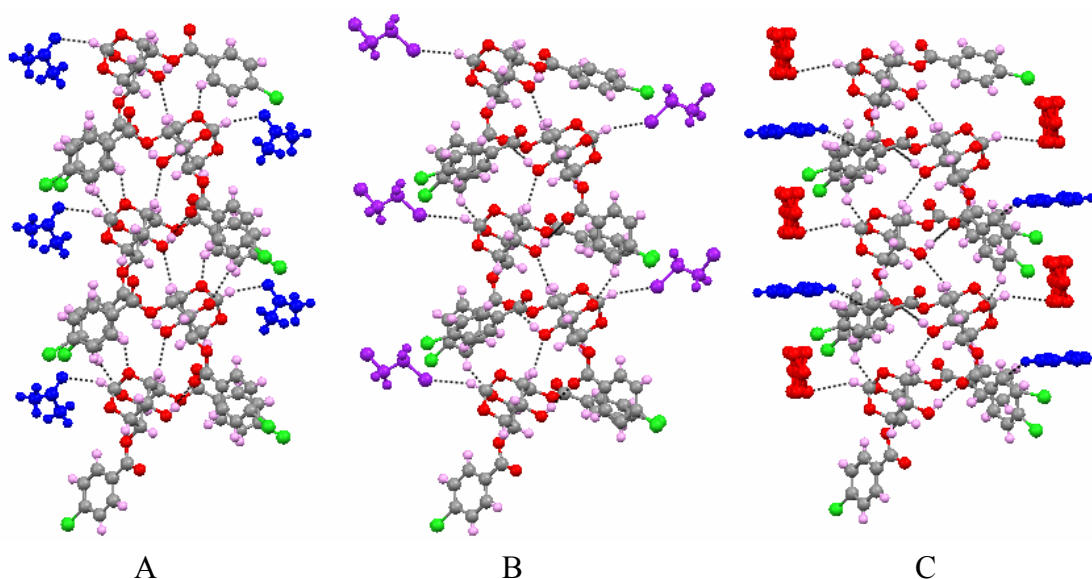


**Figure 8.32.** The solvent molecules in the three modifications A)  $P2_1/n$ , B)  $P2_1/c$  and C)  $C_2/c$ , keep the orthoformate bridge engaged in solute-solvent interactions, allowing the host molecules to assemble in helical pattern.

## 8.4 Conclusions

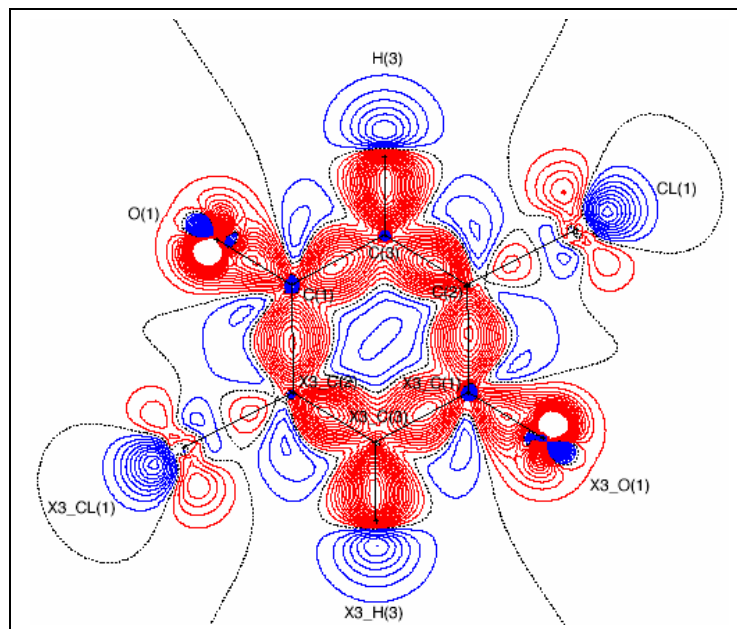
The presence of hydroxyl in **13** and **14**, changed the overall organization of the molecules due to O-H...O hydrogen bonding. But, this kept the halogen bonding contact between the halogen of the axial benzoate group and C=O of the equatorial benzoate group conserved. It is noteworthy that the same halogen-bonding interaction exists in polymorphic modifications of **13** and **14** even in the presence strong O-H...O hydrogen bonding interactions. The yield of polymorph possessing halogen-bonding contacts was more compared to the non-halogen bonded form, again suggesting the preference for the 'halogen bonding' in the molecular aggregation. Thermal conversion of Form I crystals of **13**, containing C-H...Br bridges to those containing C-Br...O=C bridges (Form II) reinforces the preference of halogen bonding over other interaction. The pseudopolymorphic behaviour of **13** and **14** that includes a whole range of organic solvents within different voids created by packing of almost identical helical self-assembly of the host is striking. Even a trace of a solvent, which can interact with the orthoformate bridge, seems to trigger the helix formation of the host, an observation almost similar to spontaneous crystallization of **3** by very low concentration of dihalomethane. However, no specificity towards size and shape of the guest solvents was observed here in contrast to that observed in case of **3** (Chapter 2).

# Chapter 9

## Part A: General Conclusion

## Part B: Charge Density Study

## Part C: Scope of Future Work



# Chapter 9

## Part A: General Conclusions

### 9.1 On exhibiting (Pseudo) Polymorphic Behaviour

The work reported in this dissertation triggered off from the observation that *myo*-inositol derivative **3** (Chapter 2) formed inclusion crystals with a very high specificity towards dihalomethane. This remarkably high affinity and dependency on  $\text{CH}_2\text{X}_2$  is one of the rare examples of molecular recognition in small molecular organic systems. The more intriguing was the nature of weak intermolecular interactions that held the guest molecules by the host system, essentially C-H $\cdots$ O and C-Cl $\cdots$ O type contacts - the later termed as ‘halogen bonding’ is what is pursued in this work and will be looked in detail in future.

The Chapters 3, 4 and 5 report the effect of synthetic modification of **3** on its high guest selectivity and specificity. However, none of the derivatives, **4**, **7** and **8**, retained this property – although, all formed the inclusion complexes with various guests, mostly with halogenated solvents! It was remarkable to see that a striking common feature in all these four derivatives was the intermolecular association that formed trifurcated centrosymmetric dimer (**Figure 9.1**). It was revealing from these structural elucidations that the zero dimensional molecular isostructurality does not guarantee any similarity in

their pseudopolymorphic or inclusion behaviour. This is because their one, two and three-dimensional organization create quite different environments that capture the guest solvents accordingly.

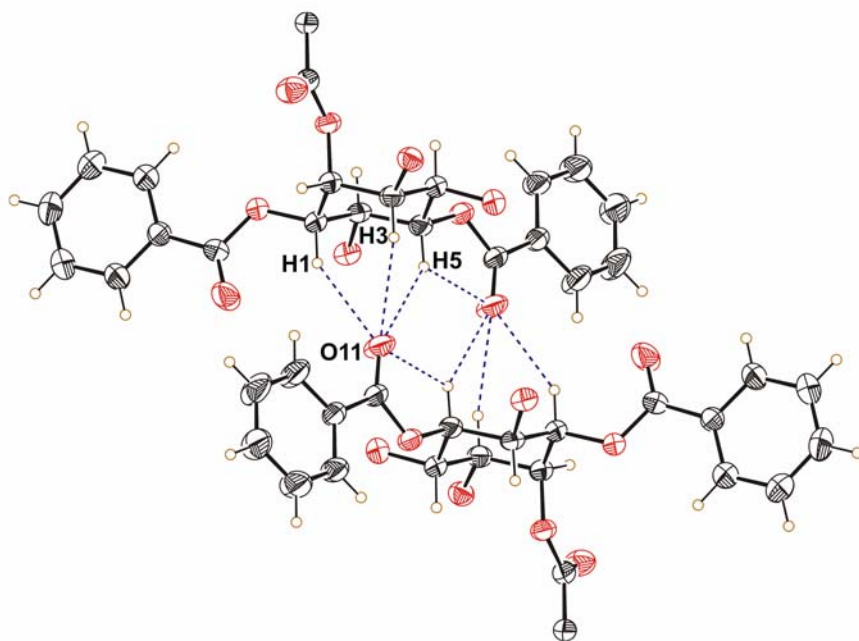


**Figure 9.1.** Centrosymmetric trifurcated C-H...O assembly.

These studies brought out a striking (and somewhat obvious!) feature pertaining to the nature of the guest binding and the stability (even specificity) of the inclusion complex crystals. The specific inclusion was observed in Chapter 2 where the guest bridges the centrosymmetric dimers (**Figure 9.2A**), further imposing its own two-fold symmetry on the supra molecular association. Whereas, the non-specific inclusions were noticed when the trifurcated dimeric synthons (**Figure 9.1**) of the host molecules created a channeled framework (**Figure 9.2B**) themselves in the crystal lattice without guest playing any structural role, as was seen in Chapters 3, 4 and 5.

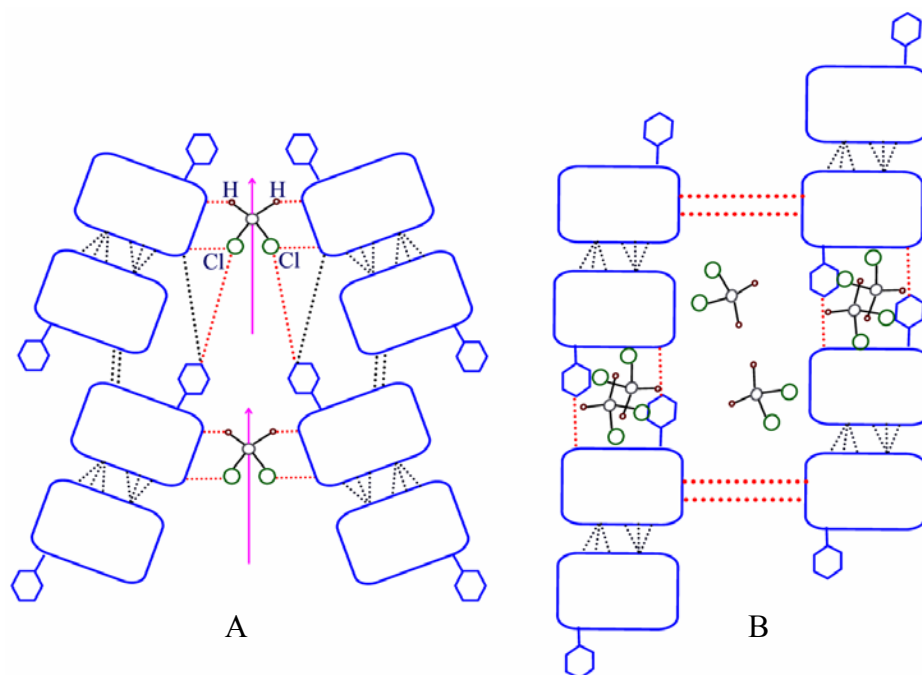


**Figure 9.2.** Cartoon representation-showing difference in association of the guest molecule with the host *myo*-inositol derivatives, A) in **3** and B) in **4**, **7** and **8**.

Chapters 6, 7 and 8 report orthoester bridged *myo*-inositol derivatives that showed remarkable polymorphic as well as pseudopolymorphic behaviour, with somewhat rare possibility of single crystal-to-crystal phase transitions between the two polymorphs. In all these ortho-bridged systems, the bridge heads tend to associate with each other via weak C-H $\cdots$ O type interactions and orientationally flexible pendant phenyl rings create the different crystalline environments. Remarkably, in all these structures, the halogen bonding was observed either between host-guest (Chapters 6 and 8) or between the molecules (Chapters 7 and 8).



The role of guest in this case is highly decisive, infact it is the initiator in the formation of the crystal itself. Although, this is seen so clearly, designing host systems that are specific to small organic molecules is not at all trivial but will always be a very challenging task. The specificity observed serendipitously in derivative **3** would be difficult to optimize further or modify for other guests. The amazingly complex task carried out by large biological molecules such as enzymes, in binding substrates having specific isomeric properties or certain chiralities will continue to provide an inspiration for designing systems that are made with specific molecular recognition in mind.

# Chapter 9

## Part B: Charge Density Study of Model Compound

### 9.2 Introduction

As electrons in an atom scatter X-rays more strongly than that of the nuclei, intensities of scattered X-rays are almost exclusively determined by the distribution of the electrons in crystals i.e. charge density. Measurement of charge densities in molecular crystals using high-resolution single crystal X-ray diffraction data has now reached a level where highly reliable experimental data that can be compared with theoretical estimations can be obtained. This has become possible because of the rapid accumulation of extremely accurate data sets due to advancement in experimental techniques, measuring devices and high-speed computation.<sup>154</sup> Several recent books, reviews and articles highlight the application of X-ray charge density analysis and developments in both experiment and theory for mapping charge densities to deduce structure property correlations.<sup>155</sup> Extraction of detailed charge density distributions of organic, organometallic, inorganic, ionic, metallic and mineral crystalline systems from X-ray

diffraction data is becoming a mature and highly productive field and is one of the most dynamic areas of modern X-ray crystallography.

It is noteworthy that crystallographic experiments allow for the identification of intermolecular interactions and with accurate data sets followed by a charge density mapping, information on charge distribution in the molecule can be analyzed. The nature of chemical interactions can be evaluated in terms of the deformation densities using Hansen and Coppens formalism<sup>156</sup> incorporated in the package XD<sup>157</sup>. In this formalism the individual atomic densities are divided into three components, the core, the spherical expansion and contraction term ( $k$ ) in the valence shell and the valence deformation in terms of density normalized spherical harmonics ( $d_{lm\pm}$ ), together with the corresponding radial expansion and contraction ( $k'$ ) of the valence shell (For details see Appendix II). The derived electron densities are then subjected to the Bader's quantum theory of 'Atoms In Molecules' (AIM),<sup>158</sup> which allows for the interpretation of detailed topological analysis that marked as local maxima at the positions of the nuclei. This theory is established as the most powerful tool to analyze and interpret the charge densities obtained from both experiment and theory. It is based on the identification of critical points (CP, classified using the Hessian matrix<sup>159</sup> of the electron density), the bond critical points (BCPs) lie along the bond path where the gradient of the electron density vanishes i. e.  $\Delta\rho_b(r) = 0$ , the mapping of bond paths which trace the inter-nuclear distance (BP, *the line of the highest electron density, referred to as the interaction line, with its length,  $R_{ij}$ , defines the "bond path" between any two atoms*). The second derivative of the electron density, the Laplacian  $\nabla^2\rho_b(r)$  that brings out the nature of intra and intermolecular interactions, for example  $\nabla^2\rho_b(r) < 0$  represents shared interactions

while  $\nabla^2\rho_b(r) > 0$  represents closed-shell interactions. The bond paths, interaction lines, and Laplacian values together represent the topology of the charge density distribution in a given molecule.

### 9.3 Charge Density and Weak Intermolecular Interactions

Evaluation of weak interactions has become an area of enormous interest since it provides the basis for supramolecular aggregation. Charge density analysis has gained immense importance in recent years, because it allows one to observe and quantify the intermolecular interactions beyond distance-angle geometry criteria. The topological analysis however, does not specify the character of the bond but only indicates the existence of a bond. In order to characterize weak and strong hydrogen bonds and to distinguish these from pure van der Waals interactions in terms of specific properties like bond order, ionicity and conjugation, the properties evaluated at the BCPs become crucial. Koch and Popelier<sup>160</sup> have proposed eight criteria to establish hydrogen bonding in particular, which allow a hydrogen bond to be distinguished from a van der Waals interaction. Among these eight criteria, the first four are sufficient with the fourth being *necessary and sufficient* to fully describe a hydrogen bond (For details see Appendix II).

In previous chapters, a significant and consistent pattern of halogen bonding interaction in molecular association and promotion of crystal growth was observed. Therefore, it was thought worthwhile to probe into this ‘halogen bridging’ interactions, namely C-halogen...O using charge density measurements. Analogous to hydrogen bonding, it was aimed to gain more insight into this bonding by examining directions of approach of C-halogen and oxygen considering their electronic orbital distribution.

#### 9.4 System Chosen for Charge Density Studies

However, the *myo*-inositol derivatives reported in thesis were rather large molecules with several phenyl rings substitutions etc. Therefore, to study the nature of the halogen bonding contact, we decided to carry out the charge density analysis on a crystal of smaller aromatic planar compound 2,5-dichloro-1,4-benzoquinone (**15**, **Figure 9.3A**). B. Rees has earlier reported the crystal structure of **15** in 1970.<sup>161</sup> The crystal packing of **15** is completely dominated by the halogen bonding contacts between the chlorine atom Cl and the carbonyl oxygen; the Cl $\cdots$ O distance (3.10 Å) is much less than the sum of van der Waals radii and the angle C-Cl $\cdots$ O is very close to linearity (164.7°). Molecules in the crystals of **15** form a herringbone type structure linked via Cl $\cdots$ O contact along the b-axis, which look like a sheet when viewed down the c-axis (**Figure 9.3B**).

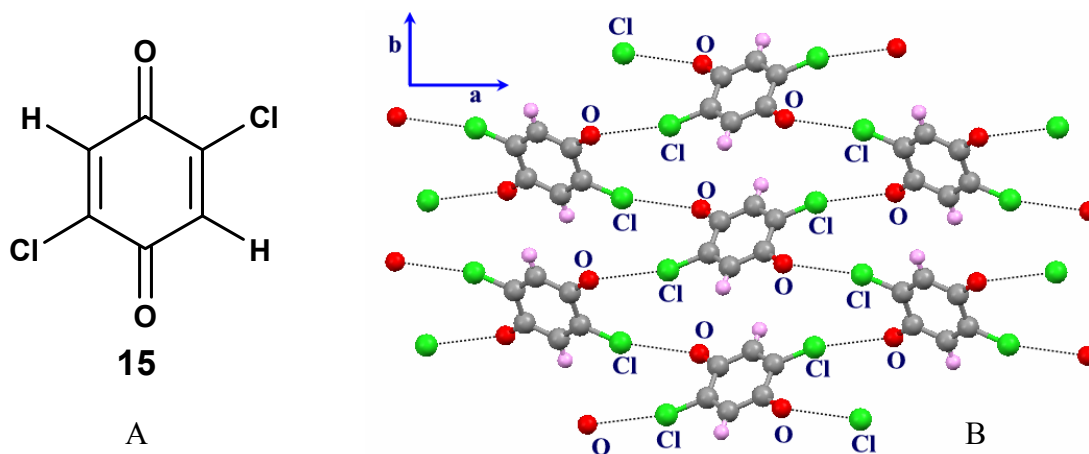


**Figure 9.3.** A) Structure of **15** and B) Molecular packing viewed down c-axis in **15**.

## 9.5 Experimental Section

### 9.5.1 Crystallization

A. R. grade 2,5-dichloro-1,4-benzoquinone<sup>161</sup> (**15**) was procured from Sigma Aldrich. Crystallization of the compound was attempted from chloroform, which gave good quality crystals on slow evaporation.

### 9.5.2 Single Crystal Data Collection and Refinement

One such crystal of a high quality (0.47 x 0.39 x 0.29 mm) was selected under Leica Polarizing microscope. High-resolution X-ray diffraction data were collected on a Bruker- AXS SMART APEX CCD diffractometer using MoK $\alpha$  radiation with the X-ray generator operating at 50 kV and 35 mA at 100 K using an Oxford cryo-system. Crystal was enclosed in a Lindemann capillary and was allowed to stabilize at the final temperature (100 K) for about an hour. The unit-cell parameters were then determined repeatedly until the estimated standard deviations in the cell dimensions did not vary beyond acceptable limits. The data were collected in several steps with different scan times (**Table 9.1**) to cover the full-sphere of reciprocal space. Different  $2\theta$  settings of the detector ( $-25^\circ$ ,  $-50^\circ$ , and  $-75^\circ$ ) and  $\varphi$  settings ( $0^\circ$ ,  $90^\circ$ ,  $180^\circ$ , and  $270^\circ$ ) of the goniometer were selected and the scanning angle  $\omega$  was set to  $0.3^\circ$  for each of the set of 606 frames. In order to perform the crystal decay corrections, an additional 60 frames were collected with  $2\theta$  settings of the detector at  $-25^\circ$ ,  $\varphi$  settings at  $0^\circ$ , giving the same exposure time as used for first set of data. The crystal to detector distance (optimized) was kept at 6.145 cm. The exposure times 10, 20, and 30 seconds were used for X-ray intensity measurements. This strategy provides high resolution ( $1.08 \text{ \AA}^{-1}$ ), large redundancy and better completeness in data sets, which are key factors required for multipole refinement

modeling in charge density analysis. The data collection was monitored using Bruker's SMART program.<sup>120</sup>

**Table 9.1:** A summary of the 100 K X-ray data collection strategy.

Run number	Starting frame number	Angle $2\theta/^\circ$	$\omega/^\circ$	$\varphi/^\circ$	$\chi/^\circ$	Axis	Angle width/ $^\circ$	Total frame numbers	Exposure time*/sec.
1	001	-25	-25	0	54.74	2	0.3	606	10
2	001	-25	-25	90	54.74	2	0.3	606	10
3	001	-25	-25	180	54.74	2	0.3	606	10
4	001	-25	-25	270	54.74	2	0.3	606	10
5	001	-50	-50	0	54.74	2	0.3	606	20
6	001	-50	-50	90	54.74	2	0.3	606	20
7	001	-50	-50	180	54.74	2	0.3	606	20
8	001	-50	-50	270	54.74	2	0.3	606	20
9	001	-75	-75	0	54.74	2	0.3	606	30
10	001	-75	-75	90	54.74	2	0.3	606	30
11	001	-75	-75	180	54.74	2	0.3	606	30
12	001	-75	-75	270	54.74	2	0.3	606	30
13	001	-25	-25	0	54.74	2	0.3	606	10

\* Depends on the diffraction quality of the crystal.

The X-ray data then reduced with the package SAINTPLUS,<sup>121</sup> which takes care of several systematic errors. Sorting, scaling, merging of the data sets, and application of empirical absorption corrections, were performed using the program SORTAV.<sup>162</sup> The

structure was solved by direct methods using SHELXS97<sup>122</sup> and refined in the spherical atom approximation (based on  $F^2$ ) using SHELXL97<sup>122</sup>. The structure of **15** refined to a good R-value (0.0295). The  $U_{ij}$ 's of all the atoms were in the range 0.03-0.05 and even the H-atom was located in difference Fourier.

## 9.6 Results and Discussion

### 9.6.1 Spherical Refinement

The 2,5-dichloro-1,4-benzoquinone<sup>160</sup> (**15**) is a planar molecule having a center of symmetry. The compound crystallizes in monoclinic space group  $P2_1/c$ . **Figure 9.4** gives the ORTEP view of the molecule drawn at 50% probability for the non-H atoms.

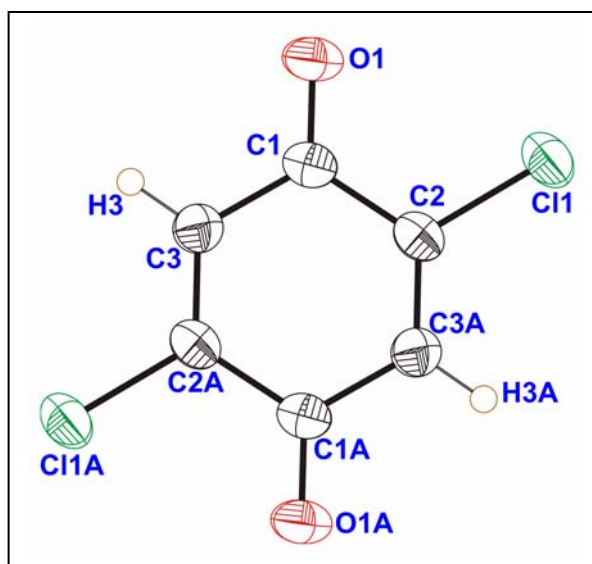


**Figure 9.4.** ORTEP view of **15** at 100 K drawn at with 50% ellipsoid probability for non-H-atoms.

The unit cell parameters, the experimental details, and the multiple refinement parameters, including the residual densities over the asymmetric unit, are listed in **Table 9.2**.



**Table 9.2:** Experimental X-ray Data of **15**

Formula	C <sub>6</sub> H <sub>2</sub> Cl <sub>2</sub> O <sub>2</sub>
Crystal size/mm	0.47 x 0.39 x 0.29
Formula weight	176.98
Crystal system	Monoclinic
Space group	P2 <sub>1</sub> /c
<i>a</i> (Å)	6.0203(12)
<i>b</i> (Å)	5.4361(11)
<i>c</i> (Å)	10.082(2)
$\alpha$ (°)	90
$\beta$ (°)	92.289(3)
$\gamma$ (°)	90
<i>V</i> (Å <sup>3</sup> )	329.69(12)
<i>Z</i>	2
<i>D</i> <sub>calc</sub> (g cm <sup>-3</sup> )	1.783
<i>F</i> (000)	176
$\mu$ (mm <sup>-1</sup> )	0.905
T <sub>min</sub> , T <sub>max</sub>	0.6758, 0.7794
(Sin $\theta$ / $\lambda$ ) <sub>max</sub> / Å <sup>-1</sup>	1.08
Reflection nos. (unique)	2363
<i>R</i> ( <i>F</i> )	0.0329
<i>R</i> <sub>w</sub> ( <i>F</i> )	0.0326
<i>S</i>	2.0335
<i>N</i> <sub>obs</sub> / <i>N</i> <sub>par</sub>	17.2482
Range of residuals (e Å <sup>-3</sup> )	-0.284, 0.387

### 9.6.2 Multipole Refinement

Multipole refinements were carried out using the module XDLSM incorporated in the software package XD.<sup>157</sup> The residual bonding density, which is not modeled in the conventional spherical refinement, is taken into account in this refinement. Scattering factors were derived from the Clementi and Roetti<sup>163</sup> wave functions for all atoms. The function minimized in the least-squares refinement was  $\sum w (|F_o|^2 - K|F_c|^2)^2$  for all reflections with  $I > 3 \sigma(I)$ . The following strategy was applied for the Multipole

refinement. Initially, only the scale factor was refined with all reflections. Next, to determine accurate positional and thermal parameters, refinement with high angle reflections ( $\sin \theta/\lambda \geq 0.8 \text{ \AA}^{-1}$ ) was performed for the non-hydrogen atoms. The positional and isotropic thermal parameters of the H atoms were then refined using low angle data ( $\sin \theta/\lambda \leq 0.8 \text{ \AA}^{-1}$ ). The positions of the H atoms in this refinement, as well as in subsequent refinements, were fixed to the average bond distance values obtained from neutron diffraction studies ( $C_{Ar} - H = 1.076 \text{ \AA}$ ).<sup>164</sup> In the subsequent stages, refinements were carried out taking into account the monopole, dipole, quadrupole, octapole, and hexadecapole populations (only for Cl) stepwise. Finally, a single k value was refined for each type of non-H atom along with the rest of the parameters (including the isotropic thermal parameters of the H atoms). For H atom the multipole expansion was truncated at the  $l_{\max} = 1$  (dipole, bond-directed) level. In order to obtain the best multipole model, only chlorine atom was allowed to refine up to the hexadecapole level, whereas for C and O multipole refinement was restricted upto octapole only. For non-H atoms, separate k and k' were allowed to refine, while for the H atoms the corresponding values were fixed at 1.2. No chemical restraints were applied during the scale factor refinement. The modules XDFFT<sup>157</sup> and XDFOUR<sup>157</sup> were used to measure the amounts of residual electron density and static deformation density. To get a quantitative description structure of the electronic structure, the module XDPROP<sup>157</sup> of the package XD<sup>157</sup> was used for topological analysis of the charge densities.

During the multipole refinement for all the atoms of **15**, the refinement went on well with expected range of values for k (value of k for Cl was 1.1542, for C and O was close to 1). However, the problem started for Cl when the radial parameter k' was

allowed to refine. The value of  $k'$  for Cl was unusually high (2.41), whereas values for C and O were 0.818 and 1.378 respectively. This hike in the  $k'$  for Cl has been perplexing, preventing us from deriving further analysis on charge density. The treatment of halogen, particularly Chlorine, is being referred to experts in the field and further work on improving the model is in progress.

The static deformation density map obtained from the theoretical structure factor generated from CRYSTAL98,<sup>165</sup> followed by multipole refinement in XD is shown in **Figure 9.5A**. The lone pairs of electrons on the oxygens and also on the chlorine atoms are well resolved. It is rather intriguing that the charge density along the C-Cl bonds is very low, which has been observed along C-F bond.<sup>166</sup> The static deformation density map obtained from the experimental structure factors (without  $k'$  refinement) shown in **Figure 9.5B** lacks the well-resolved features seen in the theoretical map although (only!) qualitatively all the features of the theoretical maps are seen.

As the multipole refinement for chlorine did not progress well, we could not analyze the topological properties of the intermolecular halogen bonding interaction. The multipole refinements, in consultation with the experts, are in progress. We have planned to work on 'halogen bridging' by charge density measurements for other heavier halogen atoms Br and I also to quantitatively determine the properties associated with halogen bonding contacts in crystals.

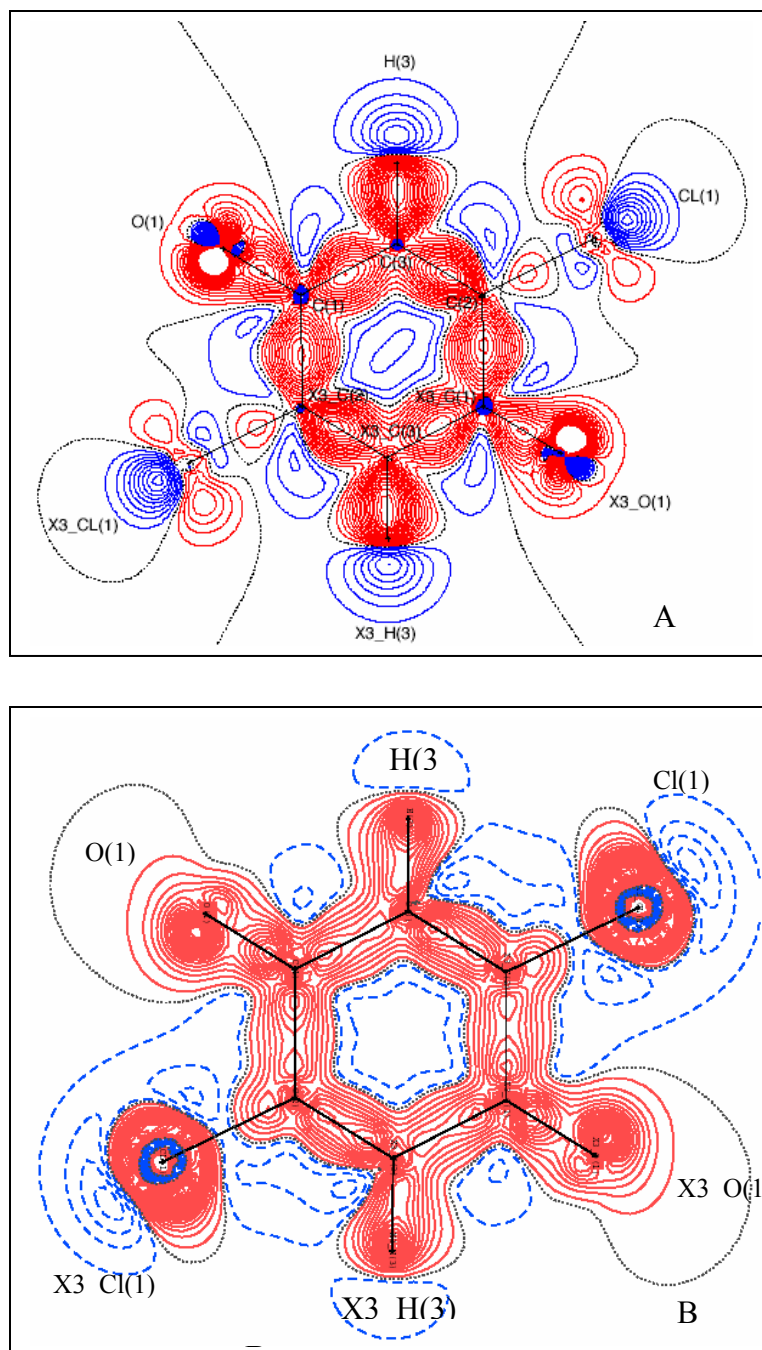


**Figure 9.5.** Static deformation density maps from, A) theoretical structure factor and B) experimental structure factor for **15**. For deformation density maps the positive (solid red lines) and negative (broken blue lines) contour starts at  $\pm 0.05 \text{ e}\text{\AA}^{-3}$  with intervals of  $\pm 0.1 \text{ e}\text{\AA}^{-3}$ , zero contours are shown as the black dotted line.

# Chapter 9

## Part C: Scope of Future Work

### 9.7 Working on Guest Specificity for Molecular Selectivity / Separations

Molecular separation is an intensively researched area because of its high applicability in chemical and pharmaceutical industries.<sup>104,105</sup> The leads obtained from the results of Chapter 2 have potential implications for exploiting the selective uptake of dihalomethane solvent. The future extension to this work is to examine whether the separations can be extended to chiral halo solvents by using chirally pure molecules of compound **3**. Also, the principles of host-guest interactions seen in these chapters are of significance in designing newer host molecules.

### 9.8 Spontaneous Resolution – Implications in Producing Organic Chiral Crystals

The spontaneous generation of chirality discussed in Chapter 3 is an enigmatic phenomenon,<sup>138</sup> which continues to fascinate chemists and biologists. The metastable crystals capable of showing optical activity can be compared with a class of crystals where the activity is due to the helical arrangement of the molecules in the entire lattice (e.g. quartz) rather than configurational or conformational<sup>167</sup> chirality of individual

molecules. Our observation of an achiral organic molecule producing a chiral crystal due to its topology of weak interactions could have relevance in asymmetric synthesis<sup>168</sup> and in designing NLO materials.<sup>169</sup>

### **9.9 Crystal-to-Crystal Phase Transitions Between Polymorphs**

Single crystal-to-crystal transformations are rather rare occurrences, which indicate the intrinsic flexibility in the crystal lattice accommodating structural changes that take place upon heating the crystals. Stabilities of pharmaceutical solids with temperature and /or with presence of solvent (water) molecules in the crystal lattice are relevant to consider in this connection. It is planned to take up some theoretical computational work that would provide some insight into molecular mechanistic pathways of transitions.

### **9.10 Insight into Halogen Bonding Interactions – its Implications in Drug Binding**

Charge density studies on model compounds (one already reported in the thesis) which possesses ‘halogen bonding’ interaction in their crystals will be extended to other halogen systems for more insight into halogen bonding contacts. Halo-substituted drugs show more activity than the non-halo counterparts in many cases. Some of these cases will be studied in detail. (PDB search is already underway).

### **9.11 Study of Other Isomers of Inositol**

Till now, we have essentially working on *myo* isomer of inositol, which produced plenty of amazing results ranging from solid state reactions,<sup>152</sup> (pseudo)polymorphism,<sup>30, 118,136</sup> to crystal-to-crystals phase transition.<sup>35g</sup> In order to pursue the similar findings, other isomers of inositol such as *scyllo* and *epi* being synthesized in our laboratory and study of their solid state reactions, (pseudo)polymorphic behaviour are underway.

# **Appendix I**

## **Lattice Energy Calculations**

# Appendix I

## Methodology

All the calculations were done applying the DREIDING force field.<sup>170</sup> The Force Field contained the necessary building blocks for the calculations of energy and force:

1) A list of atom types; 2) A list of atomic charges; 3) Atom-typing rules; 4) Functional forms for the components of the energy expression; 5) Parameters for the function terms (etc.). The Force Fields commonly used for describing molecules employ a combination of *internal coordinates* and *terms* (bond distances, bond angles, torsions, etc.) to describe part of the potential energy surface due to interactions between bonded atoms, and *nonbond terms* to describe the van der Waals and electrostatic (etc.) interactions between atoms. The functional forms range from simple quadratic forms to Morse functions, Fourier expansions, Lennard-Jones potentials, etc.

The energy expression describes the potential energy surface of a particular model as a function of its atomic coordinates.

$$E_{\text{total}} = E_{\text{valence}} + E_{\text{crosstrem}} + E_{\text{nonbond}}$$

### Valence Interactions ( $E_{\text{valence}}$ )

The energy of valence interactions is generally accounted for by *diagonal terms*, namely, bond stretching ( $E_{\text{bond}}$ ), valence angle bending ( $E_{\text{angle}}$ ), dihedral angle torsion



( $E_{\text{torsion}}$ ), and inversion (also called out-of-plane interactions) ( $E_{\text{inversion}}$  or  $E_{\text{oop}}$ ) terms, which are part of nearly all force fields for covalent systems. A Urey-Bradley term ( $E_{\text{UB}}$ ) may be used to account for interactions between atom pairs involved in 1-3 configurations (i.e., atoms bound to a common atom):

$$E_{\text{valence}} = E_{\text{bond}} + E_{\text{angle}} + E_{\text{torsion}} + E_{\text{oop}} + E_{\text{UB}}$$

### Valence Cross Terms ( $E_{\text{crossterm}}$ )

Cross terms includes the following terms: stretch-stretch, stretch-bend-stretch, bend-bend, torsion-stretch, torsion-bend-bend, bend-torsion-bend, stretch-torsion-stretch.

### Nonbonded Interactions ( $E_{\text{nonbond}}$ )

The energy of interactions between nonbonded atoms is accounted for by van der Waals ( $E_{\text{vdW}}$ ), electrostatic ( $E_{\text{Coulomb}}$ ), and hydrogen bond ( $E_{\text{hbond}}$ ) terms:

$$E_{\text{nonbond}} = E_{\text{vdW}} + E_{\text{Coulomb}} + E_{\text{hbond}}$$

Atomic charges were calculated by the Gasteiger method<sup>171</sup>

The expression used for minimizing the energy with respect to the charge on atom  $i$ :

$$q_i = \lambda - \chi_i - \Delta\chi_i / \eta_i$$

where  $\lambda$  is the Lagrange multiplier for the constraint on the total charge, which physically is the equalized electronegativity of all the atoms. The  $\Delta\chi$  term contains the geometry-independent remnant of the full Coulomb summation.

Electrostatic interactions were calculated using the Ewald summation in reciprocal space.<sup>172</sup> For all calculations, the program system "Cerius<sup>2</sup>" of Accelrys was used.<sup>173</sup>

# **Appendix II**

## **Charge Density Analysis: Overview**

# Appendix II

## II.1 Charge Densities from X-Ray Diffraction

In a typical molecule, the distance between the constituent atoms is of the order of 0.1 nm and hence X-rays, which possess wavelengths in the nanometer range, are most ideally suited to probe this regime. This allows one to see the shapes of molecules and also to visualize how they interact with each other in a molecular crystal. X-rays are scattered (in general) by the electrons in atom and hence provide the means for plotting the electron density distribution in the crystal space. The term ‘charge density’ is more appropriate<sup>155e</sup> to use than ‘electron density’ because chemically useful properties such as electrostatic potentials, molecular moments, and electric field gradients, along with the electron distribution and its topological properties are contained in X-ray diffraction experiment, which utilizes both positive and negative charges

## II.2 Elements of Charge Density Determination

The basis of X-ray structure analysis is the assumption that the atomic electron density is essentially the spherically averaged density of an isolated atom. This allows for considering the molecular crystal to be built up by independent spherical atoms, which bond together into a molecule and then rearrange following the allowed symmetry in the crystal lattice as a molecular crystal. The independent atom model (IAM)<sup>158</sup> also assumes

that the atoms in a crystal are neutral. The success of the spherical atom model has been confirmed by the large number of crystal structures that have been determined based on this assumption, where the atomic density is defined as:

$$\rho_{IAM}(\mathbf{r}) = \sum_k \rho_k^0(\mathbf{r} - \mathbf{R}_k)$$

This retains the electrons localized around a nucleus and further it assumes that the electron density in the molecule (and eventually in the crystal) is a superposition of isolated spherical densities  $\rho^0$  of isolated atoms  $k$  centered at  $\mathbf{R}_k$ . In general, diffraction is a phenomenon that keeps the average density  $\langle \rho \rangle$  as a canonical ensemble, which allows for thermal averaging as well. The thermal smearing is again restricted to the atom center and the mean square atomic displacement is expressed in terms of either harmonic or anharmonic parameters.

Further, Fourier transformation leads to the generalized structure factors,

$$F(\mathbf{H}) = \sum_k f_k(\mathbf{H}) \exp(2\pi^2 \mathbf{H}^t \mathbf{U}_k \mathbf{H}) \exp(2\pi i \mathbf{H} \mathbf{R}_k^0)$$

The IAM is effective for heavy atoms with dominant core scattering while for light atoms the directional characteristics, in terms of bonding features like valance, become more aspherical. This results in directional properties being exhibited by molecular crystals. Further, theoretical and experimental evidence showing that atoms in molecules carry partial charges necessitated improvements over the IAM.

### AII.3 The Kappa Formalism

The first extension of the IAM to allow for both valance charge transfer and expansion or contraction of the valance shell was suggested by Coppens *et. al.*<sup>174</sup> It is now called radial (kappa,  $\kappa$ ) refinement or *kappa formalism*. The basic assumption of this

model is that the electrons of the core shells are unperturbed and the atomic density is expressed as,

$$\rho_{at}(r) = \rho_{core}(r) + P_v k^3 \rho_{valence}(kr)$$

where the contribution of scattering from the core and valence shells are separated. The valence population ( $P_v$ ) and the radial parameter ( $\kappa$ ), which allows the contraction and expansion of the valence shell, are introduced in the refinement. The  $\kappa$  parameter scales the radial coordinate  $r$ ; if  $\kappa > 1$  the same density is obtained at a smaller  $r$  value and consequently the valence shell contracts and for  $\kappa < 1$  the valence shell expands. This model allows calculating the magnitude and direction of dipole moments and atomic charges and the results are found to be in good agreement with experimentally and theoretically measured values.<sup>174</sup> However, in this model the description of the nonspherical distribution of the atomic charge density is unsatisfactory.

#### AII.4 Multipole Model: Aspherical Scattering Formalism

Various groups have introduced different aspherical correction terms to the atomic model,<sup>175</sup> but the multipole expansion model suggested by Hansen and Coppens<sup>156</sup> has stood the test of time and is now the most widely used methodology. In their model, the individual atomic densities are divided into three components, the core, a spherical expansion and contraction term ( $\kappa$ ) for the valence shell, and the valence deformation, which is described in terms of density normalized spherical harmonics ( $d_{lm\pm}$ ) together with the corresponding radial expansion and contraction ( $\kappa'$ ) of the valence shell as given below,

$$\rho_{at}(r) = P_c \rho_{core}(r) + P_v k^3 \rho_{valence}(kr) + \sum_{l=0}^{l_{\max}} k'^3 R_l(k'r) \sum_{m=0}^l P_{lm\pm} d_{lm\pm}(\theta, \varphi)$$

The core ( $\rho_{\text{core}}$ ) and spherical valence ( $\rho_{\text{valence}}$ ) densities can be calculated from Hartree-Fock (HF) or relativistic HF atomic wave functions. The atomic functions are expressed in terms of the polar coordinates  $r$ ,  $\theta$ , and  $\phi$  defined on the local axes centered on each atom as shown in **Figure AII.1**.

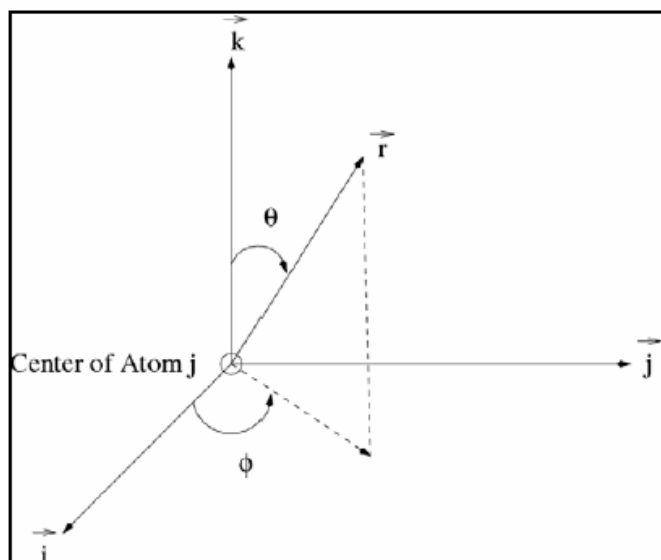


**Figure AII.1.** The definition of axes centered on atoms.

The density functions, also referred to as *multipoles*, are the product of  $r$ -dependent *radial functions* and  $\theta$ - and  $\phi$ -dependent *angular functions*. The radial function,  $R_l(\kappa' r)$  of the deformation density takes the form of normalized Slater (or Gaussian) functions,

$$R_l(\mathbf{r}) = \kappa'^3 \frac{\xi^{n_l+3}}{(n_l+2)!} (\kappa' \mathbf{r})^{n(l)} \exp(-\kappa' \xi_l \mathbf{r})$$

The angular functions are real spherical harmonic functions, which are same as those used to describe atomic orbital. The graphical representation of the functions with  $l \leq 3$  is illustrated in **Figure AII.2**.

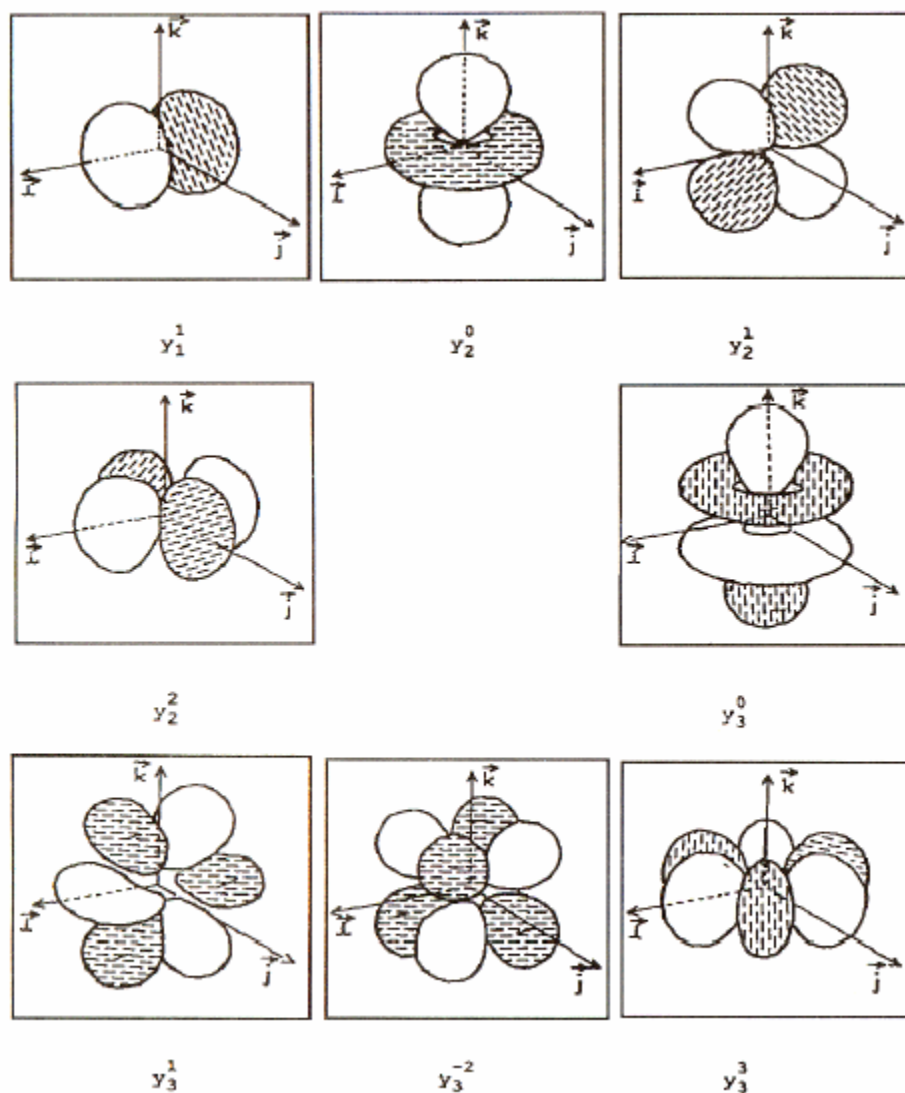


**Figure AII.2.** Schematic diagrams of multipoles ( $l_{\max} = 3$ )

### II.5 Fourier Analysis of the Charge Density Distribution

The total electron density distribution  $\rho(\mathbf{r})$  is calculated based on  $F(\mathbf{H})$ , the structure factor, by the Fourier transformation:

$$\rho(\mathbf{r}) = \int F(\mathbf{H}) \exp(-2\pi i \mathbf{H} \cdot \mathbf{r}) d\mathbf{H}$$

The difference  $\Delta\rho$  between the observed and the calculated electron density is called the *residual density*. It is a representation of the inadequacy of the multipole model and is evaluated as follows:

$$\Delta\rho(\mathbf{r}) = \rho_{obs}(\mathbf{r}) - \rho_{calc}(\mathbf{r}) = \frac{1}{V} \sum_{\mathbf{H}} \Delta F \exp(-2\pi i \mathbf{H} \cdot \mathbf{r})$$

The *deformation density*,<sup>155a,h</sup> the difference between the total density and the density calculated based on the *promolecule* density, is a representation of the valence density in the bonding regions and can be expressed as:

$$\Delta\rho(\mathbf{r}) = \rho(\mathbf{r}) - \rho_{pro}(\mathbf{r})$$

Deformation density is a measure of the deformation of the valence density into the bonding regions and the corresponding maps represent the electron density accumulated due to bonding. If the observed structure factors are used, the resulting electron density map is called a *dynamic deformation density* map, since the observed structure factors include thermal effects. The *static deformation density* map is free from thermal smearing effects and can be directly compared with the theoretical deformation density.



## AII.6 Experimental Method and Data Analysis

The accuracy and the quality of the data are highly dependent on the conditions and the strategy adopted in the diffraction experiment. In charge density studies, the data collection, processing, and refinement should be performed with enormous care, as high precision in the data is a prerequisite.<sup>176</sup> The current state of the art in data acquisition uses either conventional X-rays of fixed lower wavelength [e.g.  $\lambda(\text{MoK}\alpha) = 0.7103 \text{ \AA}$ ] or synchrotron X-rays (tunable for lower wavelength, typically  $\sim 0.4 \text{ \AA}$ ) as a source and a CCD or an IP as the detector. The success of the experiment is often determined by the quality of the crystal itself. In order to acquire high-quality diffraction data one must select a well-defined single crystal without any fractures or twinning. Another important factor is the crystal size, which should be as small as possible to reduce absorption but large enough to maximize the diffracted intensities when fully bathed in the homogenous part of the X-ray beam. It is an essential requirement that one obtains measurable data covering the entire reciprocal space up to the highest possible resolution ( $d \leq 0.5 \text{ \AA}$  or  $\sin\theta/\lambda \geq 1.0 \text{ \AA}^{-1}$ ). This is made possible through a combination of short wavelength and low temperature. A significant lowering in thermal diffuse scattering is seen in data sets collected at low temperatures (100K and below using cryosystems with  $N_2$  flow or using *He* cryostats), which allows reflections to be measured at high scattering angles. This allows one to acquire more reflections, to determine more accurate atomic positions, and to deconvolute the vibrational and bonding effects more easily. For charge density studies, the data collection strategy differs from that of a conventional spherical atom experiment. In multipole analysis, the main idea is to measure a precise data set, one that provides high resolution, large redundancy, and the best completeness in a short time. In

general, averaging over several measurements of the same or equivalent reflections improves the precision. However, the data collection strategy employed is entirely dependent on the geometry of the diffractometer being used. The most appropriate strategy for the collection of the accurate data must be judged with special care. In order to obtain accurate structure factor information, certain corrections, such as Lorentz, polarization, absorption, and crystal decay are of prime importance. Both Lorentz and polarization both factors are functions of  $2\theta$  and the exact form required depends on the geometry of the diffractometer. In practice these two corrections are generally applied together. Absorption reduces the diffracted-intensity. The amount of absorption depends on the elements present in the compound and the length of path traversed by the beam within the crystal. The program SORTAV<sup>162</sup> is extremely useful for dealing with absorption. This program can derive an empirical absorption correction by fitting real spherical harmonic functions to the empirical transmission surface as sampled by the multiple equivalent measurements.<sup>177</sup> Samples, which are exposed to intense X-ray beams for long times, are often subject to decay. The best way to confirm the amount of crystal decay is to collect a set of reflections at the end of the complete data collection under the same conditions as applied to the start of the data set. Generally, the data sets are collected in several steps and as a consequence there will be some overlap between the data sets. Finally for least-squares refinement it is necessary to merge geometrically equivalent reflections to be merged on the same scale to extract the unique reflections. The program SORTAV serves this purpose.

### AII.7 Multipole Refinement: The XD Package

The nature of chemical bonding and interactions can be evaluated in terms of the deformation densities, which are calculated based on the Hansen and Coppens multipole formalism<sup>156</sup> as described in the earlier section. A number of least squares refinement programs have been developed, and utilized by various groups.<sup>156,157,175</sup> The package, XD<sup>157</sup> is the most widely used for the analysis of experimental diffraction data. The structure of the present version of XD (Revision 4.10, Jul 23 2003) contains several components as shown in **Figure AII.3**. This package can be used for multipole refinement and hence the topological analysis of charge densities from the measured structure factors.

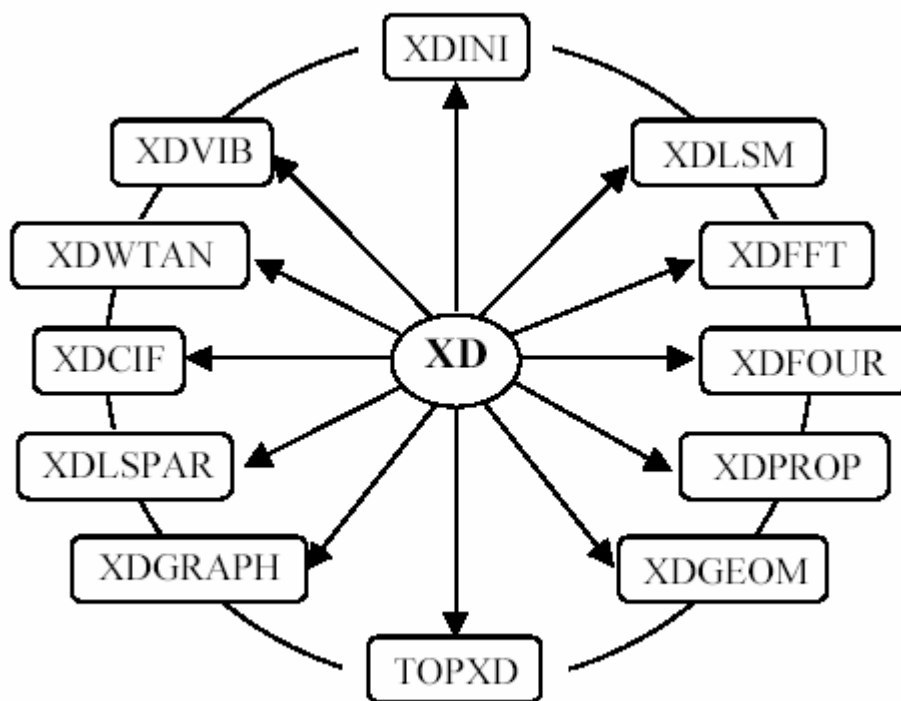


**Figure AII.3.** The structure of the present version (Revision: 4.10, Jul 23 2003) of XD

The XD manual (Version February 2004) describes the methodology and the applications of each module in detail. The module XDINI provides the interface between XD and the packages used for solving and refining the structures (spherical atom model), like for example, SHELX. It creates the master file and the required input files to run the module XDLSM, which is a full-matrix least squares program based on the Hansen & Coppens formalism.<sup>156</sup> The function minimized in the least-squares refinement is

$$\sum w \left( |F_o|^2 - K |F_c|^2 \right)^2$$

where the weighting factor  $w = 1/\sigma^2$ . In a multipole refinement, along with the conventional parameters (scale factor, positional, and thermal parameters), the charge density variables ( $P_v$ ,  $\kappa$ ) are also refined. XDLSM allows one to locate inadequacies in the model, to control refinement, and to monitor the results. During refinement various constraints such as, electro-neutrality of groups, rigid bonds etc., can be applied and a wide variety of model parameters (isotropic, anisotropic, extinction) can be used. Its present version includes multipole expansion up to the hexadecapole ( $l_{max}=4$ ) level and anharmonic treatment of the thermal motion up to the 4th order of the Gram-Charlier expansion. In general, an octopole expansion is sufficient to account for the bonding deformation density. A refinement with hexadecapole terms may improve the agreement factors, but this is often only an artifact caused by the inclusion of more parameters. In order to determine accurate positional and thermal parameters, high order ( $\sin \theta/\lambda \geq 0.8 \text{ \AA}^{-1}$ ) refinements are performed for the non-H atoms. The positional and isotropic thermal parameters of the H atoms are then refined using the lower angle data ( $\sin \theta/\lambda \leq 0.8 \text{ \AA}^{-1}$ ). In the absence of neutron data, the positions of the H atoms are set to average bond

distance values obtained from reported neutron diffraction studies.<sup>164</sup> The monopole, dipole, quadrupole, octapole, and hexadecapole populations should be refined in a stepwise manner. For all H atoms the multipole expansions are truncated at  $l_{\max} = 1$  (dipole, bond-directed) level. Next, single  $\kappa$  parameters and then single  $\kappa'$  Parameters together with  $\kappa$  for all non-H atoms should be refined. In order to achieve a stable convergence of the refinement, care must be taken in refining the very sensitive parameter,  $\kappa'$ . For each chemically different group of non-H atoms separate  $\kappa$  and  $\kappa'$  should be assigned, while for H atoms the corresponding values should be fixed at 1.2. Finally, all the multipole parameters, including the isotropic thermal parameters of the H atoms, should be refined to reach the final model of charge density distribution. The strategy of multipole refinement is very crucial and it is difficult to suggest one specific scheme. The residual bonding density, not modeled in the conventional spherical refinement, is taken into account in the multipole refinement. The module XDFFT is a three-dimensional fast Fourier transformation program, which allows determining the extrema of the residuals or the dynamic deformation density over the whole unit cell. This program is much faster than XDFOUR, which also estimates the residual and the dynamic deformation density over a given range. The static electron density, which is obtained in the form of a nuclear centered multipole expansion, can be analyzed using XDPROP. This module can be used to evaluate the one-electron properties such as net charges, electrostatic potentials, dipole moments etc. and to carry out the CP analyses and the corresponding topological analysis of the total electron density. The program XDGEOM calculates the various functions derived from the atomic coordinates together with the standard uncertainties and the symmetry related atoms in the lattice.

Additionally, it creates a crystallographic information file (CIF) and a multipole population parameter file. The quantum theory of AIM is fully incorporated in the module TOPXD,<sup>178</sup> which allows calculation of an extensive set of atomic properties, including Bader charges, dipole, and higher electrostatic moments along with atomic volume and atomic nuclear-electron potential energy by integration over atomic basins. The specific results from the programs mentioned above could be visualized via an independent graphical package, XDGRAPH, which allows for two-dimensional (contour or height field), three-dimensional (isosurface), molecule, bond path, and relief plots. The code XDLSPAR can be used to obtain the values of the parameters used in the multipole refinements and the corresponding outcomes of the refinement. Additionally, there are few XD utility programs such as XDCIF (to create an archive CIF), XDWTAN (to analyze the weighting scheme), and XDVIB [to calculate the mean square displacement amplitude (MSDA) from harmonic vibrational frequencies and normal modes]. A new module recently interfaced to the XD package is XDINTER,<sup>179</sup> which utilizes the experimental charge density approach (ECDA) and allows the evaluation of the intermolecular interaction energies and hence the lattice energy.

### **AII.8 Reliability Tests of the Multipole Model**

In addition to the R-factor and the goodness-of-fit, which is the key factors in deciding the quality of the spherical atom model, there are several factors to be considered in judging the reliability of the model in multipole refinement. The following are the main criteria used to evaluate the quality of a multipole model.

**Residual density maps:** A Fourier map, which is calculated using the Fourier coefficients  $F_{\text{obs}} - F_{\text{mult}}$ , represents the agreement between the observed and multipole model electron density. For a well-fitted model this map should be almost featureless.

**Deformation density maps:** This map visualizes the difference between the multipole and the spherical atom models and is obtained from the Fourier coefficients,  $F_{\text{mult}} - F_{\text{spherical}}$ . Location of the presence or absence of bonding and lone-pair deformation density peaks in this map illustrates the sensibility of the multipole model.

**Hirshfeld's rigid bond test**<sup>180</sup>: One of the most important tests assesses the physical significance of the thermal parameters included in the multipole model. This test assumes that in a molecular crystal the vibrational motion comes mainly from intermolecular lattice vibrations rather than from the bond-stretching amplitudes. This essentially means that the chemical bond is rigid with respect to the vibrational motion. For a pair of bonded atoms A and B, if  $Z_{A,B}$  denotes the vibration of atom A in the direction of atom B and  $Z_{B,A}$  the vibration of atom B in the direction of atom A, then they should be equal. For a rigid bond, the difference in mean square displacement amplitudes (DMSDA) should satisfy,

$$\Delta_{A,B} = Z_{A,B}^2 - Z_{B,A}^2 = 0$$

In practice, for a pair of atoms at least as heavy as carbon, the DMSDA should be less than  $0.001 \text{ \AA}^2$ . For a reliable multipole model the anisotropic displacement parameters should meet the requirements of the rigid bond test

### AII.9 Topological Analysis: Atoms in Molecule Approach

The surface features, or topology, of the charge density distribution obtained from experimental or theoretical methods can be analyzed via Bader's quantum theory of AIM.<sup>158</sup> This approach provides a pathway for comparison of the experimental electron density with the theoretically derived density in terms of the topological properties of the charge density  $\rho(\mathbf{r})$ . The topology of a scalar field, such as  $\rho(\mathbf{r})$ , which is a physical quantity, can conveniently be summarized in terms of CPs, where the first derivatives of  $\rho(\mathbf{r})$  vanishes,  $\Delta\rho(\mathbf{r}) = 0$ , indicating the position of extrema (maxima, minima, or saddles) in the  $\rho(\mathbf{r})$  at  $\mathbf{r}_c$ . In general, the theory of AIM provides a methodology for the identification of a bond between any two atoms in a molecule in terms of CPs, called bond critical points (BCP). This analysis is based on the identification of CPs, classified using the Hessian matrix of the electron density,<sup>158a, 160a</sup> which is a 3 x 3, ordered array of the second derivatives of  $\rho(\mathbf{r})$ . The Hessian matrix generates three eigenvectors, which are mutually orthogonal and coincide with the so-called *principal axis of curvature*. This suggests that each eigenvector represents an axis and the corresponding eigenvalues ( $\lambda_1$ ,  $\lambda_2$  and  $\lambda_3$  with  $\lambda_1 \leq \lambda_2 \leq \lambda_3$ ) determine the profile of the electron density along this axis. The number of nonzero curvatures of the Hessian matrix defines the *rank* associated with the CP and the *signature* of a CP is the sum of the signs of the curvatures. In general, a CP is labeled by giving both its rank and signature. It is noteworthy that the CPs in a stable molecule are all of rank 3, which gives rise to four possible type of CPs:

**(3, -3) Peaks:** all curvatures are negative and  $\rho$  is local maxima at  $\mathbf{r}_c$ .



**(3, -1) Passes or saddle points:** two negative and one positive curvature;  $\rho(\mathbf{r}_c)$  is a local maximum along two of the axes and a local minimum along the third orthogonal axis; found between every pair of nuclei linked by a chemical bond.

**(3, +1) Pales:** two positive and one negative curvatures;  $\rho(\mathbf{r}_c)$  is a local minimum along two of the axes and a local maximum along the third orthogonal axis; found at the center of a ring of bonded atoms.

**(3, +3) Pits:** all three curvatures are positive and  $\rho$  is a local minimum at  $\mathbf{r}_c$ . For intermolecular interactions, (3, -1) type CPs, and the properties of  $\rho(\mathbf{r})$  at these points, provide the chemically most useful information, and are of utmost interest. The line of the highest electron density linking any two atoms is referred to as the *bond path* (BP) and its length  $R_{ij}$ , which need not be the same as inter-atomic vector, is referred to as the *interaction line*. The BP passes through the bond critical point (BCP). The existence of a (3, -1) CP and associated BP is the topological definition of a chemical bond. For a strained system, the BPs deviate from the inter-nuclear vectors. If the charge is preferentially accumulated in a particular plane along the BP the bond will no longer be cylindrical, rather it will have an elliptical cross section ( $\lambda_1 \neq \lambda_2$ ), as is the case in a  $\pi$ -bond. A quantitative measure of the ellipticity of a bond, *bond ellipticity*, is defined as  $\varepsilon = \lambda_1 / \lambda_2 - 1$ , where  $\lambda_2$  is the curvature of smaller magnitude. For a typical cylindrical bond, as represented with a schematic diagram in **Figure AII.4**,  $\lambda_1 = \lambda_2$  and  $\varepsilon = 0$ . This is typical of a  $\sigma$ -bond, such as the C-C bond in ethane.

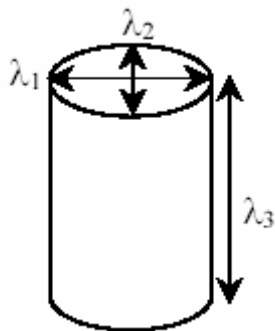


**Figure AII.4.** Schematic representations of curvatures of a chemical bond

The strength of a bond or its *bond order* is defined by the magnitude of the charge density at the BCP,  $\rho_b(\mathbf{r})$ . An important function of  $\rho(\mathbf{r})$  is its second derivative, the *Laplacian*  $\nabla^2 \rho(\mathbf{r})$ , which is a scalar quantity and is defined as the sum of the principal curvatures ( $\lambda_1 + \lambda_2 + \lambda_3$ ). It is a representation of the chemical features of the molecule. The physical significance of the Laplacian is that it represents areas of local charge concentration and depletion. If  $\nabla^2 \rho_b(\mathbf{r}) < 0$ , the density is locally concentrated resulting in shared interactions, while in the case of  $\nabla^2 \rho_b(\mathbf{r}) > 0$  the electron density is depleted representing closed-shell interactions. It is possible to observe lone pairs in the Laplacian as these appear as local maxima, *i.e.* (3, -3) CPs in the negative Laplacian. The electron densities, the Laplacian values, the interaction lines, the curvatures, and the bond ellipticities together represent the topology of the charge density distribution in a given molecule. Finally it should be noted the AIM approach could be used for both theoretical and experimental analyses.

### AII.10 Koch and Popelier's Criteria

Topological analysis does not specify the character of the bond, however, it does indicate the existence and the nature of a bond. In order to characterize a bond in terms of chemical concepts such as bond order, ionicity, conjugation, and hydrogen bonding the properties evaluated at the BCP become crucial. Based on Bader's quantum theory of AIM,<sup>158</sup> Koch and Popelier<sup>160</sup> have proposed eight criteria to establish hydrogen bonding. These criteria allow a hydrogen bond to be distinguished from a van der Waals interaction. If one or more of these criteria are not satisfied, the concerned interaction can be considered as a van der Waals interaction. Among these eight criteria, the fourth condition is considered as *necessary and sufficient* to fully describe a hydrogen bond. The following describes the eight criteria:

**Criteria 1: Topology.** Confirmation of the presence of a BCP between a donor atom and an acceptor atom linked via a BP as shown in **Figure AII.5**.

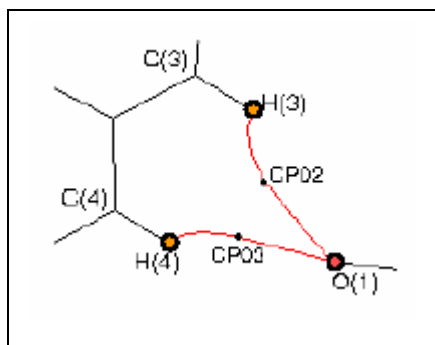


**Figure AII.5.** A schematic diagram of the location of the BCP between a donor atom and an acceptor atom along with the BP

**Criteria 2: Charge Density at the BCP.** Existence of the charge density evaluated at the BCP and its relationship with the overall hydrogen bond energy. It is possible to relate

the charge density parameters at the BCP to the local energy density  $E(\mathbf{r}_{\text{CP}})$  of the electrons by evaluating the local electronic kinetic energy density  $G(\mathbf{r}_{\text{CP}})$  and the local potential energy density  $V(\mathbf{r}_{\text{CP}})$  using the equations,<sup>158a,181</sup>

$$G(\mathbf{r}_{\text{CP}}) = \left(\frac{3}{10}\right)(3\pi^2)^{2/3}\rho^{5/3}(\mathbf{r}_{\text{CP}}) + \left(\frac{1}{6}\right)\nabla^2\rho(\mathbf{r}_{\text{CP}}),$$

$$V(\mathbf{r}_{\text{CP}}) = \left(\frac{1}{4}\right)\nabla^2\rho(\mathbf{r}_{\text{CP}}) - 2G(\mathbf{r}_{\text{CP}}), \text{ and}$$

$$E(\mathbf{r}_{\text{CP}}) = G(\mathbf{r}_{\text{CP}}) + V(\mathbf{r}_{\text{CP}})$$

**Criteria 3:** *The Laplacian of the Charge Density at BCP.* The calculated values of Laplacian,  $\nabla^2 \rho(\mathbf{r})$ , should be positive but within a sensible range and should correlate with the interaction energy.

**Criteria 4:** *Mutual Penetration of the Hydrogen and the Acceptor Atom.* Compares the non-bonded radii of the donor-hydrogen atom ( $r_D^0$ ) and the acceptor atom ( $r_A^0$ ) with their corresponding bonding radii,  $r_D$  or  $r_A$ . A schematic representation in **Figure AII.6** illustrates the concept of these two bonding radii. The nonbonding radius, the distance from the nucleus to an arbitrary charge contour (0.001 *au*), is taken to be equivalent to the gas phase van der Waals radius of the participating atoms.<sup>182</sup> The bonding radius is the distance from the nucleus to the BCP. In a typical hydrogen bond, the values of

$\Delta r_D = (r_D^0 - r_D) > \Delta r_A = (r_A^0 - r_A)$  and  $\Delta r_D + \Delta r_A > 0$  positive interpenetration. If either or both of these conditions are violated, the interaction is essentially van der Waals in nature. This condition is considered as *necessary and sufficient* to prove the existence of a hydrogen bond.

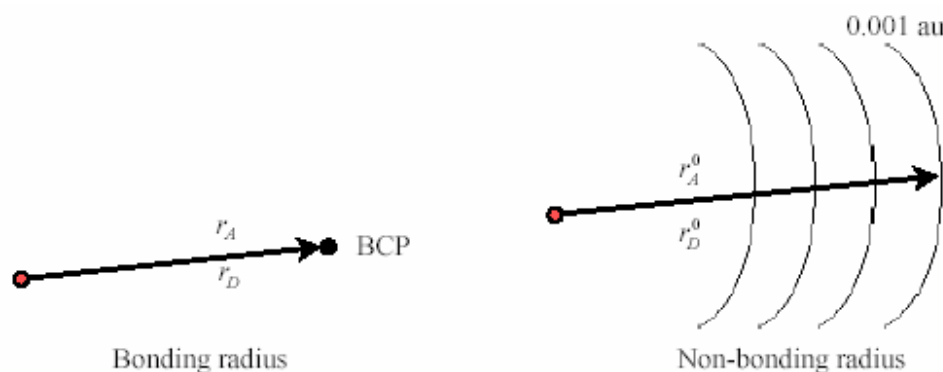


**Figure AII.6.** Schematic representation of the definition of a non-bonding and bonding radius for an atom participating in a hydrogen bond

The remaining four criteria can be obtained from integration over the atomic basins of the participating H atoms (and are more expensive to calculate). These are purely based on properties associated with the H atoms.

**Criteria 5: Loss of Charge.** The H atom loses electrons resulting in an increased net charge on the H atom. The descreening of hydrogen-bonded protons, as observed in NMR chemical shifts, follows this phenomenon.

**Criteria 6: Energetic Destabilization.** The energy of the H atom destabilized when it forms a hydrogen bond. The difference in total energy between the crystal and the bare molecule should thus be positive. This condition strongly correlates with the number 5.

**Criteria 7: Decrease in Dipolar Polarization.** There should be a decrease of the dipolar polarization (magnitude of the first moment,  $M$ ) of the H atom upon hydrogen bond formation. This essentially indicates the loss of nonbonding density on the H atom in the bare molecule.

**Criteria 8: Decrease in Volume.** The volume of the H atom should be depleted upon forming a hydrogen bond.



## References

1. G. M. Day, W. D. S. Motherwell, H. L. Ammon, S. X. M. Boerrigter, R. G. Della Valle, E. Venuti, A. Dzyabchenko, J. D. Dunitz, B. Schweizer, B. P. van Eijck, P. Erk, J. C. Facelli, V. E. Bazterra, M. B. Ferraro, D. W. M. Hofmann, F. J. J. Leusen, C. Liang, C. C. Pantelides, P. G. Karamertzanis, S. L. Price, T. C. Lewis, H. Nowell, A. Torrisi, H. A. Scheraga, Y. A. Arnautova, M. U. Schmidt and P. Verwer, *Third blind test for crystal structure prediction of small molecules*, *Acta Cryst.* **2005**, *B61*, 511.
2. A. Gavezzotti, *Acc. Chem. Res.* **1994**, *27*, 309.
3. J. D. Dunitz, *Chem. Commun.* **2003**, 545.
4. G. R. Desiraju, T. Steiner, *The Weak Hydrogen Bonds: In Structural Chemistry and Biology*, Oxford University Press: Oxford, New York, 1999 and references therein.
5. P. Munshi, T. N. Guru Row, *Crystallogr. Rev.* **2005**, *11*, 199.
6. A. D. Buckingham, *In Intermolecular forces*. Eds.: A. D. Buckingham, A. C. Legon, S. M. Roberts. Principles of molecular recognition. Blackie, London, 1993.
7. J. A. Ibers, *J. Chem. Phys.* **1964**, *40*, 402.
8. Reviews: (a) M. L. Huggins, *Angew. Chem. Int. Ed. Engl.* **1971**, *10*, 147; (b) J. C. Speakman, *Struct. Bonding* **1972**, *12*, 141; (c) L. Emsley, *Chem. Soc. Rev.* **1980**, *9*, 91; (d) G. A. Jeffrey, *Crystallogr. Rev.* **1995**, *4*, 213; (e) G. Gilli, P. Gilli, *J. Mol. Struct.* **2000**, *552*, 1; (f) T. Steiner, *Angew. Chem. Int. Ed. Engl.* **2002**, *41*, 48.
9. (a) G. R. Desiraju, *Crystal Engineering: The Design of Organic Solids*, Amsterdam: Elsevier, **1989**; (b) M. C. Etter, *Acc. Chem. Res.* **1990**, *23*, 120; (c) C. B. Aakeröy, T.

- 
- A. Evans, K. R. Seddon, I. Pálinkó, *New J. Chem.* **1999**, *23*, 145; (d) G. A. Jeffrey, *Crystallogr. Rev.* **2003**, *9*, 135; (e) T. Steiner, *Crystallogr. Rev.* **2003**, *9*, 177;
10. (a) C. B. Acheroy, K. R. Seddon, *Chem. Soc. Rev.* **1993**, *22*, 397; (b) G. A. Jeffrey, *An Introduction to Hydrogen Bonding*, Oxford Univ. Press, Oxford, **1997**.
11. R. Taylor, O. Kennard, *J. Am. Chem. Soc.* **1982**, *104*, 5063.
12. (a) L. Shimoni, H. L. Carrell, J. P. Glusker, M. M. Coombs, *J. Am. Chem. Soc.* **1994**, *116*, 816; (b) A. R. Choudhury, T. N. Guru Row, *Cryst. Growth Des.* **2004**, *4*, 47.
7. (a) M. Nishio, M. Hirota, Y. Umezawa, *The CH/ $\pi$  Interaction: Evidence, Nature and Consequences*, Wiley-VCH, 1998; (b) M. Yamakawa, I. Yamada, R. Noyori, *Angew. Chem. Int. Ed. Engl.* **2001**, *40*, 2818; (c) M. Nishio, *Cryst. Engg. Comm.* **2004**, *6*, 130.
8. C. A. Hunter, J. K. M. Sanders, *J. Am. Chem. Soc.* **1990**, *112*, 5525.
9. V. R. Pedireddi, D. S. Reddy, B. S. Goud, D. C. Craig, A. D. Rae, G. R. Desiraju, *J. Chem. Soc., Perkin Trans. 2* **1994**, 2353.
10. D. J. Sutor, *J. Chem. Soc.* **1963**, 1105.
11. (a) J. A. R. P. Sarma, G. R. Desiraju, *Acc. Chem. Res.* **1986**, *19*, 222; (b) G. R. Desiraju, *Acc. Chem. Res.* **1991**, *24*, 290; (c) G. R. Desiraju, *Acc. Chem. Res.* **1996**, *29*, 441.
12. (a) C. Pascard, *Acta Cryst.* **1995**, *D51*, 407; (b) J. P. Glusker, *Acta Cryst.* **1995**, *D51*, 418.
13. (a) G. A. Leonard, K. McAuley-Hecht, T. Brown, W. N. Hunter, *Acta Cryst.* **1995**, *D51*, 136; (b) Z. S. Derewenda, L. Lee, U. Derewenda, *J. Mol. Biol.* **1995**, *252*, 248.
14. C. A. Hunter, *Chem. Soc. Rev.* **1994**, 101.



15. M. A. Vishwamitra, R. Radhakrishnan, J. Bandekar, G. R. Desiraju, *J. Am. Chem. Soc.* **1993**, *115*, 4868.
16. M. P. Sarmah, R. G. Gonnade, M. S. Shashidhar, M. M. Bhadbhade, *Chem. Eur. J.* **2005**, *11*, 2103.
17. C. D. Tatko, M. L. Waters, *J. Am. Chem. Soc.* **2004**, *126*, 2028.
18. (a) M. Brandi, M. S. Weiss, A. Jabs, J. Suhnel, R. Hilgenfeld, *J. Mol. Biol.* **2001**, *307*, 357; (b) R. Bhattacharya, P. Chakrabarti, *J. Mol. Biol.* **2003**, *331*, 925.
19. F. H. Allen, J. A. K. Howard, V. J. Hoy, G. R. Desiraju, D. Shekhar Reddy, C. C. Wilson, *J. Am. Chem. Soc.* **1996**, *118*, 4081.
20. M. J. Jedrzejak, S. Singh, W. J. Brouillette, W. G. Laver, G. M. Air, M. Luo, *Biochem.* **1995**, *34*, 3144.
21. (a) O. Ermer, A. Eling, *J. Chem. Soc., Perkin Trans 2.* **1994**, 925; (b) F. H. Allen, V. J. Hoy, J. A. K. Howard, V. R. Thalladi, G. R. Desiraju, C. C. Wilson, G. J. McIntyre, *J. Am. Chem. Soc.* **1997**, *119*, 3477; (c) S. Kashino, M. Tomita, M. Haisa, *Acta. Cryst.* **1988**, *C44*, 780.
22. (a) F. H. Allen, C. A. Baalham, J. P. M. Lommerse, P. R. Raithby, *Acta Cryst.* **1998**, *B54*, 320; (b) J. A. Olsen, D.W. Banner, P. Seiler, U. Obst-Sander, A. D'Arcy, M. Stihle, K. Müller, F. Diederich, *Angew. Chem. Int. Ed. Engl.* **2003**, *42*, 2507; (c) J. A. Olsen, D. W. Banner, P. Seiler, B. Wagner, T. Tschopp, U. Obst-Sander, M. Kansy, K. Müller, F. Diederich, *ChemBioChem* **2004**, *5*, 666.
23. R. Paulini, K. Müller, F. Diederich, *Angew. Chem. Int. Ed. Engl.* **2005**, *44*, 1788.

24. (a) K. Manoj, K. M. Sureshan, R. G. Gonnade, M. M. Bhadbhade, M. S. Shashidhar, *Cryst. Growth Des.* **2005**, *5*, 833; (b) K. Manoj, R. G. Gonnade, M. M. Bhadbhade, M. S. Shashidhar, *Cryst. Growth Des.* **2006**, *6*, 1485.
25. O. Hassel, C. Romming, *Quart. Rev. Chem. Soc.* **1962**, *16*.
26. P. M. Lommerse, A. J. Stone, R. Taylor, F. H. Allen, *J. Am. Chem. Soc.* **1996**, *118*, 3108.
27. N. Ramasubbu, R. Parthasarathy, P. Murray-Rust. *J. Am. Chem. Soc.* **1986**, *108*, 4308.
28. H. Adams, S. L. Cockroft, C. Guardigli, C. A. Hunter, K. R. Lawson, J. Perkins, S. E. Spey, C. J. Urch, R. Ford, *ChemBioChem.* **2004**, *5*, 657.
29. (a) H.-C. Weiss, R. Boese, H. L. Smith, M. M. Haley, *Chem. Commun.* **1997**, 2403; (b) J. M. A. Robinson, B. M. Kariuki, K. D. M. Harris, D. Philip, *J. Chem. Soc., Perkin Trans. 2* **1998**, 2459; (c) R. B. Walsh, C. W. Padgett, P. Metrangolo, G. Resnati, T. W. Hanks, W. T. Pennington, *Cryst. Growth Des.* **2001**, *1*, 165; (d) E. Bosch, C. L. Barnes, *Cryst. Growth Des.* **2002**, *2*, 299; (e) J. N. Moorthy, R. Natarajan, P. Mal, P. Venugopalan, *J. Am. Chem. Soc.* **2002**, *124*, 6530; (f) F. Zordan, L. Brammer, P. Sherwood, *J. Am. Chem. Soc.* **2005**, *127*, 5979; (g) R. G. Gonnade, M. M. Bhadbhade, M. S. Shashidhar, A. K. Sanki, *Chem. Commun.* **2005**, 5870; (h) C. M. Reddy, M. T. Kirchner, R. C. Gundakaram, K. A. Padmanabhan, G. R. Desiraju, *Chem. Eur. J.* **2006**, *12*, 2222;
30. C. B. Aakeröy, T. A. Evans, K. R. Seddon, I. Palinkó, *New J. Chem.* **1999**, 145.
31. (a) C. L. D. Gibb, E. D. Stevens, B. C. Gibb, *J. Am. Chem. Soc.* **2001**, *123*, 5849; (b) J.-A. van den Berg, K. R. Seddon, *Cryst. Growth Des.* **2003**, *3*, 643.

32. (a) V. R. Thalladi, H. C. Weiss, D. Bläser, R. Boese, A. Nangia, G. R. Desiraju, *J. Am. Chem. Soc.* **1998**, *120*, 8702; (b) M. D. Prasanna, T. N. Guru Row, *J. Mol. Struct.* **2001**, *562*, 55; (c) M. D. Prasanna, T. N. Guru Row, *J. Mol. Struct.* **2001**, *559*, 255; (d) A. R. Choudhury, U. K. Urs, T. N. Guru Row, K. Nagarajan, *J. Mol. Struct.* **2002**, *605*, 71;
33. P. Dastidar, H. Krupitsky, Z. Stein, I. J. Goldberg, *J. Incl. Phenom.* **1996**, *24*, 241.
34. M. D. Prasanna, T. N. Guru Row, *Cryst. Eng.* **2000**, *3*, 135.
35. I. Saraogi, V. G. Vijay, S. Das, K. Sekar, T. N. Guru Row, *Cryst. Eng.* **2003**, *6*, 69.
36. (a) I. Csoregh, E. Weber, T. Hens, M. Czugler, *J. Chem. Soc., Perkin Trans. 2*, **1996**, 2733; (b) R. K. R. Jetti, A. Nangia, F. Xue, T. C. W. Mak, *Chem. Commun.* **2001**, 919.
37. (a) G. R. Desiraju, *Angew. Chem., Int. Ed. Engl.* **1995**, *34*, 2311; (b) D. S. Reddy, D. C. Craig, G. R. Desiraju, *J. Am. Chem. Soc.* **1996**, *118*, 4090.
38. G. R. Desiraju, R. Parthasarathi, *J. Am. Chem. Soc.* **1989**, *111*, 8725.
39. S. L. Price, A. J. Stone, J. Lucas, R. S. Rowland, A. E. Thornley, *J. Am. Chem. Soc.* **1994**, *116*, 4910.
40. N. Ramasubbu, R. Parthasarathy, P. Murray-Rust, *J. Am. Chem. Soc.* **1986**, *108*, 4308.
41. (a) G. R. Desiraju, in *Organic Solid State Chemistry*, Ed.: G. R. Desiraju, Elsevier, Amsterdam, **1987**, pp. 519-546; (b) O. Navon, J. Bernstein, V. Khodorkovsky, *Angew. Chem. Int. Ed. Engl.* **1997**, *36*, 601; (c) E. Bosch, C. L. Barnes, *Cryst. Growth Des.* **2002**, *2*, 299; (d) A. Nangia, *CrystEngComm* **2002**, *4*, 93 (e) B. K. Saha, R. K. R. Jetti, L. S. Reddy, S. Aitipamula, A. Nangia, *Cryst. Growth Des.*

- 2005, 5, 887; (f) R. Paulini, K. Müller, F. Diederich, *Angew. Chem, Int. Ed. Engl.* **2005**, 44, 1788; (g) F. Zordan, L. Brammer, P. Sherwood, *J. Am. Chem. Soc.* **2005**, 127, 5979.
42. J. M. Dumas, L. Gomel, M. Guerin, Molecular Interactions Involving Organic Halides, *The Chemistry of Functional Groups, Supplement D*, Wiley, New York, 1983, pp. 985–1020.
43. (a) S. C. Blackstock, J. P. Lorand, J. P. Kochi, *J. Org. Chem.* **1987**, 52, 1451; (b) J. S. Murray, K. Paulsen, P. Politzer, *Proc. Indian Acad. Sci.* **1994**, 106, 267; (c) A. C. Legon, *Angew. Chem. Int. Ed. Engl.* **1999**, 38, 2686; (d) P. Metrangolo, G. Resnati, *Chem. Eur. J.* **2001**, 7, 2511.
44. (a) H. A. Bent, *Chem. Rev.* **1968**, 68, 587; (b) H. A. Bent, *Solutions and Solubilities*, Eds.: M. R. J. Dack, Part II, pp. 65-93. New York: Wiley; (c) P. Huyskens, *J. Mol. Struct. (Theochem.)* **1986**, 135, 67; (d) A. C. Legon, *Chem. Commun.* **1998**, 2737; (e) A. C. Legon, *Chem. Eur. J.* **1998**, 4, 1890; (f) A. C. Legon, *Angew. Chem. Int. Ed. Engl.* **1999**, 38, 2686.
45. R. S. Mulliken, W. B. Person, *Molecular Complexes: A Lecture and Reprint Volume*, Wiley-Interscience, New York, **1969**, and references therein.
46. R. Foster, *Organic Charge-Transfer Complexes*, **1969** (Academic, London)
47. C. K. Prout, B. Kamenar, *Molecular Complexes, Elek Science* (London), 1973, Vol. 1 pp. 151–207.
48. (a) M. W. Hanna, *J. Am. Chem. Soc.* **1968**, 90, 285; (b) H. I. Bloemink, A. C. Legon, J. C. Thorn, *J. Chem. Soc. Faraday Trans.* **1994**, 90, 781; (c) H. I. Bloemink, A. C. Legon, *J. Chem. Phys.* **1995**, 103, 876; (d) H. I. Bloemink, C. M. Evans, J. H.

- Holloway, A. C. Legon, *Chem. Phys. Lett.* **1996**, 251, 275; (e) K. Hinds, A. C. Legon, J. H. Holloway, *Mol. Phys.* **1996**, 88, 673; (f) E. R. Waclawik, J. M. A. Thumwood, D. G. Lister, P. W. Fowler, A. C. Legon, *Mol. Phys.* **1999**, 97, 159.
49. F. Guthrie, *J. Chem. Soc.* **1863**, 16, 239.
50. I. Remsen, J. F. Norris, *Am. Chem. J.* **1896**, 18, 90.
51. (a) O. Hassel, C. Romming, *Quart. Rev. Chem. Soc.* **1962**, 16, 1; (b) O. Hassel, *Science* **1970**, 170, 497.
52. O. Hassel, *Structural aspects of interatomic charge-transfer bonding, Nobel Lecture*, June 9, **1970**.
53. R. N. Brown, *Acta Cryst.* **1961**, 14, 711.
54. O. Jabay, H. Pritzkow, J. Jander, *Z. Naturforsch teil*, **1977**, 32, 1416.
55. K. Padmanabhan, I. C. Paul, D. Y. Curtin, *Acta Cryst.* **1990**, C46, 88.
56. M. N. Sabesan, K. Venkatesan, *Acta Cryst.* **1971**, B27, 986.
57. R. A. Pascal Jr., D. M. Ho, *Tet. Lett.* **1992**, 33, 4707.
58. (a) A. C. Legon, *J. Chem. Soc. Faraday Trans.* **1995**, 91, 1881; (b) A. C. Legon, *Chem. Commun.* **1998**, 2737; (c) A. C. Legon, *Chem. Eur. J.* **1998**, 4, 1890; (d) A. C. Legon, *Angew. Chem. Int. Ed.* **1999**, 38, 2686; (e) A. C. Legon, *Chem. Phys. Lett.* **1999**, 314, 472.
59. (a) A. C. Legon, N. W. Howard, *J. Chem. Phys.* **1988**, 88, 4694; (b) A. C. Legon, N. W. Howard, *J. Chem. Phys.* **1987**, 86, 6722.
60. P. Murray-Rust, W. D. S. Motherwell, *J. Am. Chem. Soc.* **1979**, 101, 4374.
61. N. Ramasubbu, R. Parthasarathy, Peter Murray-Rust, *J. Am. Chem. Soc.* **1986**, 108, 4308.

62. C. Ouvrard, J.-Y. Le Questel, M. Berthelot, C. Laurence, *Acta Cryst.* **2003**, B59, 512.
63. G. Valerio, G. Raos, S. V. Meille, P. Metrangolo, G. Resnati, *J. Phys. Chem A.* **2000**, 104, 1617.
64. Q. Chu, Z. Wang, Q. Huang, C. Yan, S. J. Zhu, *J. Am. Chem. Soc.* **2001**, 123, 11069.
65. P. Romaniello, F. Lelj, *J. Phys. Chem A* **2002**, 106, 9114.
66. (a) E. Bosch, C. L. Barnes, *Cryst. Growth Des.* **2002**, 2, 299; (b) A. Chana, M. A. Concejero, M. de Frutos, M. J. Gonzalez, B. Herradon, *Chem. Res. Toxicol.* **2002**, 15, 1514.
67. J.-W. Zou, Y.-J. Jiang, M. Guo, G.-X. Hu, B. Zhang, H.-C. Liu, Q.-S. Yu, *Chem. Eur. J.* **2005**, 11, 740.
68. (a) P. Metrangolo, G. Resnati, *Chem. Eur. J.* **2001**, 7, 2511; (b) P. Metrangolo, H. Neukrich, T. Pilati, G. Resnati, *Acc. Chem. Res.* **2005**, 38, 386.
69. A. Farina, S. V. Meille, M. T. Messina, P. Metrangolo, G. Resnati, G. Vecchio, *Angew. Chem. Int. Ed. Engl.* **1999**, 38, 2433.
70. M. T. Messina, P. Metrangolo, W. Panzeri, E. Ragg, G. Resnati, *Tetrahedron Lett.* **1998**, 39, 9069.
71. (a) P. Metrangolo, C. Präsang, G. Resnati, R. Liantonio, A. C. Whitwood, D. W. Bruce, *Chem. Commun.* **2006**, 3290; (b) J. Xu, X. Liu, J. K.-P. Ng, T. Lin and C. He, *J. Mater. Chem.* **2006**, 16, 3540.
72. N. F. Cheetham, A. D. E. Pullin, *Chem. Commun.* **1967**, 233.
73. V. R. Pedireddi, J. A. R. P. Sarma, G. R. Desiraju, *J. Chem. Soc. Perkin Trans. 2* **1992**, 311; (b) G. R. Desiraju, V. R. Pedireddi, J. A. R. P. Sarma, D. E. Zacharias;

- Acta Chim. Hung.* **1993**, 451; (c) A. Ranganathan, V. R. Pedireddi, *Tetrahedron Lett.* **1998**, 1803.
74. (a) E. Corradi, S. V. Meille, M. T. Messina, P. Metrangolo, G. Resnati, *Tetrahedron Lett.* **1999**, 40, 7519; (b) P. Cardillo, E. Corradi, A. Lunghi, S. V. Meille, M. T. Messina, P. Metrangolo, G. Resnati, *Tetrahedron* **2000**, 56, 5535; (c) K. M. Sureshan, R. G. Gonnade, V. G. Puranik, M. S. Shashidhar, M. M. Bhadbhade, *Chem. Commun.* **2001**, 881; (d) F. Fontana, A. Forni, P. Metrangolo, W. Panzeri, T. Pilati, G. Resnati, *Supramol. Chem.* **2002**, 14, 47; (e) P. Metrangolo, T. Pilati, G. Resnati, Stevenazzi, *Curr. Opin. Colloid Interface Sci.* **2003**, 8, 215; (f) P. Metrangolo, T. Pilati, G. Resnati, A. Stevenazzi, *Chem. Commun.* **2004**, 1492.
75. T. Carona, R. Liantonio, T. A. Logothetic, P. Metrangolo, G. Resnati, *J. Am. Chem. Soc.* **2004**, 126, 4500.
76. P. Metrangolo, H. Neukrich, T. Pilati, G. Resnati, *Acc. Chem. Res.* **2005**, 38, 386.
77. (a) R. B. Walsh, C. W. Padgett, P. Metrangolo, G. Resnati, T. W. Hanks, W. T. Pennington, *Cryst. Growth Des.* **2001**, 1, 165; (b) A. Crihfield, J. Hartwell, D. Phelps, R. B. Walsh, J. L. Harris, J. F. Payne, W. T. Pennington, T. W. Hanks, *Cryst. Growth Des.* **2003**, 3, 313.
78. E. C. Olson, R. E. Christoffersen, Computer-Assisted Drug Design, ACS Symposium Series, No. 112, American Chemical Society, Washington DC., **1979**.
79. (a) V. Cody, P. Murray-Rust, *J. Mol. Struct.* **1984**, 112, 189. (b) L. K. Steinrauf, J. A. Hamilton, B. C. Braden, (c) J. R. Murrel, M. D. Benson, *J. Biol. Chem.* **1993**, 268, 2425.

80. E. C. Jorgensen, in C. H. Li (Ed.), *Hormonal Proteins and Peptides*, Academic Press, New York, **1978**, 6, 108.
81. M. Adler, M. J. Kochanny, B. Ye, G. Rumennik, D. R. Light, S. Biancalana, M. Whitlow, *Biochemistry* **2002**, 41, 15514.
82. J. R. Bertaccini, J. R. J. Trudell, *Anaesth.* **2002**, 89, 32.
83. P. Auffinger, F. A. Hays, E. Westhof, P. Shing Ho, *PNAS*, **2004**, 101, 16789.
84. E. De Moliner, N. R. Brown, L. N. Johnson, *Eur. J. Biochem.* **2003**, 270, 3174.
85. A. I. Kitaigorodskii, *Organic Chemical Crystallography; Consultant's Bureau*: New York, 1961. (English translation of the Russian original published by Press of the Academy of Sciences of the USSR, Moscow, 1955).
86. J. S. Moore, S. Lee, *Chem. Ind.* **1994**, 556; (b) G. B. Gardner, D. Venkataraman, J. S. Moore, S. Lee, *Nature* **1995**, 374, 792.
87. M. M. Conn, J. Jr. Rebek, *Chem. Rev.* **1997**, 97, 1647; (b) J. Jr. Rebek, *Acc. Chem. Res.* **1999**, 32, 278.
88. M. R. Caira, L. R. Nassimbeni, *Comprehensive Supramolecular Chemistry*, Eds.: J. L. Atwood, J. E. D. Davies, D. D. MacNicol, F. Vogtle, Elsevier, Oxford, 1996, Vol.6, pp.825-850.
89. (a) J. M. Lehn, *Supramolecular Chemistry: Concepts and Perspectives*, VCH Verlag, Weinheim, 1995; (b) J. Rebec. Jr., *Acc. Chem. Res.* **1999**, 32, 278.
90. (a) L. R. Nassimbeni, *Acc. Chem. Res.* **2003**, 36, 631; (b) L. R. Nassimbeni, *Supramol. Chem.* **2000**, 12, 161.
91. (a) G. R. Desiraju, in *Comprehensive Supramolecular Chemistry in Comprehensive Supramolecular Chemistry*, Eds.: J. L. Atwood, J. E. D. Davies, D. D. MacNicol, F.



- Vogtle, Elsevier, Oxford, 1996, *Vol.6*, pp.1-22; (b) R. Bishop, *Chem. Soc. Rev.* **1996**, 311-320; (c) G. R. Desiraju, T. Steiner, *The weak Hydrogen Bond In structural chemistry and Biology*, IUCr monograph, Oxford Science Publications, **1999**; (d) G. R. Desiraju, *Crystal Engineering* **1989**, Elsevier, New York; (e) V. A. Russel, C. C. Evans, W. Li, M. D. Ward, *Science* **1997**, 276, 575; (f) D. D. MacNicol, J. J. Mckendrick, D. R. Wilson, *Chem. Rev. Soc.* **1978**, 7, 65.
92. E. Weber, in *Inclusion Compounds*; Eds.: J. L. Atwood, J. E. D. Davies, D. D. MacNicol; Oxford University Press, Oxford, **1991**, *Vol. 4*, pp. 188.
93. D. J. Cram, J. M. Cram, *Container molecules and their guests*, Royal Society of Chemistry, Cambridge, **1994**.
94. F. Vogtle, in *Supramolecular Chemistry*, Wiley, Chichester, UK, **1991**, Chapter 5.
95. J. W. Steed, J. L. Atwood, *Supramolecular Chemistry*, Wiley, Chichester, UK, **2000**, Chapter 1.
96. (a) G. A. Jeffrey, *An Introduction to Hydrogen Bonding*, Oxford University Press, New York, **1997**; (b) G. A. Jeffrey, W. Saenger, *Hydrogen Bonding in Biological Structures*, Springer-Verlag, Berlin, **1991**.
97. (a) T. Kobayashi, S. Isoda and K. Kubono, in *Comprehensive Supramolecular Chemistry*, Eds.: J. L. Atwood, J. E. D. Davies, D. D. MacNicol, F. Vogtle, Elsevier, Oxford, 1996, *Vol.6*, pp.399-419; (b) E. Weber, in *Kirk-Othmer Encyclopedia of Chemical Technology*, Ed.: J. L. Kroschwitz, Wiley, New York, 1995, 4<sup>th</sup> Edn., *Vol.14* pp.122-154; (c) In *Comprehensive Supramolecular Chemistry*, Eds.: J. L. Atwood, J. E. D. Davies, D. D. MacNicol, F. Vogtle, Elsevier, Oxford, 1996, *Vol. 1-11*.

98. (a) E. Weber, *Top. Curr. Chem.* **1987**, *140*, 3; (b) D. Braga, J. Humphrey, Editorial. *CrystEngCommun.* **2003**, *5*, 1.
99. (a) M. R. Caira, L. R. Nassimbeni, F. Toda, D. Vujovic, *J. Am. Chem. Soc.* **2000**, *122*, 9367; (b) L. R. Nassimbeni, *Supramol. Chem.* **2000**, *12*, 161.
100. C. Liang, C. S. Ewig, T. R. Stouch, A. T. Hagler, *J. Am. Chem. Soc.* **1994**, *116*, 3904.
101. R. Parthasarathy, F. Eisenberg, *Biochem. J.* **1986**, *235*, 313.
102. Nomenclature Committee-IUB, *Biochem. J.* **1989**, *258*, 1.
103. B. V. L. Potter, D. Lampe, *Angew. Chem. Int. Ed. Engl.* **1995**, *34*, 1933.
104. J. R. Thomas, R. A. Dwek, T. W. Rademacher, *Biochemistry*, **1990**, *29*, 5413.
105. L. Qiao, F. Nan, M. Kunkel, A. Gallegos, G. Powis, A. P. Kozikowski, *J. Med. Chem.* **1998**, *41*, 3303.
106. (a) A. P. Kozikowski, A. H. Fauq, G. Powis, I. A. Aksoy, D. C. Melder, S. Aksoy, H. Eicjinger, *Cancer Chemother. Pharmacol.* **1991**, *29*, 95; (b) A. P. Kozikowski, A. H. Fauq, G. Powis, I. A. Aksoy, M. J. Seewald, *J. Am. Chem. Soc.* **1990**, *112*, 7403.
107. K. M. Sureshan, M. S. Shashidhar, T. Praveen, T. Das, *Chem. Rev.* **2003**, *103*, 4477.
108. H. W. Lee, Y. J. Kishi, *J. Org. Chem.* **1985**, *50*, 4402.
109. D. C. Billington, R. Baker, J. J. Kulagowski, I. M. Mawer, J. P. Vacca, S. J. deSolms, J. R. Huff, *J. Chem. Soc. Perkin Trans. 1* **1989**, 1423.
110. P. Uhlmann, A. Vasella, *Helv. Chim. Acta* **1992**, *75*, 1979.
111. K. M. Sureshan, Ph. D. Thesis-*Chemistry of Inositols: Novel synthesis of O-protected myo-inositols via myo-inositol 1,3,5-orthoesters and synthetic myo-inositol*

*derivatives as host for cations and neutral organic guests*, submitted to University of Pune, India, January 2002.

112. K. M. Sureshan, R. G. Gonnade, V. G. Puranik, M. S. Shashidhar, M. M. Bhadbhade, *Chem. Commun.* **2001**, 881.
113. DSC studies of all the solvates and polymorphs were carried out on Mettler Instrument.
114. Bruker (1998). SMART. Version 5.0. Bruker AXS Inc., Madison, Wisconsin, USA.
115. Bruker. SMART (V5.628), SAINT (V6.45a). Bruker AXS Inc. Madison, Wisconsin, USA, 2004.
116. G. M. Sheldrick, *SHELXS97, SHELXL97*: University of Göttingen, Germany. **1997**.
117. M. N. Burnett, C. K. Johnson, ORTEP III. Report ORNL-6895. Oak-Ridge National Laboratory, Oak Ridge, Tennessee, USA, 1996.
118. K. Kobayashi, K. Ishii, S. Sakamoto, T. Shirasaka, K. Yamaguchi, *J. Am. Chem. Soc.* **2003**, *125*, 10615.
119. (a) M. Fujita, S. Nagao, K. Ogura, *J. Am. Chem. Soc.* **1995**, *117*, 1649; (b) M. C. Calama, P. Timmerman, D. N. Reinhoudt, *Angew. Chem., Int. Ed.* **2000**, *39*, 755; (c) F. Hof, C. Nuckolls, J. Jr. Rebek, *J. Am. Chem. Soc.* **2000**, *122*, 4251; (d) Y. Kubota, S. Sakamoto, K. Yamaguchi, M. Fujita, *Proc. Natl. Acad. Sci. U.S.A.* **2002**, *99*, 4854.
120. A. L. Spek, PLATON – a multipurpose crystallographic tool, Utrecht University, The Netherlands, **2002**.
121. W. C. McCrone, Polymorphism in Physics and Chemistry of the Organic Solid State, Eds: D. Fox, M. M. Labes, Weissberger, Wiley Interscience, New York, **1965**, Vol. II, pp. 726-767.

122. Selected books and reviews: (a) *Polymorphism in Pharmaceutical Solids, Drugs and the Pharmaceutical Sciences*, Vol. 95, Ed.: H. G. Brittain, Marcel Dekker, Inc.: New York, 1999. (b) J. Bernstein, *Polymorphism in Molecular Crystals*; Oxford University Press: Oxford, Great Britain, 2002. (c) J. A. R. P. Sarma, G. R. Desiraju, In *Crystal Engineering: Polymorphism and Pseudopolymorphism in Organic Crystals: A Cambridge Structural Database Study*, Eds.: S. R. Seddon, M. Zaworotko, Kluwer: Norwell, MA, USA, 1999; p 325. d) T. L. Threlfall, *Analyst* **1995**, *120*, 2435; e) G. R. Desiraju, *Science* **1996**, *278*, 404.
123. Some special issues: (a) “Polymorphism and Crystallization” in *Org. Process res. & Dev.* **2000**, *4*, 371; (b) “ Polymorphism in Crystals: Fundamentals, Prediction and Industrial Practice” in *Cryst. Growth Des.* **2003**, *3*, 867; International Conferences: (c) Polymorphism in Crystals: Fundamentals, Prediction and Industrial Practice, Saddlebrook Resort, Tampa, Florida, USA, February 2003. (d) Diversity Amidst Similarity: a Multidisciplinary Approach to Polymorphs, Solvates and Phase Relationships, 35th Course: International School of Crystallography, June 9-20, Erice, Sicily, Italy, 2004.
124. T. Threlfall, *Org. Process Res. Dev.* **2000**, *4*, 384. (b) R. K. R. Jetti, R. Boese, J. A. R. P. Sarma, L. S. Reddy, P. Vishweshwar, G. R. Desiraju, *Angew. Chem. Int. Ed. Engl.* **2003**, *42*, 1963.
125. (a) A. R. Verma, P. Krishna, *Polymorphism and Polytypism in Crystals*, John Wiley, New York, **1966**, pp. 15-30; (b) W. Ostwald, *Z. Physick. Chem.* **22**, 289, 1897; (c) W. Ostwald, *Lehrbuch der Allgemeinen, Chemie 2*, W. Engelmann, Leipzig, Germany, **1896**, p.444; (d) W. Ostwald, *Grundriss der Allgemeinen, Chemie*, W. Engelmann,

- Leipzig, Germany, 1899; (e) J. W. Mullin, *Crystallization*, 3<sup>rd</sup> Ed. Butterworth Heinemann, London, UK, 1993, pp.172-201.
- 126.(a) R. M. Vrcelj, G. H.Gallagher, J. N. Sherwood, *J. Am. Chem. Soc.* **2001**, 123, 2291–2295; (b) R. J. Davey, N. Blagden, S. Righini, H. Alison, M. J. Quayle, S. Fuller, *Cryst. Growth Des.* **2001**, 1, 59 and references therein.
- 127.J. Bernstein, R. J. Davey, J.-O. Henck, *Angew. Chem. Int. Ed. Engl.* **1999**, 38, 3440.
- 128.S. M. Reed, T. J. R. Weakley, J. E. Hutchison, *Cryst. Eng.* **2000**, 3, 85.
- 129.N. Z. Stanacev, M. Kates, *J. Org. Chem.* **1961**, 26, 912.
- 130.R. G. Gonnade, M. S. Shashidhar, M. M. Bhadbhade, *Chem. Commun.* **2004**, 2530.
- 131.(a) A. Kálmán, L. Párkányi, Gy. Argay, *Acta Cryst.* **1993**, B49, 1039; (b) A. Kálmán, L. Párkányi, *Adv. Mol. Struct. Res.* **1997**, 3, 189; (c) L. Fábián, A. Kálmán, *Acta Cryst.* **1999**, B55, 1099; (d) A. Kálmán, Gy. Argay, G. Bernáth, Zs. Gyarmati, *J. Am. Chem. Soc.* **2003**, 125, 34; (e) L. Fábián, A. Kálmán, *Acta Cryst.* **2004**, B60, 547; (f) A. Kálmán, *Acta Cryst.* **2005**, B61, 536; (f) G. Bhosekar, C. Murali, R. G. Gonnade, M. S. Shashidhar, M. M. Bhadbhade, *Cryst. Growth Des.* **2005**, 5, 1977; (g) K. Manoj, R. G. Gonnade, M. M. Bhadbhade and M. S. Shashidhar, *Cryst. Growth Des.* **2006**, 6, 1485.
- 132.(a) B. S. Green, M. Lahav, D. Rabinovich, *Acc. Chem. Res.* **1979**, 12, 191; (b) J. Jacques, A. Collet, S. H. Wilen, *Enantiomers, Racemates and Resolutions*, Wiley, New York, **1981**, pp 14-23; (c) U. De Rossi, S. Dahne, S. C. J. Meskers, H. P. J. M. Dekkers, *Angew. Chem. Int. Ed. Engl.* **1996**, 35, 760; (d) H. Koshima, S. Honke and J. Fujita, *J. Org. Chem.* **1999**, 64, 3916; (e) M. Szyrszyng, E. Nowak, M. Milewska and T. Poinoski, *Tetrahedron Asymmetry* **2004**, 15, 103.

- 133.(a) E. B. Fleischer, N. Sung, S. J. Hawkinson, *J. Phys. Chem.* **1968**, 72, 4311; (b) A. Tanatani, K. Yamaguchi, I. Azumaya, R. Fukutomi, K. Shudo, H. Kagechika, *J. Am. Chem. Soc.* **1998**, 120, 6433.
- 134.H. Koshima, Y. Wang, T. Matsuura, *Mol. Cryst. Liq. Cryst.* **1996**, 277, 63.
- 135.G. Ferguson, C. Glidewell, *Acta. Cryst.* **2001**, C57, 264.
- 136.(a) T. Steiner, W. Hinrichs, W. Saenger, *Acta Cryst.* **1993**, B49, 708; (b) J. D. Dunitz, J. Bernstein, *Acc. Chem. Res.* **1995**, 28, 193; (c) M. Kaftory, M. Botoshansky, M. Kapon, V. Shteiman, *Acta Cryst.* **2001**, B57, 791; (d) D. Hashizume, N. Miki, T. Yamazaki, Y. Aoyagi, T. Arisato, H. Uchiyama, T. Endo, M. Yasui, F. Iwasakia, *Acta Cryst.* **2003**, B59, 404; (e) M. A. Fernandes, D. C. Levendis, C. B. de Koning, *Acta. Cryst.* **2004**, B60, 300 and references therein.
137. (a) S. G. Frank, *J. Pharma. Sci.* **1975**, 64, 1585; (b) M. D. Ward, A. M. Pivovar, *Current Opinion in Solid State and Mesoporous Material Science*, **1999**, 4, 581; (c) H. I. Süss, J. Hulliger, *Microporous and Mesoporous Materials* **2005**, 78, 23.
- 138.(a) A. K. Cheetham, G. Férey, T. Loiseau, *Angew. Chem. Int. Ed. Engl.* **1999**, **38**, 3268; (b) J. S. Seo, D. Whang, H. Lee, S. I. Jun, J. Oh, Y. J. Jeon, K. Kim, *Nature* **2000**, 404(6781), 982.
- 139.K. M. Sureshan, M. S. Shashidhar, *Tetrahedron Lett.* **2000**, 41, 4185.
- 140.M. P. Sarmah, Ph.D. thesis; University of Pune, Pune-2005.
- 141.K. Manoj, S. Devraj, R. G. Gonnade, M. S. Shashidhar, M. M. Bhadbhade, *Acta Cryst.* **2005**, C61, 628.
- 142.C. B. Aakeröy, A. M. Beatty, M. Tremayne, D. M. Rowe, C. C. Seaton, *Cryst. Growth Des.* **2001**, 1, 377.

- 143.S. Aitipamula, G. R. Desiraju, M. Jaskólski, A. Nangia, R. Thaimattam, *CrystEngComm* **2003**, *5*, 447.
144. Cambridge Crystals Structure Database, v5.26, November 2004.
- 145.A. I. Kitaigorodskii, *Adv. Struct. Res. Diffr. Methods* **1970**, *3*, 173.
- 146.(a) T. Praveen, U. Samanta, T. Das, M. S. Shashidhar, P. Charkrabarti, *J. Am. Chem. Soc.* **1998**, *120*, 3842; (b) M. P. Sarmah, R. G. Gonnade, M. S. Shashidhar, M. M. Bhadbhade, *Chem. Eur. J.* **2005**, *11*, 2103.
- 147.(a) M. Mazik, D. Bläser, R. Boese, *Tett. Lett.* **1999**, *40*, 4783; (b) R. Bishop, I. G. Dance, *Top. Curr. Chem.* **1988**, *149*, 137; (c) K. Tanaka, H. Osuga, Y. Kitahara, *Journal of the Chemical Society. Perkin Transactions 2*, **2000**, *12*, 2492 and references therein.
- 148.T. Koritsanszky, R. Flaig, D. Zobel, H. –G. Krane, W. Morgenroth, P. Luger, *Science* **1998**, *279*, 356; (b) R. Flaig, T. Koritsanszky, J. Janczak, H. –G. Krane, W. Morgenroth, P. Luger, *Angew. Chem. Int. Ed. Engl.* **1999**, *38*, 1397.
- 149.(a) V. G. Tsirel'son, R. P. Ozerov, *Electron Density and Bonding in Crystals*, Institute of Physics Publishing: Bristol, 1996; (c) P. Coppens, *X-ray Charge Densities and Chemical Bonding*, Oxford University Press: Oxford, UK, 1997; (c) Ed.: C. H. Schenk, *Crystallography across the Sciences*: International Union of Crystallography: Chester, UK, 1998; (d) F. L. Hirshfeld, *Crystallogr. Rev.* **1991**, *2*, 169; (e) M. A. Spackman, *Chem. Rev.* **1992**, *92*, 1769; (f) M. A. Spackman, A. S. Brown, *Annu. Rep. Prog. Chem. Sect. C: Phys. Chem.* **1994**, *91*, 175; (g) M. A. Spackman, *Annu. Rep. Prog. Chem. Sect. C: Phys. Chem.* **1997**, *94*, 177; (h) T. S. Koritsanszky, P. Coppens, *Chem. Rev.* **2001**, *101*, 1583; (i) P. Coppens, *Acta Cryst.*

- 1998**, *A54*, 779; (j) A. Martin, A. A. Pinkerton, *Acta Cryst.* **1998**, *B54*, 471; (k) A. Volkov, G. Wu, P. Coppens, *J. Synchrotron Rad.* **1999**, *6*, 1007; (l) S. Dahaoui, C. Jelsch, J. A. K. Howard, C. Lecomte, *Acta Cryst.* **1999**, *B55*, 226; (m) Y. A. Abramov, A. Volkov, G. Wu, P. Coppens, *Acta Cryst.* **2000**, *A56*, 585.
150. N. K. Hansen, P. Coppens, *Acta Cryst.* **1978**, *A34*, 909.
151. T. S. Koritsanszky, S. Howard, P. Macchi, C. Gatti, L. J. Farrugia, P. Mallinson, A. Volkov, Z. Su, T. Richter, N. K. Hansen, *XD* (version 4.10, July), *A computer program package for multipole refinement and analysis of electron densities from diffraction data*. Free University of Berlin, Germany; University of Wales, Cardiff, UK; Università di Milano, UK; CNR-ISTM, Milano, UK; University of Glasgow, UK; State University of New York, Buffalo, USA; University of Nancy, France, 2003.
152. (a) R. F. W. Bader, *Atoms in Molecules—A Quantum Theory*: Clarendon, Oxford, 1990; (b) R. F. W. Bader, *J. Phys. Chem.* **1998**, *A102*, 7314.
153. P. Coppens, *Acta Cryst.* **1998**, *A54*, 779
154. (a) P. L. A. Popelier, *Atoms in Molecules. An Introduction*: Prentice Hall, UK, pp150–153, 2000; (b) U. Koch, P. L. A. Popelier, *J. Phys. Chem.* **1995**, *99*, 9747.
155. R. Bees, *Acta Cryst.* **1970**, *B26*, 1304.
156. R. H. Blessing, *Crystallogr. Rev.* **1987**, *1*, 3.
157. E. Clementi, C. Roetti, *Atomic Data and Nuclear Data Tables.* **1974**, *14*, 177.
158. F. H. Allen, *Acta Cryst.* **1986**, *B42*, 515.
159. V. R. Saunders, R. Dovesi, C. Roetti, M. Causà, N. M. Harrison, R. Orlando, C. M. Zicovich-Wilson, *CRYSTAL98 User's Manual*, University of Torino, Torino, 1998.



- 160.(a) A. Bach, D. Lentz, P. Luger, *J. Phys. Chem. A* **2001**, *105*, 7405; (b) D. E. Hibbs, J. Overgaard, J. A. Platts, M. P. Waller, M. B. Hursthouse, *J. Phys. Chem. B* **2004**, *108*, 3663.
- 161.(a) E. B. Fleischer, N. Sung, S. J. Hawkinson, *J. Phys. Chem.* **1968**, *72*, 4311; (b) A. Tanatani, K. Yamaguchi, I. Azumaya, R. Fukutomi, K. Shudo, H. Kagechika, *J. Am. Chem. Soc.* **1998**, *120*, 6433.
- 162.(a) Suzuki, T. Fukushima, Y. Yamashita, T Miyashi, *J. Am. Chem. Soc.* **1994**, *116*, 2793; (b) M. Sakamoto, *Chem. Eur. J.* **1997**, *3*, 684; (c) B. L. Feringa, R. A. van Delden, *Angew. Chem. Int. Ed. Engl.* **1999**, *38*, 3418.
- 163.H. Koshima, Y. Wang, T. Matsuura, *Mol. Cryst. Liq. Cryst.* **1996**, *277*, 63.
- 164.S.L. Mayo, B. D. Olafson, W.A. Goddard, *J. Phys. Chem.* **1990**, *94*, 8897.
- 165.J. Gasteiger, M. Marsili, *Tetrahedron* **1980**, *36*, 3219.
- 166.P. Ewald, *Ann. Phys.* **1921**, *64*, 253.
- 167.Program package Cerius<sup>2</sup>, Version 4.9, Accelrys Ltd., 334 Cambridge Science Park, Cambridge CB4 0WN, England.
- 168.P. Coppens, T. N. Guru Row, P. Leung, E. D. Stevens, P. J. Becker, Y. W. Yang, *Acta Cryst.* **1979**, *A35*, 63.
- 169.(a) F. L. Hirshfeld, *Acta Cryst.* **1971**, *B27*, 769; (b) R. F. Stewart, *Acta Cryst.* **1976**, *A32*, 565.
- 170.P. Seiler, *Accurate Molecular Structures. Their Determination and Importance*, Eds.: A. Domenicano, I. Hargittai, Oxford University Press: Oxford, p 170. 1992.
- 171.R. H. Blessing, *Acta Cryst.* **1995**, *A51*, 33.
- 172.A. Volkov, C. Gatti, Yu. Abramov, P. Coppens, *Acta Cryst.* **2002**, *A56*, 252–258.

- 173.(a) Y. A. Abramov, A. Volkov, G. Wu, P. Coppens, *Acta Cryst.* **2000**, *A56*, 585; (b) Z. Kisiel, *PROSPE: Programs for Rotational Spectroscopy*, available from <http://info.ifpan.edu.pl/~kisiel/prospe.htm>.
- 174.F. L. Hirshfeld, *Acta Crystallogr.* **1976**, *A32*, 239.
- 175.T. Honda, I. Fujii, N. Hirayama, N. Aoyama, A. Miike, *Acta Cryst.***1996**, *C52*, 395.
- 176.(a) A. Bondi, *J. Phys. Chem.* **1964**, *68*, 441; (b) S. C. Nyburg, C. H. Faerman, *Acta Cryst.* **1985**, *B41*, 274.



## List of Publications

1. Kana. M. Sureshan, **Rajesh. G. Gonnade**, Vedavati. G. Puranik, Mysore. S. Shashidhar, Mohan. M. Bhadbhade, A highly host-guest system formed and stabilized due to concerted halogen...oxygen and C-H...O non-bonded interactions: X-ray structures of racemic 1,2,3,4,5-penta-O-benzoyl –6-O-tosyl myo-inositol - dihalomethane (CH<sub>2</sub>X<sub>2</sub>, X=Cl, Br) inclusion complexes, *Chem. Commun.* **2001**, 881-882.
2. **R. G. Gonnade**, Mohan M. Bhadbhade and Mysore S. Shashidhar, Capturing a metastable chiral polymorph of an achiral molecule hexa-O-benzoyl-myo-inositol, *Chem. Commun.* **2004**, 2530-2531.
3. **R. G. Gonnade**, M. M. Bhadbhade, M. S. Shashidhar, A. K. Sanki, Concomitant dimorphs of tri-O-[p-halobenzoyl]-myo-inositol 1,3,5-orthoformates with different halogen bonding contacts: first order crystal-to-crystal thermal phase transition of kinetic form to the thermodynamic form, *Chem Commun.* **2005**, 5870-5872.
4. Manash P. Sarmah, **Rajesh G. Gonnade**, Mysore S. Shashidhar, Mohan M. Bhadbhade Benzoyl Transfer Reactivities of racemic 2,4-di-O-acyl-myo-inositol 1,3,5-orthoesters in the Solid State: Molecular Packing and Intermolecular Interactions Correlate with the Facility of the Reaction, *Chem. Eur. J.* **2005**, *11*, 2103.
5. Gaurav Bhosekar, Chebrolu Murali, **Rajesh G. Gonnade**, Mysore S. Shashidhar, Mohan M. Bhadbhade, Identical Molecular Strings Woven Differently by Intermolecular Interactions in Dimorphs of myo-Inositol 1,3,5-Orthobenzoate *Cryst. Growth Des.* **2005**, *5*, 1977-1982.
6. K. Manoj, Kana M. Sureshan, **Rajesh G. Gonnade**, Mohan M. Bhadbhade, Mysore S. Shashidhar, Short S=O...C=O Contacts Associate Diastereomers of 2,4(6)-Di-O-benzoyl-6(4)-O-[(1*S*)-10-camphorsulfonyl]-myo-inositol 1,3,5-Orthoformate in Their Inclusion Complexes, *Cryst. Growth Des.* **2005**, *5*, 833-836.

7. K. Manoj, **Rajesh G. Gonnade**, Mohan M. Bhadbhade, Mysore S. Shashidhar, Subtle Crossover from C-H $\cdots$ O to S=O $\cdots$ C=O Short Contacts in the Association of Diastereomers of 2,4(6)-Di-*O*-benzoyl-6(4)-*O*-[(1*S*)-10-camphorsulfonyl]-*myo*-inositol 1,3,5-Orthoformate upon Formation of Pseudopolymorphs, *Cryst. Growth Des.* **2006**, *6*, 1485-1492.
8. K. Manoj, Devaraj S. **Rajesh G. Gonnade**, Mohan M. Bhadbhade, and Mysore S. Shashidhar, O-H $\cdots$ O-bridged dimers linked via C-H $\cdots$ O and C-H $\cdots$  $\pi$  interactions in 4,6-di-*O*-benzyl-*myo*-inositol 1,3,5-orthoformate, *Acta Cryst.* **2005**, *C61*, 628-630.
9. **Rajesh G. Gonnade**, Kana M. Sureshan, Mohan M. Bhadbhade, Mysore S. Shashidhar, Spontaneous Formation of Stable Inclusion Crystals of 1,2,3,4,5-*O*-benzoyl-6-*O*-tosyl *myo*-inositol induced only by Dihalomethane Solvents via C-Halogen $\cdots$ O=C and C-H $\cdots$ O Contacts (manuscript under preparation).
10. **Rajesh G. Gonnade**, Mohan M. Bhadbhade, Mysore S. Shashidhar, Pseudopolymorphic Behaviour of hexa-*O*-benzoyl *myo*-inositol: Gradual Escape of the Guest from Inclusion Crystal Lattice, (manuscript under preparation).
11. **Rajesh G. Gonnade**, Mohan M. Bhadbhade, Mysore S. Shashidhar, Pseudopolymorphic Behaviour of Racemic 1, 2, 3, 5, 6-penta-*O*-benzoyl-4-*O*-benzyl-*myo*-inositol, (manuscript under preparation).
12. **Rajesh G. Gonnade**, Mohan M. Bhadbhade, Mysore S. Shashidhar, Single Crystal to Single Crystal Phase Transition of Room Temperature Form to High Temperature Form and Solvatomorphism in Hexa-*O*-*p*-toluoyl-*myo*-inositol, (manuscript under preparation).
13. **Rajesh G. Gonnade**, Kana M. Sureshan, Mohan M. Bhadbhade, Mysore S. Shashidhar, Exploring the Inclusion Behaviour of 4,6-di-*O*-benzoyl-*myo*-inositol-1,3,5-orthoformate: Isostructurality in Host Organization and Self-Inclusion Phenomena, and Stabilities of Inclusion Crystals Correlated With Host...Guest Halogen Bonding Contacts, (manuscript under preparation).
14. **Rajesh G. Gonnade**, Mohan M. Bhadbhade, Mysore S. Shashidhar, Polymorphic and Pseudopolymorphic Behaviour of racemic 2,6-di-*O*-(*p*-halobenzoyl)-*myo*-inositol 1,3,5-orthoformates: Different Halogen Bonding Contacts in Molecular

- Associations and Crystal-to-Crystal Phase Transition, (manuscript under preparation).
15. **Rajesh G. Gonnade**, Mohan M. Bhadbhade, Mysore S. Shashidhar, Conformational Polymorphism of 2-*O*-tosyl-4,6-di-*O*-benzoyl-*myo*-inositol-1,3,5-orthoformate: Three Room Temperature Forms Transforms to High Temperature Form Upon Heating by Crystal-to-Crystal Phase Transition, (manuscript under preparation).
  16. Chebrolu Murali, Mysore S. Shashidhar, **Rajesh G. Gonnade**, Mohan M. Bhadbhade, Investigating Organization of Molecules that Facilitates Intermolecular Acyl Transfer in Crystals: Reactivity and X-Ray Structures of *O*-benzoyl-*myo*-inositol 1,3,5-orthoesters, submitted to *Eur. J. Org. Chem.* **2006**.
  17. Chebrolu Murali, Mysore S. Shashidhar, **Rajesh G. Gonnade**, Mohan M. Bhadbhade, Nucleating Reactive polymorph of non-Reactive *myo*-inositol derivative: Benzoyl Transfer Reactivity of racemic 2,4-di-*O*-benzoyl-*myo*-inositol 1,3,5-orthoacetate in the Solid State and Crystal-to-Crystal Phase Transition, (manuscript under preparation).
  18. **Rajesh G. Gonnade**, Gaurav V. Bhosekar, Manash P. Sarmah, Kana M. Sureshan, Mohan M. Bhadbhade, Mysore S. Shashidhar, Solvent induced polymorphism in *myo*-inositol 1, 3, 5 orthoesters: X-ray Structures of Four Triols and Their Polymorphs, (manuscript under preparation).

Apart from the group, crystallography service was rendered to other research group in NCL. Some selected publications of this work are given below,

19. Amol Kendhale, **Rajesh Gonnade**, Pattuparampil R. Rajamohanan and Gangadhar J. Sanjayan, Isotactic *N*-alkyl acrylamide oligomers assume self-assembled sheet structure: first unequivocal evidence from crystal structures, *Chem. Commun.* **2006**, 2756. (*published as hot article*)
20. Pranjal K. Baruah, **Rajesh Gonnade**, Usha D. Phalgune, Gangadhar J. Sanjayan, Self-Assembly with Degenerate Prototropy, *J. Org. Chem.* **2005**, 70, 6461.

21. Bapurao B. Shingate , Braja G. Hazra , Vandana S. Pore , **Rajesh G. Gonnade** and Mohan M. Bhadbhade, Ionic hydrogenation of C-20, 22-ketene dithioacetal: Stereoselective synthesis of steroidal C (20R) aldehydes, *Chem. Commun.* **2004**, 2194.
22. T. Govindaraju, **Rajesh G. Gonnade**, Mohan M. Bhadbhade, Vaijayanti A. Kumar, Krishna N. Ganesh, 1S,2R/1R,2S)-Aminocyclohexyl Glycyl Thymine PNA: Synthesis, Monomer Crystal Structures, and DNA/RNA Hybridization Studies, *Org. Lett.* **2003**, 5, 3013.
23. C. V. Ramana, S. M. Baquer, **R. G. Gonnade** and M. K. Gurjar, Expedient synthesis of tetrakis (cyclopropyl methyl) methane, *Chem. Commun.* **2002**, 614.
24. Subhash P. Chavan, Pallavi Sharma, Rasapalli, Sivappa, Mohan M. Bhadbhade, **Rajesh G. Gonnade**, and Uttam R. Kalkote, Enantioselective Synthesis of L-CCG-I, *J. Org. Chem.* **2003**, 68, 6817.

### **Paper Presented in National and International Seminars**

1. Concomitant Polymorphs Exhibiting Differences in the Halogen Bonding Contacts, **R. G. Gonnade**, M. M. Bhadbhade, M. S. Shashidhar, A. K. Sanki, *presented in XX International Union of Crystallography Congress and General Assembly held at Florence, Italy from 23<sup>rd</sup> August to 31<sup>st</sup> August 2005.*
2. Polymorphism in Ortho Esters of *myo*- Inositol: Structures of *myo*-inositol 1,3,5-orthoacetate, **Rajesh G. Gonnade**, Gaurav Bhosekar, Mysore S. Shashidhar, Mohan M. Bhadbhade, *papers presented in 34<sup>nd</sup> National Seminar on Crystallography held at Department of Chemistry, Guwahati University, Guwahati, Assam, India from 10-12 January 2005.*
3. Solvent induced polymorphism in *myo*-inositol triols: Synthesis and X-ray structures of three triols and their polymorphs, **R. G. Gonnade**, G. Bhosekar, M. P. Sarmah, C. Murali, K. M. Sureshan, M. S. Shashidhar and M. M. Bhadbhade, *papers presented in 33<sup>rd</sup> National Seminar on Crystallography held at National Chemical Laboratory, Pune, India from 8-10 January 2004.*

4. Role of Weak interactions in controlling the rate of intermolecular acyl transfer in solid-state: X-ray structures and reactivity correlation in 2,4-di-*O*-benzoyl –*myo*-inositol 1,3,5-orthoesters, **R. G. Gonnade**, M. P. Sarmah, M. S. Shashidhar, and M. M. Bhadbhade, *presented in 32<sup>nd</sup> National Seminar on Crystallography held at University of Jammu, Jammu Tawi from 24<sup>th</sup> to 26<sup>th</sup>, October 2002.*
5. Acyl transfer reactions of *myo*-inositol derivatives in the solid state and correlation with their crystal structures, **R. G. Gonnade**, M. P. Sarmah, M. S. Shashidhar, and M. M. Bhadbhade, *presented in "IV National Symposium in Chemistry" held at National Chemical Laboratory, Pune from 1<sup>st</sup> to 3<sup>rd</sup>, February 2002.*
6. A highly selective host-guest system formed and stabilised due to weak halogen...oxygen non bonded interactions: X-ray structures of racemic 1,2,3,4,5-penta-*O*-Benzoyl-6-*O*-tosyl *myo*-inositol –dihalomethane (CH<sub>2</sub>X<sub>2</sub>, X=Cl and Br), **R. G. Gonnade**, K. M. Sureshan, M. S. Shashidhar, M. M. Bhadbhade, *paper presented in "32<sup>nd</sup> International School of Crystallography held at Ettore Majorana Centre for Scientific Culture, Erice, Trapani, Sicily, Italy from 23<sup>rd</sup> may to 3<sup>rd</sup> June 2001.*
7. Role of halogen bonding in formation of stable inclusion complexes: X-ray structures of *myo*-inositol derivatives with –Dihalomethane (CH<sub>2</sub>X<sub>2</sub>, X=Cl and Br), **R. G. Gonnade**, K. M. Sureshan M. S. Shashidhar, and M. M. Bhadbhade, *paper presented in "IV Meeting of Asian Crystallographic Association" held at Indian Institute of Science, Bangalore from 18<sup>th</sup> to 21<sup>st</sup>, November 2001.*
8. Self-Assembly and molecular Recognition properties of Myo-Inositol derivatives: Structural Studies on inclusion complexes of racemic 1,2,3,4,5-Penta-*O*-Benzoyl - 6- *O*-Tosyl Myo-Inositol, **R. G. Gonnade**, M. M. Bhadbhade, K. M. Sureshan, M. S. Shashidhar, *presented in "Fifth IUPAC International Symposium on Bio-Organic Chemistry" held at National Chemical Laboratory during 30th January to 4<sup>th</sup> February 2000.*
9. Open Channel Formation with the Inclusion Of a Solvent Molecule stabilized by C-H...O interactions in the structure of racemic 1,2,3,4,5-Penta-*O*-benzoyl-6-*O*-Tosyl Myo-Inositol, **R. G. Gonnade**, M. M. Bhadbhade, K. M. Sureshan and M. S. Shashidhar, *presented in Golden Jubilee Symposium on " Small scale in space and*



*time" held at National Chemical Laboratory, Pune, India during 3<sup>rd</sup> to 5<sup>th</sup> November 1999.*

### **Talks Delivered**

1. 'Role of halogen bonding in formation of stable inclusion complexes: x-ray structures of myo-inositol derivatives with dihalomethanes (CH<sub>2</sub>X<sub>2</sub>, X= Cl, Br)' at 32<sup>nd</sup> National Seminar on Crystallography held at Department of Physics, University of Jammu, Jammu Tawi from 24 -26, October 2002.
2. 'Halogen bonding interactions as a decisive factor in the formation and stability of inclusion crystals: synthesis and structures of inclusion complexes of myo-inositol derivatives with alkyl halides as guests' at 33<sup>nd</sup> National Seminar on Crystallography held at National Chemical Laboratory, Pune from 8-10 January 2004.
3. 'Halogen bonding interactions in promotion of crystal growth: Structures of myo-inositol derivatives and a survey of CCDC of halo solvated inclusion complexes.' at 34<sup>nd</sup> National Seminar on Crystallography held at Department of Chemistry, Guwahati University, Guwahati, Assam, India from 10-12 January 2005.

### **Awards**

1. Best poster award at 34<sup>th</sup> National Seminar on crystallography held at Department of Chemistry, Guwahati University, Guwahati, Assam, India from 10 -12 January 2005.
2. Best poster award at 32<sup>nd</sup> International School of crystallography '*Strength from Weakness, Consequences of Weak Interactions in Molecules, Supramolecules and Crystals*' held at Erice, Sicily, Italy from 23<sup>rd</sup> May 2001-3<sup>rd</sup> June 2001.
3. Best poster award in the electron microscopy meeting organized by electron microscopy society of India, held at Punjab University, Chandigarh, India on 9-11 February 2001.

*"Thus, the task is, not so much to see what no one  
has yet seen; but to think what nobody has yet  
thought, about that which everybody sees."*

- Erwin Schrodinger